AUGUST 2026
VOLUME 85
ISSUE
8

ANNALS OF THE RHEUMATIC DISEASES

THE EULAR JOURNAL

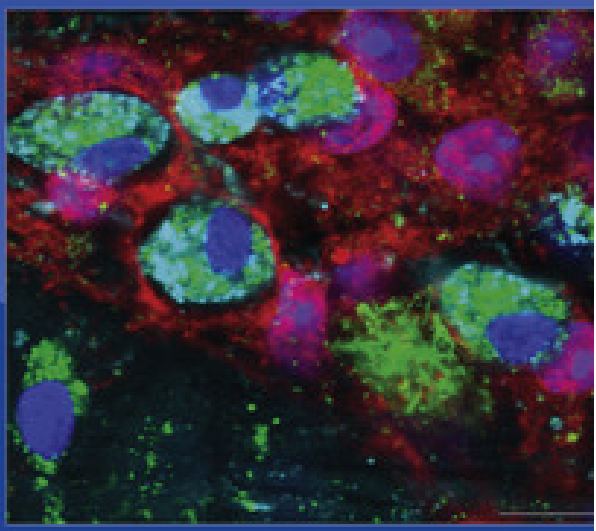

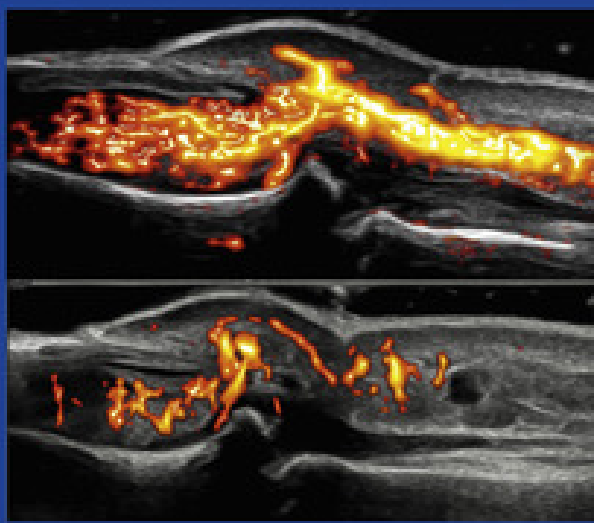

ELSEVIER

eular
EUROPEAN ALLIANCE OF ASSOCIATIONS FOR RHEUMATOLOGY

The home of innovative rheumatology research

Ann Rheum Dis 85 (2026) 1445–1449

Contents lists available at ScienceDirect

Annals of the Rheumatic Diseases

journal homepage: https://www.sciencedirect.com/journal/annals-of-the-rheumatic-diseases

Viewpoint

Subclinical psoriatic arthritis: concepts, dilemmas, and research needs

Fadi Kharouf[1,2,3], Pankti Mehta[1,2,4], Virginia Carrizo Abarza[1,2], Richard J. Cook[5], Vinod Chandran[1,2,4,6], Denis Poddubnyy[1,2,4,*]

[1] *Gladman Krembil Psoriatic Arthritis Program, Centre for Prognosis Studies in the Rheumatic Diseases, Schroeder Arthritis Institute, University Health Network, Toronto, ON, Canada*
[2] *Division of Rheumatology, Department of Medicine, University of Toronto, Toronto, ON, Canada*
[3] *Rheumatology Unit, Department of Medicine, Hadassah Medical Center and Faculty of Medicine, Hebrew University of Jerusalem, Jerusalem, Israel*
[4] *Institute of Medical Science, University of Toronto, Toronto, ON, Canada*
[5] *Department of Statistics and Actuarial Science, University of Waterloo, Waterloo, ON, Canada*
[6] *Department of Laboratory Medicine and Pathobiology, University of Toronto, Toronto, ON, Canada*

ARTICLE INFO

Article history:
Received 26 December 2025
Received in revised form 10 February 2026
Accepted 11 March 2026

ABSTRACT

Psoriatic arthritis (PsA) develops in up to one-third of patients with psoriasis (PsC), yet increasing attention is now focused on a putative subclinical phase preceding overt arthritis. Several conceptual frameworks describe the PsC–PsA transition, including the pragmatic definition proposed by the European Alliance of Associations for Rheumatology, which defines subclinical PsA as arthralgia and/or imaging abnormalities in the absence of clinical synovitis. However, the absence of validated serological biomarkers, the marked clinical heterogeneity of PsA, the frequent occurrence of nonspecific musculoskeletal symptoms, and the limited specificity of imaging findings complicate risk stratification and may lead to misclassification and overtreatment. Lessons from rheumatoid arthritis highlight both the potential and the pitfalls of applying prevention paradigms to subclinical disease. This viewpoint critically appraises current definitions of subclinical PsA, discusses therapeutic and trial-design implications, and outlines key research priorities, including longitudinal PsC cohorts, advanced and molecular imaging, and multiomic biomarker discovery. Future progress depends on developing robust risk-stratification models that capture the full spectrum of psoriatic disease and enable targeted prevention strategies while minimising unnecessary intervention. At the same time, caution is warranted against broad expansion of the 'subclinical' disease state concept, as it may dilute disease definitions, increase overdiagnosis, and divert attention from improving early and accurate identification of clinically meaningful PsA.

INTRODUCTION

Psoriatic arthritis (PsA) is a chronic inflammatory disease that develops in up to one-third of individuals with psoriasis (PsC) [1]. The clinical diagnosis is typically made once overt musculoskeletal inflammation, such as arthritis, enthesitis, dactylitis, or axial disease, becomes apparent [1,2]. Recently, attention has been directed to a so-called 'subclinical' phase of PsA [3–5], motivated by observations that many patients with PsC experience musculoskeletal symptoms or demonstrate imaging abnormalities before PsA becomes clinically evident [4,6,7]. Beyond musculoskeletal symptoms and imaging findings,

*Correspondence to Dr Denis Poddubnyy, University Health Network - Toronto Western Hospital, 399 Bathurst St, Toronto, ON M5T 2S8, Canada.
E-mail address: denis.poddubnyy@utoronto.ca (D. Poddubnyy).
Handling editor Josef S. Smolen.

https://doi.org/10.1016/j.ard.2026.03.011

several clinical and demographic factors have been associated with increased risk of progression from PsC to PsA, including severe skin disease, nail involvement, obesity, family history, and genetic susceptibility, although their predictive value at the individual level remains limited [1,3,8,9].

The concept of subclinical PsA presents potential opportunities but also poses a dilemma for modern rheumatology. Early identification may enable interventions that prevent progression to established PsA, thus preserving function and quality of life [1,4]. At the same time, the lack of a clear definition risks misclassification and overtreatment and may divert attention from efforts to improve the early and accurate recognition of clinically meaningful PsA. This viewpoint critically appraises the current understanding of subclinical PsA and potential avenues for future research to enhance clinical care.

THE CURRENT CONCEPT AND DEFINITIONS

Several working groups have proposed frameworks to study the PsC–PsA transition, each using distinct terminology and thresholds for 'subclinical disease' [3,8,9]. The Scher model [8] describes a 5-stage process: (1) PsC with risk factors such as human leukocyte antigen B*27 (*HLA-B*27*) genotype, obesity, or severe skin disease; (2) preclinical PsA with immune activation; (3) asymptomatic subclinical PsA with imaging abnormalities; (4) prodromal PsA with arthralgia and fatigue; and (5) clinically diagnosed PsA [8]. This model remains conceptual, as the immune, radiologic, and molecular subclinical events that precede PsA onset have yet to be fully characterised. The Preventing Arthritis in a Multicenter Psoriasis At-Risk (PAMPA) consensus (2021) proposed an alternative framework for the PsC–PsA transition, classifying PsC patients into 3 groups: those with risk factors, those with asymptomatic synovio-entheseal imaging abnormalities, and those with unexplained musculoskeletal symptoms [9]. This represents a more pragmatic approach that emphasises 'synovio-entheseal inflammation' as a hallmark of PsA, although its operational definitions remain to be explored.

The European Alliance of Associations for Rheumatology (EULAR) task force (2023) offered the most pragmatic definition of subclinical PsA, primarily for use in clinical trials: arthralgia and/or imaging abnormalities in the absence of clinical synovitis [3]. In its framework for the PsC–PsA transition, the task force distinguished long-term risk factors (e.g., PsC severity, obesity, family history) from short-term factors (eg, arthralgia, imaging changes) [3]. Clinical synovitis was considered the hallmark of transition to established PsA, while arthralgia and imaging findings served as early warning signs [3]. This approach helps clarify disease evolution, as the absence of reliable biomarkers makes it challenging to detect underlying immune abnormalities in the preclinical stage, unlike in rheumatoid arthritis (RA) [10,11].

Although overlapping, these frameworks diverge on what constitutes the threshold of PsA versus 'preclinical' or 'subclinical' disease, with important consequences for research and clinical decision-making. Furthermore, terms such as 'preclinical,' 'prodromal,' and 'subclinical' PsA are often used interchangeably [3,8,9], further complicating clarity in trial design and clinical practice.

LESSONS FROM PRECLINICAL RA

In RA, a preclinical phase is recognised in individuals with serological autoimmunity (anti-citrullinated protein antibodies [ACPA] or rheumatoid factor), arthralgia, and subclinical synovitis detectable by ultrasound or magnetic resonance imaging (MRI) but without clinically detectable swollen joints [11,12]. EULAR/American College of Rheumatology risk-stratification criteria define such at-risk cohorts, reporting progression rates of ~12% within 1 year and ~21% within 2 years [11]. MRI markedly enhances predictive accuracy (area under the curve ≈ 0.93), whereas ultrasound adds little when layered onto optimised clinical and serological models [11]. Importantly, these criteria are intended to standardise the identification of research cohorts, not to serve as clinical guidelines for initiating treatment [11].

Prevention trials in RA suggest that while complete prevention remains challenging, interventions can delay disease progression or improve symptoms and imaging [13–17]. Two major challenges underlie these variable results: (1) phenotypic noise: arthralgia and imaging abnormalities are often nonspecific, reflecting osteoarthritis or mechanical changes; and (2) some individuals may already have clinically silent RA, meaning that interventions may treat very early disease rather than truly prevent its onset.

These experiences caution against uncritical expansion of pre-disease concepts, particularly in PsA, where the absence of validated biomarkers, marked clinical heterogeneity, and frequent comorbidities together amplify the risks of misclassification and inappropriate intervention.

IMPLICATIONS FOR PSC–PSA TRANSITION

The same challenges apply to psoriatic disease, with additional complexity. PsA lacks validated serological markers analogous to ACPA and features broader clinical heterogeneity: peripheral enthesitis and axial involvement may occur without synovitis [1]. Moreover, musculoskeletal symptoms in PsC are common, often nonspecific, and frequently influenced by comorbidities, such as osteoarthritis and obesity [1,6,8,18]. Imaging modalities, including ultrasound and MRI, can detect early inflammatory changes, although their predictive value remains incompletely defined. Indeed, they detect synovio-entheseal inflammation in over 45% of PsC patients [5,19,20], yet a significantly smaller proportion progress to PsA [1]. This underscores the potentially limited specificity of imaging, as detected abnormalities may reflect mechanical or degenerative changes rather than true inflammation. Although imaging is valuable for identifying inflammatory changes, its predictive role across various modalities in asymptomatic or minimally symptomatic patients remains uncertain [21].

The EULAR framework defined clinically evident synovitis as the hallmark of transition to PsA [3]. However, several limitations challenge this definition: (1) clinical joint examination has limited reliability, particularly in mild disease, risking underdetection in the absence of imaging [22]; (2) the marked heterogeneity of PsA means that peripheral enthesitis or axial involvement may occur without overt synovitis, and current synovitis-centred definitions therefore overlook entheseal and axial disease, failing to capture the full clinical spectrum of PsA [1,23–25]; and (3) patients with arthralgia and imaging abnormalities may have already developed PsA, challenging the concept of truly 'subclinical' disease. Furthermore, some at-risk individuals may progress rapidly to clinically apparent PsA after triggers such as trauma, without a discernible transition phase [3].

THERAPEUTIC IMPLICATIONS

The central question is whether and how to intervene in the subclinical phase. This challenge aligns with the emerging concept of disease interception, which seeks to modify disease trajectory through intervention at subclinical or at-risk stages before the onset of clinically manifest inflammatory arthritis [5]. In psoriatic disease, observational data and prevention-oriented initiatives, including PAMPA-related efforts, reflect growing interest in interception strategies, although methodological limitations continue to constrain the strength and clinical applicability of available evidence [26–30].

Some patients with PsC and arthralgia may already have true subclinical inflammatory disease. Early intervention in these individuals could potentially prevent progression to established PsA, thereby reducing joint damage and preserving quality of life. However, questions remain as to whether musculoskeletal symptoms in a patient with PsC can truly be considered 'subclinical,' and, more importantly, whether this stage may already be too advanced to prevent transition to clinically apparent arthritis. Conversely, expanding treatment to all patients with arthralgia and/or imaging abnormalities risks overtreatment. Thus, the challenge lies in distinguishing patients with true subclinical inflammation, or, ideally, those at risk of developing it who could benefit from early intervention, from individuals with nonspecific findings (eg, degenerative changes), to balance the potential benefits of prevention against the risks of unnecessary therapy. Given current limitations in prediction, a pragmatic priority is to improve early and accurate identification of clinically relevant PsA and to define reliable predictors of progression within PsC, rather than further expanding poorly defined pre-disease categories.

RETHINKING SUBCLINICAL PSA: TOWARDS CLEAR DEFINITIONS

Clinical trials evaluating the impact of disease-modifying antirheumatic drugs on PsA risk in PsC patients require clear, validated, and reliable definitions of patient groups before enrolment. EULAR's definition of subclinical PsA provides a reference [3], but broad inclusion risks enrolling heterogeneous cohorts and diluting the predictive value of such trials. As in RA, imprecisely defined 'at-risk' PsA cohorts may encompass:

1. Patients with early PsA lacking overt synovitis;
2. Patients with musculoskeletal symptoms due to degenerative or mechanical causes; and
3. Patients truly transitioning towards PsA (Figure).

Without appropriate stratification, this heterogeneity may obscure treatment effects and increase the risk of trial failure. A practical study design might enrol PsC patients without musculoskeletal complaints at baseline, then enrich the cohort using risk markers such as nail disease, obesity, or severe skin involvement, explicitly excluding symptomatic patients.

In clinical practice, the population transitioning from subclinical disease to clinically manifest PsA appears to be limited in size and challenging to identify prospectively, given the often narrow time window before overt PsA develops. Clearer descriptive terminology is required to differentiate clinically and prognostically distinct patient groups, with explicit incorporation of imaging findings, such as:

1. PsC with nonspecific musculoskeletal symptoms (arthralgia without objectively detectable inflammation).
2. PsC with imaging abnormalities alone.
3. PsC with both arthralgia and imaging abnormalities—this group likely includes patients who have already transitioned to PsA.

This approach avoids premature disease labelling while still acknowledging risk and guiding monitoring strategies based on the patient's current clinical profile.

Future frameworks for the PsC–PsA transition must capture the full disease spectrum, including enthesitis and axial disease, using imaging capable of detecting inflammation across these domains. Parallel translational research should prioritise biomarker discovery and validation to enable robust risk stratification, analogous to ACPA in RA. Ultimately, the goal is not additional terminology, but a conceptual and methodological framework that minimises misclassification, accounts for heterogeneity, and targets intervention to those most likely to benefit.

IMPLICATIONS FOR RESEARCH

Key priorities for future research include improved understanding and identification of early markers of PsA development

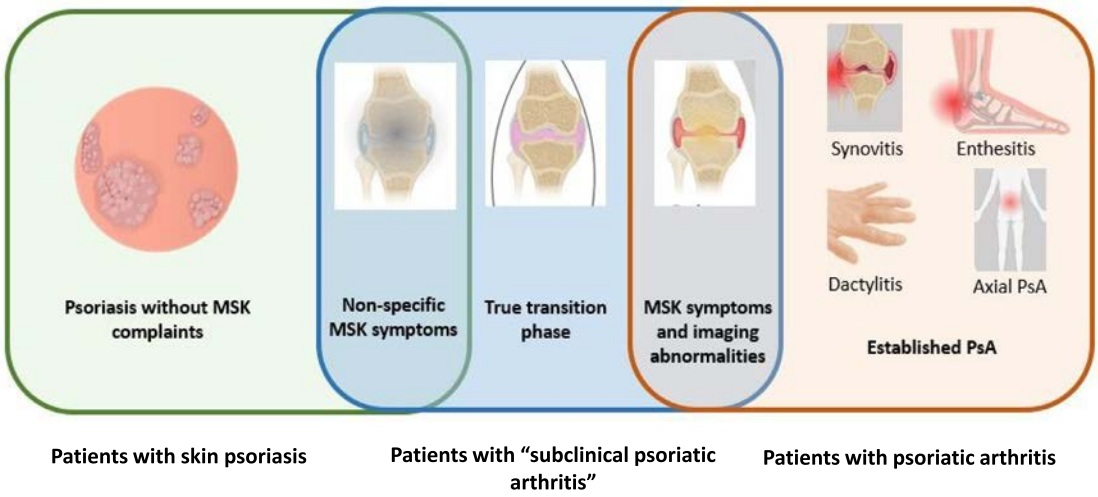

Figure. Illustration of the subgroups comprising the spectrum of psoriatic disease, including the current 'subclinical PsA' definition. MSK, musculoskeletal; PsA, psoriatic arthritis.

in patients with PsC, enabling individualised risk stratification. This will likely require the development of longitudinal inception cohorts of patients with recent-onset PsC, integrating detailed clinical phenotyping with advanced imaging modalities, such as MRI. In parallel, comprehensive molecular risk profiling should be pursued, encompassing soluble biomarkers, genetic susceptibility factors, transcriptomic signatures, metabolomic profiles, and other emerging molecular readouts relevant to PsA pathogenesis. In addition to conventional imaging, molecular imaging using tracers targeting key immunopathological pathways may offer the opportunity to visualise immunologically driven inflammation and thereby improve early and accurate diagnosis of PsA, which remains a major unmet need in the field. Finally, PsA prevention trials should carefully exclude individuals with established imaging abnormalities or overt musculoskeletal symptoms, to avoid conflating early treatment with true disease prevention and to focus on individuals who are genuinely at risk of developing clinically manifest PsA.

CONCLUSIONS

The notion of subclinical PsA has received increased attention, but the concept of early disease remains ambiguous. Some 'subclinical' patients may already meet PsA criteria; others may never progress, as their symptoms may be unrelated to psoriatic disease. Restricting the diagnosis to synovitis oversimplifies a heterogeneous disease, whereas inaccurate interpretation of symptoms or imaging can lead to overdiagnosis. Continued expansion of loosely defined preclinical categories risks diluting disease definitions and exposing patients to unnecessary investigation or treatment without clear clinical benefit.

For trials, the EULAR framework provides a pragmatic yet imperfect foundation that requires development. In practice, descriptive terminology based on risk factors, symptoms, and imaging better captures uncertainty while avoiding premature labelling.

Progress will depend on improving early and accurate diagnosis of clinically meaningful PsA and on developing robust risk-stratification models within PsC cohorts to identify those truly at risk of progression. Rather than further expanding broadly defined pre-disease categories, future efforts should prioritise diagnostic precision and clinically meaningful risk prediction to ensure that earlier identification of PsA improves patient outcomes without increasing overdiagnosis or unnecessary treatment.

Contributors

All authors made significant contributions to the conception and design of this study. All authors reviewed and approved the final manuscript.

Funding

The Gladman Krembil Psoriatic Arthritis Program is funded by a grant from the Krembil Foundation and the Schroeder Arthritis Institute. Vinod Chandran is supported by the Dr Dafna D. Gladman Chair in Psoriatic Arthritis Research, a joint Hospital-University Named Chair between the University of Toronto, the University Health Network, and the UHN Foundation. Denis Poddubnyy is supported by a grant from the Krembil Foundation.

Competing interests

FK, PM, VCA, and RJC have no conflicts of interest. VC has received research grants from AbbVie, Eli Lilly, and Johnson and Johnson, and has received honoraria for advisory board member roles from AbbVie, Bristol-Myers Squibb, Eli Lilly, Fresenius Kabi, Johnson and Johnson, Novartis, Takeda, and UCB. His spouse is an employee of AstraZeneca. He serves as a member of the board of directors of GRAPPA and is its co-Vice President. DP has received research support from AbbVie, Eli Lilly, Johnson and Johnson, Novartis, Pfizer, and UCB; consulting fees from AbbVie, Eli Lilly, GlaxoSmithKline, Greywolf Therapeutics, Johnson and Johnson, Merck, Moonlake, Novartis, Pfizer, and UCB; and speaker fees from AbbVie, Canon, Celltrion, Eli Lilly, Globemed, Johnson and Johnson, Medscape, Novartis, Peervoice, Pfizer, and UCB. He serves as a member of the executive committee of ASAS and the steering committee of GRAPPA.

Patient consent for publication

Not applicable.

Ethics approval

Not applicable.

Provenance and peer review

Not commissioned; externally peer reviewed.

Orcid

Fadi Kharouf: http://orcid.org/0000-0002-3540-0341
Denis Poddubnyy: http://orcid.org/0000-0002-4537-6015

REFERENCES

[1] Kharouf F, Gladman DD. Advances in the management of psoriatic arthritis in adults. BMJ 2024;387:e081860.
[2] Kharouf F, Gladman DD. Treatment controversies in spondyloarthritis and psoriatic arthritis: focus on biologics and targeted therapies. Expert Rev Clin Immunol 2024;20(11):1381–400.
[3] Zabotti A, De Marco G, Gossec L, Baraliakos X, Aletaha D, Iagnocco A, et al. EULAR points to consider for the definition of clinical and imaging features suspicious for progression from psoriasis to psoriatic arthritis. Ann Rheum Dis 2023;82(9):1162–70.
[4] Zabotti A, Fagni F, Gossec L, Giovannini I, Sticherling M, Tullio A, et al. Risk of developing psoriatic arthritis in psoriasis cohorts with arthralgia: exploring the subclinical psoriatic arthritis stage. RMD Open 2024;10(2):e004314.
[5] López-Medina C, McGonagle D, Gossec L. Subclinical psoriatic arthritis and disease interception—where are we in 2024? Rheumatology (Oxford) 2025;64(1):56–64.
[6] Eder L, Polachek A, Rosen CF, Chandran V, Cook R, Gladman DD. The development of psoriatic arthritis in patients with psoriasis is preceded by a period of nonspecific musculoskeletal symptoms: a prospective cohort study. Arthritis Rheumatol 2017;69(3):622–9.
[7] Zabotti A, McGonagle DG, Giovannini I, Errichetti E, Zuliani F, Zanetti A, et al. Transition phase towards psoriatic arthritis: clinical and ultrasonographic characterisation of psoriatic arthralgia. RMD Open 2019;5(2):e001067.
[8] Scher JU, Ogdie A, Merola JF, Ritchlin C. Preventing psoriatic arthritis: focusing on patients with psoriasis at increased risk of transition. Nat Rev Rheumatol 2019;15(3):153–66.
[9] Perez-Chada LM, Haberman RH, Chandran V, Rosen CF, Ritchlin C, Eder L, et al. Consensus terminology for preclinical phases of psoriatic arthritis for use in research studies: results from a Delphi consensus study. Nat Rev Rheumatol 2021;17(4):238–43.
[10] Veale DJ, Fearon U. What makes psoriatic and rheumatoid arthritis so different? RMD Open 2015 Apr;1(1):e000025.

[11] van Steenbergen HW, Doornkamp F, Alivernini S, Backlund J, Codreanu C, Cohen SB, et al. EULAR/American College of Rheumatology risk stratification criteria for development of rheumatoid arthritis in the risk stage of arthralgia. Arthritis Rheumatol 2026;78(3):523–36.
[12] Petrovská N, Prajzlerová K, Vencovský J, Šenolt L, Filková M. The pre-clinical phase of rheumatoid arthritis: From risk factors to prevention of arthritis. Autoimmun Rev 2021;20(5):102797.
[13] Gerlag DM, Safy M, Maijer KI, Tang MW, Tas SW, Starmans-Kool MJF, et al. Effects of B-cell directed therapy on the preclinical stage of rheumatoid arthritis: the PRAIRI study. Ann Rheum Dis 2019;78(2):179–85.
[14] Deane KD, Striebich CC, Feser ML, O'Dell JR, James JA, Sparks JA, et al. A phase 2 trial of hydroxychloroquine in individuals at risk for rheumatoid arthritis. Arthritis Rheumatol 2025. Published online August 29. doi: 10.1002/art.43366.
[15] Krijbolder DI, Verstappen M, Van Dijk BT, Dakkak YJ, Burgers LE, Boer AC, et al. Intervention with methotrexate in patients with arthralgia at risk of rheumatoid arthritis to reduce the development of persistent arthritis and its disease burden (TREAT EARLIER): a randomised, double-blind, placebo-controlled, proof-of-concept trial. Lancet 2022;400(10348):283–94.
[16] Dumoulin QA, Krijbolder DI, Visser K, Lard LR, van der Helm-van Mil AHM. Development of rheumatoid arthritis after methotrexate in anticitrullinated protein antibody-negative people with clinically suspect arthralgia at risk of rheumatoid arthritis: 4-year data from the TREAT EARLIER trial. Lancet Rheumatol 2024;6(12):e827–36.
[17] Cope AP, Jasenecova M, Vasconcelos JC, Filer A, Raza K, Qureshi S, et al. Abatacept in individuals at high risk of rheumatoid arthritis (APIPPRA): a randomised, double-blind, multicentre, parallel, placebo-controlled, phase 2b clinical trial. Lancet 2024;403(10429):838–49.
[18] Kharouf F, Gao S, Pereira D, Cook RJ, Chandran V, Gladman DD. Degenerative disc disease in young adults with psoriatic arthritis. J Rheumatol 2025;52(6):583–9.
[19] Acquacalda E, Albert C, Montaudie H, Fontas E, Danre A, Roux CH, et al. Ultrasound study of entheses in psoriasis patients with or without musculoskeletal symptoms: a prospective study. Joint Bone Spine 2015;82(4):267–71.
[20] Erdem CZ, Tekin NS, Sarikaya S, Erdem LO, Gulec S. MR imaging features of foot involvement in patients with psoriasis. Eur J Radiol 2008;67(3):521–5.
[21] Dubash SR, De Marco G, Wakefield RJ, Tan AL, McGonagle D, Marzo-Ortega H. Ultrasound imaging in psoriatic arthritis: what have we learnt in the last five years? Front Med 2020;7:487.
[22] Gazel U, Solmaz D, Ayan G, Ivory C, Karsh J, Aydin SZ. Accuracy of physical examination to detect synovial and extra-synovial pathologies in psoriatic arthritis in comparison to ultrasonography. J Clin Med 2020;9(9):2929.
[23] Kaeley GS, Eder L, Aydin SZ, Gutierrez M, Bakewell C. Enthesitis: a hallmark of psoriatic arthritis. Semin Arthritis Rheum 2018;48(1):35–43.
[24] Kharouf F, Mehta P, Gao S, Pereira D, Cook R, Gladman DD, et al. Comparative analysis of disease outcomes: Early vs. late transition from psoriasis to psoriatic arthritis. Semin Arthritis Rheum 2025;71:152639.
[25] Poddubnyy D, Jadon DR, Van den Bosch F, Mease PJ, Gladman DD. Axial involvement in psoriatic arthritis: an update for rheumatologists. Semin Arthritis Rheum 2021;51(4):880–7.
[26] Kharouf F, Anacleto-Dabarno M, Cook RJ, Chandran V, Poddubnyy D. Understanding the transition from psoriasis to psoriatic arthritis: the role of targeted therapy. EULAR Rheumatol Open 2026;2(1):58–61.
[27] Gisondi P, Bellinato F, Targher G, Idolazzi L, Girolomoni G. Biological disease-modifying antirheumatic drugs may mitigate the risk of psoriatic arthritis in patients with chronic plaque psoriasis. Ann Rheum Dis 2022;81(1):68–73.
[28] Meer E, Merola JF, Fitzsimmons R, Love TJ, Wang S, Shin D, et al. Does biologic therapy impact the development of PsA among patients with psoriasis? Ann Rheum Dis 2022;81(1):80–6.
[29] Gisondi P, Bellinato F, Galeone C, Turati F, Idolazzi L, Zabotti A, et al. Risk of developing psoriatic arthritis in patients with psoriasis initiating treatment with different classes of biologics. Ann Rheum Dis 2025 Mar;84(3):435–41.
[30] Haberman RH, MacFarlane KA, Catron S, Samuels J, Blank RB, Toprover M, et al. Efficacy of guselkumab, a selective IL-23 inhibitor, in Preventing Arthritis in a Multicentre Psoriasis At-Risk cohort (PAMPA): protocol of a randomised, double-blind, placebo controlled multicentre trial. BMJ Open 2022;12(12):e063650.

Ann Rheum Dis 85 (2026) 1450–1462

Contents lists available at ScienceDirect

Annals of the Rheumatic Diseases

journal homepage: https://www.sciencedirect.com/journal/annals-of-the-rheumatic-diseases

Inflammatory arthritis

RA and PsA synovial tissue single-cell analysis demonstrates differential fibroblast populations with distinct phenotypes and functional capacities

Órla Tynan[1], Aenea A.I. Brugman[1], Conor M. Smith[2], Mary Canavan[3], Aoife M. O'Rourke[3], Achilleas Floudas[4,5], Dumitru Anton[1], Siobhán Wade[1], Sonia Sundanum[6], Jean M. Fletcher[2,7], Carl Orr[6], Douglas J. Veale[6], Ursula Fearon[1,6,*]

[1] *Molecular Rheumatology, Trinity Biomedical Sciences Institute, Trinity College Dublin, Dublin, Ireland*
[2] *School of Biochemistry and Immunology, Trinity College Dublin, Dublin, Ireland*
[3] *Translational Immunopathology, Schools of Biochemistry and Immunology and Medicine, Trinity College Dublin, Dublin, Ireland*
[4] *Life Sciences Institute, Dublin City University, Dublin, Ireland*
[5] *Medical School, University of Ioannina, Ioannina, Greece*
[6] *EULAR Centre of Excellence, Centre for Arthritis and Rheumatic Diseases, St Vincent's University Hospital, Dublin, Ireland*
[7] *School of Medicine, Trinity Biomedical Sciences Institute, Trinity College Dublin, Dublin, Ireland*

ARTICLE INFO

Article history:
Received 18 December 2025
Received in revised form 4 March 2026
Accepted 11 March 2026

ABSTRACT

Objectives: This study determines the phenotypic and functional characteristics that define distinct fibroblast-like synoviocyte (FLS) populations in rheumatoid arthritis (RA) vs psoriatic arthritis (PsA).

Methods: Single-cell RNA sequencing and multiparametric flow cytometry analysis (21 markers) were performed on RA and PsA synovial cell suspensions to determine FLS phenotype/function. Podoplanin (PDPN)$^+$ FLS and sorted THY1$^+$ FLS vs THY1$^-$ FLS function in RA vs PsA was assessed by flow cytometry, enzyme-linked immunosorbent assay (ELISA), quantitative real -time quantitative polymerase chain reaction (qPCR), and metabolic analysis ex vivo, in vitro, and in the presence of verteporfin (Hippo signalling blockade).

Results: Flow analysis of PDPN$^+$ FLS demonstrated significant increases in human leukocyte antigen (HLA)-DR$^+$, yes-associated protein (YAP)$^+$, cadherin 11 (Cad11)$^+$, and phosphorylated protein S6$^+$ FLS in RA (all $P < .05$), while CD55 was increased in PsA-FLS ($P < .001$). Polyfunctionality demonstrated enhanced coexpression of Cad11$^+$CD44$^+$HLA-DR$^+$ICAM-1$^+$ FLS ($P < .01$) and CD44$^+$HLA-DR$^+$ICAM-1$^+$VCAM-1$^+$ FLS ($P < .05$) in RA, whereas PsA-FLS exhibited increased coexpression of pAKT$^+$pmTOR$^+$ ($P < .01$). THY1$^+$ FLS populations were dominant in RA ($P < .05$), while THY1$^-$ FLS were dominant in PsA ($P < .05$), with differential angiogenic, chemokine, and matrix metalloproteinase expression observed. THY1$^+$FAP$^+$ FLS correlated with disease activity score (DAS28) ($r = 0.55$, $P < .05$) and synovitis ($r = 0.54$, $P < .05$). Further flow analysis identified 6 main distinct FLS populations, with enrichment of THY1$^+$CD34$^-$CD55$^-$FAP$^+$ FLS and THY1$^+$CD34$^+$CD55$^-$FAP$^+$ FLS in RA ($P < .05$), while PsA displayed enrichment of THY1$^+$CD34$^-$CD55$^+$FAP$^+$ FLS ($P < .05$) and THY1$^-$CD34$^-$CD55$^+$FAP$^+$ FLS ($P < .001$). Immune/adhesive markers were significantly higher in RA subpopulations, whereas metabolic/osteogenic markers were higher in PsA subpopulations. ScRNA-seq

*Correspondence to Dr. Ursula Fearon.
E-mail address: fearonu@tcd.ie (U. Fearon).
Handling editor Josef S. Smolen.

https://doi.org/10.1016/j.ard.2026.03.010

identified 16 distinct FLS clusters, with 3 sublining clusters enriched in RA compared with PsA, including *THY1^{hi}POSTN^{+}*, *THY1^{hi}CXCL12^{+}CHI3L2^{+}*, and *THY1^{hi}CXCL12^{+}APOE^{+}*. Pathway enrichment analysis identified heightened Hippo signalling in RA *THY1^{hi}POSTN^{+}* FLS, and blockade of this signalling inhibited FLS pathogenic function.

Conclusions: RA and PsA possess distinct FLS populations with unique functional and metabolic properties, which may facilitate improved understanding of disease pathogenesis and therapeutic response.

WHAT IS ALREADY KNOWN ON THIS TOPIC

- Previous global single-cell RNA sequencing analysis identified the existence of 11 clusters of FLS in RA and PsA synovial tissue with differential dominance of these clusters between both disease pathotypes.
- THY1^{+}FAP^{+} FLS clusters are enriched in RA while THY1^{-}FAP^{-} FLS clusters are enriched in PsA.

WHAT THIS STUDY ADDS

- For the first time, distinct clusters of synovial fibroblasts (FLS), exhibiting differential functional dominance, were identified in RA vs PsA.
- In-depth flow cytometric analysis, alongside ex vivo analysis, identified enrichment of THY1^{+} FLS subsets in RA with these FLS exhibiting potent immune and angiogenic roles while THY1^{-} FLS subsets were dominant in PsA, demonstrating greater invasive and metabolic capacity.
- Single-cell RNA sequencing of RA and PsA synovial cells identified 16 transcriptionally distinct FLS clusters, with enrichment of three sub-lining clusters in RA compared to PsA: *THY1^{hi}POSTN^{+}*, *THY1^{hi}CXCL12^{+}CHI3L2^{+}*, and *THY1^{hi}CXCL12^{+}APOE^{+}*.
- RA FLS of the *THY1^{hi}POSTN^{+}* cluster demonstrated enrichment of several metabolic/inflammatory pathways including Hippo signalling, blockade of which led to a reduction in FLS pathogenicity.

HOW THIS STUDY MIGHT AFFECT RESEARCH, PRACTICE OR POLICY

- Importantly, identifying these distinct FLS signatures that differ between RA and PsA may provide a unique opportunity to better understand divergent pathogenic mechanisms, with important implications for therapeutic response and targeted intervention.

INTRODUCTION

Rheumatoid arthritis (RA) and psoriatic arthritis (PsA) are 2 of the most prevalent forms of inflammatory arthritis (IA), characterised by synovial inflammation and subsequent cartilage destruction and bone erosion [1–4]. While the 2 arthropathies share common inflammatory features, distinct differences exist at the clinical, molecular, cellular, immunological, and genetic levels [1–3]. The most distinct differences include the presence/absence of autoantibodies, patterns of synovial vascularity, immune cell infiltrates, joint involvement, and differential therapeutic responses, highlighting the disparity between the 2 diseases [1,3]. Moreover, suboptimal responses and failure to achieve disease remission are frequently observed in both patient cohorts, emphasising the need to better understand the differential cellular predominance and subsequent interactions that underpin these 2 distinct forms of IA.

Fibroblast-like synoviocytes (FLS) are a critical resident stromal cell type that assume key roles in homeostatic joint maintenance related to both structural and functional aspects [5,6]. However, the transformation of FLS into a pathogenic phenotype is a hallmark characteristic of IA. Once activated, FLS secrete a plethora of proinflammatory cytokines, chemokines, matrix metalloproteinases (MMPs), and bone-destructive factors, which facilitate the regulation of pathogenic immune cell responses and the invasive phenotype of FLS [7–10]. This is further exacerbated by FLS's adoption of a defective metabolic state and their capacity to rapidly expand and proliferate, constructing stromal networks while simultaneously resisting apoptosis, all disease-related properties that enable them to fulfil their role as facilitators of chronic inflammation and joint damage [11–16].

Contrary to previous views that considered FLS to be predominantly homogeneous in phenotype and function, significant emphasis in recent years has been placed on stratifying discrete populations of FLS using the key markers THY1, CD55, proteoglycan 4 (PRG4), and CD34, alongside epigenetic patterns, which have identified distinct FLS clusters within the synovium [9,17–24]. In particular, THY1^{+} expression is associated with sublining (SL) FLS, while THY1^{-}, along with CD55^{hi} expression, is associated with lining layer (LL) FLS [19]. Additional studies have defined CD34^{-}THY1^{+} FLS as perivascular FLS due to their close proximity to the underlying vasculature and their role in immune cell recruitment [9,20]. Moreover, an elegant study by Croft et al [21] identified fibroblast activation protein (FAP)-α^{+}THY1^{+} immune-effector FLS in the synovial SL and FAPα^{+}-THY1^{-} bone and cartilage destructive fibroblasts restricted to the synovial LL. However, to date, the majority of studies have focused on delineating FLS subpopulations and their contribution to RA pathogenesis, with a stark absence of studies examining the role that FLS subsets play in perpetuating PsA disease development and progression. Moreover, differences in the FLS transcriptional profile and their impact on distinct disease mechanisms in RA vs PsA remain unexplored.

The influence of neighbouring cells and environmental cues in promoting and maintaining distinct FLS phenotypes is increasingly recognised [22,24,25]. Micheroli et al [22] extended this concept by linking defined FLS clusters to specific RA pathotypes (fibroid, myeloid, and lymphoid), with a dominant stromal/fibroblast signature (fibroid/pauci-immune) associated with treatment resistance, underscoring the need to better understand FLS heterogeneity [22,26]. This was further supported by comprehensive synovial profiling, which stratified RA tissue into 6 cell-type abundance phenotypes [24]. Furthermore, Wei et al [25] eloquently demonstrated that endothelial cells (ECs) drive FLS to adopt a THY1^{+} phenotype through NOTCH signalling, an effect lost upon removal from the joint microenvironment. Moreover, FLS gene expression patterns and proliferative capacity can be affected by repeated culturing processes, supporting the notion that environmental cues are essential for phenotypic maintenance [20,27,28].

Given the pivotal role of FLS in joint destruction, this study combined multiparametric flow cytometry and single-cell RNA

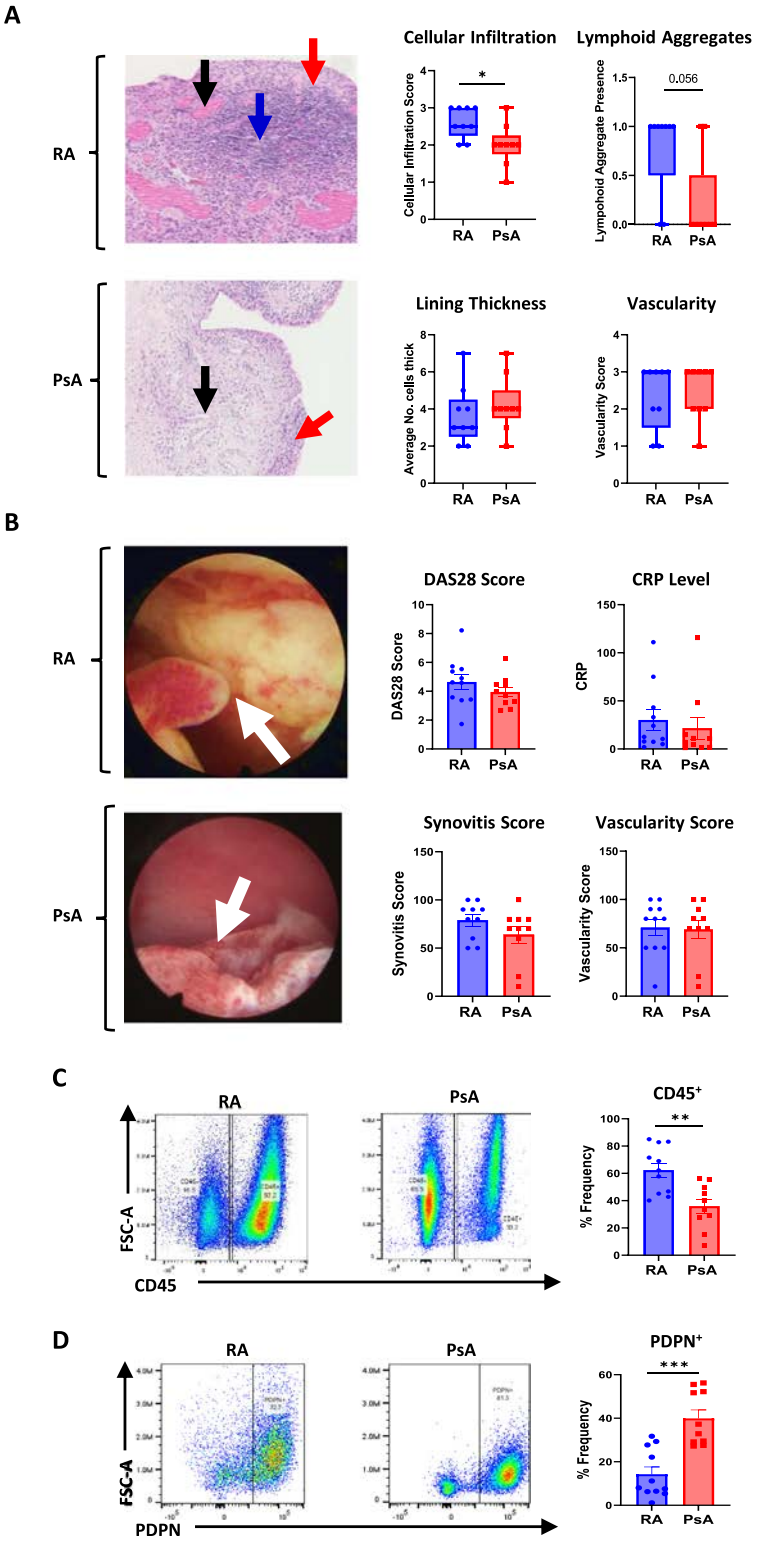

Figure 1. Podoplanin (PDPN)$^{+}$ fibroblast-like synoviocyte (FLS) expression in rheumatoid arthritis (RA) and psoriatic arthritis (PsA) synovial tissue. A, Representative haematoxylin and eosin staining of RA and PsA synovium showing intact tissue morphology and cell–cell contact with the lining layer (red arrows), blood vessels (black arrows), lymphoid aggregates (blue arrow), and synovial infiltrate clearly visible at 10 × magnification. Representative whiskers and box plots quantifying the indicated features in RA (n = 9) and PsA (n = 9) synovial biopsies. All data are presented as median (IQR) using the Mann-Whitney U test; *$P \leq .05$. B, Representative macroscopic images showing RA and PsA synovial tissue. Representative bar graphs comparing disease activity score (DAS28), C-reactive protein (CRP) level, synovitis score, and vascularity score in RA (n = 11) and PsA (n = 10) individuals. Representative flow cytometry plots and accompanying frequency (of live cells) bar graph quantification showing the expression of (C) CD45 and (D) PDPN in RA vs PsA synovial tissue (n = 10-11). FSC, forward scatter.

sequencing (scRNA-seq) to define phenotypic and functional differences between RA and PsA-FLS subsets. Ex vivo functional assays further demonstrate the transient nature of these phenotypes and clarify their distinct contributions to disease pathogenesis.

METHODS

All methodology, statistical analysis, and demographics for the patients used are included in Supplementary Methods 1-13 and Supplementary Tables S1-S9.

RESULTS

Histopathological differences in RA and PsA synovial tissue correspond with differences in immune and FLS population frequency

Representative haematoxylin and eosin staining of RA and PsA tissue demonstrated that cellular infiltration was significantly higher in RA than in PsA ($P < .05$), with increased lymphoid aggregates in RA ($P < .056$) (Fig 1A). Increased vascularity scores, with a trend towards increased LL thickness, were observed in PsA compared with RA (Fig 1A). Importantly,

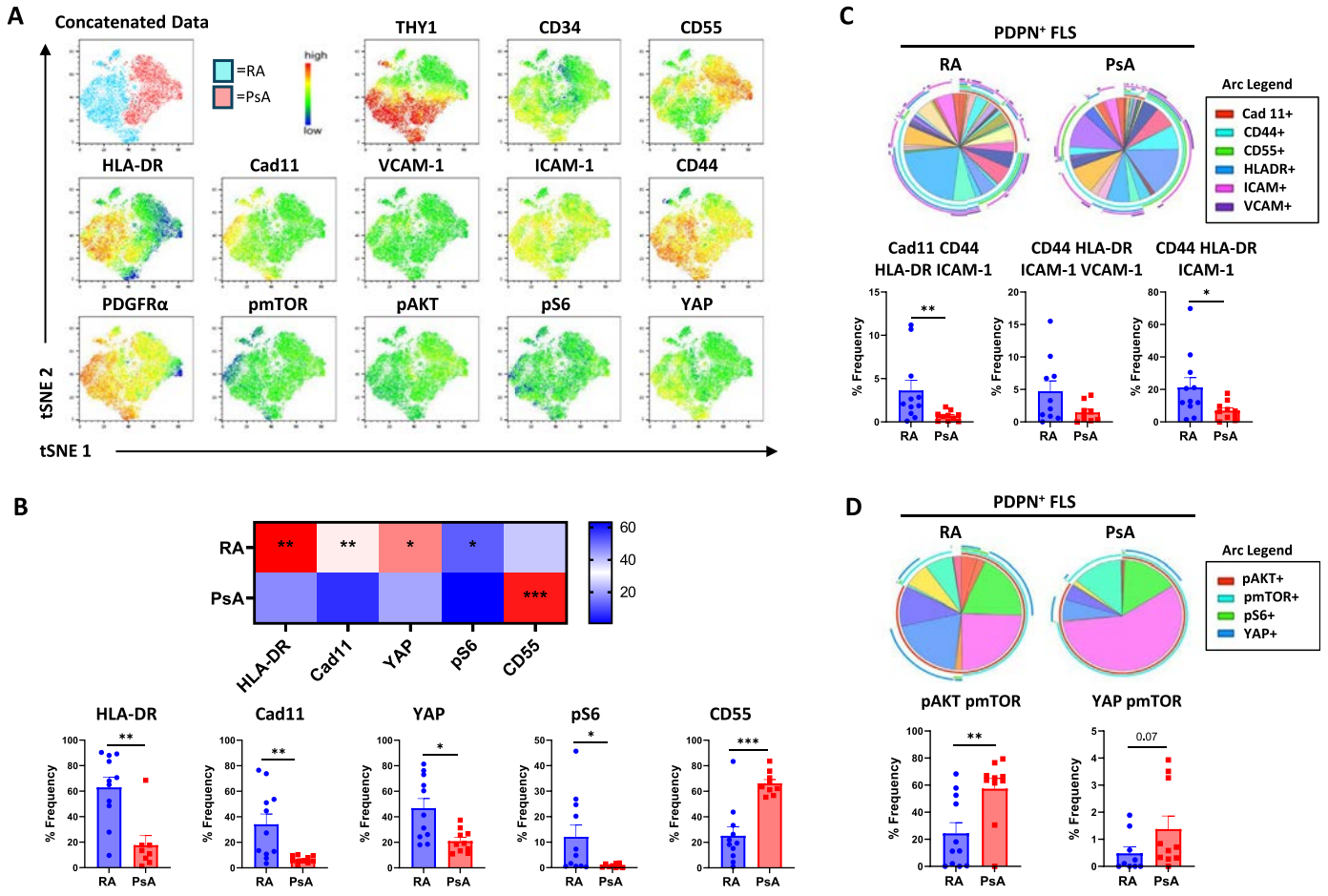

Figure 2. Rheumatoid arthritis (RA) and psoriatic arthritis (PsA) podoplanin (PDPN)$^+$ fibroblast-like synoviocytes (FLS) exhibit different functional capacities. A, Multiparametric flow cytometry data of PDPN$^+$ FLS subjected to the t-distributed stochastic neighbour embedding (t-SNE) algorithm following data concatenation of 1 RA and 1 PsA synovial tissue. Data concatenation and relative expression of the indicated parameters are shown. B, Bar graphs and accompanying heatmap quantifying differences in the frequency of the indicated markers in RA (n = 11) and PsA (n = 10) synovial tissue. Visual representation of multidimensional flow cytometry data. Simplified Presentation of Incredibly Complex Evaluations (SPICE) analysis was performed to identify polyfunctionality of PDPN$^+$ FLS in synovial tissue from RA (n = 11) and PsA (n = 10). Each pie segment indicates the different combinations of (C) immune and (D) metabolic/invasive marker expression, as denoted in the legends of Supplementary Figures S3 and S4. The surrounding pie arcs indicate the specific markers expressed in each pie segment. Representative bar graphs depict the quantification of coexpressed markers that differ between RA and PsA-FLS. Data are presented as mean ± SEM using the Mann-Whitney U test; *P < .05, **P < .01, ***P < .001. Cad11, cadherin 11; HLA, human leukocyte antigen; ICAM-1, intercellular adhesion molecule-1; pAKT, phospho-protein kinase B; PDGFR, platelet-derived growth factor receptor; pmTOR, phosphorylated mechanistic target of rapamycin; pS6, phosphorylated protein S6; VCAM-1, vascular cell adhesion molecule-1; YAP, yes-associated protein.

no significant differences in clinical parameters, disease activity score (DAS28), C-reactive protein (CRP), macroscopic synovitis, macroscopic vascularity, gender (male vs female), age, treatment, or disease duration were observed between RA and PsA (Fig 1B and Supplementary Fig S1). Representative flow cytometry plots of the percentage frequency of CD45$^{+/-}$ cells and podoplanin (PDPN)$^{+/-}$ cells in RA vs PsA synovial tissue cell suspensions are shown in Figure 1C. A significantly higher frequency of CD45$^+$ cells in RA than in PsA was observed (P < .01), which parallels the pattern observed in the analysis of histological cellular infiltrates (Fig 1A,C). Consistent with this, the frequency of PDPN$^+$ cells was significantly higher in PsA than in RA (P < .001) (Fig 1D).

Differential phenotype and function of PDPN$^+$ FLS within the RA and PsA synovium

Although FLS are known to be central instigators of joint damage, no study to date has directly examined and compared RA-FLS and PsA-FLS phenotypes and functions ex vivo. The flow cytometry gating strategy to identify PDPN$^+$ FLS populations is shown in Supplementary Figure S2. Initially, we conducted an unbiased, unsupervised analysis using t-distributed stochastic neighbour embedding (t-SNE) following pregating on PDPN$^+$ FLS [21,22]. Total PDPN$^+$ FLS were subjected to the t-SNE algorithm following data concatenation (Fig 2A). Analysis identified higher expression of THY1, human leukocyte antigen (HLA)-DR, cadherin 11 (Cad11), platelet-derived growth factor receptor (PDGFR)-α, and yes-associated protein (YAP) in RA-FLS, while higher expression of CD55 and phospho-protein kinase B (pAKT) was observed in PsA-FLS (Fig 2A). Quantification demonstrated a significantly higher percentage frequency of HLA-DR (P < .01), Cad11 (P < .01), YAP (P < .05), and phosphorylated protein S6 (pS6) (P < .05) in RA-FLS, and a significantly higher frequency of CD55 (P < .001) in PsA-FLS (Fig 2B). Moreover, examination of the functional capacity of THY1$^-$CD55$^+$ LL-FLS vs THY1$^+$CD55$^-$ SL-FLS in general revealed a significantly higher frequency of Cad11, HLA-DR, and YAP (all P <

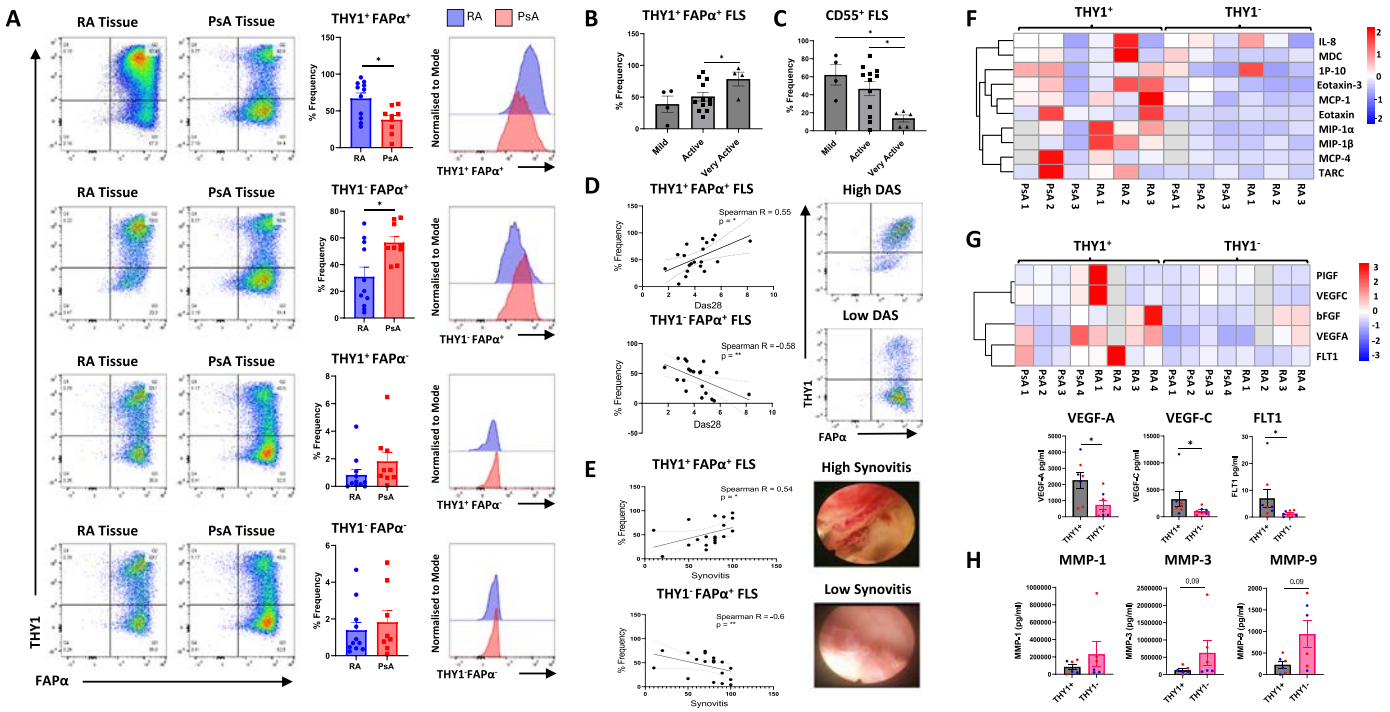

Figure 3. Differential frequency of THY1 fibroblast activation protein (FAP)-α fibroblast-like synoviocyte (FLS) populations in rheumatoid arthritis (RA) vs psoriatic arthritis (PsA). A, Representative flow cytometry dot plots, bar graphs, and relative histograms demonstrating quantification of the percentage frequency of THY1 FAPα FLS populations in RA (n = 11) and PsA (n = 9) synovial tissue. Bar graphs showing the (B) percentage frequency of THY1$^+$FAPα^+ FLS and (C) the percentage frequency of CD55$^+$ FLS in inflammatory arthritis (IA) mild vs active vs very active disease (n = 20). Mild disease: disease activity score (DAS) > 3.2; active disease: DAS = 3.2 to 5.1; very active disease: DAS > 5.1. Data are presented as mean ± SEM using the Mann-Whitney U test; *$P < .05$. D, Spearman pairwise correlation plot and representative flow dot plots of THY1$^+$FAPα^+ and THY1$^-$FAPα^+ FLS frequency in high vs low disease activity in IA (n = 20) synovial tissue. E, Spearman pairwise correlation plot and representative macroscopic images showing the relationship between THY1$^+$FAPα^+ and THY1$^-$FAPα^+ FLS frequency and the extent of synovitis in IA (n = 20) synovial tissue. F, Clustered heatmap displaying the scaled expression of chemotactic factors measured by meso scale discovery (MSD) analysis in the supernatants of sorted THY1$^+$ vs THY1$^-$ FLS in RA and PsA synovial tissue (n = 6) collected after 48 h. G, Clustered heatmap and accompanying bar graphs representing the secretion of angiogenic mediators from the sorted synovial tissue of THY1$^+$ vs THY1$^-$ FLS, as measured by MSD assay (n = 6). H, Bar graphs representing quantification of matrix metalloproteinases (MMPs) excreted from sorted THY1$^+$ vs THY1$^-$ FLS, as measured by MSD assay (n = 6). RA donors are depicted as blue dots, and PsA donors as red dots. All data are presented as mean ± SEM using the Wilcoxon signed-rank test; *$P < .05$. bFGF, basic fibroblast growth factor; Flt, fms-like tyrosine kinase; IL, interleukin; IP, interferon-gamma-induced protein; MCP, monocyte chemoattractant protein; MDC, macrophage-derived chemokine; MIP, macropahge inflammatory protein; PIGF, placental growth factor; TARC, thymus and activation-regulated chemokine; VEGF, vascular endothelial growth factor.

.05) in SL-FLS compared with the LL-FLS (Supplementary Fig S3). Next, to more accurately recapitulate their in vivo state, PDPN$^+$ FLS polyfunctionality was analysed using the Simplified Presentation of Incredibly Complex Evaluations (SPICE) algorithm, which allows multiple parameters to be visualised concurrently (Supplementary Figs S4 and S5). RA patients demonstrated a significantly enhanced coexpression of several immune and adhesive markers, including Cad11$^+$CD44$^+$HLA-DR$^+$ICAM-1$^+$ ($P < .01$), CD44$^+$HLA-DR$^+$ICAM-1$^+$VCAM-1$^+$, and CD44$^+$HLA-DR$^+$ICAM-1$^+$ ($P < .05$) (Fig 2C). Moreover, PsA patients demonstrated enhanced dual coexpression of metabolic/invasive markers, including phosphorylated mechanistic target of rapamycin (pmTOR)$^+$pAKT$^+$ ($P < .01$) and YAP$^+$pmTOR$^+$ (Fig 2D). These results suggest that both RA-FLS and PsA-FLS differ in their polyfunctional capacity in terms of immune and metabolic function.

The dominance of THY1$^+$ FLS differs between RA and PsA synovium

THY1 expression has been used in the literature to delineate FLS into LL and SL subsets, each with characteristic immune-related and bone-degradative functions [21]. Therefore, to identify potential differences in the dominance of LL- vs SL-FLS in RA vs PsA, flow cytometry analysis was performed ex vivo using the gating strategy outlined in Supplementary Figures S6 and S7. For the first time, a significantly higher frequency of THY1$^+$FAPα^+ FLS was observed in RA ($P < .05$), while THY1$^-$FAPα^+ FLS were significantly higher in PsA ($P < .05$) (Fig 3A). Conversely, the THY1$^+$FAPα^- FLS and THY1$^-$FAPα^- FLS populations exhibited similar frequencies in both RA and PsA (Fig 3A). The percentage frequency of THY1$^+$FAPα^+ FLS was associated with increased DAS28 in IA ($P < .05$), whereas that of CD55$^+$ FLS showed an inverse relationship with DAS28 ($P < .05$), findings that were mirrored when stratified by disease status (Fig 3B,C, and Supplementary Fig S8). A significant positive correlation was observed between the percentage frequency of THY1$^+$FAPα^+ FLS and DAS28 ($P < .05$), and macroscopic synovitis ($P < .05$), suggesting a more potent role for THY1$^+$ FLS in driving IA inflammation (Fig 3D,E). Interestingly, when stratified by disease status, there appeared to be a stronger correlation between the percentage frequency of RA THY1$^+$FAPα^+ FLS and both DAS28 and synovitis than with PsA, although these results were limited by the number of patients (Supplementary Fig S8). Next, THY1$^+$ FLS and THY1$^-$ FLS were sorted from synovial biopsies (n = 6) and cultured, and the spontaneous release of several proinflammatory, angiogenic, and invasive mediators was assessed in the cultured supernatants.

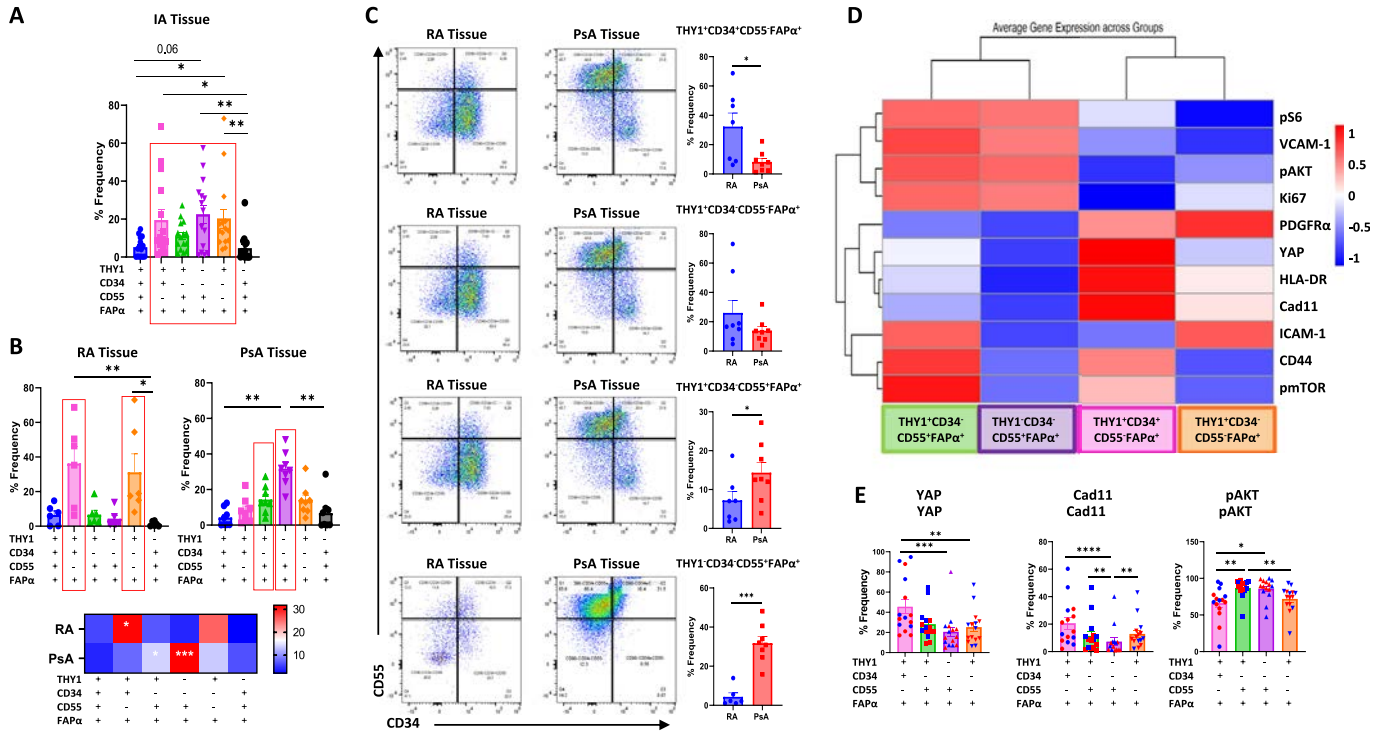

Figure 4. Differential expression of THY1-CD34-CD55-fibroblast activation protein (FAP)-α–expressing fibroblast-like synoviocyte (FLS) clusters in rheumatoid arthritis (RA) vs psoriatic arthritis (PsA). A, Bar graph demonstrating differences in the percentage frequency of populations identified by flow cytometry analysis in inflammatory arthritis (IA) synovial tissue (n = 15). B, Bar graphs and accompanying heatmap of the frequency of each of the FLS populations when separated by disease status, RA (n = 7), and PsA (n = 8). All data are presented as mean ± SEM using Friedman's test; *P < .05, **P < .01. C, Representative flow cytometry dot plots and accompanying bar graphs demonstrating quantification of the frequency of THY1-CD34-CD55-FAPα FLS populations in RA (n = 7) and PsA (n = 8) synovial tissue. Data are presented as mean ± SEM using the Mann-Whitney U test; *P < .05, ***P < .001. D, Hierarchical clustered heatmap and (E) bar graphs quantifying differences in the average expression of the indicated functional, metabolic, and immune markers in IA synovial tissue (n = 15). RA is indicated by blue dots and PsA by red dots. Data are presented as mean ± SEM using Friedman's test; *P < .05, **P < .01, ***P < .001, ****P < .0001. Cad11, cadherin 11; HLA, human leukocyte antigen; ICAM-1, intercellular adhesion molecule-1; pAKT, phospho-protein kinase B; PDGFR, platelet-derived growth factor receptor; pmTOR, phosphorylated mechanistic target of rapamycin; pS6, phosphorylated protein S6; VCAM-1, vascular cell adhesion molecule-1; YAP, yes-associated protein.

Interestingly, while chemokine levels were highly donor-specific, as depicted in Figure 3F and Supplementary Figure S9, THY1$^+$ FLS in both disease states exhibited greater expression of monocyte chemotactic protein (MCP)-1, MCP-4, eotaxin, eotaxin-3, interferon-gamma-induced protein (IP)-10, macrophage inflammatory protein (MIP)-1α, MIP-1β, thymus and activation-regulated chemokine (TARC), and macrophage-derived chemokine (MDC) compared with THY1$^-$ FLS, supporting the hypothesis that they assume a more immune-mediating role. Furthermore, angiogenic mediators, including vascular endothelial growth factor (VEGF)-A, VEGF-C, and Flt1, were significantly higher in THY1$^+$ FLS than in THY1$^-$ FLS (all P < .05) (Fig 3G). In contrast, although the extent varied across individual donors, higher expression of MMP-1, MMP-3, and MMP-9 in the THY1$^-$ FLS than in the THY1$^+$ FLS subset was observed, with this difference more pronounced in PsA THY1$^-$ FLS (Fig 3H). Collectively, these data imply stronger chemotactic/angiogenic functions of the THY1$^+$ FLS population, while THY1$^-$ FLS, associated with PsA, exhibit greater invasive MMP expression.

Differential expression of THY1, CD34, CD55, and FAPα-expressing FLS clusters in RA vs PsA, with distinct pathogenic function

To further expand on differences in dominant FLS subsets between RA and PsA, the markers CD55 and CD34 were incorporated alongside THY1 and FAPα to provide more detailed analyses of distinct FLS populations in RA vs PsA. The gating strategy implemented is shown in Supplementary Figures S6 and S7, yielding 6 distinct FLS subsets (Fig 4A). Enrichment in THY1$^+$CD34$^+$CD55$^-$FAPα^+ FLS (P < .05) and THY1$^+$CD34$^-$CD55$^-$FAPα^+ FLS was demonstrated in RA, while PsA displayed enrichment in THY1$^-$CD34$^-$CD55$^+$FAPα^+ FLS (P < .001) and, unexpectedly, a THY1$^+$ intermediate (INT) population, THY1$^+$CD34$^-$CD55$^+$FAPα^+ FLS (P < .05) (Fig 4B,C). The THY1$^+$CD34$^+$CD55$^+$FAPα^+ FLS and THY1$^-$CD34$^+$CD55$^+$FAPα^+ FLS populations were relatively similar between RA and PsA and had lower frequencies, leading to their exclusion from further analysis (Fig 4B). A higher percentage frequency of pS6, VCAM-1, pAKT, and Ki67 was observed in the 2 PsA-dominant populations, whereas PDGFRα, YAP, HLA-DR, and Cad11 were markedly higher in the 2 RA-dominant populations (Fig 4D). Interestingly, the frequency of markers expressed by the THY1$^-$CD34$^-$CD55$^+$FAPα^+ PsA-enriched subset (purple) was nearly the inverse of the 2 RA-enriched THY1$^+$ subsets (pink and orange), with high-frequency expression in the THY1$^-$ subset and low-frequency expression in the 2 RA-enriched THY1$^+$ subsets, and vice versa (Fig 4D). However, as shown in the heatmap in Figure 4D, the PsA-enriched THY1$^+$CD34$^-$CD55$^+$FAPα^+ FLS population (green) exhibited expression levels of specific markers that overlapped with those of the other 3 populations, suggesting it may possess greater INT functionality. Both YAP and Cad11 were significantly higher in the RA-dominant populations, particularly THY1$^+$CD34$^+$CD55$^-$FAPα^+ FLS (Fig 4E). Conversely, pAKT

was significantly higher in PsA-FLS, specifically THY1$^+$CD34$^-$CD55$^+$FAPα^+ (Fig 4E). Collectively, these data indicate the presence of 6 distinct FLS populations based on expression of the surface markers THY1, CD34, CD55, and FAPα, with THY1$^-$CD55$^+$ LL-FLS dominant in PsA and THY1$^+$ SL-FLS dominant in RA. Importantly, the expression of specific markers differed across clusters, further defining the function of each cluster across disease states, with these clusters being differentially enriched for RA vs PsA.

RA- and PsA-FLS at passage 0 exhibit differential functional characteristics, with FLS expansion resulting in the loss/gain of specific markers

To determine whether the identified unique phenotypic profiles of FLS are retained following removal from the joint microenvironment, ex vivo experiments were performed on passage 0 (P0) FLS. While MMP-1 and MMP-3 levels were higher in the synovial fluid than in the serum of patients with RA and PsA, no differences in MMP-1 and MMP-3 levels were observed in either compartment between RA and PsA donors (Supplementary Fig S10), possibly due to the cumulative production from other cell types within the joint microenvironment. However, significantly higher levels of MMP-1 and MMP-3 messenger RNA were observed specifically in PsA-FLS compared with RA-FLS ($P <$ .05), mirroring the single-cell data (Fig 5A). Although highly donor-dependent, angiogenic mediators were comparable between the 2 arthropathies, except for basic fibroblast growth factor (bFGF) in PsA ($P <$ .01) (Fig 5B and Supplementary Fig S11A). Interestingly, interleukin (IL)-8 and eotaxin-3 demonstrated a trend towards increased levels in PsA, whereas IP-10 was higher in RA (Fig 5C and Supplementary Fig S11B). These data suggest that both RA-FLS and PsA-FLS have the capacity to differentially recruit peripheral immune cells in response to chemokine gradients. Furthermore, metabolic analysis indicated a slightly greater preference for glycolysis in PsA-FLS compared with RA-FLS at P0 (Fig 5D). Additionally, trends towards increased levels of several glycolytic mediators in P0-FLS were observed, including hypoxia inducible factor (HIF)-1α, hexokinase 2 (HK2), pyruvate kinase M2 (PKM2), glucose transporter type 1 (GLUT-1), and glyceraldehyde 3-phosphate dehydrogenase (GAPDH) (Fig 5E). However, the addition of IL-1β resulted in greater glycolytic metabolic capacity (extracellular acidification rate) in RA-FLS compared with PsA-FLS ($P <$ .001), with the energy map clearly depicting a greater shift towards an energetic profile in RA-FLS than in PsA-FLS (Fig 5F). In order to determine whether the FLS phenotype is affected by repeated culturing, flow cytometry analysis was performed on FLS across 3 consecutive passages (P0, P1, P2). Representative flow plots of fluorescence minus one controls used to determine boundaries are shown in Supplementary Figure S12. The percentage frequency and median fluorescent intensity (MFI) of HLA-DR and CD55 decreased across consecutive passages (Fig 5G,H), with a comparable reduction observed in both disease states. Furthermore, CD34 and intercellular adhesion molecule 1 (ICAM-1) displayed opposite trends, with increases in the percentage frequency and MFI for both markers across passages (Fig 5I,J). Cumulatively, these results indicate that both RA-FLS and PsA-FLS alter their phenotypic profiles across passages, with a loss/gain of markers once removed from inflammatory influences within the joint microenvironment. Moreover, after culturing sorted THY1$^+$ and THY1$^-$ FLS for 7 days, there was a significant reduction in the amount of THY1$^-$ FLS that remained negative for this marker in both disease states, suggesting that FLS phenotype is indeed transient, with convergence towards a common THY1$^+$ phenotype upon removal from the influence of the synovial joint (Supplementary Fig S13). However, as shown in Figure 5, even with this loss of FLS diversity in expanded FLS, they still retain imprinted functions that differ between the 2 diseases.

ScRNA-seq analysis of FLS populations in RA and PsA synovium

Using a previously published global scRNA-seq synovial tissue dataset comparing RA and PsA [23], we reanalysed it, focusing only on FLS, and provided a unique atlas of FLS subsets across both disease states. This targeted reanalysis enabled higher-resolution clustering, improved detection of cellular heterogeneity and transitional states, and greater sensitivity in identifying condition-specific gene expression and pathway activity. By minimising background noise from unrelated cell types in the global analysis, this approach provided a more in-depth analysis of the distinct FLS cell populations in the synovium and their contributions to disease. Nonlinear stochastic uniform manifold approximation and projection analysis identified 16 distinct FLS subclusters in the IA synovium (Fig 6A). FLS clusters were further characterised using gene expression analysis of the top differentially expressed genes (DEGs) per cluster, alongside hierarchical clustering analysis (Fig 6B,C, and Supplementary Fig S14). Using these various methods of analysis, FLS clusters were further classified into distinct subgroups, with an initial delineation into 3 primary categories: SL with high *THY1* expression, LL with high *PRG4* and *CD55* expression, and INT (Fig 6C,D, and Supplementary Fig S15).

The SL population contained 2 subclusters: *THY1^{hi}CXCL12$^+$* and *THY1^{hi}POSTN$^+$* (cluster 3), with the latter possessing a cluster marker gene signature indicative of a central role in cytoskeletal and extracellular matrix (ECM) regulation, as denoted by high collagen gene expression. Furthermore, the *THY1^{hi}CXCL12$^+$* subcluster was further segregated based on distinct DEGs into *VCAN$^+$* (cluster 1), *IER2$^+$* (cluster 8), *CHI3L2$^+$* (cluster 9), *APOE$^+$* (cluster 10), and *CCL2$^+$* (cluster 12), all with gene signatures implicated in distinct functions related to ECM regulation, inflammatory responses, signalling, and lipid metabolism (Supplementary Fig S16) [29–32]. Moreover, the LL population was further subdivided into 3 predominant phenotypes based on cluster marker genes: an MMP group, a homeostatic group, and an inflammatory group (Fig 6D and Supplementary Fig S17). The MMP group exhibited upregulated expression of genes involved in ECM turnover and tissue remodelling, classified into the *PRG4^{hi}MMP1$^+$* (cluster 5), *PRG4^{hi}MMP3$^+$* (cluster 6), and *PRG4^{hi}TIMP1$^+$* (cluster 13) subclusters. Two homeostatic clusters were identified, with high expression of genes related to homeostasis maintenance: *PRG4^{hi}CLIC5$^+$* (cluster 0), containing high expression of classical LL markers, including *PRG4* and *CD55*, and *PRG4^{hi}MTIG$^+$* (cluster 11), characterised by an abundance of genes related to heavy metal detoxification, which have been shown to assist in immunosuppression in RA mouse models [33]. Finally, the remaining LL subgroup consisted of clusters associated with inflammatory gene signatures and was subdivided into a *PRG4^{hi}CXCL8$^+$* group (cluster 2) with high chemoattractant gene expression; a *PRG4^{hi}INHBA$^+$* group (cluster 7), which has been associated with a 'pain-associated FLS' phenotype; and a *CSN1S1$^+$* group (cluster 15), which was grouped with cluster 0 [34,35]. The remaining FLS clusters were defined as INT due to their similarities to both SL and LL gene expression of *THY1, CD55*, and *PRG4* (Supplementary Fig S18). For the first cluster, high expression of genes implicated in

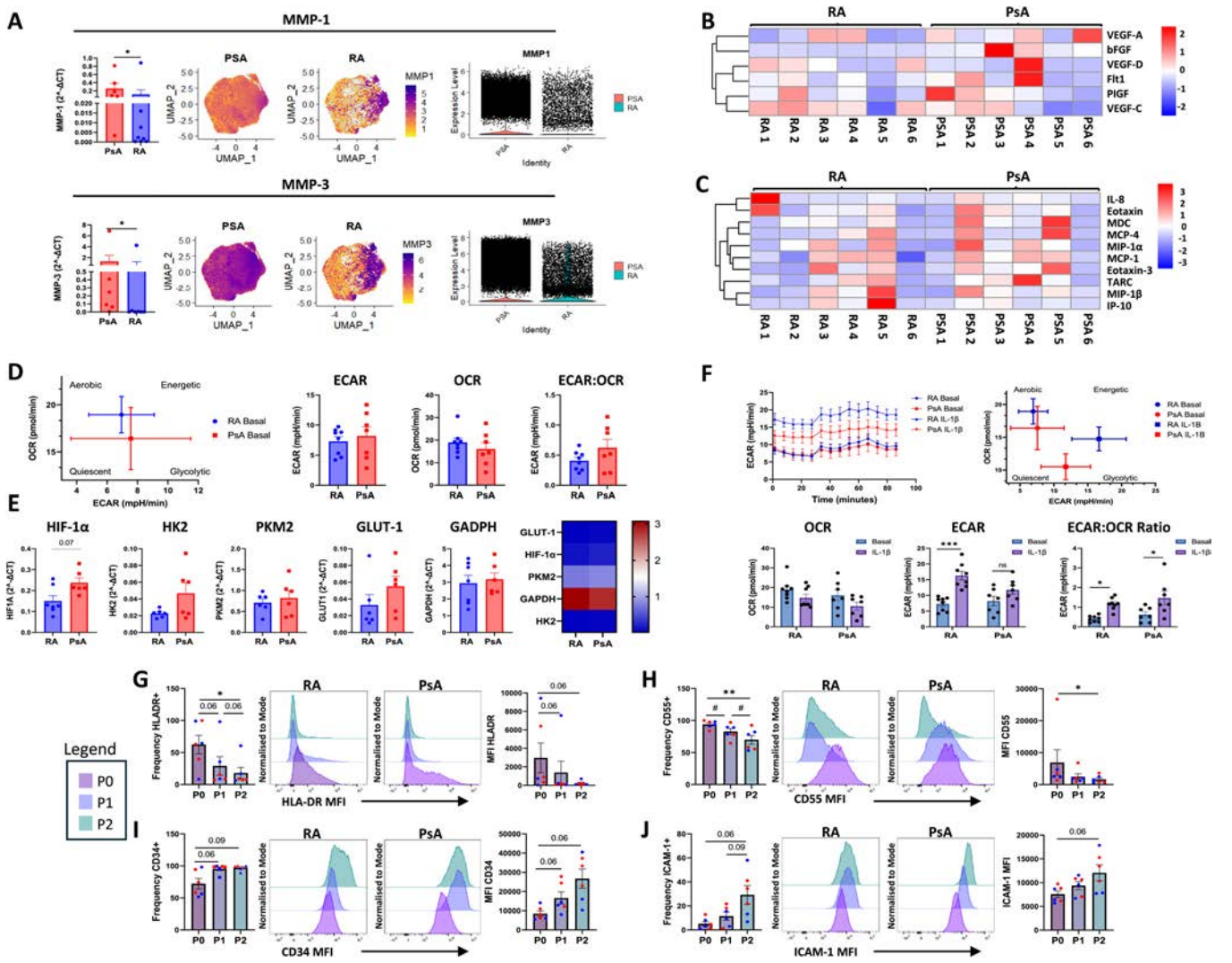

Figure 5. Rheumatoid arthritis (RA) and psoriatic arthritis (PsA) fibroblast-like synoviocytes (FLS) at passage 0 (P0) exhibit distinct functional capacities ex vivo, converging towards common phenotypes upon expansion. A, Bar graphs showing messenger RNA (mRNA) expression of matrix metalloproteinase (MMP)-1 and MMP-3 in unstimulated P0 RA (n = 8) and PsA (n = 6) FLS, and single-cell RNA sequencing (scRNA-seq) uniform manifold approximation and projections (UMAPs) and violin plot representations depicting gene expression of MMP-1 and MMP-3 in PsA vs RA-FLS. Normalisation to the housekeeping gene RPLP0 was used to generate ΔCT values. Data are presented as mean ± SEM using the Mann-Whitney U test; $*P < .05$ significantly different from each other. Clustered heatmaps depicting the scaled expression of (B) angiogenic factors and (C) chemokines in the supernatants of P0 RA-FLS and PsA-FLS (n = 6 each), as determined by meso scale discovery (MSD) analysis. D, Representative energy map and accompanying bar graphs showing baseline extracellular acidification rate (ECAR), baseline oxygen consumption rate (OCR), and the ECAR:OCR ratio in RA (n = 8) and PsA (n = 7) P0 FLS under basal conditions, as determined by Seahorse metabolic analysis, before and after injections of oligomycin, carbonyl cyanide-p-trifluoromethoxyphenylhydrazone (FCCP), and antimycin A/rotenone. E, Bar graphs and representative heatmap showing quantification of gene mRNA expression of hypoxia-inducible factor 1-alpha (HIF-1α), hexokinase 2 (HK2), pyruvate kinase M2 (PKM2), glucose transporter type 1 (GLUT-1), and glyceraldehyde 3-phosphate dehydrogenase (GAPDH) in RA (n = 7) and PsA (n = 6) FLS under baseline conditions. Data are presented as ΔCT, normalised to the housekeeping control RPLP0. F, Average ECAR profile, representative energy map, and bar graphs quantifying baseline OCR, ECAR, and the ECAR:OCR ratio of RA and PsA-FLS (n = 6-8) at baseline and following 24-hour interleukin (IL)-1β (1 ng/mL) stimulation, as determined by Seahorse metabolic analysis. Significance was determined by two-way analysis of variance (ANOVA) with Tukey's multiple comparisons test; $*P < .05$, $**P < .01$, $***P < .001$. Bar graphs depicting the changes in frequency expression, representative histograms, and bar graphs showing median fluorescent intensity (MFI) of the markers (G) human leukocyte antigen (HLA)-DR, (H) CD55, (I) CD34, and (J) intercellular adhesion molecule-1 (ICAM-1) across passages 0 to 2 (P0, P1, and P2) in RA vs PsA-FLS (n = 3 each). RA is indicated by blue dots, and PsA is indicated by red dots. Data are presented as mean ± SEM using Friedman's test (*) or the Wilcoxon signed-rank test (#) as appropriate; $*^{(\#)}P < .05$, $**^{(\#\#)}P < .01$. bFGF, basic fibroblast growth factor; Flt, fms-like tyrosine kinase; IP, interferon-gamma-induced protein; MCP, monocyte chemoattractant protein; MDC, macrophage-derived chemokine; MIP, macropahge inflammatory protein; PlGF, placental growth factor; TARC, thymus and activation-regulated chemokine; VEGF, vascular endothelial growth factor.

immune response regulation and antigen processing, including *HLA-DR* and *CD74,* resulted in its designation as *HLA-DR^{hi}* (cluster 4). The final cluster was defined as *TM4SF1^{+}* (cluster 14), with a gene signature associated with epithelial-mesenchymal transition [36].

Subsequent analysis demonstrated significant enrichment (all $P < .05$) of the clusters *THY1^{hi}POSTN^{+}* (cluster 3), *THY1^{hi}CXCL12^{+}CHI3L2^{+}* (cluster 9), and *THY1^{hi}CXCL12^{+}APOE^{+}* (cluster 10) in RA; importantly, all were SL clusters, thus mirroring the RA THY1^{+} dominance identified by flow cytometry (Fig 6E,F, and Supplementary Fig S19). Conversely, consistent with the flow cytometry analysis, the LL clusters *PRG4^{hi}CLIC5^{+}* and *PRG4^{hi}MMP3^{+}* were enriched for PsA, along with the INT cluster denoted as *HLA-DRA^{hi}* (Fig 6F). The

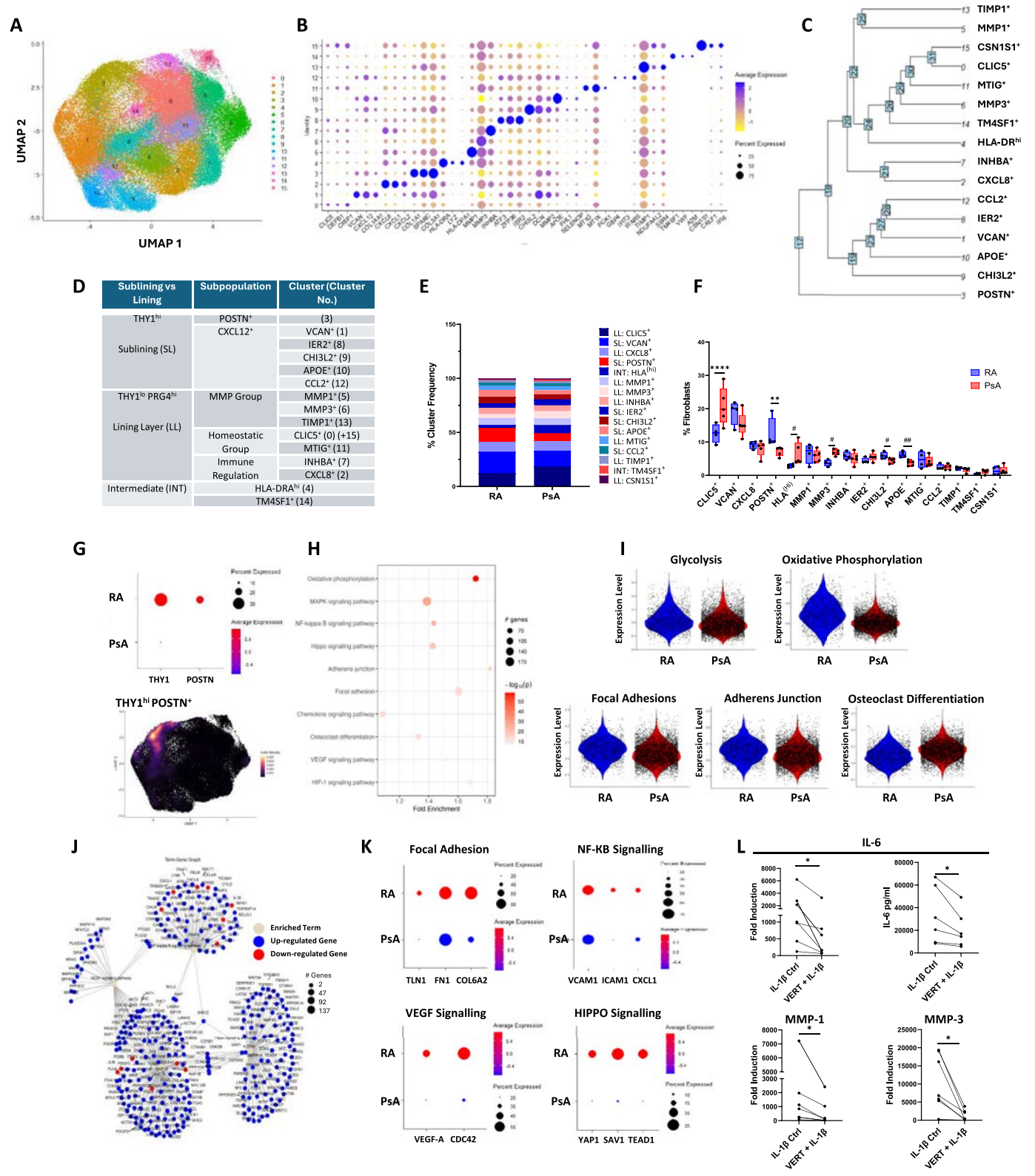

Figure 6. Single-cell RNA sequencing (scRNA-seq) analysis showing fibroblast-like synoviocyte (FLS) heterogeneity in synovial tissue from rheumatoid arthritis (RA) and psoriatic arthritis (PsA). A, Uniform manifold approximation and projection (UMAP) representation of 16 synovial tissue FLS clusters in RA (n = 4) and PsA (n = 5), identified by high-dimensionality scRNA-seq analysis. B, Dot plot showing the top differentially expressed genes (DEGs) per identified cluster. C, Proposed classification and (D) hierarchical clustering of human synovial tissue FLS. E, Proportional cluster abundance and (F) representative whiskers and box plot depicting differences in the frequency of the specific clusters between patients with RA (n = 4) and those with PsA (n = 5). Two-way analysis of variance (ANOVA) with Sidak's multiple comparisons test (*) and the Mann-Whitney U test ($^{\#}$) were used to determine significance; $^{*(\#)}P < .05$, $^{**(\#\#)}P < .01$, $^{***}P < .001$, $^{****}P < .0001$. G, Dot plot and UMAP illustrating THY1^{hi}POSTN^{+} messenger RNA (mRNA) expression in synovial tissue from RA and PsA-FLS. H, Analysis of pathways enriched in THY1^{hi}POSTN^{+} FLS in RA (n = 4) and PsA (n = 5) synovial tissue; colour intensity represents significance, and dot size denotes the number of genes within each pathway that are differentially expressed. I, Violin plots representing the expression scores of gene modules related to the indicated pathways in the THY1^{hi}POSTN^{+} cluster in RA vs PsA. J, Term plot of the indicated pathways with significant enrichment in RA compared with PsA-FLS. Blue indicates upregulation of specific genes, and red indicates downregulation within the pathway in RA compared with PsA. Dot size represents the statistical significance of the change.

remaining clusters showed comparable expression levels between RA and PsA (Fig 6F).

Differential function of the THY1^{hi}POSTN^{+} FLS cluster between RA and PsA

Further analysis focused specifically on the RA-enriched SL *THY1^{hi}POSTN^{+}* cluster to further characterise its function and determine whether RA-FLS and PsA-FLS within this cluster exhibit different functional properties (Fig 6G and Supplementary Fig S20). Pathway enrichment analysis identified several pathogenic pathways enriched in the RA *THY1^{hi}POSTN^{+}* cluster compared with PsA, including oxidative phosphorylation, Hippo-YAP signalling, and MAPK signalling (Fig 6H). Bioinformatic characterisation of gene modules based on the Kyoto Encyclopedia of Genes and Genomes (KEGG) metabolic reference pathways revealed enhanced levels of oxidative phosphorylation, glycolysis, and focal adhesions in the *THY1^{hi}POSTN^{+}* RA-FLS cluster compared with PsA-FLS (Fig 6I). Conversely, osteoclast differentiation genes were higher in the PsA *THY1^{hi}POSTN^{+}* FLS cluster, implying a more bone-degradative role in PsA. Differential expression of specific members of the nuclear factor (NF)-κB, VEGF, and Hippo-YAP signalling pathways, as well as focal adhesions in RA vs PsA *THY1^{hi}POSTN^{+}* FLS, is shown in Figure 6J. Furthermore, Figure 6K demonstrates increased expression of several key mediators involved in the Hippo-YAP pathway in RA *THY1^{hi}POSTN^{+}* FLS compared with PsA, including YAP1, salvador family WW domain containing protein 1 (SAV1), and transcriptional enhanced associate domain (TEAD), as well as mediators involved in focal adhesion, NF-κB, and VEGF signalling. To further assess the involvement of the Hippo-YAP pathway in driving the pathogenic behaviour of the *THY1^{hi}POSTN^{+}* FLS cluster in RA, FLS were treated with verteporfin in the presence/absence of IL-1β. Verteporfin significantly inhibited IL-1β–induced IL-6 at both the gene and protein levels ($P < .05$), as well as MMP-1 and MMP-3 ($P < .05$) (Fig 6L). Cumulatively, these results suggest that at a highly specific cluster scale, differences in frequency, in addition to differences in FLS functionality within the same cluster, can be detected between RA and PsA disease states, thereby introducing differential pathways to target preferentially.

DISCUSSION

While FLS heterogeneity is increasingly recognised, most studies focus on RA-FLS, with little known about PsA-FLS. THY1^{+} FLS were enriched in RA, while THY1^{-} FLS predominated in PsA, with distinct functional profiles: THY1^{+} FLS showed higher angiogenic and chemokine activity, whereas THY1^{-} FLS had elevated MMPs. Flow cytometry identified 6 FLS subsets, with specific populations enriched in RA (THY1^{+}CD34^{+}CD55^{-}FAPα^{+} and THY1^{+}CD34^{-}CD55^{-}FAPα^{+}) vs PsA (THY1^{-}CD34^{-}CD55^{+}FAPα^{+} and THY1^{+}CD34^{-}CD55^{+}FAPα^{+}). Ex vivo studies showed that RA-dominant populations drive immune responses, while PsA populations have higher matrix-degradative activity. Phenotypic features were maintained at P0 but diminished by P2. ScRNA-seq identified 16 FLS clusters, with 3 SL clusters enriched in RA (*THY1^{hi}POSTN^{+}*, *THY1^{hi}CXCL12^{+}CHI3L2^{+}*, and *THY1^{hi}CXCL12^{+}APOE^{+}*). Bioinformatics indicated that Hippo-YAP signalling was enriched in *THY1^{hi}POSTN^{+}* RA-FLS and that its blockade inhibited their pathogenicity.

Interestingly, although the proportion of CD45^{+} immune cells was higher in RA, a significantly higher frequency of PDPN^{+} FLS was detected in PsA. Furthermore, significantly higher expression of the markers HLA-DR, Cad11, YAP, and pS6 was observed on PDPN^{+} RA-FLS, whereas PsA-FLS were enriched for CD55. Consistent with this, previous studies have demonstrated that HLA-DR is a characteristic marker of THY1^{+} RA-FLS and that elevated levels of Cad11 have been previously associated with RA-FLS invasive behaviour [9,17,20]. Moreover, higher levels of YAP, a protein with diverse functions, including regulation of cell motility, growth, proliferation, and differentiation, have been demonstrated in the RA synovium [37,38]. Conversely, the higher CD55 expression in PsA-FLS implies an enrichment of LL-FLS in PsA compared with RA. Furthermore, in the context of biological relevance, greater coexpression of immune-related markers was observed on RA-FLS, whereas PsA-FLS showed greater coexpression of metabolic and invasive markers, indicating differences in FLS pathogenic functionality across disease states.

Analysis of THY1 expression on PDPN^{+} FLS revealed enrichment of THY1^{+} FLS in RA, while THY1^{-} FLS were enriched in PsA. Consistent with the observed enrichment of THY1^{+} FLS in RA, Croft et al [21] also identified an expanded population of PDPN^{+}FAPα^{+}THY1^{+} immune-effector FLS in RA compared with osteoarthritis (OA). At a functional level, higher expression of MCP-1, MCP-4, eotaxin, eotaxin-3, IP-10, MIP-1α, MIP-1β, and TARC was observed in THY1^{+} FLS than in THY1^{-} FLS. THY1^{+} FLS are strongly associated with immune-effector functions and increased secretion of proinflammatory mediators, and positively correlate with the proportion of infiltrated leukocytes [20,21,39]. THY1^{+}FAPα^{+} FLS were positively correlated with DAS28 and synovitis, corroborating their central role in perpetuating synovial inflammation. Moreover, a higher angiogenic propensity of THY1^{+} FLS was observed, consistent with previous studies that have shown a direct positive correlation between the number of THY1^{+} mesenchymal stem cells and the extent of angiogenesis [40]. Additionally, studies of human and collagen-induced arthritis mouse models suggest that THY1^{-} LL-FLS exhibit a greater propensity to mediate structural bone and cartilage damage, consistent with the higher expression of MMP-1, MMP-3, and MMP-9 observed in THY1^{-} FLS [20,21]. Therefore, the ECM-degradative role of THY1^{-} FLS (enriched in

K, Dot plots showing important mediators involved in focal adhesion and nuclear factor (NF)-κB, VEGF, and Hippo signalling pathways. L, Line graphs showing the mRNA and protein expression of interleukin (IL)-6, and the mRNA expression of matrix metalloproteinase (MMP)-1 and MMP-3, as determined by real-time polymerase chain reaction (qPCR) and enzyme-linked immunosorbent assay (ELISA), respectively, in RA-FLS (n = 7) cultured with the inhibitor verteporfin (VERT) (50 nM) and IL-1β (1 ng/mL). Data are presented as mean ± SEM using the Wilcoxon signed-rank test; *$P < .05$. APOE, apolipoprotein E; CCL, C-C motif chemokine ligand; CHI3L2, chitinase-3-like protein 2; CSN1S1, casein alpha S1; CLIC5, chloride intracellular channel 5; CXCL, chemokine (C-X-C motif) ligand; HLA, human leukocyte antigen; HIF-1, hypoxia inducible factor-1; ICAM-1, intercellular adhesion molecule-1; IER2, immediate early response 2; INHBA, inhibin subunit beta A; INT, intermediate; LL, lining layer; MT1G, metallothionein 1G; POSTN, periostin; SL, sublining; SAV1, salvador family WW domain containing protein 1; TEAD1, TEA domain transcription factor 1; TIMP1, tissue inhibitor of metalloproteinases 1; TM4SF1, transmembrane 4 L six family member 1; YAP, yes-associated protein; VEGF; vascular endothelial growth factor; VCAM-1, vascular cell adhesion molecule-1; VCAN, versican.

PsA) suggests that THY1$^-$ FLS may play a more prominent role in PsA.

Subsequent in-depth characterisation of FLS subsets, focusing on the markers THY1, CD34, CD55, and FAPα, identified 6 distinct FLS subsets, with 2 of these, both notably THY1$^+$CD55$^-$, enriched in the RA cohorts, further corroborating the enrichment of SL-FLS in RA [9,19–22]. Moreover, one of these populations was CD34$^-$, which correlated with the RA-enriched CD34$^-$THY1$^+$ 'perivascular' subset, named for its location surrounding the deep SL capillary structures [9,20]. In alignment with this more 'immune-regulatory' role of the THY1$^+$ SL-FLS clusters, matched histological sections demonstrated significantly higher immune cell infiltration and lymphoid aggregate presence in RA compared with PsA, thus reinforcing the dominance of more immune-related SL-FLS in RA [41,42]. Conversely, PsA was enriched for THY1$^-$CD34$^-$CD55$^+$FAPα^+ and, interestingly, a THY1$^+$ population THY1$^+$CD34$^-$CD55$^+$FAPα^+. Previous studies identified THY1$^-$CD55$^+$ FLS as the classic LL phenotype, supporting the observed increase in LL thickness in PsA synovium at the histological level [19,20,22]. However, the THY1$^+$CD55$^+$ FLS subset enriched in PsA was of particular interest due to its 'intermediate' characteristics, a finding that validates the notion that FLS phenotypes can exist along a dynamic gradient [25].

While the ex vivo flow cytometry analysis demonstrated differences in FLS function between RA and PsA, we next examined whether these differences are maintained in FLS expanded in vitro. To address this, experiments were conducted on FLS at P0 to recapitulate their behaviour within the joint as closely as possible. While differences in the expression of chemokines and angiogenic factors were highly patient- and, indeed, mediator-specific, significantly higher expression of MMP-1 and MMP-3 was observed in PsA-FLS, consistent with scRNA-seq data and previous studies [43,44]. Interestingly, increased glycolysis in PsA-FLS compared with RA-FLS was observed, along with a trend towards increased HIF-1α, HK2, and GLUT-1, indicating a PsA preferential skew towards glycolysis that could be related to the higher pAKT identified in PsA-dominant subsets. However, following IL-1β stimulation, RA-FLS exhibited a more robust glycolytic response. This differential metabolic response to stimulation has been shown previously, albeit in the context of different disease states, with platelet-derived growth factor inducing a significantly lower glycolytic response in OA-FLS than in RA-FLS [45].

Although we have shown differences in enriched FLS populations between RA and PsA, with functional differences retained ex vivo at P0, thereby reinforcing the influence of the 'imprinted-aggressor' phenotype, the ability of these differences to be sustained through further expansion remains unanswered [46]. Therefore, the expression of several surface markers on expanded RA-FLS and PsA-FLS across consecutive passages (P0-P2) was characterised, demonstrating a gradual elevation in CD34 and ICAM-1 expression, while FLS expression of CD55 and HLA-DR showed a stepwise decrease across increasing passages. These results support studies demonstrating that cell removal from the cues/stimuli surrounding them in the joint microenvironment can directly impact their phenotypic profile and corresponding functional behaviour [25,27,28]. Indeed, previous research has shown that once removed from the innate positional cues of neighbouring ECs, the transcriptional profiles of the LL/SL-FLS converge and they lose their proximity to specific poles, a finding mirrored in this data, with a gradual convergence across passages towards a common phenotype [25].

Furthermore, scRNA-seq analysis demonstrated diversity across FLS subsets in the RA and PsA synovium, with 16 distinct clusters identified. Consistent with previous single-cell analyses, demarcation into clear LL vs SL subsets was performed based on *THY1, PRG4,* and *CD55* [9,19–22,24,47]. Interestingly, all RA-dominant populations were of SL origin, aligning with the flow cytometry data. Enrichment of 2 *CXCL12*$^+$ subsets in RA supports previous studies identifying a *CXCL12*$^+$*HLA-DR*^{hi} subset in RA-SL, which expresses genes related to collagen and immune regulation [9,22,39]. In our study, specific enrichment of the *CXCL12*$^+$*APOE*$^+$ and *CXCL12*$^+$*CHI3L2*$^+$ subsets was observed; the latter was previously identified in scRNA-seq analysis of healthy homeostatic FLS clusters and exhibited significant enrichment in the disease state, thereby reinforcing its pathogenic role [47]. Moreover, the RA-enriched *THY1*^{hi}*POSTN*$^+$ cluster was of particular interest due to its higher frequency in the tissue. The *POSTN* gene is strongly associated with RA pathogenesis, with recent studies suggesting that *POSTN* is a central gene with high abundance in the RA synovium, where it is associated with blood vessels and macrophage expansion [48]. Analysis of this specific cluster in RA compared with PsA identified enrichment of several pathways, including focal adhesion/adherens junctions, which are fundamental for facilitating cell migration, as well as oxidative phosphorylation, Hippo-YAP signalling, and MAPK signalling. Indeed, blockade of Hippo-YAP signalling resulted in suppression of FLS proinflammatory responses, suggesting that the *THY1*^{hi}*POSTN*$^+$ cluster is not only more abundant in RA but also has a pathogenic function. This introduces the notion that at a very specific cluster level, FLS within the same cluster may exhibit slightly different functionality depending on the disease state.

Moreover, although our findings are supported by complementary single-cell and functional assays, additional studies incorporating spatial transcriptomics will be important for validating and extending these findings in the native tissue context. However, previous eloquent studies examining the anatomical location of these 2 FLS subtypes have demonstrated that THY1$^+$ FLS are anatomically localised in the synovial SL, whereas THY1$^-$ FLS are localised in the LL, further supporting our data [18,25].

In summary, distinct FLS clusters differ between RA and PsA and exhibit unique transcriptomic and functional properties that shape disease pathogenesis. However, once removed from their native in vivo environment, FLS gradually undergo phenotypic changes, converging towards a common phenotype in both diseases. Further study of FLS subsets may reveal disease-specific mechanisms and enable more precise therapeutic strategies.

Competing interests

All authors declare they have no competing interests.

CRediT authorship contribution statement

Órla Tynan: Writing – review & editing, Writing – original draft, Software, Methodology, Formal analysis, Data curation, Conceptualization. **Aenea A.I. Brugman:** Writing – review & editing, Validation, Methodology, Formal analysis, Data curation. **Conor M. Smith:** Writing – review & editing, Methodology, Formal analysis, Data curation. **Mary Canavan:** Writing – review & editing, Formal analysis, Data curation. **Aoife M. O'Rourke:** Writing – review & editing, Formal analysis, Data curation. **Achilleas Floudas:** Writing – review & editing, Methodology, Data curation. **Dumitru Anton:** Writing – review &

editing, Methodology, Data curation. **Siobhán Wade:** Writing – review & editing, Methodology, Data curation. **Sonia Sundanum:** Writing – review & editing, Methodology, Data curation. **Jean M. Fletcher:** Writing – review & editing, Methodology, Data curation. **Carl Orr:** Writing – review & editing, Methodology, Data curation. **Douglas J. Veale:** Supervision, Methodology, Investigation, Funding acquisition, Formal analysis, Data curation, Conceptualization. **Ursula Fearon:** Writing – review & editing, Writing – original draft, Validation, Supervision, Resources, Project administration, Methodology, Investigation, Funding acquisition, Formal analysis, Data curation, Conceptualization.

Acknowledgements

We would like to thank all the patients who consented to be involved in this study.

Funding

This work was supported by Arthritis Ireland, the Centre for Arthritis and Rheumatic Diseases (CARD), the Health Research Board (HRB), and Science Foundation Ireland (SFI).

Patient consent for publication

Not applicable.

Ethics approval

The study was approved by the Institutional Ethics Committees of St Vincent's University Hospital UCD and Tallaght University Hospital, TCD. Participants gave informed consent to participate in the study before taking part.

Provenance and peer review

Not commissioned; externally peer reviewed.

Data availability statement

All data needed to evaluate the conclusions in the paper are present in the paper and/or the Supplementary Materials. All RNA-seq data are available in a public, open-access repository.

Supplementary materials

Supplementary material associated with this article can be found in the online version at doi:10.1016/j.ard.2026.03.010.

REFERENCES

[1] Veale DJ, Fearon U. What makes psoriatic and rheumatoid arthritis so different? RMD Open 2015;1(1):e000025.
[2] Veale DJ, Fearon U. The pathogenesis of psoriatic arthritis. Lancet 2018 Jun 2;391(10136):2273–84.
[3] Merola JF, Espinoza LR, Fleischmann R. Distinguishing rheumatoid arthritis from psoriatic arthritis. RMD Open 2018;4(2):e000656.
[4] Gravallese EM, Firestein GS. Rheumatoid arthritis - common origins, divergent mechanisms. N Engl J Med 2023 Feb 9;388(6):529–42.
[5] Ospelt C. Synovial fibroblasts in 2017. RMD Open 2017;3(2):e000471.
[6] Koliaraki V, Prados A, Armaka M, Kollias G. The mesenchymal context in inflammation, immunity and cancer. Nat Immunol 2020 Sep;21(9):974–82.
[7] Pap T, Müller-Ladner U, Gay RE, Gay S. Fibroblast biology. Role of synovial fibroblasts in the pathogenesis of rheumatoid arthritis. Arthritis Res 2000;2(5):361–7.
[8] Tolboom TC, Pieterman E, van der Laan WH, Toes RE, Huidekoper AL, Nelissen RG, et al. Invasive properties of fibroblast-like synoviocytes: correlation with growth characteristics and expression of MMP-1, MMP-3, and MMP-10. Ann Rheum Dis 2002 Nov;61(11):975–80.
[9] Zhang F, Wei K, Slowikowski K, Fonseka CY, Rao DA, Kelly S, et al. Defining inflammatory cell states in rheumatoid arthritis joint synovial tissues by integrating single-cell transcriptomics and mass cytometry. Nat Immunol 2019 Jul;20(7):928–42.
[10] Kondo N, Kuroda T, Kobayashi D. Cytokine networks in the pathogenesis of rheumatoid arthritis. Int J Mol Sci 2021 Oct 10;22(20):10922.
[11] Lee SY, Kwok SK, Son HJ, Ryu JG, Kim EK, Oh HJ, et al. IL-17-mediated Bcl-2 expression regulates survival of fibroblast-like synoviocytes in rheumatoid arthritis through STAT3 activation. Arthritis Res Ther 2013 Feb 20;15(1):R31.
[12] Hu F, Yang S, Zhao D, Zhu S, Wang Y, Li J. Moderate extracellular acidification inhibits capsaicin-induced cell death through regulating calcium mobilization, NF-κB translocation and ROS production in synoviocytes. Biochem Biophys Res Commun 2012 Jul 20;424(1):196–200.
[13] Biniecka M, Canavan M, McGarry T, Gao W, McCormick J, Cregan S, et al. Dysregulated bioenergetics: a key regulator of joint inflammation. Ann Rheum Dis 2016 Dec;75(12):2192–200.
[14] Bustamante MF, Garcia-Carbonell R, Whisenant KD. Guma M. Fibroblast-like synoviocyte metabolism in the pathogenesis of rheumatoid arthritis. Arthritis Res Ther 2017;19(1):110.
[15] Pucino V, Certo M, Varricchi G, Marone G, Ursini F, Rossi FW, et al. Metabolic checkpoints in rheumatoid arthritis. Front Physiol 2020;11:347.
[16] Hanlon MM, Canavan M, Barker BE, Fearon U. Metabolites as drivers and targets in rheumatoid arthritis. Clin Exp Immunol 2022 Jun 11;208(2):167–80.
[17] Kemble S, Croft AP. Critical role of synovial tissue-resident macrophage and fibroblast subsets in the persistence of joint inflammation. Front Immunol 2021;12:715894.
[18] Croft AP, Naylor AJ, Marshall JL, Hardie DL, Zimmermann B, Turner J, et al. Rheumatoid synovial fibroblasts differentiate into distinct subsets in the presence of cytokines and cartilage. Arthritis Res Ther 2016 Nov 18;18(1):270.
[19] Stephenson W, Donlin LT, Butler A, Rozo C, Bracken B, Rashidfarrokhi A, et al. Single-cell RNA-seq of rheumatoid arthritis synovial tissue using low-cost microfluidic instrumentation. Nat Commun 2018 Feb 23;9(1):791.
[20] Mizoguchi F, Slowikowski K, Wei K, Marshall JL, Rao DA, Chang SK, et al. Functionally distinct disease-associated fibroblast subsets in rheumatoid arthritis. Nat Commun 2018 Feb 23;9(1):789.
[21] Croft AP, Campos J, Jansen K, Turner JD, Marshall J, Attar M, et al. Distinct fibroblast subsets drive inflammation and damage in arthritis. Nature 2019 Jun;570(7760):246–51.
[22] Micheroli R, Elhai M, Edalat S, Frank-Bertoncelj M, Bürki K, Ciurea A, et al. Role of synovial fibroblast subsets across synovial pathotypes in rheumatoid arthritis: a deconvolution analysis. RMD Open 2022 Jan;8(1):e001949.
[23] Floudas A, Smith CM, Tynan O, Neto N, Krishna V, Wade SM, et al. Distinct stromal and immune cell interactions shape the pathogenesis of rheumatoid and psoriatic arthritis. Ann Rheum Dis 2022 Aug 11;81(9):1224–42.
[24] Zhang F, Jonsson AH, Nathan A, Millard N, Curtis M, Xiao Q, et al. Deconstruction of rheumatoid arthritis synovium defines inflammatory subtypes. Nature 2023 Nov;623(7987):616–24.
[25] Wei K, Korsunsky I, Marshall JL, Gao A, Watts GFM, Major T, et al. Notch signalling drives synovial fibroblast identity and arthritis pathology. Nature 2020 Jun;582(7811):259–64.
[26] Rivellese F, Surace AEA, Goldmann K, Sciacca E, Çubuk C, Giorli G, et al. Rituximab versus tocilizumab in rheumatoid arthritis: synovial biopsy-based biomarker analysis of the phase 4 R4RA randomized trial. Nat Med 2022 Jun;28(6):1256–68.
[27] Zimmermann T, Kunisch E, Pfeiffer R, Hirth A, Stahl HD, Sack U, et al. Isolation and characterization of rheumatoid arthritis synovial fibroblasts from primary culture–primary culture cells markedly differ from fourth-passage cells. Arthritis Res 2001;3(1):72–6.
[28] Neumann E, Riepl B, Knedla A, Lefèvre S, Tarner IH, Grifka J, et al. Cell culture and passaging alters gene expression pattern and proliferation rate in rheumatoid arthritis synovial fibroblasts. Arthritis Res Ther 2010;12(3):R83.
[29] Tullai JW, Schaffer ME, Mullenbrock S, Sholder G, Kasif S, Cooper GM. Immediate-early and delayed primary response genes are distinct in function and genomic architecture. J Biol Chem 2007 Aug 17;282(33):23981–95.
[30] Wight TN, Kang I, Evanko SP, Harten IA, Chang MY, Pearce OMT, et al. Versican-a critical extracellular matrix regulator of immunity and inflammation. Front Immunol 2020;11:512.
[31] Vogt LM, Kwasniewicz E, Talens S, Scavenius C, Bielecka E, Ekdahl KN, et al. Apolipoprotein E triggers complement activation in joint synovial fluid of rheumatoid arthritis patients by binding C1q. J Immunol 2020 May 15;204(10):2779–90.
[32] Khmelevskaya A, Houtman M, Bürki K, Pauli C, Mohammadian H, Angeli M, et al. POS1201 CHI3L1 and CHI3L2 represent two highly specific synovial

fibroblast-related biomarkers in seropositive and negative rheumatoid arthritis. Ann Rheum Dis 2024;83(Suppl 1):590.
[33] Sun J, Li L, Li L, Ding L, Liu X, Chen X, et al. Metallothionein-1 suppresses rheumatoid arthritis pathogenesis by shifting the Th17/Treg balance. Eur J Immunol 2018 Sep;48(9):1550–62.
[34] Nanus DE, Badoume A, Wijesinghe SN, Halsey AM, Hurley P, Ahmed Z, et al. Synovial tissue from sites of joint pain in knee osteoarthritis patients exhibits a differential phenotype with distinct fibroblast subsets. EBioMedicine 2021 Oct;72:103618.
[35] Vordenbäumen S, Braukmann A, Petermann K, Scharf A, Bleck E, von Mikecz A, et al. Casein α s1 is expressed by human monocytes and upregulates the production of GM-CSF via p38 MAPK. J Immunol 2011 Jan 1;186(1):592–601.
[36] Wei Y, Shen X, Li L, Cao G, Cai X, Wang Y, et al. TM4SF1 inhibits apoptosis and promotes proliferation, migration and invasion in human gastric cancer cells. Oncol Lett 2018 Nov;16(5):6081–8.
[37] Caire R, Audoux E, Courbon G, Michaud E, Petit C, Dalix E, et al. YAP/TAZ: key players for rheumatoid arthritis severity by driving fibroblast like synoviocytes phenotype and fibro-inflammatory response. Front Immunol 2021;12:791907.
[38] Barker BE, Hanlon MM, Marzaioli V, Smith CM, Cunningham CC, Fletcher JM, et al. The mammalian target of rapamycin contributes to synovial fibroblast pathogenicity in rheumatoid arthritis. Front Med (Lausanne) 2023;10:1029021.
[39] Alivernini S, MacDonald L, Elmesmari A, Finlay S, Tolusso B, Gigante MR, et al. Distinct synovial tissue macrophage subsets regulate inflammation and remission in rheumatoid arthritis. Nat Med 2020 Aug;26(8):1295–306.
[40] Zeng F, Gao M, Liao S, Zhou Z, Luo G, Zhou Y. Role and mechanism of CD90$^+$ fibroblasts in inflammatory diseases and malignant tumors. Mol Med 2023 Feb 6;29(1):20.
[41] Veale D, Yanni G, Rogers S, Barnes L, Bresnihan B, Fitzgerald O. Reduced synovial membrane macrophage numbers, ELAM-1 expression, and lining layer hyperplasia in psoriatic arthritis as compared with rheumatoid arthritis. Arthritis Rheum 1993 Jul;36(7):893–900.
[42] Alivernini S, Firestein GS, McInnes IB. The pathogenesis of rheumatoid arthritis. Immunity 2022 Dec 13;55(12):2255–70.
[43] Gao W, McGarry T, Orr C, McCormick J, Veale DJ, Fearon U. Tofacitinib regulates synovial inflammation in psoriatic arthritis, inhibiting STAT activation and induction of negative feedback inhibitors. Ann Rheum Dis 2016 Jan;75(1):311–5.
[44] O'Brien A, Hanlon MM, Marzaioli V, Wade SC, Flynn K, Fearon U, et al. Targeting JAK-STAT signalling alters PsA synovial fibroblast pro-inflammatory and metabolic function. Front Immunol 2021;12:672461.
[45] Kvacskay P, Yao N, Schnotz JH, Scarpone R, Carvalho RA, Klika KD, et al. Increase of aerobic glycolysis mediated by activated T helper cells drives synovial fibroblasts towards an inflammatory phenotype: new targets for therapy? Arthritis Res Ther 2021 Feb 15;23(1):56.
[46] Bottini N, Firestein GS. Duality of fibroblast-like synoviocytes in RA: passive responders and imprinted aggressors. Nat Rev Rheumatol 2013 Jan;9(1):24–33.
[47] Faust HJ, Cheng TY, Korsunsky I, Watts GFM, Gal-Oz ST, Trim WV, et al. Adipocyte associated glucocorticoid signaling regulates normal fibroblast function which is lost in inflammatory arthritis. Nat Commun 2024;15:9859.
[48] Li W, Li Z, Zou Z, Liu X, Li X. Integrated single-cell and bulk RNA sequencing identifies POSTN as a potential biomarker and therapeutic target for rheumatoid arthritis. Gene 2024 Nov 30;928:148798.

Ann Rheum Dis 85 (2026) 1463–1476

Contents lists available at ScienceDirect

Annals of the Rheumatic Diseases

journal homepage: https://www.sciencedirect.com/journal/annals-of-the-rheumatic-diseases

Inflammatory arthritis

Psoriatic arthritis monocyte DNA methylomes bridge joint and skin inflammatory pathways across rheumatoid arthritis and psoriasis

Cristina Gómez-Pereira[1], Anna Guiomar Ferreté-Bonastre[1], Ana Belén Azuaga[2], Mónica Munera-Campos[3], Celia Lourdes Calvillo[1], Julio Ramírez[2], Octavio Morante-Palacios[4], Carlos de la Calle-Fabregat[1,5], Laura Ciudad[1], Eva Martínez-Cáceres[6,7], Manel Esteller[8,9,10,11,12], José Manuel Carrascosa[3], Juan D Cañete[2], Esteban Ballestar[1,13,*]

[1] *Epigenetics and Immune Disease Group, Josep Carreras Leukaemia Research Institute (IJC), Badalona, Barcelona, Spain*
[2] *Arthritis Unit, Rheumatology Department, Hospital Clinic, FCRB and IDIBAPS, Barcelona, Spain*
[3] *Department of Dermatology, Hospital Universitari Germans Trias i Pujol, Departament de Medicina, Universitat Autonoma de Barcelona (UAB), Germans Trias i Pujol Research Institute (IGTP), Badalona, Barcelona, Spain*
[4] *Early Oncology Data Science, AstraZeneca, Barcelona, Spain*
[5] *Université Paris-Saclay, Gustave Roussy, U1356 Next Generation Immuno-Oncology Research, Villejuif, France*
[6] *Immunology Division, Laboratori Clínic de la Metropolitana Nord, Germans Trias i Pujol University Hospital and Research Institute, Badalona, Spain*
[7] *Department of Cellular Biology, Physiology and Immunology, Universitat Autònoma de Barcelona, Cerdanyola del Vallès, Spain*
[8] *Cancer Epigenetics Group, Josep Carreras Leukaemia Research Institute (IJC), Badalona, Barcelona, Spain*
[9] *Centro de Investigacion Biomedica en Red Cancer (CIBERONC), Madrid, Spain*
[10] *Institucio Catalana de Recerca i Estudis Avançats (ICREA), Barcelona, Spain*
[11] *Physiological Sciences Department, School of Medicine and Health Sciences, University of Barcelona (UB), Barcelona, Spain*
[12] *Cancer Epigenetics Group, Sant Pau Research Institute (IRSantPau), Barcelona, Spain*
[13] *Epigenetics in Inflammatory and Metabolic Diseases Laboratory, Health Science Center (HSC), East China Normal University (ECNU), Shanghai, China*

ARTICLE INFO

Article history:
Received 10 October 2025
Received in revised form 12 March 2026
Accepted 17 March 2026

ABSTRACT

Objectives: Immune-mediated inflammatory diseases share clinical, genetic, and immunological features, but their specific molecular drivers are not fully defined. Psoriatic arthritis (PsA) exemplifies this overlap, bridging the joint pathology of rheumatoid arthritis (RA) with the skin involvement of psoriasis (PsO). We investigated shared and disease-specific epigenomic traits across the RA-PsA-PsO spectrum, focusing on monocyte DNA methylation and transcriptional programmes.
Methods: We compared genome-wide DNA methylation profiles from peripheral blood monocytes from patients with RA, PsA, PsO, undifferentiated arthritis, and matched healthy donors. We correlated DNA methylation changes with joint- and skin-associated disease activity indices (Disease activity score in 28 joints and body surface area) and analysed for transcription factor motif and pathway enrichment. Single-cell RNA sequencing datasets of monocytes from RA, PsA, and PsO were incorporated to validate and extend epigenomic findings at the transcriptional level in monocyte subsets.

*Correspondence to Dr Esteban Ballestar.
E-mail address: eballestar@carrerasresearch.org (E. Ballestar).
Handling editor Josef S Smolen.
Anna Guiomar Ferreté-Bonastre and Ana Belén Azuaga contributed equally.
Juan D Cañete and Esteban Ballestar share senior authorship.

https://doi.org/10.1016/j.ard.2026.03.018

Results: Across RA, PsA, and PsO, we identified a common methylation signature enriched in enhancers and immune regulatory pathways, implicating transcription factors such as interferon regulatory factors, signal transducer and activator of transcription proteins, Krüppel-like factors, and CCAAT/enhancer-binding proteins. PsA exhibited a dual epigenomic profile, sharing features with both RA and PsO, including Major histocompatibility complex (MHC) class II-related loci and fibroblast growth factor receptor signalling. The dual disease activity component of PsA correlated with methylation changes linked to inflammasome components, on the one hand, and cytokine signalling (interleukin [IL]-23/IL-17, IL-7, IL-2), on the other. Single-cell transcriptomic analysis confirmed convergent alterations in antigen presentation, interferon responses, nuclear factor kappa B (NF-κB) signalling, and fibroblast-associated genes, while highlighting PsA-specific transcriptional signatures.
Conclusions: Monocyte epigenomes reveal shared inflammatory programmes across RA, PsA, and PsO, with PsA occupying a dual molecular state with joint and skin autoimmunity. Integration with single-cell transcriptomes underscores common and distinct pathogenic pathways in PsA, providing insights into underlying disease mechanisms and classification.

WHAT IS ALREADY KNOWN ON THIS TOPIC

- Rheumatoid arthritis (RA), psoriatic arthritis (PsA) and psoriasis (PsO) share genetic and inflammatory pathways, complicating disease classification.
- PsA shows overlapping clinical features with RA and PsO, but its molecular basis remains poorly defined.
- Epigenetic changes in immune cells, including monocytes, contribute to Immune-mediated inflammatory diseases (IMID) pathogenesis.

WHAT THIS STUDY ADDS

- Identifies a shared monocyte DNA methylation signature across RA, PsA and PsO, enriched in immune regulatory pathways.
- Demonstrates that PsA exhibits a dual epigenomic and transcriptomic profile bridging RA and PsO.
- Reveals coordinated dysregulation of key transcription factor networks and inflammatory pathways.
- Links joint-based and skin-based disease activity to distinct methylation programmes.

HOW THIS STUDY MIGHT AFFECT RESEARCH, PRACTICE OR POLICY

- Supports refined molecular classification of IMIDs, particularly PsA.
- Provides a basis for epigenetic biomarkers to stratify patients and identify PsO individuals at risk of PsA.
- Highlights circulating monocytes as accessible indicators of systemic inflammatory states.
- Identifies candidate pathways for therapeutic targeting across IMIDs.

INTRODUCTION

Immune-mediated inflammatory diseases (IMIDs) represent a major challenge due to the striking overlap in their clinical manifestations and underlying genetic susceptibilities. Diseases such as rheumatoid arthritis (RA), psoriatic arthritis (PsA), and psoriasis (PsO) may affect different organs, yet they share genetic risk factors, networks of immune dysregulation, and inflammatory pathways that blur traditional diagnostic boundaries.

Chronic inflammatory arthritis is a group of disorders that primarily affect the joints and substantially impact patients' quality of life. Early stages of arthritis, including the so-called undifferentiated arthritis (UA), can last for years before progressing into RA or PsA, among others.

RA is a chronic systemic inflammatory disorder that primarily affects diarthrodial joints, leading to inflammation and tissue damage [1], which is characterised by immune cell infiltration, synovial lining hyperplasia, pannus formation, and destruction of cartilage and bone. Overall, the genetic factor is the most contributing risk for RA. Genetic variants in the human leukocyte antigen (HLA)-DR locus are associated with an increased risk of RA through citrullinated peptide presentation to CD4+ T cells, resulting in T-cell activation and proinflammatory cytokine production.

On the other hand, PsO is a chronic inflammatory disease of the skin, recognisable by whitish erythematous or red scaly patches and excessive skin exfoliation due to increased keratinocyte proliferation [2]. Its prevalence is 2% to 3% in the general population. PsO is characterised by interleukin-17 (IL-17)-dominant abnormal innate and acquired immunity, with hyperproliferation and aberrant differentiation of epidermal keratinocytes. Over 100 genetic loci have been associated with PsO susceptibility, of which HLA-C*06:02, IL12B, IL23A, and IL17RA are among the most well-studied [3].

PsA offers a key example of how conditions within this spectrum can associate seemingly distinct diseases, linking the joint-centred pathology of RA with the skin manifestations of PsO. Like RA, PsA potentially causes chronic synovial inflammation, joint damage, and disability; however, it lacks typical RA autoantibodies and often presents with asymmetric joint involvement, dactylitis, enthesitis, and spondylitis. Its close association with PsO reflects shared genetic and immunologic drivers, including dysregulation of the IL-23/IL-17 axis, differentiating it from the predominantly autoantibody-driven processes of RA. In addition, approximately 30% of patients with PsO develop PsA [4]. Many PsA cases are misdiagnosed as UA or RA because of overlapping clinical patterns, particularly in the early stages.

Autoimmunity occurs when immune tolerance is disrupted due to alterations in the immune system that cause proliferation of autoreactive T and B lymphocyte populations in response to autoantigens. The abnormal function of the adaptive immune system is triggered by the innate immune response. In this regard, cells of the mononuclear phagocyte system also play crucial roles in autoimmunity progression. Monocytes are early effectors and responders of inflammation and differentiate into macrophages or dendritic cells after travelling through the blood to the tissues. Many studies show that different monocyte subsets can also contribute to the pathogenesis of IMIDs.

In addition to genetic determinants, epigenetic alterations, including DNA methylation in cell types involved in autoimmune pathogenesis, such as monocytes, provide valuable information about underlying pathogenic mechanisms, help identify

specific markers, enable earlier detection of pathology, and reveal therapeutic targets.

In this study, we examined shared and disease-specific epigenetic features in monocytes across the RA-PsA-PsO spectrum, focusing on distinctive DNA methylation traits of PsA. We further identified genes and pathways associated with these changes and integrated public single-cell RNA sequencing (scRNA-seq) data to validate and extend the findings at the transcriptional level.

METHODS

Details of the patient cohorts included in this study, a description of the experimental methods, including DNA methylation and scRNA-seq analyses, as well as the statistical analyses applied, are provided in the online supplementary material.

RESULTS

A common DNA methylation signature in the RA-PsA-PsO spectrum

To investigate common features in the DNA methylation signatures of monocytes from RA, PsA, and PsO, as well as their relationship to those in UA, we first performed a differential analysis comparing the entire patient group with healthy donor (HD) monocytes. For this analysis, all patient entities were considered together as a single group of patients with IMID, and only samples from individuals with moderate or high disease activity were included (Fig 1A,B and Supplementary Table S1). We identified 92 differentially methylated positions (DMPs) with an adjusted *P* value of <0.05 and a differential beta-value of >0.1. Unsupervised clustering led to the segregation of these DMPs into 2 clusters: cluster 1 (36 hypomethylated DMPs in the 4 IMID groups compared with HD) and cluster 2 (56 hypermethylated DMPs in the 4 IMID groups compared with HD) (Fig 1C,D and Supplementary Table S2.1). Although this analysis considered all pathological conditions as a single entity, unique patterns emerged across diseases. UA samples showed the most distinct profile relative to HD, whereas PsA and PsO displayed subtler differences and were highly similar to each other.

In addition to this analysis, we performed the same comparison including patients with low activity and remission (Supplementary Figure S1A,B and Supplementary Table S2.2). In this case, a total of 39 DMPs were identified, supporting that most differences arise when comparing patient samples with active disease. When we conducted a contrast comparing only low disease activity/remission vs HD, we identified only 1 DMP, supporting the interpretation that the vast majority of the methylation changes observed are associated with high disease activity. Furthermore, to assess how many differences were associated with disease state independently of activity, we designed a model that included activity as an additional covariate, yielding 23 DMPs (*P* value < 0.05) (Supplementary Fig S1C,D and Supplementary Table S2.3). Some interesting genes annotated to these DMPs include *SLC40A1* in cluster 1 and *IGLL5* in cluster 2 (Supplementary Fig S1E). *SLC40A1* encodes ferroportin-1 (FPN1), involved in cellular iron efflux. Its expression decreases in response to IL-6, increases intracellular iron, and potentially enhances the proliferation of RA synovial fibroblasts [5]. The *IGLL5* gene encodes a member of the immunoglobulin superfamily, a key component of the B cell receptor signalling pathway that plays an important role in immune regulation. It is upregulated in RA and is likely involved in its pathogenesis [6].

For the initial DNA methylation analysis, which included only samples with moderate to high activity, we examined the distribution of DMPs in relation to gene bodies and cytosine −phosphate−guanine (CpG) islands (Fig 1E). Most DMPs were located outside CpG islands (CGIs) in both clusters 1 and 2. In addition, the majority were found in distal intergenic and intronic regions. ChromHMM analysis further associated these DMPs with specific chromatin states (Fig 1F). The only regions significantly enriched for our CpGs were enhancers.

We then performed transcription factor (TF) binding motif enrichment analysis using Hypergeometric Optimization of Motif EnRichment (HOMER) in the regions comprising these DMPs to identify potential TFs that may contribute to the observed DNA methylation changes (Fig 1G and Supplementary Table S3.1). Among the hypomethylated DMPs (cluster 1), we found significant enrichment of consensus binding sequences for several factors, including nuclear factor interleukin 3 regulated (NFIL3) and CCAAT/enhancer-binding proteins (CEBPs). Notably, NFIL3 has been linked to inflammatory conditions such as RA [7], and several CEBP family members are critical for myeloid cell development and activation [8]. In the hypermethylated DMP cluster (cluster 2), TF binding motif enrichment analysis revealed a strong involvement of interferon-related factors (IRFs), particularly IRF8, which has been associated with inflammatory diseases in response to proinflammatory stimuli [9].

We also performed gene ontology (GO) analysis of the genes closest to the identified DMPs (Fig 1H and Supplementary Table S4) to identify functionally relevant gene categories. We observed important differences in the pathways enriched in each cluster. Although both clusters showed significant enrichment for functions related to T-cell regulation and activation, they differed in the specific interleukin pathways represented. Cluster 1 DMPs were associated with negative regulation of IL-12 and IL-10 secretion, as well as with the response to IL-1. IL-12 is a proinflammatory cytokine secreted by myeloid lineage cells such as monocytes, macrophages, and dendritic cells, which induces a Th1 response in T cells and promotes interferon-gamma (IFN-γ) production [10]. In contrast, IL-10 is an anti-inflammatory cytokine with an autoregulatory role when secreted by monocytes. The pathways enriched among cluster 2 DMPs involved interleukins such as IL-7 and IL-2. Elevated concentrations of IL-7 have been reported in RA, where it promotes the differentiation of monocytes into macrophages and osteoclasts, thereby contributing to proinflammatory bone-damaging functions [11] Similarly, the proinflammatory cytokine IL-2 promotes T-cell proliferation and contributes to cartilage and joint damage [12].

Cluster 1 DMPs were annotated to genes such as Krüppel-like factor (*KLF)2,* transmembrane 4 L six family member 20 (*TM4SF20), LRIG1*, and *FAM20A* (Fig 1I). The TF KLF2 is expressed in basal monocytes but is downregulated upon activation or differentiation, thereby modulating these processes [13]. KLF2 has also been hypothesised to attenuate arthritis by epigenetically regulating the nuclear factor kappa B (NF-κB) pathway [14]. In addition, *LRIG1* expression has been shown to regulate the suppressive properties of T cells, thereby preventing autoimmunity [15]. In cluster 2, several significant DMPs were

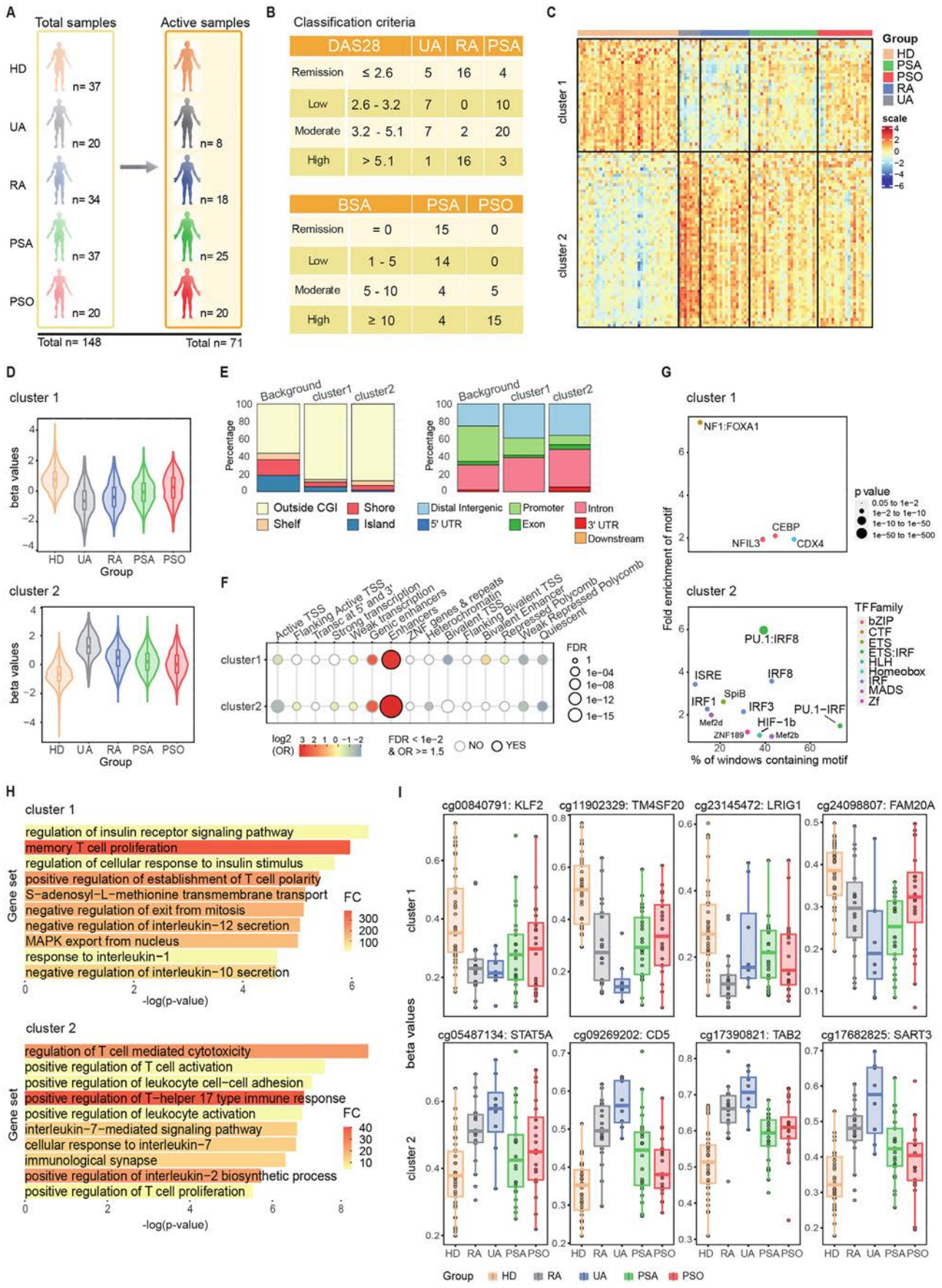

Figure 1. Differential methylation analysis between HD and all diseases. (A) Scheme summarising the number of patients in each cohort, including the total number of samples and the samples in disease cohorts after selecting only the active ('Moderate' and 'High'). (B) Table of the classification criteria for both activity indexes, DAS28 and BSA, and the number of samples for each level of activity: 'Remission', 'Low', 'Moderate', 'High'. (C) Heatmap representing 92 DMPs (FDR < 0.05, $|\Delta\beta| > 0.1$) among HD (n = 37), UA (n = 8), RA (n = 18), PsA (n = 25), and PsO (n = 20), with only active samples filtered. (D) Violin plots showing the beta values for each cohort. (E) Barplot describing the percentage of CpGs from our DMPs that fall in a certain type of genomic position, both in relation to the CpG islands or the functional genomic region. (F) ChromHMM associates the CpGs

annotated to genes such as signal transducer and activator of transcription (*STAT)5A, CD5, TAB2*, and *SART3*.

PsA shares disease-specific methylation features with both RA and PsO

We next performed a pairwise comparison of RA, PsA, and PsO monocyte DNA methylation profiles, identifying 566 DMPs (P value < 0.01 and $|\Delta\beta| > 0.1$), which grouped into 4 clusters. Examination of the heatmap and the violin plots (Fig 2A,B and Supplementary Table S2.4) revealed that DNA methylation levels in PsA and PsO samples within cluster 1 (312 CpGs) and cluster 3 (163 CpGs) are very similar, with the former being hypermethylated and the latter hypomethylated. In contrast, in cluster 2 (33 CpGs), the methylation levels of RA and PsA samples were more similar to each other than to those of PsO.

Enrichment analysis of TF binding motifs across the 4 clusters revealed the potential involvement of several relevant TF. For example, cluster 1 showed binding motifs for STAT4 and SMAD family member 4 (SMAD4) (Fig 2C and Supplementary Table S3.2), with STAT4 reported to be dysregulated in several autoimmune diseases.

Inspection of the genes annotated to DMPs from the 4 clusters revealed several important candidates. Figure 2D shows 2 representative genes from each cluster, which are described below. In cluster 1, where both PsA and PsO are hypermethylated compared with RA, *FGF12* (fibroblast growth factor 12) encodes a member of the FGF family involved in diverse biological processes, including cell growth and tumour progression. *RLF* encodes a zinc finger−containing protein implicated in transcriptional activation and epigenetic modification [16]. In cluster 2, where RA and PsA are hypomethylated compared with PsO, we identified *SLC50A1*, which encodes a glucoside transmembrane transporter. This cluster also included a DMP annotated to *HLA-DRB1*. Several SNPs in *HLA-DRB1* have been associated with PsO risk, and hypomethylation of this gene has been implicated in PsO pathogenesis [17]. *HLA-DRB1* hypomethylation has been associated with increased expression and PsO severity. In cluster 3, where both PsA and PsO are hypomethylated compared with RA, we identified genes like *FGFR2* and *PRDM1*, which regulate natural killer T cell memory differentiation and effector function [18]. Finally, in cluster 4, hypermethylated in PsA, we identified *PCDH9-AS2*, a PCDH9 Antisense RNA 2, and *METRNL*.

GO analysis (Fig 2E and Supplementary Table S5) of clusters 1 and 3 showed enrichment in the HLA region, one of the most genetically diverse regions of the genome. Interestingly, we also found enrichment of the fibroblast growth factor receptor (FGFR) signalling pathway, whose membrane-bound receptors are activated by fibroblast growth factors.

We then performed a new pairwise comparison including RA, PsA, and, in this case, UA to explore the potential relationship between untreated UA cases and 2 distinct forms of chronic inflammatory arthritis. Supplementary Figure S2 summarises these results, where we obtained 1081 DMPs (FDR < 0.05 and $|\Delta\beta| > 0.1$) (Supplementary Table S2.5) grouped into 4 distinct clusters, all of which indicated that UA displays more extreme methylation values. HOMER analysis (Supplementary Fig S2C and Supplementary Table S3.3) revealed, in cluster 1, the presence of several IRF proteins, including IRF2, which negatively regulates type I IFN signalling and stimulates inflammatory reactive oxygen species production and the expression of tumour necrosis factor (TNF), IL-1β, and IL-6 [19]. Moreover, IRF2 has been reported to promote RANKL-induced osteoclast differentiation by modulating the NF-κB-NFATc1 signalling pathway [20]. Other examples include several members of the transcriptional enhancer factor family (TEAD), TEAD4, in cluster 3, which is typically expressed in skeletal muscle.

The pathways enriched across the 4 clusters were all related to immune system activation and cytokine production (Supplementary Table S6). In cluster 3, IL-3 was identified, an important mediator of haematopoiesis that also inhibits TNF-α-induced bone resorption and prevents inflammatory arthritis in mice [21].

The dual disease activity component of PsA is reflected in the monocyte DNA methylomes

We also investigated the relationship between DNA methylation and disease activity, measured by the disease activity score in 28 joints (DAS28) for RA and PsA, and by body surface area (BSA) for PsO and PsA (Supplementary Methods). This analysis allowed us to explore the impact of distinct components of disease activity arising from joint and skin lesions, which are potentially reflected when analysing peripheral monocytes in PsA. Figure 3 shows the results of the Spearman's correlation analysis between sample methylation patterns and disease activity indices (DAS28 or BSA). Significant CpGs were classified as hypermethylated or hypomethylated based on their methylation values, in relation to DAS28 and BSA (Fig 3A,D). From these CpGs, we further investigated the associated TF and pathways.

In the GO analysis of the Spearman's test for DAS28 (RA + PsA) (Fig 3B and Supplementary Table S7), the hypermethylated DMPs were primarily enriched for immune system activation and regulation functions, as well as cytokine signalling pathways. We also observed enrichment for IFN-γ production and natural killer activation, among others. GO analysis of hypomethylated DMPs mainly highlighted an involvement of the nucleotide-binding domain and Leucine-rich Repeat containing (NLR) family pyrin domain containing 1 (NLRP1) inflammasome complex. Inflammasomes are cytoplasmic protein assemblies that drive inflammation as part of host defence. Disruptions in the NLRP1 pathway have been associated with both PsA [22] and RA [23]. In addition, the Janus kinase−signal transducer and activator of transcription (JAK-STAT) pathway emerged as crucial in IMID pathogenesis due to its central role in the downstream signalling that regulates inflammatory

statistically with a genomic region for each cluster. (G) Significantly enriched TF motifs for the selected DMPs were identified by HOMER. (H) GO significant pathways obtained with GREAT. (I) Boxplots showing the significant genes associated with the CpGs from each cluster. BSA, body surface area; bZIP, basic leucine zipper; CDX4, caudal type homeobox 4; CEBP, CCAAT/enhancer-bindng proteins; CpG, cytosine−phosphate−guanine (dinucleotide); CTF, CCCTC-binding transcription factor; CGI, CpG island; DMP, differentially methylated position; DAS28, disease activity score using 28 joints; ETS, E26 transformation-specific (family of transcription factors); FC, fold change; FDR, false discovery rate; GO, gene ontology; GREAT, Genomic Regions Enrichment of Annotations Tool; HD, healthy donor; HIF, hypoxia-inducible factor; HLH, helix−loop−helix; HOMER, Hypergeometric Optimization of Motif EnRichment; IRF, interferon regulatory factor; ISRE, interferon-stimulated response element; KLF, Krüppel-like factor; MADS, MCM1, AGAMOUS, DEFICIENS, SRF (transcription factor family); MAPK, mitogen-activated protein kinase; NFIL3, nuclear factor, interleukin 3 regulated; OR, odds ratio; PsA, psoriatic arthritis; PsO, psoriasis; RA, rheumatoid arthritis; TF, transcription factor; TSS, transcription start site; UA, undifferentiated arthritis; UTR, untranslated region.

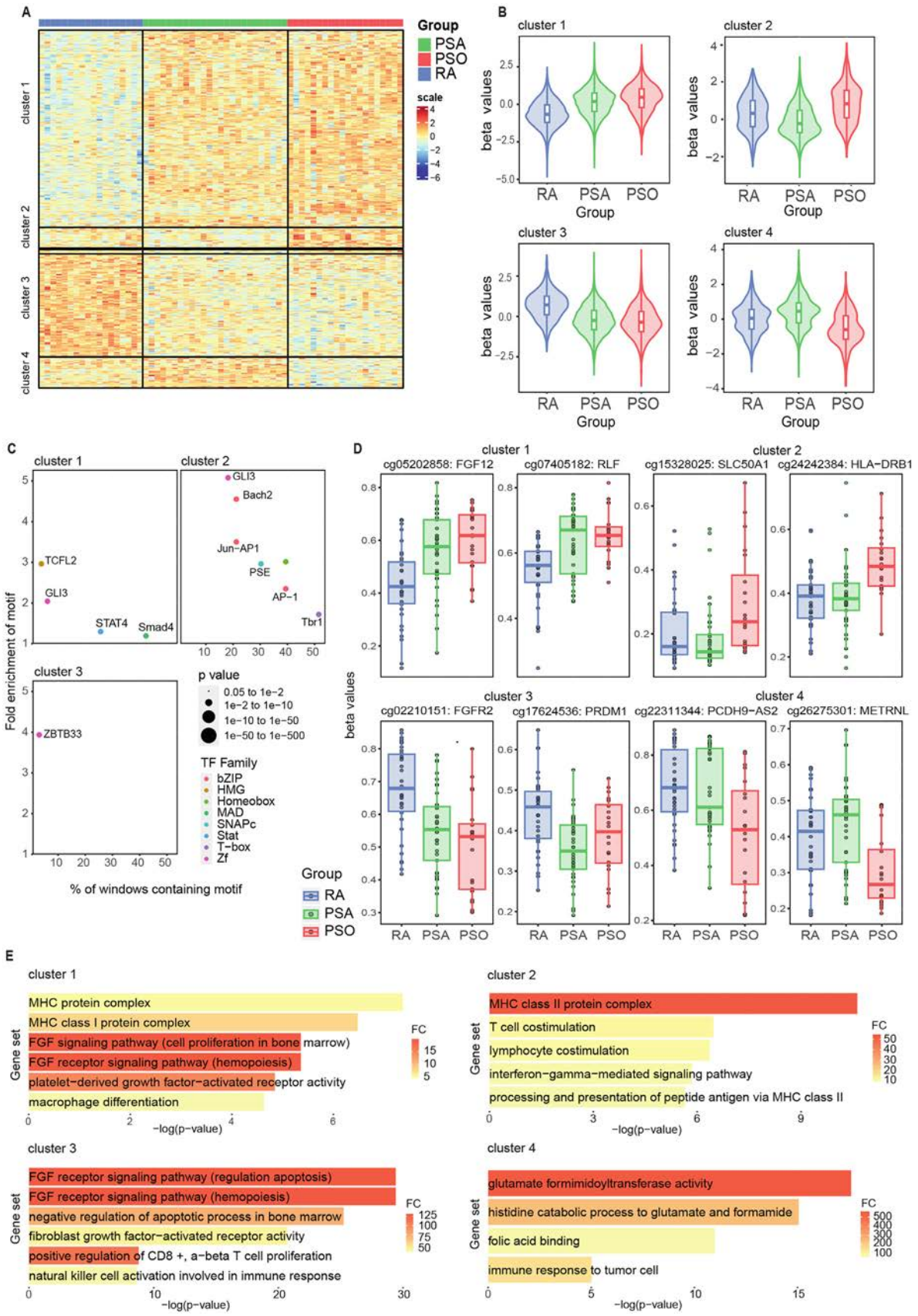

Figure 2. Differential methylation analysis between RA, PsA, and PsO. (A) Heatmap representing 566 CpGs (P value < 0.01, $|\Delta\beta| > 0.1$) between RA (n = 18), PsA (n = 25) and PsO (n = 20), with only active samples filtered. (B) Violin plots representing, for the 4 selected clusters, the beta values for each cohort. (C) Representation for the significantly enriched TF from the first 3 clusters. (D) Selection of the most significant genes associated with CpGs from each cluster. (E) GO-enriched pathways for each cluster, analysed by GREAT. bZIP, basic leucine zipper (domain); CpG, cytosine−phosphate−guanine (dinucleotide); FC, fold change; FGFR, fibroblast growth factor receptor; GO, gene ontology; GREAT, Genomic Regions Enrichment of Annotations Tool; HLA, human leukocyte antigen; HMG, High Mobility Group (protein family/domain); MAD, MAX dimerization protein; METRNL, meteorin-like protein; MHC, major histocompatibility complex; PCDH9, protocadherin 9; PsA, psoriatic arthritis; PSE, proximal sequence element; PsO, psoriasis; PRDM1, PR/SET domain 1; RLF, rearranged L-myc fusion gene; RA, rheumatoid arthritis; SLC, solute carrier (family of membrane transporters); SNAPc, small nuclear RNA activating protein complex; STAT4, signal transducer and activator of transcription 4; TF, transcription factor; TCFL2, transcription factor 7 like 2.

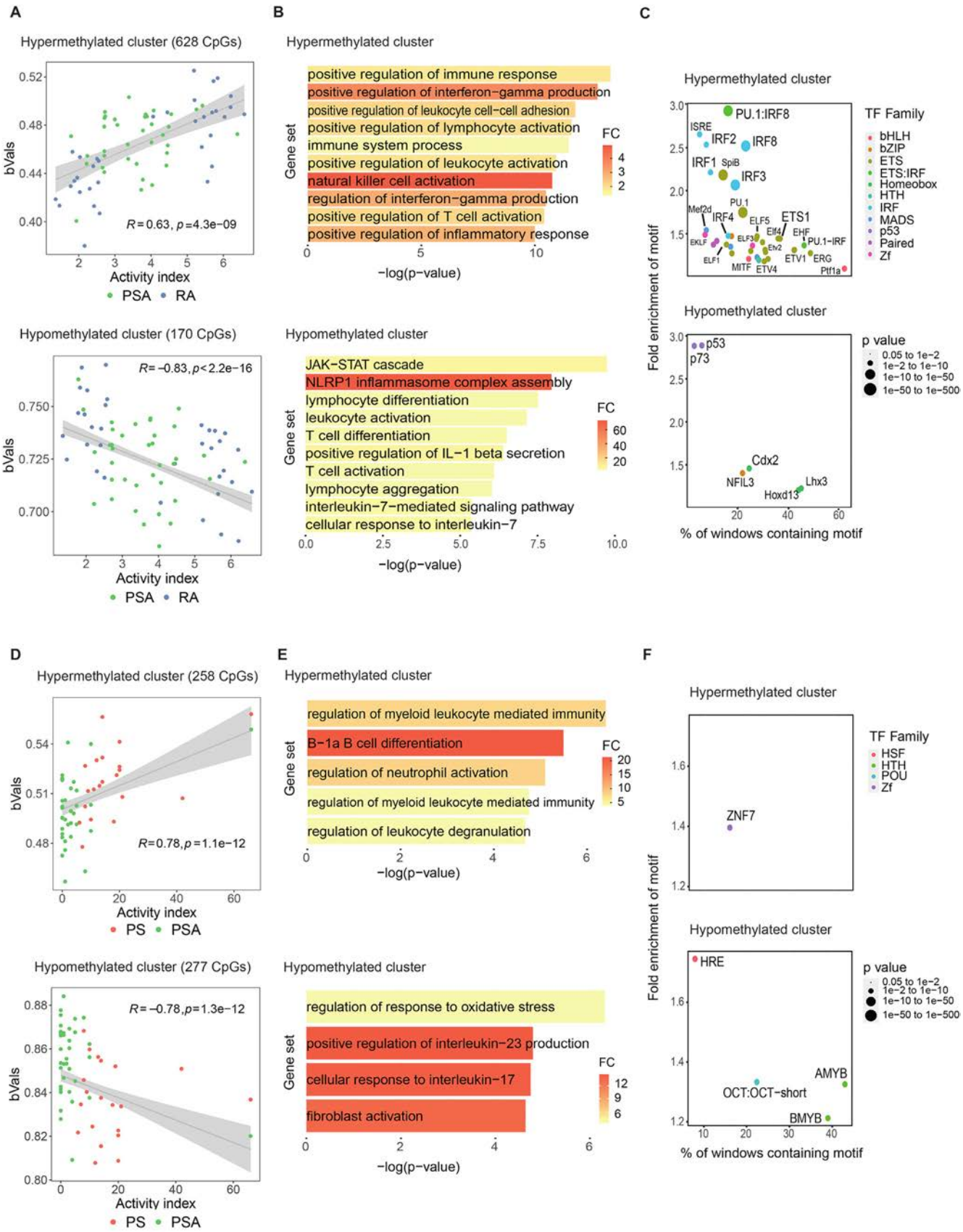

Figure 3. Correlation analysis of DNA methylation and activity indexes (DAS28 and BSA). (A) Two scatter plots of the correlation between the activity index, DAS28 in this case, and the beta values of the statistically significant CpGs, for the hypermethylated ones (628 CpGs) and for hypomethylated (170 CpGs). CpGs significantly correlated with disease activity were selected using a nominal *P* value threshold (*P* value < 0.001) without multiple testing correction and were used for downstream functional enrichment analyses (see Methods). (B) The enriched GO pathways resulted from GREAT for each cluster. (C) The significant TF analysed by HOMER. (D) Two scatter plots of the correlation between the activity index, BSA in this case, and the beta values of the statistically significant CpGs, for the hypermethylated ones (258 CpGs) and for hypomethylated (277 CpGs). (E) The enriched GO pathways resulted from GREAT for each cluster. (F) The significant TF analysed by HOMER. bHLH, basic helix−loop−helix; BSA, body surface area; bZIP, basic leucine zipper; CpG, cytosine−phosphate−guanine; DAS28, disease activity score using 28 joints; ETS, E26 transformation-specific;

responses, and JAK inhibitors have been approved for the treatment of these diseases [24].

Enrichment analysis of TF binding motifs across the hypermethylated and hypomethylated clusters in relation to DAS28 revealed highly relevant TFs (Fig 3C and Supplementary Table S3.4). In the hypermethylated cluster, TF binding motifs included members of the IRF and E26 transformation-specific (ETS) families. In the hypomethylated cluster, p53 was enriched. An immunopathologic study of p53 expression in synovial tissue from patients with RA and PsA has demonstrated its association with bone erosion in RA, but not in PsA [25].

Spearman's correlation with BSA, the skin-related disease activity score in PsA and PsO also revealed interesting pathways. In this case, GO analysis highlighted several pathways related to immune system activation specific for these conditions (Fig 3E,F, also Supplementary Tables S3.5 and S8). In particular, the hypomethylated cluster in relation to BSA was enriched for IL-23 production and response to IL-17 (Fig 3E). These 2 cytokines are critical in chronic inflammatory pathways, both in the synovium and skin lesions of patients with PsA. IL-23 promotes the survival and expansion of Th17 cells through its receptor IL23R, and the Th17-mediated inflammatory response involves the signalling adaptor TRAF3 interacting protein 2 (TRAF3IP2). The IL23/IL-17 axis also induces abnormal proliferation of keratinocytes, causing skin PsO [26].

Finally, we inspected the genes to which the CpGs identified by Spearman's correlation with DAS28 and BSA were annotated (Supplementary Fig S3A). For RA and PsA samples stratified by DAS28, we identified both hypermethylated and hypomethylated genes. Among them, *WNT8A*, encoding a regulator of the Wnt signalling pathway, was hypermethylated in RA. Dysregulation of this pathway has been implicated in fibroblast-like synoviocyte activation, synovial hyperplasia, and joint destruction, underscoring its contribution to RA pathogenesis [27]. We also observed differential methylation in *CD5*, consistent with previous evidence showing that $CD5^+$ B cells are increased in RA and display distinctive features, including spontaneous upregulation of CD5 expression *in vitro*, which is specifically downregulated by IL-4 [28]. In addition, methylation of *STAT5A* was detected; this TF plays a unique role in $CD4^+$ T cells, where its knockdown specifically downregulates the survival factor Bcl-X, distinguishing it from STAT5B [29]. IL-7-driven arthritis is characterised by an increase in IL-7R+ macrophages, which contribute to disease severity by promoting the differentiation of inflammatory M1 macrophages and bone-eroding osteoclasts [30].

For PsA and PsO samples, correlating with activity through the BSA index, we identified additional genes of interest (Supplementary Fig S3B). As previously described, IRF8 showed disease-related alterations. We also found evidence of dysregulation of IL-13, which has been shown to have variable activity in PsO, with stronger genetic and receptor associations in PsA, highlighting its role in patient heterogeneity [31]. On the other hand, IL-13 can also be dysregulated in RA [32].

scRNA-seq analysis in the RA-PsA-PsO spectrum reveals specific features in different monocyte subsets

Finally, we compared the transcriptome profiles of RA, PsA, and PsO to investigate their dysregulation across different monocyte subsets. To this end, we integrated 2 scRNA-seq datasets [33,34] comprising a total of 20 RA, 28 PsA, 24 PsO, and 33 HD samples. The integrated Seurat object was then filtered for monocyte populations defined by the markers $FUT4^-$, $ITGAM^+$, and $CD33^+$ (Fig 4A), equivalent to their respective encoded genes using for the sorting of the patient samples used for the DNA methylation study. Supplementary Figure S4A displays the same uniform manifold approximation and projection (UMAP) separated by condition (HD, RA, PsA, and PsO) to illustrate the groupwise distribution of cells. The identified clusters were annotated as distinct monocyte subtypes based on canonical markers such as CD14 and CD16, along with additional subtype-defining markers (Fig 4B). Supplementary Figure S4B quantifies these distributions, showing the relative proportions of each monocyte subtype across the 4 groups.

In parallel with the DNA methylation analyses, we first performed a differential expression analysis for each monocyte cluster, comparing HDs with all disease groups combined (RA, PsA, and PsO) using the integrated scRNA-seq data (Fig 4C and Supplementary Table S9.1). An overlap of differentially expressed genes (DEGs) across clusters was observed, comprising 5204 upregulated genes and 5339 downregulated genes (Supplementary Fig S4C).

The results of this analysis are shown in Figure 4C as volcano plots of the DEGs identified in this comparison (Supplementary Table S9.1), highlighting both upregulated and downregulated genes across monocyte clusters for RA, PsA, and PsO. A considerable proportion of these genes belong to the KLF family, including *KLF4*, previously associated with PsO [35]. While increased KLF4 expression in psoriatic skin has been interpreted as a compensatory response to abnormal keratinocyte behaviour, in our data, KLF4 was consistently downregulated in disease groups (RA, PsA, and PsO) across all clusters. Finally, CD68, a macrophage marker expressed in synovial tissue, has been proposed as a biomarker for evaluating treatment effectiveness in RA [36].

In contrast, the upregulation of STAT4 observed in several clusters may represent a functional consequence of risk-associated STAT4 haplotypes, linking genetic predisposition with enhanced inflammatory signalling in RA [37]. Moreover, *KLF12* has been identified as a susceptibility gene in RA genome-wide association studies [38], and its upregulation in our dataset further supports a potential role in disease pathogenesis. In the classical 1 and intermediate monocyte clusters, chemokine-like factor (CKLF) was detected, in line with reports showing significantly elevated CKLF1 levels in patients with RA, osteoarthritis, and axial spondylarthritis compared with controls [39]. In addition, CD247, encoding the T-cell receptor zeta chain, was upregulated in all clusters except the intermediate subset, in line with previous genome-wide evidence linking CD247 polymorphisms to RA risk [40].

We then performed GO analysis on the upregulated DEGs from the comparison of RA+PsA+PsO vs HD, where we observed enrichment for immune-related processes such as antigen presentation, T-cell activation, phagocytosis, interferon activity, and NF-κB signalling, with different trends across clusters for the upregulated genes (Fig 4D (top) and Supplementary Table S10). These categories were differentially enriched in different monocyte subsets (Fig 4D, top). The major histocompatibility (MHC) complex

FC, fold change; GO, gene ontology; GREAT, Genomic Regions Enrichment of Annotations Tool; HOMER, Hypergeometric Optimization of Motif EnRichment; HRE, hypoxia response element; HSF, heat shock factor; HTH, helix–turn–helix; IRF, interferon regulatory factor; JAK, Janus Kinase; MADS, MCM1, AGAMOUS, DEFICIENS, SRF; NFIL3, nuclear factor, interleukin 3 regulated; NLRP1, NLR family pyrin domain containing 1; OCT, octamer-binding transcription factor; POU, pit-oct-unc (domain family); PsA, psoriatic arthritis; RA, rheumatoid arthritis; STAT, signal transducer and activator of transcription; TF, transcription factor.

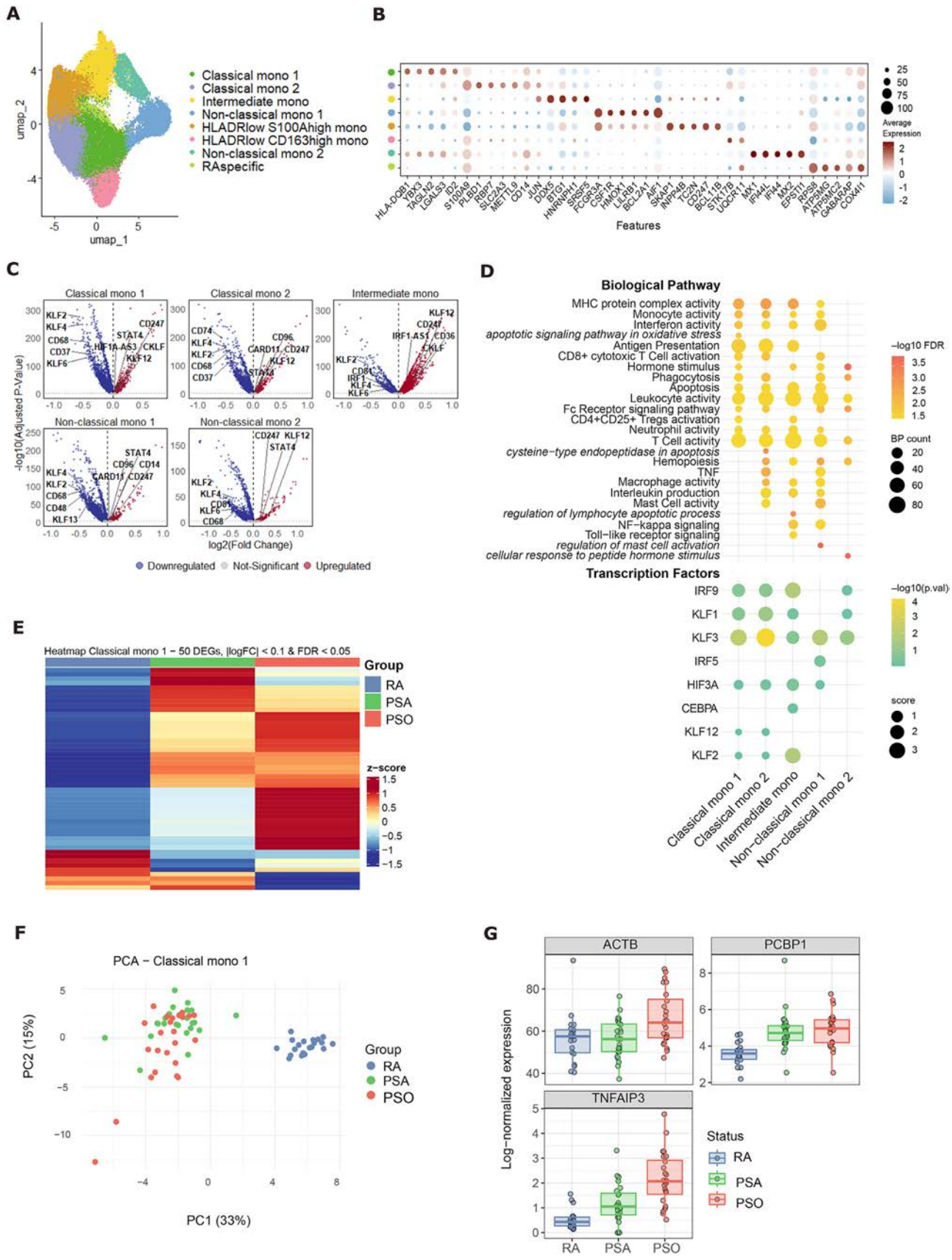

Figure 4. scRNA-seq analysis of public databases. (A) UMAP with the integrated samples of RA, PsA, and PsO from 2 public databases, with a total of 77.655 cells classified according to their specific monocyte subcluster. (B) Dotplot with the specific markers to characterise the different monocyte subclusters. (C) Volcano plot of the 5 principal monocyte clusters, representing both upregulated and downregulated DEGs from the HD vs All comparison, with 5 examples of the most relevant for each of them. (D) GO and TF enrichment analysis of upregulated DEGs from monocyte subsets (HD vs All). Top: biological pathways grouped into general categories, with *BP count* indicating the number of specific pathways included and −log10(FDR) showing the most significant value. Terms in italics highlight pathways specific to individual clusters. Bottom: enriched TFs, with circle size representing −log10(adjusted *P* value) and colour indicating enrichment score. (E) Heatmap showing the expression of 50 DEGs from Classical Mono 1 across RA, PsA, and PsO samples that were obtained from their pairwise comparison (|logFC| > 0.1, FDR < 0.05). (F) PCA of the 50 DEGs from Classical

was significantly enriched across the monocyte clusters, strongly associated with RA, particularly through HLA-DRB1 [41]. Intermediate monocyte populations showed enrichment for NF-κB signalling and Toll-like receptor (TLR) signalling. TLRs are expressed in the inflamed joints of patients with RA and are also contributors to chronic inflammatory skin diseases such as PsO [42].

TF enrichment analysis of the upregulated DEGs (Fig 4D and Supplementary Table S11) identified IRFs (IRF9, IRF5, IRF2), KLF family members (KLF1, KLF3, KLF2), CEBPA, and hypoxia-inducible factor 3 alpha (HIF3A). Aligning with the GO analysis, this analysis showed some differences among monocyte subsets. IRF9 contributes to RA progression by regulating macrophage polarisation through proteasome subunit alpha type 5 (PSMA5) [43]. IRF5 promotes inflammatory arthritis by driving proinflammatory cytokine production downstream of the RNA-sensing receptors TLR7 and TLR3, implicating endogenous RNA ligands in RA pathogenesis [44]. Another study suggested that HIF3A may act as a negative regulator of chondrocyte hypertrophy and thus play a protective role in joint homeostasis [45]. Finally, KLF3, which is essential for epidermal differentiation and barrier formation through enhancer activation, may be particularly relevant in PsO, where impaired keratinocyte differentiation is a defining pathogenic feature [46].

In addition, we examined the downregulated DEGs from the HD vs RA + PsA + PsO comparison (Supplementary Fig S4D and Supplementary Table S10), which revealed enrichment for processes including monocyte activity, regulation of apoptosis, MHC class I and II protein activity, TNF signalling, phagocytosis, antigen presentation, T-cell and leukocyte activity, interferon responses, NF-κB and p38 mitogen-activated protein kinase (MAPK) signalling, and TLR and neutrophil functions.

Along these downregulated pathways, we also examined the TF sets associated with the regulation of these genes (Supplementary Fig S4D and Supplementary Table S10). Notably, NF-κB is a central regulator in RA and PsA, not only driving inflammation but also influencing Th1 responses, synovial fibroblast activation, and osteoclast-mediated bone resorption, with animal models supporting NF-κB inhibition as a therapeutic target [47]. It is also a key mediator in PsO, by driving both keratinocyte dysfunction and immune cell-mediated inflammation. Similarly, hypoxia-inducible factor-1 (HIF-1) is aberrantly expressed in RA and PsA joints [48]. In PsO, elevated HIF-1α in keratinocytes and serum promotes angiogenesis, keratinocyte hyperproliferation, and immune dysregulation [49]. Finally, enhanced nuclear localisation of C/EBPβ in synovial fibroblasts and macrophages from RA tissue, particularly within the synovial lining, suggests that its activation contributes to chronic inflammation and highlights C/EBPβ as a potential therapeutic target [50].

To further investigate disease-specific transcriptional signatures, we performed a pairwise comparison of RA, PsA, and PsO within the Classical Mono 1 cluster, identifying 50 DEGs with significant expression differences. Figure 4E presents a heatmap of z-score values for these DEGs (Supplementary Table S9.2), showing the average expression in each group (RA, PsA, PsO, in this order). Unlike previous analyses that compared HDs with disease groups, this analysis focuses on differences across the 3 diseases. The heatmap reveals that RA exhibits the most distinct expression profile, characterised by widespread downregulation. PsA shows a dual pattern: some clusters mirror the downregulation observed in RA, whereas others align more closely with the upregulation seen in PsO. PsO, in contrast, generally maintains upregulated expression for many genes that are downregulated in RA.

A principal component analysis (PCA) of the 50 DEGs from the Classical Mono 1 cluster revealed a distinct separation of RA samples, whereas PsO and PsA samples cluster together (Fig 4F), providing a clear visual representation of the expression patterns observed in the heatmap. In the corresponding PCAs for the remaining monocyte clusters (Classical Mono 2, Non-Classical 1, Non-Classical 2, and Intermediate) (Supplementary Fig S4E), the pattern mirrors that of Classical Mono 1, with RA separating distinctly from PsA and PsO. Notably, in the Intermediate cluster, RA samples are positioned closer to PsA and PsO, diverging from the separation pattern observed in other clusters.

We selected relevant genes from the Classical Mono 1 cluster that displayed expression patterns potentially explaining the behaviour of PsA in relation to RA or PsO (Fig 4G). Actin beta (*ACTB*), which encodes β-actin, a key cytoskeletal component, shows a PsA expression pattern more similar to RA. Its altered regulation may contribute to the actin rearrangements that drive synovial fibroblast activation in TNF-mediated arthritis, promoting proliferation, migration, and resistance to apoptosis [51]. Poly(rC)-binding protein 1 (*PCBP1*), a canonical RNA-binding protein and potential biomarker of RA, exhibits a PsA pattern closer to PsO and may contribute to disease development [52]. Polymorphisms in tumour necrosis factor alpha-induced protein 3 (TNFAIP3) are associated with increased susceptibility to IMIDs such as RA, PsA, and PsO, with the PsO risk haplotype being distinct from that of other IMIDs [53].

Finally, analysis of the Non-Classical Mono 1 cluster revealed that *IFITM3*, an interferon-inducible transmembrane protein, shows haplotype-specific associations with RA susceptibility and exhibits a similar expression pattern in PsA and PsO, while RA remains distinct, supporting a potential role for IFITM3 in RA pathogenesis (Supplementary Fig S4F) [54].

DISCUSSION

In this study, we studied the monocyte DNA methylome and transcriptome profiles from several related IMIDs—RA, PsA, and PsO—together with UA and HD, to investigate both shared and disease-specific molecular traits. Our analysis revealed that all groups share common alterations in the monocyte DNA methylomes. Most importantly, differences emerged between disease groups, particularly when we stratified by the DAS28 and BSA datasets. Of particular interest is the exploration of distinct hallmarks that set PsA apart from RA and PsO.

PsA remains an understudied IMID and is often misdiagnosed as seronegative RA or UA, or even as noninflammatory arthritis. Clinical evaluation relies not only on physical examination and

Mono 1 of the pairwise comparison from RA, PsA, and PsO. (G) Boxplots showing log-normalised expression of selected genes across RA, PsA, and PsO groups. ACTB, actin beta; BP, biological process; CEBPA, CCAAT/enhancer-binding protein alpha; DEG, differentially expressed gene; FDR, false discovery rate; GO, gene ontology; HD, healthy donor; HIF, hypoxia-inducible factor; IRF, interferon regulatory factor; KLF, Krüppel-like factor; logFC, log fold change; MHC, major histocompatibility complex; NF, nuclear factor; PCA, principal component analysis; PsA, psoriatic arthritis; PsO, psoriasis; PCBP1, poly(rC)-binding protein 1; RA, rheumatoid arthritis; scRNA-seq, single-cell RNA sequencing; STAT4, signal transducer and activator of transcription 4; TF, transcription factor; TNF, tumour necrosis factor; TNFAIP3, tumour necrosis factor alpha-induced protein 3; Treg, regulatory T cell; UMAP, uniform manifold approximation and project.

patient history but also on established classification criteria [55], which helps clinicians recognise the characteristic features unique to PsA. Several studies have also identified genetic risk factors specific to PsA, including amino acid variants within HLA-B and polymorphisms in the *IL23R* gene [56].

The IL-23/IL-17 axis plays a central role in PsA and PsO; however, gene expression patterns in PsA skin and synovium are clearly distinct. Skin displays a stronger IL-17 gene signature, whereas both tissues show comparable TNF and IFN-γ signatures. These findings align with clinical trial data demonstrating that IL-17 and IL-23 inhibitors yield better results in PsA skin than in PsA joints [57].

RA and PsA also display a substantial overlap, although there are ongoing efforts to delineate their differences. A clinical study identified several serum cytokines as markers for both diseases: PsA was associated with elevated levels of IL-1β, IL-6, IL-17, IL-22, IL-23, IFN-γ, and TNF-α, whereas RA showed elevated levels of IL-1, IL-6, IL-22, IL-33, TNF-α, chemokine ligand 11, and chemokine C-X-C motif ligand 13 [58].

Our DNA methylation and scRNA-seq analyses revealed consistent alterations in key TF families (Krüppel-like factors, signal transducer and activator of transcription proteins, IRFs, and CEBPs) and immune pathways in the HD vs all comparison. For instance, KLF2 was hypomethylated, while KLF2, KLF4, and KLF6 were downregulated, suggesting that these normally protective factors lose their anti-inflammatory function in disease. In contrast, genes such as KLF12 and STAT4 were upregulated, indicating potential proinflammatory roles. IRFs and CEBPs likewise showed coordinated changes across both molecular layers, pointing to enhanced interferon signalling, monocyte differentiation, and inflammatory cytokine regulation. At the pathway level, both datasets highlighted NF-κB activity, antigen presentation, cytokine responses, and T-cell activation, with MHC class II (HLA-DRB1) consistently implicated. Together, these findings suggest that the HD vs all comparison captures a shared inflammatory signature across RA, PsA, and PsO: downregulated or hypomethylated genes likely represent protective mechanisms lost in disease, while upregulated or hypermethylated genes reflect disease-promoting activity.

In the RA vs PsA vs PsO comparison, both analyses revealed that PsA shares molecular features with RA and PsO, often displaying a dual profile. Convergence was observed in pathways related to fibroblast function, MHC antigen presentation, and interferon signalling. In the methylation data, FGF12 and FGFR-related pathways were enriched, indicating dysregulation of fibroblast growth and signalling that may drive synovial tissue inflammation and remodelling. Consistently, scRNA-seq identified DEGs such as ACTB and PCBP1, which modulate cytoskeletal dynamics and gene expression in fibroblasts, supporting disease-specific fibroblast activation. For the MHC complex, methylation analysis showed hypomethylation of HLA-DRB1 and enrichment of MHC-related pathways, while scRNA-seq data revealed differential expression of antigen-processing and presentation genes across disease groups, reinforcing the role of MHC-mediated immune activation in RA, PsA, and PsO. Notably, several loci associated with DMPs identified in this study fall within genomic regions previously implicated by GWAS in RA, PsA, and PsO (eg, HLA-DRB1 and IL-23/IL-17-related pathways), supporting consistency between the epigenetic alterations observed here and known genetic susceptibility mechanisms. Finally, interferon-related pathways were highlighted in both datasets: methylation analyses showed enrichment for IRF family members, key regulators of type I interferon responses, and inflammatory signalling, while scRNA-seq confirmed altered interferon activity through differential expression of IFITM3, an interferon-inducible gene. An important question is whether the observed methylation changes reflect disease-specific regulatory programmes or differences in monocyte activation associated with disease activity. Correlation analyses with DAS28 and BSA indicate that part of the methylation variation relates to general inflammatory activation, as CpGs were enriched in pathways linked to interferon signalling, NF-κB responses, cytokine signalling, and inflammasome components. However, pairwise disease comparisons and integration with scRNA-seq data revealed disease-specific regulatory patterns and monocyte transcriptional programmes, with PsA displaying a dual profile bridging RA and PsO. Together, these findings suggest that monocyte methylation patterns reflect both shared activation-dependent inflammation and disease-specific regulatory alterations.

Our integrative analyses highlight the pivotal role of monocyte subsets in shaping disease-specific features across RA, PsA, and PsO. In RA, classical monocytes were linked to osteoclastogenic and joint-destructive programmes, whereas PsO-associated monocytes emphasised keratinocyte-driven inflammatory circuits. PsA exhibited a distinctive dual profile, with contributions from both classical and nonclassical subsets converging on fibroblast growth factor signalling, antigen presentation, and interferon-related pathways. This molecular duality may underlie PsA's heterogeneous clinical spectrum and persistent diagnostic ambiguity, reinforcing its identity as a true bridge disease. By delineating subset-specific epigenomic and transcriptional signatures, our work establishes a framework for refining disease classification and identifying therapeutic targets uniquely relevant to PsA. Although direct gene-level concordance between DMP-associated genes and DEGs was limited, both datasets showed consistent alterations in key TF families (KLF, STAT, IRF, CEBP) and immune pathways, indicating convergence at the regulatory network level rather than a simple CpG-gene relationship.

An important clinical challenge relates to the interception and prevention of PsA in patients with PsO, as PsA typically manifests several years after the onset of PsO. This delay has spurred efforts to identify biomarkers that could guide early therapeutic intervention, including timely use of biologics, before irreversible joint damage occurs. However, robust predictive markers for PsA development are currently lacking. Our data, which highlight dual hybrid monocyte epigenomic traits in PsA bridging RA and PsO, raise the possibility that such molecular signatures may help refine risk stratification in patients with PsO who are at increased risk of progression to PsA. Although our present study was not designed to address prediction directly, and patients with established PsA were analysed separately from PsO, the identification of PsA-specific pathways (eg, FGFR signalling, MHC class II-related loci, interferon-driven programmes) may provide a framework for future longitudinal studies aimed at defining epigenomic or transcriptomic biomarkers of PsA transition. Together, these findings highlight systemic monocyte epigenomic programmes that differentiate RA, PsA, and PsO while also revealing shared inflammatory mechanisms across these conditions.

An important consideration is that DNA methylation profiling was performed in circulating monocytes rather than in tissue-resident cells within inflamed synovium or psoriatic skin. Although this approach cannot fully capture tissue-specific epigenetic imprinting that may arise after monocyte infiltration and differentiation within local inflammatory niches, the study was designed to investigate systemic

immune programming across RA, PsA, and PsO using a clinically accessible compartment. Circulating monocytes therefore provide a valuable window into shared and disease-specific inflammatory pathways operating at the systemic level. Accordingly, the epigenetic signatures identified here should be interpreted as reflecting systemic monocyte states rather than tissue-specific regulatory programmes. Future studies integrating matched blood and tissue epigenomic profiling will help clarify how these systemic programmes relate to local inflammatory microenvironments.

CRediT authorship contribution statement

Cristina Gómez-Pereira: Writing – review & editing, Writing – original draft, Investigation, Formal analysis. **Anna Guiomar Ferreté-Bonastre:** Investigation, Formal analysis. **Ana Belén Azuaga:** Resources, Investigation. **Mónica Munera-Campos:** Resources, Investigation. **Celia Lourdes Calvillo:** Methodology, Formal analysis. **Julio Ramírez:** Resources, Investigation. **Octavio Morante-Palacios:** Resources, Investigation. **Carlos de la Calle-Fabregat:** Methodology, Investigation. **Laura Ciudad:** Investigation. **Eva Martínez-Cáceres:** Investigation. **Manel Esteller:** Investigation. **José Manuel Carrascosa:** Resources, Investigation, Funding acquisition. **Juan D Cañete:** Resources, Investigation, Funding acquisition, Conceptualization. **Esteban Ballestar:** Writing – review & editing, Writing – original draft, Supervision, Resources, Investigation, Funding acquisition, Conceptualization.

Acknowledgements

We thank the CERCA Programme/Generalitat de Catalunya and the Josep Carreras Foundation for institutional support. The authors thank all the patients who graciously donated their time and samples for arthritis and psoriasis research.

Funding

EB was funded by the Spanish Ministry of Science and Innovation (MICINN; grant numbers PID2020-117212RB-I00/AEI/10.13038/501100011033). JMC was funded by the European Academy of Dermatology and Venereology (grant number PPRC-2021-2) and Instituto de Salud Carlos III (FIS grant number PI21/01139). JDC was funded by the Innovative Medicines Initiative 2 Joint Undertaking (JU) under grant agreement no. 101007757 (HIPPOCRATES). The JU receives support from the European Union's Horizon 2020 research and innovation program and EFPI. The JU is not responsible for any use that may be made of the information it contains. ABA received a Kern grant from the Catalan Society of Rheumatology.

Competing interests

All authors declare they have no competing interests.

Patient consent for publication

Not applicable.

Ethics approval

The study was approved by the ethical committees of all institutions involved in this study. Participants gave informed consent to participate in the study before taking part.

Provenance and peer review

Not commissioned; externally peer reviewed.

Data availability statement

Methylation data for this publication have been deposited in NCBI's Gene Expression Omnibus and are accessible through GEO accession number GSE326371.

Declaration of generative AI and AI-assisted technologies in the writing process

During the preparation of this work, the authors used ChatGPT in order to revise grammar. After using this tool, the authors reviewed and edited the content as needed and take full responsibility for the content of the publication.

Patient and public involvement

Patients and/or the public were not involved in the design, or conduct, or reporting, or dissemination plans of this research.

Supplementary materials

Supplementary material associated with this article can be found, in the online version, at doi:10.1016/j.ard.2026.03.018.

Orcid

Mónica Munera-Campos: http://orcid.org/0000-0002-2227-2993
Juan D Cañete: http://orcid.org/0000-0003-2606-0573
Esteban Ballestar: http://orcid.org/0000-0002-1400-2440

REFERENCES

[1] Zhang F, Jonsson AH, Nathan A, Millard N, Curtis M, Xiao Q, et al. Deconstruction of rheumatoid arthritis synovium defines inflammatory subtypes. Nature 2023;623:616–24. doi: 10.1038/S41586-023-06708-Y.
[2] Shi Z, Liu Z, Wei Y, Zhang R, Deng Y, Li D. The role of dermal fibroblasts in autoimmune skin diseases. Front Immunol 2024;15:1379490. doi: 10.3389/FIMMU.2024.1379490.
[3] Armstrong AW, Blauvelt A, Callis Duffin K, Huang YH, Savage LJ, Guo L, et al. Psoriasis. Nat Rev Dis Primers 2025;11:45. doi: 10.1038/S41572-025-00630-5.
[4] Saalfeld W, Mixon AM, Zelie J, Lydon EJ. Differentiating psoriatic arthritis from osteoarthritis and rheumatoid arthritis: a narrative review and guide for advanced practice providers. Rheumatol Ther 2021;8:1493–517. doi: 10.1007/S40744-021-00365-1.
[5] Torres A, Pedersen B, Guma M. Solute carrier nutrient transporters in rheumatoid arthritis fibroblast-like synoviocytes. Front Immunol 2022;13:984408. doi: 10.3389/FIMMU.2022.984408.
[6] Wu B, He Y, Yang D, Liu RX. Identification of hub genes and therapeutic drugs in rheumatoid arthritis patients. Clin Rheumatol 2021;40:3299–309. doi: 10.1007/S10067-021-05650-6.
[7] Du J, Zheng L, Chen S, Wang N, Pu X, Yu D, et al. NFIL3 and its immunoregulatory role in rheumatoid arthritis patients. Front Immunol 2022;13:950144. doi: 10.3389/FIMMU.2022.950144.
[8] Wedel A, Ziegler-Heitbrock HW. The C/EBP family of transcription factors. Immunobiology 1995;193:171–85. doi: 10.1016/S0171-2985(11)80541-3.
[9] Salem S, Salem D, Gros P. Role of IRF8 in immune cells functions, protection against infections, and susceptibility to inflammatory diseases. Hum Genet 2020;139:707–21. doi: 10.1007/S00439-020-02154-2.
[10] Tait Wojno ED, Hunter CA, Stumhofer JS. The immunobiology of the interleukin-12 family: room for discovery. Immunity 2019;50:851–70. doi: 10.1016/j.immuni.2019.03.011.

[11] Meyer A, Parmar PJ, Shahrara S. Significance of IL-7 and IL-7R in RA and autoimmunity. Autoimmun Rev 2022;21:103120. doi: 10.1016/j.autrev.2022.103120.
[12] Kozanidou VI, Theocharis AD, Georgiadis A, Voulgari PV, Drosos AA, Karamanos NK. Signal transduction by IL-2 and its receptors as target in treatment of rheumatoid arthritis. Curr Drug Targets Immune Endocr Metabol Disord 2005;5:41–50. doi: 10.2174/1568008053174741.
[13] Das M, Lu J, Joseph M, Aggarwal R, Kanji S, McMichael BK, et al. Kruppel-like factor 2 (KLF2) regulates monocyte differentiation and functions in mBSA and IL-1β-induced arthritis. Curr Mol Med 2012;12:113–25. doi: 10.2174/156652412798889090.
[14] Jha P, Das H. KLF2 in regulation of NF-κB-mediated immune cell function and inflammation. Int J Mol Sci 2017;18:2383. doi: 10.3390/IJMS18112383.
[15] Moon JS, Ho CC, Park JH, Park K, Shin BY, Lee SH, et al. Lrig1-expression confers suppressive function to CD4+ cells and is essential for averting autoimmunity via the Smad2/3/Foxp3 axis. Nat Commun 2023;14:5382. doi: 10.1038/S41467-023-40986-4.
[16] Harten SK, Oey H, Bourke LM, Bharti V, Isbel L, Daxinger L, et al. The recently identified modifier of murine metastable epialleles, rearranged L-Myc Fusion, is involved in maintaining epigenetic marks at CpG island shores and enhancers. BMC Biol 2015;13:21. doi: 10.1186/S12915-015-0128-2.
[17] Zong W, Ge Y, Han Y, Yang X, Li Q, Chen M. Hypomethylation of HLA-DRB1 and its clinical significance in psoriasis. Oncotarget 2017;8:12323–32. doi: 10.18632/ONCOTARGET.12468.
[18] Tian G, Barragan GA, Yu H, Martinez-Amador C, Adaikkalavan A, Rios X, et al. PRDM1 Is a key regulator of the NKT-cell central memory program and effector function. Cancer Immunol Res 2025;13:577–90. doi: 10.1158/2326-6066.CIR-24-0259.
[19] Balendran T, Lim K, Hamilton JA, Achuthan AA. Targeting transcription factors for therapeutic benefit in rheumatoid arthritis. Front Immunol 2023;14:1196931. doi: 10.3389/FIMMU.2023.1196931.
[20] Kim I, Kim JH, Kim K, Seong S, Lee KB, Kim N. IRF2 enhances RANKL-induced osteoclast differentiation via regulating NF-κB/NFATc1 signaling. BMB Rep 2021;54:482–7. doi: 10.5483/BMBREP.2021.54.9.070.
[21] Yogesha SD, Khapli SM, Srivastava RK, Mangashetti LS, Pote ST, Mishra GC, et al. IL-3 inhibits TNF-alpha-induced bone resorption and prevents inflammatory arthritis. J Immunol 2009;182:361–70. doi: 10.4049/JIMMUNOL.182.1.361.
[22] Juneblad K, Kastbom A, Johansson L, Rantapää-Dahlqvist S, Söderkvist P, Alenius GM. Association between inflammasome-related polymorphisms and psoriatic arthritis. Scand J Rheumatol 2021;50:206–12. doi: 10.1080/03009742.2020.1834611.
[23] Wang T, Zhu CL, Wang S, Mo LW, Yang GD, Hu J, et al. Role of NLRP3 and NLRP1 inflammasomes signaling pathways in pathogenesis of rheumatoid arthritis. Asian Pac J Trop Med 2014;7:827–31. doi: 10.1016/S1995-7645(14)60145-0.
[24] Xue C, Yao Q, Gu X, Shi Q, Yuan X, Chu Q, et al. Evolving cognition of the JAK-STAT signaling pathway: autoimmune disorders and cancer. Signal Transduct Target Ther 2023;8:204. doi: 10.1038/S41392-023-01468-7.
[25] Salvador G, Sanmarti R, Garcia-Peiró A, Rodríguez-Cros JR, Muñoz-Gómez J, Cañete JD. p53 expression in rheumatoid and psoriatic arthritis synovial tissue and association with joint damage. Ann Rheum Dis 2005;64:183–7. doi: 10.1136/ard.2004.024430.
[26] Vecellio M, Hake VX, Davidson C, Carena MC, Wordsworth BP, Selmi C. The IL-17/IL-23 axis and its genetic contribution to psoriatic arthritis. Front Immunol 2021;11:596086. doi: 10.3389/FIMMU.2020.596086.
[27] Sen M. Wnt signalling in rheumatoid arthritis. Rheumatology (Oxford) 2005;44:708–13. doi: 10.1093/RHEUMATOLOGY/KEH553.
[28] Hidaka T, Kitani A, Hara M, Harigai M, Suzuki K, Kawaguchi Y, et al. IL-4 down-regulates the surface expression of CD5 on B cells and inhibits spontaneous immunoglobulin and IgM-rheumatoid factor production in patients with rheumatoid arthritis. Clin Exp Immunol 1992;89:223–9. doi: 10.1111/J.1365-2249.1992.TB06936.X.
[29] Jenks JA, Seki S, Kanai T, Huang J, Morgan AA, Scalco RC, et al. Differentiating the roles of STAT5B and STAT5A in human CD4+ T cells. Clin Immunol 2013;148:227–36. doi: 10.1016/j.clim.2013.04.014.
[30] Kim SJ, Chang HJ, Volin MV, Umar S, Van Raemdonck K, Chevalier A, et al. Macrophages are the primary effector cells in IL-7-induced arthritis. Cell Mol Immunol 2020;17:728–40. doi: 10.1038/S41423-019-0235-Z.
[31] Swindell WR, Xing X, Stuart PE, Chen CS, Aphale A, Nair RP, et al. Heterogeneity of inflammatory and cytokine networks in chronic plaque psoriasis. PLoS One 2012;7:e34594. doi: 10.1371/JOURNAL.PONE.0034594.
[32] Iwaszko M, Biały S, Bogunia-Kubik K. Significance of interleukin (IL)-4 and IL-13 in inflammatory arthritis. Cells 2021;10:3000. doi: 10.3390/CELLS10113000.
[33] Liu J, Kumar S, Hong J, Huang ZM, Paez D, Castillo M, et al. Combined single cell transcriptome and surface epitope profiling identifies potential biomarkers of psoriatic arthritis and facilitates diagnosis via machine learning. Front Immunol 2022;13:835760. doi: 10.3389/FIMMU.2022.835760.
[34] Wu X, Liu Y, Jin S, Wang M, Jiao Y, Yang B, et al. Single-cell sequencing of immune cells from anticitrullinated peptide antibody positive and negative rheumatoid arthritis. Nat Commun 2021;12:4977. doi: 10.1038/S41467-021-25246-7.
[35] Kim KJ, Park S, Park YH, Ku SH, Cho EB, Park EJ, et al. The expression and role of Krüppel-like factor 4 in psoriasis. Ann Dermatol 2014;26:675–80. doi: 10.5021/AD.2014.26.6.675.
[36] Bresnihan B, Pontifex E, Thurlings RM, Vinkenoog M, El-Gabalawy H, Fearon U, et al. Synovial tissue sublining CD68 expression is a biomarker of therapeutic response in rheumatoid arthritis clinical trials: consistency across centers. J Rheumatol 2009;36:1800–2. doi: 10.3899/JRHEUM.090348.
[37] Remmers EF, Plenge RM, Lee AT, Graham RR, Hom G, Behrens TW, et al. STAT4 and the risk of rheumatoid arthritis and systemic lupus erythematosus. N Engl J Med 2007;357:977–86. doi: 10.1056/NEJMOA073003.
[38] Julià A, Ballina J, Cañete JD, Balsa A, Tornero-Molina J, Naranjo A, et al. Genome-wide association study of rheumatoid arthritis in the Spanish population: KLF12 as a risk locus for rheumatoid arthritis susceptibility. Arthritis Rheum 2008;58:2275–86. doi: 10.1002/ART.23623.
[39] Tao K, Tang X, Wang B, Li RJ, Zhang BQ, Lin JH, et al. Distinct expression of chemokine-like factor 1 in synovium of osteoarthritis, rheumatoid arthritis and ankylosing spondylitis. J Huazhong Univ Sci Technolog Med Sci 2016;36:70–6. doi: 10.1007/S11596-016-1544-4.
[40] Teruel M, McKinney C, Balsa A, Pascual-Salcedo D, Rodriguez-Rodriguez L, Ortiz AM, et al. Association of CD247 polymorphisms with rheumatoid arthritis: a replication study and a meta-analysis. PLoS One 2013;8:e68295. doi: 10.1371/JOURNAL.PONE.0068295.
[41] Ge C, Weisse S, Xu B, Dobritzsch D, Viljanen J, Kihlberg J, et al. Key interactions in the trimolecular complex consisting of the rheumatoid arthritis-associated DRB1*04:01 molecule, the major glycosylated collagen II peptide and the T-cell receptor. Ann Rheum Dis 2022;81:480–9. doi: 10.1136/annrheumdis-2021-220500.
[42] Sun L, Liu W, Zhang LJ. The role of toll-like receptors in skin host defense, psoriasis, and atopic dermatitis. J Immunol Res 2019;2019:1824624. doi: 10.1155/2019/1824624.
[43] Guan Y, Li X, Yang H, Xu S, Shi L, Liu Y, et al. Role and mechanism of IRF9 in promoting the progression of rheumatoid arthritis by regulating macrophage polarization via PSMA5. Heliyon 2024;10:e35589. doi: 10.1016/j.heliyon.2024.e35589.
[44] Duffau P, Menn-Josephy H, Cuda CM, Dominguez S, Aprahamian TR, Watkins AA, et al. Promotion of inflammatory arthritis by interferon regulatory factor 5 in a mouse model. Arthritis Rheumatol 2015;67:3146–57. doi: 10.1002/ART.39321.
[45] Markway BD, Cho H, Zilberman-Rudenko J, Holden P, McAlinden A, Johnstone B. Hypoxia-inducible factor 3-alpha expression is associated with the stable chondrocyte phenotype. J Orthop Res 2015;33:1561–70. doi: 10.1002/JOR.22930.
[46] Jones J, Chen Y, Tiwari M, Li J, Ling J, Sen GL. KLF3 mediates epidermal differentiation through the epigenomic writer CBP. iScience. 2020;23:101320. doi:10.1016/j.isci.2020.101320
[47] Makarov SS. NF-kappa B in rheumatoid arthritis: a pivotal regulator of inflammation, hyperplasia, and tissue destruction. Arthritis Res 2001;3:200–6. doi: 10.1186/AR300.
[48] Li H, Wu QY, Teng XH, Li ZP, Zhu MT, Gu CJ, et al. The pathogenesis and regulatory role of HIF-1 in rheumatoid arthritis. Cent Eur J Immunol 2023;48:338–45. doi: 10.5114/CEJI.2023.134217.
[49] Zhu WJ, Li P, Wang L, Xu YC. Hypoxia-inducible factor-1: a potential pharmacological target to manage psoriasis. Int Immunopharmacol 2020;86:106689. doi: 10.1016/j.intimp.2020.106689.
[50] Pope RM, Lovis R, Mungre S, Perlman H, Koch AE. Haines GK 3rd. C/EBPβ in rheumatoid arthritis: correlation with inflammation, not disease specificity. Clin Immunol 1999;91:271–82. doi: 10.1006/clim.1999.4723.
[51] Vasilopoulos Y, Gkretsi V, Armaka M, Aidinis V, Kollias G. Actin cytoskeleton dynamics linked to synovial fibroblast activation as a novel pathogenic principle in TNF-driven arthritis. Ann Rheum Dis 2007;66:iii23–8. doi: 10.1136/ard.2007.079822.
[52] Cao X, Li P, Song X, Shi L, Qin L, Chen D, et al. PCBP1 is associated with rheumatoid arthritis by affecting RNA products of genes involved in immune response in Th1 cells. Sci Rep 2022;12:8398. doi: 10.1038/S41598-022-12594-7.
[53] Nititham J, Taylor KE, Gupta R, Chen H, Ahn R, Liu J, et al. Meta-analysis of the TNFAIP3 region in psoriasis reveals a risk haplotype that is distinct from other autoimmune diseases. Genes Immun 2015;16:120–6. doi: 10.1038/GENE.2014.75.

[54] Lee SY, Yu JI, Chae SC. Associations of ifitm3 haplotypes with rheumatoid arthritis in a Korean population. Genes Genom 2012;34:493–8. doi: 10.1007/s13258-011-0241-8.
[55] Taylor W, Gladman D, Helliwell P, Marchesoni A, Mease P, Mielants H, et al. Classification criteria for psoriatic arthritis: development of new criteria from a large international study. Arthritis Rheum 2006;54:2665–73. doi: 10.1002/ART.21972.
[56] Soomro M, Stadler M, Dand N, Bluett J, Jadon D, Jalali-Najafabadi F, et al. Comparative genetic analysis of psoriatic arthritis and psoriasis for the discovery of genetic risk factors and risk prediction modeling. Arthritis Rheumatol 2022;74:1535–43. doi: 10.1002/ART.42154.
[57] Belasco J, Louie JS, Gulati N, Wei N, Nograles K, Fuentes-Duculan J, et al. Comparative genomic profiling of synovium versus skin lesions in psoriatic arthritis. Arthritis Rheumatol 2015;67:934–44. doi: 10.1002/ART.38995.
[58] Merola JF, Espinoza LR, Fleischmann R. Distinguishing rheumatoid arthritis from psoriatic arthritis. RMD Open 2018;4:e000656. doi: 10.1136/RMDOPEN-2018-000656.

Ann Rheum Dis 85 (2026) 1477–1485

Contents lists available at ScienceDirect

Annals of the Rheumatic Diseases

journal homepage: https://www.sciencedirect.com/journal/annals-of-the-rheumatic-diseases

Inflammatory arthritis

Intra-articular injection of autologous tolerogenic dendritic cells modifies the synovial immune landscape in rheumatoid and inflammatory arthritis

Ioana Nicorescu[1], Amanda Thomson[1,2], George Merces[3,4], Jack F. Harrison[1,5], Ben Barron-Millar[1], Arthur G. Pratt[1,5,6], Amy E. Anderson[1,5,6], Julie Diboll[1,5,6], Kenneth S. Rankin[1], Domenico Somma[6,7], Mariola Kurowska-Stolarska[6,7], Luke J. Jones[6,8], Andrew Filer[6,8,9,10], David McDonald[2,3], Andrew Filby[2,3], John D. Isaacs[1,5,6], Catharien M.U. Hilkens[1,5,6,*]

[1] *Translational and Clinical Research Institute, Faculty of Medical Sciences, Newcastle University, Newcastle upon Tyne, UK*
[2] *Flow Cytometry Core Facility, Faculty of Medical Sciences, Newcastle University, Newcastle upon Tyne, UK*
[3] *Biosciences Institute, Innovation, Methodology and Application (IMA) Research Theme, Faculty of Medical Sciences, Newcastle University, Newcastle upon Tyne, UK*
[4] *Image Analysis Unit, Faculty of Medical Sciences, Newcastle University, Newcastle upon Tyne, UK*
[5] *National Institute for Health Research (NIHR) Newcastle Biomedical Research Centre and NIHR Clinical Research Facility, Newcastle upon Tyne NHS Foundation Trust, Newcastle upon Tyne, UK*
[6] *Research into Inflammatory Arthritis Centre Versus Arthritis (RACE), UK*
[7] *School of Infection and Immunity, University of Glasgow, Glasgow, UK*
[8] *National Institute for Health Research (NIHR) Birmingham Biomedical Research Centre and NIHR Clinical Research Facility, University Hospitals Birmingham NHS Foundation Trust, Birmingham, UK*
[9] *Rheumatology Research Group, School of Infection, Inflammation and Immunology, University of Birmingham, Birmingham, UK*
[10] *Birmingham Tissue Analytics, Institute of Translational Medicine, University of Birmingham, Birmingham, UK*

ARTICLE INFO

Article history:
Received 13 February 2025
Received in revised form 11 December 2025
Accepted 5 January 2026

ABSTRACT

Objectives: In our previously reported trial of intra-articular tolerogenic dendritic cells (tolDC) as a treatment to restore immune tolerance in autoimmune arthritis, high doses of cells appeared to stabilise knee symptoms, although no systemic clinical or immunomodulatory effects were observed. We therefore sought to understand how tolDC affected the local synovial immune landscape.

Methods: Synovial biopsies were taken at baseline and 14 days after intra-articular injection of tolDC or, as a control, saline washout. Histopathological analyses (Krenn evaluation and pathotype) and multiparametric imaging mass cytometry (IMC) were performed on paired synovial tissues from 7 participants (5 tolDC-treated and 2 controls), selected based on tissue availability at both time points. The IMC panel included 27 antibodies defining lymphoid, myeloid, and stromal cells.

Results: We observed no changes in the histopathology or the overall distribution of broadly classified cell populations (myeloid, lymphoid, and stromal) before and after tolDC administration.

*Correspondence to Professor Catharien M U Hilkens.
E-mail address: catharien.hilkens@newcastle.ac.uk (C.M.U. Hilkens).

Handling editor Josef S. Smolen.

Ioana Nicorescu and Amanda Thomson contributed equally.

https://doi.org/10.1016/j.ard.2026.01.004

Furthermore, the proportions of $CD4^+$ and $CD8^+$ T cells were not altered, with no indication that tolDC had induced regulatory T cells within the synovium. However, we found a significant increase in a subset of myeloid cells expressing high levels of the inflammation resolution marker Mer tyrosine kinase ($MerTK^{High}$), which positively correlated with tolDC dose. Moreover, the percentages of total $MerTK^+$ myeloid cells inversely correlated with arthroscopic synovitis scores at both time points.

Conclusions: The tolDC-induced increase in synovial Myeloid $MerTK^{High}$ cells may have local immune modulatory effects and provide promising evidence for an effect of tolDC treatment on the synovial immune landscape.

WHAT IS ALREADY KNOWN ON THIS TOPIC

- In our phase I safety study of intra-articular tolerogenic dendritic cell (tolDC) therapy for autoimmune arthritis, no changes were documented in the overall disease activity of systemic immunological parameters. However, there was a trend for improved knee symptoms in those receiving the highest dose. A follow-on study with ^{111}Indium-labelled tolDC showed that these cells remain in the joint, possibly explaining the local rather than systemic effects of this cell therapy.

WHAT THIS STUDY ADDS

- Utilising high-parameter mass cytometry imaging on synovial biopsies taken before and 14 days after tolDC therapy, we show a tolDC dose-dependent increase in a subset of myeloid cells that express high levels of the inflammation resolution marker Mer tyrosine kinase (MerTK). Furthermore, we show that the number of $MerTK^+$ myeloid cells inversely correlates with the arthroscopic synovitis score.

HOW THIS STUDY MIGHT AFFECT RESEARCH, PRACTICE OR POLICY

- Our study underlines the importance of defining changes in the immune landscape both locally and systemically to provide a better understanding of how advanced therapies, such as tolerogenic cell therapies, exert their immunomodulatory effects. The study also gives further credence to $MerTK^+$ myeloid cells playing a role in the resolution of synovial inflammation.

INTRODUCTION

The last 2 decades have seen major improvements in the clinical management of rheumatoid arthritis (RA), with earlier diagnosis and advancements in disease-modifying antirheumatic drugs leading to milder disease courses [1]. Despite remission being an achievable state, current treatments do not robustly reinstate immune tolerance, and patients often flare after treatment cessation. Thus, novel treatments that aim to restore immune tolerance are currently under development, including tolerogenic dendritic cell (tolDC) therapy, classified as an advanced therapy investigational medicinal product (ATIMP). Pathfinder trials have proved the safety of tolDC therapies for RA and other autoimmune diseases, such as type 1 diabetes, Crohn's disease, and multiple sclerosis [2–10]. tolDCs are thought to exert their immunoregulatory actions mainly through the modulation of T cells, eg, by inducing anti-inflammatory cytokine profiles and the promotion of regulatory T cells [11–20]. We have confirmed the feasibility and safety of tolDC intra-articular injection in the inflamed knee of patients with autoimmune arthritis, in the Autologous Tolerogenic Dendritic Cells for Rheumatoid and Inflammatory Arthritis (AuToDeCRA) phase I safety trial [10]. Although there was a trend for sustained resolution of synovitis in patients receiving the highest dose of tolDC (10 million cells), we could not detect any changes in systemic immunological parameters or overall disease activity. A follow-on study with ^{111}Indium-labelled tolDC injected intra-articularly showed that these cells remain in the joint, possibly explaining the local rather than systemic effects of this cell therapy [21]. Ongoing efficacy trials by our and other groups are now addressing optimal tolDC dosage and route of administration ([17,22] and trial ISRCTN14999554). As a consequence, the immunoregulatory mechanisms exerted by tolDC after *in vivo* administration are a critical area for investigation—monitoring changes in local and systemic immune biomarkers, including local tissue changes at the site of disease, will provide the most robust evidence for efficacy [23]. The recent development of spatial technologies and improvements in analysis pipelines have increased the understanding of cellular landscapes and interactions in health and disease. In this study, we used imaging mass cytometry (IMC) to evaluate the cellular synovial landscape following tolDC treatment.

METHODS

Participants, synovial biopsies, and histopathology

This study forms part of the AuToDeCRA clinical trial (NCT01352858 and [10]), which included a total of 13 participants (10 receiving tolDC and 3 controls). The trial protocol was approved by the Medicines and Healthcare products Regulatory Agency and by the National Research Ethics Committee North East (Sunderland) (EudraCT number: 2011-001582-41). The trial was conducted according to the International Council for Harmonisation of Technical Requirements for Pharmaceuticals for Human Use Good Clinical Practice and the Declaration of Helsinki. Participant inclusion and exclusion criteria are detailed in the original study [10]. Briefly, participants had inflammatory arthritis, including an inflamed knee joint with an effusion. tolDC treatment was added to stable disease-modifying anti-rheumatic drug therapies, and glucocorticoid injections were not permitted for at least 6 weeks prior to baseline. The study started in February 2012 with the first participant receiving tolDC treatment in July 2012 and the last participant being treated in May 2014; clinical follow-up of participants was 3 months. Autologous tolDC, loaded with autologous synovial fluid as the source of autoantigen, were administered via intra-articular injection into an inflamed knee joint, following saline washout. Participants received a single injection of 1×10^6, 3×10^6, or 10×10^6 viable tolDC; control participants received a joint washout with saline but were not treated with tolDC. Synovial biopsies were obtained via arthroscopic examination, before tolDC injection (baseline) and 14 days after (day 14), and further processed for formalin fixation and paraffin embedding (FFPE) preservation. FFPE blocks were stored at room temperature in a low-humidity environment and away from direct light.

Haematoxylin and eosin (H&E) staining was carried out by the National Health Service (NHS) histopathology service, and images of slides were archived. Histopathological analysis was performed according to the Krenn grading system and the pathotype scoring method previously described [24–26]. Of the 13 trial participants, 7 had good quality synovial tissue samples (5 tolDC-treated, 2 controls) available at both time points and were therefore included in the IMC analysis. These samples were distributed across all 4 treatment groups. Patient demographics of AuToDeCRA participants included in the IMC study are shown in Supplementary Table S1.

IMC

A panel of 27 markers was designed to investigate the cellular diversity of the synovial tissue environment, and to include major lineage subsets, such as myeloid, lymphoid, and stromal cells. All antibodies were optimised individually by standard immunofluorescence microscopy, using 4-μm-thick FFPE tonsil and synovium sections (data not shown). Validated antibodies were conjugated to lanthanide metals using MaxPar Conjugation kits (Standard BioTools), according to the manufacturer's instructions. Final IMC panel details can be found in Supplementary Table S2. Freshly sliced 4-μm-thick FFPE synovium sections were dewaxed in xylene and rehydrated through graded alcohols (100%, 90%, 70%, 50%). Antigen retrieval was performed for 20 minutes in a microwavable pressure cooker pot with Tris-EDTA, at pH 9. Nonspecific binding was blocked with 3% bovine serum albumin, followed by an overnight incubation with the IMC antibody panel, as well as iridium to identify nuclei. Selected regions of interest (ROIs) ranging between 0.2 and 1 mm^2 were ablated on the Hyperion imaging mass cytometer. One slide was prepared per patient, containing the paired baseline and day 14 synovial tissues. A maximum of 2 ROIs were selected per tissue sample. ROI selection was performed by a single trained operator for each slide to ensure consistency in the selection process. Ablation energy was set at 2 dB with a laser frequency of 200 Hz. Signal of pulverised tissue containing the spatial coordinates of each antibody was used to generate single-channel images, which were exported as MCD files.

IMC data analysis

Data analysis was performed according to the OPTimised Imaging Mass cytometry AnaLysis (OPTIMAL) framework [27], a method for IMC analysis developed on tonsil tissue, with a 27-marker panel and also used successfully to analyse the cellular landscape of postmortem COVID-19 lung biopsies [28]. Files in MCD format were exported as multichannel 16-bit TIFF images for each ROI and processed for segmentation and transformation into single-cell data. Information on the number of ROIs, cell counts, and total imaged area are provided in Supplementary Table S3. Segmentation was carried out with CXCR3 as a membrane marker, and Iridium-193 signal for nuclei detection, following processing using a custom Ilastik model to enhance the separation of nuclei in dense regions. Single-cell converted data were arcsin (co-factor of 1) and Z-scale transformed. Single-cell data from each ROI were converted into individual FCS files, which were further analysed in FCSExpress (DeNovo Software). A total of 75,934 events (single cells) were subject to FlowSOM clustering, in combination with the pairwise controlled manifold approximation projection (PACMAP) dimensionality reduction approach, to project clusters in reduced dimensions for phenotypic exploration. Clusters representing the cell subsets in the synovium were annotated based on marker expression and merged based on similarity. As an additional quality control step, a plot with centroid x on the x-axis and centroid y on the y-axis (location of each cell in the tissue slide) was generated. Each cluster was highlighted on the ROI, and the raw IMC signal from the strongest marker was viewed to confirm whether the annotated clusters matched the marker expression at the same location on the tissue. The relative percentages of clusters were calculated based on the total number of cells within each ROI. A Wilcoxon matched-pairs signed rank test was used to test differences in cell abundance between time points. Pearson tests were performed to measure linear correlations between variables. Statistical significance was calculated in Graphpad Prism. Spatial analysis was carried out as elaborated in the OPTIMAL framework, to create interaction heatmaps [27]. A disk pixel expansion was performed using an expansion of 5 pixels to identify the area for cellular neighbourhood analysis. Next, a Monte Carlo simulation was applied to generate cellular interaction heatmaps and to compare defined cellular organisation to randomised alternatives.

RESULTS

tolDC treatment does not change the synovial tissue histopathological score

We previously reported that intra-articular injection with autologous tolDC did not lead to detectable changes in systemic clinical or immunomodulatory parameters [10]. However, clinical arthroscopic assessment before biopsy collection (synovitis, hypertrophy, vascularity) at day 14 had shown a reduced synovitis score in 2 participants who had received 10×10^6 tolDC, and a third participant treated with the same tolDC dose declined arthroscopy due to improvement of symptoms. We therefore addressed the question of whether tolDC treatment had changed the immune landscape locally, within the synovial tissues of the injected knee joints. We first performed histopathological analyses of archived H&E images of synovial tissue biopsies taken at baseline and day 14 of the tolDC trial. Overall, we found no consistent differences in the Krenn scores or pathotypes before and after tolDC administration (Table), with immune cell infiltrates remaining present within the 14-day period after tolDC injection. However, these data provide no information on the identity and functional status of synovial immune cells.

tolDC administration does not modify global synovial tissue cell type composition at the 14-day time point

To investigate whether tolDC treatment affected synovial cell composition, we performed IMC on 7 paired (baseline and day 14) synovial samples, including samples from all treatment groups (Table). Following cell segmentation and single-cell transformation (Fig 1A-D), 75,934 cells underwent dimensionality reduction and cluster annotation. We identified 14 clusters in 51,382 events, with main synovial cell clusters including stromal, lymphoid and myeloid. The remaining events were annotated as unclassified due to insufficient expression of markers included in the panel. Figure 1E,F shows the PACMAP projection representing all annotated clusters, as well as the heatmap with Z-score marker values for each individual cluster. The majority of the annotated clusters were of myeloid lineage in all treatment groups (Fig 1G). Global percentages of cells classified as myeloid did not change significantly between baseline and day 14 within individual paired biopsies. Percentages of lymphocytes ($CD4^+$ T cells, $CD8^+$ T cells and B cells; Fig 1H), and

Table
Histopathological analysis of AuToDeCRA participants included in the IMC study

Participant no.	tolDC treatment	Arthroscopic synovitis (baseline)	Arthroscopic synovitis (day 14)	Krenn baseline	Krenn day 14	Pathotype baseline	Pathotype day 14
3	1×10^6	3[a]	3	High-grade synovitis	High-grade synovitis	Lymphoid	Lymphoid
5	3×10^6	2	3	High-grade synovitis	High-grade synovitis	Lymphoid	Lymphoid
6	Untreated[b]	2	2	No synovitis	Low-grade synovitis	Pauci-immune	Lymphoid
7	3×10^6	4	3	Low-grade synovitis	No synovitis	Diffuse	Pauci-immune
9	3×10^6	1	2	High-grade synovitis	High-grade synovitis	Lymphoid	Lymphoid
11	Untreated	3	3	Low-grade synovitis	Low-grade synovitis	Pauci-immune	Pauci-immune
12	10×10^6	3	1	High-grade synovitis	High-grade synovitis	Pauci-immune	Diffuse

AuToDeCRA, Autologous Tolerogenic Dendritic Cells for Rheumatoid and Inflammatory Arthritis; IMC, imaging mass cytometry; tolDC, tolerogenic dendritic cell. Arthroscopic synovitis was assessed on a 5-point scale (0-4, with 0 representing no synovial activity and 4 representing maximum synovial activity).
[a] Arthroscopic synovitis score was completed during the arthroscopic procedure before the collection of the synovial biopsy.
[b] Untreated: participants receiving a joint washout only.

nonimmune cells (stromal, endothelial, and CXCR3$^+$ cells; Fig 1I) varied across biopsies, but no discernible pattern emerged in terms of how tolDC treatment affected the presence of these broadly classified cell types.

MerTK$^+$ myeloid cell phenotype is increased at day 14 and inversely correlates with arthroscopic synovitis

We next investigated whether specific phenotypes (clusters) within the major cell subsets (myeloid, lymphoid, and stromal) were affected by tolDC treatment. Percentages of annotated clusters were compared between the 2 time points for all individual donors. No significant changes in activated CD4$^+$, CD4$^+$, or CD8$^+$ T cell percentages were detected between baseline and day 14 (Fig 2A-C). A significant decrease in podoplanin$^+$ fibroblasts and in a myeloid population positive for CCR2 (myeloid CCR2$^+$) was consistently observed at day 14 for all treatment groups, including the 2 participants who had received a washout only (Fig 2D,E), suggesting the effect may have been due to the joint irrigation procedure. The variations in percentage for the other annotated cell clusters are detailed in the Supplemental material (Supplementary Fig S1).

Because Mer tyrosine kinase (MerTK)-expressing synovial macrophages have been shown to be associated with remission in RA [29], we included this marker in the IMC panel. The proportion of overall MerTK-positive myeloid cells did not significantly change from baseline to day 14 (data not shown). However, we identified a significant increase in a cluster of myeloid cells expressing high levels of MerTK (Myeloid MerTK^{High}) at day 14 in the 2 higher dose groups (3×10^6 and 10×10^6 tolDC), with the highest increase observed in participant 12, treated with 10×10^6 tolDC (Fig 2F). Interestingly, percentages of all MerTK$^+$ myeloid cells (including MerTK^{High} and MerTK^{Low}) inversely correlated with the arthroscopic synovitis score (Fig 2G). Similarly, ratios of Myeloid MerTK^{High} to Myeloid MerTK^{Low} percentages were significantly higher at day 14, and this 'shift' from MerTK^{Low} to MerTK^{High} expressing myeloid cells was more prominent at the higher tolDC doses (Fig 2H), suggesting the possibility that the observed shift in MerTK expression was not due to joint irrigation per se. Furthermore, the difference (Δ) in MerTK^{High} normalised absolute numbers, between day 14 and baseline, positively correlated with the tolDC dose (Fig 2I).

We next looked at the spatial distribution of MerTK-expressing myeloid cells within the synovium, as this may provide further insight into how these cells act. By plotting the annotated clusters on a centroid x and y graph (as in Fig 1D), we observed that localisation of myeloid cells expressing MerTK was varied (Supplementary Fig S2). In some biopsies, these cells were found nearby potential lymphatic vessels, as evidenced by colocalisation of MerTK with lymphatic vessel endothelial hyaluronan receptor 1 (LYVE-1; raw signal, Supplementary Fig S2A), while other biopsies showed a prevalence in the lining layer (Supplementary Fig S2B) or dispersed throughout the synovium (Supplementary Fig S2C).

The spatial interactions between the Myeloid MerTK^{High} cluster and other annotated clusters were generated in the form of an interaction heatmap (Supplementary Fig S2D). Biopsies from all 5 tolDC-treated participants were grouped and compared with biopsies from the 2 untreated participants. No differences were seen in the Myeloid MerTK^{High} cluster interactions between the 2 groups, with increased endothelial cell interactions seen at day 14 for both groups. In addition, Myeloid MerTK^{High} cluster interactions with CD4$^+$ T cells were seen at both time points for the tolDC-treated group.

Because tolDC are characterised by expression of MerTK (Supplementary Fig S3A-C), we considered the possibility that they have the capacity to (1) enhance the expression of this marker by myeloid cells in a contact-dependent manner (eg, through intercellular membrane exchange or release of MerTK-enhancing mediators), and/or (2) survive for 14 days. Coculturing of tolDC with autologous CD14$^+$ monocytes did not enhance cell-surface expression of MerTK by the monocytes (Supplementary Fig S3D,E). However, interestingly, we found that a large portion of tolDC (40%–60%) survived for 14 days and retained expression of MerTK in culture medium that was devoid of the typical dendritic cell-survival factor GM-CSF (Supplementary Fig S3F-H). Addition of inflammatory arthritis synovial fluid during tolDC culture did not affect tolDC survival nor MerTK expression (Supplementary Fig S3F-H). Given that tolDC, in addition to MerTK, also has other markers in common with the Myeloid MerTK^{High} cluster (incl. CD1c and CD32; Fig 1F and data not shown), these data are supportive of the possibility that the observed enhancement of MerTK^{High} myeloid cells after intra-articular injection represents, at least partly, surviving tolDC.

DISCUSSION

This study investigated whether intra-articular tolDC administration affected the synovial immune landscape and whether this could shed light on the immunoregulatory actions that these cells may exert locally, within the synovium. We could not find any evidence of changes in the adaptive immune subsets, but, interestingly, we found that the myeloid compartment contained an increased proportion of cells expressing high levels of MerTK after higher tolDC doses (Myeloid MerTK^{High}).

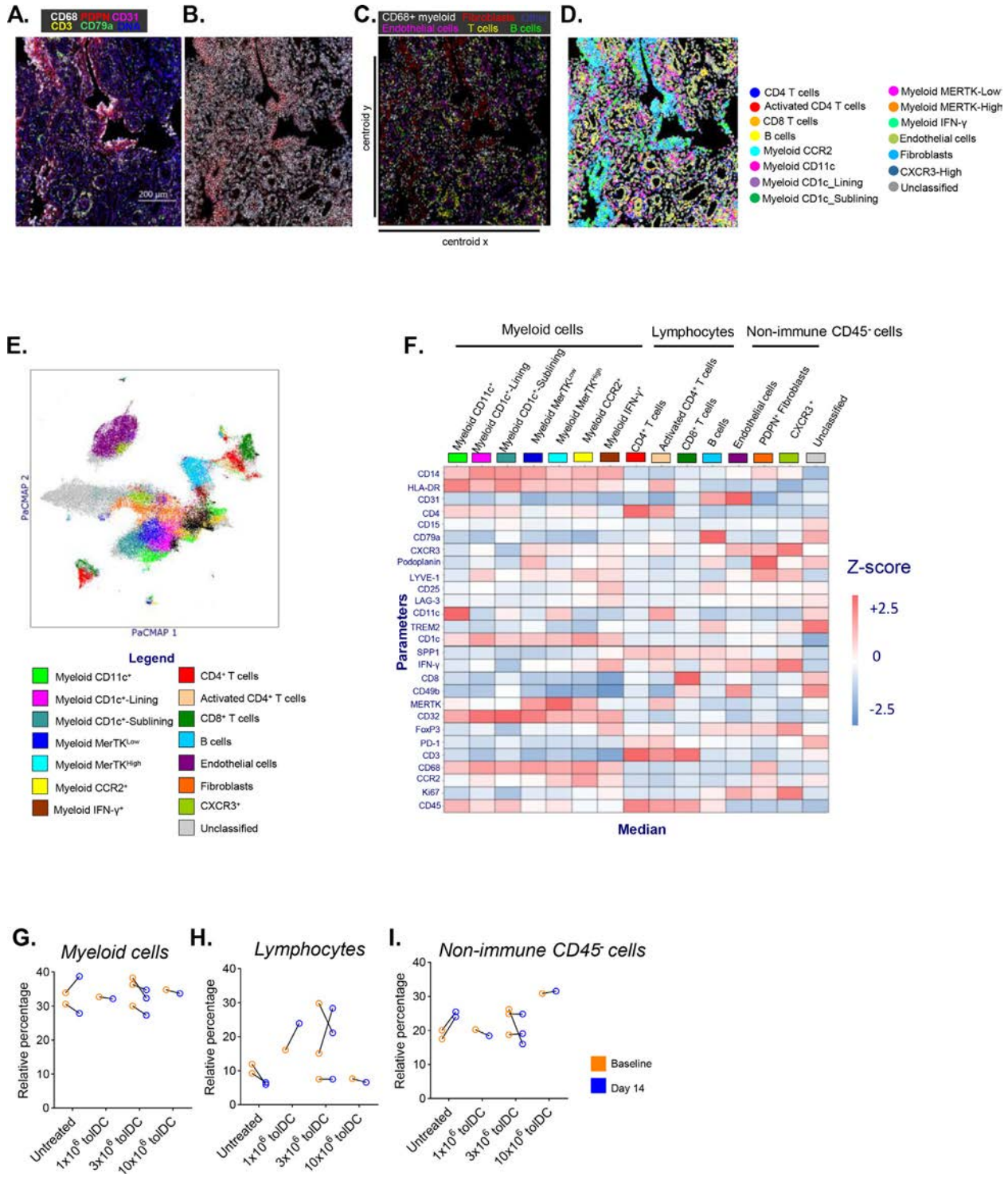

Figure 1. Phenotyping of synovial cell subsets before and after tolDC intra-articular administration. (A) IMC raw signal for selected markers on a representative synovial region. (B) Segmentation mask with identified cells based on a membrane marker and nuclei. (C) Spatial rendering of selected annotated subsets with spatial location added on centroid x and y coordinates. (D) Mask with all annotated subsets on the original tissue region. (E) PACMAP projection of all 15 annotated subsets. (F) Heatmap representing annotated subsets and Z-score of relative IMC marker expression. (G-I) Relative percentages of myeloid, lymphoid, and stromal/nonimmune cells for all treatment groups, at baseline and day 14 after tolDC treatment. Baseline: synovial biopsy collected before tolDC administration. Day 14: synovial biopsy collected 14 days after tolDC administration. Untreated: washout-only procedure. 1×10^6 tolDC: Washout and tolDC injected at 1×10^6 dose; 3×10^6 tolDC: Washout and tolDC injected at 3×10^6 dose; 10×10^6 tolDC: Washout and tolDC injected at 10×10^6 dose. IFN, interferon; IMC, imaging mass cytometry; LYVE-1, lymphatic vessel endothelial hyaluronan receptor 1; MerTK, Mer tyrosine kinase; PACMAP, pairwise controlled manifold approximation projection; PD-1, programmed cell death protein 1; PDPN, podoplanin; tolDC, tolerogenic dendritic cell.

MerTK has been described as playing a role in resolving inflammation, eg, through efferocytosis of dead cells, production of proresolving mediators, and inhibition of T cell activation [30–32]. Alivernini et al [29] previously demonstrated that high proportions of MerTK$^+$ synovial macrophages were associated with remission in RA and that these cells were particularly enriched for negative regulators of inflammation. Notably, they also found that a low proportion of MerTK$^+$ synovial

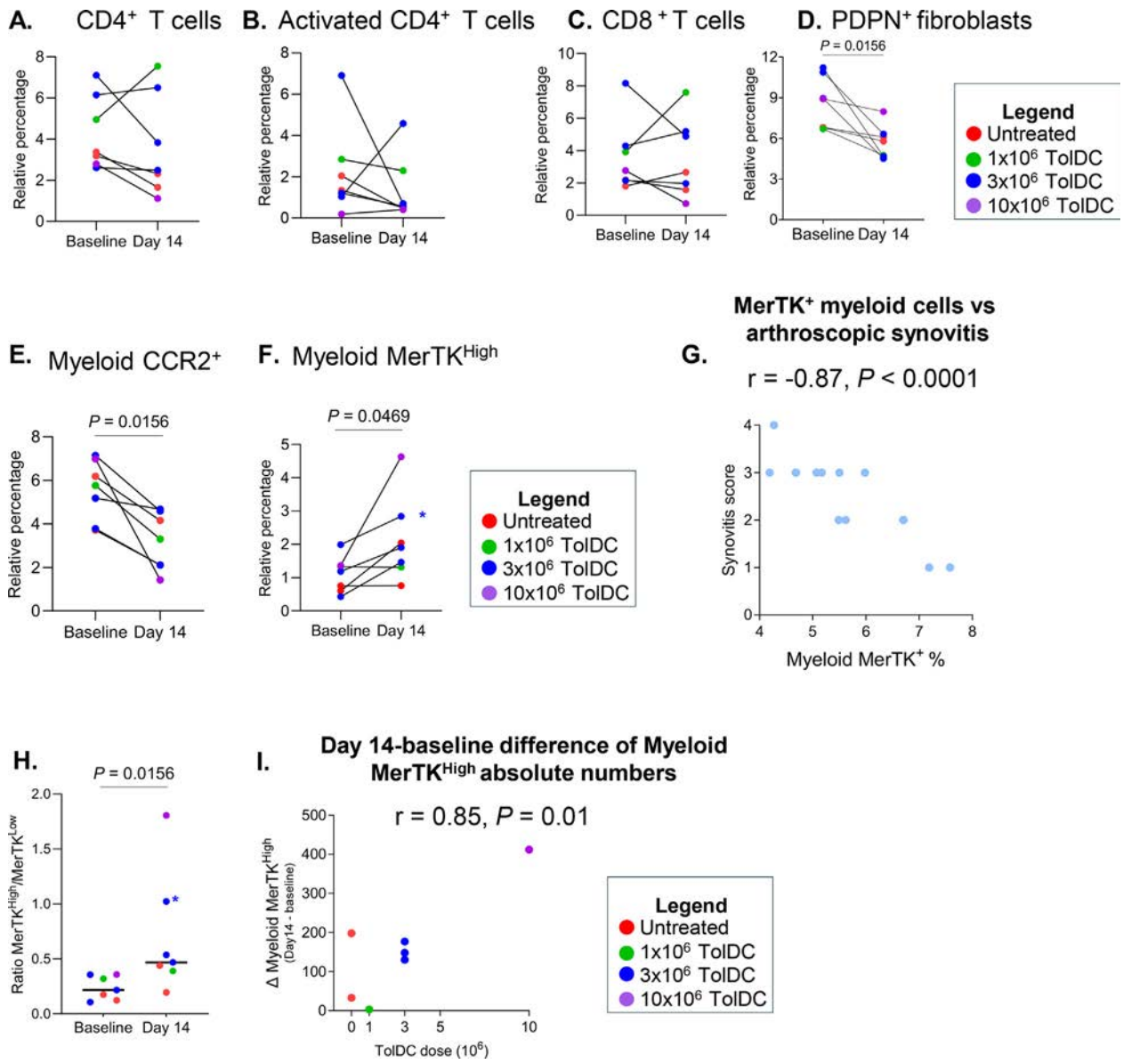

Figure 2. Quantitative analysis of annotated cellular subsets in synovial biopsies. (A-F) Changes in percentages of selected annotated subsets after tolDC treatment. *Denotes study participant 9 (received an intra-articular injection with steroids at day 7) in plot F. (G) Pearson correlation of arthroscopic synovitis score against the percentage of total MerTK^{+} myeloid cells. (H) Ratios of percentages of Myeloid MerTK^{High} cells on Myeloid MerTK^{Low} cells, at baseline and day 14. (I) Pearson correlation of difference (day 14—baseline) of MerTK^{High}/MerTK^{Low} ratios. MerTK, Mer tyrosine kinase; PDPN, podoplanin; tolDC, tolerogenic dendritic cell.

macrophages in remission patients was associated with an enhanced risk of the disease flaring after termination of treatment. Our observation that the number of MerTK^{+} synovial myeloid cells inversely correlated with the arthroscopic synovitis score of study participants in the AuToDeCRA trial, who were all selected for having knee effusions, adds to the notion that these cells may be important in regulating synovial inflammation.

The shift from MerTK^{Low} to MerTK^{High} myeloid cells was most evident in participants receiving the higher doses of tolDC. Of the 2 washout-only participants, 1 showed a similar shift, suggesting that this procedure may have contributed to the observation in tolDC recipients. Additionally, participant 9 received intra-articular glucocorticoids (a known driver of MerTK expression) on day 7 after tolDC injection as their synovitis had not settled after washout and tolDC administration, complicating the interpretation of this participant's data.

The possibility that the Myeloid MerTK^{High} cluster may (partially) represent surviving tolDC is an interesting notion that may explain why the increase in absolute numbers of this cluster was proportionate to the injected tolDC dose, although it cannot explain their appearance in a control (washout only) participant. The possibility that these administered cells migrated into the synovial membrane is encouraging, particularly in the context of data from others that MerTK^{High} synovial myeloid cells associate with drug-free remission, which is the ultimate hope for a tolerogenic therapy such as tolDC [29]. Nevertheless, this notion will need to be validated by further clinical trials, eg, by comparing the transcriptional profiles of our therapeutic tolDC with this cluster and/or by tracking migration/location of the injected tolDC by magnetic resonance imaging of ^{19}F-labelled tolDC or by reporter gene-based molecular imaging [17,21]. Regardless of their origin, it is encouraging that intra-articular tolDC treatment may increase the presence of a myeloid cell type associated with inflammation resolution.

We have previously shown that tolDC act through modulation of CD4^{+} T cell responses, including induction of T regulatory type 1 (Tr1) cells *in vitro* [11,33] and *in vivo*, in the collagen-induced arthritis mouse model [14]. Our initial focus

was, therefore, to investigate whether tolDC treatment modulated the number and/or functional features of $CD4^+$ T cells. All identified $CD4^+$ T cells expressed programmed cell death protein 1 (PD-1), whereas increased expression of HLA-DR, interferon (IFN)-γ, CXCR3, and CD11c was seen in a small proportion of $CD4^+$ T cells, annotated as activated $CD4^+$ T cells. This cluster also exhibited FoxP3 expression, indicating the presence of more phenotypically diverse cell populations within the same cluster. However, no discernible patterns were observed between the different treatment groups. In addition, the marker LAG-3, which had been included as a marker for Tr1 cells, was not detected on any of the T cell clusters, suggesting that tolDC treatment did not support Tr1 induction in the synovium. It is possible that T cell modulatory effects by tolDC occur more efficiently in secondary lymphoid tissues, rather than the inflamed synovium, in which T cells are terminally differentiated and refractory to modulation [34]. For the ongoing AuToDeCRA 2 trial, we are therefore comparing different routes of tolDC injection, ie, intranodal (into an inguinal lymph node), intradermal, or intra-articular, and performing lymph node aspirates before and after therapy.

Histopathological assessments of cell infiltrate and inflammatory aggregates are useful indicators of the general extent of immune cell abundances. We noted, however, that histopathology scores did not always align with the synovitis score during arthroscopic evaluation (eg, participants 7 and 12). The arthroscopic score was based on the evaluation of overall synovitis in the knee, whereas the histopathology analysis scored biopsies collected from selected areas with visibly increased synovitis, contributing to the incongruence between both assessments. Since the biopsy site typically does not correspond to the area examined during the arthroscopic procedure, data interpretation is more challenging. Mussawy et al [35] demonstrated that synovitis can vary across different regions of joint topography, which may help explain this observation. Expanding the size of the tissue biopsy and/or the collection of multiple biopsies should provide a more robust understanding of cell dynamics at a spatial level.

A limitation of this study is that paired biopsies were only available from a limited number of trial participants, with differing background therapies. Within this context, however, it is perhaps more remarkable that we have documented a possible dose-response relationship in the number of synovial $MerTK^{High}$ myeloid cells and an inverse correlation with arthroscopic synovitis. Small sample numbers and heterogeneity could, however, have contributed to the lack of consistency in localisation and intercellular interactions of the Myeloid $MerTK^{High}$ subset.

A major strength of this study comes from analysing the histopathology of synovial tissues derived from a unique experimental medicine study testing a novel cell therapy; because of the complexity of these types of studies, sample sizes are inherently small. Nonetheless, our study was carefully conducted and incorporated paired synovial biopsies taken pre- and post-tolDC treatment, as well as paired biopsies from control participants who had received a joint washout only. Another strength comes from applying a high-parametric spatial imaging technology that enabled an in-depth analysis of immune cell subsets *in situ*, thereby providing a novel and unexpected insight into how autologous tolDC treatment modifies the synovial immune cell landscape.

In conclusion, this study shows, for the first time, that intra-articular injection of autologous tolDC is associated with an increase in a synovial myeloid subset that expresses high levels of the inflammation resolution molecule MerTK. Our study underlines the importance of defining changes in the immune landscape both locally and systemically to provide a better understanding of how ATIMPs, such as tolerogenic cell therapies, exert their immunomodulatory effects. The study also gives further credence to the role of $MerTK^+$ myeloid cells in resolving synovial inflammation.

Competing interests

AGP reports a relationship with GSK that includes: funding grants. KSR reports a relationship with Stryker Conferences that includes: speaking and lecture fees. JDI reports a relationship with GSK that includes: consulting or advisory and funding grants. JDI reports a relationship with Pfizer that includes: consulting or advisory and funding grants. JDI reports a relationship with AbbVie Inc that includes: consulting or advisory. JDI reports a relationship with AnaptysBio Inc that includes: consulting or advisory. JDI reports a relationship with Annexon Biosciences that includes: consulting or advisory. JDI reports a relationship with AstraZeneca UK Limited that includes: consulting or advisory. JDI reports a relationship with Bristol Myers Squibb Co that includes: consulting or advisory. JDI reports a relationship with Cyxone that includes: consulting or advisory. JDI reports a relationship with Dragonfly Therapeutics, Inc. that includes: consulting or advisory. JDI reports a relationship with Eli Lily that includes: consulting or advisory. JDI reports a relationship with Galapagos that includes: consulting or advisory. JDI reports a relationship with Gilead Sciences Ltd that includes: consulting or advisory. JDI reports a relationship with Istesso Ltd that includes: consulting or advisory. JDI reports a relationship with Janssen Pharmaceuticals Inc that includes: consulting or advisory. JDI reports a relationship with Kenko International that includes: consulting or advisory. JDI reports a relationship with Kira Biotech that includes: consulting or advisory. JDI reports a relationship with Ono Pharma that includes: consulting or advisory. JDI reports a relationship with Revelo Biotherapeutics that includes: consulting or advisory. JDI reports a relationship with Roche that includes: consulting or advisory. JDI reports a relationship with Sail that includes: consulting or advisory. JDI reports a relationship with Sanofi that includes: consulting or advisory. JDI reports a relationship with Sonoma Biotherapeutics Inc that includes: consulting or advisory. JDI reports a relationship with Topas that includes: consulting or advisory. JDI reports a relationship with UCB that includes: consulting or advisory. CMUH reports a relationship with GSK that includes: consulting or advisory and funding grants. All other authors declare they have no competing interests.

CRediT authorship contribution statement

Ioana Nicorescu: Writing – original draft, Visualization, Investigation, Formal analysis. **Amanda Thomson:** Writing – review & editing, Investigation. **George Merces:** Writing – review & editing, Visualization, Methodology, Formal analysis. **Jack F. Harrison:** Formal analysis, Investigation. **Ben Barron-Millar:** Investigation, Funding acquisition. **Arthur G. Pratt:** Writing – review & editing, Funding acquisition. **Amy E. Anderson:** Writing – review & editing. **Julie Diboll:** Resources. **Kenneth S. Rankin:** Resources. **Domenico Somma:** Resources. **Mariola Kurowska-Stolarska:** Writing – review & editing. **Luke J. Jones:** Formal analysis. **Andrew Filer:** Writing – review & editing. **David McDonald:** Methodology. **Andrew Filby:** Methodology, Funding acquisition. **John D. Isaacs:** Writing – review & editing, Resources, Funding acquisition, Conceptualization. **Catharien M.U. Hilkens:** Writing – review & editing, Supervision, Funding acquisition, Conceptualization.

Acknowledgements

We thank the Newcastle University Flow Cytometry Core Facility for advice and for running the samples on the Hyperion instrument, and Emma Foster (Image Analysis Unit/Bioimaging Unit) for assistance with initial image processing and segmentation. We thank Gillian Bell and Richard Reece for obtaining the synovial biopsies and Bethany Hunter and Dagmar Scheel-Toellner for providing advice on antibody optimisation for synovial tissues.

Funding

This work has received funding from Arthritis UK grant no 18155, 21811 and 22072, the European Union's Horizon 2020 research and innovation programme under grant agreement No 860003, and the JGWP Foundation. The National Institute for Health and Care Research (NIHR) Newcastle Biomedical Research Centre (BRC) is a partnership between Newcastle Hospitals NHS Foundation Trust and Newcastle University, funded by the NIHR. This research was funded by the NIHR Newcastle Biomedical Research Centre awarded to the Newcastle upon Tyne Hospitals NHS Foundation Trust, Newcastle University and Cumbria, Northumberland, Tyne and Wear Foundation Trust, and the NIHR Birmingham BRC. The views expressed are those of the author(s) and not necessarily those of the NIHR or the Department of Health and Social Care.

Patient consent for publication

Not applicable.

Ethics approval

Ethics committee approved.

Provenance and peer review

Not commissioned; externally peer reviewed.

Data availability statement

The imaging mass cytometry data generated in this study have been deposited at https://doi.org/10.25405/data.ncl.c.7890872

Supplementary materials

Supplementary material associated with this article can be found in the online version at doi:10.1016/j.ard.2026.01.004.

Orcid

Ioana Nicorescu: http://orcid.org/0000-0002-5043-3280
Amanda Thomson: http://orcid.org/0000-0001-9633-9604
George Merces: http://orcid.org/0000-0001-7116-2451
Arthur G. Pratt: http://orcid.org/0000-0002-9909-8209
Amy E. Anderson: http://orcid.org/0000-0003-0532-623X
Kenneth S. Rankin: http://orcid.org/0000-0001-6302-0269
Mariola Kurowska-Stolarska: http://orcid.org/0000-0003-2124-7777
Andrew Filer: http://orcid.org/0000-0001-8164-6249
Andrew Filby: http://orcid.org/0000-0001-9078-4360
John D. Isaacs: http://orcid.org/0000-0002-6103-7056
Catharien M.U. Hilkens: http://orcid.org/0000-0003-2283-8886

REFERENCES

[1] Gravallese EM, Firestein GS. Rheumatoid arthritis — common origins, divergent mechanisms. N Engl J Med 2023;388(6):529–42. doi: 10.1056/NEJMra2103726.
[2] Benham H, Nel HJ, Law SC, Mehdi AM, Street S, Ramnoruth N, et al. Citrullinated peptide dendritic cell immunotherapy in HLA risk genotype-positive rheumatoid arthritis patients. Sci Transl Med 2015;7(290) 290ra87. doi: 10.1126/scitranslmed.aaa9301.
[3] Jauregui-Amezaga A, Cabezón R, Ramírez-Morros A, España C, Rimola J, Bru C, et al. Intraperitoneal administration of autologous tolerogenic dendritic cells for refractory Crohn's disease: a phase I study. J Crohns Colitis 2015;9(12):1071–8. doi: 10.1093/ecco-jcc/jjv144.
[4] Giannoukakis N, Phillips B, Finegold D, Harnaha J, Trucco M. Phase I (safety) study of autologous tolerogenic dendritic cells in type 1 diabetic patients. Diabetes Care 2011;34(9):2026–32. doi: 10.2337/dc11-0472.
[5] Kurochkina Y, Tyrinova T, Leplina O, Tikhonova M, Sizikov A, Sulutian A, et al. The effect of tolerogenic dendritic cells in patients with rheumatoid arthritis: a small pilot trial. Ann Rheum Dis 2019;78(Suppl 2):364. doi: 10.1136/annrheumdis-2019-eular.2965.
[6] Nikolic T, Zwaginga JJ, Uitbeijerse BS, Woittiez NJ, de Koning EJ, Aanstoot H-J, et al. Safety and feasibility of intradermal injection with tolerogenic dendritic cells pulsed with proinsulin peptide-for type 1 diabetes. Lancet Diabetes Endocrinol 2020;8(6):470–2. doi: 10.1016/s2213-8587(20)30104-2.
[7] Nikolic T, Suwandi JS, Wesselius J, Laban S, Joosten AM, Sonneveld P, et al. Tolerogenic dendritic cells pulsed with islet antigen induce long-term reduction in T-cell autoreactivity in type 1 diabetes patients. Front Immunol 2022;13:1054968. doi: 10.3389/fimmu.2022.1054968.
[8] Zubizarreta I, Flórez-Grau G, Vila G, Cabezón R, España C, Andorra M, et al. Immune tolerance in multiple sclerosis and neuromyelitis optica with peptide-loaded tolerogenic dendritic cells in a phase 1b trial. Proc Natl Acad Sci U S A 2019;116(17):8463–70. doi: 10.1073/pnas.1820039116.
[9] Willekens B, Presas-Rodriguez S, Mansilla MJ, Derdelinckx J, Lee WP, Nijs G, et al. Tolerogenic dendritic cell-based treatment for multiple sclerosis (MS): a harmonised study protocol for two phase I clinical trials comparing intradermal and intranodal cell administration. BMJ Open 2019;9(9):e030309. doi: 10.1136/bmjopen-2019-030309.
[10] Bell GM, Anderson AE, Diboll J, Reece R, Eltherington O, Harry RA, et al. Autologous tolerogenic dendritic cells for rheumatoid and inflammatory arthritis. Ann Rheum Dis 2017;76(1):227–34. doi: 10.1136/annrheumdis-2015-208456.
[11] Anderson AE, Sayers BL, Haniffa MA, Swan DJ, Diboll J, Wang XN, et al. Differential regulation of naive and memory CD4+ T cells by alternatively activated dendritic cells. J Leukoc Biol 2008;84(1):124–33. doi: 10.1189/jlb.1107744.
[12] Jansen MAA, Spiering R, Ludwig IS, van Eden W, Hilkens CMU, Broere F. Matured tolerogenic dendritic cells effectively inhibit autoantigen specific $CD4^+$ T cells in a murine arthritis model. Front Immunol 2019;10:2068. doi: 10.3389/fimmu.2019.02068.
[13] Navarro-Barriuso J, Mansilla MJ, Quirant-Sánchez B, Teniente-Serra A, Ramo-Tello C, Martínez-Cáceres EM. Vitamin D3-induced tolerogenic dendritic cells modulate the transcriptomic profile of T $CD4^+$ cells towards a functional hyporesponsiveness. Front Immunol 2020;11:599623. doi: 10.3389/fimmu.2020.599623.
[14] Stoop JN, Harry RA, von Delwig A, Isaacs JD, Robinson JH, Hilkens CM. Therapeutic effect of tolerogenic dendritic cells in established collagen-induced arthritis is associated with a reduction in Th17 responses. Arthritis Rheum 2010;62(12):3656–65. doi: 10.1002/art.27756.
[15] Ten Brinke A, Martinez-Llordella M, Cools N, Hilkens CMU, van Ham SM, Sawitzki B, et al. Ways forward for tolerance-inducing cellular therapies- an AFACTT perspective. Front Immunol 2019;10:181. doi: 10.3389/fimmu.2019.00181.
[16] Kleijwegt FS, Laban S, Duinkerken G, Joosten AM, Koeleman BP, Nikolic T, et al. Transfer of regulatory properties from tolerogenic to proinflammatory dendritic cells via induced autoreactive regulatory T cells. J Immunol 2011;187(12):6357–64. doi: 10.4049/jimmunol.1101638.
[17] Mansilla MJ, Hilkens CMU, Martínez-Cáceres EM. Challenges in tolerogenic dendritic cell therapy for autoimmune diseases: the route of administration. Immunother Adv 2023;3(1) ltad012. doi: 10.1093/immadv/ltad012.
[18] Suwandi JS, Nikolic T, Roep BO. Translating mechanism of regulatory action of tolerogenic dendritic cells to monitoring endpoints in clinical trials. Front Immunol 2017;8:1598. doi: 10.3389/fimmu.2017.01598.
[19] Lee W-P, Willekens B, Cras P, Goossens H, Martínez-Cáceres E, Berneman ZN, et al. Immunomodulatory effects of 1,25-dihydroxyvitamin D3 on dendritic cells promote induction of T cell hyporesponsiveness to myelin-derived antigens. J Immunol Res 2016;2016(1):5392623. doi: 10.1155/2016/5392623.
[20] Van Delen M, Janssens I, Dams A, Roosens L, Ogunjimi B, Berneman ZN, et al. Tolerogenic dendritic cells induce apoptosis-independent T cell hyporesponsiveness of SARS-CoV-2-Specific T cells in an antigen-specific manner. Int J Mol Sci 2022;23(23):15201. doi: 10.3390/ijms232315201.

[21] Cooke F, Neal M, Wood MJ, de Vries IJM, Anderson AE, Diboll J, et al. Fluorine labelling of therapeutic human tolerogenic dendritic cells for ^{19}F-magnetic resonance imaging. Front Immunol 2022;13:988667. doi: 10.3389/fimmu.2022.988667.

[22] Stoppelenburg AJ, Schreibelt G, Koeneman B, Welsing P, Breman E-J, Lammers L, et al. Design of TOLERANT: phase I/II safety assessment of intranodal administration of HSP70/mB29a self-peptide antigen-loaded autologous tolerogenic dendritic cells in patients with rheumatoid arthritis. BMJ Open 2024;14(9):e078231. doi: 10.1136/bmjopen-2023-078231.

[23] Baker KF, Sim JPX, Isaacs JD. Biomarkers of tolerance in immune-mediated inflammatory diseases: a new era in clinical management? Lancet Rheumatol 2021;3(5):e371–82. doi: 10.1016/S2665-9913(21)00069-2.

[24] Krenn V, Morawietz L, Burmester GR, Kinne RW, Mueller-Ladner U, Muller B, et al. Synovitis score: discrimination between chronic low-grade and high-grade synovitis. Histopathology 2006;49(4):358–64. doi: 10.1111/j.1365-2559.2006.02508.x.

[25] Lewis MJ, Barnes MR, Blighe K, Goldmann K, Rana S, Hackney JA, et al. Molecular portraits of early rheumatoid arthritis identify clinical and treatment response phenotypes. Cell Rep 2019;28(9):2455–70 .e5. doi: 10.1016/j.celrep.2019.07.091.

[26] Zhang F, Jonsson AH, Nathan A, Millard N, Curtis M, Xiao Q, et al. Deconstruction of rheumatoid arthritis synovium defines inflammatory subtypes. Nature 2023;623(7987):616–24. doi: 10.1038/s41586-023-06708-y.

[27] Hunter B, Nicorescu I, Foster E, McDonald D, Hulme G, Fuller A, et al. OPTIMAL: an OPTimized imaging mass cytometry anaLysis framework for benchmarking segmentation and data exploration. Cytometry A 2024;105(1):36–53. doi: 10.1002/cyto.a.24803.

[28] Milross L, Hunter B, McDonald D, Merces G, Thomson A, Hilkens CMU, et al. Distinct lung cell signatures define the temporal evolution of diffuse alveolar damage in fatal COVID-19. EBioMedicine 2023;99:104945. doi: 10.1016/j.ebiom.2023.104945.

[29] Alivernini S, MacDonald L, Elmesmari A, Finlay S, Tolusso B, Gigante MR, et al. Distinct synovial tissue macrophage subsets regulate inflammation and remission in rheumatoid arthritis. Nat Med 2020;26(8):1295–306. doi: 10.1038/s41591-020-0939-8.

[30] Cabezón R, Carrera-Silva EA, Flórez-Grau G, Errasti AE, Calderón-Gómez E, Lozano JJ, et al. MERTK as negative regulator of human T cell activation. J Leukoc Biol 2015;97(4):751–60. doi: 10.1189/jlb.3A0714-334R.

[31] Cai B, Kasikara C, Doran AC, Ramakrishnan R, Birge RB. Tabas I. MerTK signaling in macrophages promotes the synthesis of inflammation resolution mediators by suppressing CaMKII activity. Sci Signal 2018;11(549):eaar3721. doi: 10.1126/scisignal.aar3721.

[32] Chakraborty S, Singh A, Wang L, Wang X, Sanborn MA, Ye Z, et al. Trained immunity of alveolar macrophages enhances injury resolution via KLF4-MERTK-mediated efferocytosis. J Exp Med 2023;220(11):e20221388. doi: 10.1084/jem.20221388.

[33] Spiering R, Jansen MAA, Wood MJ, Fath AA, Eltherington O, Anderson AE, et al. Targeting of tolerogenic dendritic cells to heat-shock proteins in inflammatory arthritis. J Transl Med 2019;17(1):375. doi: 10.1186/s12967-019-2128-4.

[34] Isomäki P, Luukkainen R, Lassila O, Toivanen P, Punnonen J. Synovial fluid T cells from patients with rheumatoid arthritis are refractory to the T helper type 2 differentiation-inducing effects of interleukin-4. Immunology 1999;96(3):358–64. doi: 10.1046/j.1365-2567.1999.00712.x.

[35] Mussawy H, Zustin J, Luebke AM, Strahl A, Krenn V, Rüther W, et al. The histopathological synovitis score is influenced by biopsy location in patients with knee osteoarthritis. Arch Orthop Trauma Surg 2022;142(11):2991–7. doi: 10.1007/s00402-021-03889-x.

Ann Rheum Dis 85 (2026) 1486–1494

Contents lists available at ScienceDirect

Annals of the Rheumatic Diseases

journal homepage: https://www.sciencedirect.com/journal/annals-of-the-rheumatic-diseases

Rheumatoid arthritis

Progression from symptom onset to rheumatoid arthritis: is the trajectory similar in anticitrullinated protein antibody-positive and -negative disease? A comparative longitudinal study

Mitra Hosseini Malekroudi[1,*], Stijn Claassen[1], Hanna W. van Steenbergen[1], Elise van Mulligen[1,2], Annette H.M. van der Helm-van Mil[1,2]

[1] *Department of Rheumatology, Leiden University Medical Center, Leiden, Zuid-Holland, The Netherlands*
[2] *Department of Rheumatology, Erasmus University Medical Center, Leiden, Zuid-Holland, The Netherlands*

ARTICLE INFO

Article history:
Received 15 September 2025
Received in revised form 25 February 2026
Accepted 25 April 2026

ABSTRACT

Objectives: The period between symptom onset and the development of rheumatoid arthritis (RA) is a putative window for disease modification. It is insufficiently known whether anticitrullinated protein antibody (ACPA)-positive and ACPA-negative disease develop similarly in this symptomatic pre-RA period. We therefore studied this trajectory in developing ACPA-positive and ACPA-negative RA and compared timelines and inflammation-related markers.

Methods: We studied 173 (n = 87 ACPA-negative and n = 86 ACPA-positive) patients with clinically suspected arthralgia (CSA) who all developed RA. Time from symptom onset to presentation with CSA, and from CSA presentation to RA development were compared. Longitudinal inflammatory trajectories were assessed by studying clinical measures (morning stiffness and tender joints), laboratory (C-reactive protein [CRP]), and imaging (hand/foot-magnetic resonance imaging) markers.

Results: ACPA-positive patients had a longer time between symptom onset and presentation with CSA, but a shorter time from CSA presentation until RA development ($p = 0.006$ and $p = 0.014$, respectively). ACPA-negative patients had more morning stiffness at symptom onset ($p = 0.024$), at CSA presentation ($p = 0.006$) and until RA development ($p = 0.017$). Likewise, ACPA-negative patients had more hand pain at symptom onset, more tender hand joints at CSA presentation ($p < 0.001$) and until RA development ($p < 0.001$). In contrast, ACPA-positive patients showed a faster increase in CRP level ($p = 0.006$) and subclinical joint inflammation the year before developing RA, which was due to a significantly greater increase in forefoot inflammation ($p = 0.043$).

Conclusions: From symptom onset to RA development, ACPA-negative and ACPA-positive disease differ in timelines, morning stiffness severity, and location of inflammation in hands/feet. These differences may reflect differences in underlying inflammatory mechanisms and may suggest that different preventive strategies are required to intervene in the development of ACPA-positive and ACPA-negative RA.

*Correspondence to Dr. Mitra Hosseini Malekroudi, Department of Rheumatology, Leiden University Medical Center, Leiden 2300 RC, The Netherlands.
E-mail address: s.m.hosseini_malekroudi@lumc.nl (M.H. Malekroudi).
Handling editor Josef Smolen.

https://doi.org/10.1016/j.ard.2026.04.011

WHAT IS ALREADY KNOWN ON THIS TOPIC

- Rheumatoid arthritis (RA) has 2 subgroups: anticitrullinated protein antibody (ACPA)-positive and ACPA-negative RA. These 2 groups have different environmental and genetic risk factors.
- It is known that both forms of RA have a symptomatic predisease phase, but it is unknown whether there are differences in inflammatory markers and progression to RA between ACPA-positive and ACPA-negative disease.

WHAT THIS STUDY ADDS

- This study adds to the understanding of differences in the symptomatic pre-RA phase of ACPA-positive and ACPA-negative disease. Symptoms of ACPA-negative RA include more severe morning stiffness and increased symptoms and tenderness in the hand joints. ACPA-negative RA has a longer time between the onset of clinically suspect arthralgia (CSA) and progression to RA.
- On the other hand, ACPA-positive patients develop RA more rapidly after presentation with CSA; they also have a more rapid increase in C-reactive protein and subclinical joint inflammation (particularly in the feet) during this period.

HOW THIS STUDY MIGHT AFFECT RESEARCH, PRACTICE OR POLICY

- These differences point to differences in biological processes in the symptomatic pre-RA phase that may warrant further investigation.
- Moreover, the presence of pathophysiological differences suggests that secondary prevention may be differentially effective in patients with developing ACPA-positive and ACPA-negative RA.

INTRODUCTION

The pathophysiology of the development of rheumatoid arthritis (RA) is still incompletely understood. It is known that most patients have a symptomatic at-risk phase preceding RA development that can last for a long time [1–3]. In developing anticitrullinated protein antibody (ACPA)-positive RA, autoantibodies can appear approximately 10 years before diagnosis; subsequent maturation of the autoantibody response occurs approximately 5 years before diagnosis, which is followed by a rise in cytokines in the systemic circulation [4]. Most patients are then still asymptomatic. Symptoms occur more shortly before diagnosis. During this symptomatic pre-RA phase, subclinical joint inflammation may occur, which may subsequently progress to clinical arthritis and diagnosis of RA. The pathophysiology of ACPA-negative RA is even less well understood. Also, there is a preceding phase of systemic inflammation, which is followed by local subclinical joint inflammation [4,5]. Insight into the pathophysiological trajectory of the development of RA and the timing of processes within it is crucial for designing interventions aimed at influencing the course of developing RA.

There is increasing evidence that ACPA-positive and ACPA-negative RA are different. Differences in the severity of the course of classified RA, in terms of radiological progression, chance of achieving disease-modifying antirheumatic drugs (DMARD)-free remission [6], and response to treatment, have long been known. Although the overall clinical phenotype at RA diagnosis is similar [7], studies using sensitive imaging techniques have revealed subtle differences at diagnosis, with ACPA-positive RA more likely to have foot involvement, including intermetatarsal bursitis [8]. Furthermore, risk factors differ, with smoking and the human leukocyte antigen (HLA)-shared epitope being known risk factors for ACPA-positive RA [9,10]. Fewer genetic and environmental risk factors are known for ACPA-negative RA, but lifelong exposure to oestrogens and/or the decline in oestrogen levels after menopause may play a role in its pathophysiology [11–13]. There are therefore differences between the 2 RA entities in terms of risk factors for the development and progression of the disease.

It is so far unknown whether there are also differences in the symptomatic stage of arthralgia that precedes RA. This symptomatic stage is important because it is presumed to be a window for disease interception or disease modification. Therefore, it is important to understand the inflammatory processes occurring in this pre-RA period. Based on the observed differences at RA diagnosis and in the course after RA diagnosis, we hypothesise that ACPA-positive and ACPA-negative RA also differ in the symptomatic pre-RA period. To investigate this, we conducted an in-depth longitudinal study of the trajectory from symptom onset to RA development, comparing timelines and inflammation-related markers (obtained from physical examination, laboratory measurements, and joint imaging) during the development of ACPA-positive and ACPA-negative RA.

METHODS

Patients

We studied all patients who developed clinically apparent inflammatory arthritis (IA) and were included in the observational Leiden clinically suspect arthralgia (CSA)-cohort between April 2012 and December 2024 and in the placebo arm of the TREAT Early Arthralgia to Reverse or Limit Impending Exacerbation to Rheumatoid arthritis (TREAT EARLIER) trial [14]. The CSA cohort is an inception cohort including patients older than 18 with arthralgia of the small joints for less than 1 year, which is considered suspicious of progression to RA based on the clinical judgement of the rheumatologist and without any prior knowledge of the autoantibody status. Patients were excluded if they had clinically apparent arthritis or if another reason for the arthralgia was more likely (eg, fibromyalgia and osteoarthritis) [15]. The TREAT EARLIER trial is a randomised, double-blind, placebo-controlled clinical trial that included patients with CSA with subclinical joint inflammation on magnetic resonance imaging (MRI). Patients in both datasets were recruited from rheumatology outpatient clinics. Consecutive patients with CSA presenting to the Leiden rheumatology outpatient clinic were included in the observational CSA cohort. Identification of CSA was done at the first visit, when the results of additional investigations (laboratory and imaging) were not yet known. Moreover, autoantibody status was generally unknown at this first visit because Dutch primary care guidelines explicitly discourage ordering these tests (https://www.nhg.org/standaarden/volledig/nhg-standaard-artritis).

Likewise, following a regional educational campaign, general practitioners were advised to refer patients based on clinical suspicion of arthritis, without prior laboratory testing [16]. Hence, patients with CSA were referred to the rheumatology outpatient clinic and identified as CSA by rheumatologists without knowledge of ACPA status. The same applied to the patients with CSA included in the TREAT EARLIER trial. The fact that referral was not based on or influenced by ACPA allowed us to compare the pre-RA period of both ACPA-positive or ACPA-negative disease.

In both studies, ACPA was determined at inclusion, and positivity was defined as a level of ≥ 7 IU/mL (EliA CCP, Phadia).

In the CSA cohort, patients were followed after 4, 12, and 24 months according to protocolised visits; thereafter, visits were left to the treating rheumatologists. In the TREAT EARLIER trial, participants were followed with visits every 4 months for up to 24 months and then, according to the treating rheumatologist, with data collected for up to 5 years after treatment. In both studies, patients were seen between these protocolised visits if they reported any signs of IA development. In both datasets, patients were not treated with DMARDs and corticosteroids before clinically apparent IA developed.

From both datasets with consecutively included patients with CSA, we studied only the patients who progressed to clinically apparent IA over time. IA was defined as the presence of swollen joint count (SJC66) ≥ 1 on physical examination by the rheumatologist. In sensitivity analysis, the development of RA was studied, defined as IA plus fulfilment of the 2010- or 1987-classification criteria for RA.

Research protocols for the Leiden CSA cohort and the TREAT EARLIER trial were approved by the local Medical Ethics Committee of the Leiden University Medical Center. The TREAT EARLIER trial was also registered with EudraCT (2014-004472-35) and the Netherlands Trial Register (NTR4853-trial-NL4599). Written informed consent was also signed by all the patients before participation.

Assessment of timelines

We studied the period from CSA onset to the development of RA. Data collection was similar at inclusion in the CSA cohort and the TREAT EARLIER trial. At inclusion, patients filled out a questionnaire about symptom onset, which comprised information about calendar dates, as well as the location and type of symptoms at symptom onset. In addition, data were collected at inclusion, after which patients were longitudinally followed until IA/RA development. Timelines were assessed by subtracting calendar dates and 2 time periods were defined: from symptom duration to first presentation with CSA (date of inclusion minus date of symptom onset), and from CSA presentation to IA development.

Assessment of inflammatory markers

At the initial presentation with CSA, patients completed a questionnaire about the onset of symptoms, including the location and type of initial symptoms (as mentioned above). In addition, several markers related to inflammation were studied at presentation with CSA and during follow-up; these were obtained from patients themselves (morning stiffness), through physical examination of the joints (tender joints), laboratory measurements (C-reactive protein [CRP]), and MRI scans of the joints (subclinical joint inflammation). We studied all these patients in the mentioned datasets for 2 years after inclusion.

Morning stiffness

During all study visits, the following question was asked about morning stiffness: 'How was the stiffness in your joints when you woke up yesterday?' the answers were expressed on a Visual Analogue Scale (VAS), and assessed by having the patient mark a point on a line representing a range of stiffness, from 'none' to 'very severe' (range 0-10). The distance of the mark from the 'none' end of the line was then measured, in centimetres, and the value represented the severity of the morning stiffness.

Tender joint count 68

The tender joint count (TJC) based on 68 joints (TJC68) was assessed by physical examination. The TJC68 was studied as a whole, and for more in-depth analyses, we compared groups of joints, grouping them as hand joints (including metacarpophalangeal joints [MCP] 1-5, proximal interphalangeal joints 1-5, distal interphalangeal joints 2-5, and the wrists), foot joints (including metatarsophalangeal joints [MTP] 1-5, and large joints (including shoulders, elbows, hips, knees, and ankles).

CRP

CRP levels were measured at each study visit and reported in milligrams per litre (mg/L).

Subclinical joint inflammation

Subclinical joint inflammation was assessed using unilateral contrast-enhanced 1.5 T MRI scans of hands and feet. The scans were made at inclusion, at IA/RA development in the CSA cohort and TREAT EARLIER trial, and also after 4- and 12-month follow-up in the TREAT EARLIER trial (if IA was still absent). Wrist, MCP (2-5), and MTP (1-5) joints were scored according to Rheumatoid Arthritis Magnetic Resonance Imaging Score (RAMRIS) for osteitis, synovitis, and tenosynovitis [17]. The same scanner, scan protocol, and scoring methodology were used in both studies. Inter- and intrareader interclass correlation coefficients were high (≥ 0.90) (Supplementary S1 and S2).

Statistical analysis

Comparisons between ACPA-positive and ACPA-negative groups at a single time point were done with the Mann-Whitney U test and Chi-square tests as appropriate. For a longitudinal analysis, a negative binomial model was used for TJCs and CRP, due to overdispersion (ie, variance larger than the mean). To assess the course of morning stiffness over time, a linear mixed model was applied as the outcome was normally distributed and after checking the assumptions by examining residuals using a Q-Q plot and a histogram with a normal curve. For the course of subclinical joint inflammation (count data), a Poisson regression model was used. As MRI-detected joint inflammation is known to increase with age [18], the analyses for MRI-detected subclinical inflammation were corrected for age; the other analyses were uncorrected. The described models were selected based on graphical inspection of the raw data and comparison of Akaike's Information Criterion and Bayesian Information Criterion. In all described models, the time of IA development was set as zero, with the negative time points indicating assessments in the pre-disease period. A random intercept was included to account for repeated measures within individuals. We also used an unstructured covariance matrix to flexibly account for the relationships between repeated measurements within the same person. The results from both the Poisson and negative binomial models are presented as incidence rate ratios (IRRs) and are interpreted on a multiplicative scale. An IRR > 1 indicates an increased rate of the outcome associated with the predictor, whereas an IRR < 1 shows a decreased rate.

Two sensitivity analyses were performed. First, analyses were repeated in the subgroup of patients who fulfilled the classification criteria for RA (presence of joint swelling on physical examination by the rheumatologist plus fulfilment of the 2010 or 1987 criteria). Second, analyses were repeated for autoantibody positivity rather than ACPA positivity. Here, autoantibody negativity was defined as negativity for both ACPA and rheumatoid

factor (RF), and autoantibody-positive patients had either one of these or both autoantibodies.

Statistical analyses were performed using IBM SPSS Statistics version 29.0.0.0 (Build 241) and Stata/SE 16.1 for Windows. A 2-tailed p-value of < 0.05 was considered statistically significant.

RESULTS

Patient characteristics

In total, 173 patients presented with CSA and progressed to clinically apparent IA; all these patients were studied. Of these, 142 were included in the observational CSA cohort and 31 in the placebo arm of the TREAT EARLIER trial. In total, 102 of the 140 patients (73%) with complete data for the European Alliance of Associations for Rheumatology (EULAR) CSA criteria fulfilled ≥ 3 criteria. In addition, 87 were ACPA negative and 86 ACPA positive at presentation with CSA. All remained ACPA negative and ACPA positive, respectively, until clinical arthritis development. Proportions of ACPA-negative and ACPA-positive patients who did not progress to clinical arthritis are shown in Supplementary S3. In both ACPA groups, 72% of the patients were female. The mean age at inclusion was 46 years (SD 13) for ACPA-negative patients and 49 years (SD 13) for ACPA-positive patients. Further baseline characteristics of the patients are provided in Table 1.

Assessment of timelines

ACPA-positive RA had a longer time between symptom onset and presentation with CSA; the median period was 24 weeks (IQR: 13-52) compared with 16 weeks (IQR: 7-28) in ACPA-negative RA (p = 0.006). Conversely, ACPA-positive RA had a shorter time between CSA presentation and development of IA; the median period was 12 weeks (IQR 4-55) compared with 21 weeks (IQR 9-69) in ACPA-negative RA (p = 0.014) (Fig 1). The total time between symptom onset and IA development in ACPA negative and positive CSA was 62 weeks (IQR: 25-120) and 56 (IQR: 26-111) (p = 0.77), respectively. This indicates that although the total symptomatic pre-RA period was not significantly different in length, it takes longer in ACPA-positive RA before patients present to rheumatological care with a CSA phenotype, but shorter to progress to clinically apparent IA.

Assessment of inflammatory markers

Inflammatory symptoms

At symptom onset in ACPA-negative RA, symptoms started significantly more often in the small joints (79% vs 62% in ACPA positive) and tended to present more often in the upper extremities (69% vs 52% in ACPA positive). Together, this suggests that symptoms more often started in the hand joints in ACPA-negative RA. Furthermore, in ACPA-negative disease, patients had more often morning stiffness (70%, vs 54% in ACPA-positive disease, p = 0.024) at symptom onset. At presentation with CSA, ACPA-negative patients also had more severe morning stiffness (mean VAS 6 vs 5 [on a 0-10 range], p = 0.006). Longitudinal analysis to and including IA development showed that ACPA-negative disease remained to have more severe morning stiffness than ACPA-positive disease (p = 0.017) (Fig 2).

Table 1
Patient characteristics at symptom onset and at presentation with CSA

	ACPA-negative (n = 87)	ACPA-positive (n = 86)	p-value
Age (mean ± SD)	46 ± 13	49 ± 13	0.23
Female n %	72	72	0.96
Characteristics at symptom onset			
Symptom started with (%):			
• Pain	95	97	1.00
• Loss of function	38	36	0.80
• Stiffness	70	54	0.024
Localisation at symptom onset (%):	79	62	0.045
• Small joints (hand/foot)	9	14	
• Large joints	12	23	
• Both			
Localisation at symptom onset[a] (%):	69	52	0.073
• Upper extremities	12	13	
• Lower extremities	16	29	
• Both			
Patients' characteristics at presentation with CSA			
VAS morning stiffness (mean,SD)	6 (2.4)	5 (2.7)	0.006
TJC 68 (median,IQR)	5 (3-10)	3 (1-6)	<0.001
• Hand joints (incl wrist)	3 (1-6)	1 (0-3)	<0.001
• Foot joints	0 (0-3)	0 (0-2)	0.28
• Large joints[b]	0 (0-2)	0 (0-1)	0.018
[c]Positive rheumatoid factor (RF) %	18	92	<0.001
CRP (median, IQR)	3 (3-8)	4 (3-8)	0.52
MRI total inflammation (median, IQR)	5 (2-10)	6 (3-13)	0.35

ACPA, anticitrullinated protein antibodies; CRP, C-reactive protein; CSA, clinically suspect arthralgia; MRI, magnetic resonance imaging; TJC, tender joint count; VAS, Visual Analogue Scale.
[a] Totals may not equal 100% because of missing values.
[b] Large joints are shoulder, elbow, hip, knee, and ankle.
[c] Positive RF is defined as ≥ 3.5 IU/mL.

Tender joints

At physical examination at presentation with CSA, ACPA-negative patients had more tender joints; the median was 5 (IQR: 3-10), compared with 3 (IQR: 1-6; *P* < .001), and a difference remained over time (*P* = .001, Fig 3A). Separating this for the different joint regions (hands/feet/large joints) revealed that this difference was based on a greater number of tender hand joints in ACPA-negative disease than ACPA-positive disease, median 3 (IQR: 1-6) vs 1 (IQR: 0-3), respectively, at CSA presentation (p < 0.001) and over time (p < 0.001, Fig 3B). Hence, in line with the results at symptom onset, ACPA-negative

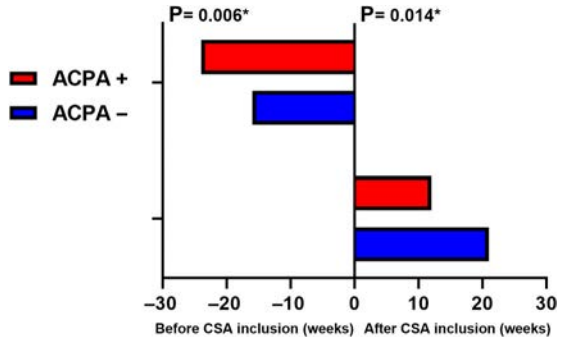

Figure 1. Time between symptom onset and presentation with CSA, and between CSA presentation until development of clinical arthritis, stratified by ACPA. Bars represent median values; statistically significant differences were observed both before (p = 0.006*) and after CSA inclusion (p = 0.014*) between ACPA+ and ACPA− groups. ACPA, anticitrullinated protein antibodies; CSA, clinically suspect arthralgia.

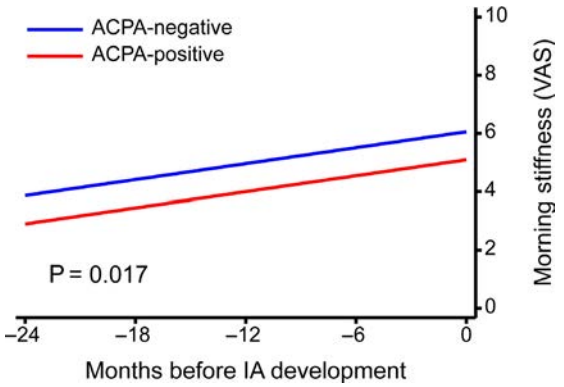

Figure 2. Course of morning stiffness until the development of clinical arthritis. The data presented were collected at presentation with CSA up to the development of clinically apparent inflammatory arthritis. For comparability, the time of clinical arthritis development was set as time zero. Morning stiffness was measured using a VAS scale ranging from 0 to 10. ACPA-negative patients had significantly more severe morning stiffness: −0.96; 95% CI, −1.76 to −0.17; p = 0.017. ACPA, anticitrullinated protein antibodies; CSA, clinically suspect arthralgia; IA, inflammatory arthritis; VAS, Visual Analogue Scale.

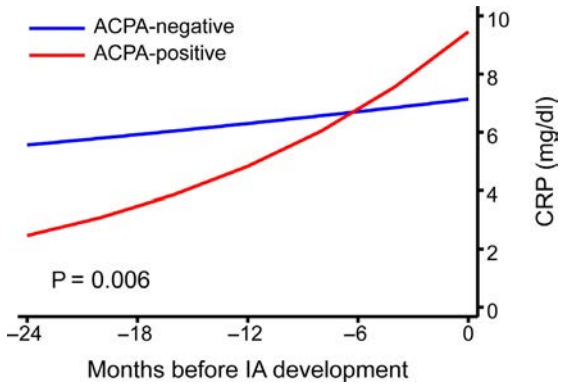

Figure 4. Course of CRP over time until the development of clinical arthritis. The data presented were collected at the presentation with CSA to the development of clinically apparent inflammatory arthritis. For comparability, the time of clinical arthritis development was set as time zero. ACPA-positive patients had a faster increase before clinical arthritis development: (IRR: 1.05; 95% CI: 1.01-1.08; p = 0.006). ACPA, anticitrullinated protein antibodies; CRP, C-reactive protein; CSA, clinically suspect arthralgia; IA, inflammatory arthritis; IRR, incidence rate ratio.

disease had more involved hand joints in the predisease period than ACPA-positive disease. Although tender large joints were infrequent, they occurred slightly more often in ACPA-negative disease over time (p = 0.001), whereas there was no significance in the number of tender foot joints over time (Supplementary S4).

CRP

The CRP levels at presentation with CSA were not significantly different between the ACPA groups (Table 1). However, longitudinal analysis with time of clinical arthritis development set as zero time showed that the CRP level increased more rapidly in the months before diagnosis in ACPA-positive disease compared with the ACPA-negative disease (p = 0.006; Fig 4).

Subclinical joint inflammation

Finally, we studied the course of subclinical joint inflammation from presentation with CSA to and including clinical arthritis development. As with CRP, the severity of subclinical joint inflammation was not statistically significantly different at presentation with CSA (Table 1). However, longitudinal analyses with clinical arthritis development set as zero time demonstrated that ACPA-positive patients showed a trend towards faster increase in the total level of subclinical joint inflammation (Fig 5A, p = 0.062); a difference which was statistically significantly different when studying subclinical joint inflammation in the foot only (Fig 5B, p = 0.043). The course of subclinical inflammation in the hands was not statistically significant (Supplementary S5).

Sensitivity analysis

Two sensitivity analyses were performed. As ACPA-negative patients can be RF positive, the longitudinal analyses from CSA onset to clinical arthritis development were repeated in the patients who were autoantibody positive and autoantibody negative (102 vs 71, respectively), whereby autoantibody negativity was defined as RF negative and ACPA negative. The results were similar, although the statistical significance for CRP level over time was lost, whereas the difference in total subclinical

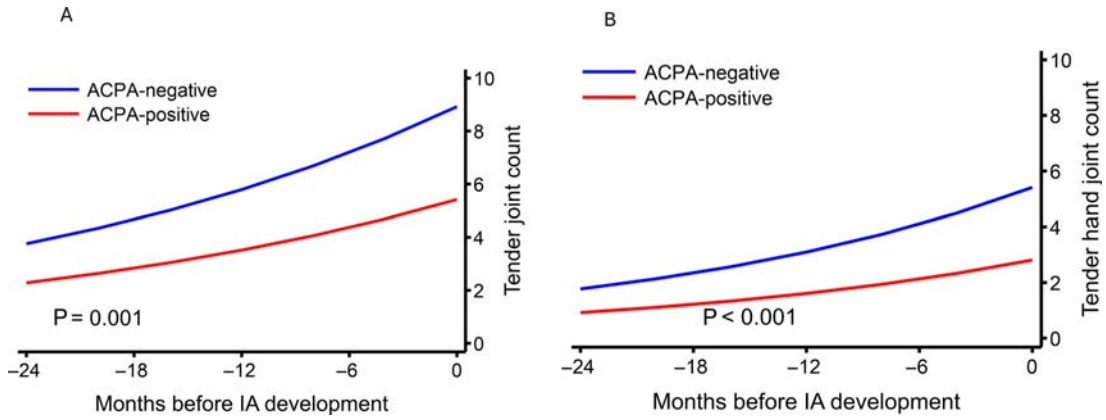

Figure 3. Course of the total tender joints (A) and tender hand joints (B) until development of clinical arthritis. The data presented were collected at the presentation with CSA until the development of clinically apparent inflammatory arthritis. For comparability, the time of clinical development was set as time zero. In (A), the total TJC68 was studied (IRR: 0.61; 95% CI: 0.45-0.82; *P* = 0.001). In B, the TJC of the hand joints (metacarpophalangeal joints [MCP] 1-5, proximal interphalangeal joints [PIP] 1-5, distal interphalangeal joints [DIP] 2-5, and the wrists) was studied, which was also significantly higher in ACPA-negative patients (IRR: 0.52; 95% CI: 0.37-0.72; p < 0.001). ACPA, anticitrullinated protein antibodies; CSA, clinically suspect arthralgia; IA, inflammatory arthritis; IRR, incidence rate ratio; TJC, tender joint count.

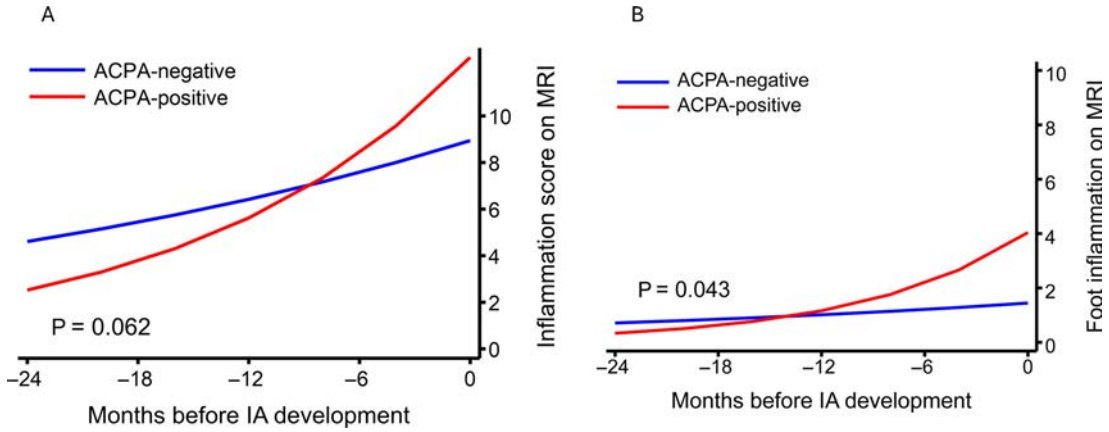

Figure 5. Course of subclinical joint inflammation until development of clinical arthritis, presented for total inflammation (A), and for the feet only (B). The data presented were collected at the presentation with CSA until the development of clinically apparent inflammatory arthritis. For comparability, the time of clinical arthritis development was set as time zero. The models are corrected for age at inclusion. An interaction term was added for time and ACPA status in all the models. In (A), the total MRI inflammation score (sum of synovitis, tenosynovitis, and BME) was studied (IRR: 1.04; 95% CI: 1.00-1.08; p = 0.062). In (B), subclinical inflammation in the feet is presented, which was significantly higher in ACPA-positive patients (IRR: 1.08; 95% CI: 1.00-1.16; p = 0.043). The scores in hands did not differ significantly between ACPA-positive and ACPA-negative patients over time (IRR: 1.03; 95% CI: 0.98-1.08; p = 0.28). ACPA, anticitrullinated protein antibodies; BME, Bone marrow oedema; CSA, clinically suspect arthralgia; IA, inflammatory arthritis; IRR, incidence rate ratio; MRI, magnetic resonance imaging.

inflammation on MRI became statistically significantly higher in seropositive patients. (Supplementary S6).

Analyses were repeated in patients who progressed to RA (defined as IA plus fulfilment of classification criteria at clinical arthritis development or the first year thereafter). At IA development, 85 patients had ACPA-positive RA and 50 had ACPA-negative RA. During follow-up, an additional 11 ACPA-negative patients fulfilled RA criteria, resulting in 146 patients (84%) classified as RA. The results of the analysis were similar (Supplementary S7).

Among the remaining patients with IA, 22 (13%) were classified as undifferentiated arthritis, and 5 received alternative diagnoses (4 psoriatic arthritis and 1 gout).

DISCUSSION

The pathophysiological trajectory leading to RA is not fully understood. Although insights have been gained by studying the autoantibody response in developing ACPA-positive RA, the pathophysiology of ACPA-negative RA remains elusive. Furthermore, for both subgroups of RA, the timelines and sequence of inflammatory events from symptom onset to development of RA are not known. The current study is one of the largest to date that has studied patients from the symptomatic risk stage through to the development of clinical arthritis. We demonstrated that ACPA-positive RA has a longer period from symptom onset to presentation with a CSA phenotype, but a shorter symptom duration to clinical arthritis development. In contrast, ACPA-negative RA more often started with morning stiffness and experienced more hand symptoms and hand joint tenderness throughout the symptomatic course until clinical arthritis developed. Altogether, these findings show that the progression patterns and inflammatory trajectories differ between the 2 RA entities.

Previous studies have demonstrated that the autoantibody response matures in the asymptomatic stage and that several autoantibody characteristics seem to be stable during the transition from CSA to clinical arthritis/RA [11,19–23]. This study has increased the knowledge about the development of ACPA-positive RA by showing that subclinical inflammation had a sharper increase in the 6 to 12 months before diagnosis than in ACPA-negative RA. It was also observed that the time between CSA and RA development is shorter in ACPA-positive subgroups. The time interval and the increase in inflammation may be related, as the steepness may be greater when the time to the development of RA is shorter. However, this is not the only reason, because subclinical inflammation in the feet increased more in the ACPA-positive group, whereas this was not the case for subclinical inflammation in the hands. The higher frequency of foot involvement in developing ACPA-positive disease is in line with results from a study with MRI at RA diagnosis, which showed that ACPA-positive patients had more MRI-detected inflammation in the feet, including more inflamed intermetatarsal bursae [8].

In ACPA-negative RA, the onset of symptoms before presentation with CSA tended to be somewhat shorter; however, the time to progression to RA was longer. This suggests that a potential symptomatic window for intervention in ACPA-negative CSA is longer. It is striking that ACPA-negative RA differed in 2 aspects from the onset of the symptoms: more severe morning stiffness and more hand involvement. We found this both in retrospectively asking about the onset of the symptoms and in the prospective observation until clinical arthritis development. ACPA-negative RA had more tender joints at the time of diagnosis. This result aligns with results reported in early RA, showing that ACPA-negative RA had higher swollen and TJCs [8,24]. It has sometimes been suggested that this was due to the 2010 classification criteria, which require more inflamed joints to be present to achieve 6 points [25–27]. Our data suggest that this is not the only explanation; the difference in TJC is present throughout the symptomatic predisease phase and also at the presentation with clinical arthritis/IA, even without the 2010 criteria being applied. Therefore, it appears to be a difference not due to the criteria but rather intrinsic to the ACPA-negative RA entity.

Misclassification in ACPA-negative RA is often mentioned as a threat to ACPA-negative disease. We tried to prevent this problem at the inclusion level by not including the patients who were likely to have other diagnoses (eg, signs of osteoarthritis, fibromyalgia, and psoriasis). In addition, we were careful in defining the endpoint; we studied not only patients who developed IA,

but also RA according to the classification criteria, which yielded similar results. As a result, we believe that misclassification of developing ACPA-negative RA in this study is unlikely to be a problem.

ACPA-negative RA remained ACPA negative in the whole trajectory. We performed a sensitivity analysis in evolving seronegative RA, which showed similar results. It is sometimes questioned if evolving ACPA-negative RF-negative patients carry other autoantibodies such as anticarbamylated and antiacetylated protein antibodies. However, these antibodies are rare in ACPA-negative RF-negative at-risk individuals [28,29].

Our study convincingly showed differences in timelines between CSA onset and RA development. This supports a previous analysis from our group [30], but now in a larger dataset, and strengthened by more in-depth clinical and imaging data over time. Interestingly, a study on proteomics of evolving RA showed differences between ACPA-positive and ACPA-negative RA. These differences in markers from the systemic circulation were already present 1 or 2 decades before the diagnosis; for example, APCA-positive RA had an increase in interleukin-10 almost 2 decades before diagnosis [31]. Taken together, the data from others and ours support the proposition that ACPA-positive and ACPA-negative RA are distinct diseases with differences in development.

A question that arises is why the course of the TJC in the feet does not differ significantly between the ACPA-positive and ACPA-negative groups, even though the ACPA-positive group shows significantly higher foot involvement on MRI. It may well be that MRI is a much more sensitive measure for foot inflammation than physical evaluation of tender joints. Consequently, the increase in MRI may have been more difficult to detect at physical examination when evaluating joint tenderness. Another explanation could be that the TJC is also influenced by noninflammatory mechanisms. Comorbid pain or central sensitisation may be present in a pre-RA phase and could amplify pain perception, whereas it is not compatible with imaging findings [32]. This would mean that such pain trajectories are more often present in the foot of ACPA-negative patients, hence diminishing the difference of inflammation-related pain in the forefoot. A previous study did indeed reveal that patients with ACPA-negative RA experience a higher disease burden at the group level, which is not explained by local subclinical joint inflammation [33]. Whether this explanation is valid, is subject to further research.

A limitation of our study was that the number of serial MRIs differed between the 2 datasets; 2 per patient in the CSA cohort and more in the TREAT EARLIER trial, according to differences in the study protocols. Differences in the number of MRIs were not associated with ACPA status. Consequently, it is unlikely to have significantly impacted the observed differences between ACPA groups over time. Another limitation is that symptom duration before CSA presentation was patient reported and may be subject to recall bias. However, this bias is unlikely to be largely influenced by ACPA status and is unlikely to provide a major influence on the findings. Finally, we studied largely clinical and imaging measures of inflammation. Regarding markers of systemic inflammation, we only studied CRP. More inflammatory markers were not yet available in our data. Therefore, further studies on systemic markers (eg, such as the study reporting differences in IL-10 in predisease stage ACPA-positive and ACPA-negative RA) [31] may provide more insight into the differences between the development of ACPA-positive and ACPA-negative RA.

A strength of this study is the inclusion of regional incident patients with CSA. The distribution of ACPA positivity was similar to that observed in several early arthritis cohorts, where half of the population was also ACPA positive. This argues against a relevant selection bias [34]. In addition, our study, to the best of our knowledge, is one of the largest longitudinal investigations in the CSA stage, with data available from symptom onset to the development of IA/RA, comparing the ACPA-positive and ACPA-negative trajectories.

This study deepens our knowledge about the symptomatic phase that precedes RA. The differences observed may point towards yet unresolved differences in autoimmune and inflammatory molecular processes. The presence of differences in pathophysiology would also imply that patients with evolving ACPA-positive and ACPA-negative RA may respond differently to interventions in this stage. Indeed, the long-term effects of methotrexate in the TREAT EARLIER study showed differential treatment effectiveness for interventions during the development of ACPA-positive and ACPA-negative disease, with the highest durable effectiveness in the ACPA-negative group [35,36]. Further translational studies are needed to unravel the molecular differences between the 2 groups and determine the differences that are important for establishing the chronicity of the disease in both groups.

In conclusion, we have shown that the development of ACPA-negative and ACPA-positive RA differs in timelines, severity of morning stiffness, and location of inflammation in the hands/feet during the symptomatic pre-RA phase. These differences may reflect differences in underlying inflammatory mechanisms and suggest that different preventive strategies are needed to intervene in the development of ACPA-positive and ACPA-negative RA.

Competing interests

The authors have declared no conflicts of interest.

Contributors

All authors interpreted the data and wrote the report. SMHM performed the analyses. All authors have approved the final version of the manuscript.

Funding

This work was supported by the Dutch Arthritis Society.

Patient consent for publication

Not applicable

Ethics approval

Ethics approval was obtained from the Medical Ethics Committee of the Leiden University Medical Center

Provenance and peer review

Not commissioned; externally peer reviewed

Data availability statement

Requests for data can be made to the corresponding author, and requests will be considered on an individual basis.

Supplementary materials

Supplementary material associated with this article can be found in the online version at doi:10.1016/j.ard.2026.04.011.

Orcid

Mitra Hosseini Malekroudi: http://orcid.org/0000-0002-3462-6904
Stijn Claassen: http://orcid.org/0009-0006-6299-7653
Hanna W. van Steenbergen: http://orcid.org/0000-0002-3251-0238
Elise van Mulligen: http://orcid.org/0000-0003-1900-790X
Annette H.M. van der Helm-van Mil: http://orcid.org/0000-0001-8572-1437

REFERENCES

[1] Paul BJ, Kandy HI, Krishnan V. Pre-rheumatoid arthritis and its prevention. Eur J Rheumatol. 2017;4(2):161–5.
[2] Claassen S, Boeren AMP, Khidir SJH, van Steenbergen HW, van der Helm-van Mil AHM. Is rheumatoid arthritis always preceded by a symptomatic at-risk phase of arthralgia? RMD Open 2024;10(4):e004714.
[3] Gerlag DM, Raza K, van Baarsen LG, Brouwer E, Buckley CD, Burmester GR, et al. EULAR recommendations for terminology and research in individuals at risk of rheumatoid arthritis: report from the Study Group for Risk Factors for Rheumatoid Arthritis. Ann Rheum Dis. 2012;71(5):638–41.
[4] Heutz JW, Toes REM, van der Helm-van Mil AHM. Time sequence of autoimmune processes in the trajectory to rheumatoid arthritis development: what do we know? RMD Open 2025;11(2):e005377.
[5] Li K, Wang M, Zhao L, Liu Y, Zhang X. ACPA-negative rheumatoid arthritis: from immune mechanisms to clinical translation. EBioMedicine 2022;83:104233.
[6] Matthijssen XME, Niemantsverdriet E, Huizinga TWJ, van der Helm-van Mil AHM. Enhanced treatment strategies and distinct disease outcomes among autoantibody-positive and -negative rheumatoid arthritis patients over 25 years: a longitudinal cohort study in the Netherlands. PLoS Med. 2020;17(9):e1003296.
[7] van der Helm-van Mil AH, Verpoort KN, Breedveld FC, Toes RE, Huizinga TW. Antibodies to citrullinated proteins and differences in clinical progression of rheumatoid arthritis. Arthritis Res Ther. 2005;7(5):R949–58.
[8] DA Ton, van Dijk BT, van Steenbergen HW, van der Helm-van Mil AHM. Forefoot inflammation in recent-onset ACPA-positive and ACPA-negative RA: clinically similar, but different in underlying inflamed tissues. RMD Open 2024;10(4):e004722.
[9] Murphy D, Mattey D, Hutchinson D. Anti-citrullinated protein antibody positive rheumatoid arthritis is primarily determined by rheumatoid factor titre and the shared epitope rather than smoking per se. PLoS One 2017;12(7):e0180655.
[10] Too CL, Yahya A, Murad S, Dhaliwal JS, Larsson PT, Muhamad NA, et al. Smoking interacts with HLA-DRB1 shared epitope in the development of anti-citrullinated protein antibody-positive rheumatoid arthritis: results from the Malaysian Epidemiological Investigation of Rheumatoid Arthritis (MyEIRA). Arthritis Res Ther. 2012;14(2):R89.
[11] Heutz JW, Boeren AMP, Claassen S, van Mulligen E, de Jong PHP, van der Helm-van Mil AHM. Shorter reproductive time span and early menopause increase the risk of ACPA-negative inflammatory arthritis in postmenopausal women with clinically suspect arthralgia. Rheumatology (Oxford) 2025;64(6):3451–7.
[12] De Stefano L, D'Onofrio B, Manzo A, Montecucco C, Bugatti S. The genetic, environmental, and immunopathological complexity of autoantibody-negative rheumatoid arthritis. Int J Mol Sci. 2021;22(22):12386.
[13] Verpoort KN, van Gaalen FA, van der Helm-van Mil AH, Schreuder GM, Breedveld FC, Huizinga TW, et al. Association of HLA-DR3 with anti-cyclic citrullinated peptide antibody-negative rheumatoid arthritis. Arthritis Rheum. 2005;52(10):3058–62.
[14] Krijbolder DI, Verstappen M, van Dijk BT, Dakkak YJ, Burgers LE, Boer AC, et al. Intervention with methotrexate in patients with arthralgia at risk of rheumatoid arthritis to reduce the development of persistent arthritis and its disease burden (TREAT EARLIER): a randomised, double-blind, placebo-controlled, proof-of-concept trial. Lancet 2022;400(10348):283–94.
[15] van Steenbergen HW, van Nies JA, Huizinga TW, Bloem JL, Reijnierse M, van der Helm-van Mil AH. Characterising arthralgia in the preclinical phase of rheumatoid arthritis using MRI. Ann Rheum Dis. 2015;74(6):1225–32.
[16] van Nies JA, Brouwer E, van Gaalen FA, Allaart CF, Huizinga TW, Posthumus MD, et al. Improved early identification of arthritis: evaluating the efficacy of Early Arthritis Recognition Clinics. Ann Rheum Dis. 2013;72(8):1295–301.
[17] Østergaard M, Peterfy C, Conaghan P, McQueen F, Bird P, Ejbjerg B, et al. OMERACT Rheumatoid Arthritis Magnetic Resonance Imaging Studies. Core set of MRI acquisitions, joint pathology definitions, and the OMERACT RA-MRI scoring system. J Rheumatol. 2003;30(6):1385–6.
[18] Nieuwenhuis WP, Mangnus L, van Steenbergen HW, Newsum EC, Huizinga TW, Reijnierse M, et al. Older age is associated with more MRI-detected inflammation in hand and foot joints. Rheumatology (Oxford). 2016;55(12):2212–9.
[19] van Beers JJ, Willemze A, Jansen JJ, Engbers GH, Salden M, Raats J, et al. ACPA fine-specificity profiles in early rheumatoid arthritis patients do not correlate with clinical features at baseline or with disease progression. Arthritis Res Ther. 2013;15(5):R140.
[20] Kissel T, Hafkenscheid L, Wesemael TJ, Tamai M, Kawashiri SY, Kawakami A, et al. IgG anti−citrullinated protein antibody variable domain glycosylation increases before the onset of rheumatoid arthritis and stabilizes thereafter: a cross-sectional study encompassing ~ 1,500 samples. Arthritis Rheumatol. 2022;74(7):1147–58.
[21] de Brito Rocha S, Baldo DC, Andrade LEC. Clinical and pathophysiologic relevance of autoantibodies in rheumatoid arthritis. Adv Rheumatol. 2019;59(1):2.
[22] Rönnelid J, Turesson C, Kastbom A. Autoantibodies in rheumatoid arthritis −laboratory and clinical perspectives. Front Immunol. 2021;12:685312.
[23] R Hiwa, Ohmura K, Nakabo S, Terao C, Murakami K, Nakashima R, et al. Only rheumatoid factor-positive subset of anti-citrullinated peptide/protein antibody-negative rheumatoid arthritis may seroconvert to anti-citrullinated peptide/protein antibody-positive. Int J Rheum Dis. 2017;20(6):731–6.
[24] Pertsinidou E, Saevarsdottir S, Manivel VA, Klareskog L, Alfredsson L, Mathsson-Alm L, et al. In early rheumatoid arthritis, anticitrullinated peptide antibodies associate with low number of affected joints and rheumatoid factor associates with systemic inflammation. Ann Rheum Dis. 2024;83(3):277–87.
[25] Fautrel B, Combe B, Rincheval N, Dougados M, Scientific Committee ESPOIR. Level of agreement of the 1987 ACR and 2010 ACR/EULAR rheumatoid arthritis classification criteria: an analysis based on ESPOIR cohort data. Ann Rheum Dis. 2012;71(3):386–9.
[26] Steiner G, Van Hoovels L, Csige D, Gatto M, Iagnocco A, Szekanecz Z. Should ACR/EULAR criteria be revised changing the RF and ACPA scores? Autoimmun Rev. 2024;23(1):103421.
[27] Nordberg LB, Lillegraven S, Aga AB, Sexton J, Olsen IC, Lie E, et al. Comparing the disease course of patients with seronegative and seropositive rheumatoid arthritis fulfilling the 2010 ACR/EULAR classification criteria in a treat-to-target setting: 2-year data from the ARCTIC trial. RMD Open 2018;4(2):e000752.
[28] Wouters F, Niemantsverdriet E, Salioska N, Dorjée AL, Toes REM, van der Helm-van Mil AHM. Do autoantibody-responses mature between presentation with arthralgia suspicious for progression to rheumatoid arthritis and development of clinically apparent inflammatory arthritis? A longitudinal serological study. Ann Rheum Dis. 2021;80(4):540–2.
[29] Boeters DM, Trouw LA, van der Helm-van Mil AHM, van Steenbergen HW. Does information on novel identified autoantibodies contribute to predicting the progression from undifferentiated arthritis to rheumatoid arthritis: a study on anti-CarP antibodies as an example. Arthritis Res Ther. 2018;20(1):94.
[30] Burgers LE, van Steenbergen HW, Ten Brinck RM, Huizinga TW, van der Helm-van Mil AH. Differences in the symptomatic phase preceding ACPA-positive and ACPA-negative RA: a longitudinal study in arthralgia during progression to clinical arthritis. Ann Rheum Dis. 2017;76(10):1751–4.
[31] Rachid Zaim S, Savage AK, Gillespie MA, Castillo JD, Bennett C, Torgerson TR, et al. Serum proteomic signatures before the diagnosis of rheumatoid arthritis: evolving biologic pathways and specific periods of disease development. Arthritis Rheumatol. 2025;77(9):1166–78.
[32] Mesci N, Mesci E, Kandemir EU, Kulcu DG, Celik T. Impact of central sensitization on clinical parameters in patients with rheumatoid arthritis. North Clin Istanb. 2024;11(2):140–6.

[33] Khidir SJH, Krijbolder DI, Glas HK, van Mulligen E, van der Helm-van Mil AHM. Patient burden and joint inflammation during development of RA from arthralgia: is it similar in ACPA-positive and ACPA-negative disease? Rheumatology (Oxford) 2024;63(9):2336–44.
[34] Niemantsverdriet E, Dougados M, Combe B, van der Helm-van Mil AHM. Referring early arthritis patients within 6 weeks versus 12 weeks after symptom onset: an observational cohort study. Lancet Rheumatol. 2020;2(6):e332–8.
[35] Dumoulin QA, Krijbolder DI, Visser K, Lard LR, van der Helm-van Mil AHM. Development of rheumatoid arthritis after methotrexate in anticitrullinated protein antibody-negative people with clinically suspect arthralgia at risk of rheumatoid arthritis: 4-year data from the TREAT EARLIER trial. Lancet Rheumatol. 2024;6(12):e827–36.
[36] Dumoulin QA, van Steenbergen HW, Krijbolder DI, Visser W, Böhringer S, van der Helm – van Mil AHM. OP0324 long-term sustainability of methotrexate intervention in anticitrullinated protein antibody-positive and autoantibody-negative arthralgia patients at increased risk for rheumatoid arthritis on disease development and disease burden; 5 year results from the TREAT EARLIER trial. Ann Rheum Dis. 2025;84:260–1.

Ann Rheum Dis 85 (2026) 1495–1506

Contents lists available at ScienceDirect

Annals of the Rheumatic Diseases

journal homepage: https://www.sciencedirect.com/journal/annals-of-the-rheumatic-diseases

Rheumatoid arthritis

Dual dynamics of persistence and recruitment characterise the ACPA-expressing B cell response in rheumatoid arthritis

Renee van de Wetering[1,*], Shachi Mujumdar[1], Linda M. Slot[1], Arieke S.B. Kampstra[1], Sanne Kroos[1], Rian Schopmeijer[1], Sam Neppelenbroek[1], Cynthia M. Fehres[1], Mirjam H.M. Heemskerk[2], Hans U. Scherer[1], René E.M. Toes[1]

[1] *Department of Rheumatology, Leiden University Medical Center, Leiden, The Netherlands*
[2] *Department of Hematology, Leiden University Medical Center, Leiden, The Netherlands*

ARTICLE INFO

Article history:
Received 21 January 2026
Received in revised form 30 March 2026
Accepted 31 March 2026

ABSTRACT

Objectives: Rheumatoid arthritis, a prototypic autoimmune disease, is characterised by the presence of anticitrullinated protein antibodies (ACPAs). Unlike responses to recall antigens, ACPA-expressing B cells display a continuous phenotype of recent activation, even in patients with sustained clinical remission, indicating that these cells are continuously activated over long periods without 'dying out' or acquiring a resting or anergic phenotype. To elucidate whether this persistent activation reflects ongoing stimulation of the same B cell clones or recruitment of new cells, we longitudinally analysed ACPA B cell dynamics.

Methods: ACPA-expressing B cells were isolated using tetramer-based flow cytometry. One thousand five hundred eighty-one B cell receptor sequences were determined by Smart-Seq2-based immunoglobulin-gene amplification and paired heavy/light-chain Sanger sequencing. Antigen reactivity was validated by producing and testing 414 monoclonal antibodies.

Results: The data obtained show that ACPA repertoires are polyclonal with oligoclonal expansions and skewed variable gene usage, increased lambda-to-kappa ratios, and extensive somatic mutations. Clonal phylogenetic analysis revealed the presence of highly mutated clones persisting over time, coexisting with newly appearing, lowly mutated expanded families. Remarkably, multiple clonal families could be traced over a period of 8 years.

Conclusions: These observations demonstrate that the ACPA-expressing B cell population includes persistent and newly recruited cells that together fuel this ongoing autoimmune response. These data provide insights into B cell autoreactivity and its seemingly exhaustless persistence in a prominent human autoimmune disease by indicating that human autoreactive B cell populations are not static but continuously reshape under chronic antigen stimulation.

INTRODUCTION

Rheumatoid arthritis (RA) is a chronic autoimmune disease characterised by the presence of autoantibodies directed against (self-)proteins that have been post-translationally modified by citrullination. The clinical success of B cell depleting therapies such as rituximab firmly established B cells as critical mediators of disease [1]. However, the intricacies of disease onset and chronicity remain incompletely understood.

*Correspondence to Renee van de Wetering, Department of Rheumatology, Leiden University Medical Center, Leiden, The Netherlands.
E-mail address: r.van_de_wetering@lumc.nl (R. van de Wetering).
Handling editor Josef Smolen.

https://doi.org/10.1016/j.ard.2026.03.033

WHAT IS ALREADY KNOWN ON THIS TOPIC

- The anticitrullinated protein antibodies (ACPAs)-expressing B cell response in Rheumatoid arthritis (RA) is highly active and proliferative, seemingly without becoming quiescent or exhausted, also in patients that are in clinical remission.
- ACPA B cells participate in ongoing autoimmune responses in RA, but the mechanisms sustaining their persistence are unclear.

WHAT THIS STUDY ADDS

- The ACPA B cell population includes both long-lived clones persisting for years and newly recruited B cells.

HOW THIS STUDY MIGHT AFFECT RESEARCH, PRACTICE OR POLICY

- It demonstrates that human autoreactive B cell responses are not static, supporting research into mechanisms sustaining chronic autoimmunity.
- Identifying persistent autoreactive clones and their antigenic drivers may inform the sites involved in their activation and strategies for targeted B cell therapy in RA.

The adaptive immune system generates antibody diversity through assembly of immunoglobulin heavy (IGH) and light-chain (LC) (IGK and IGL) variable (V), diversity (D) and joining (J) genes in the process of V(D)J recombination during B cell development, creating a vast primary, naïve repertoire estimated to comprise up to 3×10^{15} potential B cell receptors (BCRs) [2]. Upon antigen encounter, activated B cells typically undergo somatic hypermutation (SHM) and affinity maturation in germinal centres (GCs), further diversifying the antibody repertoire while selecting for high-affinity variants. In the case of RA, anticitrullinated protein antibodies (ACPAs) are the hallmark antibody response. ACPA-expressing memory B cells express markers indicating proliferation, such as Ki-67, and costimulatory molecules, also in patients with longstanding disease [3–5]. Their BCRs harbour extensive SHM indicative of selection [6]. These findings, together with the variable presence of ACPA-secreting plasmablasts, indicate that the ACPA-expressing B cell response is continuously activated [7]. Remarkably, despite the presumed continuous presence of autoantigen, these B cell responses do not seem to become anergic or extinguish over time. This contrasts with T cell responses under chronic antigen exposure in infection or malignancy, which often become exhausted and functionally anergic, although there is little information on exhaustion of (antigen-specific) autoreactive T cells in RA [8]. At present, the cellular dynamics underlying the persistently activated phenotype of the ACPA-expressing B cell response, or of any autoimmune B cell response exposed to constant antigenic stimulation, remains elusive. In principle, one could expect these responses to stabilise or resolve over time, rather than persist in an active state. Understanding repertoire dynamics could reveal whether RA pathogenesis is driven by the continuous recruitment and activation of new autoreactive B cell clones, or by the persistent expansion and maintenance of established autoreactive clones.

Previous analysis of the secreted ACPA-IgG revealed that the autoreactive repertoire is highly diverse yet dominated by a few abundant clones [9]. Here, we set out to characterise the stability and dynamics of the cellular response by conducting a longitudinal analysis of ACPA-BCR repertoires in established patients with RA. Through paired heavy chain (HC) and LC BCR sequencing of single-cell sorted ACPA-expressing B cells from 10 individuals across 3 timepoints spanning 1 year, as well as previously collected data from several patients, we observed a polyclonal repertoire with oligoclonal expansions and demonstrated both clonal persistence and continuous recruitment of ACPA-expressing B cells into the autoreactive repertoire.

METHODS

Primary material

Patient blood samples were obtained after obtaining written informed consent from patients diagnosed with ACPA-positive RA visiting the outpatient clinic of the Department of Rheumatology at Leiden University Medical Center (LUMC), Leiden, The Netherlands. Patients treated with B cell–modifying agents were excluded. All patient information can be found in Supplementary Table S1. This study was approved by the ethical review board of the LUMC (protocol P17.151). Patients were selected to represent both high and low circulating numbers of ACPA-expressing B cells. Patients or the public were not involved in the design of the study.

Cell sorting

Peripheral blood mononuclear cells (PBMCs) were isolated from 45 mL of peripheral blood by Ficoll-Paque gradient centrifugation. Double-positive cyclic citrullinated peptide (CCP)2-tetramer-binding B cells were isolated as single cells from PBMCs using a fluorescence-activated cell sorter (FACS Aria, BD Biosciences) using a 100-µm nozzle. The antibody panel consisted of a violet LIVE/DEAD cell stain kit (ThermoFisher Scientific), anti-CD3 Pacific Blue (UCHT1, BD Biosciences), anti-CD14 Pacific Blue (M5E2, BD Biosciences), anti-CD19 APC-Cy7 (SJ25C1, BD Biosciences), anti-CD20 AF700 (2H7, Biolegend), anti-CD27 PE-Cy7 (M-T271, BD Biosciences), anti-IgG BV510 (G18-145, BD Biosciences), anti-IgD FITC (IA6-2, BD Biosciences), and antigen-tetramers (CCP2-streptavidin-BV605, CCP2-streptavidin-APC, CArgP2-extravidin-PE). All antibodies and their used dilutions are listed in Supplementary Table S2.

BCR sequencing

For the workup from sorted cells to polymerase chain reaction (PCR) products, the Smart-Seq2 protocol was used [10]. Single B cells were sorted into a PCR plate containing an mRNA lysis mix consisting of Triton X-100 (0.2% vol/vol), recombinant RNAse inhibitor (Takara Bio), dNTPs (2.5 mM, Thermo Scientific), and oligo dT30VN primer (2.5 µM). After the sort, plates were spun down before adding cDNA mix consisting of nuclease-free water, SMARTScribe Reverse Transcriptase (Takara Bio), RNAse inhibitor (Takara Bio), DTT (20 mM, Takara Bio), 5× First-Strand Buffer (Takara Bio), Betaine (1.8 M), and template switching oligo primer (6 µM). cDNA was preamplified using the KAPA HiFi HotSTart ReadyMix (KAPA Biosystems) and an ISPCR oligo. Products were then purified using AMPure XP beads (Beckman Coulter) at a 0.8:1 ratio before BCR-specific amplification using the Anchoring Reverse Transcription of Immunoglobulin Sequences and Amplification by Nested (ARTISAN) PCR as described previously [11]. HC and LC PCR products were sequenced by Sanger sequencing using chain- and sometimes leader-specific primers (provided in Supplementary Table S3) on Applied Biosystems 96-capillary (ABI3730) systems (LGTC Facility; Macrogen). Productive, full-length sequences were processed with IMGT/(High)V-QUEST [12]. The isotype of each BCR was determined by index sort analysis and/

or successful amplification with its respective chain-specific primers.

BCR sequences from ACPA-expressing B cells characterised in our prior study were included in this analysis [13]. Briefly, ACPA specificity was confirmed by culturing sorted single B cells and testing culture supernatants for reactivity against citrullinated antigens by ELISA. Although the protocol from cultured cells to cDNA synthesis differed from that used for newly sorted cells in this study, BCR amplification, sequencing, and data analysis were performed using the same approach.

Identification of B cell clonotypes

B cell clones were defined as sequences containing the same IGHV gene, IGHJ gene, and 80% nucleotide identity (based on the Hamming distance determined in our dataset) in Ig HC CDR3s of the same length using the Change-O Python package [14]. Analyses were also performed using even more stringent clone definitions with 85% and 90% nucleotide sequence similarity, with no substantial differences observed. All further analyses were performed in R (R version 4.4.3, http://www.r-project.org).

Monoclonal antibody production

Human monoclonal antibodies (mAbs) were either generated using plasmid cloning ('full-scale') as described previously [15], or with the Rapid Assembly, Transfection and Production of Immunoglobulins (RATP-Ig) method [16]. For full-scale productions, full-length BCR sequences retrieved from the sequencing of the ARTISAN PCR products were cloned into pcDNA3.1 (+) expression vector and transfected into Freestyle 293-F cells (Gibco) using Opti-MEM (Gibco) medium and 293Fectin (Thermo Fisher). Supernatants were harvested 5 to 6 days after transfection. For the RATP-Ig method, which entails the production of recombinant HC and LC-expressing linear DNA cassettes that are directly transfected into HEK cells, we adapted the original plasmid cassettes kindly provided by Daniel Douek (National Institutes of Health) to be compatible with our ARTISAN PCR products. Amplicons of these adapted plasmids were first synthesised by PCR using Phusion Flash High-Fidelity PCR Master Mix (ThermoFisher), run on a 1% agarose gel and extracted using the NucleoSpin Gel and PCR Clean-up kit (Macherey-Nagel). These products were digested with DpnI (New England Biolabs) and amplified further to create clean stocks for use in the following assemblies. For all assemblies (IGHG1, IGHA1/IGHA2, IGHM, IGK, and IGL), we combined (i) a linear DNA fragment containing a cytomegalovirus (CMV) promotor with overlapping 3′ ends including the template switching oligo sequence with (ii) our linear HC or LC ARTISAN PCR product, and (iii) a linear DNA fragment containing the remainder of the matching constant region and a poly-A tail sequence. These ligated fragments were assembled into linear expression cassettes using NEBuilder HiFi DNA Assembly Mastermix (New England BioLabs). If no gel extraction was described, PCR products were purified using AMPure XP Beads at a 1:1 ratio. Amplified HC and LC cassettes were cotransfected into HEK FreestyleTM 293-F cells following a scaled-down protocol of our full transfection conditions, in 6/12/24/28/96-well plates depending on the specific experiment. Cells were cultured at 37°C and 8% CO_2 with shaking (varying rotation speeds depending on the plate size) for 5 to 6 days before supernatants were clarified by centrifugation and harvested. For mAb production, representative members of each clonal family were prioritised, and multiple mAbs from the same clonotypes showed consistent ELISA profiles, and thus specificity was inferred for all members of that clonal family.

Antibody measurements by ELISA

Monoclonal antibodies

Total IgG, IgA, and IgM were assessed by enzyme-linked immunosorbent assay (ELISA) (A80-100, 102, and 104, Bethyl Laboratories). For the in-house peptide ELISAs, Corning 384 well microplates (3700, Sigma Aldrich) were coated overnight with streptavidin (Invitrogen) and incubated with biotinylated modified (Citrulline [Cit], Homocitrulline [HCit], and Acetyllysine [Ace]), or unmodified (Arginine [Arg], Lysine [Lys]) CXP2 (Patent EP2071335) synthesised at the LUMC facility, with X being the modification, for example, CCP2 for cyclic citrullinated peptide 2 and CArgP2 for its Arg control. The samples (Freestyle 293 transfected supernatant) were preincubated for 1 h at a 1:1 dilution with an horseradish peroxidase (HRP)-conjugated Goat antihuman IgG + IgM + IgA HC and LC antibody (DAKO) before addition to the plate. Subsequently, plates were incubated overnight before detection with ABTS the following morning (cross-linking ELISA). Samples with an optical density (OD) value higher than 2 times the blank were considered positive. In cases where the total isotype ELISA was negative and the antigen-specific cross-linking ELISA was positive (the latter being more sensitive), the mAb was marked as positive for the posttranslational modification (PTM).

Serum

ACPA (aU/mL) were measured in an in-house ELISA, in which 384-well microplates were coated with streptavidin and incubated with biotinylated CCP2 or its Arg control (CArgP2). Serum samples were serially diluted (1:50, 1:200, 1:400, and 1:800) in phosphate buffered saline (PBS), 1% bovine serum albumin (BSA), 0.05% Tween, along with a serially diluted in-house serum control used for a standard curve, and incubated for 1 hour at room temperature. After washing and an hour incubation with Rabbit antihuman IgG-HRP (DAKO), samples were incubated with ABTS substrate.

Rheumatoid Factor IU/mL were measured in an in-house ELISA, where 384 well microplates were coated with antihuman IgG (Jackson Immunoresearch) at 10 μg/mL at 4° overnight. After blocking with PBS 1% BSA, samples were added at a 1:100 dilution in PBS with 1% BSA and 0.05% Tween, together with a serial dilution of the N/T rheumatology control SL/2 (200 IU/mL Siemens) to create a standard curve. HRP-labelled Goat antihuman IgM (Millipore AP114P, 10 mg/mL) was used for the detection of the RF-IgM antibodies in combination with ABTS substrate. As the highest value for the standard used is 200 IU/mL, samples at a similar or higher OD value than the highest concentration of our standard are indicated with ≥200 in the patient characteristics in Supplementary Table S1.

Statistical analysis

Statistical analyses were performed using R. Where applicable, details about the statistical tests used are indicated in the figure legends. Given the limited sample size for some donors and the varying sequence quality control success rates across individuals (Supplementary Fig 1), we deemed our data unfit to perform formal statistical analyses of repertoire diversity and stability, such as Shannon or Gini-Simpson Diversity indexes.

To assess the likelihood that certain clones were only detected at 1 timepoint, we calculated the hypergeometric probability under the null hypothesis of random sampling across timepoints:

$$P(X \geq n) = C(K, n) / C(N, n)$$

Where,

N = total sequences analysed
K = total sequences at a specific timepoint
n = clone size
X = number of clone sequences found at that timepoint

RESULTS

Longitudinal isolation and sequencing of ACPA-expressing B cells

We collected peripheral blood from 14 individuals with established, ACPA-positive RA at 3 sequential timepoints, spaced 6 months apart (Supplementary Table S1). Patient selection excluded treatment with B cell–modifying therapies during the study time. Four donors were lost to follow-up and excluded from data analysis. Across the timepoints of the other 10 donors, 3559 single B cells were sorted using CCP2-tetramers, of which 1581 yielded high-quality HC sequences suitable for downstream analysis (Supplementary Fig S1). Interpatient variability in the number of cells sorted was substantial, ranging from 0 to 479 cells per donor per timepoint, reflecting the heterogeneous nature of the circulating ACPA-expressing B cell response across patients.

Clonal definitions and verification of ACPA-reactivity

To obtain first insights into temporal stability, we assessed clonal relationships among sequences. B cell clonal lineages were defined as sharing identical IGHV and IGHJ genes and having equal CDR3 lengths with ≥80% nucleotide identity [14]. Sequences were categorised as following: (i) *singleton*, a unique BCR sequence observed at a single timepoint, (ii) *nonrecurring clone*, clonally related sequences detected at only 1 timepoint, (iii) *recurring clone*, clonally related sequences observed at 2 timepoints, and (iv) *persistent clone*, clonally related sequences detected at all 3 timepoints. Across all donors, at least 50% of sequences were singletons (Fig 1A,B). However, persistent clones were also detected, predominantly in patients from whom higher cell numbers were isolated (Fig 1C,D). Most B cells in the B cell population enriched for ACPA-expressing B cells were IgG$^+$ (subclass distribution: IgG1 > IgG2 > IgG4 > IgG3)

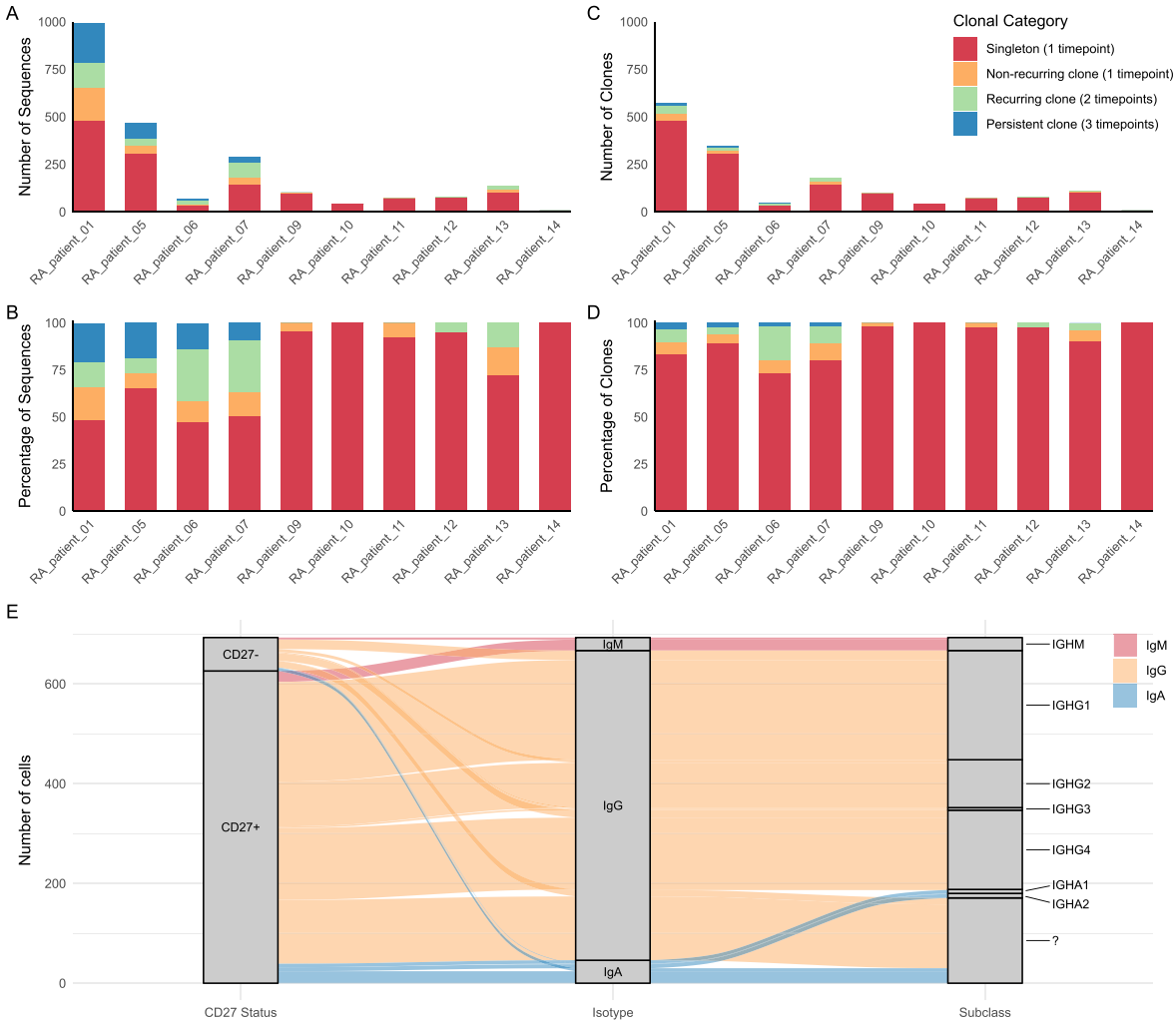

Figure 1. BCR sequences and clonal families of single-cell sorted CCP2-tetramer$^{+\,+}$ cells. (A-D) Numbers and proportions of sequences and BCR Vh unique clones per patient, coloured according to their presence across timepoints. (E) CD27 FACS status, PCR-determined isotype, and sequencing subclass assignments for all verified ACPA-reactive sequences. ACPA, anticitrullinated protein antibodies; BCR, B cell receptor; CCP, cyclic citrullinated peptide; IgG/A/M, immunoglobulin G, A or M; PCR, polymerase chain reaction; RA, rheumatoid arthritis; VH, heavy chain variable regio.

and CD27$^+$, consistent with a switched memory B cell phenotype (Fig 1E). We anticipated the possibility that not all B cells in this population were citrullinated-antigen-reactive. Therefore, we validated antigen specificity using a high-throughput mAb production pipeline (RATP-Ig [16]). Out of 576 selected sequences, 414 (72%) were successfully expressed as mAbs. The majority of clonally related IgG and IgA sequences tested positive on the citrullinated antigen ELISA (Supplementary Fig S2). A large part of the IgM sequences, however, did not, with one-third recognising streptavidin used to link the peptides and fluorochromes in the tetrameric reagent. Based on these data, further analyses were restricted to validated ACPA sequences and their clonal families. To enable robust longitudinal analysis, we also established a minimum threshold of sequences per patient. Accordingly, subsequent analysis focused on the 4 patients from whom ≥15 ACPA-validated sequences were available at each of the 3 timepoints (Fig 2A).

General characteristics of ACPA-expressing BCRs

For downstream analyses focusing on repertoire features, clonally related sequences were collapsed so that each clone was represented once. In healthy repertoires, the average κ/λ ratio is 2:1. As κ LCs are rearranged before λ chains during B cell development, lambda skewing can suggest multiple rounds of receptor editing to escape autoreactive κ configurations [17]. Overall, ACPA-expressing B cells were enriched in λ usage with a near equal κ/λ distribution (Fig 2B, κ 55.3% vs λ 44.7%) rather than the 2:1 ratio observed in healthy repertoires, consistent with our previous findings [13,18]. The average CDR3 length in our dataset was 15.7 amino acids (Fig 2C), comparable with the general human average CDR3 length of ∼15 aa [17,19]. We next analysed V-gene usage patterns, as skewed utilisation of particular V-gene segments can reflect structural predispositions for recognition of certain antigens [20]. These analyses revealed enrichment of specific variable gene segments among BCRs of ACPA-expressing B cells. More specifically, HC genes IGHV3-49, IGHV4-39, and IGHV7-4-1 showed statistically significant overrepresentation in this dataset (Fig 2D). LC usage was similarly skewed, with overrepresentation of IGKV4-1, IGLV1-44, and IGLV6-57 (Fig 2E). Together, these findings indicate that BCRs of ACPA-expressing B cells are characterised by an increased λ-usage compared with average repertoires, and biased V-gene segment selection, consistent with selective pressures shaping B cell repertoires.

Temporal dynamics of clonal families over 1 year

We next focused on the temporal dynamics within clonal families to obtain insight into the changes of the ACPA-expressing B cell repertoire over time. Patient 1 contributed the largest dataset, with 992 sorted cells (686 analysed: 154 at T = 0, 200 at 6 months, and 332 at 1 year). In this patient, we found 14 clones present at each of the 3 timepoints (Fig 3A). Clonal tree

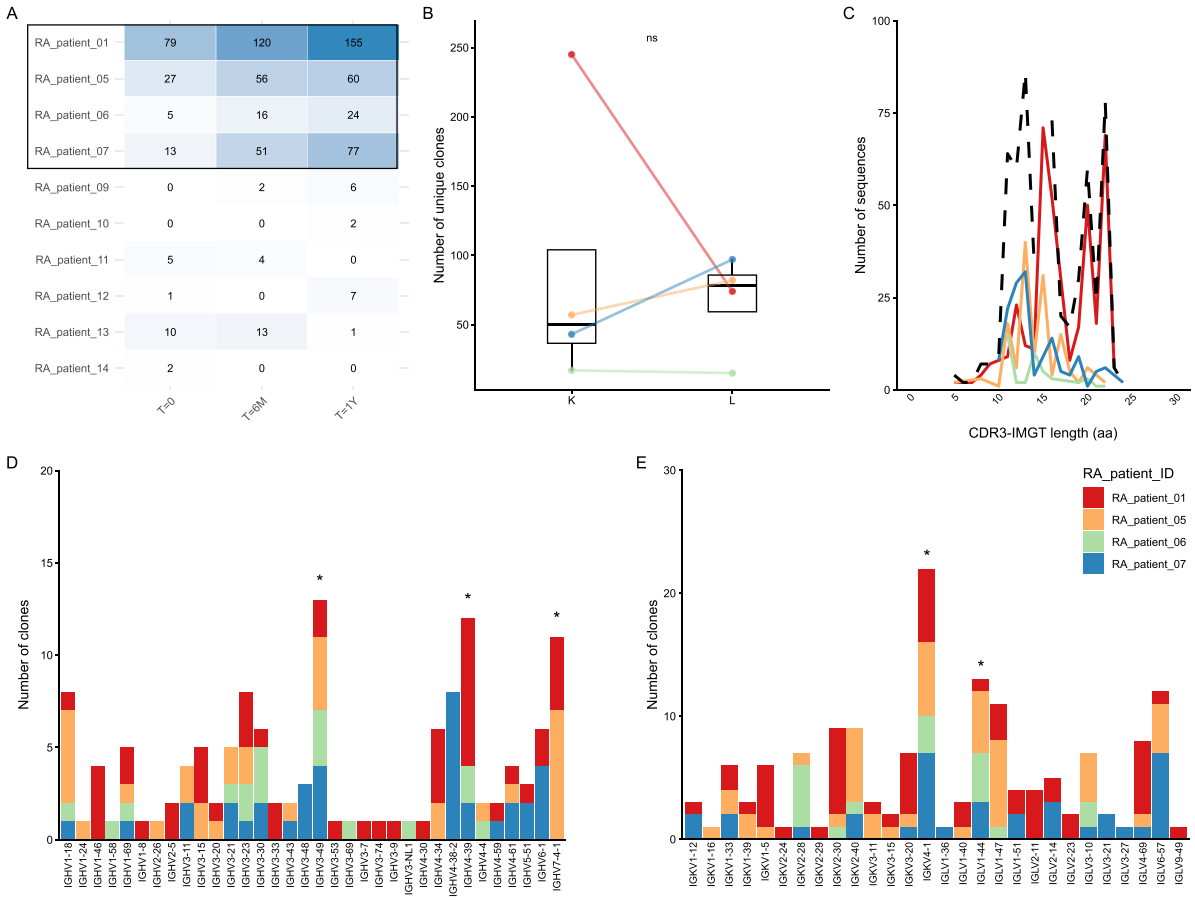

Figure 2. General characteristics of BCRs of ACPA-expressing B cells. (A) Number of cells per patient per timepoint after quality assessment and verification of ACPA-reactivity. (B) κ and λ light-chain usage across donors (Wilcoxon signed-rank test; $P = .313$). (C) Distribution of heavy chain CDR3 lengths across donors. (D,E) IGHV and IGHK/IGKL gene usage across donors, with statistically significant differences indicated by asterisks (Chi-squared test with Bonferroni correction; $P \leq .05$).

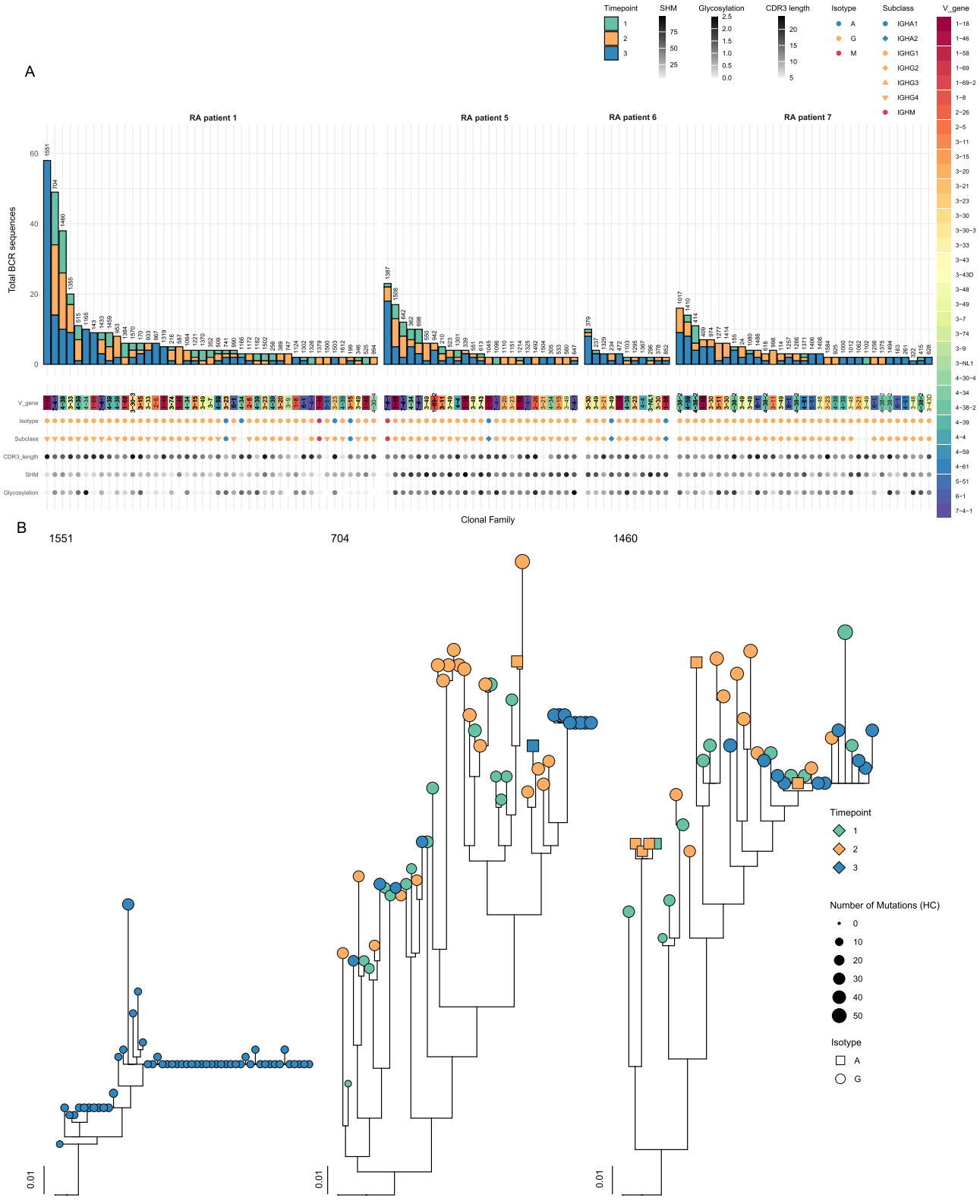

Figure 3. Clonal families and their characteristics across patients and timepoints. (A) Clonal families (singletons not shown) verified as citrulline-reactive across individual patients, grouped per clonal family and coloured per timepoint. For each clonal family, the majority or average heavy chain sequence features are shown in metadata below the clonal family bars, including IGHV gene usage, isotype and subclass, CDR3 length, somatic hypermutation load, and the number of N-glycosylation sites within the variable domain. Analyses were also performed using even more stringent clone definitions with 85% and 90% nucleotide sequence similarity, with no substantial differences observed. (B) Phylogenetic trees of selected clonal families from patient 1 with RA, indicating the timepoint of each heavy chain sequence, isotype, and the number of mutations relative to the inferred common ancestor. The inferred common ancestor is located on the left, and the length of each branch proportionally matches the number of mutations present between 2 antibody nodes. (C) Average number of nucleotide mutations and (D) number of N-glycosylation sites for all heavy chain sequences within a clonal family, per patient. SHM, somatic hypermutation.

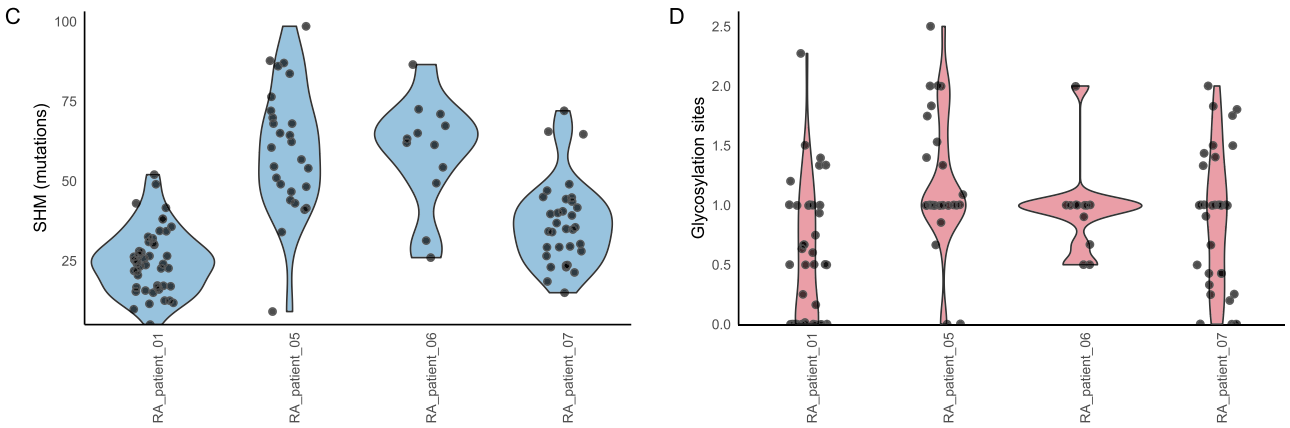

Figure 3. Continued.

reconstruction demonstrated nonlinear evolutionary patterns within these clonal families, with sequences from earlier timepoints occasionally exhibiting greater mutational distances than variants found at later timepoints (Fig 3B). Next to IgG, IgM and IgA BCR sequences could be detected in multiple clades of sizeable clonal families (examples in Fig 3B). The average number of somatic mutations per clone was 25.9 in this patient (Fig 3C). Consistent with previous observations, numerous N-linked glycosylation sites were identified in the HC BCRs of ACPA-expressing B cells (Fig 3D). Such sites are associated with disease prognosis and modified BCR-signalling [21,22]. Intriguingly, 1 dominant clone in patient 1 was detected exclusively at timepoint 3. Given its representation by 58 sequences (8.5% of the total), the likelihood that this family would have remained undetected at earlier timepoints within the dataset is exceedingly low (hypergeometric probability = 5×10^{-19}), suggesting emergence between timepoints 2 and 3. In line with the notion that this clone was recently expanded, phylogenetic tree analysis revealed that this clone harboured fewer SHMs compared with established persistent lineages (Fig 3B). This dominant clone was also the main exception in terms of CD20-expression, as a substantial proportion was CD20-negative (41%), suggesting the presence of recently activated plasmablasts (Supplementary Fig S3). Similarly, several other clones within this patient were only detected at the third timepoint, pointing towards a broad new recruitment of autoreactive B cells into the response.

To verify these observations, we analysed data from patients 5, 6, and 7 as these patients reached our cutoff of ≥15 verified ACPA-reactive BCR sequences per timepoint. Also, in these patients, evidence of clonal stability was observed within the ACPA-expressing B cell population, with both persistent and recurring clones detected in all 3 individuals. In general, the average number of somatic mutations per clone in these 3 donors was higher than in patient 1 (52.0 vs 25.9 in patient 1, Fig 3C), as was the average number of HC N-linked glycosylation sites (0.99 vs 0.56 in patient 1, Fig 3D). These findings demonstrate that while certain clonal lineages persist over extended periods, new clones continue to emerge throughout the disease course.

Long-term persistence of autoreactive B cell clones for years

Patients 5 and 7 also participated in a study analysing BCRs of ACPA-expressing B cells ~6 years before the start of the current study [13]. Remarkably, when analysing the datasets together, we identified clonal families spanning the entire timespan (Fig 4, Supplementary Fig S5A). Several IgG sequences recovered from these earlier samples of patients 5 and 7 revealed both clones that remained identical and others that had accumulated further mutations (Supplementary Fig S5B), indicating that certain autoreactive lineages can simultaneously maintain stability and continue to evolve over time. Notably, the largest persistent clone in patient 5 (clone 1387, 7 nt/5 aa mutations in most members) was of the IgM isotype and members of that same BCR clone were also detected in the earlier sequencing data, demonstrating long-term persistence of these clonal B cells. Together, these data reveal that ACPA-expressing clonal families can persist and evolve over many years, whereas new clones continue to arise throughout disease, highlighting the dual dynamics of stability and renewal within the autoreactive B cell repertoire.

DISCUSSION

The clinical response to B cell–targeting therapies highlights the importance of B cells in many human autoimmune diseases. This is also the case for ACPA$^+$ RA, a common autoimmune disease that harbours a continuously active, proliferative autoreactive B cell response to a plethora of posttranslationally modified (self-)antigens [3]. In this longitudinal study, we show that the pool of ACPA-expressing B cells in the circulation of people with RA is maintained through dual dynamics: the recruitment of novel autoreactive B cell clones into the autoimmune response, and the long-term persistence of established clonal families. To our knowledge, our findings provide the first evidence that autoreactive B cell responses in humans are not static but continuously reshape by evolving longstanding, as well as newly occurring, clonal families. A deeper understanding of these dynamics may inform the development of next-generation therapies, including antigen-specific B cell depletion strategies or interventions targeting the metabolic fitness that sustains autoreactive clones.

We have previously described that ACPA-expressing B cell responses exhibit a highly active and proliferative phenotype, as ACPA-expressing B cells in blood abundantly display markers of activation and proliferation [3–5]. The phenotype of ACPA-expressing B cells is therefore reminiscent of pathogen-reactive B cell responses shortly (7-28 days) after booster vaccination and/or infection. However, following this initial response, virus-reactive B cell responses typically adopt a quiescent phenotype as a consequence of a strong reduction of antigen expression due to antigen clearance. By analogy, we consider it most likely that B cell responses to autoantigens occur under

distinctive conditions, and that the persistent proliferative phenotype of ACPA-expressing B cells reflects a continuous encounter with citrullinated (self-)antigens. The observation that the continuous proliferative phenotype of the ACPA B cell response does not appear to lead to B cell exhaustion is intriguing. In fact, we now show a striking persistence of multiple ACPA-expressing B cell clones and clonal families, with some detected over a timespan of up to 8 years. Our observation of persistent ACPA-expressing clones suggests that, in established disease, these B cells are not subjected to effective peripheral inhibitory checkpoints and maintain an activated status. This contrasts with T cells, where prolonged antigen exposure during chronic infection or malignancy frequently drives cells towards exhaustion [23–26]. Importantly, contrary to T cells, no analogous exhaustion phenotype for human B cells has been defined [27,28]. Inhibitory markers previously proposed to be indicators of B cell exhaustion have since been reassigned as defining features of the double negative 2 (DN2) B cell subset—a population also expanded in autoimmune diseases and following SARS-CoV-2 infection, of which the exact function is yet unknown [29–33]. Together, this implies that *bona fide* B cell exhaustion may not occur in (autoreactive) B cell populations.

In RA, the anatomical sites and quantity of citrullinated antigen exposure that shape ACPA-expressing B cell fate decisions remain unclear. To the best of our knowledge, this is also not known for other human autoimmune diseases, as no antigen-specific autoreactive B cell responses have previously been studied for BCR repertoire dynamics in time. Nonetheless, the presumed persistent antigenic stimulation thought to be present in RA creates an immunological environment that may not be directly comparable to other biological contexts such as those present after infection. Pathogen-specific B cell responses, both vaccine-induced and acute, have been extensively characterised but often represent acute, local, and time-limited immune challenges that are fundamentally different from chronic autoimmune responses [34–36]. Likewise, most chronic viruses, such as Epstein-Barr virus or Varicella Zoster Virus, 'hide' and antigen persists within restricted cellular reservoirs and defined locations after establishment. Nonetheless, although BCR repertoires from chronic infections may not provide a direct comparator to the autoimmune disease setting, it would be informative to analyse these responses antigen specifically, as such analyses have seldom been performed [37–39]. This is particularly important because the dynamics of antigen-specific responses will likely be obscured within (longitudinal) total BCR repertoire studies, especially in the context of ongoing inflammation in individuals with chronic infections or autoimmune diseases [17,37–45].

Despite the fundamental differences in antigenic context, findings from antigen-specific BCR repertoire studies of virus-specific B cells, such as those directed against influenza and SARS-CoV-2, appear unexpectedly similar to our observations. Hemagglutinin-specific clones following influenza vaccination can be repeatedly reactivated, with clonotype lineages remaining detectable for months during the recall response, whereas the repertoire continues to mutate and reshape to recognise novel epitopes [31,46,47]. Some SARS-CoV-2-reactive B cells also seem to remain active after infection and vaccination, with members of shared progenitor clones continuing to diversify over the course of months or even 1 year after infection, presumably driven by sustained antigen retention within GCs [35,48–51]. In addition, a study on vaccinia-specific B cells in the spleen decades after vaccination suggested that affinity-driven selection of the BCR repertoire can persist far beyond the acute

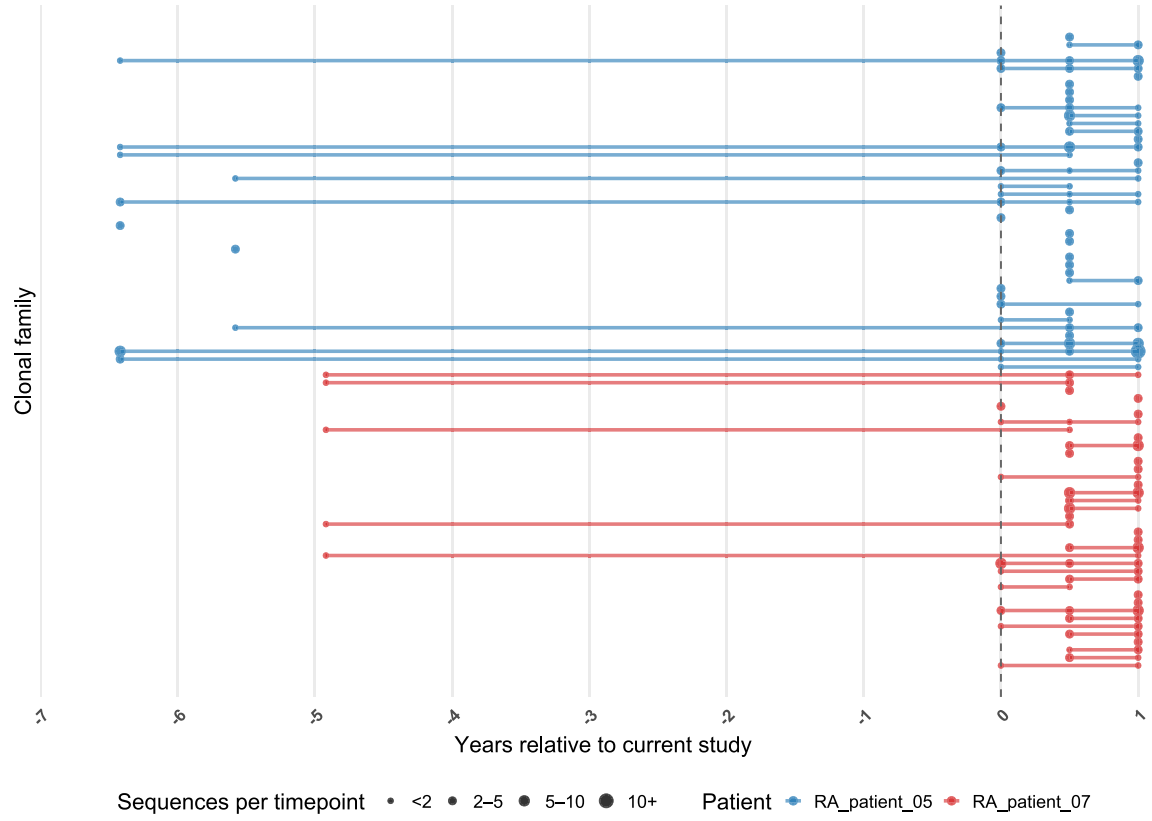

Figure 4. Clones detected across years. The number of BCR Vh sequences in a clonal family detected at each timepoint across years, relative to the start of the current study (T = 1 is 0 years). For patient 5 (blue), sequences were collected at 2 earlier timepoints (6.5 and 5.5 years before the start of this study), and for patient 7 (red), there was 1 timepoint 5 years prior. For both patients, very few BCR sequences were obtained at the earlier timepoints.

response [52]. Collectively, these observations indicate that chronic (autoimmune) B cell responses share features with 'acute' pathogen-directed responses, as in both cases, evolving clonal families can persist after repeated antigen exposure. In 'acute' pathogen-directed responses, this phenomenon has been attributed to the persistence of small quantities of antigen, such as antigen retained on follicular dendritic cells in GCs, which appears sufficient to drive continuous BCR maturation [53,54]. Interestingly, this notion might also explain another feature both responses have in common: the continued emergence of new clonal families, which in viral infections is thought to result from the recruitment of naïve B cells into GCs in tissues or lymph nodes [55]. By analogy, similar processes may contribute to the ongoing diversification of the ACPA-expressing B cell response, albeit potentially operating in distinct anatomical sites, such as the synovial tissue [56].

Together, these observations raise the possibility that (other) principles established for pathogen-specific recall responses may also apply to autoreactive PTM-directed B cell responses. ACPA-expressing B cells have previously been described as promiscuous in antigen recognition and broadly cross-reactive towards several PTMs, such as homocitrulline (HCit) and acetyllysine (Ace), on a broad range of protein backbones [15,57,58]. Conceptually, this could parallel features of original antigenic sin, in which early-imprinted B cell lineages dominate subsequent antigen-specific responses until new antigenic variants diverge sufficiently to recruit additional naïve or memory B cells [47,59]. Translating this framework to autoimmunity, a primary breach of tolerance to a single PTM on a specific protein backbone might seed long-lived progenitor lineages that persist and expand, whereas newly arising clones may reflect recruitment in response to distinct PTM-modified epitopes encountered over time [60]. Consistent with this idea, we identified numerous clones with exclusive citrullinated-antigen-reactivity, and larger clonal families showed a trend towards reduced cross-reactivity (Supplementary Fig S6A,B), suggesting that clonal expansion may be associated with highly focused antigen recognition. However, our assessment of PTM-antigen recognition was limited to 3 modifications expressed on the same peptide backbone, and we cannot exclude the possibility that rare cross-reactive branches within clonal families existed that were not captured in our analysis, as reported in other studies [57,58,61]. In this context, the persistence of IgM clone 1387 in patient 5 over multiple years without isotype switching may similarly indicate early clonal expansion during disease onset, followed by its progressive outcompetition by higher-affinity ACPA-expressing B cells and their secreted antibodies. Although this interpretation is speculative given the current data, it would mimic pathways thought to be operative in the prevention of Rhesus D antagonism in which Rhesus-negative women are given high-affinity anti-D IgG to prevent the induction or propagation of anti-D B cell responses.

Supporting the notion of ongoing recruitment of clones, we detected both mutated and unmutated ACPA-expressing B cells, including 3 naïve (IgD^+CD27^-) B cells expressing germline-rearranged IgM sequences, 2 of which were cross-reactive with HCit. This also demonstrates that B cells can have intrinsic citrullinated-antigen-reactivity in the absence of somatic mutations and potentially give rise to new clonal lineages. Alternatively, new autoreactive lineages can emerge through epitope spreading [62]. This is, however, difficult to show as we do not know which (PTM-)proteins may have shaped the ACPA-reactive clonotypes. Together, our findings suggest that on the BCR level, ACPA-expressing B cell responses share key features with pathogen-specific recall responses, including the coexistence of persistent, continuously evolving clonal lineages alongside ongoing recruitment of newly arising clones with potentially distinct specificities.

Our study has several limitations. It was designed to reflect the heterogeneity of the RA population by including both donors with typically low ACPA-expressing B cell frequencies and selected donors with abundant autoreactive B cells. The infrequency of ACPA-expressing B cells in most patients inherently limits sequencing depth and complicates distinguishing biological variation from potential sampling effects. The trend towards greater clonal persistence in donors with higher cell numbers (Fig 1C,D) may reflect the technical challenges in repertoire coverage for donors with lower ACPA-expressing B cell frequencies in blood [40,41,63]. Therefore, we included only patients with ≥15 verified citrullinated-antigen-reactive BCR sequences per timepoint in the longitudinal clonal analyses. Nonetheless, when we studied the overall repertoire characteristics and included sequences from all patients, this remained consistent with those of the 4 individuals analysed in detail (Supplementary Fig S3). To maximise the number of antigen-specific B cells per donor, we did not sequence total B cell repertoires as comparators, precluding direct assessment of ACPA-specific repertoire features against the broader polyclonal background. Our stringent verification pipeline ensured that analysed sequences represent *bona fide* Cit-reactive clones, albeit at the cost of total sequence yield. As 72% of selected sequences were successfully expressed as mAb, expanded clones were more likely to yield successful mAb production. Therefore, the dataset may be biased towards larger families, and we refrained from direct comparisons between singletons and expanded clones, although investigating in detail why certain clones expand successfully while others remain infrequent could reveal intrinsic features that confer proliferative or survival advantages to specific autoreactive B cell lineages. Similarly, our analysis focused on circulating PBMCs and excluded synovial or lymphoid tissue B cells, where local ACPA-expressing populations may reside [9,56,64]. We also cannot exclude that a newly detected clone at a certain timepoint was an established clone that egressed from a target tissue before detection. In addition, our antigen-specific staining approach omitted fixation and permeabilisation to preserve mRNA integrity for sequencing, potentially limiting detection of ACPA-producing plasmablasts or plasma cells with low surface BCR expression [7].

In conclusion, by combining stringent validation of Cit specificity with longitudinal repertoire analysis, this study offers novel insights into the clonal behaviour of ACPA-expressing B cells in RA. Our data demonstrate that autoreactive B cell populations are not static as they continuously reshape under chronic antigen stimulation. Autoreactive B cell populations not only persist over time but also recruit new B cell clones that fuel the response. These data provide insights into the biology of B cell autoreactivity and its remarkable, seemingly exhaustless persistence in a prominent human autoimmune disease.

Acknowledgements

We thank Natasja Dolezal, Robert Cordfunke, and Dr. J.W. Drijfhout (Leiden University Medical Center, Leiden) for providing all peptides. Flow cytometry was performed at the Flow Cytometry Core Facility of the Leiden University Medical Center. We also thank Dr. Daniel Douek and his team at the NIH for providing the starting materials and detailed protocols for the RATP-Ig. We also thank Eva Maria Stork for the discussion and

Dr. Yasuo Nagafuchi for input on clonal analysis and coding logic.

Contributors

RvdW contributed to conceptualisation, methodology, software, validation, formal analysis, investigation, resources, data curation, writing—original draft, writing—review & editing, visualisation, and project administration. SM contributed to investigation, validation, and writing—review & editing. LMS contributed to conceptualisation, investigation, resources, writing—original draft, writing—review & editing, and supervision. ASBK contributed to investigation and writing—review & editing. SK contributed to investigation and writing—review & editing. RS contributed to investigation and writing—review & editing. SN contributed to conceptualisation, data curation, and writing—review & editing. CMF contributed to conceptualisation, methodology, and writing—review & editing, supervision. MHMH contributed to writing—review & editing and supervision. HUS contributed to conceptualisation, resources, writing—review & editing, and supervision. REMT contributed to conceptualisation, methodology, writing—original draft, writing—review & editing, supervision, and funding acquisition.

Funding

REMT is the recipient of a European Research Council (ERC) Advanced Grant (AdG2019-884796). HUS is the recipient of a NWO-ZonMW VIDI grant (project 09150172010067), a NWO-ZonMW OffRoad Grant (project 451001012), and received support from the Dutch Arthritis Foundation (projects 15-2-402 and 18-1-205, as well as LLP-5). This work was cosupported by funding from the Dutch Arthritis Society and co-funded by the PPP Allowance made available by Health Holland, Top Sector Life Sciences & Health, to the Association of Collaborating Health Foundations (SGF) to stimulate public-private partnerships (LSHM22042-SGF).

Competing interests

All authors declare they have no competing interests.

Patient consent for publication

Not applicable.

Ethics approval

This study was approved by the ethical review board of the Leiden University Medical Center (protocol number P17.151).

Provenance and peer review

Not commissioned; externally peer reviewed.

Data availability statement

All data presented in the article are available upon reasonable request. All data relevant to the study are included in the article or uploaded as supplementary information.

Supplementary materials

Supplementary material associated with this article can be found in the online version at doi:10.1016/j.ard.2026.03.033.

Orcid

Renee van de Wetering: http://orcid.org/0000-0001-5330-5113
Linda M. Slot: http://orcid.org/0000-0002-7993-5831
Arieke S.B. Kampstra: http://orcid.org/0000-0001-8840-7443
Sanne Kroos: http://orcid.org/0000-0001-8900-1285
Rian Schopmeijer: http://orcid.org/0009-0009-1517-8307
Sam Neppelenbroek: http://orcid.org/0000-0002-9582-2837
Cynthia M. Fehres: http://orcid.org/0000-0001-9020-1591
Mirjam H.M. Heemskerk: http://orcid.org/0000-0001-6320-9133
Hans U. Scherer: http://orcid.org/0000-0002-5700-5617
René E.M. Toes: http://orcid.org/0000-0002-9618-6414

REFERENCES

[1] Edwards JC, Szczepanski L, Szechinski J, Filipowicz-Sosnowska A, Emery P, Close DR, et al. Efficacy of B-cell-targeted therapy with rituximab in patients with rheumatoid arthritis. N Engl J Med 2004;350:2572–81. doi: 10.1056/NEJMoa032534.
[2] Briney B, Inderbitzin A, Joyce C, Burton DR. Commonality despite exceptional diversity in the baseline human antibody repertoire. Nature 2019;566:393–7. doi: 10.1038/s41586-019-0879-y.
[3] Blomberg NJ, Kristyanto H, Verstappen M, Neppelenbroek S, van der Helm-van Mil AHM, Toes REM, et al. Autoreactive B cells in extremes of rheumatoid arthritis disease phenotypes. Ann Rheum Dis 2026;85(2):388–90. doi: 10.1016/j.ard.2025.05.006.
[4] Neppelenbroek S, Blomberg NJ, Kampstra ASB, van der Hem JGK, Huizinga TWJ, Toes REM, et al. Autoreactive B cells remain active despite clinical disease control in rheumatoid arthritis. J Autoimmun 2024;149:103320. doi: 10.1016/j.jaut.2024.103320.
[5] Kristyanto H, Blomberg NJ, Slot LM, van der Voort EIH, Kerkman PF, Bakker A, et al. Persistently activated, proliferative memory autoreactive B cells promote inflammation in rheumatoid arthritis. Sci Transl Med 2020;12(570): eaaz5327. doi: 10.1126/scitranslmed.aaz5327.
[6] Vergroesen RD, Slot LM, van Schaik BDC, Koning MT, Rispens T, van Kampen AHC, et al. N-Glycosylation site analysis of citrullinated antigen-specific B-cell receptors indicates alternative selection pathways during autoreactive B-cell development. Front Immunol 2019;10:2092. doi: 10.3389/fimmu.2019.02092.
[7] Reijm S, Kwekkeboom JC, Blomberg NJ, Suurmond J, van der Woude D, Toes RE, et al. Autoreactive B cells in rheumatoid arthritis include mainly activated CXCR3 + memory B cells and plasmablasts. Jci Insight 2023;8(20): e172006. doi: 10.1172/jci.insight.172006.
[8] Wherry EJ. T cell exhaustion. Nat Immunol 2011;12(6):492–9. doi: 10.1038/ni.2035.
[9] Stork EM, van Rijswijck DMH, van Schie KA, Hoek M, Kissel T, Scherer HU, et al. Antigen-specific Fab profiling achieves molecular-resolution analysis of human autoantibody repertoires in rheumatoid arthritis. Nat Commun 2024;15(1):3114. doi: 10.1038/s41467-024-47337-x.
[10] Picelli S, Faridani OR, Björklund AK, Winberg G, Sagasser S, Sandberg R. Full-length RNA-seq from single cells using Smart-seq2. Nat Protoc 2014;9 (1):171–81. doi: 10.1038/nprot.2014.006.
[11] Koning MT, Kiełbasa SM, Boersma V, Buermans HPJ, van der Zeeuw SAJ, van Bergen CAM, et al. ARTISAN PCR: rapid identification of full-length immunoglobulin rearrangements without primer binding bias. Br J Haematol 2017;178(6):983–6. doi: 10.1111/bjh.14180.
[12] Alamyar E, Duroux P, Lefranc MP, Giudicelli V. IMGT((R)) tools for the nucleotide analysis of immunoglobulin (IG) and T cell receptor (TR) V-(D)-J repertoires, polymorphisms, and IG mutations: IMGT/V-QUEST and IMGT/HighV-QUEST for NGS. Methods Mol Biol 2012;882:569–604. doi: 10.1007/978-1-61779-842-9_32.
[13] Slot LM, Vergroesen RD, Kerkman PF, Staudinger E, Reijm S, van Dooren HJ, et al. Light chain skewing in autoantibodies and B-cell receptors of the

citrullinated antigen-binding B-cell response in rheumatoid arthritis. PLoS One 2021;16(3):e0247847. doi: 10.1371/journal.pone.0247847.
[14] Gupta NT, Vander Heiden JA, Uduman M, Gadala-Maria D, Yaari G, Kleinstein SH. Change-O: a toolkit for analyzing large-scale B cell immunoglobulin repertoire sequencing data. Bioinformatics 2015;31(20):3356–8. doi: 10.1093/bioinformatics/btv359.
[15] Kissel T, Reijm S, Slot LM, Cavallari M, Wortel CM, Vergroesen RD, et al. Antibodies and B cells recognising citrullinated proteins display a broad cross-reactivity towards other post-translational modifications. Ann Rheum Dis 2020;79(4):472–80. doi: 10.1136/annrheumdis-2019-216499.
[16] Lima NS, Musayev M, Johnston TS, Wagner DA, Henry AR, Wang L, et al. Primary exposure to SARS-CoV-2 variants elicits convergent epitope specificities, immunoglobulin V gene usage and public B cell clones. Nat Commun 2022;13(1):7733. doi: 10.1038/s41467-022-35456-2.
[17] Aterido A, López-Lasanta M, Blanco F, Juan-Mas A, García-Vivar ML, Erra A, et al. Seven-chain adaptive immune receptor repertoire analysis in rheumatoid arthritis reveals novel features associated with disease and clinically relevant phenotypes. Genome Biol. 2024;25(1):68. doi: 10.1186/s13059-024-03210-0.
[18] Coleclough C, Perry RP, Karjalainen K, Weigert M. Aberrant rearrangements contribute significantly to the allelic exclusion of immunoglobulin gene expression. Nature 1981;290(5805):372–8. doi: 10.1038/290372a0.
[19] Zhang Y, Lee TY. Revealing the immune heterogeneity between systemic lupus erythematosus and rheumatoid arthritis based on multi-omics data analysis. Int J Mol Sci 2022;23(9):5166. doi: 10.3390/ijms23095166.
[20] Pushparaj P, Nicoletto A, Sheward DJ, Das H, Castro Dopico X, Perez Vidakovics L, et al. Immunoglobulin germline gene polymorphisms influence the function of SARS-CoV-2 neutralizing antibodies. Immunity 2023;56(1):193–206.e197. doi: 10.1016/j.immuni.2022.12.005.
[21] Kissel T, Hafkenscheid L, Wesemael TJ, Tamai M, Kawashiri SY, Kawakami A, et al. IgG anti-citrullinated protein antibody variable domain glycosylation increases before the onset of rheumatoid arthritis and stabilizes thereafter: a cross-sectional study encompassing ~1500 samples. Arthritis Rheumatol 2022;74(7):1147–58. doi: 10.1002/art.42098.
[22] Kissel T, Ge C, Hafkenscheid L, Kwekkeboom JC, Slot LM, Cavallari M, et al. Surface Ig variable domain glycosylation affects autoantigen binding and acts as threshold for human autoreactive B cell activation. Sci Adv 2022;8(6):1759.
[23] Klenerman P, Zinkernagel RM. What can we learn about human immunodeficiency virus infection from a study of lymphocytic choriomeningitis virus? Immunol Rev 1997;159:5–16. doi: 10.1111/j.1600-065x.1997.tb01003.x.
[24] Moskophidis D, Lechner F, Pircher H, Zinkernagel RM. Virus persistence in acutely infected immunocompetent mice by exhaustion of antiviral cytotoxic effector T cells. Nature 1993;362(6422):758–61. doi: 10.1038/362758a0.
[25] den Boer AT, Diehl L, van Mierlo GJ, van der Voort EI, Fransen MF, Krimpenfort P, et al. Longevity of antigen presentation and activation status of APC are decisive factors in the balance between CTL immunity versus tolerance. J Immunol 2001;167(5):2522–8. doi: 10.4049/jimmunol.167.5.2522.
[26] Toes RE, Offringa R, Blom RJ, Melief CJ, Kast WM. Peptide vaccination can lead to enhanced tumor growth through specific T-cell tolerance induction. Proc Natl Acad Sci U S A 1996;93(15):7855–60. doi: 10.1073/pnas.93.15.7855.
[27] Zikherman J, Parameswaran R, Weiss A. Endogenous antigen tunes the responsiveness of naive B cells but not T cells. Nature 2012;489(7414):160–4. doi: 10.1038/nature11311.
[28] Dizon BLP, Holla P, Mutic EC, Schaughency P, Pierce SK. Human naive B cells show evidence of anergy and clonal redemption following vaccination. NPJ Vaccines 2025;10(1):96. doi: 10.1038/s41541-025-01133-w.
[29] Sosa-Hernández VA, Torres-Ruíz J, Cervantes-Díaz R, Romero-Ramírez S, Páez-Franco JC, Meza-Sánchez DE, et al. B Cell Subsets as severity-associated signatures in COVID-19 patients. Front Immunol 2020;11:611004. doi: 10.3389/fimmu.2020.611004.
[30] Moir S, Ho J, Malaspina A, Wang W, DiPoto AC, O'Shea MA, et al. Evidence for HIV-associated B cell exhaustion in a dysfunctional memory B cell compartment in HIV-infected viremic individuals. J Exp Med 2008;205(8):1797–805. doi: 10.1084/jem.20072683.
[31] Ellebedy AH, Jackson KJ, Kissick HT, Nakaya HI, Davis CW, Roskin KM, et al. Defining antigen-specific plasmablast and memory B cell subsets in human blood after viral infection or vaccination. Nat Immunol 2016;17(10):1226–34. doi: 10.1038/ni.3533.
[32] Wei C, Anolik J, Cappione A, Zheng B, Pugh-Bernard A, Brooks J, et al. A new population of cells lacking expression of CD27 represents a notable component of the B cell memory compartment in systemic lupus erythematosus. J Immunol 2007;178(10):6624–33. doi: 10.4049/jimmunol.178.10.6624.
[33] Wing E, Sutherland C, Miles K, Gray D, Goodyear CS, Otto TD, et al. Double-negative-2 B cells are the major synovial plasma cell precursor in rheumatoid arthritis. Front Immunol 2023;14:1241474. doi: 10.3389/fimmu.2023.1241474.
[34] Galson JD, Trück J, Fowler A, Clutterbuck EA, Münz M, Cerundolo V, et al. Analysis of B cell repertoire dynamics following hepatitis B vaccination in humans, and enrichment of vaccine-specific antibody sequences. EBioMedicine 2015;2(12):2070–9. doi: 10.1016/j.ebiom.2015.11.034.
[35] Scharf L, Axelsson H, Emmanouilidi A, Mathew NR, Sheward DJ, Leach S, et al. Longitudinal single-cell analysis of SARS-CoV-2-reactive B cells uncovers persistence of early-formed, antigen-specific clones. JCI Insight 2023;8(1):e165299. doi: 10.1172/jci.insight.165299.
[36] Khatri I, Diks AM, van den Akker EB, Oosten LEM, Zwaginga JJ, Reinders MJT, et al. Longitudinal dynamics of human B-cell response at the single-cell level in response to Tdap vaccination. Vaccines (Basel) 2021;9(11):1352. doi: 10.3390/vaccines9111352.
[37] Setliff I, McDonnell WJ, Raju N, Bombardi RG, Murji AA, Scheepers C, et al. Multi-donor longitudinal antibody repertoire sequencing reveals the existence of public antibody clonotypes in HIV-1 infection. Cell Host Microbe 2018;23(6):845–54 .e846. doi: 10.1016/j.chom.2018.05.001.
[38] Moir S, Malaspina A, Ogwaro KM, Donoghue ET, Hallahan CW, Ehler LA, et al. HIV-1 induces phenotypic and functional perturbations of B cells in chronically infected individuals. Proc Natl Acad Sci U S A 2001;98(18):10362–7. doi: 10.1073/pnas.181347898.
[39] Wang C, Liu Y, Xu LT, Jackson KJ, Roskin KM, Pham TD, et al. Effects of aging, cytomegalovirus infection, and EBV infection on human B cell repertoires. J Immunol. 192(2):603-11. doi:10.4049/jimmunol.1301384
[40] Phad GE, Pinto D, Foglierini M, Akhmedov M, Rossi RL, Malvicini E, et al. Clonal structure, stability and dynamics of human memory B cells and circulating plasmablasts. Nat Immunol. 23(7):1076-85. doi:10.1038/s41590-022-01230-1
[41] Mikelov A, Alekseeva EI, Komech EA, Staroverov DB, Turchaninova MA, Shugay M, et al. Memory persistence and differentiation into antibody-secreting cells accompanied by positive selection in longitudinal BCR repertoires. Elife 2022;11:e79254. doi: 10.7554/eLife.79254.
[42] Galson JD, Trück J, Fowler A, Münz M, Cerundolo V, Pollard AJ, et al. In-depth assessment of within-individual and inter-individual variation in the b cell receptor repertoire. Front Immunol 2015;6:531. doi: 10.3389/fimmu.2015.00531.
[43] Bashford-Rogers RJM, Smith KGC, Thomas DC. Antibody repertoire analysis in polygenic autoimmune diseases. Immunology 2018;155(1):3–17. doi: 10.1111/imm.12927.
[44] Cowan GJM, Miles K, Capitani L, Giguere SSB, Johnsson H, Goodyear C, et al. In human autoimmunity, a substantial component of the B cell repertoire consists of polyclonal, barely mutated IgG(+ve) B cells. Front Immunol 2020;11:395. doi: 10.3389/fimmu.2020.00395.
[45] Wang Y, Lloyd KA, Melas I, Zhou D, Thyagarajan R, Lindqvist J, et al. Rheumatoid arthritis patients display B-cell dysregulation already in the naive repertoire consistent with defects in B-cell tolerance. Sci Rep 2019;9(1):19995. doi: 10.1038/s41598-019-56279-0.
[46] Nellore A, Zumaquero E, Scharer CD, Fucile CF, Tipton CM, King RG, et al. A transcriptionally distinct subset of influenza-specific effector memory B cells predicts long-lived antibody responses to vaccination in humans. Immunity 2023;56:847–63 .e848. doi: 10.1016/j.immuni.2023.03.001.
[47] Andrews SF, Chambers MJ, Schramm CA, Plyler J, Raab JE, Kanekiyo M, et al. Activation dynamics and immunoglobulin evolution of pre-existing and newly generated human memory b cell responses to influenza hemagglutinin. Immunity 2019;51(2):398–410.e395. doi: 10.1016/j.immuni.2019.06.024.
[48] Jacob-Dolan C, Lifton M, Powers OC, Miller J, Hachmann NP, Vu M, et al. B cell somatic hypermutation following COVID-19 vaccination with Ad26.COV2.S. iScience 2024;27(4):109716. doi: 10.1016/j.isci.2024.109716.
[49] Zurbuchen Y, Michler J, Taeschler P, Adamo S, Cervia C, Raeber ME, et al. Human memory B cells show plasticity and adopt multiple fates upon recall response to SARS-CoV-2. Nat Immunol 2023;24(6):955–65. doi: 10.1038/s41590-023-01497-y.
[50] Sokal A, Chappert P, Barba-Spaeth G, Roeser A, Fourati S, Azzaoui I, et al. Maturation and persistence of the anti-SARS-CoV-2 memory B cell response. Cell 2021;184:1201–13 .e1214. doi: 10.1016/j.cell.2021.01.050.
[51] Gaebler C, Wang Z, Lorenzi JCC, Muecksch F, Finkin S, Tokuyama M, et al. Evolution of antibody immunity to SARS-CoV-2. Nature 2021;591(7851):639–44. doi: 10.1038/s41586-021-03207-w.
[52] Chappert P, Huetz F, Espinasse MA, Chatonnet F, Pannetier L, Da Silva L, et al. Human anti-smallpox long-lived memory B cells are defined by dynamic interactions in the splenic niche and long-lasting germinal center imprinting. Immunity 2022;55(10):1872–90 .e1879. doi: 10.1016/j.immuni.2022.08.019.
[53] Heesters BA, Myers RC, Carroll MC. Follicular dendritic cells: dynamic antigen libraries. Nat Rev Immunol 2014;14(7):495–504. doi: 10.1038/nri3689.
[54] Laidlaw BJ, Ellebedy AH. The germinal centre B cell response to SARS-CoV-2. Nat Rev Immunol 2022;22(1):7–18. doi: 10.1038/s41577-021-00657-1.

[55] Guillaume SM, Foster WS, San Martín Molina I, Watson EM, Innocentin S, Kennedy GM, et al. Lung B cells in ectopic germinal centers undergo affinity maturation. Proc Natl Acad Sci U S A 2025;122(14):e2416855122. doi: 10.1073/pnas.2416855122.

[56] Willemze A, Shi J, Mulder M, Stoeken-Rijsbergen G, Drijfhout JW, Huizinga TW, et al. The concentration of anticitrullinated protein antibodies in serum and synovial fluid in relation to total immunoglobulin concentrations. Ann Rheum Dis 2013;72(6):1059–63. doi: 10.1136/annrheumdis-2012-202747.

[57] Kongpachith S, Lingampalli N, Ju CH, Blum LK, Lu DR, Elliott SE, et al. Affinity maturation of the anti-citrullinated protein antibody paratope drives epitope spreading and polyreactivity in rheumatoid arthritis. Arthritis Rheumatol 2019;71(4):507–17. doi: 10.1002/art.40760.

[58] Biersteker R, Athanasiadou A, van der Meulen S, van Wesemael TJ, Slot LM, Kissel T, et al. Insights into the detection of AMPA cross-reactivity: comparing cyclic peptide- to protein-based assays. Arthritis Res Ther 2025;27(1):138. doi: 10.1186/s13075-025-03591-y.

[59] Schiepers A, van 't Wout MFL, Greaney AJ, Zang T, Muramatsu H, Lin PJC, et al. Molecular fate-mapping of serum antibody responses to repeat immunization. Nature 2023;615(7952):482–9. doi: 10.1038/s41586-023-05715-3.

[60] van Mourik AG, Johansson L, van Wesemael TJ, Maurits MP, Kokkonen H, Rönnelid J, et al. Autoantibody clusters in rheumatoid arthritis are not driven by antigen specificity or isotype. RMD Open 2025;11(2):e005291. doi: 10.1136/rmdopen-2024-005291.

[61] Titcombe PJ, Wigerblad G, Sippl N, Zhang N, Shmagel AK, Sahlström P, et al. Pathogenic citrulline-multispecific B cell receptor clades in rheumatoid arthritis. Arthritis Rheumatol 2018;70(12):1933–45. doi: 10.1002/art.40590.

[62] Cornaby C, Gibbons L, Mayhew V, Sloan CS, Welling A, Poole BD. B cell epitope spreading: mechanisms and contribution to autoimmune diseases. Immunol Lett 2015;163(1):56–68. doi: 10.1016/j.imlet.2014.11.001.

[63] Lee H, Yoo DK, Han J, Kim KH, Noh J, Lee Y, et al. Optimization of peripheral blood volume for in silico reconstitution of the human B-cell receptor repertoire. FEBS Open Bio 2022;12(9):1634–43. doi: 10.1002/2211-5463.13467.

[64] Elliott SE, Kongpachith S, Lingampalli N, Adamska JZ, Cannon BJ, Blum LK, et al. B cells in rheumatoid arthritis synovial tissues encode focused antibody repertoires that include antibodies that stimulate macrophage TNF-alpha production. Clin Immunol 2020;212:108360. doi: 10.1016/j.clim.2020.108360.

Ann Rheum Dis 85 (2026) 1507–1519

Contents lists available at ScienceDirect

Annals of the Rheumatic Diseases

journal homepage: https://www.sciencedirect.com/journal/annals-of-the-rheumatic-diseases

Rheumatoid arthritis

Anti-PAD4 antibodies link autoimmunity to PAD4 with CTL-associated rheumatoid arthritis

Kusuma Ananth[1], Katharine B Moosic[2], Eduardo Gomez-Banuelos[1], Hong Wang[1], Isabel Trejo-Zambrano[1], Ramona Johnson[1], Jessica Marie Kirschmann[3,4], Tess Deddens[2], Omar Elghawy[2], Bryna Shemo[2], William H Robinson[3,4], Donald Kimpel[5], Clifton O Bingham[1], David J Feith[2], Brendan Antiochos[1], Felipe Andrade[1], Thomas P Loughran Jr[2,**], Erika Darrah[1,*]

[1] *Division of Rheumatology, Johns Hopkins University School of Medicine, Baltimore, MD, USA*
[2] *Division of Hematology/Oncology, Department of Medicine, University of Virginia School of Medicine, Charlottesville, VA, USA*
[3] *Division of Immunology and Rheumatology, Stanford School of Medicine, Stanford, CA, USA*
[4] *The Geriatric Research, Education, and Clinical Center, Veterans Affairs Palo Alto Health Care System, Palo Alto, CA, USA*
[5] *Division of Rheumatology & Immunology, Department of Medicine, University of Virginia School of Medicine, Charlottesville, VA, USA*

ARTICLE INFO

Article history:
Received 23 December 2025
Received in revised form 14 April 2026
Accepted 15 April 2026

ABSTRACT

Objectives: We aimed to study the serologic, genetic, and immunologic underpinnings associated with cytotoxic T lymphocytes (CTLs) in rheumatoid arthritis (RA), using T-large granular lymphocytic leukaemia with comorbid RA (T-LGLL/RA) as a model of CTL-linked RA.

Methods: We used blood samples and paired clinical data from patients with RA, T-LGLL/RA, T-LGLL and healthy controls. Serological characterisation was performed using anti-cyclic citrullinated peptide 3.1 (anti-CCP3.1) enzyme-linked immunosorbent assay, multiplex RA autoantigen array, and radiolabelled peptidylarginine deiminase type III and IV (PAD4) immunoprecipitations. Genetic characterisation was performed using *PADI4* single nucleotide polymorphism TaqMan genotyping assays and droplet digital polymerase chain reaction for signal transducer and activator of transcription 3 (*STAT3*) mutations. Multiparameter flow cytometry and pentamer binding assays were performed to immunophenotype CTLs and characterise PAD4-specific CTLs, respectively.

Results: Patients with T-LGLL/RA had enhanced anticitrullinated protein antibody responses compared with RA, and a strikingly higher frequency of anti-PAD4 antibodies (60% vs 27%, $P < .0001$). Among patients with T-LGLL, *PADI4* single nucleotide polymorphisms were associated with anti-PAD4−positive RA (20% vs 3%, $P = .02$), and anti-PAD4 antibody levels were inversely correlated with absolute neutrophil count (Spearman's rho = −0.236; $P = .02$). Activating *STAT3* mutations were associated with anti-PAD4 antibodies in both T-LGLL/RA (90% vs 74%, $P = .047$) and RA (39% vs 9%, $P = .002$). Flow cytometric characterisation of CTLs showed that anti-PAD4−positive RA was enriched for CD57+, CD7 low, T effector memory cells re-expressing CD45RA (TEMRA) CTLs. Furthermore, PAD4-specific CTLs were detected in anti-PAD4+ patients with RA and expressed elevated levels of CD69, CD57, and KLRG1, and a TEMRA phenotype.

*Correspondence to Dr Erika Darrah, Division of Rheumatology, Johns Hopkins University School of Medicine, Baltimore, MD, USA.
**Correspondence to Dr Thomas P Loughran, Division of Hematology/Oncology, Department of Medicine, University of Virginia School of Medicine, Charlottesville, VA, USA.
E-mail addresses: tl7cs@uvahealth.org (T.P. Loughran), edarrah1@jhmi.edu (E. Darrah).
Handling editor Josef Smolen

https://doi.org/10.1016/j.ard.2026.04.006

Conclusions: These data demonstrate a mechanistic link between autoimmunity to PAD4 and CTL-associated disease in RA.

WHAT IS ALREADY KNOWN ON THIS TOPIC

- Previous studies have shown that CD8+ T cells infiltrate the synovial joints in rheumatoid arthritis (RA). These cells have evidence of clonal expansion and express an activated, chronically stimulated phenotype. Similar expansions of clonal CD8 + T cells are observed in T-large granular lymphocytic leukaemia (T-LGLL), a disease in which RA occurs with high frequency. Mechanistically, cytotoxic T lymphocytes (CTLs) have been linked to autoantigen production and activation of effector pathways in RA.

WHAT THIS STUDY ADDS

- Here, we used T-LGLL with comorbid RA (T-LGLL/RA) as a model of CTL-associated RA to understand the role of CTLs in RA. Specifically, we identified anti-peptidylarginine deiminase type IV (PAD4) antibodies, a marker associated with erosive disease in the general RA population, as highly enriched in the T-LGLL/RA population. Next, we studied the subset of patients with RA with anti-PAD4 antibodies and found that they share features of T-LGLL/RA, including increased frequency of activating signal transducer and activator of transcription 3 (*STAT3*) mutations and frequency of CD57+, CD7 low and T effector memory cells re-expressing CD45RA CD8+ T cells. Finally, we identified PAD4 as a novel target of CD8+ T cells in anti-PAD4 antibody−positive patients with RA, suggesting a potential mechanism wherein CTLs may target PAD4-expressing cells in RA. In conclusion, this study suggests PAD4-directed autoimmune responses as markers of CTL-associated RA.

HOW THIS STUDY MIGHT AFFECT RESEARCH, PRACTICE OR POLICY

- We identified anti-PAD4 antibodies as a biomarker of RA development in the setting of T-LGLL, which may be used for screening purposes to identify patients with RA at risk for future T-LGLL development. Our work opens the opportunity to further research the precise effector mechanisms of CTLs in RA within the distinct subset of patients with RA with anti-PAD4 antibodies. Furthermore, our discovery that autoimmunity to PAD4 is linked to features of CTL-associated RA highlights the potential of anti-PAD4 antibodies as a serological biomarker to identify patients who may benefit from treatments that antagonise the STAT3 signalling pathway or CTL effector functions.

INTRODUCTION

Rheumatoid arthritis (RA) is a chronic autoimmune disease targeting synovial joints, resulting in destruction of articular cartilage and bone [1]. Although the aetiology of RA is unknown, there has been substantial progress, largely fuelled by the discovery that citrullinated proteins are enriched in RA joints and are major targets of autoantibodies, known as anticitrullinated protein antibodies (ACPAs) in up to 80% of patients with RA [2−6]. In addition to targeting citrullinated substrates, 23% to 45% of patients with RA harbour autoantibodies against peptidylarginine deiminase type IV (PAD4) isoenzyme, which are associated with destructive joint disease [7−10]. There is also growing evidence for CD8+ cytotoxic T lymphocytes (CTLs) in RA pathogenesis, both as generators of citrullination-associated autoantigens and as autoimmune effectors [11−14].

As generators of citrullination-associated antigens, the CTL effector molecules, perforin and granzyme B, can induce the production of RA autoantigens via their activity on target cells 11,13]. Perforin-mediated neutrophil lysis induces hyperactivation of peptidylarginine deiminases (PADs) and the production of citrullinated autoantigens in a process known as leukotoxic hypercitrullination (LTH) [11]. In addition, PAD4 is a substrate of granzyme B, which enhances presentation of immunogenic PAD4 peptides capable of stimulating PAD4-specific CD4+ T cells from patients with RA [12]. The complement pathway, which can be activated by granzyme K released by CTLs, can promote both tissue damage and the production of citrullinated antigens [11,14].

Several studies have also shed light on the involvement of CTLs in RA as autoimmune effectors. Activated and chronically stimulated T effector memory cells re-expressing CD45RA (TEMRA) and effector memory CTLs have been identified in the RA synovium [15,16], and there is evidence of their oligoclonal expansion [17]. Levels of granzymes A, B, and M are elevated in RA synovial fluid, which provide evidence of CTL degranulation [18,19]. Furthermore, Moon et al [20] demonstrated that in response to citrullinated vimentin, CTLs in patients with ACPA-positive RA proliferate, upregulate CD69, and secrete granzyme B and interferon gamma (IFNγ).

Further evidence of the role of CTLs in RA is demonstrated through the lymphoproliferative disorder T-large granular lymphocytic leukaemia (T-LGLL), which is characterised by the clonal expansion of morphologically distinct CTLs known as large granular lymphocytes (LGLs) [21,22]. LGLs express a terminal effector memory phenotype and high levels of FS-7-associated surface antigen (Fas), indicative of chronic antigen stimulation [23]. They commonly harbour activating somatic mutations in the signal transducer and activator of transcription 3 (*STAT3*) gene that promote the expression of prosurvival genes [24,25]. Neutropenia is a hallmark feature of T-LGLL, but its aetiology remains uncertain [21]. Although RA occurs in around 1% of the global population [26], it occurs in 17% to 36% of patients with T-LGLL [27] (hereafter T-LGLL with comorbid RA [T-LGLL/RA]). The high incidence of RA in T-LGLL suggests that clonally expanded CTLs play a role in RA induction, but the mechanistic link between T-LGLL and RA has not been defined.

In this study, we studied T-LGLL/RA as a model of CTL-associated RA to gain mechanistic insights into the role of CTLs in RA. First, we probed whether common features of RA were present in T-LGLL/RA and discovered that autoantibodies targeting citrullination-associated antigens are enhanced in T-LGLL/RA. Notably, we identified anti-PAD4 antibodies to be highly prevalent in the T-LGLL/RA population, suggesting seropositivity to PAD4 as a marker of CTL-associated RA. We then investigated whether the subset of patients with RA with anti-PAD4 antibodies (anti-PAD4−positive RA) shared immunologic or haematologic features of T-LGLL/RA. These studies revealed that patients with anti-PAD4−positive RA harboured CTLs enriched in the *STAT3* activating mutations, with phenotypic similarities to LGLs, and specific for PAD4 peptides. Together, our data support the hypothesis that anti-PAD4 autoimmunity is a mechanistic marker of an endotype of RA linked to chronically activated CTLs.

METHODS

This study used blood samples and paired clinical data from patients with RA, T-LGLL/RA, T-LGLL, and healthy controls (HCs). Serological characterisation was performed using the anti-cyclic citrullinated peptide 3.1 (anti-CCP3.1) enzyme-linked immunosorbent assay, a multiplex RA autoantigen array [28], and by immunoprecipitation of radiolabelled PAD3 and PAD4 generated by *in vitro* coupled transcription/translation immunoprecipitation (IVTT-IP) [8]. Genetic characterisation was performed using *PADI4* single nucleotide polymorphism (SNP) genotyping, and droplet digital polymerase chain reaction (ddPCR) of the *STAT3* gene [29]. Flow cytometry was performed to immunophenotype CTLs from each patient or control group, and a pentamer binding assay was performed to detect and characterise PAD4-specific CTLs. Detailed methods can be found in Supplemental Data S1.

RESULTS

ACPAs in patients with T-LGLL/RA have higher frequency, levels, and antigenic diversity than RA

To define serological features of CTL-associated RA, we studied 2 cohorts of patients with RA (1 from the University of Virginia [UVA; n = 150] and 1 from Johns Hopkins University [n = 230]) (characteristics in Supplemental Table S1) and compared them to a cohort of patients with T-LGLL/RA (n = 94) and a cohort of patients with T-LGLL (n = 95) as a control of CTL-driven disease without RA (characteristics in Supplemental

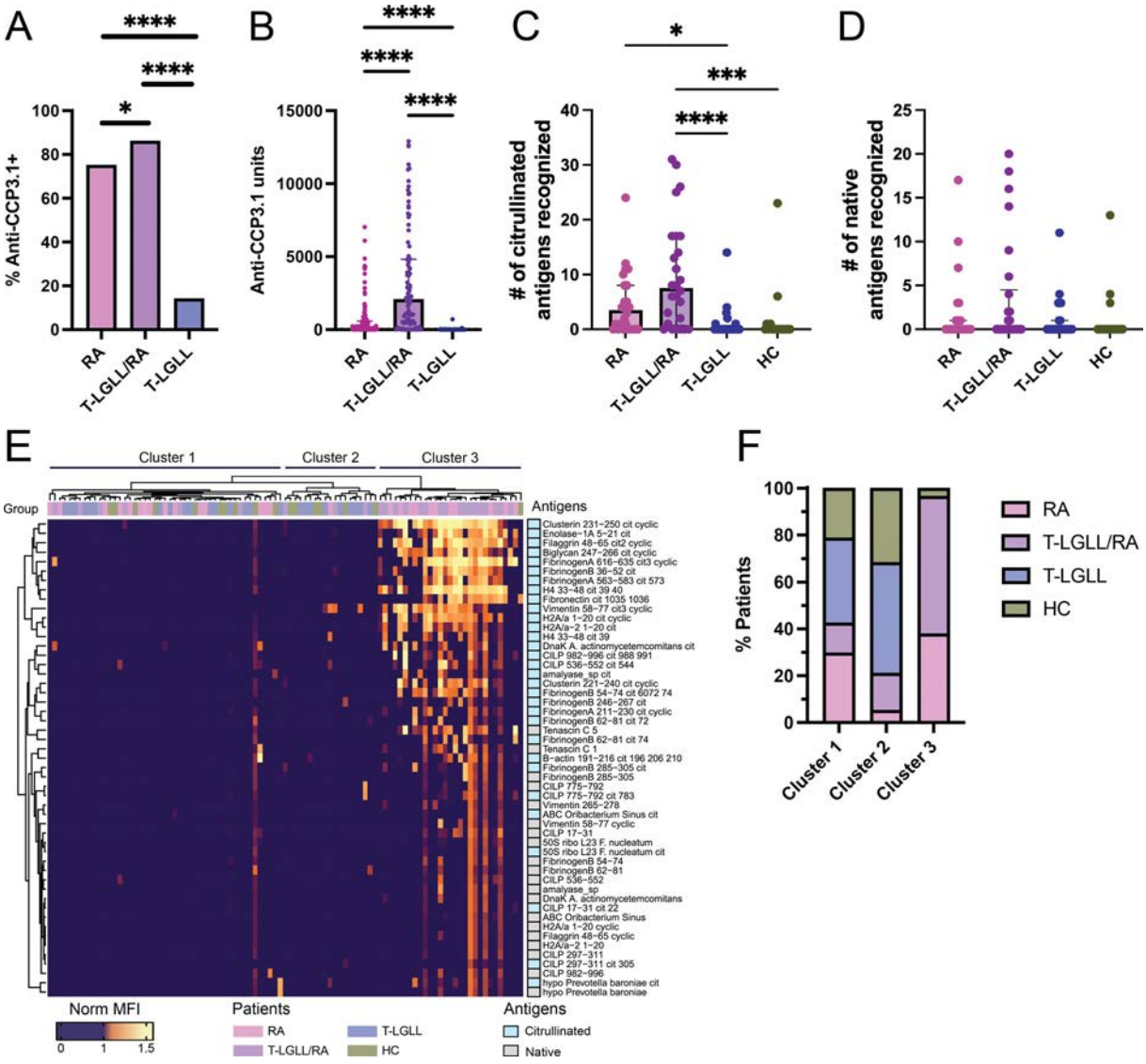

Figure. 1. Patients with T-LGLL/RA have higher frequency, antibody levels, and antigenic diversity of ACPAs compared with RA or T-LGLL. (A) Bar graphs show the percentage of patients with anti-CCP3.1 + in each group, as measured by CCP3.1 ELISA, where the cutoff for positivity was 20 units. RA (UVA cohort; n = 145), T-LGLL/RA (n = 94), and T-LGLL (n = 95). (B) Anti-CCP3.1 levels are shown for patients with anti-CCP3.1 positive. RA (UVA cohort; n = 109), T-LGLL/RA (n = 81), and T-LGLL (n = 13). Results of the RA antigen multiplex array are shown in (C-F), and include RA (JHU cohort; n = 26), T-LGLL/RA (n = 26), T-LGLL (n = 26), and HC (n = 17). (C) The number of citrullinated antigens and (D) the number of native antigens recognised by each patient or control are shown. Recognition of each antigen was defined as greater than the 95th percentile of antigen recognition score by HC sera. Bar graphs show the median with interquartile range. (E) A heatmap was generated to cluster patients or controls based on reactivity to RA antigens and to cluster antigens based on recognition by sera. (F) A bar graph shows the percentage of patients or controls that comprise each cluster. *$P < .05$, ***$P < .001$, and ****$P < .0001$. ACPA; anti-citrullinated protein antibody; HC, healthy control; JHU, Johns Hopkins University; MFI, mean fluorescence intensity; RA, rheumatoid arthritis; T-LGLL, T-large granular lymphocytic leukaemia; UVA, University of Virginia.

Table S2). Since perforin from cytotoxic granules can induce LTH in neutrophils [11], and neutropenia is a common feature of T-LGLL/RA [21], we hypothesised that patients with T-LGLL/RA may have higher prevalence and levels of antibodies targeting citrullinated autoantigens. First, we analysed ACPAs using the anti-CCP3.1 test, which evaluates immunoglobulin (Ig)G and IgA, and found that these antibodies are more frequent in T-LGLL/RA (86%) than in RA (75%, $P = .049$) or T-LGLL (14%, $P < .0001$; Fig 1A). Strikingly, ACPA levels were 7 times higher in T-LGLL/RA (median [IQR], 2484 U [817.9-5842 U]) compared with RA (338.8 U [89.12-772.1 U]), $P < .0001$), and 100 times higher than in T-LGLL (24.99 U [21.64-32.44 U], $P < .0001$) (Fig 1B), indicating an enhanced humoral immune response to citrullinated autoantigens in T-LGLL/RA.

The enhanced ACPA response in patients with T-LGLL/RA could be driven either by high antibody levels targeting a restricted set of antigens or by recognition of a wider breadth of citrullinated proteins. To assess this, we characterised the fine autoantibody specificities present in T-LGLL/RA, RA, T-LGLL, or HCs against a multiplex antigen array of 51 common RA antigens, including 25 citrullinated peptides, 13 native peptides, 6 citrullinated proteins, and 7 native proteins (Supplemental Table S3). In this analysis, sera from patients with T-LGLL/RA recognised a similar number of citrullinated antigens (median [IQR], 7.5 [0.75-17]) as compared with RA alone (3.5 [0-8]) ($P = .71$). However, sera from patients with T-LGLL/RA did recognise a significantly greater number of citrullinated antigens than T-LGLL (0 [0-0.25], $P < .0001$) and HC (0 [0-0.5], $P = .0004$) (Fig 1C). There was no difference in the recognition of native antigens between any of the 4 groups (Fig 1D). Hierarchical clustering based on reactivity of responders and recognition of antigens identified 3 main groups (Fig 1E). Cluster 3 represents patients with the highest reactivity to RA antigens, which largely consists of patients with T-LGLL/RA (58.6%), followed by patients with RA (37.9%), and HC (3.4%) (Fig 1E,F). These data indicate that ACPAs in patients with T-LGLL/RA recognise a wide diversity of citrullinated antigens and are more frequent and found at higher levels than in those with RA, demonstrating that CTL-associated RA is associated with more robust ACPA responses.

Patients with T-LGLL/RA have higher frequency and levels of anti-PAD4 antibodies than patients with RA

The augmented ACPA response in T-LGLL/RA suggests that these patients may generate immune responses to a wider array of citrullination-associated autoantigens such as PAD4. Anti-PAD4 antibodies are highly specific for RA [7,8,30,31] and associate with ACPAs [30] and more severe and erosive joint disease [32,33]. IVTT-IP demonstrated that anti-PAD4 antibodies were twice as frequent in T-LGLL/RA than in RA (60% vs 27%, $P < .0001$) (Fig 2A). Among patients with anti-PAD4 positive, median anti-PAD4 levels in T-LGLL/RA were significantly higher than in RA (0.84 [0.70-1.01] vs 0.59 [0.29-0.87], respectively, $P < .0001$) (Fig 2B). Interestingly, anti-PAD4 antibodies were strikingly more frequent in T-LGLL/RA than T-LGLL (60% vs 2%, $P < .0001$), indicating that anti-PAD4 antibodies are highly specific for RA in the setting of T-LGLL (Fig 2A) and may be a unique serological marker of CTL-associated RA.

Anti-PAD4 antibodies are predominantly found in ACPA-positive RA [30]: in our cohorts, 97.7% of patients with anti-PAD4−positive RA were anti-CCP3.1 positive, and 100% of anti-PAD4−positive patients with T-LGLL/RA were anti-CCP3.1 positive (Supplemental Table S4). Thus, we sought to determine whether anti-PAD4 antibodies are overrepresented in patients with T-LGLL/RA compared with patients with RA, independent of ACPA positivity. Logistic regression analysis showed that even after accounting for ACPA positivity, patients with T-LGLL/RA were 3.69 times more likely to have anti-PAD4 antibodies than patients with RA (Supplemental Table S5).

Similarly, anti-PAD4 antibodies are associated with RA duration [34,35], and in both our RA and T-LGLL/RA cohorts, patients with anti-PAD4 positive had a significantly longer RA

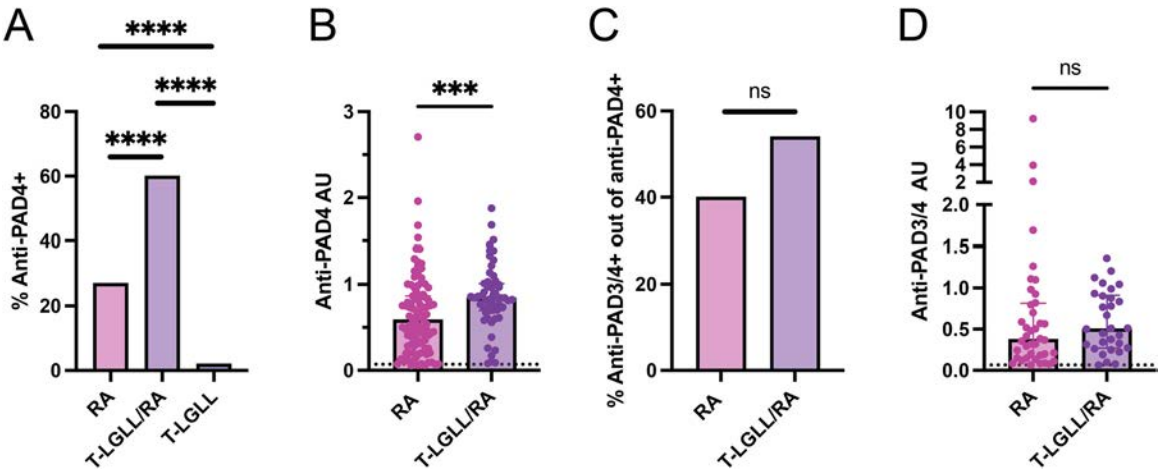

Figure. 2. Patients with T-LGLL/RA have higher frequency and levels of anti-PAD4 antibodies and have anti-PAD3/4 cross-reactive antibodies. (A) Frequency of anti-PAD4 antibodies, as measured by IVTT-IP, where the cutoff for positivity was defined as 0.07 AU. RA (UVA and JHU cohorts; n = 375), T-LGLL/RA (n = 94), and T-LGLL (n = 95). (B) Anti-PAD4 arbitrary units (AUs) in patients with anti-PAD4+ RA (UVA and JHU cohorts; n = 100) and anti-PAD4+ T-LGLL/RA (n = 56). T-LGLL was omitted because n = 2. The dotted line representing 0.07 AU is the cutoff for anti-PAD4 positivity. (C) Frequency of anti-PAD3/4 cross-reactive antibodies out of patients with anti-PAD4+, as measured by IVTT-IP, where the cutoff for positivity was defined as 0.065 AU. RA (UVA and JHU cohorts; n = 100), T-LGLL/RA (n = 56). T-LGLL was omitted because n = 2. (D) Anti-PAD3/4 AU in anti-PAD3/4+ RA (UVA and JHU cohorts; n = 40) and anti-PAD3/4+ T-LGLL/RA (n = 30). The dotted line representing 0.065 is the cutoff for anti-PAD3/4 positivity. Median with interquartile range is shown. ns = not significant, ***$P < .001$, and ****$P < .0001$. IVTT-IP, *in vitro* coupled transcription/translation immunoprecipitation; JHU, Johns Hopkins University; PAD3, peptidylarginine deiminase type III; PAD4, peptidylarginine deiminase type IV; RA, rheumatoid arthritis; T-LGLL, T-large granular lymphocytic leukaemia; UVA, University of Virginia.

duration than patients with anti-PAD4 negative (Supplemental Fig S1A,B). Since patients with T-LGLL/RA have longer RA duration than patients with sporadic RA (Supplemental Fig S1C), we performed generalised linear models to probe whether T-LGLL/RA have higher frequency and levels of anti-PAD4 antibodies than RA, independent of RA duration. After accounting for RA duration, patients with T-LGLL/RA were 2.66 times more likely to be anti-PAD4 positive than patients with RA (Supplemental Table S6), and anti-PAD4−positive T-LGLL/RA had 35% higher levels of anti-PAD4 antibodies than anti-PAD4−positive RA (Supplemental Table S7). Thus, higher frequency and levels of anti-PAD4 antibodies are a feature of T-LGLL/RA, independent of ACPA positivity and RA disease duration. Of note, anti-PAD4 antibodies were associated with an extended interval between RA and T-LGLL diagnoses in the T-LGLL/RA group, with anti-PAD4 antibody−positive individuals, being diagnosed with T-LGLL an average of 17.41±10.27 years after their RA diagnosis compared with 10.86±10.85 years in anti-PAD4 negative individuals ($P = .013$) (Supplemental Table S2). RA was diagnosed before T-LGLL in the majority of cases, with only 18% (5/28) of anti-PAD4 negative and 5% (2/42) of anti-PAD4−positive individuals receiving a diagnosis of T-LGLL before RA (Fisher's exact $P = .10$).

Given the profound enrichment of anti-PAD4 antibodies in T-LGLL/RA, we next assessed the prevalence and function of anti-PAD3/4 cross-reactive antibodies, a unique subset of anti-PAD4 antibodies with the capacity to activate PAD4 enzymatic function by reducing its calcium requirements [8]. Among patients with anti-PAD4 positive, a similar percentage of patients with T-LGLL/RA and RA had anti-PAD3/4 antibodies (Fig 2C), and among patients with anti-PAD3/4 positive, levels were comparable between patients with T-LGLL/RA and RA (Fig 2D). In addition, in an *in vitro* histone H3 citrullination assay, purified IgG from patients with anti-PAD3/4−positive T-LGLL/RA activated PAD4 to a similar degree as IgG from patients with anti-PAD3/4−positive RA, demonstrating that anti-PAD3/4 antibodies possess the same functional capacity in both diseases (Supplemental Fig S2). These data indicate that humoral autoimmunity to PAD4 is a feature of T-LGLL/RA, suggesting that T-LGLL/RA and anti-PAD4−positive RA may share mechanistic features.

PADI4 *SNPs are associated with the presence of anti-PAD4 antibodies in T-LGLL/RA*

Three SNPs in the *PADI4* gene, termed the 'susceptible haplotype' [7,9,36], are strongly associated with RA development and have been reported to associate with anti-PAD4 antibodies in some RA populations [7,37,38]. We sought to determine whether the susceptible haplotype is associated with anti-PAD4 antibodies in the setting of T-LGLL/RA. Patients with T-LGLL/RA or RA were genotyped for the 3 SNPs (rs11203366 [A163G], rs11203367 [C245T], and rs874881 [C335G]) that comprise the susceptible haplotype (GTG) [7,36].

Patients with anti-PAD4−positive T-LGLL/RA were 9.21 times more likely to be homozygous for the susceptible haplotype than patients with anti-PAD4−negative T-LGLL/RA (95% CI, 1.45-101.8; $P = .02$) (Table 1). A similar, though non-significant, trend was observed when restricting the analysis to Caucasians, the largest racial group in our cohorts, with anti-PAD4+ T-LGLL/RA being 5.85 times as likely to be homozygous for the susceptible haplotype as compared with patients with anti-PAD4−negative T-LGLL/RA (95% CI, 0.82-66.40; $P = .087$) (Supplemental Table S8). There was no association between anti-PAD4 positivity and the susceptible haplotype in the RA cohort as a whole or when restricting to Caucasians (Table 1). In summary, homozygosity for the susceptible haplotype associates with anti-PAD4 antibodies in patients with T-LGLL/RA, suggesting that *PADI4* SNPs may predispose patients with T-LGLL/RA to the breach of immune tolerance to PAD4.

Absolute neutrophil count negatively correlates with anti-PAD4 antibodies in T-LGLL/RA

Neutropenia is a hallmark feature of T-LGLL/RA, but its aetiology remains uncertain [39]. Since neutrophils express PAD4 and can be a source of autoantigens in RA [11], we sought to determine whether anti-PAD4 antibodies are associated with neutropenia in T-LGLL/RA and RA. As expected, the T-LGLL and T-LGLL/RA cohorts had a similar degree of neutropenia (median [IQR] absolute neutrophil count [ANC] 1180 [675-2255] and 1200 [387-2350] neutrophils/mm^3, respectively), defined as ANC below 1500 neutrophils/mm^3, and the RA group had normal neutrophil levels (median [IQR] ANC 4176 [3150-5640] neutrophils/mm^3) (Fig 3A).

The frequency of neutropenia was similar between anti-PAD4−positive vs anti-PAD4 negative T-LGLL/RA (66.07% vs 52.63%, $P = .20$), and although severe neutropenia (defined as ANC <500 neutrophils/mm^3) was 2-fold more frequent in anti-PAD4 positive than patients with anti-PAD4 negative T-LGLL/RA, it did not achieve statistical significance (32.14% vs 15.79%, $P = .09$) (Supplemental Table S9). Similarly, median ANC was comparable between patients with anti-PAD4−positive and anti-PAD4−negative T-LGLL/RA (median [IQR] of 1005 [135-2298] and 1460 [605-2713] neutrophils/mm^3, respectively, $P = .14$) (Fig 3B). However, when assessing the relationship between anti-PAD4 antibodies and ANC as continuous variables, we observed a modest yet statistically significant negative correlation between ANC and anti-PAD4 levels in T-LGLL/RA (Spearman's r = −0.2358, $P = .02$) (Fig 3C).

Table 1
Homozygosity for *PADI4* susceptible haplotype single nucleotide polymorphisms (SNPs) is associated with anti-PAD4 antibodies in T-LGLL/RA

Patient group	Susceptible haplotype	*P*	OR	95% CI	Homozygous for susceptible haplotype	*P*	OR	95% CI
T-LGLL/RA								
Anti-PAD4+ (n = 54)	63% (34)	.2	1.79	0.78-4.28	20% (11)	*.02	9.21	1.45-101.8
Anti-PAD4- (n = 37)	49% (18)				3% (1)			
RA								
Anti-PAD4+ (n = 57)	77% (44)	.73	1.16	0.57-2.32	28% (16)	.27	1.53	0.79-3.08
Anti-PAD4- (n = 172)	74% (128)				20% (35)			

OR, odds ratio; PAD4, peptidylarginine deiminase type IV; *PADI4*, peptidylarginine deiminase type IV; RA, rheumatoid arthritis; T-LGLL, T-large granular lymphocytic leukaemia.

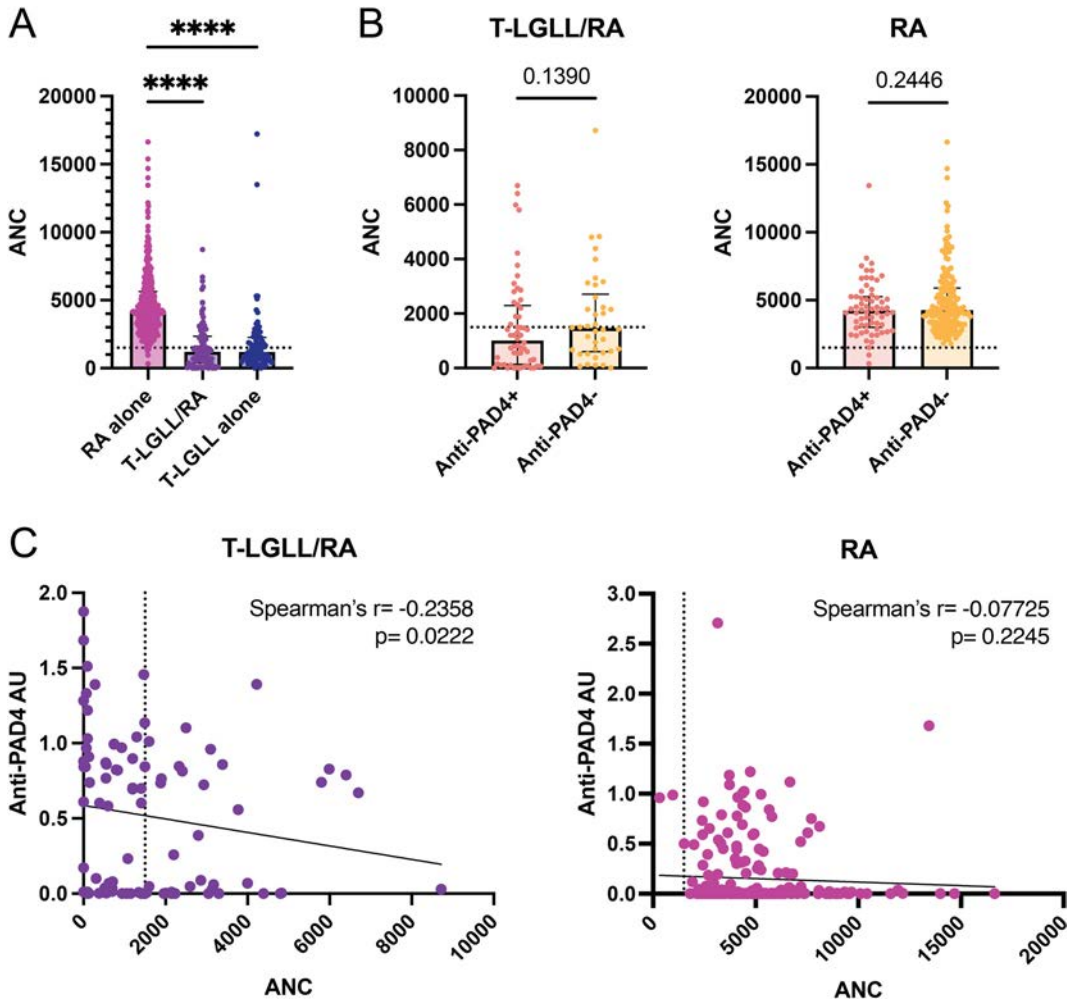

Figure. 3. ANC is negatively correlated with anti-PAD4 antibodies in T-LGLL/RA. (A) ANC is shown in RA (UVA and JHU cohorts; n = 359), T-LGLL/RA (n = 94), and T-LGLL (n = 93). (B) ANC is shown for patients with anti-PAD4+ and anti-PAD4- T-LGLL/RA (left; anti-PAD4+ T-LGLL/RA [n = 56], anti-PAD4- T-LGLL/RA [n = 38]) and patients with RA (right; anti-PAD4+ RA [n = 64], anti-PAD4- RA [n = 185]). Bar graphs show the median with the interquartile range, and the dotted line at 1500 neutrophils/mm^3 represents the cutoff for neutropenia. (C) Scatter plots show ANC vs anti-PAD4 AU for patients with T-LGLL/RA (left; n = 94) or RA (right; UVA and JHU cohorts; n = 249). Only patients with RA for whom ANC was measured within 30 days of collecting serum for PAD4 antibody testing were included in panel C. The solid line represents a best-fit line with simple linear regression. Spearman's r and *P*-values are shown. ****$P < .0001$. ANC, absolute neutrophil count; AU, arbitrary unit; IVTT-IP, *in vitro* coupled transcription/translation immunoprecipitation; JHU, Johns Hopkins University; PAD4, peptidylarginine deiminase type IV; RA, rheumatoid arthritis; T-LGLL, T-large granular lymphocytic leukaemia; UVA, University of Virginia.

In patients with RA, ANC was comparable between anti-PAD4−positive vs anti-PAD4−negative patients (median [IQR] of 4215 [3008-5260] vs 4260 [3235-5895] neutrophils/mm^3, respectively, $P = .25$, Fig 3B), and there was no correlation between ANC and anti-PAD4 levels (Spearman's r = −0.07725, $P = .22$) (Fig 3C). Of note, only 2 patients with RA had neutropenia, and both were anti-PAD4 positive (Supplemental Table S9). Our results suggest that humoral immune responses against PAD4 may be linked to lower ANC in patients with T-LGLL/RA, supporting the hypothesis that neutrophils could represent a cellular reservoir of citrullination-associated autoantigens in this subset of patients.

STAT3 *mutations are associated with anti-PAD4 antibodies in T-LGLL/RA and RA*

As *STAT3* mutations in CTLs are a common feature of T-LGLL and are enriched in T-LGLL/RA [24,40,41], we assessed whether *STAT3* mutations and anti-PAD4 antibodies are associated in T-LGLL/RA. We used ddPCR to detect the 2 most common *STAT3* mutations—D661Y and Y640F—in peripheral blood mononuclear cells (PBMCs) of patients with T-LGLL/RA. At least 1 *STAT3* mutation was found in 83% of patients with T-LGLL/RA: 58% had the D661Y mutation and 70% had the Y640F mutation. The frequency of *STAT3* mutations was higher in anti-PAD4 positive than patients with anti-PAD4−negative T-LGLL/RA (90% vs 74%, $P = .047$). This difference appeared to be largely driven by the D661Y mutation with 71% of patients with anti-PAD4−positive T-LGLL/RA harbouring this mutation, as compared with 39% of anti-PAD4 negative T-LGLL/RA ($P = .005$), whereas the frequency of patients with T-LGLL/RA with the Y640F mutation was similar between patients with anti-PAD4 positive vs anti-PAD4 negative (77% vs 61%, $P = .11$) (Table 2). This links activating *STAT3* mutations with the presence of anti-PAD4 antibodies in patients with T-LGLL/RA.

Since activating *STAT3* mutations have recently been identified in CTLs of patients with RA [29], we probed the relationship between activating *STAT3* mutations and anti-PAD4 antibodies in RA (UVA cohort), using data from Moosic et al [29]. Interestingly, 16% harboured at least 1 *STAT3* mutation; 8% had the D661Y, and 10% had the Y640F mutation. Patients with anti-PAD4−positive RA had a higher prevalence of *STAT3* mutations compared with patients with anti-PAD4−negative RA (39% vs

Table 2
***STAT3* mutations are present in a subset of patients with RA and associated with anti-PAD4 antibodies**

Patient group	*STAT3* mut	*P*	D661Y mut	*P*	Y640F mut	*P*
T-LGLL/RA (n = 90)	83% (75)		58% (52)		70% (63)	
Anti-PAD4+ (n = 52)	90% (47)	*.047	71% (37)	**.0047	77% (40)	.108
Anti-PAD4− (n = 38)	74% (28)		39% (15)		61% (23)	
RA (n = 98)	16% (16)		8% (8)		10% (10)	
Anti-PAD4+ (n = 23)	39% (9)	**.002	26% (6)	**.0019	22% (5)	.052
Anti-PAD4− (n = 75)	9% (7)		3% (2)		7% (5)	

PAD4, peptidylarginine deiminase type IV; RA, rheumatoid arthritis; *STAT3*, signal transducer and activator of transcription 3; T-LGLL, T-large granular lymphocytic leukaemia.
* $P < .05$.
** $P < .01$.

9%, $P = .002$). The D661Y mutation was found in 26% of anti-PAD4 positive RA, and the Y640F mutation was found in 22% of anti-PAD4 positive RA, as compared with 3% ($P = .002$) and 7% ($P = .05$) of anti-PAD4 negative RA, respectively (Table 2). These data indicate that humoral autoimmunity to PAD4 is linked to activating *STAT3* mutations in CTLs of both patients with T-LGLL/RA and RA.

Characterisation of CTL phenotypes in anti-PAD4 positive RA

Given the striking enrichment of anti-PAD4 antibodies in patients with T-LGLL/RA and increased frequency of CTLs harbouring *STAT3* mutations in anti-PAD4 positive RA, we addressed whether CTLs in anti-PAD4 positive RA might share features of LGLs. The LGL phenotype varies between patients and can include expression of CD57, NK markers CD16 and CD56, and reduced expression of pan-T cell markers CD5 and CD7 [42−47]. The expression of these LGL markers, as well as typical lineage and activation markers, was assessed in PBMCs from T-LGLL (n = 5), anti-PAD4 positive T-LGLL/RA (n = 3), anti-PAD4 positive RA (n = 10), anti-PAD4 negative RA (n = 10), and HCs (n = 10) via flow cytometry (Supplemental Table S10).

Dimensional reduction analysis was performed to generate a uniform manifold approximation and projection of CTLs consisting of 8 clusters based on expression of the 11 markers assessed (Fig 4A,B). Clusters 6 and 8 were overrepresented in T-LGLL (13.62% and 18.81%, respectively) and T-LGLL/RA (18.62% and 27.77%, respectively) (Fig 4C,D). Cluster 6 represents human leukocyte antigen (HLA)-DR+ CD38+ CD5 low, CD7 low TEMRA cells. Cluster 8 is similar to cluster 6 and also includes CD57 high cells (Fig 4B). The phenotypes present in clusters 6 and 8 are consistent with the known phenotype of LGLs [42]. Cluster 7 represents CD57 high, CD7 low, TEMRA cells, without any other defining features (Fig 4B-D), and comprised 16.23% of the CTLs in anti-PAD4 positive RA. Although LGLs are not overrepresented in this disease subset, patients with anti-PAD4−positive RA had a numerically higher proportion of CD57 high CD7 low TEMRA cells (cluster 7) than anti-PAD4−negative RA or HCs, indicating the presence of chronically stimulated CTLs, similar to T-LGLL and T-LGLL/RA.

Patients with Anti-PAD4+ RA have PAD4-specific CTLs that express CD69, CD57, KLRG1, and a TEMRA phenotype

Previous studies have shown oligoclonality of CTLs in RA, specifically among CD57+ CD8+ T cells [48,49], and have identified CTLs specific for citrullinated antigens [20]. This, along with our data linking anti-PAD4 antibodies with CTL involvement in RA, led us to hypothesise that PAD4 may be a target of antigen-specific CTLs in anti-PAD4 positive RA. To assess the existence of PAD4-specific CTLs in RA, high-resolution HLA class I sequencing was first performed to identify major histocompatibility complex class I alleles present at high frequency in our cohort. This analysis revealed that the most common allele in our RA cohort was HLA-A*02:01 (present in 49% of patients). The Net-CTL 1.2 Algorithm was used to predict 9-amino acid long peptides of the susceptible variant of the PAD4 protein that could bind to the HLA-A2 supertype (Supplemental Table S11). Each PAD4 peptide predicted to bind to the HLA-A2 supertype was individually tested using Multiparameter Fluorospot with PBMCs from 2 patients with HLA-A*02:01−positive anti-PAD4−positive RA and 1 HLA-A*02:01 positive HC. Eight of the 22 PAD4 peptides tested were found to elicit a greater or equal coexpression of IFN-γ and Granzyme B in either patient with anti-PAD4−positive RA than the HC and were selected for subsequent analysis (Supplemental Fig S3).

These 8 PAD4 peptides (40, 105, 109, 263, 271, 285, 312, and 534) and a pool of all 22 PAD4 peptides predicted to bind HLA-A2 supertype were tested in a peptide stimulation assay to measure their ability to induce degranulation and activation of CTLs (flow panels are shown in Supplemental Table S12 and gating strategy is shown in Supplemental Fig S6). All PBMCs used in this assay were from HLA-A*02:01 positive individuals. Patients with anti-PAD4−positive RA had a significantly higher percentage of CTLs that degranulated in response to Peptide 105 (KALLYLTGV) with a median (95% CI) of 0.1 (0.03-0.57) than anti-PAD4−negative RA (0.0 [0.0-0.08], $P = .04$), or HCs (0.0 [0.0-0.03], $P = .03$). We observed a similar trend with Peptide 263 (GLITLTISL), with a median (95% CI) of 0.12 (0.0-0.54) in anti-PAD4−positive RA, compared with 0.01 (0.0-0.25) ($P = .29$) in anti-PAD4−negative RA, and 0.0 (0.0-0.06) ($P = .09$) in HC (Fig 5A). The PAD4 peptide pool also demonstrated a similar trend: 0.52 (0.18-0.77) in anti-PAD4−positive RA, compared with 0.25 (0.0-0.43) ($P = .27$) in anti-PAD4−negative RA and 0.05 (0.02-0.31) ($P = .11$) in HC (Fig 5A). None of the other PAD4 peptides tested induced CTL degranulation or activation (Supplemental Fig S4).

To identify the presence of PAD4-specific CTLs in anti-PAD4−positive RA, a pentamer binding assay was performed using HLA-A*02:01 pentamers with either the KALLYLTGV or GLITLTISL peptides (both peptides induced CTL degranulation in patients with anti-PAD4−positive RA [Fig 5A]). The flow panel used for the pentamer binding assay is shown in Supplemental Table S13, and the gating strategy is shown in Supplemental Fig S7. All PBMCs used in this assay were from HLA-A*02:01−positive individuals. A significantly higher percentage of CD8+ T cells from patients with anti-PAD4−positive RA bound the KALLYLTGV pentamer (median [95% CI] of 0.32 [0.23-0.47]) than anti-PAD4−negative RA (0.13 [0.05-0.25], $P = .02$) or HC

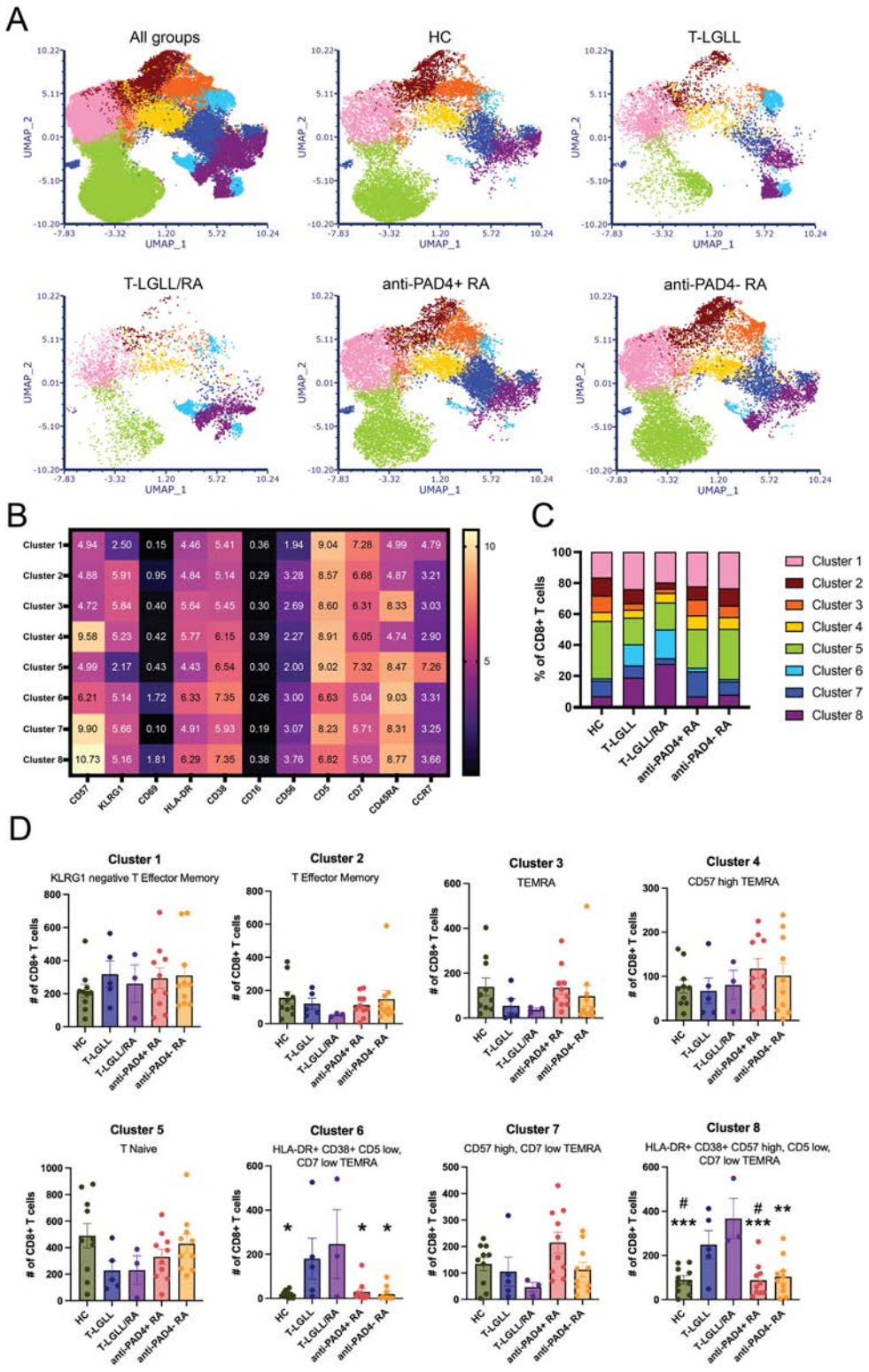

Figure. 4. Phenotypic analysis of CD8+ T cells in T-LGLL, T-LGLL/RA, anti-PAD4+ RA, anti-PAD4- RA, and HC. (A) Colour dot plots show UMAPs generated using T-LGLL (n = 5), T-LGLL/RA (n = 3), anti-PAD4+ RA (JHU cohort; n = 10), anti-PAD4- RA (JHU cohort; n = 10), and HC (n = 10). The first UMAP shows all patients and controls, and subsequent UMAPs show each group separately. (B) A heat map shows the scaled MFI of each of the 11 markers within each of the 8 clusters. (C) The stacked bar graph shows the percentage of each cluster that was found in each disease group. (D) Bar graphs show number of CD8+ T cells in each disease group within each cluster. Each data point represents 1 patient, and mean with SEM is shown. *$P < .05$, **$P < .01$, and ***$P < .001$ with T-LGLL/RA as the comparator group; # = $P < .05$ with T-LGLL as the comparator group. ANC, absolute neutrophil count; AU, arbitrary unit; HC, healthy control; JHU, Johns Hopkins University; MFI, mean fluorescence intensity; PAD4, peptidylarginine deiminase type IV; RA, rheumatoid arthritis; T-LGLL, T-large granular lymphocytic leukaemia; UMAP, uniform manifold approximation and projection; UVA, University of Virginia.

(0.12 [0.06-0.19], $P = .049$) (Fig 5B). We did not observe binding to the GLITLTISL PAD4 pentamer or the HIV pentamer above the no pentamer negative control (Fig 5B). Of the patients with anti-PAD4−positive RA tested, 88% had CTLs specific for the KALLYLTGV peptide, compared with only 25% of anti-PAD4 −negative RA ($P = .02$) and 20% of HC ($P = .03$), where positivity was defined as greater than the 95th percentile of pentamer positive CD8+ T cells in HC subjects.

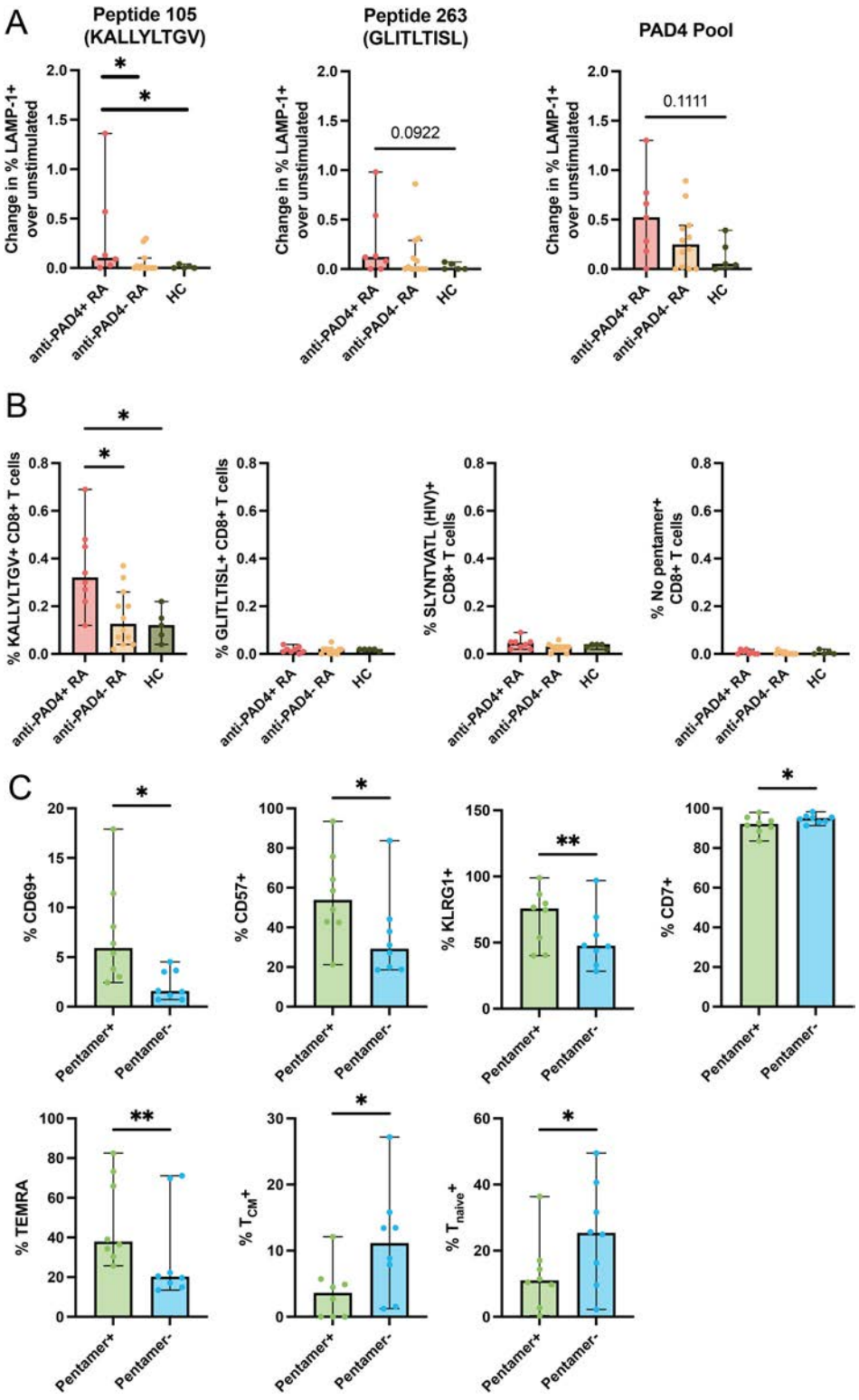

Figure. 5. Patients with anti-PAD4 + RA have PAD4-specific CD8 + T cells that express CD69, CD57, KLRG1, and a TEMRA phenotype. (A) Bar graphs show the percentage of CD8 + T cells that express LAMP-1 when stimulated with PAD4 peptide 105 (KALLYLTGV), PAD4 peptide 263 (GLITLTISL), or a pool of 22 PAD4 peptides predicted to bind HLA-A2, after subtracting the percentage of LAMP-1 + cells in the unstimulated condition. PBMCs from patients with HLA-A*02:01−positive anti-PAD4 + RA (JHU cohort; n = 7), patients with anti-PAD4− RA (JHU cohort; n = 12), and HC (n = 5) were included in this analysis (B) Bar graphs show the percentage of CD8 + T cells that bound the KALLYLTGV pentamer, GLITLTISL pentamer, negative control HIV pentamer (SLYNTVATL), or that stained positive for PE in the no pentamer condition (negative control). PBMCs from HLA-A*02:01 positive patients with anti-PAD4 + RA (JHU cohort; n = 8), patients with anti-PAD4− RA (JHU cohort; n = 12), and HC (n = 5) were included in this analysis. (C) Bar graphs show the percentage of CD8 + T cells in patients with anti-PAD4 + RA (JHU cohort; n = 8) that were positive or negative for the KALLYLTGV pentamer that expressed CD69, CD57, KLRG1, CD7, or a TEMRA, T_{CM}, or T_{naive} phenotype. Median with 95% CI is shown for all bar graphs. *P < .05, **P < .01. HC, healthy control; HLA-A2, human leukocyte antigen serotype A2; JHU, Johns Hopkins University; LAMP-1, lysosomal associated membrane protein 1; PAD4, peptidylarginine deiminase type IV; PBMCs, peripheral blood mononuclear cells; PE, R-Phycoerythrin; RA, rheumatoid arthritis; T-LGLL, T-large granular lymphocytic leukaemia; TEMRA, T effector memory cells re-expressing CD45RA.

In patients with anti-PAD4+ RA, a greater percentage of KALLYLTGV-positive vs KALLYLTGV-negative CTLs expressed CD69 (median of 5.90% vs 1.56%, $P = .02$), CD57 (53.74% vs 29.16%, $P = .02$), KLRG1 (75.62% vs 47.48%, $P = .008$), and a TEMRA phenotype (37.76% vs 20.10%, $P = .008$), which are indicative of chronic activation and are expressed by LGLs (Fig 5C). Notably, a lower percentage of KALLYLTGV-positive cells expressed CD7, a marker downregulated in LGLs (92.06% vs 94.94%, $P = .04$), or were T_{cm} (3.59% vs 11.12%, $P = .04$) or T_{naive} (10.94% vs 25.31%, $P = .02$) cells (Fig 5C). In addition, a higher percentage of KALLYLTGV-positive cells compared with KALLYLTGV-negative cells expressed activation markers CD137, HLA-DR, CD38, and LGL marker CD56, and a lower percentage expressed CD5, a pan-T cell marker downregulated in LGLs, but these did not reach significance (Supplemental Fig S5). These data reveal that patients with anti-PAD4 antibodies harbour PAD4-specific CTLs that express features of chronically antigen-stimulated cells.

DISCUSSION

Our work reveals striking serologic and haematologic similarities between T-LGLL/RA and anti-PAD4−positive RA that suggest a shared CTL-associated mechanism. Here, we identified that anti-PAD4 antibodies were significantly enriched in patients with T-LGLL/RA relative to T-LGLL and spontaneous RA, demonstrating that anti-PAD4 antibodies are highly specific serological biomarkers of an RA endotype linked to pathogenic CTLs. This is strengthened by our findings that patients with anti-PAD4 positive with RA harboured CTLs with increased rates of *STAT3* activating mutations, features of chronically antigen-stimulated TEMRA cells, and reactivity to PAD4 peptides. Clinically, the enrichment of anti-PAD4 antibodies in T-LGLL/RA and their association with a prolonged interval between RA and subsequent T-LGLL diagnosis suggest that anti-PAD4 antibodies may identify patients with RA with chronic PAD4-driven CTL stimulation who are at higher risk for future T-LGLL development. Together, our data suggest that T-LGLL in the RA population occurs on a continuum, with T-LGLL/RA representing an extreme end of the spectrum of CTL-associated RA enriched in autoimmunity to citrullinated antigens and PAD4.

In this study, we found that homozygosity for the susceptible haplotype of *PADI4* is enriched in patients with T-LGLL/RA who developanti-PAD4 antibodies. The *PADI4* susceptible haplotype has been shown to associate with anti-PAD4 antibodies in 1 RA cohort [7], but this was not observed in other RA cohorts [37,38], and was not seen in the group of patients with RA included in our study. The functional consequences of the *PADI4* polymorphisms associated with RA development remain unclear, with hypotheses including stabilising PAD4 mRNA [7,9,36]. Although our study focused on the relationship between 3 specific polymorphisms in the *PADI4* gene and the development of anti-PAD4 antibodies in T-LGLL/RA, it is possible that other SNPs within the *PADI4* gene or in nearby genes as part of an extended haplotype may also increase the genetic risk for developing autoimmunity to PAD4 as well as T-LGLL more broadly. In this regard, studies on the effects of *PADI4* SNPs have not yet extended to understanding the relationship between the susceptible haplotype and cellular immunity to PAD4. Future studies aimed at more broadly understanding the immunologic significance of *PADI4* SNPs to the breach of tolerance to PAD4 are warranted.

Our data show that patients with anti-PAD4+ RA harbour CTLs enriched for features reminiscent of LGLs including *STAT3* mutations and a chronically antigen-stimulated TEMRA phenotype. These genetic and immunological similarities between T-LGLL/RA and RA provide compelling evidence linking humoral autoimmunity to PAD4 with CTL-associated RA. The enrichment in *STAT3* mutations in patients with anti-PAD4−positive T-LGLL/RA or patients with RA could support the persistence and accumulation of autoreactive CTLs in these patients. In fact, there is evidence of oligoclonal CD8+ CD57+ granzyme+ T cells in the RA synovium [17,50,51], and CTLs specific for citrullinated antigens have been identified in RA [20]. Importantly, our study in patients with anti-PAD4+ RA adds PAD4 as a novel target of CTLs, which can degranulate in response to cognate antigen recognition, and express an activated, antigen experienced, and chronically stimulated phenotype. Future studies are needed to further define the functionality of PAD4-specific CTLs and their ability to kill PAD4-expressing cells *in vitro* and *in vivo*.

The mechanistic roles of anti-PAD4 antibodies and PAD4-specific CTLs in RA remain to be determined. Given that we observed a modest negative correlation between ANC and anti-PAD4 antibodies in T-LGLL/RA, and the only 2 patients with RA with neutropenia were anti-PAD4 positive, 1 hypothesis is that anti-PAD4 antibodies may directly target and contribute to the killing of neutrophils, which are highly abundant in the RA joint and express surface PAD4 [52], via antibody dependent cellular cytotoxicity or complement-dependent cytotoxicity [53]. Furthermore, our data that PAD4-specific CTLs are present in the peripheral blood of patients with anti-PAD4−positive RA suggest that CTLs may also target PAD4-expressing neutrophils through recognition of PAD4 peptides displayed on surface major histocompatibility complex class I, leading to perforin-mediated neutrophil hypercitrullination and cell death [11]. Certainly, other factors may also contribute to neutropenia in patients with T-LGLL/RA and in T-LGLL who do not develop RA or anti-PAD4 immune responses [39]. Studies have shown that sera of patient with T-LGLL have increased levels of soluble Fas ligand and enhanced capacity to induce apoptosis in neutrophils *ex vivo* [53,54]. Bone marrow abnormalities in patients with T-LGLL have also been described, with fibrosis, hypercellularity, and lymphocyte infiltration reported in some patients [39]. Thus, neutropenia in T-LGLL/RA is likely multifactorial, with PAD4-directed autoimmunity representing 1 of several possible mechanisms contributing to reduced neutrophil counts in these patients. In patients with T-LGLL who do not develop RA, it is likely that the other mechanisms are dominant and that these patients lack the requisite genetic risk factors and contributing environmental exposures needed to break immune tolerance to citrullination-associated antigens and develop RA.

Although it is still unknown whether subclinical T-LGLL or RA develops first in patients who ultimately receive both diagnoses, we have identified anti-PAD4 antibodies as a biomarker of T-LGLL/RA. Our results highlight serologic, genetic, and haematologic factors linked to CTL-associated RA and reveal the presence of autoreactive PAD4-specific CTLs in patients with RA with humoral autoimmunity to PAD4. These findings reveal CTLs as a common mechanistic link between the anti-PAD4 autoantibody positive subset of RA and RA occurring in the setting of T-LGLL.

CONCLUSIONS

Here, we demonstrated that patients with T-LGLL/RA have a high prevalence of anti-PAD4 antibodies, identifying anti-PAD4 antibodies as a biomarker of RA in the T-LGLL population. We additionally found that anti-PAD4 positivity in sporadic RA is

associated with activating *STAT3* mutations and PAD4-specific CTLs that bear phenotypic similarities to LGLs. This study provides evidence that humoral autoimmunity to PAD4 is a marker of CTL-associated RA.

Competing interests

ED is currently an employee of AstraZeneca and may own shares and/or restricted stock of AstraZeneca. ED and FA are authors on licensed patent no. 8975033, entitled 'Human autoantibodies specific for PAD3 which are cross-reactive with PAD4 and their use in the diagnosis and treatment of rheumatoid arthritis and related diseases' and on a pending patent application no. WO2024233251A2, entitled 'Human monoclonal antibodies that enhance pad4 for use in autoimmune diseases'. FA has received consulting fees from RheumaLogics. TPL has received Scientific Advisory Board membership, consultancy fees, honoraria, and/or stock options from Keystone Nano, Flagship Labs 86, Dren Bio, Recludix Pharma, Kymera Therapeutics, Nouveau Biosciences, and CancerRx. DJF has received research funding, honoraria, and/or stock options from AstraZeneca, Dren Bio, Recludix Pharma, and Kymera Therapeutics. COB has served as a consultant for AbbVie, BMS, Eli Lilly, Janssen, Pfizer, and Sanofi. DK has served on the Aurinia Lupus Center Advisory Board, and Clinical Advisory Board for Landos Biopharma; and is a member of the Amgen Speaker's Bureau. All other authors have declared no conflicts of interest.

CRediT authorship contribution statement

Kusuma Ananth: Writing – review & editing, Writing – original draft, Visualization, Investigation, Formal analysis, Data curation, Conceptualization. **Katharine B Moosic:** Writing – review & editing, Investigation, Formal analysis, Data curation. **Eduardo Gomez-Banuelos:** Writing – review & editing, Visualization, Formal analysis. **Hong Wang:** Writing – review & editing, Investigation, Formal analysis. **Isabel Trejo-Zambrano:** Writing – review & editing, Investigation. **Ramona Johnson:** Writing – review & editing, Formal analysis. **Jessica Marie Kirschmann:** Writing – review & editing, Investigation. **Tess Deddens:** Writing – review & editing, Data curation. **Omar Elghawy:** Writing – review & editing, Formal analysis. **Bryna Shemo:** Writing – review & editing, Data curation. **William H Robinson:** Writing – review & editing, Investigation. **Donald Kimpel:** Writing – review & editing, Resources. **Clifton O Bingham:** Writing – review & editing, Resources, Funding acquisition. **David J Feith:** Writing – review & editing, Investigation. **Brendan Antiochos:** Writing – review & editing, Writing – original draft, Resources. **Felipe Andrade:** Writing – review & editing, Funding acquisition, Conceptualization. **Thomas P Loughran Jr:** Writing – review & editing, Resources, Funding acquisition. **Erika Darrah:** Writing – review & editing, Writing – original draft, Visualization, Investigation, Funding acquisition, Formal analysis, Conceptualization.

Acknowledgements

We thank Christopher Thoburn and the Sidney Kimmel Comprehensive Cancer Center (SKCCC) Immune Monitoring Core (IMC), funded by the Sidney Kimmel Cancer Center National Cancer Institute P30 CA006973 Center Grant, for performing Multiparameter Fluorospot experiments. We thank Marilyn C. Towns and Michelle Jones at the Johns Hopkins Division of Rheumatology for collecting samples of patients with RA and performing chart reviews. We thank John Schroeder at the Johns Hopkins School of Medicine for providing PBMCs from healthy donor leukopaks. We thank Alexander Girgis for advising on the statistical analyses. We thank Matthew Schmachtenberg, Heather Robinette, and Carey Thomas for technical support of the LGL leukaemia cohorts at University of Virginia. We thank all the patients and healthy donors who donated blood for this study.

Funding

This study was funded by the National Institute of Allergy and Infectious Diseases (NIAID), and the National Institute of Arthritis and Musculoskeletal and Skin Diseases (NIAMS) at the National Institutes of Health (NIH) grant numbers R01AR079404, P30AR070254, and R21AI188438. Jerome L. Greene Foundation, the Patient Centered Outcomes Research Institute (PCORI) Pilot Project Award IP2-PI000737, and the P30AR053503 funded the collection of patient samples. The study was also funded by the R01CA178393 as well as the Bess Family Charitable fund, a gift from a generous anonymous donor, and Scarlet Feather Fund sponsorship for the T-cell Orphan Blood Cancer Research Initiative (TOBCRI). Part of this work was presented at AAI 2023 and FOCIS 2025. The content of this study is solely the responsibility of the authors and does not necessarily represent the official views of the National Institutes of Health.

Patient consent for publication

Not applicable.

Ethics approval

This study was approved by the Institutional Review Boards at Johns Hopkins University School of Medicine and at University of Virginia.

Provenance and peer review

Not commissioned; externally peer reviewed.

Supplementary materials

Supplementary material associated with this article can be found in the online version at doi:10.1016/j.ard.2026.04.006.

Orcid

Kusuma Ananth: http://orcid.org/0000-0002-0361-3465
Erika Darrah: http://orcid.org/0000-0003-1119-0279

REFERENCES

[1] Darrah E, Andrade F. Rheumatoid arthritis and citrullination. Curr Opin Rheumatol 2018;30(1):72–8. doi: 10.1097/BOR.0000000000000452.
[2] Schellekens GA, de Jong BA, van den Hoogen FH, van de Putte LB, van Venrooij WJ. Citrulline is an essential constituent of antigenic determinants recognized by rheumatoid arthritis-specific autoantibodies. J Clin Invest. 1998;101(1):273–81. doi: 10.1172/JCI1316.
[3] Lutteri L, Malaise M, Chapelle J. Comparison of second- and third-generation anti-cyclic citrullinated peptide antibodies assays for detecting rheumatoid arthritis. Clin Chim Acta 2007;386(1):76–81. doi: 10.1016/j.cca.2007.08.002.
[4] dos Anjos LME, Pereira IA, d 'Orsi E, Seaman AP, Burlingame RW, Morato EF. A comparative study of IgG second- and third-generation anti-cyclic citrullinated peptide (CCP) ELISAs and their combination with IgA third-generation

CCP ELISA for the diagnosis of rheumatoid arthritis. Clin Rheumatol. 2009;28(2):153–8. doi: 10.1007/s10067-008-0999-5.
[5] Masson-Bessière C, Sebbag M, Girbal-Neuhauser E, Nogueira L, Vincent C, Senshu T, et al. The major synovial targets of the rheumatoid arthritis-specific antifilaggrin autoantibodies are deiminated forms of the alpha- and beta-chains of fibrin. J Immunol. 2001;166(6):4177–84. doi: 10.4049/jimmunol.166.6.4177.
[6] Matsuo K, Xiang Y, Nakamura H, Masuko K, Yudoh K, Noyori K, et al. Identification of novel citrullinated autoantigens of synovium in rheumatoid arthritis using a proteomic approach. Arthritis Res Ther. 2006;8(6):R175. doi: 10.1186/ar2085.
[7] Harris ML, Darrah E, Lam GK, Bartlett SJ, Giles JT, Grant AV, et al. Association of autoimmunity to peptidyl arginine deiminase type 4 with genotype and disease severity in rheumatoid arthritis. Arthritis Rheum. 2008;58(7):1958–67. doi: 10.1002/art.23596.
[8] Darrah E, Giles JT, Ols ML, Bull HG, Andrade F, Rosen A. Erosive rheumatoid arthritis is associated with antibodies that activate PAD4 by increasing calcium sensitivity. Sci Transl Med 2013;5(186):186ra65. doi: 10.1126/scitranslmed.3005370.
[9] Curran AM, Naik P, Giles JT, Darrah E. PAD enzymes in rheumatoid arthritis: pathogenic effectors and autoimmune targets. Nat Rev Rheumatol. 2020;16(6):301–15. doi: 10.1038/s41584-020-0409-1.
[10] Darrah E, Martinez-Prat L, Mahler M. Clinical utility of antipeptidyl arginine deiminase type 4 antibodies. J Rheumatol. 2019;46(3):329–30. doi: 10.3899/jrheum.180905.
[11] Romero V, Fert-Bober J, Nigrovic PA, Darrah E, Haque UJ, Lee DM, et al. Immune-mediated pore-forming pathways induce cellular hypercitrullination and generate citrullinated autoantigens in rheumatoid arthritis. Sci Transl Med. 2013;5(209):209ra150. doi: 10.1126/scitranslmed.3006869.
[12] Darrah E, Kim A, Zhang X, Boronina T, Cole RN, Fava A, et al. Proteolysis by Granzyme B enhances presentation of autoantigenic peptidylarginine deiminase 4 epitopes in rheumatoid arthritis. J Proteome Res. 2017;16(1):355–65. doi: 10.1021/acs.jproteome.6b00617.
[13] Romero V, Darrah E, Andrade F. Generation of distinct patterns of rheumatoid arthritis autoantigens by peptidylarginine deiminase types 2 and 4 during perforin-induced cell damage. Arthritis Rheumatol. 2020;72(6):912–8. doi: 10.1002/art.41196.
[14] Donado CA, Theisen E, Zhang F, Nathan A, Fairfield ML, Rupani KV, et al. Granzyme K activates the entire complement cascade. Nature 2025;641(8061):211–21. doi: 10.1038/s41586-025-08713-9.
[15] Cho B, Sim JH, Park JA, Kim HW, Yoo WH, Lee SH, et al. Characterization of effector memory CD8+ T cells in the synovial fluid of rheumatoid arthritis. J Clin Immunol. 2012;32(4):709–20. doi: 10.1007/s10875-012-9674-3.
[16] Savola P, Kelkka T, Rajala HL, Kuuliala A, Kuuliala K, Eldfors S, et al. Somatic mutations in clonally expanded cytotoxic T lymphocytes in patients with newly diagnosed rheumatoid arthritis. Nat Commun. 2017;8:15869. doi: 10.1038/ncomms15869.
[17] Masuko-Hongo K, Sekine T, Ueda S, Kobata T, Yamamoto K, Nishioka K, et al. Long-term persistent accumulation of CD8+ T cells in synovial fluid of rheumatoid arthritis. Ann Rheum Dis. 1997;56(10):613–21. doi: 10.1136/ard.56.10.613.
[18] Tak PP, Spaeny-Dekking L, Kraan MC, Breedveld FC, Froelich CJ, Hack CE. The levels of soluble granzyme A and B are elevated in plasma and synovial fluid of patients with rheumatoid arthritis (RA). Clin Exp Immunol. 1999;116(2):366–70. doi: 10.1046/j.1365-2249.1999.00881.x.
[19] Shan L, van den Hoogen LL, Meeldijk J, Kok HM, Jongeneel LH, Boes M, et al. Increased intra-articular granzyme M may trigger local IFN-λ1/IL-29 response in rheumatoid arthritis. Clin Exp Rheumatol. 2020;38(2):220–6. doi: 10.55563/clinexprheumatol/ffb107.
[20] Moon J, Younis S, Ramadoss NS, Iyer R, Sheth K, Sharpe O, et al. Cytotoxic CD8+ T cells target citrullinated antigens in rheumatoid arthritis. Nat Commun 2023;14(1):319. doi: 10.1038/s41467-022-35264-8.
[21] Zhang R, Shah MV, Loughran TP. The root of many evils: indolent large granular lymphocyte leukaemia and associated disorders. Hematol Oncol. 2010;28(3):105–17. doi: 10.1002/hon.917.
[22] Lamy T, Loughran TP. How I treat LGL leukemia. Blood 2011;117(10):2764–74. doi: 10.1182/blood-2010-07-296962.
[23] Yang J, Epling-Burnette PK, Painter JS, Zou J, Bai F, Wei S, et al. Antigen activation and impaired Fas-induced death-inducing signaling complex formation in T-large-granular lymphocyte leukemia. Blood 2008;111(3):1610–6. doi: 10.1182/blood-2007-06-093823.
[24] Koskela HLM, Eldfors S, Ellonen P, van Adrichem AJ, Kuusanmäki H, Andersson EI, et al. Somatic STAT3 Mutations in Large Granular Lymphocytic Leukemia. N Engl J Med. 2012;366(20):1905–13. doi: 10.1056/NEJMoa1114885.
[25] Epling-Burnette PK, Liu JH, Catlett-Falcone R, Turkson J, Oshiro M, Kothapalli R, et al. Inhibition of STAT3 signaling leads to apoptosis of leukemic large granular lymphocytes and decreased Mcl-1 expression. J Clin Invest. 2001;107(3):351–62. doi: 10.1172/JCI9940.
[26] Smolen JS, Aletaha D, Barton A, Burmester GR, Emery P, Firestein GS, et al. Rheumatoid arthritis. Nat Rev Dis Primers 2018;4:18001. doi: 10.1038/nrdp.2018.1.
[27] Moosic KB, Ananth K, Andrade F, Feith DJ, Darrah E, Loughran TP. Intersection between large granular lymphocyte leukemia and rheumatoid arthritis. Front Oncol. 2022;12:869205. doi: 10.3389/fonc.2022.869205.
[28] Sokolove J, Bromberg R, Deane KD, Lahey LJ, Derber LA, Chandra PE, et al. Autoantibody epitope spreading in the pre-clinical phase predicts progression to rheumatoid arthritis. PLoS One 2012;7(5):e35296. doi: 10.1371/journal.pone.0035296.
[29] Moosic KB, Olson TL, Freijat M, Khalique S, Hamele CE, Shemo B, et al. Activating STAT3 mutations in CD8+ T-cells correlate to serological positivity in rheumatoid arthritis. Front Immunol. 2024;15:1466276. doi: 10.3389/fimmu.2024.1466276.
[30] Zhang G, Xu J, Du D, Liu Y, Dai L, Zhao Y. Diagnostic values, association with disease activity and possible risk factors of anti-PAD4 in rheumatoid arthritis: a meta-analysis. Rheumatology (Oxford) 2024;63(4):914–24. doi: 10.1093/rheumatology/kead545.
[31] Navarro-Millán I, Darrah E, Westfall AO, Mikuls TR, Reynolds RJ, Danila MI, et al. Association of anti-peptidyl arginine deiminase antibodies with radiographic severity of rheumatoid arthritis in African Americans. Arthritis Res Ther. 2016;18(1):241. doi: 10.1186/s13075-016-1126-7.
[32] Nissinen R, Paimela L, Julkunen H, Tienari PJ, Leirisalo-Repo M, Palosuo T, et al. Peptidylarginine deiminase, the arginine to citrulline converting enzyme, is frequently recognized by sera of patients with rheumatoid arthritis, systemic lupus erythematosus and primary Sjögren syndrome. Scand J Rheumatol. 2003;32(6):337–42. doi: 10.1080/03009740410004990.
[33] Zhao J, Zhao Y, He J, Jia R, Li Z. Prevalence and significance of anti-peptidylarginine deiminase 4 antibodies in rheumatoid arthritis. J Rheumatol. 2008;35(6):969–74.
[34] Pollmann S, Stensland M, Halvorsen EH, Sollid LM, Kvien TK, Fleckenstein B, et al. Anti-PAD4 autoantibodies in rheumatoid arthritis: levels in serum over time and impact on PAD4 activity as measured with a small synthetic substrate. Rheumatol Int. 2011;32(5):1271–6. doi: 10.1007/s00296-010-1765-y.
[35] Cappelli LC, Hines D, Wang H, Bingham CO, Darrah E. Anti-peptidylarginine deiminase 4 autoantibodies and disease duration as predictors of treatment response in rheumatoid arthritis. ACR Open Rheumatol. 2024;6(2):81–90. doi: 10.1002/acr2.11630.
[36] Suzuki A, Yamada R, Chang X, Tokuhiro S, Sawada T, Suzuki M, et al. Functional haplotypes of PADI4, encoding citrullinating enzyme peptidylarginine deiminase 4, are associated with rheumatoid arthritis. Nat Genet. 2003;34(4):395–402. doi: 10.1038/ng1206.
[37] Reyes-Castillo Z, Palafox-Sánchez CA, Parra-Rojas I, Martínez-Bonilla GE, del Toro-Arreola S, Ramírez-Dueñas MG, et al. Comparative analysis of autoantibodies targeting peptidylarginine deiminase type 4, mutated citrullinated vimentin and cyclic citrullinated peptides in rheumatoid arthritis: associations with cytokine profiles, clinical and genetic features. Clin Exp Immunol. 2015;182(2):119–31. doi: 10.1111/cei.12677.
[38] Guderud K, Mæhlen MT, Nordang GBN, Viken MK, Andreassen BK, Molberg Ø, et al. Lack of association among peptidyl arginine deiminase type 4 autoantibodies, PADI4 polymorphisms, and clinical characteristics in rheumatoid arthritis. J Rheumatol. 2018;45(9):1211–9. doi: 10.3899/jrheum.170769.
[39] Calabretto G, Teramo A, Barilà G, Vicenzetto C, Gasparini VR, Semenzato G, et al. Neutropenia and large granular lymphocyte leukemia: from pathogenesis to therapeutic options. Cells 2021;10(10):2800. doi: 10.3390/cells10102800.
[40] Teramo A, Barilà G, Calabretto G, Ercolin C, Lamy T, Moignet A, et al. STAT3 mutation impacts biological and clinical features of T-LGL leukemia. Oncotarget 2017;8(37):61876–89. doi: 10.18632/oncotarget.18711.
[41] Barilà G, Teramo A, Calabretto G, Vicenzetto C, Gasparini VR, Pavan L, et al. Stat3 mutations impact on overall survival in large granular lymphocyte leukemia: a single-center experience of 205 patients. Leukemia 2020;34(4):1116–24. doi: 10.1038/s41375-019-0644-0.
[42] Assmann JLJC, Leon LG, Stavast CJ, van den Bogaerdt SE, Schilperoord-Vermeulen J, Sandberg Y, et al. miR-181a is a novel player in the STAT3-mediated survival network of TCRαβ+ CD8+ T large granular lymphocyte leukemia. Leukemia 2022;36(4):983–93. doi: 10.1038/s41375-021-01480-2.
[43] Lundell R, Hartung L, Hill S, Perkins SL, Bahler DW. T-cell large granular lymphocyte leukemias have multiple phenotypic abnormalities involving pan-T-cell antigens and receptors for MHC molecules. Am J Clin Pathol. 2005;124(6):937–46.
[44] Lamy T, Moignet A, Loughran Jr TP. LGL leukemia: from pathogenesis to treatment. Blood 2017;129(9):1082–94. doi: 10.1182/blood-2016-08-692590.

[45] O'Malley DP. T-cell large granular leukemia and related proliferations. Am J Clin Pathol. 2007;127(6):850–9. doi: 10.1309/A8FHDA0VVRJ05GJP.
[46] Giudice V, D'Addona M, Montuori N, Selleri C. The value of flow cytometry clonality in large granular lymphocyte leukemia. Cancers (Basel) 2021;13 (18):4513. doi: 10.3390/cancers13184513.
[47] Costa RO, Bellesso M, Chamone DAF, Ruiz MA, Hallack Neto AE, Aldred VL, et al. T-cell large granular lymphocytic leukemia: treatment experience with fludarabine. Clinics (Sao Paulo) 2012;67(7):745–8. doi: 10.6061/clinics/2012(07)07.
[48] Hall FC, Thomson K, Procter J, McMichael AJ, Wordsworth BP. TCR beta spectratyping in RA: evidence of clonal expansions in peripheral blood lymphocytes. Ann Rheum Dis. 1998;57(5):319–22. doi: 10.1136/ard.57.5.319.
[49] Hingorani R, Monteiro J, Furie R, Chartash E, Navarrete C, Pergolizzi R, et al. Oligoclonality of V beta 3 TCR chains in the CD8+ T cell population of rheumatoid arthritis patients. J Immunol. 1996;156(2):852–8.
[50] Dupuy d'Angeac A, Monier S, Jorgensen C, Gao Q, Travaglio-Encinoza A, Bologna C, et al. Increased percentage of CD3+, CD57+ lymphocytes in patients with rheumatoid arthritis. Correlation with duration of disease. Arthritis Rheum. 1993;36(5):608–12. doi: 10.1002/art.1780360506.
[51] Zhang F, Wei K, Slowikowski K, Fonseka CY, Rao DA, Kelly S, et al. Defining inflammatory cell states in rheumatoid arthritis joint synovial tissues by integrating single-cell transcriptomics and mass cytometry. Nat Immunol. 2019;20(7):928–42. doi: 10.1038/s41590-019-0378-1.
[52] Zhang L, Yuan Y, Xu Q, Jiang Z, Chu C. Contribution of neutrophils in the pathogenesis of rheumatoid arthritis. J Biomed Res. 2020;34(2):86–93. doi: 10.7555/JBR.33.20190075.
[53] Liu JH, Wei S, Lamy T, Epling-Burnette P, Starkebaum G, Djeu J, et al. Chronic neutropenia mediated by Fas ligand. Blood 2000;95(10):3219–22. doi: 10.1182/blood.V95.10.3219.
[54] Tanaka M, Suda T, Haze K, Nakamura N, Sato K, Kimura F, et al. Fas ligand in human serum. Nat Med. 1996;2(3):317–22. doi: 10.1038/nm0396-317.

Ann Rheum Dis 85 (2026) 1520–1529

Contents lists available at ScienceDirect

Annals of the Rheumatic Diseases

journal homepage: https://www.sciencedirect.com/journal/annals-of-the-rheumatic-diseases

Rheumatoid arthritis

Risk of first and second primary keratinocyte cancers in relation to treatment of rheumatoid arthritis with JAKi, TNFi, and non-TNFi bDMARDs—a Swedish nationwide study

Viking Huss[1,2,*], Hannah Bower[1], Martin Björklund[1], Karin Hellgren[1], Thomas Frisell[1], Benedicte Delcoigne[1], Daniela Di Giuseppe[1], Johan Askling[1,2], on behalf of the ARTIS group [#]

[1] *Clinical Epidemiology Division, Department of Medicine Solna, Karolinska Institutet, Stockholm, Sweden*
[2] *Rheumatology, Theme Inflammation and Ageing, Karolinska University Hospital, Stockholm, Sweden*

ARTICLE INFO

Article history:
Received 24 October 2025
Received in revised form 23 January 2026
Accepted 16 February 2026

ABSTRACT

Objectives: This study aims to assess the risks of primary and second primary keratinocyte cancers (KCs) in patients with rheumatoid arthritis (RA) and in relation to treatment with biologic disease-modifying antirheumatic drugs (bDMARDs) or targeted synthetic disease-modifying antirheumatic drugs.

Methods: Nationwide cohort study of patients treated with Janus kinase inhibitors (JAKi), tumour necrosis factor inhibitor (TNFi), or non-TNFi bDMARDs, using data from the Swedish Rheumatology Quality Register linked to other registers including the National Cancer Register, 2012 through 2023. Adjusted hazard ratios (HRs) were estimated via Cox regression using TNFi as reference.

Results: We identified 21,756 unique patients with RA. Based on 155 incident KC with JAKi, 458 with non-TNFi and 766 with TNFi, the HR for JAKi vs TNFi was 1.39 (1.16-1.68), corresponding to 1 extra KC case per every 244 patients per year. For non-TNFi vs TNFi, the HR was 0.96 (0.86-1.08). By subtype, the HR for JAKi vs TNFi was 1.41 (1.13-1.75) for basal cell carcinoma and 1.49 (1.09-2.05) for squamous cell carcinoma (SCC). For abatacept vs etanercept, the HR for SCC was 1.48 (1.11-1.97). The HR for a second primary KC was 1.31 (0.94-1.82) for JAKi and 0.94 (0.75-1.17) for non-TNFi bDMARD vs TNFi.

Conclusions: Patients treated with JAKi have an elevated risk of KC compared with patients treated with TNFi. Although the class of non-TNFi bDMARDs is not associated with increased KC risk, we repeated a drug-specific signal of increased risk for SCC with abatacept.

INTRODUCTION

Keratinocyte cancer (KC), with its 2 main subtypes, basal cell cancer (BCC) and squamous cell skin cancer (SCC), is the most common malignancy in the general population and comprises the vast majority of all 'nonmelanoma skin cancers' [1]. Established risk factors for KC include skin complexion, exposure to UV radiation, and therapeutic immunosuppression such as

*Correspondence to Dr Viking Huss, Clinical Epidemiology Division T2:01, Karolinska University Hospital Solna, Stockholm, Sweden.
E-mail address: viking.huss@ki.se (V. Huss).
Handling editor Josef S. Smolen.
[#] The ARTIS Study Group: Katerina Chatzidionysiou, Alf Kastbom, Ann Knight, Anna Deminger, Anna Södergren, Carl Tureson, Gerd-Marie Alenius, Helena Forsblad -d'Elia, Johan Askling, Johan Wallman, Lars Klareskog, Lotta Ljung, Nils Feltelius, and Valgerdur Sigurdardottir

https://doi.org/10.1016/j.ard.2026.02.015

WHAT IS ALREADY KNOWN ON THIS TOPIC

- Patients with rheumatoid arthritis (RA) are at increased risk of keratinocyte cancer (KC, a.k.a. nonmelanoma skin cancer) compared with the general population. Whether this increased risk varies with biologic or targeted synthetic disease-modifying antirheumatic drug (b/tsDMARDs) treatment is unknown, especially for Janus kinase inhibitors (JAKi). For abatacept, signals of a possible risk increase have been reported.

WHAT THIS STUDY ADDS

- For JAKi, we noted a higher incidence of first ever as well as second primary KC compared with tumour necrosis factor inhibitor (TNFi), which in turn showed a higher incidence than b/tsDMARD-naïve RA, among which the incidence was higher than that in the general population. In absolute terms, these increased KC risks would translate into 1 extra case of a first primary KC per year per every: 244 patients treated with JAKi vs TNFi, 667 patients treated with TNFi vs b/tsDMARD-naïve RA, and 526 individuals with b/tsDMARD-naïve RA vs the general population. For the class of non-TNFi bDMARDs, no overall risk increase was observed; however, the signal for squamous cell skin cancer in patients treated with abatacept was repeated.

HOW THIS STUDY MIGHT AFFECT RESEARCH, PRACTICE OR POLICY

- Our study supports the Oral Rheumatoid Arthritis Trial (ORAL) surveillance trial signal of an increased risk for KC with tofacitinib, extending it to the class of JAKi vs TNFi. We provide relative and absolute risk data on subtype-specific, second primary KC and time-dependent risks by time in relation to other b/tsDMARDs, and contextualise these risks by providing information on the relative and absolute scale on KC risks in b/tsDMARD-naïve RA and in the general population. Regular skin cancer screening may be advisable, especially in patients with prior KC starting treatment with b/tsDMARDs.

following organ transplantation [2–4]. In contrast to their high—and increasing—incidence, the mortality from KC is low, in the order of <1 per 100,000 cases [5]. Previous studies in patients with rheumatoid arthritis (RA) naïve to biologic/targeted synthetic disease-modifying antirheumatic drugs (b/tsDMARDs) have reported a 20%-80% increased risk of KC compared with the general population [6–9]. Concerns have been raised that the immune-modulatory properties of b/tsDMARDs might further increase the already elevated KC risk in RA [10]. For tumour necrosis factor inhibitor (TNFi), several studies have examined risks of KC, with somewhat inconsistent results; some studies pointing towards increased risks [11,12], others not [6,13]. Data on KC risks in relation to treatment with non-TNFi bDMARDs are scarce, and as with TNFi, results are somewhat conflicting. For abatacept, a meta-analysis of 6 observational studies did not find a statistically increased risk of KC (hazard ratio [HR]: 1.11, 95% CI: 0.98-1.26) compared with other b/tsDMARD [14]. However, a previous study from our group found an increased risk of KC with abatacept vs TNFi (HR: 2.12, 95% CI: 1.14-3.95) [15]. A meta-analysis by Xie et al [16] reported no signals of increased risks with rituximab and tocilizumab.

For Janus kinase inhibitors (JAKi), the Oral Rheumatoid Arthritis Trial (ORAL) surveillance safety trial found a signal of an almost doubled risk of KC with tofacitinib compared with TNFi. The extent to which this signal is study-, drug-, or class-specific remains unclear [17]. In a previous study from our group, based on 1967 JAKi-treated patients with RA followed for a median of 1.95 years, we reported an increased risk of KC (HR: 1.39, 95% CI: 1.01-1.91) based on 59 KC events in the JAKi cohort vs TNFi [18]. By contrast, a meta-analysis by Olivera et al [19] and 2 (shorter) recent observational US cohort studies [20,21] found no increased risk of KC with JAKi treatment. So far, available studies on risks for KC with JAKi vs TNFi have not presented data by subtype (SCC or BCC). Similarly, whether the association between JAKi and KC is similar or different in patients with a history of KC is not studied. The latter is highly clinically important for risk mitigation strategies, especially since the baseline absolute risks of KC are about 2- to 10-fold higher in individuals with a history of KC [7–9,22].

The primary aim was to estimate the incidence of KC overall and by subtypes in patients with RA initiating JAKi or non-TNFi bDMARDs compared with TNFi. Our secondary aim was to estimate the risk of a second primary KC in patients with RA who had a history of KC before their b/tsDMARD treatment start. To contextualise our findings, we put these incidences in relation to those in patients with b/tsDMARD-naïve RA and to those in the general population.

METHODS

Design and setting

We performed a nationwide cohort study (January 1, 2012 through December 31, 2023) using the Swedish Rheumatology Quality Register (SRQ) linked to the National Cancer Register and other national registers (Supplementary Table S1).

Participants

We identified all individuals in Sweden above 18 years of age registered with a diagnosis of RA in SRQ and/or in the National Patient Register (NPR) (Supplementary Table S2). To minimise misclassification, we required 2 or more registrations with a diagnosis code for RA in NPR. At least 1 of these visits had to be from an internal medicine or rheumatology department. The second of the 2 visits served as the date of inclusion. Through this, we identified virtually all patients with RA alive in Sweden during the study period. For comparison purposes, we also identified a random sample of individuals from the general population.

Exposure

In SRQ, we identified all treatment initiations for all individual b/tsDMARDs: (i) JAKi (baricitinib, filgotinib, tofacitinib, and upadacitinib), (ii) non-TNFi bDMARD (abatacept, rituximab, sarilumab, and tocilizumab), and (iii) TNFi (adalimumab, certolizumab pegol, etanercept, golimumab, and infliximab). We used the Prescribed Drug Register (PDR) to verify that treatment episodes recorded in SRQ corresponded to actually dispensed drugs. In analyses by drug class, each individual drug initiation (the first treatment episode of each individual b/tsDMARD) was included. Accordingly, patients who initiated treatment with 1 JAKi and later with a second (different) JAKi contributed both treatment episodes to the JAKi class. Similarly, a patient who was first treated with, eg, etanercept, then with rituximab, followed by upadacitinib contributed to the TNFi, non-TNFi, and JAKi classes, respectively. Nonmedical switch to the same drug (originator to biosimilar) was not counted as a treatment discontinuation. Treatment interruptions shorter than

90 days (183 days for rituximab) were considered as the same treatment episode. Patients with RA unexposed to b/tsDMARDs were considered as b/tsDMARD-naïve up until their first start of a b/tsDMARD, but not thereafter and thus censored from the b/tsDMARD-naïve cohort at that time point.

Follow-up

The start of follow-up for each treatment exposure cohort was the date of treatment initiation. Start of follow-up for the b/tsDMARD-naive cohort was the first date of entry criteria fulfilment during the study period, provided the patient was b/tsDMARD naïve at this date. For the general population subjects, the start of follow-up was the date of the matched patient's first treatment initiation. We applied an ever-treated approach in which each individual was followed until any occurrence of the outcome, death, emigration from Sweden, or the end of the study period. Thus, 1 outcome could be attributed to more than 1 treatment.

Outcomes

Outcomes were defined as first ever: (i) KC of any subtype, (ii) any SCC, (iii) *in situ* SCC, (iv) invasive SCC, and (v) BCC. In the main analysis, patients with a history of any previous invasive cancer (including KC) were excluded (Supplementary Table S3). Individuals who, during follow-up, developed a cancer other than the 1 under study were not censored. SCC was identified through ICD codes in the National Cancer Register. BCC was identified through the BCC register (Supplementary Table S4). For the analysis of the second primary KC, we performed the same analyses but restricted to patients with a history of a first KC (of any subtype) before treatment start.

Statistical methods

For each cohort, we calculated crude and age- and sex-standardised incidence rates, weighted against the age/sex distribution in the TNFi cohort. We used Cox proportional hazards models to estimate HRs using time since treatment initiation as time scale. In the class-specific analysis, we used the class of TNFi as reference. In the drug-specific analysis, we used etanercept as a reference. Models were first adjusted for age and sex. Fully adjusted HRs were additionally adjusted for line of therapy, comorbidities (diabetes, heart failure, ischaemic heart disease, hospitalised infections, lung disease, kidney failure, joint surgery, organ transplantation, and benign skin disorders), disability and sick leave, educational level, use of concomitant medications (csDMARD, steroids, and topical steroid creams), RA disease-related factors (DAS28CRP, disease duration, and seropositivity), and smoking status (Supplementary Table S5). HRs were not estimated where the number of observed events in each cohort was less than 5. Supplementary Table S6 describes missing data. We applied a missing indicator approach where missing data for a variable were coded as a separate category. In addition, we conducted alternative analyses using a complete case approach as well as a sensitivity analysis excluding variables with non-negligible proportions of missing (here: DAS28CRP, CRP, and smoking) and performed a sensitivity analysis with an IPTW weighted model for the main outcome and subtypes (Supplementary Tables S7-S9). As a measure of absolute risk increase, approximate numbers needed to harm were calculated as: 1/(age- and sex-standardised incidence rate in the exposed group—age- and sex-standardised incidence rate in the referent group, assuming stable incidences over time [23]. Stata 16.1 and R 4.5.1 were used for the analyses.

Additional analyses

We performed analyses stratified by time since treatment initiation (0 to ≤1 year, 1 to ≤2 years, 2 to ≤3 years, 3 to ≤4 years, 4 to ≤5 years, and ≥5 years), by age at treatment initiation (18-59, 60-74, and 75+ years of age), by number of previously initiated b/tsDMARDs (0, 1-2, and ≥3) and by time on active treatment (0 to ≤1 year, 1 to ≤2 years, 2 to ≤3 years, 3 to ≤4 years, 4 to ≤5 years, and ≥5 years). We limited the study period to January 1, 2017-2020 and 2017-2023, respectively. We restricted the analyses to individuals who had accumulated at least 1 year of continuous treatment, thus starting follow-up at day 366. We evaluated a 90- and 180-day lag period, and changed the main analysis from ever-treated to an on-drug analysis in which follow-up ended at the discontinuation of the treatment episode in question. The study was approved by the Swedish Ethics Review Authority 2023-03804-01.

Patients and public involvement

Patients and/or the public were not involved in the design, or conduct, or reporting, or dissemination plans of this research.

RESULTS

We identified a total of 21,756 unique individuals with RA, without any history of organ transplantation or any history of previous cancer, who started at least 1 b/tsDMARD. Of these, 2936 initiated a JAKi, 7280 a non-TNFi bDMARD, and 15,359 a TNFi. A total of 5834 patients contributed to more than 1 b/tsDMARD cohort. We identified 65,218 patients who contributed to the b/tsDMARD-naïve cohort (14,212 of these also contributed to the b/tsDMARD cohorts). For each b/tsDMARD treatment initiation, 5 general population comparators (n = 163,909) from the total population register were identified, which are matched based on age, sex, and vital status at the date of at the date of first identification of RA. In the main analysis, the median (IQR) follow-up times were 3.8 years (2.2-5.3) for JAKi initiators, 6.6 years (3.4-9.1) for non-TNFi bDMARD, and 5.8 years (3.0-8.9) for TNFi (Table 1 and Supplementary Table S10).

Occurrence, relative, and absolute risks of first-ever KC

The age- and sex-standardised incidence rates in the 3 b/tsDMARD cohorts were all higher than in the b/tsDMARD-naïve cohort, with 12.9/1000-person-years for JAKi, 9.1 for non-TNFi bDMARDs, 8.8 for TNFi, and 7.3 for b/tsDMARD-naïve RA, which in turn was higher than the 5.4 for the general population subjects (Table 2). For JAKi vs TNFi, the fully adjusted overall HR was 1.39 (1.16-1.68), corresponding to 1 additional case of KC for every 244 patients treated with JAKi vs a TNFi per year (Table 2). For non-TNFi bDMARDs vs TNFi, the corresponding HR was 0.96 (0.86-1.08). Comparing the pattern of fully adjusted HRs from the main model with the 3 alternative Cox models suggested small between-model variations, taking statistical precision into account (Supplementary Table S7).

Table 1
Baseline characteristics of the study cohorts of Swedish patients with RA initiating b/tsDMARD treatment

Cohort	No. of treatment episodes	No. of patients	Median follow-up, y (IQR [25th percentile-75th percentile])	Age (y), median	Female, %	Disease duration (y), median	No. of treatment episodes 0 previous b/tsDMARDs	No. of treatment episodes 1-2 previous b/tsDMARDs	No. treatment episodes 3+ previous b/tsDMARDs
JAKi	3416	2936	3.8 (2.2-5.3)	58	81	12.6	392	1265	1279
Baricitinib	1798	1716	4.7 (3.6-5.5)	59	81	12.3	249	695	772
Filgotinib	152	89	0.6 (0.3-0.9)	54	76	11.8	6	50	33
Tofacitinib	462	339	4.9 (3.3-6.2)	57	78	12.0	49	121	169
Upadacitinib	1004	792	2.0 (1.4-2.6)	57	81	12.4	88	399	305
Non-TNFi bDMARD	9381	7280	6.6 (3.4-9.1)	61	78	10.5	1931	3936	1412
Abatacept	3465	2750	6.0 (2.7-8.8)	61	79	10.8	635	1512	603
Rituximab	2917	2310	6.9 (4.3-9.4)	63	75	11.4	880	1114	316
Sarilumab	629	378	1.6 (2.5-3.9)	60	77	9.7	41	237	100
Tocilizumab	2371	1842	7.5 (4.6-9.6)	58	79	9.5	375	1073	393
TNFi	20,065	15,359	5.8 (3.0-8.9)	57	76	6.1	12,211	2338	495
Adalimumab	7212	5284	3.2 (1.8-4.9)	57	75	5.6	4007	786	153
Certolizumab	1591	1213	9.9 (8.2-10.9)	55	80	7.7	824	271	119
Etanercept	7776	6071	5.9 (3.6-7.7)	57	77	5.9	5186	816	88
Golimumab	1401	1063	9.3 (8.4-10.5)	57	76	8.6	656	310	97
Infliximab	2085	1728	8.0 (6.1-10.2)	57	74	5.7	1538	155	38

bDMARD, biologic disease-modifying antirheumatic drug; JAKi, Janus kinase inhibitor; TNFi, tumour necrosis factor inhibitor; tsDMARD, targeted synthetic disease-modifying antirheumatic drug.
Extended information on baseline characteristics is provided in Supplementary Table S10.

Occurrence, relative, and absolute risks of first-ever KC—by time since treatment initiation

Table 3 presents analyses stratified by time since treatment initiation. Figure displays the corresponding Kaplan-Meier failure curve. For JAKi vs TNFi, numerically increased risks were found in most follow-up intervals after around 15 months. At 4 years, patients treated with JAKi (4.9% crude cumulative incidence) had a 2.4% higher absolute risk of KC vs TNFi and its 2.5% crude cumulative incidence, corresponding to 1 extra KC case for every 41 patients treated with JAKi instead of TNFi for 4 years. For non-TNFi bDMARD vs TNFi, we observed no pattern of increased risk in any of the time intervals.

Occurrence, relative, and absolute risks of first-ever KC—by subtype

For SCC, the fully adjusted HR for JAKi vs TNFi was 1.49 (1.09-2.05) and 1.10 (0.91-1.32) for non-TNFi bDMARD vs TNFi. For BCC, the fully adjusted HR for JAKi vs TNFi was 1.41 (1.13-1.75) and 0.92 (0.80 -1.05) for non-TNFi bDMARD vs TNFi (Table 2).

Occurrence, relative risk of first-ever KC of any subtype—by individual b/tsDMARDs

Table 4 and Supplementary Table S11 display the fully adjusted HR for KC by individual b/tsDMARDs using etanercept as reference. For all KC, we noted increased HRs for baricitinib 1.50 (1.19-1.89), tofacitinib 1.69 (1.16-2.45), and infliximab 1.27 (1.05-1.54). Regarding specific subtypes, SCC risk was increased HRs for baricitinib 1.54 (1.03-2.30), abatacept 1.48 (1.11-1.97), and infliximab 1.45 (1.06-1.98). For BCC, we noted increased HR with baricitinib 1.62 (1.24-2.12) and tofacitinib 1.79 (1.16-2.78). The above-mentioned signal for abatacept appeared specific to SCC; HR: 1.52 (1.05-2.19) for *in situ* SCC and 1.52 (0.99-2.33) for invasive SCC, whereas no increased risk was found for BCC: 1.07 (0.87-1.33).

Occurrence, relative, and absolute risk of second primary KC

Overall, the incidence rates of second primary KC were approximately 10-fold higher than those for first-ever KC (Tables 2 and 5). The fully adjusted HR for a second KC was 1.31 (0.94-1.82) for JAKi vs TNFi, corresponding to 1 extra case per 17 patients per year. The corresponding HR for non-TNFi bDMARD vs TNFi was 0.94 (0.75-1.17) (Table 5).

Additional analyses

Analyses by age at treatment initiation (Supplementary Table S12) and by previous number of b/tsDMARDs (Supplementary Table S13) revealed a U-shaped risk pattern of HRs for all KC and BCC. The results of analyses with a 90-day and 180-day latency period (Supplementary Table S14), and those restricting the study period to 2017-2020 and 2017-2023 (Supplementary Table S15), also fell close to the main analysis. The on-drug analysis, the analyses by time on active treatment, and the analyses restricted to individuals who had been on treatment for at least 1 year resulted in, if anything, higher HRs compared with the main analysis (Supplementary Tables S16-S18).

DISCUSSION

In this nationwide observational cohort study on risks of KC in patients with RA in relation to b/tsDMARD treatment, we confirmed an increased risk of KC in b/tsDMARD-naive RA vs the general population and an increased risk in TNFi-treated vs b/tsDMARD-naive RA. We observed that patients initiating treatment with JAKi, but not patients initiating treatment with the class of non-TNFi bDMARDs, had a higher incidence of KC compared with those initiating a TNFi. However, drug-specific analyses confirmed a signal for elevated SCC risk with abatacept. Additional analyses suggested that the elevated KC incidence with JAKi was a class rather than drug-specific effect, that it applied (at least numerically) also to patients with a history of a previous KC, and that it remained or was accentuated with increasing follow-up or time since treatment initiation.

Table 2
Number of treatment episodes, incident events, incidences, and relative risks of first primary KC, overall and by KC subtype

Cohort	No. of treatment episodes	No. of patients	No. of events	Crude incidence per 1000 PY	Age/sex-standardised incidence per 1000 PY	Age-sex adjusted HR[a]	Fully adjusted HR[b]	No. needed to harm (1 extra KC case per 1-y treatment vs reference)
All KC								
JAKi	3416	2936	155	14.7	12.9	1.67 (1.40-1.99)	1.39 (1.16-1.68)	JAKi vs TNFi = 244
Non-TNFi bDMARD	9381	7279	458	10.4	9.1	1.04 (0.93-1.17)	0.96 (0.86-1.08)	n/a
TNFi	20,065	15,044	766	8.8	8.8	1 (reference)	1 (reference)	TNFi vs b/tsDMARD-naive RA = 667
b/tsDMARD-naïve RA	65,218	65,218	5027	8.8	7.3	0.75 (0.69-0.80)	n/a	b/tsDMARD-naive RA vs gen pop = 526
General population	163,909	163,909	4016	5.5	5.4	0.61 (0.57-0.66)	n/a	n/a
All SCC								
JAKi	3416	2936	55	5.2	4.2	1.80 (1.35-2.42)	1.49 (1.09-2.05)	JAKi vs TNFi = 833
Non-TNFi bDMARD	9381	7279	196	4.4	3.8	1.21 (1.00-1.45)	1.10 (0.91-1.32)	n/a
TNFi	20,065	15,044	271	3.0	3.0	1 (reference)	1 (reference)	TNFi vs b/tsDMARD-naive RA = 3333
b/tsDMARD-naïve RA	65,218	65,218	2057	3.5	2.7	0.75 (0.66-0.86)	n/a	b/tsDMARD-naive RA vs gen pop = 909
General population	163,909	163,909	1206	1.6	1.6	0.52 (0.45-0.59)	n/a	n/a
In situ SCC								
JAKi	3416	2936	42	3.9	3.1	2.52 (1.80-3.55)	2.06 (1.43-2.98)	JAKi vs TNFi = 714
Non-TNFi bDMARD	9381	7279	113	2.5	2.2	1.20 (0.94-1.52)	1.16 (0.93-1.46)	n/a
TNFi	20,065	15,044	158	1.8	1.7	1 (reference)	1 (reference)	TNFi vs b/tsDMARD-naive RA = 10,000
b/tsDMARD-naïve RA	65,218	65,218	1164	1.9	1.6	0.70 (0.59-0.84)	n/a	b/tsDMARD-naive RA vs gen pop = 1429
General population	163,909	163,909	659	0.8	0.9	0.48 (0.40-0.58)	n/a	n/a
Invasive SCC								
JAKi	3416	2936	21	1.9	1.8	1.77 (1.11-2.82)	1.20 (0.75-1.93)	JAKi vs TNFi = 2000
Non-TNFi bDMARD	9381	7279	92	2.0	1.7	1.33 (1.01-1.75)	1.05 (0.79-1.38)	n/a
TNFi	20,065	15,044	115	1.3	1.3	1 (reference)	1 (reference)	TNFi vs b/tsDMARD-naive RA = 5000
b/tsDMARD-naïve RA	65,218	65,218	879	1.5	1.1	0.68 (0.56-0.83)	n/a	b/tsDMARD-naive RA vs gen pop = 2000
General population	163,909	163,909	497	0.6	0.6	0.49 (0.40-0.60)	n/a	n/a
BCC								
JAKi	3416	2936	113	10.6	9.6	1.65 (1.35-2.02)	1.41 (1.13-1.75)	JAKi vs TNFi = 526
Non-TNFi bDMARD	9381	7279	312	7.0	6.2	0.97 (0.84-1.11)	0.92 (0.80-1.05)	n/a
TNFi	20,065	15,044	568	6.5	6.5	1 (reference)	1 (reference)	TNFi vs b/tsDMARD-naive RA = 833
b/tsDMARD-naïve RA	65,218	65,218	3622	6.3	5.3	0.75 (0.68-0.82)	n/a	b/tsDMARD-naive RA vs gen pop = 909
General population	163,909	163,909	3102	4.3	4.2	0.65 (0.59-0.70)	n/a	n/a

b/tsDMARD, biologic/targeted synthetic disease-modifying antirheumatic drug; BCC, basal cell carcinoma; csDMARD, conventional synthetic disease-modifying antirheumatic drugs; DAS28CRP, disease activity score 28-joint count C reactive protein; HR, hazard ratio; JAKi, Janus kinase inhibitor; KC, keratinocyte cancer; n/a, analyses not performed; PY, person-years; RA, rheumatoid arthritis; SCC, squamous cell carcinoma; TNFi, tumour necrosis factor inhibitor.

[a] Age-sex adjusted HR was adjusted for age and sex.

[b] Fully adjusted HR: HR was adjusted for age, sex, line of therapy, disability and sick leave, comorbidities (diabetes, heart failure, ischaemic heart disease, hospitalised infections, lung disease, kidney failure, joint surgery, organ transplantation, benign skin disorders), disability and sick leave, socioeconomic status, educational level, use of concomitant medications (csDMARDs, steroids and topical steroid cream), RA disease-related factors (DAS28CRP, disease duration, seropositivity), calendar year, smoking status and with missing categories included for those variables with missing information.

Our observation that patients with RA treated with JAKi had an increased risk of KC (of any subtype) compared with TNFi blends well with findings from the ORAL surveillance trial, which reported close to doubled risk for KC with tofacitinib compared with etanercept or adalimumab. That trial included patients with at least 1 cardiovascular risk factor failing methotrexate and who were largely b/tsDMARD-naive (89%) [17]. Conversely, our JAKi cohort had considerably more b/tsDMARD exposures (12% b/tsDMARD-naïve), suggesting that the association observed in the ORAL surveillance trial was not limited to the trial population under study but was also detectable in a real-world setting. However, a meta-analysis by Olivera et al [19] of (considerably shorter) JAKi trials did not find a statistically significant risk for KC in patients with RA (pooled analysis from 11 RA trials) treated with JAKi (1.12, 95% CI: 0.39-3.24). Two observational cohort studies from the United States, where the follow-up times for JAKi were 2.3 years and less than 1 year, respectively, did not find any increased risk of KC with tofacitinib vs other bDMARDs (HR: 1.02, 95% CI: 0.69-1.50) and vs TNFi (HR: 1.15, 95% CI: 0.96-1.39), respectively [20,21]. In a previous report from our group, we described an increased risk for KC in patients with RA treated with JAKi vs TNFi (HR: 1.39, 95% CI: 1.01-1.91). Our current study, performed in a considerably extended dataset with more individuals treated with JAKi (2936 vs 1967), longer median follow-up time for JAKi (3.8 years vs 1.95 years) and more than twice as many incident KC events in the JAKi class (155 vs 59) as in our previous assessment confirms and strengthens this signal [18].

Our current study included analysis by KC subtype. We observed an increased risk for BCC with JAKi. For SCC, the

Table 3
Relative risks for first-ever KC by time since treatment initiation and KC subtype

Cohort	0-1 y Fully adjusted HR[a]/no. events	1-2 y Fully adjusted HR[a]/no. events	2-3 y Fully adjusted HR[a]/no. events	3-4 y Fully adjusted HR[a]/no. events	4-5 y Fully adjusted HR[a]/no events	5+ y Fully adjusted HR[a]/no events
All KC						
JAKi	0.78 (0.51-1.20) n = 25	1.81 (1.27-2.58) n = 45	1.95 (1.35-2.82) n = 41	1.45 (0.95-2.20) n = 29	1.78 (1.13-2.78) n = 25	1.0 (0.50-1.97) n = 9
Non-TNFi bDMARD	0.81 (0.61-1.10) n = 70	1.20 (0.90-1.60) n = 82	1.37 (1.03-1.81) n = 90	0.89 (0.66-1.20) n = 67	0.97 (0.70-1.33) n = 64	0.87 (0.72-1.04) n = 199
TNFi	1 (reference) n = 142	1 (reference) n = 116	1 (reference) n = 110	1 (reference) n = 122	1 (reference) n = 106	1 (reference) n = 371
All SCC						
JAKi	0.79 (0.37-1.70) n = 8	3.13 (1.74-5.62) n = 20	1.80 (0.97-3.35) n = 15	1.28 (0.58-2.80) n = 8	2.20 (1.08-4.41) n = 11	n/a n ≤ 5
Non-TNFi bDMARD	0.82 (0.49-1.37) n = 23	1.63 (0.98-2.75) n = 30	1.76 (1.14-2.71) n = 46	0.89 (0.52-1.53) n = 21	0.85 (0.49-1.48) n = 21	1.03 (0.80-1.34) n = 106
TNFi	1 (reference) n = 42	1 (reference) n = 28	1 (reference) n = 40	1 (reference) n = 35	1 (reference) n = 36	1 (reference) n = 154
In situ SCC						
JAKi	1.02 (0.41-2.50) n = 6	4.14 (2.00-8.58) n = 15	2.27 (0.98-5.24) n = 9	1.70 (0.66-4.37) n = 6	2.45 (1.10-5.49) n = 9	n/a n = <5
Non-TNFi bDMARD	0.85 (0.43-1.68) n = 13	0.83 (0.36-1.97) n = 8	2.42(1.33-4.43) n = 28	1.18 (0.60-2.32) n = 15	0.47 (0.21-1.06) n = 8	1.19(0.85-1.64) n = 73
TNFi	1 (reference) n = 23	1 (reference) n = 15	1 (reference) n = 18	1 (reference) n = 19	1 (reference) n = 25	1 (reference) n = 93
Invasive SCC						
JAKi	n/a n ≤ 5	2.70 (1.16-6.30) n = 10	1.54 (0.66-3.56) n = 8	n/a n ≤ 5	n/a n ≤ 5	n/a n ≤ 5
Non-TNFi bDMARD	0.58 (0.22-1.55) n = 6	1.79 (0.86-3.70) n = 17	1.30 (0.69-2.48) n = 19	n/a n ≤ 5	1.10 (0.49-2.50) n = 11	0.92 (0.64-1.35) n = 53
TNFi	1 (reference) n = 14	1 (reference) n = 13	1 (reference) n = 20	1 (reference) n = 11	1 (reference) n = 13	1 (reference) n = 77
BCC						
JAKi	0.92 (0.56-1.50) n = 20	1.48 (0.95-2.30) n = 27	2.13 (1.38-3.28) n = 30	1.52 (0.94-2.46) n = 22	1.54 (0.90-2.6) n = 17	1.32 (0.66-2.66) n = 9
Non-TNFi bDMARD	0.83 (0.59-1.18) n = 49	1.07 (0.76-1.50) n = 54	1.16 (0.82-1.67) n = 52	0.96 (0.69-1.36) n = 53	0.99 (0.70-1.41) n = 51	0.79 (0.64-0.98) n = 129
TNFi	1 (reference) n = 103	1 (reference) n = 90	1 (reference) n = 78	1 (reference) n = 93	1 (reference) n = 86	1 (reference) n = 272

BCC, basal cell carcinoma; bDMARD, biologic disease-modifying antirheumatic drug; csDMARD, conventional synthetic disease-modifying antirheumatic drugs; DAS28CRP, disease activity score 28-joint count C reactive protein; JAKi, Janus kinase inhibitor; KC, keratinocyte cancer, n/a, analyses not performed; PY, person-years; RA, rheumatoid arthritis; SCC, squamous cell carcinoma; TNFi, tumour necrosis factor inhibitor.

[a] Fully adjusted HR: HR was adjusted for age, sex, line of therapy, disability and sick leave, comorbidities (diabetes, heart failure, ischaemic heart disease, hospitalised infections, lung disease, kidney failure, joint surgery, organ transplantation, and benign skin disorders), disability and sick leave, socioeconomic status, educational level, use of concomitant medications (csDMARDs, steroids, and topical steroid cream), RA disease-related factors (DAS28CRP, disease duration, and seropositivity), calendar year, smoking status, and missing categories included for those variables with missing information.

results were mixed, with significant risks observed for all SCC and *in situ* but not for invasive SCCs. To our knowledge, subtype-specific analyses for JAKi vs TNFi have not been presented previously, but relative risks by KC subtype have been studied in patients with RA naïve to b/tsDMARDs compared with the general population; a Danish study by Mellemkjaer et al [9] reported elevated risks for BCC (RR 1.3, 95% CI: 1.1-1.4) as well as for SCC (RR: 1.4, 95% CI: 1.1-1.9). Also, a previous study from our group reported similar results with a fully adjusted HR of 1.22 (95% CI: 1.07-1.41) for BCC and 1.88 (95% CI: 1.74-2.03) for SCC [8]. There are also studies on TNFi compared with patients with b/tsDMARD-naïve RA; a British cohort study by Mercer et al [7] did not find increased risks for BCC (HR: 0.95, 95% CI: 0.53-1.71) nor for SCC (HR: 1.16, 95% CI: 0.35-3.84). Similarly, a previous study by our group did not confirm any elevated risk for SCC (but for BCC) with TNFi (HR: 1.09, 95% CI: 0.84-1.42) [8,15].

When stratifying our analysis by time since treatment initiation, we observed that the risk curves (JAKi vs TNFi) started to deviate at approximately 15 months, similar to the findings from the German RABBIT registry study regarding overall malignancy, by Schaefer et al [24], underscoring the need for sufficient observation time to capture the latency period of malignancies associated with JAKi treatment.

A further observation in our study was that the increased risk of KC was specific to the class of JAKi and not to non-TNFi bDMARDs (rituximab, abatacept, tocilizumab, and sarilumab). However, drug-specific analysis revealed a safety signal for abatacept. While the pooled results for abatacept (all KC) were reassuring, we identified an increased risk of SCC with abatacept vs etanercept. This finding replicates a previous signal reported by our group, which showed a doubled risk of SCC (based on 17 events) in patients treated with abatacept vs TNFi [15]. Our current study, using a considerably larger dataset, strengthens the evidence for an association between abatacept and SCC, noting that the risk increase was specific to SCC (both *in situ* and invasive) with no corresponding signal for BCC. By contrast, a recent study by Simon et al [14] presenting pooled estimates from 6 observational studies did not show an increased risk for KC in patients with RA treated with abatacept compared with other b/tsDMARDs. Finally, all b/tsDMARD-exposed cohorts had higher incidence rates for KC overall compared with b/tsDMARD-naïve

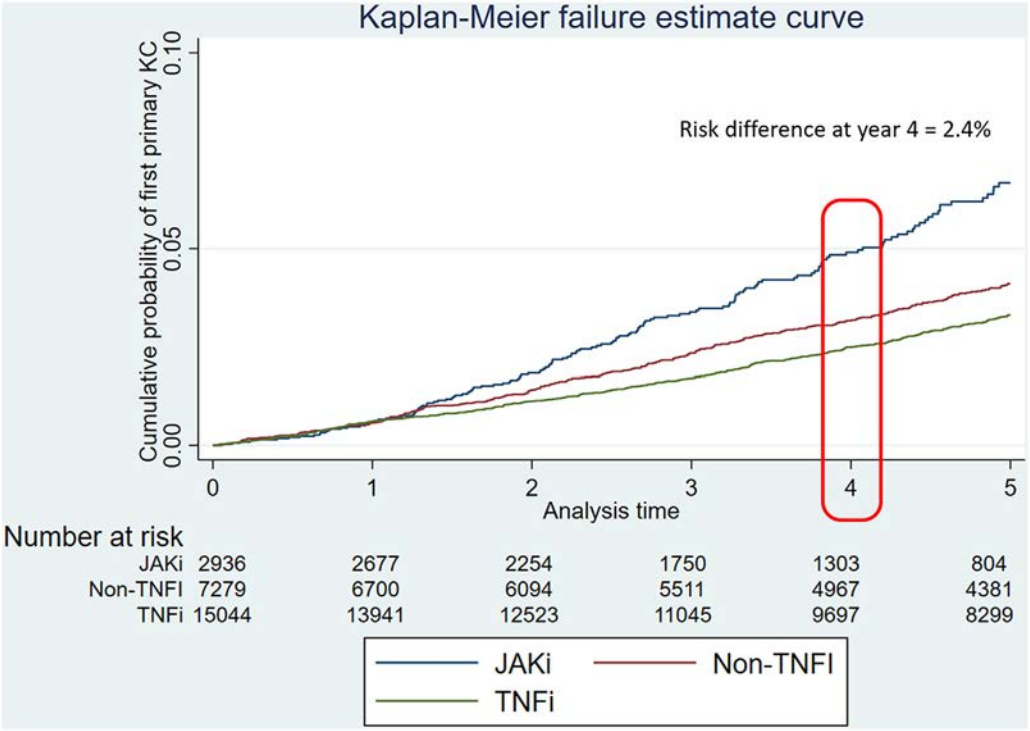

Figure. Kaplan-Meier failure estimate curve (age/sex-standardised cumulative incidence) for first primary KC, in patients with RA initiating treatment with JAKi, TNFi, or non-TNFi bDMARDs. bDMARD, biologic synthetic disease-modifying antirheumatic drug; JAKi, Janus kinase inhibitor; KC, keratinocyte cancer; RA, rheumatoid arthritis; TNFi; tumour necrosis factor inhibitor.

patients, who in turn had higher rates than the general population.

Among patients with a history of KC before treatment start, we observed a signal of increased risk of a second primary KC (JAKi vs TNFi). Data on the risk of a second primary KC are so far limited. This remains a clinically relevant group to identify, as individuals with RA and a history of KC represent a potential risk group when considering further immunosuppressive treatment.

Our study has some limitations. Although skin complexion and exposure to UV radiation are well-known risk factors for KC, we did not have information on these. That said, to bias the HRs in the between-drug analyses, patients treated with JAKi, TNFi, and non-TNFi bDMARDs would need to have different UV

Table 4

Number of treatment episodes, incident events, incidences and relative risks of a first-ever KC, by individual b/tsDMARDs using etanercept as reference

Cohort	No. of treatment episodes	No. of patients	No. of events	Crude incidence per 1000 PY	Age/sex-standardised incidence per 1000 PY	Age-sex adjusted HR[a]	Fully adjusted HR[b]
All KC							
Baricitinib	1798	1716	113	15.2	13.2	1.74 (1.40-2.18)	1.50 (1.19-1.89)
Filgotinib	152	89	0	n/a	n/a	n/a	n/a
Tofacitinib	463	339	25	16.6	15.3	2.12 (1.41-3.18)	1.69 (1.16-2.45)
Upadacitinib	1004	792	17	11.1	10.3	1.59 (0.97-2.61)	1.23 (0.77-1.96)
Abatacept	3465	2750	178	11.5	10.4	1.23 (1.02-1.48)	1.15 (0.96-1.38)
Rituximab	2917	2310	170	11.4	9.1	1.10 (0.91-1.34)	1.03 (0.86-1.24)
Sarilumab	629	378	8	7.9	6.9	1.04 (0.51-2.09)	0.91 (0.53-1.55)
Tocilizumab	2370	1841	102	8.2	8.2	0.96 (0.76-1.20)	0.89 (0.72-1.10)
Adalimumab	6796	4946	160	8.0	8.4	1.03 (0.85-1.25)	1.05 (0.89-1.26)
Certolizumab	1591	1214	99	9.3	9.9	1.17 (0.89-1.40)	1.12 (0.90-1.39)
Etanercept	7776	6090	284	8.3	8.3	1 (reference)	1 (reference)
Golimumab	1401	1063	89	9.7	9.7	1.17 (0.92-1.49)	1.09 (0.87-1.37)
Infliximab	2086	1731	134	10.4	10.2	1.18 (0.96-1.45)	1.27 (1.05-1.54)

BCC, basal cell carcinoma; b/tsDMARD, biologic/targeted synthetic disease-modifying antirheumatic drug; csDMARD, conventional synthetic disease-modifying antirheumatic drugs; DAS28CRP, disease activity score 28-joint count C reactive protein; HR, hazard ratio; KC, keratinocyte cancer; n/a, analyses not performed; PY, person-years; RA, rheumatoid arthritis.

Extended information on KC by each outcome definition; all KC, all SCC, *in situ* SCC, invasive SCC, and BCC, is presented in Supplementary Table S11.

[a] Age-sex adjusted HR was adjusted for age and sex.

[b] Fully adjusted HR: HR was adjusted for age, sex, line of therapy, disability and sick leave, comorbidities (diabetes, heart failure, ischaemic heart disease, hospitalised infections, lung disease, kidney failure, joint surgery, organ transplantation, and benign skin disorders), disability and sick leave, socioeconomic status, educational level, use of concomitant medications (csDMARD, steroids and topical steroid cream), RA disease-related factors (DAS28CRP, disease duration, seropositivity), calendar year, smoking status, and missing categories included for those variables with missing information.

Table 5
Number of treatment episodes, events, incidences, and relative risks of a second KC, in individuals with a history of a primary KC

Cohort	No. of treatment episodes	No. of patients	No. of events	Crude incidence per 1000 PY	Age/sex-standardised incidence per 1000 PY	Age-sex adjusted HR[a]	Fully adjusted HR[b]	No. needed to harm (1 extra KC case per 1-y treatment vs reference)
All KC								
JAKi	222	190	83	145.0	150.9	1.48 (1.17-1.89)	1.31 (0.94-1.82)	JAKi vs TNFi = 17
Non-TNFi bDMARD	614	508	208	94.6	92.5	0.99 (0.83-1.17)	0.94 (0.75-1.17)	n/a
TNFi	948	779	317	92.7	92.7	1 (reference)	1.0 (reference)	TNFi vs b/tsDMARD-naive RA = 63
b/tsDMARD-naïve RA	2800	2800	1247	82.0	76.8	0.85 (0.74-0.97)	n/a	b/tsDMARD-naive RA vs gen pop = 103
General population	6859	6859	1799	67.3	67.1	0.71 (0.62-0.81)	n/a	n/a

bDMARD, biologic disease-modifying antirheumatic drug; csDMARD, conventional synthetic disease-modifying antirheumatic drugs; DAS28CRP, disease activity score 28-joint count C reactive protein; HR, hazard ratio; JAKi, Janus kinas inhibitor; KC, keratinocyte cancer; n/a, analyses not performed; PY; person-years; RA, rheumatoid arthritis; TNFi, tumour necrosis factor inhibitor; tsDMARD, targeted synthetic disease-modifying antirheumatic drug.

[a] Age-sex adjusted HR was adjusted for age and sex.

[b] Fully adjusted HR: HR was adjusted for age, sex, line of therapy, disability and sick leave, comorbidities (diabetes, heart failure, ischaemic heart disease, hospitalised infections, lung disease, kidney failure, joint surgery, organ transplantation, and benign skin disorders), disability and sick leave, socioeconomic status, educational level, use of concomitant medications (csDMARD, steroids, and topical steroid cream), RA disease-related factors (DAS28CRP, disease duration, and seropositivity), calendar year, smoking status, and missing categories included for those variables with missing information.

exposures, or skin types. We observed notable differences in baseline characteristics, with JAKi initiators having longer disease duration and more extensive treatment history than TNFi initiators. We adjusted for line of therapy and disease duration, performed analyses stratified by previous b/tsDMARD use, and employed alternative specifications of the Cox model, all of which resulted in qualitatively similar main results. For the main analysis, we used an ever-treated approach (mimicking an 'intention to treat') where follow-up stopped at the end of the study period, death or migration, whichever occurred first. However, many patients initiating JAKi therapy were previously treated with TNFi, meaning that the HRs for JAKi, often used as later line of therapy, also include person-time on other and preceding b/tsDMARDs, potentially skewing HRs downwards in an ever-treated approach, attributing incident events to all preceding drug exposures. To address this, we conducted a sensitivity analysis using an on-drug approach (similar to an 'as treated' approach), which assesses risk linked to active treatment. This more restrictive analysis resulted in reduced person-time and fewer events, limiting its interpretability but did not challenge the findings from the main analysis. To remove the influence of biologically less plausible short induction times, we conducted an additional sensitivity analysis restricting the analysis to patients who remained on treatment for at least 365 days (starting follow-up at day 366). This analysis did not weaken the HRs for all KC and SCC; if anything, the opposite.

A central question is whether malignancy risks in RA treated with b/tsDMARDs are driven by the medication or by the underlying inflammation, and the net balance between the 2. In our study, both the JAKi group and the non-TNFi-bDMARD group were likely more 'refractory' to treatment than the TNFi group, yet while we observed a signal for KC in the JAKi group, none was observed in the non-TNFi group (with the exception of SCC risk with abatacept). The absence of a signal in the latter group argues against (albeit does not demonstrate) that the observed increase in risk with JAKi would only be a question about disease severity, but certainly does not exclude the possibility of an interaction of the 2, here: that any (true) effects of JAKi on KC risk would be particularly pronounced in patients with a higher underlying KC risk due to factor associated with their more severe RA.

Our study has several strengths. We used nationwide registers with high validity and coverage (SRQ, around 85% of all RA in Sweden) [25]. Using SRQ, NPR, and PDR ensured accurate exposure data for the vast majority of Swedish patients with b/tsDMARD-treated RA. Additionally, our median follow-up for JAKi (3.8 years) is comparable to the ORAL surveillance trial (4.0 years) [17]. We were additionally able to evaluate the risk for KC by subtype (BCC and SSC), risks of KC in patients with RA treated with JAKi or non-TNFi bDMARD per class and per drug, and risks of KC in patients with a history of KC whose baseline risk is 10-fold higher. Also, we performed several sensitivity analyses that supported the robustness of our findings.

In conclusion, our results add to the concern regarding the risk of developing KC (of any subtype and order) in patients with RA treated with a JAKi compared with TNFi, with absolute risk differences for a primary KC in the order of 4.9% (JAKi) vs 2.5% (TNFi) at 4 years of follow-up. By contrast, our results do not link the class of non-TNFi bDMARDs with increased KC risks. However, at the drug-specific level, we confirmed a signal for an increased risk of SCC with abatacept. Considering that b/tsDMARD-treated patients with RA are at increased risk for KC compared to both b/tsDMARD-naïve patients and the general population, it would seem prudent to focus skin cancer vigilance on advanced treatments in general rather than on specific drugs, especially in patients with a history of KC.

Competing interests

VH has no competing interests to declare. KH is part-time employed at the Swedish Medical Products Agency. The views expressed in this paper are the personal views of the authors and not necessarily the views of the Government agency. JA has had or have research agreements with AbbVie, AstraZeneca, BMS, Eli Lilly, MSD, Pfizer, Roche, Samsung Bioepis, Sanofi, and UCB, mainly in the context of safety monitoring of biologics via ARTIS/Swedish Biologics Register.

Acknowledgements

The following were members of the ARTIS Study Group during study completion:

Katerina Chatzidionysiou (Department of Medicine Solna, Karolinska Institutet), Alf Kastbom (Department of Biomedical and Clinical Sciences, Linköping University), Ann Knight (Department of Medical Sciences, Uppsala University), Anna Deminger (Department of Rheumatology and Inflammation Research, Sahlgrenska Academy, University of Gothenburg),

Anna Södergren (Department of Public Health and Clinical Medicine/Rheumatology, Umeå University, 901 87 Umeå, Sweden), Carl Turesson (Rheumatology, Department of Clinical Sciences, Malmö, Lund University), Gerd-Marie Alenius (Department of Public Health and Clinical Medicine/Rheumatology, Umeå University), Helena Forsblad-d'Elia (Department of Rheumatology and Inflammation Research, Sahlgrenska Academy, University of Gothenburg), Eva Baecklund (Department of Medical Sciences, Uppsala University), Johan Askling (Department of Medicine Solna, Karolinska Institutet), Johan K. Wallman (Department of Clinical Sciences Lund, Rheumatology, Skåne University Hospital, Lund University, Lund, Sweden.), Lars Klareskog (Department of Medicine Solna, Karolinska Institutet), Lotta Ljung (Department of Medicine Solna, Karolinska Institutet), Nils Feltelius (Swedish Medical Products Agency, Department of Public Health and Caring Sciences, Uppsala University), and Valgerdur Sigurdardottir (Department of Rheumatology, Falun Hospital, Centre for Clinical Research, Dalarna, Uppsala University, Falun, Sweden).

We also would like to thank all Swedish patients with RA and rheumatologists for entering data into the Swedish Rheumatology Quality Register.

Contributors

VH, HB, MB, KH, TF, BD, DDG, and JA had full access to all the data in the study and participated in the design of the study. HB, MB, and VH conducted the statistical analyses. All authors participated in designing the analyses and in the interpretation of the results. All authors contributed to the drafting of the manuscript.

Funding

This work was supported by funding from the Karolinska Institute Region Stockholm funds (FoUI-1000733), the Swedish Research Council (2023-01827), the Swedish Cancer Society (22 2208 Pj), Vinnova (2024-01145), ERA PerMed ScandRA (2021-00757), and NORDFORSK (90825). TF was supported by the Swedish Research Council (2021-01418). Funders had no impact on the design or interpretation of the study or its results.

Patient consent for publication

Not applicable.

Ethics approval

The study was approved by the Swedish Ethics Review Authority 2023-03804-01.

Provenance and peer review

Not commissioned; externally peer-reviewed.

Supplementary materials

Supplementary material associated with this article can be found in the online version at doi:10.1016/j.ard.2026.02.015.

Orcid

Viking Huss: http://orcid.org/0000-0002-9764-6435

REFERENCES

[1] Almahroos M, Kurban AK. Ultraviolet carcinogenesis in nonmelanoma skin cancer. Part I: incidence rates in relation to geographic locations and in migrant populations. Skinmed 2004;3(1):29–35 quiz 35-6.
[2] Adami J, Gäbel H, Lindelöf B, Ekström K, Rydh B, Glimelius B, et al. Cancer risk following organ transplantation: a nationwide cohort study in Sweden. Br J Cancer 2003;89(7):1221–7.
[3] Lindelöf B, Sigurgeirsson B, Gäbel H, Stern RS. Incidence of skin cancer in 5356 patients following organ transplantation. Br J Dermatol 2000;143 (3):513–9.
[4] Leiter U, Eigentler T, Garbe C. Epidemiology of skin cancer. Adv Exp Med Biol 2014;810:120–40.
[5] Andersson EM, Paoli J, Wastensson G. Incidence of cutaneous squamous cell carcinoma in coastal and inland areas of Western Sweden. Cancer Epidemiol 2011;35(6):e69–74.
[6] Dreyer L, Mellemkjær L, Andersen AR, Bennett P, Poulsen UE, Juulsgaard Ellingsen T, et al. Incidences of overall and site specific cancers in TNFα inhibitor treated patients with rheumatoid arthritis and other arthritides - a follow-up study from the DANBIO Registry. Ann Rheum Dis 2013;72(1): 79–82.
[7] Mercer LK, Green AC, Galloway JB, Davies R, Lunt M, Dixon WG, et al. The influence of anti-TNF therapy upon incidence of keratinocyte skin cancer in patients with rheumatoid arthritis: longitudinal results from the British Society for Rheumatology Biologics Register. Ann Rheum Dis 2012;71 (6):869–74.
[8] Raaschou P, Simard JF, Asker Hagelberg C, Askling J, ARTIS Study Group. Rheumatoid arthritis, anti-tumour necrosis factor treatment, and risk of squamous cell and basal cell skin cancer: cohort study based on nationwide prospectively recorded data from Sweden. BMJ 2016;352:i262.
[9] Mellemkjaer L, Linet MS, Gridley G, Frisch M, Møller H, Olsen JH. Rheumatoid arthritis and cancer risk. Eur J Cancer 1996;32A(10):1753–7.
[10] Balkwill F. Tumour necrosis factor and cancer. Nat Rev Cancer 2009;9 (5):361–71.
[11] Amari W, Zeringue AL, McDonald JR, Caplan L, Eisen SA, Ranganathan P. Risk of non-melanoma skin cancer in a national cohort of veterans with rheumatoid arthritis. Rheumatology (Oxford) 2011;50(8):1431–9.
[12] Chakravarty EF, Michaud K, Wolfe F. Skin cancer, rheumatoid arthritis, and tumor necrosis factor inhibitors. J Rheumatol 2005;32(11):2130–5.
[13] Haynes K, Beukelman T, Curtis JR, Newcomb C, Herrinton LJ, Graham DJ, et al. Tumor necrosis factor α inhibitor therapy and cancer risk in chronic immune-mediated diseases. Arthritis Rheum 2013;65(1):48–58.
[14] Simon TA, Dong L, Suissa S, Michaud K, Pedro S, Hochberg M, et al. Abatacept and non-melanoma skin cancer in patients with rheumatoid arthritis: a comprehensive evaluation of randomised controlled trials and observational studies. Ann Rheum Dis 2024;83(2):177–83.
[15] Wadström H, Frisell T, Askling J, Anti-Rheumatic Therapy in Sweden (ARTIS) Study Group. Malignant neoplasms in patients with rheumatoid arthritis treated with tumor necrosis factor inhibitors, tocilizumab, abatacept, or rituximab in clinical practice: a nationwide cohort study from Sweden. JAMA Intern Med 2017;177(11):1605–12.
[16] Xie W, Yang X, Huang H, Gao D, Ji L, Zhang Z. Risk of malignancy with non-TNFi biologic or tofacitinib therapy in rheumatoid arthritis: a meta-analysis of observational studies. Semin Arthritis Rheum 2020;50(5):930–7.
[17] Ytterberg SR, Bhatt DL, Mikuls TR, Koch GG, Fleischmann R, Rivas JL, et al. Cardiovascular and cancer risk with tofacitinib in rheumatoid arthritis. N Engl J Med 2022;386(4):316–26.
[18] Huss V, Bower H, Hellgren K, Frisell T, Askling J, behalf of the ARTIS group. Cancer risks with JAKi and biological disease-modifying antirheumatic drugs in patients with rheumatoid arthritis or psoriatic arthritis: a national real-world cohort study. Ann Rheum Dis 2023;82:911–9.
[19] Olivera PA, Lasa JS, Bonovas S, Danese S, Peyrin-Biroulet L. Safety of Janus kinase inhibitors in patients with inflammatory bowel diseases or other immune-mediated diseases: a systematic review and meta-analysis. Gastroenterology 2020;158(6) 1554-73.e12.
[20] Kremer JM, Bingham 3rd CO, Cappelli LC, Greenberg JD, Madsen AM, Geier J, et al. Postapproval comparative safety study of tofacitinib and biological disease-modifying antirheumatic drugs: 5-year results from a United States-based rheumatoid arthritis registry. ACR Open Rheumatol 2021;3(3):173–84.
[21] Khosrow-Khavar F, Kim SC, Lee H, Lee SB, Desai RJ. Tofacitinib and risk of cardiovascular outcomes: results from the Safety of TofAcitinib in Routine care patients with Rheumatoid Arthritis (STAR-RA) study. Ann Rheum Dis 2022;81(6):798–804.
[22] Duarte AF, Sousa-Pinto B, Haneke E, Correia O. Risk factors for development of new skin neoplasms in patients with past history of skin cancer: a survival analysis. Sci Rep 2018;8(1):15744.

[23] Citrome L, Ketter TA. When does a difference make a difference? Interpretation of number needed to treat, number needed to harm, and likelihood to be helped or harmed. Int J Clin Pract 2013;67(5):407–11.
[24] Schaefer M, Purschke A, Zietemann V, Rudi T, Meissner Y, Richter A, et al. Comparative risk of incident malignancies in rheumatoid arthritis patients treated with Janus kinase inhibitors or bDMARDs: observational data from the German RABBIT register. Ann Rheum Dis 2025;84:1779–90.
[25] Wadström H, Eriksson JK, Neovius M, Askling J, ARTIS Study Group. How good is the coverage and how accurate are exposure data in the Swedish Biologics Register (ARTIS)? Scand J Rheumatol 2015;44(1):22–8.

Ann Rheum Dis 85 (2026) 1530–1542

Contents lists available at ScienceDirect

Annals of the Rheumatic Diseases

journal homepage: https://www.sciencedirect.com/journal/annals-of-the-rheumatic-diseases

Psoriatic arthritis

Composite outcome measures that successfully differentiate active treatments from placebo in psoriatic arthritis trials: a GRAPPA-OMERACT systematic review and network meta-analysis

Tommy K Annfeldt[1,*], Mina N Händel[1,2], Tobias Haugegaard[1,3], Marius Henriksen[1], Laura C Coates[4], Alexis Ogdie[5,6], William Tillett[7,8], Niti Goel[9], Dafna D Gladman[10,11], Ana-Maria Orbai[12], Maarten de Wit[13], Vibeke Strand[14], Philip J Mease[15,16], Oliver FitzGerald[17], Philip S Helliwell[18], Peter Tugwell[19], Ying-Ying Leung[20,21], Robin Christensen[1,3,22]

[1] *Section for Biostatistics and Evidence-Based Research, The Parker Institute, Bispebjerg and Frederiksberg Hospital, Copenhagen, Denmark*
[2] *Research Unit OPEN at Department of Clinical Research, University of Southern Denmark, Odense, Denmark*
[3] *Research Unit of Rheumatology, Department of Clinical Research, University of Southern Denmark, Odense University Hospital, Denmark*
[4] *Nuffield Department of Orthopaedics, Rheumatology and Musculoskeletal Sciences, University of Oxford, Oxford, UK*
[5] *Department of Medicine/Rheumatology, University of Pennsylvania Perelman School of Medicine, Philadelphia, PA, USA*
[6] *Department of Epidemiology and Biostatistics, University of Pennsylvania Perelman School of Medicine, Philadelphia, PA, USA*
[7] *Department of Life Sciences, Centre for Therapeutic Innovation, University of Bath, Bath, UK*
[8] *Royal National Hospital for Rheumatic Diseases, University of Bath, Bath, UK*
[9] *Patient Research Partner and Department of Medicine, Duke University School of Medicine, Durham, NC, USA*
[10] *Division of Rheumatology, Department of Medicine, University of Toronto, Toronto, ON, Canada*
[11] *Schroeder Arthritis Institute, Krembil Research Institute, Toronto Western Hospital, University Health Network, Toronto, ON, Canada*
[12] *Psoriatic Arthritis Program, Johns Hopkins Arthritis Center, Division of Rheumatology, Johns Hopkins University School of Medicine, Baltimore, MD, USA*
[13] *GRAPPA Patient Research Partner, The Netherlands*
[14] *Division of Immunology/Rheumatology, Stanford University, Palo Alto, CA, USA*
[15] *Swedish Medical Center/Providence St. Joseph Health, Seattle, WA, USA*
[16] *University of Washington School of Medicine, Seattle, WA, USA*
[17] *UCD Conway Institute, School of Medicine, University College Dublin, Belfield, Dublin, Ireland.*
[18] *LIRMM, University of Leeds, Leeds, UK*
[19] *Department of Medicine, University of Ottawa, Ottawa, ON, Canada*
[20] *Singapore General Hospital, Singapore, Singapore*
[21] *Duke-NUS Medical School, Singapore, Singapore*
[22] *Cochrane Denmark & Centre for Evidence-Based Medicine Odense (CEBMO), Department of Clinical Research, University of Southern Denmark, Denmark*

*Correspondence to Tommy Kok Annfeldt, Section for Biostatistics and Evidence-Based Research, The Parker Institute, Bispebjerg and Frederiksberg Hospital, Copenhagen, Denmark.

E-mail address: Tommy.Kok.Annfeldt@regionh.dk (T.K. Annfeldt).

Ying-Ying Leung and Robin Christensen are co-senior authors.

https://doi.org/10.1016/j.ard.2026.05.013

ARTICLE INFO

Article history:
Received 19 October 2025
Received in revised form 9 May 2026
Accepted 11 May 2026

Handling editor Josef S Smolen

ABSTRACT

Objectives: To identify which composite outcome measure most effectively distinguishes active treatments from placebo in randomised controlled trials (RCTs) of biologic or targeted synthetic disease-modifying antirheumatic drugs (b- or tsDMARDs) for psoriatic arthritis (PsA).

Methods: A systematic literature review (PROSPERO ID: CRD42024578203) of Cochrane Central Register of Controlled Trials and PubMed identified RCTs comparing b- or tsDMARDs with placebo reporting ≥2 of 7 composite outcome measures shortlisted for evaluation by the Group for Research and Assessment of Psoriasis and Psoriatic Arthritis–Outcome Measures in Rheumatology (GRAPPA-OMERACT) working group (American College of Rheumatology Response Criteria [ACR], Composite Psoriatic Disease Activity Index [CPDAI], Disease Activity index for PSoriatic Arthritis [DAPSA], Minimal Disease Activity [MDA], Psoriatic Arthritis Disease Activity Score [PASDAS], and 3- and 4-Visual Analogue Scale [VAS]). Discriminant capacities were assessed using odds ratio (OR) for binary outcomes, with continuous outcomes converted from standardised mean differences and analysed through network and multivariate meta-analysis techniques.

Results: Of 2483 references, 24 trials were included (43 randomised comparisons). CPDAI was rarely reported, and no RCTs reported 3-VAS and 4-VAS. The main network meta-analysis showed differences in discriminant properties for DAPSA vs ACR20 (OR: 0.80; 95% CI: 0.66-0.97; favouring ACR20), DAPSA vs MDA (OR: 0.71; 0.57-0.87; favouring MDA), and PASDAS vs DAPSA (OR: 1.35; 1.10-1.66; favouring PASDAS). Supported by multivariate meta-analysis: MDA (OR: 5.06; 4.20-6.09), ACR20 (OR: 4.01; 3.41-4.73), PASDAS (OR:3.70; 3.00-4.56), DAPSA (OR: 3.02; 2.44-3.75), and CPDAI (OR: 1.86; 0.95-3.64). Sensitivity analyses confirmed a pattern of consistent numerical advantages for MDA and PASDAS. Exploratory analyses showed ACR70 had more discriminant capacity than ACR20 and DAPSA but not ACR50, MDA, and PASDAS.

Conclusions: ACR20, MDA, and PASDAS demonstrated greater discriminant capacity than DAPSA. Exploratory analyses suggested greater discriminant capacity for ACR70 compared with ACR20 and DAPSA but not with ACR50, MDA or PASDAS.

WHAT IS ALREADY KNOWN ON THIS TOPIC

- Composite outcome measures can measure several domains in one combined measure.
- Composite outcome measures add statistical efficiency when they are used as outcome measures in randomised controlled trials (RCTs).
- The Group for Research and Assessment of Psoriasis and Psoriatic Arthritis–Outcome Measures in Rheumatology (GRAPPA-OMERACT) working group has shortlisted 7 composite outcome measures (American College of Rheumatology Response Criteria [ACR], Composite Psoriatic Disease Activity Index [CPDAI], Disease Activity index for PSoriatic Arthritis [DAPSA], Minimal Disease Activity [MDA], Psoriatic Arthritis Disease Activity Score [PASDAS], and 3- and 4 Visual Analogue Scale) to be evaluated for their use in RCTs comparing a biologic or targeted synthetic disease-modifying antirheumatic drug (b- or tsDMARD) against placebo in people with psoriatic arthritis (PsA).
- It is not known which composite outcome measure is best at separating experimental intervention from a placebo-comparator in RCTs comparing a b- or tsDMARD against placebo in people with PsA.

WHAT THIS STUDY ADDS

- This study provides an evidence-based comparison of the discriminant capacity of the composite outcome measures shortlisted by the GRAPPA-OMERACT working group, for use in RCTs comparing a b- or tsDMARD against placebo in people with PsA. An evidence-based evaluation of the shortlisted composite outcome measures could facilitate consensus on the most relevant primary outcome measure for future RCTs evaluating experimental interventions against a placebo-comparator in people with PsA.

HOW THIS STUDY MIGHT AFFECT RESEARCH, PRACTICE OR POLICY

- Given that MDA, followed by PASDAS consistently showed a pattern of numerically higher discriminant capacity across the primary and sensitivity analyses, this study indicates that they might be more relevant endpoints relative to ACR20 in PsA RCT settings.

INTRODUCTION

Psoriatic arthritis (PsA) is a chronic inflammatory disease with manifestations affecting the skin, nails, peripheral joints, spine, and entheses. Patients are affected by a variety of symptoms arising from these aspects to various degrees [1]. Hence, for people living with PsA, the impact of the disease and the subsequent response to therapy are related to improvement in a combination of several domains. Composite outcome measures are attractive options to measure disease activity in multiple domains and response to experimental therapy in randomised controlled trials (RCTs) because they measure several domains and offer increased statistical efficiency by avoiding multiplicity issues [2]. According to Outcome Measures in Rheumatology (OMERACT), composite outcome measures may be implemented either as a composite outcome domain (COD) measured by a dichotomous instrument, which comprises multiple components and is evaluated by determining whether one, several, or all specified components are present in each individual. It is summarised as achieving vs not achieving the COD [3]. Alternatively, a composite outcome measure can be applied as a multi-outcome domain (MOD) measured by a continuous instrument, wherein a single aggregated score is calculated for each individual based on assessments across all domains within the MOD [3]. There are several validated COD and MOD instruments for use in PsA RCTs [4]; however, it is not known which instrument possesses the most discriminant capacity to separate the experimental therapy group from the placebo-comparator group.

Since the update of the PsA core domain set in 2016 [5], the Group for Research and Assessment of Psoriasis and Psoriatic Arthritis (GRAPPA)-OMERACT working group has been assessing the measurement properties of various COD and MOD instruments used to evaluate the net benefit of an experimental therapy, relative to an active- or placebo-comparator [5]. The working group has proposed a list of COD and MOD instruments to evaluate for use in PsA RCTs which includes: Minimal Disease

Activity (MDA) [6] Disease Activity index for PSoriatic Arthritis (DAPSA) [7], American College of Rheumatology Response Criteria (ACR) [8], Psoriatic Arthritis Disease Activity Score (PASDAS) [9], Composite Psoriatic Disease Activity Index (CPDAI) [10], and 3- or 4-visual analogue scales (VASs) [4,11,12]. The American Food and Drug Administartion (FDA) and the European Medicines Agency (EMA) have historically supported ACR20 as the primary efficacy endpoint to be used in PsA RCTs [13]. Therefore, the final list of instruments to be evaluated for their discriminant capacities in RCTs includes the 2 COD instruments ACR20 and MDA, and 5 MOD instruments DAPSA, PASDAS, CPDAI, 3-VAS, and 4-VAS. An evidence-based evaluation of the shortlisted instruments could facilitate consensus on the most appropriate primary outcome measure for future RCTs evaluating experimental interventions against a placebo-comparator [4].

This study was conducted as part of the GRAPPA-OMERACT working group's agenda to evaluate PsA composite outcome measures used in RCTs. The objective was to identify which composite outcome measure most effectively distinguished active treatments from placebo in RCTs evaluating biologic or targeted synthetic disease-modifying antirheumatic drugs (b- or tsDMARDs) in people with PsA. In this context, our aim was not to evaluate within-person change, but rather to assess the RCT discrimination on a group level for each composite outcome measure as defined by the OMERACT Handbook [14].

METHODS

This study was a systematic literature review and network meta-analysis of the comparative discriminant capacities of composite outcome measures in published RCTs in PsA. In accordance with OMERACT guidance and recommendations from the European Alliance of Associations for Rheumatology (formerly known as the European League Against Rheumatism) [15], patient research partners (NG and MDW) were involved from the project start. Study selection, assessment of eligibility criteria, data extraction, and statistical analyses were performed as described in the protocol (Supplementary file) submitted to the International Prospective Register of Systematic Reviews PROSPERO on 2024-Aug-09 (ID: CRD42024578203). The protocol followed the recommendations in Preferred Reporting Items for Systematic Reviews and Meta-Analysis Protocols [16], and the study findings are reported according to the PRISMA checklist (Supplementary file) [16].

Identification of eligible trials

Eligible trials were identified through systematic literature searches in the Cochrane Central Register of Controlled Trials (CENTRAL) for RCTs and MEDLINE (via PubMed) for RCTs from inception to September 16, 2024; in addition, experts in the field were consulted to identify additional trials. The search strategies for PubMed and CENTRAL are described in the protocol and focused on identifying trials which aimed to compare the effect of a b- or tsDMARD to a placebo-comparator for the treatment of PsA. Included b- or tsDMARDs, where those with an approved label in the EU and United States to treat PsA [17–19]. Eligible trials had to report results for at least 2 of the 7 shortlisted composite outcome measures in a PsA population.

All references were uploaded into Covidence [20], and duplicates were removed. Two reviewers (TKA and MNH) independently screened titles and abstracts to identify references for full-text review. Full-text published articles were again independently reviewed by the same reviewers. In case of disagreement, consensus was reached through discussion and consulting with a third reviewer (RC) if needed. Risk of bias assessment was performed using the updated Cochrane Collaboration tool (RoB2) [21]. Two reviewers (TKA and MNH) independently assessed each trial and reached consensus through discussions. The overall risk of bias for a study was determined as 'low risk of bias', 'some concerns', or 'high risk of bias' accordingly [21]. The Excel tool available from www.riskofbias.com was used to facilitate the RoB2 process.

Data extraction process

Data were extracted from journal articles and ClinicalTrials.gov onto a predefined form (Supplementary file) by TKA and verified for accuracy by MNH. In cases where data were incomplete, study authors were contacted. For studies with multiple publications reporting the same data, the original publication was used for extraction. Missing outcome data were visualised as an empty line in the forest plots. All efficacy data were extracted at the end of the placebo-controlled period.

For continuous instruments, we extracted the mean change from baseline to the end of the placebo-controlled period, along with the reported measures of variance. These data were used to calculate standardised mean differences (SMD) (Cohen's d) [22]. For binary instruments, we extracted the number of patients achieving the outcome and the total number of patients randomised to each group. These data were used to estimate odds ratios (ORs) and their variances. From the included trials, we extracted the sample sizes, female proportion, mean age, disease duration, proportion with prior exposure to b- or tsDMARDs, early escape (yes/no), and funding source. The relevant extracted data were transferred to an evidence synthesis document created in Microsoft Excel, where we calculated the summary measures as introduced below.

Statistical analysis

The SMD between intervention- and placebo-comparator groups with the corresponding SE was chosen as the summary measure for quantifying the discriminant capacity of the continuous instruments (DAPSA, PASDAS, CPDAI, 3-VAS, and 4-VAS). It was calculated by dividing the difference between the change in the intervention and the placebo group by the pooled SD for that trial. Where the SD was not reported, it was estimated based on measures of variation or precision published. For the binary instruments (ACR20 and MDA) the OR was chosen as the summary measure, calculated based on the number of events and total participants in the intervention and placebo groups. Where there was more than one randomised comparison (ie, several doses) within a trial, the number of participants in the placebo group was divided by the number of comparisons for the analysis. Data were coded so that an SMD > 0 and an OR > 1 indicated a beneficial effect of the experimental intervention compared with placebo. This facilitated a standardised way of assessing the discriminant capacity of the included composite outcome measures [23,24]. The greater the size of the SMD, or the higher the OR, the stronger the discriminant capacity of the instrument within any given trial. To enable comparisons between binary and continuous instruments, SMDs were converted to their corresponding OR following the method described by Chinn [25]. Similarly, the ORs were converted to their corresponding SMDs. Consequently, all 7 composite outcome measures were analysed as both ORs and SMDs with 95% CIs.

Forest plots displaying the logOR with 95% CIs for binary instruments and SMD with 95% CIs for continuous instruments were produced to visually display the discriminant capacity and the magnitude of missing data for each measure. The number of rows per study in each forest plot corresponds to the number of comparisons in that study, eg, if a study includes 2 doses of the experimental intervention against 1 placebo-comparator, data were coded as 2 mutually independent randomised comparisons 1 row for each dose compared with placebo). Since the purpose of the forest plots was to visually display the missing data, we did not calculate or display the pooled summary measures.

Quantitative evidence synthesis

The relative discriminant capacities of the composite outcome measures were compared through a multiple-treatment network meta-analysis approach using both indirect and direct analysis, which allowed us to model the net benefit of each outcome measure. Making valid inferences based on network meta-analysis techniques requires a consideration of both the direct and indirect evidence contributing to the network meta-analysis effect estimates (NMA estimates). Robustness of the inference was supported if the direct estimates for a comparison between 2 specific measures fell within the 95% CI derived from the corresponding network. The present meta-analysis was specifically vulnerable to selective outcome reporting bias, and therefore multivariate meta-analysis was used as a sensitivity analysis [26]. Multivariate meta-analysis is a technique developed by Kirkham et al. [26] specifically to reduce the impact of outcome reporting bias in systematic reviews. This method combines results from different studies by considering how their outcomes are related and maximizes use of the available evidence while reducing potential bias from selective reporting [26].

To assess the robustness of the findings and the impact of trial-level heterogeneity, additional sensitivity analyses not prespecified in the protocol were performed. First, to further assess selective outcome reporting bias, we stratified the analysis by trials reporting fewer (ie, 2) vs more (ie, ≥3) than half of the 5 outcome measures with available data. Second, to assess outcome-availability bias, we restricted the dataset to trials reporting at least ACR20, MDA, DAPSA, and PASDAS concurrently. Third, to ensure temporal alignment, we repeated the analysis restricted to trials with data extracted at week 24. This week-24 dataset was then stratified (1) by the presence vs absence of early escape, and (2) the proportion of participants previously exposed to b- or tsDMARD therapy (≥50% vs <50% of participants). To explore the discriminant capacity of ACR50/70, we expanded the network and multivariate meta-analyses to include these outcomes alongside the prespecified outcomes. Lastly, we excluded the active-controlled arm from a trial that contributed both placebo-controlled and active-controlled comparisons. All sensitivity analyses were performed using the same random-effects network meta-analytic framework as the primary analysis. All statistical analyses and visualisations were performed using RStudio version 4.3.0 [27].

RESULTS

Systematic literature search

We identified 1653 and 830 references through PubMed and CENTRAL, respectively. After removal of duplicates, 2082 titles

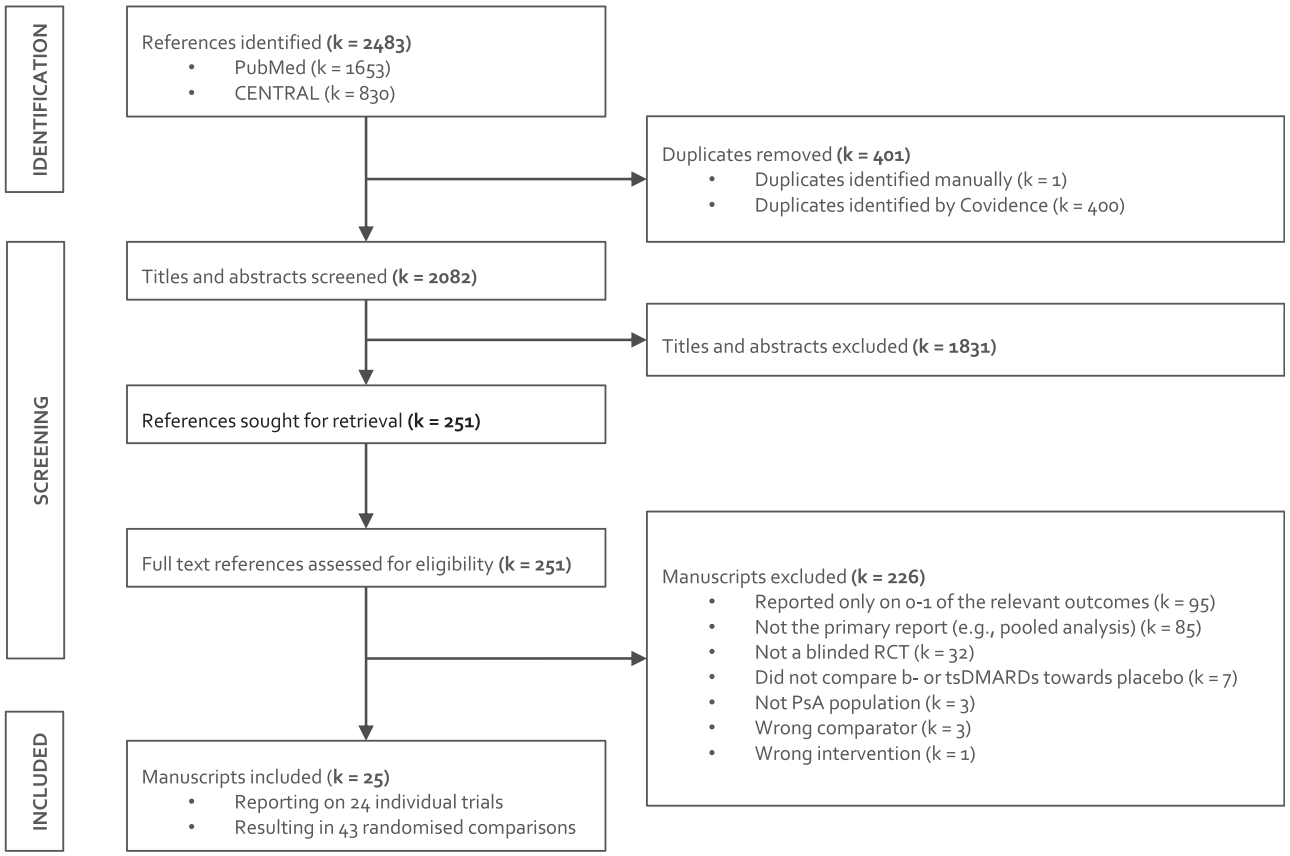

Figure 1. Flow chart illustrating the systematic literature search and manuscript selection process. bDMARD, biologic disease-modifying antirheumatic drugs; CENTRAL, Cochrane Central Register of Controlled Trials; PSA, psoriatic arthritis; RCT, randomised controlled trials.

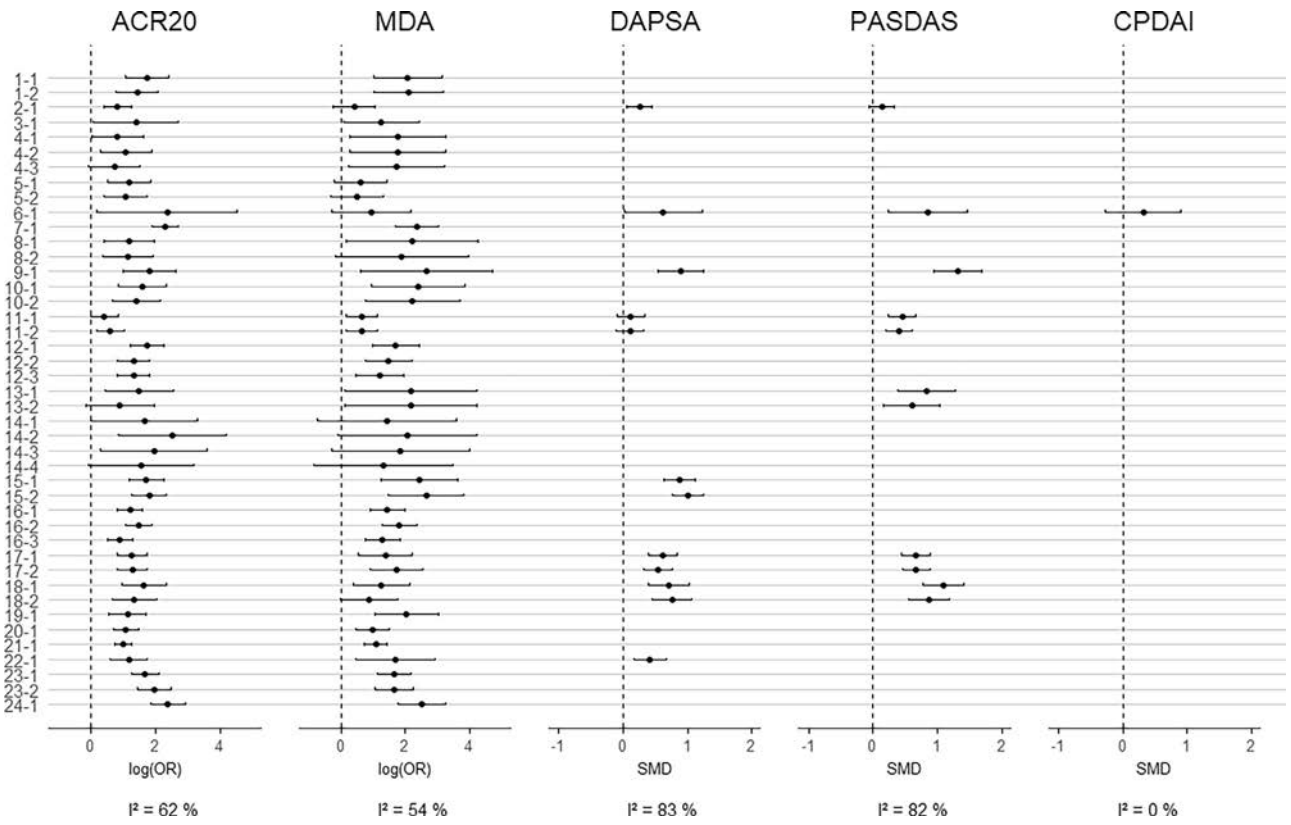

Figure 2. Forest plots displaying the randomised comparisons of the ACR20 and MDA log odds ratios (OR) including 95% CI and the DAPSA, PASDAS and CPDAI standardised mean differences (SMDs) including the 95% CI. 1-1 refers to the first comparison in study ID#1 and 1-2 refers to the second comparison in study ID#1; ACR, American College of Rheumatology Response Criteria; CPDAI, Composite Psoriatic Disease Activity Index; DAPSA, Disease Activity index for Psoriatic Arthritis; I^2, the proportion of total variability in effect estimates across studies that is due to heterogeneity rather than chance; MDA, Minimal Disease Activity; PASDAS, Psoriatic Arthritis Disease Activity Score.

and abstracts were screened, and 251 articles were retrieved for full-text screening, of which 25 articles reporting on 24 trials, corresponding to 43 randomised comparisons, were eligible for this analysis (Fig 1); references excluded following full-text review can be found in the online supplementary file.

The included trials (Table 1) involved 12,000 participants across both treatment naïve and b- and tsDMARD-experienced populations. All 24 trials reported ACR20 and MDA, 7 trials reported PASDAS, 6 trials reported DAPSA, and 1 trial reported CPDAI. No trials reported 3-VAS and 4-VAS; hence, data for 5 outcome measures (2 COD and 3 MOD) were available for analysis. Two trials were investigator-initiated of which 1 was sponsored by a pharmaceutical company. The remaining 22 studies were initiated and sponsored by the pharmaceutical industry. All studies were multicentre trials with 3 to 281 trial sites included. All 24 trials achieved a low risk of bias rating (Supplementary file) and consistently reported results of the outcome measures they had prospectively registered on ClinicalTrials.gov.

Quantitative evidence synthesis

Figure 2 shows the combined forest plot displaying results from 24 RCTs, with each row representing a unique comparison. Composite outcome measures are illustrated by the logORs with 95% CIs plotted for COD instruments (ACR20, MDA), and SMDs with 95% CIs for MOD instruments (DAPSA, PASDAS, and CPDAI). Empty rows within outcome columns indicate that the corresponding trial did not report that specific measure. The included RCTs allowed for up to 43 randomised direct comparisons between ACR20 and MDA; 11 between ACR20, PASDAS, and DAPSA, respectively; 11 between MDA, PASDAS, and DAPSA respectively; and 8 between DAPSA and PASDAS. One study reported CPDAI, resulting in one randomised comparison between CPDAI, DAPSA, PASDAS, ACR20, and MDA, respectively. Since no study reported the 3-VAS and 4-VAS, they are not included in the figures.

Unlike conventional network meta-analysis, which compares treatments across trials, the present network used nodes to represent outcome measures, with the connections quantifying the

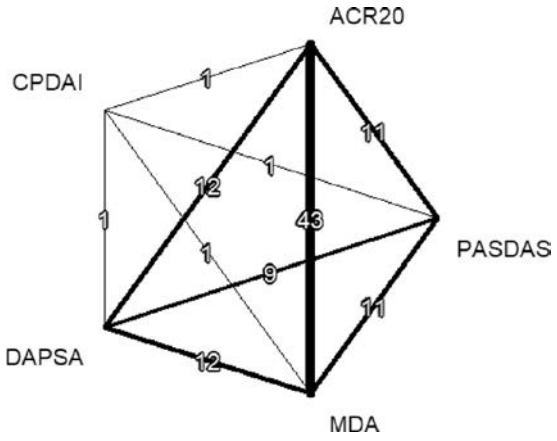

Figure 3. Network graph visualising the direct comparisons. The numbers on and the thickness of each line refer to the number of randomised comparisons between each outcome measure. ACR, American College of Rheumatology Response Criteria; CPDAI, Composite Psoriatic Disease Activity Index; DAPSA, Disease Activity index for PSoriatic Arthritis; MDA, Minimal Disease Activity; PASDAS, Psoriatic Arthritis Disease Activity Score.

Table 1

Characteristics of the trials and randomised comparisons eligible for the quantitative evidence synthesis

Author, year	Study ID#	Study acronym NCT#	N total	Study population	Outcomes reported	Experimental Intervention (n)	Comparator (n) total	Early escape: (Yes/No)	Timepoint for data extraction	Funding source
Mease PJ, 2014 [28]	1	RAPID-PsA NCT01087788	409	% Female: 55.4 Mean age (y): 47.5 Mean disease duration (y): 8.5 % Prior b-, tsDMARD exposure: 19.5	ACR20 MDA	Certolizumab pegol 400 mg LD, then 200 mg q2wk, n = 138 Certolizumab pegol 400 mg LD, then 400 mg q4wk, n = 135	Placebo, n = 136	Yes	Week 24	UCB Pharma
Mease PJ, 2017 [29]	2	ASTREA NCT01860976	424	% Female: 60.0 Mean age (y): 50.4 Mean disease duration (y): 8.6 % Prior b-, tsDMARD exposure: 61.1	ACR20 MDA DAPSA PASDAS	Abatacept 125 mg qwk, n = 213	Placebo, n = 211	Yes	Week 24	Bristol-Meyers Squibb
van Mens LJJ, 2019 [30]	3	NA NCT01871649	51	% Female: 25.4 Mean age (y): 46.7 Mean disease duration (y): 0.5 % Prior b-, tsDMARD exposure: 0	ACR20 MDA	Golimumab 50 mg q4wk, n = 26	Placebo, n = 25	No	Week 12	Investigator initiated study supported by MSD
Mease PJ, 2017 [31]	4	OPAL Broaden NCT01877668	422	% Female: 53.3 Mean age (y): 47.9 Mean disease duration (y): 6.1 % Prior b-, tsDMARD exposure: 2.8	ACR20 MDA	Tofacitinib 5 mg twice daily, n = 107 Tofacitinib 10 mg twice daily, n = 104 Adalimumab 40 mg q2wk, n = 106	Placebo, n = 105	No	Week 24	Pfizer
Gladman D, 2017 [32]	5	Opal Beyond NCT01882439	394	% Female: 55.3 Mean age (y): 49.9 Mean disease duration (y): 9,4 % Prior b-, tsDMARD exposure: 100	ACR20 MDA	Tofacitinib 5 mg twice daily, n = 131 Tofacitinib 10 mg twice daily, n = 132	Placebo, n = 131	No	Week 24	Pfizer
Vieira-Sousa E, 2020 [33]	6	GO-DACT NCT02065713	44	% Female: 16 Mean age (y): 49.16 Mean disease duration (y): 5.3 % Prior b-, tsDMARD exposure:0	ACR20 MDA DAPSA PASDAS CPDAI	Golimumab 50 mg q4wk, n = 21	Placebo, n = 23	No	Week 24	Investigator initiated, funding not reported
Kavanaugh A, 2017 [34]	7	GO-VIBRANT NCT02181673	479	% Female: 48.0 Mean age (y): 46.2 Mean disease duration (y): 5.8 % Prior b-, tsDMARD exposure: 0	ACR20 MDA	Golimumab 2 mg/kg at weeks 0 and 4 and then q8wk, n = 240	Placebo, n = 239	Yes	Week 24	Janssen
Kivitz AJ, 2019 [35]	8	FUTURE 4 NCT02294227	341	% Female: 58.0 Mean age (y): 49.0 Mean disease duration (y): 6.0 % Prior b-, tsDMARD exposure: 23.8	ACR20 MDA	Secukinumab 150 mg at weeks 0, 1, 2, and 3 then q4wk, n = 114 Secukinumab 150 mg q4wk, n = 113	Placebo, n = 114	Yes	Week 16	Novartis
Deodhar A, 2018 [36] & Helliwell PS, 2020 [37]	9	NA NCT02319759	149	% Female: 49.5 Mean age (y): 45.8 Mean disease duration (y): 6.8 % Prior b-; tsDMARD exposure: 8.5	ACR20 MDA PASDAS DAPSA	Guselkumab 100 mg at week 0 and 4 and then q8wk, n = 100	Placebo, n = 49	Yes	Week 24	Janssen
Nash P, 2017 [38]	10	SPIRIT-P2 NCT02349295	363	% Female: 53.3 Mean age (y): 51.9 Mean disease duration (y): 10.3 % Prior b-; tsDMARD exposure: 100	ACR20 MDA	Ixekizumab 80 mg q2wk, n = 123 Ixekizumab 80 mg q4wk, n = 122	Placebo, n = 118	Yes	Week 24	Eli Lilly and Company

(*continued on next page*)

Table 1 (*Continued*)

Author, year	Study ID#	Study acronym NCT#	N total	Study population	Outcomes reported	Experimental Intervention (n)	Comparator (n) total	Early escape: (Yes/No)	Timepoint for data extraction	Funding source
Mease PJ, 2019 [39]	11	SEAM-PsA NCT02376790	851	% Female: 50.7 Mean age (y): 48.4 Mean disease duration (y): 4.4 % Prior b-, tsDMARD exposure: 0	ACR20 MDA PASDAS DAPSA	Etanercept 50 mg qwk, n = 284 Etanercept 50 mg qwk + MTX 20 mg qwk, n = 283	Placebo + MTX 20 mg qwk, n = 284	No	Week 24	Amgen Inc
Mease PJ, 2018 [40]	12	FUTURE 5 NCT02404350	996	% Female: 49.6 Mean age (y): 48.8 Mean disease duration (y): 6.6 % Prior b-, ts-DMARD exposure: 29.6	ACR20 MDA	Secukinumab 300 mg at week 1, 2, and 3 then q4wk, n = 222 Secukinumab 150 mg at week 1, 2, and 3 then q4wk, n = 220 Secukinumab 150 mg q4ek, n = 222	Placebo, n = 332	Yes	Week 16	Novartis
Nguyen T, 2020 [41]	13	CHOICE NCT02798211	258	% Female: 50.3 Mean age (y): 52.1 Mean disease duration (y): 3,6 % Prior b-, tsDMARD exposure: o	ACR20 MDA PASDAS	Secukinumab 300 mg at week 0, 1, 2, and 3 then q4wk, n = 103 Secukinumab 150 mg at week 0, 1, 2, and 3 then q4wk, n = 103	Placebo, n = 52	No	Week 16	Novartis
Ritchlin CT, 2020 [42]	14	BE ACTIV NCT02969525	206	% Female: 49.0 Mean age (y): 49.3 Mean disease duration (y): 7.1 % Prior b-, tsDMARD exposure: 19	ACR20 MDA	Bimekizumab 16 mg q4wk, n = 41 Bimekizumab 160 mg q4wk, n = 41 Bimekizumab 320 mg LD and then 160 mg q4w, n = 41 Bimekizumab 320 mg q4wk, n = 41	Placebo, n = 42	No	Week 12	UCB Pharma
Mease PJ, 2021 [43]	15	SELECT-PsA 2 NCT03104374	641	% Female: 54.3 Mean age (y): 53.4 Mean disease duration (y): 10.1 % Prior b-, tsDMARD exposure: 92.0	ACR20 MDA DAPSA	Upadacitinib 15 mg daily, n = 211 Upadacitinib 30 mg daily, n = 218	Placebo, n = 212	Yes	Week 24	AbbVie Inc
McInnes IB, 2021 [44]	16	SELECT-PsA 1 NCT03104400	1704	% Female: 53.2 Mean age (y): 50.1 Mean disease duration (y): 6.1 % Prior b-, tsDMARD exposure:0	ACR20 MDA	Upadacitinib 15 mg daily, n = 429 Upadacitinib 30 mg daily, n = 423 Adalimumab 40mg q2wk, n = 429	Placebo, n = 423	Yes	Week 24	AbbVie Inc
Mease PJ, 2020 [45]	17	DISCOVER -2 NCT03158285	739	% Female: 47.3 Mean age (y): 45.7 Mean disease duration (y): 5.5 % Prior b-, tsDMARD exposure: 0	ACR20 MDA PASDAS DAPSA	Guselkumab 100 mg, q4wk, n = 245 Guselkumab 100 mg at week 0 and 4 and them q8wk, n = 248	Placebo, n = 247	Yes	Week 24	Janssen
Deodhar A, 2020 [46]	18	DISCOVER -1 NCT03162796	381	% Female: 48.7 Mean age (y): 48.4 Mean disease duration (y): 6.7 % Prior b-, tsDMARD exposure: 31	ACR20 MDA PASDAS DAPSA	Guselkumab 100 mg q4wk, n = 128 Guselkumab 100mg at week 0 and 5 and then q8wk, n = 127	Placebo, n = 126	Yes	Week 24	Janssen
Leng X, 2023 [47]	19	NA NCT03486457	204	% Female: 40.1 Mean age (y): 44.6 Mean disease duration (y):4.3 % Prior b-, tsDMARD exposure: 13.2	ACR20 MDA	Tofacitinib 5 mg twice daily, n = 136	Placebo, n = 86	No	Week 12	Pfizer
Östör A, 2022 [48]	20	KEEPsAKE 2 NCT03671148	443	% Female: 51.1 Mean age (y): 52.5 Mean disease duration (y): 8.2 % Prior b-, tsDMARD exposure: 46.5	ACR20 MDA	Risankizumab 150mg at week 0, 4, and 16, n = 224	Placebo, n = 219	No	Week 24	AbbVie Inc

(*continued on next page*)

Table 1 (*Continued*)

Author, year	Study ID#	Study acronym NCT#	N total	Study population	Outcomes reported	Experimental Intervention (n)	Comparator (n) total	Early escape: (Yes/No)	Timepoint for data extraction	Funding source
Kristensen LE, 2022 [49]	21	KEEPsAKE 1 NCT03675308	964	% Female: 49.6 Mean age (y): 52 Mean disease duration (y): 7.1 % Prior b-, tsDMARD exposure: o	ACR20 MDA	Risankizumab 150 mg at week 0, 4, and 16, n = 483	Placebo, n = 481	Yes	Week 24	AbbVie Inc
Coates LC, 2022 [50]	22	COSMOS NCT03796858	285	% Female: 50.0 Mean age (y): 49.0 Mean disease duration (y): 8.5 % Prior b-, tsDMARD exposure: 100	ACR20 MDA DAPSA	Guselkumab 100 mg at week 0 and 4 and then q8wk, n = 189	Placebo, n = 96	Yes	Week 24	Janssen
McInnes IB, 2023 [51]	23	BE OPTIMAL NCT03895203	852	% Female: 52.2 Mean age (y): 48.7 Mean disease duration (y): 5.9 % Prior b-, tsDMARD exposure: 0	ACR20 MDA	Bimekizumab 160 mg q4wk, n = 431 Adalimumab 40 mg q2wk, n = 140	Placebo, n = 281	No	Week 16	UCB Pharma
Merola JF, 2023 [52]	24	BE COMPLETE NCT03896581	400	% Female: 53.0 Mean age (y): 50.7 Mean disease duration (y): 9.4 % Prior b-, tsDMARD exposure: 12	ACR20 MDA	Bimekizumab 160 mg q4wk, n = 267	Placebo, n = 133	No	Week 16	UCB Pharma

ACR, American College of Rheumatology Response Criteria; CPDAI, Composite Psoriatic Disease Activity Index; DAPSA, Disease Activity index for PSoriatic Arthritis; LD, loading dose; NCT, clinicaltrials.gov identifier MDA, Minimal Disease Activity; MTX, methotrexate; NA, not applicable; PASDAS, Psoriatic Arthritis Disease Activity Score; q2wk, once every other week; q4wk; once every 4 weeks; q8wk, once every 8 weeks; qwk; once every week; tsDMARD, targeted synthetic disease-modifying antirheumatic drugs.

number of randomised comparisons available between each pair. The network graph (Fig 3) illustrates the number of randomised comparisons available between each pair of measures. Each line represents direct evidence, with the thickness proportional to the number of comparisons; numbers on the lines indicate the exact count of randomised comparisons informing each assessment.

As illustrated in Table 2, all direct estimates fell within the 95% CI of the network meta-analysis estimates, thus confirming the robustness of the inference made from the model. Differences in the discriminant capacity were observed for DAPSA vs ACR20 (NMA estimate = 0.80, 95% CI 0.66-0.97; favouring ACR20), DAPSA vs MDA (NMA estimate = 0.71, 95% CI 0.57-0.87; favouring MDA), and PASDAS vs DAPSA (NMA estimate = 1.35, 95% CI 1.10-1.66; favouring PASDAS). Trends consistently placed MDA as the most discriminant measure and favoured PASDAS over ACR20. Comparisons between CPDAI and other instruments resulted in wide CIs indicating imprecision, likely due to limited data being available for CPDAI. The direction of effects was consistent between direct and network estimates (Table 2), with the SMD analysis (Supplementary file) confirming the OR-based analysis.

Including ACR50/70 in the network meta-analysis showed greater discriminant capacity for ACR70 than ACR20 and DAPSA, but not vs ACR50, MDA, or PASDAS. ACR50 outperformed DAPSA only. Robustness was not confirmed for ACR50 vs DAPSA or PASDAS. PASDAS showed greater discriminant capacity compared with ACR20 (Table 3). Forest plots are included in the supplementary file.

The multivariate meta-analysis (Table 4) enabled presentation of estimates in a direct manner that largely confirmed the results derived from the network meta-analysis. Again, MDA (OR: 5.06; 95% CI: 4.20-6.09) was the most discriminant outcome measure, this time followed by ACR20 (OR: 4.01; 95% CI: 3.41-4.73), then PASDAS (OR: 3.70; 95% CI: 3.00-4.56), DAPSA (OR: 3.02; 95% CI: 2.44-3.75), and lastly CPDAI (OR: 1.86; 95% CI: 0.95-3.64).

Including ACR50/70 in the multivariate meta-analysis yielded wide and overlapping 95% CIs for all comparisons (Table 5).

Restricting the dataset to trials reporting ACR20, MDA, DAPSA, and PASDAS concurrently, to those with data extracted at week 24, or to week-24 trials stratified by early escape rules or by prior b- or tsDMARD exposure (≥50% vs <50%) did not materially alter the direction or relative magnitude of the estimates. In all analyses, direct estimates fell within the corresponding 95% CIs of the network estimates. No reversals of statistically significant contrasts from the network meta-analysis were observed. Full numerical results are available in the supplementary file.

DISCUSSION

This study aimed to identify which composite outcome measure most effectively differentiated active treatment from placebo in the setting of PsA RCTs. Network meta-analysis showed that MDA, ACR20, and PASDAS all discriminated experimental drug from placebo better than DAPSA with 95% CIs excluding one. The pairwise comparisons of MDA, ACR20, and PASDAS, respectively, had overlapping 95% CIs and contrasts involving CPDAI were imprecise because of sparse data. The multivariate meta-analysis, which accounted for correlations across measures, confirmed these patterns, again identifying MDA as most discriminant, followed by ACR20 and PASDAS. Although effect

Table 2
Network meta-analysis using OR comparing discriminant capacity of ACR20, MDA, DAPSA, PASDAS, and CPDAI

Comparison	NMA estimate	95% CIs	Direct estimate	95% CIs	Robustness Yes/No
MDA vs ACR20	1.13	0.97-1.31	1.14	0.98-1.32	Yes
[a]DAPSA vs ACR20	0.80	0.66-0.97	0.79	0.64-0.96	Yes
PASDAS vs ACR20	1.08	0.88-1.32	1.04	0.83-1.31	Yes
CPDAI vs ACR20	0.47	0.13-1.64	0.17	0.02-1.91	Yes
[a]DAPSA vs MDA	0.71	0.57-0.87	0.71	0.55-0.94	Yes
PASDAS vs MDA	0.96	0.76-1.19	1.06	0.80-1.41	Yes
CPDAI vs MDA	0.41	0.76-1.19	0.68	0.13-3.50	Yes
[a]PASDAS vs DAPSA	1.35	1.10-1.66	1.35	1.09-1.67	Yes
CPDAI vs DAPSA	0.58	0.17-2.04	0.57	0.12-2.68	Yes
CPDAI vs PASDAS	0.43	0.12-1.52	0.38	0.08-1.78	Yes

ACR, American College of Rheumatology Response Criteria; CPDAI, Composite Psoriatic Disease Activity Index; DAPSA, Disease Activity index for PSoriatic Arthritis; MDA, Minimal Disease Activity; NMA, network meta-analysis; OR, odds ratio; PASDAS, Psoriatic Arthritis Disease Activity Score.
An NMA estimate >1 indicates that the comparator listed on the left demonstrates greater discriminant capacity.
[a] Comparisons where the 95% CIs exclude 1. Direct, Inference is based on trials that compared the measures head-to-head.

Table 3
Exploratory network meta-analysis comparing discriminant capacity of ACR20/50/70, MDA, DAPSA, PASDAS, and CPDAI

Comparison	NMA estimate	95% CIs	Direct estimate	95% CIs	Robustness Yes/No
ACR50 vs ACR20	1.13	0.98-1.29	1.13	0.98-1.29	Yes
[a]ACR70 vs ACR20	1.23	1.08-1.54	1.23	1.07-1.53	Yes
MDA vs ACR20	1.10	0.95-1.27	1.10	0.95-1.28	Yes
DAPSA vs ACR20	0.91	0.76-1.08	0.80	0.65-0.97	Yes
[a]PASDAS vs ACR20	1.24	1.02-1.50	1.06	0.84-1.33	Yes
CPDAI vs ACR20	0.55	0.17-1.83	0.24	0.03-2.03	Yes
ACR70 vs ACR50	1.15	0.95-1.38	1.15	0.95-1.39	Yes
MDA vs ACR50	0.97	0.83-1.14	0.95	0.81-1.12	Yes
DAPSA vs ACR50	0.81	0.67-0.97	1.02	0.81-1.28	No
PASDAS vs ACR50	1.11	0.90-1.35	1.44	1.13-1.85	No
CPDAI vs ACR50	0.49	0.15-1.63	0.41	0.08-2.12	Yes
MDA vs ACR70	0.85	0.70-1.03	0.83	0.68-1.01	Yes
[a]DAPSA vs ACR70	0.70	0.57-0.87	0.68	0.50-0.92	Yes
PASDAS vs ACR70	0.96	0.76-1.21	1.02	0.74-1.39	Yes
CPDAI vs ACR70	0.43	0.13-1.42	0.70	0.13-3.69	Yes
DAPSA vs MDA	0.83	0.68-1.01	0.74	0.57-0.97	Yes
PASDAS vs MDA	1.13	0.92-1.40	1.10	0.83-1.46	Yes
CPDAI vs MDA	0.50	0.15-1.67	0.72	0.14-3.58	Yes
[a]PASDAS vs DAPSA	1.36	1.11-1.67	1.35	1.09-1.67	Yes
CPDAI vs DAPSA	0.61	0.18-2.02	0.57	0.12-2.68	Yes
CPDAI vs PASDAS	0.45	0.13-1.48	0.38	0.08-1.78	Yes

ACR, American College of Rheumatology Response Criteria; CPDAI, Composite Psoriatic Disease Activity Index; DAPSA, Disease Activity index for PSoriatic Arthritis; MDA, Minimal Disease Activity; NMA, network meta-analysis; OR, odds ratio; PASDAS, Psoriatic Arthritis Disease Activity Score.
An NMA estimate >1 indicates that the comparator listed on the left demonstrates greater discriminant capacity.
[a] Comparisons where the 95% CIs exclude 1. Direct: Inference is based on trials that compared the measures head-to-head.

sizes were modest and 95% CIs overlapped, the network- and multivariate meta-analysis together with the sensitivity analyses indicated a numerical advantage for MDA with PASDAS generally emerging as the second most discriminant measure. Taken together, these complementary approaches strengthen confidence in the findings, highlighting modest but directionally consistent differences in performance across measures. Although differences in discriminant capacity between composite outcome measures were modest in absolute terms, they may still have practical implications for primary endpoint selection in future PsA RCTs. For example, an NMA estimate of 0.71 for DAPSA vs MDA indicates that DAPSA has approximately 29% lower ability to distinguish active treatment from placebo compared with MDA, that is, MDA demonstrated 40% higher discriminant capacity relative to DAPSA. As endpoints with higher discriminant capacity generally require smaller sample sizes to achieve the same statistical power, differences of this magnitude could meaningfully influence statistical power and reduce the number of patients needed to detect a meaningful treatment effect.

Our results should be interpreted as differences in how effectively each measure captures treatment effects in the RCT framework, not as indicators of differential clinical benefit in routine practice. Interpreting discriminant capacity must consider both the relative measure and the absolute response rates underlying each outcome. ACR20 represents a low threshold for improvement and may yield relatively high placebo response rates, which can offset the contrast between intervention and placebo-comparator. MDA, however, is a more stringent target with low placebo response rates, making between-group differences more detectable. This difference in hurdle height could contribute to the moderately higher ORs observed for MDA. In addition to the discriminant capacity, a relevant outcome measure should reflect what is important for people living with the condition. Although all 5 shortlisted composite outcome measures include peripheral joint activity, PASDAS also includes enthesitis and

Table 4
Multivariate meta-analysis comparing discriminant capacity of ACR20, MDA, DAPSA, PASDAS, and CPDAI

Outcome	OR	95% CIs	k
MDA	5.06	4.20-6.09	43
ACR20	4.01	3.41-4.73	43
PASDAS	3.70	3.00-4.56	11
DAPSA	3.02	2.44-3.75	12
CPDAI	1.86	0.95-3.64	1

ACR, American College of Rheumatology Response Criteria; CPDAI, Composite Psoriatic Disease Activity Index; DAPSA, Disease Activity index for PSoriatic Arthritis; k, the number of randomised comparisons included; MDA, Minimal Disease Activity; OR, odds ratio; PASDAS, Psoriatic Arthritis Disease Activity Score.

Table 5
Exploratory multivariate meta-analysis comparing discriminant capacity of ACR20/50/70, MDA, DAPSA, PASDAS, and CPDAI

Outcome	OR	95% CIs	k
ACR70	4.78	3.64-6.29	43
MDA	4.34	3.65-5.17	43
ACR50	4.12	3.50-4.86	43
PASDAS	4.09	3.18-5.26	11
ACR20	3.58	3.07-4.16	43
DAPSA	2.92	2.25-3.79	12
CPDAI	2.03	1.05-3.93	1

ACR, American College of Rheumatology Response Criteria; CPDAI, Composite Psoriatic Disease Activity Index; DAPSA, Disease Activity index for PSoriatic Arthritis; k, the number of randomised comparisons included; MDA, Minimal Disease Activity; OR, odds ratio; PASDAS, Psoriatic Arthritis Disease Activity Score.

dactylitis, whereas MDA incorporates enthesitis and skin activity, which is a hallmark of PsA and considered important by people with the condition [5]. These structural differences likely influence their observed discriminant capacities, reflecting alignment between the instrument and the clinical expression of treatment benefit. Nonetheless, it also underscores the importance of selecting outcome measures that match the therapeutic targets and the multidimensional nature of PsA. Therefore, the higher discriminant capacity observed for MDA and PASDAS relative to ACR20 might reflect their multidomain structure.

Exploratory analyses suggested greater discriminant capacity for ACR70 than for ACR20 and DAPSA, whereas comparisons against MDA and PASDAS showed overlapping 95% CIs indicating no difference. This may be truly no difference or an insufficient statistical power to demonstrate the differences. However, the selection of an appropriate composite outcome measure for an RCT should incorporate considerations beyond RCT discrimination. In line with the OMERACT filter 2.2, this includes assessment of truth, discrimination, and feasibility, alongside the intended purpose [53]. Based on systematic review and Delphi consensus, DAPSA, MDA, and PASDAS have demonstrated consistent measurement-property evidence and achieved support for domain match by the GRAPPA-OMERACT group [54]. In contrast, consensus on domain match has not been achieved for ACR20/50/70, limiting their suitability as standalone primary endpoints in PsA RCTs [54]. Nevertheless, ACR response criteria may remain useful as legacy measures to facilitate comparison with the extensive existing PsA trial literature. At the same time, it will be important for future PsA trials to incorporate PsA-specific composite outcome measures as primary endpoints and to report not only on continuous values but also the proportions of patients achieving PASDAS- and DAPSA-defined remission and low disease activity. Routine reporting of these stringent, PsA-relevant endpoints will facilitate further evidence generation and support more comprehensive comparative evaluations in the future.

We are mindful of a few limitations of our study. Most included trials were industry-sponsored regulatory trials. As a result, the discriminant capacity identified here reflects performance within this specific trial population, mostly patients with polyarthritis, and may not fully generalise to the broader clinical spectrum of PsA encountered in routine practice. In addition, because the focus of this analysis was outcome-level discriminant capacity rather than estimating intervention effect sizes, the network estimates should be interpreted as indicators of within-trial separation between active treatment and placebo, averaged across RCTs, rather than as population-specific estimates of treatment efficacy. The number of available comparisons varied markedly across instruments, with MDA and ACR20 being reported in all included trials, whereas PASDAS, DAPSA, and particularly CPDAI were reported far less frequently. This imbalance reflects the historical landscape of PsA RCTs and regulatory requirements for inclusion of ACR20. Since the intent for the development of 3-VAS and 4-VAS was their use in clinical practice or longitudinal studies, and because the included RCTs were published between 2014 and 2023, with initiation of the trials predating the introduction of 3-VAS and 4-VAS in 2021 [11,12], their absence from the dataset would be expected. Similarly, we are cognisant that there was only 1 study reporting CPDAI, and hence more data are needed to analyse the discriminant capacity of CPDAI in RCTs. DAPSA and PASDAS were originally developed and validated as continuous instruments with remission and low disease activity cut-off values introduced later to support clinical interpretation [7,9]. As this analysis focused on evaluating the discriminant capacity in the RCT setting, the prespecified protocol did not include these cut-off values. However, as these cut-off values also represent stringent responder criteria, like MDA, future analyses should examine their comparative discriminant capacity to provide a more comprehensive evaluation across stringent PsA-specific composite outcome measures. To evaluate the impact of trial-level heterogeneity and confounding factors, we performed a set of additional sensitivity analyses. First, restricting the dataset to trials reporting at least ACR20, MDA, DAPSA, and PASDAS, which yielded effect estimates consistent with the main analysis. Second, limiting the dataset to trials reporting data at week 24 ensured temporal alignment across measures, yielding discriminant capacity estimates that were highly consistent with the main analysis. Third, stratifying week-24 trials by the presence vs absence of early escape showed no meaningful changes in relative performance. Finally, stratifying week-24 trials by prior b- or tsDMARD exposure (>50% vs <50%) demonstrated stable direction and magnitude across the strata. Collectively, these analyses indicate that differences in outcome availability, timepoints, early-escape policies, and prior treatment exposure did not materially influence the comparative patterns observed in the main analysis, suggesting that the results are transferable to future PsA RCTs.

Using a network meta-analytic framework to compare outcome measures is not a traditional application. However, a recent publication comparing physical functioning outcomes in PsA demonstrated that this approach can be successfully applied to compare measurement instruments [55]. Comparing binary and continuous measures was a methodological challenge requiring a common summary measure. In line with recommendations from the Cochrane Handbook for Systematic Reviews of Interventions [56], we addressed this by converting SMDs into ORs using Chinn's conversion factor [25]. Recognising that this process could potentially reduce the precision of the estimates, we also performed the reverse conversion (ie, transforming ORs into SMDs) and repeated the analysis, which confirmed the OR-based results. The agreement between the OR-

and SMD-based analyses, as well as the consistency observed when comparing original and converted estimates for both binary and continuous outcomes, supports the robustness of our findings and strengthens the confidence in the validity of our comparative analyses across different outcome types. In network meta-analyses, inconsistency should reflect disagreement between direct and indirect comparisons of the included composite outcome measures. High inconsistency would indicate that the relative discriminant capacity of 2 measures differs depending on whether it is estimated directly from trials reporting both outcomes or indirectly via a third measure. Such findings would question the assumption of generalisability and may arise from differences in trial populations, design, or selective outcome reporting. However, in the present analysis, including sensitivity analyses, all direct estimates fell within the 95% CIs, indicating robustness in the model.

Conclusion

Among the 5 shortlisted composite outcome measures with available data, ACR20, MDA, and PASDAS all demonstrated greater discriminant capacity than DAPSA. Exploratory analyses suggested greater discriminant capacity for ACR70 compared with ACR20 and DAPSA but not with ACR50, MDA or PASDAS. Limited data were available for CPDAI, and no data were available for 3-VAS and 4-VAS.

Acknowledgements

We thank the Parker Institute, Bispebjerg and Frederiksberg Hospital, and the OMERACT Technical Advisory Group (TAG) for their guidance.

Contributors

TKA: conceptualization, methodology, investigation, data curation, writing – original draft, writing – review & editing, and visualisation. MNH: conceptualisation, methodology, investigation, data curation, writing – original draft, writing – review & editing, and visualisation. TH: conceptualisation, methodology, data curation, formal analysis, writing – original draft, writing – review & editing, and visualisation. MH: conceptualisation, methodology, and writing – review & editing. LCC: conceptualisation, methodology, and writing – review & editing. AO: conceptualisation, methodology, and writing – review & editing. WT: conceptualisation, methodology, and writing – review & editing. NG: conceptualisation, methodology, and writing – review & editing. DDG: conceptualisation, methodology, and writing – review & editing. AMO: conceptualisation, methodology, and writing – review & editing. MW: conceptualisation, methodology, and writing – review & editing. VS: conceptualisation, methodology, and writing – review & editing. PJM: conceptualisation, methodology, and writing – review & editing. OF: conceptualisation, methodology, and writing – review & editing. PSH: conceptualisation, methodology, and writing – review & editing. PT: conceptualisation, methodology, and writing – review & editing. Y-YL: conceptualisation, methodology, writing – review & editing, and writing – review & editing supervision. RC: conceptualisation, methodology, investigation, writing – original draft, writing – review & editing, and supervision.

Funding

The Parker Institute, Bispebjerg and Frederiksberg Hospital is supported by a core grant from the Oak Foundation (OCAY-24-074-OFIL). This research was carried out on behalf of the OMERACT Technical Advisory Group which had no role in study design, data collection, data synthesis, data interpretation, and writing the report or the decision to submit the manuscript for publication.

Apart from above, this research project received no grant from any funding agency in the public, commercial, or not-for-profit sectors.

Competing interests

TKA is an employee of Ascendis Pharma, and a minority shareholder of Eli Lilly, Biogen, and Ascendis Pharma. MNH has no competing interests to declare. TH has no competing interests to declare. MH is advisory board member Leo Pharma and Thuasne. LCC has received grants/research support from AbbVie, Amgen, Janssen, and UCB; worked as a paid consultant for AbbVie, Amgen, Bristol Myers Squibb, Eli Lilly, Enlivex, Janssen, Moonlake, Novartis, Pfizer, Takeda, and UCB; and has been paid as a speaker for AbbVie, Amgen, Eli Lilly, Janssen, Novartis, Pfizer, and UCB. AO has no competing interests to declare. WT received research grants, consulting fees, speaking fees, and/or honoraria from AbbVie, Amgen, BMS, Celgene, Eli Lilly, GSK, Janssen, MSD, Novartis, Ono Pharma, Pfizer, and UCB Pharma. NG is a minority shareholder in UCB and Abcuro. DDG has received grants and/or consulting fees from AbbVie, Amgen, BMS, Eli Lilly, Fresenius Kabi, Janssen, Johnson & Johnson, Novartis, Pfizer, and UCB. A-MO has no competing interests to declare. MW: No competing interests to declare. VS is a founding member of the executive committee of Outcome Measures in Rheumatology (OMERACT) [1992 – present], an international consensus organization that develops and validates outcome measures in rheumatology RCTs and LOS, and has received arms-length funding from as many as 36 sponsors. PJM received research grants, consultation fees, and/or speaker honoraria from AbbVie, Amgen, Astra Zeneca, Biogen, Bristol Myers, Century, Cullinan, Eli Lilly, Inmagene, Johnson & Johnson, Merck, Moonlake Pharma, Novartis, Oruka, Pfizer, Spyre, SUN Pharma, Takeda, and UCB. OF received grants from Novartis, UCB, Pfizer, BMS, AbbVie, Lilly, and Johnson & Johnson. PSH has no conflicts to declare other than the fact that the PASDAS and MDA are licensed by the University of Leeds. PT has no competing interests to declare. Y-YL received speaker fee from AbbVie, DKSH, Janssen, Novartis, and Pfizer. All of these were outside of the submitted work. RC has received reports providing consulting on biostatistical matters, including trial design and statistical inference, for ZPD A/S (ScanDroitin), Image Analysis Ltd (trading as IAG, Image Analysis Group, UK), Compass Communications Ltd, and Ascendis Pharma A/S, with payments made directly to him as an individual. He serves as consultant/editor for Osteoarthritis and Cartilage and Acta Orthopaedica; holds leading roles in OMERACT; serves as statistical advisor to BMJ Open; is a member of the GRADE Working Group; and serves as editor for Arthritis Care & Research, Arthritis Research & Therapy, and the Cochrane Collaboration.

Patient consent for publication

Not applicable.

Ethics approval

Not applicable.

Provenance and peer review

Not commissioned; externally peer reviewed.

Declaration of generative AI and AI-assisted technologies in the writing process

A bespoke ChatGPT-based large language model configured for literature searches in PubMed and CENTRAL was used during protocol development to suggest an initial search string (described in the protocol). The suggested output was then evaluated and adjusted by the first author (TKA) and subsequently reviewed by all authors. No AI-assisted technologies were used during the preparation of this manuscript.

Supplementary materials

Supplementary material associated with this article can be found, in the online version, at doi:10.1016/j.ard.2026.05.013.

Orcid

Tommy K Annfeldt: http://orcid.org/0009-0001-8402-3917

REFERENCES

[1] Stober C. Pathogenesis of psoriatic arthritis. Best Pract Res Clin Rheumatol. 2021;35(2):101694. doi: 10.1016/j.berh.2021.101694.
[2] Freemantle N, Calvert M, Wood J, Eastaugh J, Griffin C. Composite outcomes in randomized trials greater precision but with greater uncertainty? [Internet]. Report. Available from: https://jamanetwork.com/
[3] Wells GA, Tugwell P, Tomasson G, Guillemin F, Maxwell LJ, Shea BJ, et al. Composite outcomes at OMERACT: multi-outcome domains and composite outcome domains. Semin Arthritis Rheum. 2021;51(6):1370–7. doi: 10.1016/j.semarthrit.2021.11.001.
[4] Leung YY, Tillett W, de Wit M, Orbai AM, Coates LC, FitzGerald O, et al. Initiating evaluation of composite outcome measures for psoriatic arthritis: 2022 updates from the GRAPPA-OMERACT Working Group. J Rheumatol. 2023;50:53–7. doi: 10.3899/jrheum.2023-0530.
[5] Orbai AM, De Wit M, Mease P, Shea JA, Gossec L, Leung YY, et al. International patient and physician consensus on a psoriatic arthritis core outcome set for clinical trials. Ann Rheum Dis. 2017 Apr;76(4):673–80. doi: 10.1136/annrheumdis-2016-210242.
[6] Coates LC, Fransen J, Helliwell PS. Defining minimal disease activity in psoriatic arthritis: a proposed objective target for treatment. Ann Rheum Dis. 2010 Jan;69(1):48–53. doi: 10.1136/ard.2008.102053.
[7] Schoels M, Aletaha D, Funovits J, Kavanaugh A, Baker D, Smolen JS. Application of the DAREA/DAPSA score for assessment of disease activity in psoriatic arthritis. Ann Rheum Dis. 2010 Aug;69(8):1441–7. doi: 10.1136/ard.2009.122259.
[8] Felson D, Aletaha D, Anderson J, Bathon J, Boers M, Bombardier C, et al. A proposed revision to the ACR20: the hybrid measure of American College of Rheumatology response. Arthritis Care Res (Hoboken). 2007 Mar;57(2):193–202. doi: 10.1002/art.22552.
[9] Helliwell PS, FitzGerald O, Fransen J, Gladman DD, Kreuger GG, Callis-Duffin K, et al. The development of candidate composite disease activity and responder indices for psoriatic arthritis (GRACE project). Ann Rheum Dis. 2013 Jun;72(6):986–91. doi: 10.1136/ANNRHEUMDIS-2012-201341.
[10] Mumtaz A, Gallagher P, Kirby B, Waxman R, Coates LC, Veale JD, et al. Development of a preliminary composite disease activity index in psoriatic arthritis. Ann Rheum Dis. 2011 Feb;70(2):272–7. doi: 10.1136/ARD.2010.129379.
[11] Tillett W, FitzGerald O, Coates LC, Packham J, Jadon DR, Massarotti M, et al. Composite measures for clinical trials in psoriatic arthritis: testing pain and fatigue modifications in a UK multicenter study. J Rheumatol Suppl. 2021 Jun;97:39–44. doi: 10.3899/jrheum.201674.
[12] Tillett W, FitzGerald O, Coates LC, Packham J, Jadon DR, Massarotti M, et al. Composite measures for routine clinical practice in psoriatic arthritis: testing of shortened versions in a UK multicenter study. J Rheumatol Suppl. 2021 Jun;97:45–9. doi: 10.3899/jrheum.201675.
[13] CHMP. Committee for Medicinal Products for human use (CHMP) guideline on clinical investigation of medicinal products for the treatment of psoriatic arthritis draft agreed by the efficacy working party adoption by CHMP for release for consultation end of CONSU... [Internet]. 2004 [cited 2026 Mar 29]. Available from: http://www.emea.europa.eu.
[14] Beaton D, Maxwell L, Grosskleg S, Shea B, Tugwell P, editors. The OMERACT handbook for establishing and implementing core outcomes in clinical trials across the spectrum of rheumatologic conditions [Internet]. 2.1. OMERACT; 2021 [cited 2026 Jan 21]. Available from: https://omeract.org/wp-content/uploads/2025/11/Handbook-June-2021-1.pdf
[15] de Wit M, Aouad K, Elhai M, Benavent D, Bertheussen H, Blackburn S, et al. EULAR recommendations for the involvement of patient research partners in rheumatology research: 2023 update. Ann Rheum Dis. 2024 Oct;83(11):e225566. doi: 10.1136/ARD-2024-225566.
[16] Page MJ, Moher D, Bossuyt PM, Boutron I, Hoffmann TC, Mulrow CD, et al. PRISMA 2020 explanation and elaboration: updated guidance and exemplars for reporting systematic reviews. BMJ. 2021;372:n160. doi: 10.1136/bmj.n160.
[17] Singh JA, Guyatt G, Ogdie A, Gladman DD, Deal C, Deodhar A, et al. Special article: 2018 American College of Rheumatology/National Psoriasis Foundation guideline for the treatment of psoriatic arthritis. Arthritis Rheumatol. 2019 Jan;71(1):5–32. doi: 10.1002/art.40726.
[18] Gossec L, Baraliakos X, Kerschbaumer A. EULAR recommendations for the management of psoriatic arthritis with pharmacological therapies: 2019 update. Helena Marzo-Ortega. 2020;79:32. doi:10.1136/annrheumdis-2020-217159
[19] Coates LC, Soriano ER, Corp N, Bertheussen H, Callis Duffin K, Campanholo CB, et al. Group for Research and Assessment of Psoriasis and Psoriatic Arthritis (GRAPPA): updated treatment recommendations for psoriatic arthritis 2021. Nat Rev Rheumatol. 2022 Aug;18(8):465–79. doi: 10.1038/s41584-022-00798-0.
[20] Covidence systematic review software [Internet] Melbourne, Australia: Veritas Health Innovation; 2024 [cited 2024 Sep 16] Available from www.covidence.org.
[21] Sterne JAC, Savović J, Page MJ, Elbers RG, Blencowe NS, Boutron I, et al. RoB 2: A revised tool for assessing risk of bias in randomised trials. BMJ. 2019;366. doi: 10.1136/bmj.l4898.
[22] Wells G, Li T, Maxwell L, Maclean R, Tugwell P. Responsiveness of patient reported outcomes including fatigue, sleep quality, activity limitation, and quality of life following treatment with abatacept for rheumatoid arthritis. Ann Rheum Dis 2008 Feb;67(2):260–5. doi: 10.1136/ard.2007.069690.
[23] Guyatt GH, Oxman AD, Santesso N, Helfand M, Vist G, Kunz R, et al. GRADE guidelines: 12. Preparing summary of findings tables - binary outcomes. J Clin Epidemiol. 2013 Feb;66(2):158–72. doi: 10.1016/j.jclinepi.2012.01.012.
[24] Guyatt GH, Thorlund K, Oxman AD, Walter SD, Patrick D, Furukawa TA, et al. GRADE guidelines: 13. Preparing summary of findings tables and evidence profiles - continuous outcomes. J Clin Epidemiol. 2013 Feb;66(2):173–83. doi: 10.1016/j.jclinepi.2012.08.001.
[25] Chinn S. A simple method for converting an odds ratio to effect size for use in meta-analysis. Stat Med. 2000 Nov;19(22):3127–31. doi: 10.1002/1097-0258(20001130)19:22<3127::AID-SIM784>3.0.CO;2-M.
[26] Kirkham JJ, Riley RD, Williamson PR. A multivariate meta-analysis approach for reducing the impact of outcome reporting bias in systematic reviews. Stat Med. 2012 Sep;31(20):2179–95. doi: 10.1002/sim.5356.
[27] RStudio Team. RStudio: Integrated Development Environment for R, version 2023.06.0. Boston, MA: RStudio, PBC; 2023.
[28] Mease PJ, Fleischmann R, Deodhar AA, Wollenhaupt J, Khraishi M, Kielar D, et al. Effect of certolizumab pegol on signs and symptoms in patients with psoriatic arthritis: 24-week results of a Phase 3 double-blind randomised placebo-controlled study (RAPID-PsA). Ann Rheum Dis. 2014;73(1):48–55. doi: 10.1136/annrheumdis-2013-203696.
[29] Mease PJ, Gottlieb AB, van der H D, FitzGerald O, Johnsen A, Nys M, et al. Efficacy and safety of abatacept, a T-cell modulator, in a randomised, double-blind, placebo-controlled, phase III study in psoriatic arthritis. Ann Rheum Dis. 2017;76(9):1550–8. doi: 10.1136/annrheumdis-2016-210724.
[30] van MLJ J, de JH M, Fluri I, Nurmohamed MT, van de SMG H, Kok M, et al. Achieving remission in psoriatic arthritis by early initiation of TNF inhibition: a double-blind, randomised, placebo-controlled trial of golimumab plus methotrexate versus placebo plus methotrexate. Ann Rheum Dis. 2019;78(5):610–6. doi: 10.1136/annrheumdis-2018-214746.
[31] Mease P, Hall S, FitzGerald O, van der H D, Merola JF, Avila-Zapata F, et al. Tofacitinib or adalimumab versus placebo for psoriatic arthritis. N Engl J Med. 2017;377(16):1537–50. doi: 10.1056/NEJMoa1615975.

[32] Gladman D, Rigby W, Azevedo VF, Behrens F, Blanco R, Kaszuba A, et al. Tofacitinib for psoriatic arthritis in patients with an inadequate response to TNF inhibitors. N Engl J Med. 2017;377(16):1525–36. doi: 10.1056/NEJMoa1615977.

[33] Vieira-Sousa E, Alves P, Rodrigues AM, Teixeira F, Tavares-Costa J, Bernardo A, et al. GO-DACT: a phase 3b randomised, double-blind, placebo-controlled trial of GOlimumab plus methotrexate (MTX) versus placebo plus MTX in improving DACTylitis in MTX-naive patients with psoriatic arthritis. Ann Rheum Dis. 2020;79(4):490–8. doi: 10.1136/annrheumdis-2019-216500.

[34] Kavanaugh A, Husni ME, Harrison DD, Kim L, Lo KH, Leu JH, et al. Safety and efficacy of intravenous golimumab in patients with active psoriatic arthritis: results through week twenty-four of the GO-VIBRANT Study. Arthritis Rheumatol. 2017;69(11):2151–61. doi: 10.1002/art.40226.

[35] Kivitz AJ, Nash P, Tahir H, Everding A, Mann H, Kaszuba A, et al. Efficacy and safety of subcutaneous secukinumab 150 mg with or without loading regimen in psoriatic arthritis: results from the FUTURE 4 Study. Rheumatol Ther. 2019;6(3):393–407. doi: 10.1007/s40744-019-0163-5.

[36] Deodhar A, Gottlieb AB, Boehncke WH, Dong B, Wang Y, Zhuang Y, et al. Efficacy and safety of guselkumab in patients with active psoriatic arthritis: a randomised, double-blind, placebo-controlled, phase 2 study. Lancet. 2018;391(10136):2213–24. doi: 10.1016/S0140-6736(18)30952-8.

[37] Helliwell PS, Deodhar A, Gottlieb AB, Boehncke WH, Xu XL, Xu S, et al. Composite measures of disease activity in psoriatic arthritis: comparative instrument performance based on the efficacy of guselkumab in an interventional phase II trial. Arthritis Care Res (Hoboken). 2020;72(11):1579–88. doi: 10.1002/acr.24046.

[38] Nash P, Kirkham B, Okada M, Rahman P, Combe B, Burmester GR, et al. Ixekizumab for the treatment of patients with active psoriatic arthritis and an inadequate response to tumour necrosis factor inhibitors: results from the 24-week randomised, double-blind, placebo-controlled period of the SPIRIT-P2 phase 3 trial. Lancet. 2017;389(10086):2317–27. doi: 10.1016/S0140-6736(17)31429-0.

[39] Mease PJ, Gladman DD, Collier DH, Ritchlin CT, Helliwell PS, Liu L, et al. Etanercept and methotrexate as monotherapy or in combination for psoriatic arthritis: primary results from a randomized, controlled phase III trial. Arthritis Rheumatol. 2019;71(7):1112–24. doi: 10.1002/art.40851.

[40] Mease P, van der H D, Landewé R, Mpofu S, Rahman P, Tahir H, et al. Secukinumab improves active psoriatic arthritis symptoms and inhibits radiographic progression: primary results from the randomised, double-blind, phase III FUTURE 5 study. Ann Rheum Dis. 2018;77(6):890–7. doi: 10.1136/annrheumdis-2017-212687.

[41] Nguyen T, Churchill M, Levin R, Valenzuela G, Merola JF, Ogdie A, et al. Secukinumab in United States Biologic-Naïve patients with psoriatic arthritis: results from the randomized, placebo-controlled CHOICE study. J Rheumatol. 2022;49(8):894–902. doi: 10.3899/jrheum.210912.

[42] Ritchlin CT, Kavanaugh A, Merola JF, Schett G, Scher JU, Warren RB, et al. Bimekizumab in patients with active psoriatic arthritis: results from a 48-week, randomised, double-blind, placebo-controlled, dose-ranging phase 2b trial. Lancet. 2020;395(10222):427–40. doi: 10.1016/S0140-6736(19)33161-7.

[43] Mease PJ, Lertratanakul A, Anderson JK, Papp K, V den B F, Tsuji S, et al. Upadacitinib for psoriatic arthritis refractory to biologics: SELECT-PsA 2. Ann Rheum Dis. 2021;80(3):312–20. doi: 10.1136/annrheumdis-2020-218870.

[44] McInnes IB, Anderson JK, Magrey M, Merola JF, Liu Y, Kishimoto M, et al. Trial of upadacitinib and adalimumab for psoriatic arthritis. N Engl J Med. 2021;384(13):1227–39. doi: 10.1056/NEJMoa2022516.

[45] Mease PJ, Rahman P, Gottlieb AB, Kollmeier AP, Hsia EC, Xu XL, et al. Guselkumab in biologic-naive patients with active psoriatic arthritis (DISCOVER-2): a double-blind, randomised, placebo-controlled phase 3 trial. Lancet. 2020;395(10230):1126–36. doi: 10.1016/S0140-6736(20)30263-4.

[46] Deodhar A, Helliwell PS, Boehncke WH, Kollmeier AP, Hsia EC, Subramanian RA, et al. Guselkumab in patients with active psoriatic arthritis who were biologic-naive or had previously received TNFα inhibitor treatment (DISCOVER-1): a double-blind, randomised, placebo-controlled phase 3 trial. Lancet. 2020;395(10230):1115–25. doi: 10.1016/S0140-6736(20)30265-8.

[47] Leng X, Lin W, Liu S, Kanik K, Wang C, Wan W, et al. Efficacy and safety of tofacitinib in Chinese patients with active psoriatic arthritis: a phase 3, randomised, double-blind, placebo-controlled study. RMD Open. 2023;9:1. doi: 10.1136/rmdopen-2022-002559.

[48] Östör A, V den B F, Papp K, Asnal C, Blanco R, Aelion J, et al. Efficacy and safety of risankizumab for active psoriatic arthritis: 24-week results from the randomised, double-blind, phase 3 KEEPsAKE 2 trial. Ann Rheum Dis. 2022;81(3):351–8. doi: 10.1136/annrheumdis-2021-221048.

[49] Kristensen LE, Keiserman M, Papp K, McCasland L, White D, Lu W, et al. Efficacy and safety of risankizumab for active psoriatic arthritis: 24-week results from the randomised, double-blind, phase 3 KEEPsAKE 1 trial. Ann Rheum Dis. 2022;81(2):225–31. doi: 10.1136/annrheumdis-2021-221019.

[50] Coates LC, Gossec L, Theander E, Bergmans P, Neuhold M, Karyekar CS, et al. Efficacy and safety of guselkumab in patients with active psoriatic arthritis who are inadequate responders to tumour necrosis factor inhibitors: results through one year of a phase IIIb, randomised, controlled study (COSMOS). Ann Rheum Dis. 2022;81(3):359–69. doi: 10.1136/annrheumdis-2021-220991.

[51] McInnes IB, Asahina A, Coates LC, Landewé R, Merola JF, Ritchlin CT, et al. Bimekizumab in patients with psoriatic arthritis, naive to biologic treatment: a randomised, double-blind, placebo-controlled, phase 3 trial (BE OPTIMAL). Lancet. 2023;401(10370):25–37. doi: 10.1016/S0140-6736(22)02302-9.

[52] Merola JF, Landewé R, McInnes IB, Mease PJ, Ritchlin CT, Tanaka Y, et al. Bimekizumab in patients with active psoriatic arthritis and previous inadequate response or intolerance to tumour necrosis factor-α inhibitors: a randomised, double-blind, placebo-controlled, phase 3 trial (BE COMPLETE). Lancet. 2023;401(10370):38–48. doi: 10.1016/S0140-6736(22)02303-0.

[53] Maxwell LJ, Beaton DE, Boers M, D'Agostino MA, Conaghan PG, Grosskleg S, et al. The evolution of instrument selection for inclusion in core outcome sets at OMERACT: Filter 2.2. Semin Arthritis Rheum. 2021 Dec;51(6):1320–30. doi: 10.1016/J.SEMARTHRIT.2021.08.011.

[54] Ribeiro AL, Annfeldt TK, Gladman DD, Tillett W, Orbai AM, Leung YY. Composite outcome measures for psoriatic arthritis: project updates 2024. J Rheumatol. 2025 Aug jrheum.2025-0268. doi: 10.3899/JRHEUM.2025-0268.

[55] Leung YY, Haugegaard T, Annfeldt TK, Holland R, Strand V, Mease P, et al. Determining the best discriminatory physical functioning outcome measurement instrument for psoriatic arthritis trials: a meta-epidemiological study. Semin Arthritis Rheum. 2026 Apr;77:152907. doi: 10.1016/J.SEMARTHRIT.2025.152907.

[56] Higgins JP, Green S. Cochrane Handbook for Systematic Reviews of Interventions | Cochrane Training [Internet]. 5.1.0 (March 2011). Higgins JP, Green S, editors. [cited 2024 Apr 24]. Available from: https://training.cochrane.org/handbook/current

Ann Rheum Dis 85 (2026) 1543–1555

Contents lists available at ScienceDirect

Annals of the Rheumatic Diseases

journal homepage: https://www.sciencedirect.com/journal/annals-of-the-rheumatic-diseases

Axial spondyloarthritis

An app-based nonpharmacological intervention improves patient-reported disease activity, functionality, and quality of life in patients with axial spondyloarthritis: a randomised controlled trial

Patrick-Pascal Strunz[1,*], Matthias Froehlich[1], Tobias Heusinger[2], Maxime le Maire[2], Anna Fleischer[3], Karsten Sebastian Luetkens[4], Patricia Possler[2], Michael Gernert[1], Hannah Labinsky[1], Ottar Gadeholt[1], Robert Leppich[5], Astrid Schmieder[6], Ludwig Hammel[7], Billy Sperlich[8], Hermann Einsele[9], Marc Schmalzing[1]

[1] *Department of Internal Medicine 2, Rheumatology/Clinical Immunology, University Hospital Wuerzburg, Wuerzburg, Germany*
[2] *Medical Faculty, University of Wuerzburg, Wuerzburg, Germany*
[3] *Department of Internal Medicine 2, Psychosomatic Medicine, University Hospital Wuerzburg, Wuerzburg, Germany*
[4] *Department of Diagnostic and Interventional Radiology, University Hospital Wuerzburg, Wuerzburg, Germany*
[5] *Department of Computer Science, University of Wuerzburg, Wuerzburg, Germany*
[6] *Department of Dermatology, Venereology, and Allergology, University Hospital Wuerzburg, Wuerzburg, Germany*
[7] *Deutsche Vereinigung Morbus Bechterew e. V., Schweinfurt, Germany*
[8] *Integrative and Experimental Exercise Science and Training, Institute for Sports Science, University of Wuerzburg, Wuerzburg, Germany*
[9] *Department of Internal Medicine 2, University Hospital Wuerzburg, Wuerzburg, Germany*

ARTICLE INFO

Article history:
Received 4 November 2025
Received in revised form 16 February 2026
Accepted 17 February 2026

ABSTRACT

Objectives: No app-based nonpharmacological intervention has yet demonstrated to meaningfully improve disease activity, functional status, and disease-specific quality of life in axial spondyloarthritis (axSpA). We evaluated *Axia*, a CE-marked smartphone application designed for axSpA, that combines personalised exercise therapy, patient education, and disease management, supported by gamification for long-term adherence.

Methods: To evaluate its clinical efficacy, a 12-week monocentric randomised controlled interventional trial was conducted involving 200 patients with axSpA with stable pharmacotherapy. Patients were randomised (1:1) to either using *Axia* (intervention group [IG]) or standard of care (control group [CG]).

Results: A total of 186 participants (mean age 50.61 years, 66% females, 56% with radiographic axSpA, mean Bath Ankylosing Spondylitis Disease Activity Index [BASDAI] 5.17, and 58% received biologicals or Janus kinase inhibitors) completed the study (95 in the IG and 91 in the CG). Compared to CG, participants in the IG demonstrated significant improvements in BASDAI (analysis of covariance [ANCOVA]-estimated group difference: −1.508, $P < .001$), Bath Ankylosing Spondylitis Functional Index (−1.139; $P < .001$), and Ankylosing Spondylitis Quality of Life questionnaire (−2.297; $P < .001$), all exceeding minimal clinically important difference thresholds. A significantly higher proportion of patients in the IG achieved an Assessment of

*Correspondence to Dr. Patrick-Pascal Strunz, Department of Medicine II, Rheumatology/Clinical Immunology, University Hospital Wuerzburg, Wuerzburg, Germany.

E-mail address: Strunz_p@ukw.de (P.-P. Strunz).

Handling editor Josef S. Smolen.

https://doi.org/10.1016/j.ard.2026.02.016

Spondyloarthritis International Society (ASAS)20 response compared to the CG (51% vs 9%; $P < .001$), and the ASAS40 response rate was also higher (23% vs 3%; $P < .001$). No concerning safety signals were observed.

Conclusions: These findings support the potential of *Axia* as a safe and effective nonpharmacological intervention to further improve the state of care of patients with axSpA in addition to conventional anti-inflammatory pharmacotherapy.

WHAT IS ALREADY KNOWN ON THIS TOPIC

- Exercise therapy and patient education are key recommendations in axial spondyloarthritis (axSpA) care, but long-term adherence is often poor, and scalable access is limited.
- No app-based intervention in axSpA has yet demonstrated clinically meaningful improvements in disease activity in a randomised controlled trial.

WHAT THIS STUDY ADDS

- In a 12-week randomised controlled trial (n = 186), an app-based, axSpA-specific digital intervention ('Axia') as add-on to stable pharmacotherapy significantly improved patient-perceived disease activity (Bath Ankylosing Spondylitis Disease Activity Index), functionality (Bath Ankylosing Spondylitis Functional Index), and quality of life (Ankylosing Spondylitis Quality of Life questionnaire) vs standard of care alone.
- Assessment of Spondyloarthritis International Society 20/40 response rates were markedly higher in the app-usage group than in the control group.

HOW THIS STUDY MIGHT AFFECT RESEARCH, PRACTICE OR POLICY

- These findings suggest that an axSpA-specific app-based intervention could serve as an accessible and scalable form of nonpharmacological therapy as add-on to routine care.
- Digital interventions may help to close the long-standing implementation gap between guideline-recommended nonpharmacological therapies and their real-world clinical practice.

INTRODUCTION

Nonpharmacological interventions such as physical activity and patient education are a cornerstone in the management of axial spondyloarthritis (axSpA), an inflammatory rheumatic and musculoskeletal disease (iRMD) characterised by chronic inflammation of the axial skeleton [1]. In particular, home-based exercise (HbE) has been shown to improve disease activity, physical function, and quality of life [2,3], and is thus strongly recommended in national and international guidelines [4–6].

However, the effective translation of these recommendations in real-world clinical practice remains a major challenge, as a considerable proportion of patients underutilise or fail to adhere to exercise therapy [7]. This lack of sustained engagement has far-reaching consequences, as patients who do not engage in regular exercise interventions are more likely to experience progressive functional and mobility limitations, higher disease activity, and poorer disease-related quality of life [8].

Mobile healthcare apps may offer a scalable solution to this gap by delivering structured and individualised interventions directly to patients in their everyday environments [9,10]. In doing so, they may reduce key barriers to adherence, including limited access to physiotherapy, time constraints, and motivational challenges [11,12]. However, no app-based intervention in rheumatology has yet demonstrated clinically meaningful improvements in robust clinical endpoints in a randomised controlled trial (RCT) with a substantial sample size [13]. This evidentiary gap currently limits their integration into standard care pathways.

To address these gaps, *Axia* was developed by a start-up of 2 medical students in collaboration with the University Hospital of Wuerzburg and the German axSpA patient self-help association [14]. Axia provides axSpA-specific HbE and structured patient education, complemented by additional disease self-management tools. Gamification elements are integrated to enhance engagement and maximise adherence to therapy [14].

To prove Axia's efficacy, we conducted the Bechterew-App Trial, a 3-phase RCT involving 200 patients with axSpA with stable pharmacotherapy (German registry of clinical trials [DRKS], DRKS-ID: DRKS00033783).

METHODS

Study design

The Bechterew-App Trial was designed as a monocentric, prospective RCT with remote nationwide recruitment to evaluate the efficacy of the medical app *Axia* in patients with axSpA receiving stable pharmacotherapy. The RCT was conducted under the sponsorship of the University Hospital of Wuerzburg. Following baseline assessment, participants were randomised in a 1:1 ratio to either the intervention group (IG) or the control group (CG). Randomisation was stratified based on whether or not participants were receiving 1 session of individual physiotherapy per week (yes/no).

Participants in the IG received access to *Axia* for a 12-week period in addition to standard of care (SOC). The CG received SOC alone. SOC included pharmacological and nonpharmacological treatment as recommended by their treating physicians. Participants were intended to stay on stable physical therapy and pharmacotherapy during the trial; however, treating physicians were free to change pharmacotherapy on the basis of their own decision in case of flares or side-effects (rescue medication). Participants with switches of antirheumatic pharmacotherapy were excluded from the per-protocol (PP) analysis. Neither participants nor investigators were blinded.

The study was conducted in accordance with the Declaration of Helsinki and Good Clinical Practice guidelines. The study protocol was approved by the ethics committee of the medical faculty of the University of Wuerzburg, Wuerzburg (DE/EKBY13) (Date July 31, 2023, No. 92/23-am). The trial was prospectively registered at the German Clinical Trials Register (DRKS, DRKS-ID: DRKS00033783), date of first registry March 1, 2024. The corresponding consolidated standards of reporting trials (CONSORT) statement can be found in our Supplementary File.

Patient and public involvement

Patients with axSpA and representatives of the national German patient self-help association (Deutsche Vereinigung Morbus

Bechterew [DVMB]) were involved in the development of *Axia*, including the definition of patient-relevant content (exercise therapy, self-management support, and education) and usability testing. Patients and DVMB representatives were not involved in the RCT design, the selection of outcomes, the analysis, or the interpretation of data. However, they contributed to the recruitment process by supporting outreach to potential participants. The results of this study will be communicated back to the patient community in an accessible summary via the DVMB. Further details on patient and public involvement are provided in the Supplementary Material.

Participants

Candidates were eligible for participation in the Bechterew-App Trial if they were at least 18 years old, not pregnant, and had a confirmed diagnosis of axSpA. Furthermore, they had to be on stable axSpA-specific pharmacotherapy for 8 weeks before baseline (Supplementary Material for detailed definitions), a Bath Ankylosing Spondylitis Disease Activity Index (BASDAI) of at least 3.5 was mandatory at baseline, and participants were excluded if they had already been engaged in high levels of physical exercise. Finally, candidates must have sufficient digital literacy skills defined by the regular use of a messenger service. A comprehensive list of inclusion and exclusion criteria is provided in the Supplementary Material.

Intervention

The intervention consisted of using the medical smartphone application *Axia* over a 12-week period. *Axia* is a German language, disease-specific, and patient-tailored medical app developed for individuals with axSpA.

Axia is a Conformité Européenne (CE) class I medical device certified under the European Medical Device Regulation. Axia and its functions have already been described in detail elsewhere [14]. The content and the features of Axia, as well as its onboarding process, are presented in Figure 1 and in detail in the Supplementary Figures S1-S4.

Primary and secondary endpoints and their assessment

The coprimary endpoints were changes in patient-reported disease activity (measured by BASDAI), disease-specific functionality (assessed by Bath Ankylosing Spondylitis Functional Index [BASFI]), and axSpA-specific quality of life (assessed by Ankylosing Spondylitis Quality of Life [ASQoL] questionnaire) after 12 weeks, comparing the IG with the CG. All 3 instruments are standard patient-reported outcome measures (PROM) routinely used in axSpA care and pharmacological trials. Literature-based minimal clinically important differences (MCIDs), predefined in the study protocol, were as follows: a reduction of ≥1.0 point or ≥22.5% in BASDAI, ≥0.7 points or ≥17.5% in BASFI [15], and ≥1.8 points in ASQoL (equivalent to 10% of the total scale range) [16].

As patients are familiar with answering these questionnaires in clinical routine, no specific training was required. All PROMs were digitalised within an electronic Case Report Form (eCRF) and completed independently by participants at home, without access to previous responses or interaction with study personnel. Baseline and week-12 assessments were made available via email invitations. To simulate real-world conditions, no financial compensation or additional incentives were provided.

Secondary endpoints included self-efficacy (Allgemeine Selbstwirksamkeit Kurzskala [German language questionnaire for self-efficacy]), health literacy (German version of the 16-Item European Health Literacy Survey Questionnaire), global pain (numeric rating scale), patient global assessment of disease activity (PtGA), and self-reported adherence to exercise therapy (Exercise Adherence Rating Scale). All secondary measures were collected via eCRF at baseline and week 12.

In addition, the Assessment of Spondyloarthritis International Society (ASAS)20 and ASAS40 response rates were calculated. ASAS20 response was defined as an improvement of at least 20% and at least 1 unit (on a 0-10 scale) from baseline in 3 of 4 domains (spinal pain [BASDAI question 2], spinal inflammation [mean of BASDAI questions 5 and 6], physical function [BASFI], and PtGA), with no worsening in the remaining domain (defined as a deterioration of ≥20% and ≥1 unit). ASAS40 response required an improvement of at least 40% and 2 units in 3 of the 4 domains without any worsening in the fourth.

At week 12, participants were also asked via open-ended questions about adverse events (AEs) and their willingness to continue with *Axia* in the follow-up phases of the trial.

Sample size calculation

A sample size of 160 patients (80 patients per group) was determined to provide 90% power to detect differences in the coprimary outcomes between CG and IG at a significance level of $\alpha = 0.05$ using baseline- and multiplicity-adjusted analysis of covariance (ANCOVA). To account for an expected drop-out rate of 20%, 40 participants were added. Further information on sample size calculation is reported in our Supplementary Material.

Randomisation

The randomisation method was stratified block randomisation (ratio 1:1) in randomly defined blocks of 4 or 6. The stratification factor was regular individual physiotherapy (defined as 4 sessions per month on average during the 3 months preceding study inclusion vs no/less regular individual physiotherapy sessions before the study). Separate randomisation lists were generated by the independent Clinical Trial Center at the University Hospital Wuerzburg (ZKSW) for each stratum and implemented in a secure allocation software. The study team was blinded to the allocation sequence, and group assignment was revealed only after eligibility confirmation and entry of participant data into the system.

Statistical analysis

The primary analysed population was the intention-to-treat (ITT) population. Due to the use of mandatory fields within the eCRF, data completeness was 100% for all participants who completed the trial; missing values occurred only for the single individual lost to follow-up after 12 weeks.

Primary and secondary outcomes were analysed by ANCOVA models, adjusted for the respective baseline value, comparing the IG and CG after 12 weeks. Due to the slightly higher proportion of women in the IG compared to the CG, additional ANCOVA adjustments were made for sex (biological sex), besides the adjustment for baseline values. Descriptive statistics, including mean and SD, were used to summarise baseline characteristics. To address multiple testing and accumulation of

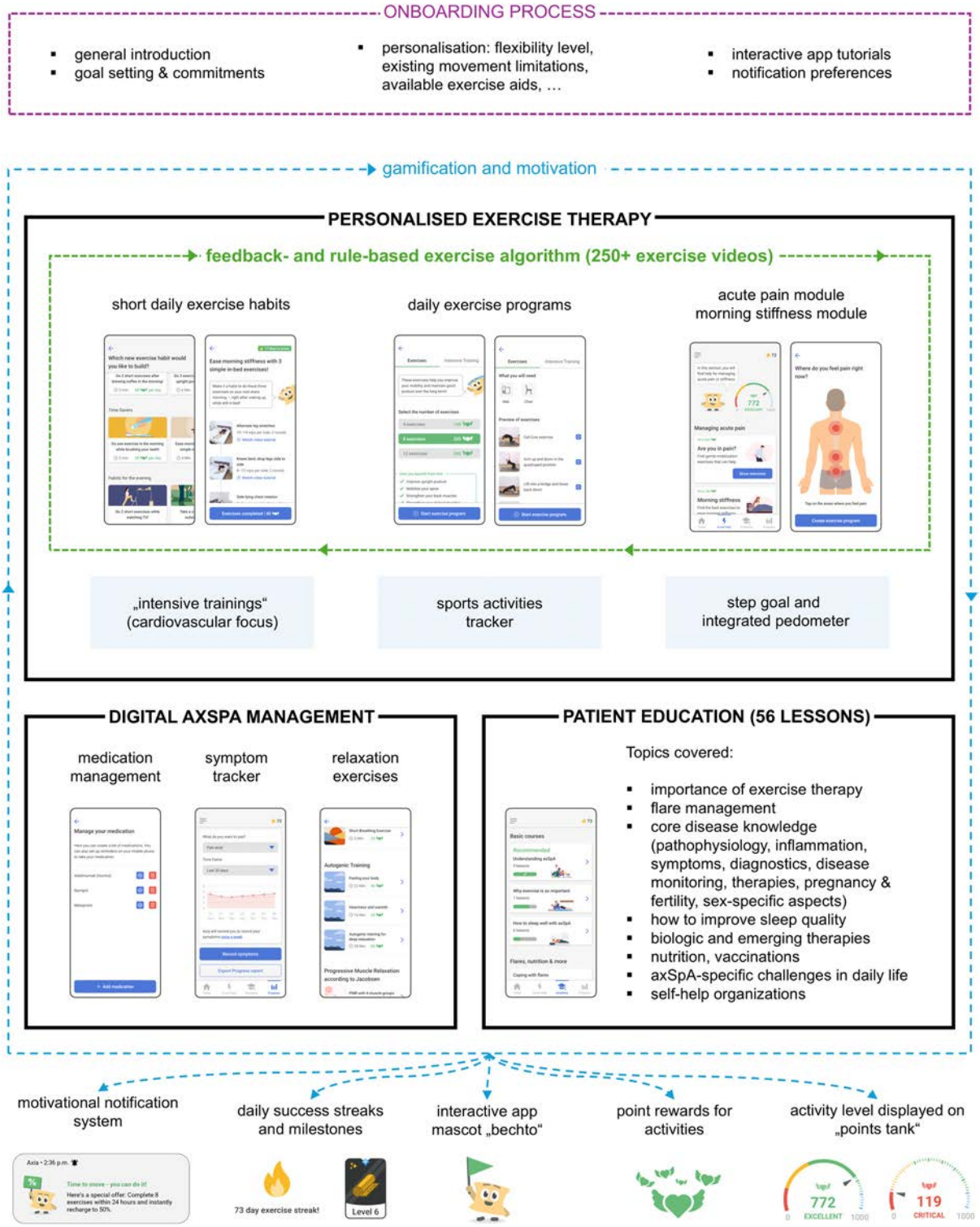

Figure 1. Onboarding process and key functional components of Axia. The figure shows the onboarding process (purple box), exercise functions as core components (central black box), and patient education and disease management functions (lower black boxes). Gamification elements (blue arrows) support treatment adherence. Navigation through Axia and representative slides of functional areas are provided in the Supplementary Material.

alpha errors, the Benjamini-Hochberg method was used to adjust the significance level. The primary endpoint was considered achieved if the statistical analysis using the baseline-adjusted ANCOVA described above, together with the Benjamini-Hochberg adjustment, showed a statistically significant improvement ($P < .05$) in at least 1 of the 3 coprimary outcomes.

Differences in ASAS20 and ASAS40 response rates between both groups were analysed by the Chi-square test. For all analyses, Prism and R were used. The statistical analysis plan is presented in detail in our Supplementary File.

RESULTS

Recruitment and baseline characteristics

Participants were recruited in Germany between March 2024 and December 2024 with the support of patient self-help

associations, social media, and rheumatology practices. The recruitment process is described in detail in the Supplementary Material. Of 453 individuals screened for eligibility, 200 were enrolled and randomised 1:1 to receive either *Axia* or SOC for 12 weeks.

The primary outcome assessment was conducted at week 12 and was completed by 186 participants; baseline characteristics for the ITT population are reported for the 187 participants with available baseline data (Table 1, Supplementary Table S1). The main reason for discontinuation was withdrawal of informed consent (n = 13); 1 participant was lost to follow-up (Fig 2).

Blockwise randomisation within the physiotherapy stratum (yes/no) ensured an equal distribution of participants with and without physiotherapy between IG and CG. Apart from a slightly higher proportion of female participants in the IG, no relevant differences were observed. Age, use of biological disease-modifying antirheumatic drugs (bDMARDs) or targeted synthetic

Table 1
Baseline characteristics

Characteristic	Intervention (n = 95)	Control (n = 92)	Total (n = 187)
Mean age, y (SD)	50.36 (12.07)	50.63 (11.35)	50.49 (11.69)
BASDAI, absolute (SD)	5.32 (1.31)	5.02 (1.26)	5.17 (1.29)
Female proportion, n (%)	70 (74%)	54 (59%)	124 (66%)
Radiographic axSpA, n (%)	59 (62%)	45 (49%)	104 (56%)
Nonradiographic axSpA, n (%)	36 (38%)	47 (51%)	83 (44%)
Peripheral involvement, n (%)	16 (17%)	31 (34%)	47 (25%)
HLA-B27 status, n (%)			
HLA-B27 positive, n (%)	47 (49%)	53 (58%)	100 (53%)
HLA-B27 negative, n (%)	11 (12%)	9 (10%)	20 (11%)
Not reported, n (%)	37 (39%)	30 (33%)	67 (36%)
Pharmacotherapy			
NSAIDs, n (%)	52 (55%)	57 (62%)	109 (58%)
bDMARD or tsDMARD usage, n (%)	53 (56%)	55 (60%)	108 (58%)
Physical therapy			
Professional physiotherapy			
Once per week, n (%)	53 (56%)	55 (60%)	108 (58%)
No physiotherapy, n (%)	42 (44%)	37 (40%)	79 (42%)
Other forms of exercise and physical therapy			
Home-based exercise, n (%)	37 (39%)	38 (41%)	75 (40%)
Functional training, n (%)	29 (31%)	31 (34%)	60 (32%)
Other sports, n (%)	30 (32%)	31 (34%)	61 (33%)
Disease duration			
0-2 y, n (%)	11 (12%)	14 (15%)	25 (13%)
2-10 y, n (%)	28 (29%)	29 (32%)	57 (30%)
>10 y, n (%)	56 (59%)	49 (53%)	105 (56%)
Comorbidities			
SpA-related comorbidities, n (%)	26 (27%)	33 (36%)	59 (32%)
Inflammatory bowel disease, n (%)	8 (8%)	6 (7%)	14 (7%)
Ulcerative colitis, n (%)	2 (2%)	2 (2%)	4 (2%)
Crohn's disease, n (%)	2 (2%)	3 (3%)	5 (3%)
Not classified, n (%)	4 (4%)	1 (1%)	5 (3%)
Psoriasis, n (%)	4 (4%)	15 (16%)	19 (10%)
Uveitis, n (%)	14 (15%)	12 (13%)	26 (14%)
Chronic pain syndrome/fibromyalgia, n (%)	16 (17%)	12 (13%)	28 (15%)
Other comorbidities			
Cardiovascular disease, n (%)	42 (44%)	48 (52%)	90 (48%)
Pulmonary disease, n (%)	13 (14%)	8 (9%)	21 (11%)
Dermatologic disease, n (%)	7 (7%)	9 (10%)	16 (9%)
Endocrine/metabolic disease, n (%)	47 (49%)	51 (55%)	98 (52%)
MSK disease, n (%)	59 (62%)	55 (60%)	114 (61%)
Hip OA, n (%)	9 (9%)	7 (8%)	16 (9%)
Knee OA, n (%)	5 (5%)	3 (3%)	8 (4%)
OA of the fingers, n (%)	7 (7%)	6 (7%)	13 (7%)
Basal thumb OA, n (%)	2 (2%)	3 (3%)	5 (3%)
Other forms of OA, n (%)	3 (3%)	1 (1%)	4 (2%)
Other degenerative MSK disease, n (%)	10 (11%)	8 (9%)	18 (10%)
Degenerative spinal disorders, n (%)	23 (24%)	27 (29%)	50 (27%)
History of cancer, n (%)	8 (8%)	1 (1%)	9 (5%)
Gastroenteric disease, n (%)	13 (14%)	13 (14%)	26 (14%)
Psychiatric/neurologic disorders, n (%)	22 (23%)	21 (23%)	43 (23%)
Other disorders, n (%)	14 (15%)	21 (23%)	35 (19%)
Non-SpA-related comorbidities in total, n	225	227	452
Unknown due to data deletion, n (%)	5 (5%)	8 (9%)	13 (7%)
No comorbidity, n (%)	16 (17%)	14 (15%)	30 (16%)

axSpA, axial spondyloarthritis; BASDAI, Bath Ankylosing Spondylitis Disease Activity Index; bDMARD, biological disease-modifying antirheumatic drug; HLA, human leukocyte antigen; MSK, musculoskeletal; NSAID, non-steroidal anti-inflammatory drug; OA, osteoarthritis; SpA, spondyloarthritis; tsDMARD, targeted synthetic disease-modifying antirheumatic drug.
The individual comorbidity categories are further detailed in the Supplementary Table S1, which can be found in the Supplementary Material.

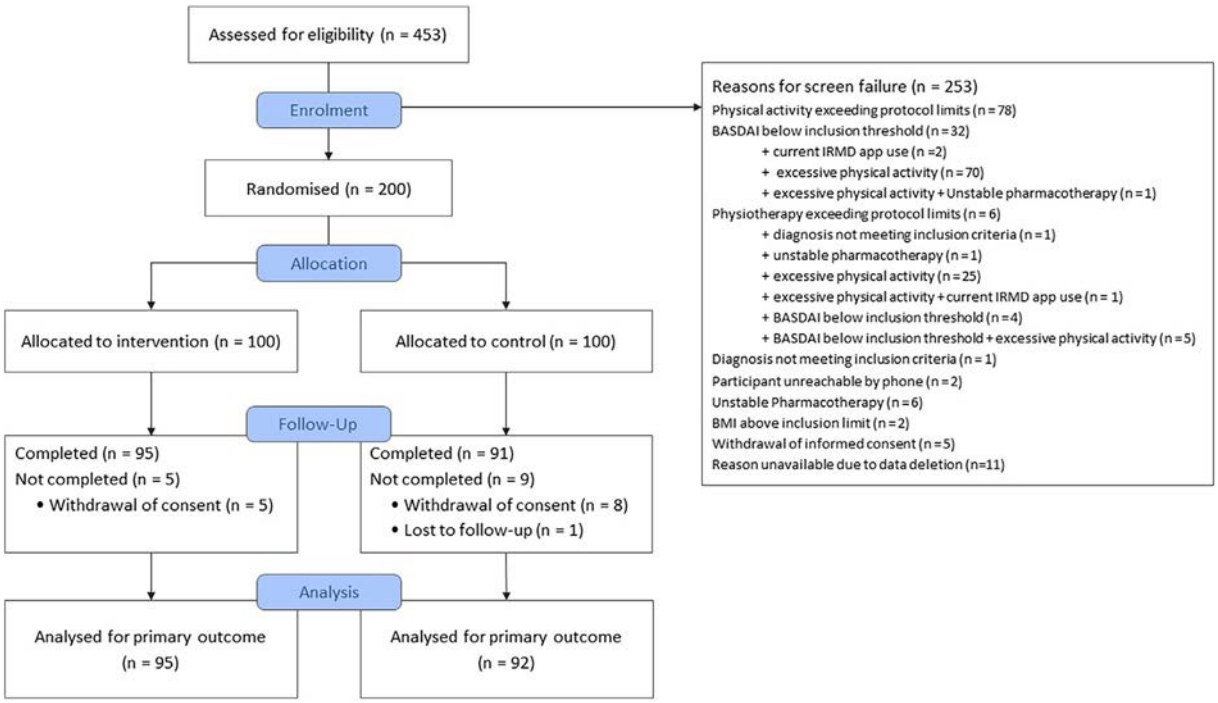

Figure 2. CONSORT flow diagram of the trial. BASDAI, Bath Ankylosing Spondylitis Disease Activity Index; BMI, body mass index; Consort, consolidated standards of reporting trials; iRMD, inflammatory rheumatic and musculoskeletal disease.

disease-modifying antirheumatic drugs, and exercise behaviour were well balanced between both groups.

Primary outcomes

After 12 weeks, participants in the *Axia* IG showed significantly greater improvements in BASDAI (ANCOVA-estimated group difference, adjusted for baseline values and sex: −1.508; 95% CI: −1.874 to −1.142; $P < .001$), BASFI (−1.139; 95% CI: −1.524 to −0.755; $P < .001$), and ASQoL (−2.297; 95% CI: −2.983 to −1.610; $P < .001$) (Fig 3). All effects exceeded their respective MCID thresholds. Effect sizes were large across all primary outcomes, with Cohen's *d* values of 1.20 for BASDAI, 0.87 for BASFI, and 0.97 for ASQoL.

Participants were instructed to remain on stable antirheumatic pharmacotherapy and physiotherapy during the trial to minimise the potential influence of treatment changes. Nevertheless, some treatment switches occurred. To assess their impact, the primary outcomes of the PP population were compared to the ITT population. Effect estimates in the PP population were numerically higher and consistent in direction with the ITT analysis, indicating that protocol deviations, including treatment modifications, had no substantial impact on the results (Supplementary Table S2). Physiotherapy use remained stable from baseline to week 12 in both groups (CG: from 60% to 64%; IG: from 56% to 62%).

Participants in the IG who increased their HbE by more than 60 min/wk on average achieved a markedly better response in the primary outcomes (Table 2). Responder analyses revealed that significantly more participants in the IG achieved improvements exceeding the predefined MCIDs compared with the CG (BASDAI: 67% vs 18%; BASFI: 67% vs 22%; ASQoL: 60% vs 28%; all $P < .001$).

Secondary outcomes

Secondary outcomes included response rates according to the ASAS20 and ASAS40 criteria, as well as changes in global pain, PtGA, self-efficacy, self-reported exercise adherence, and health literacy.

After 12 weeks of app use, significantly more participants in the IG met the ASAS20 (51% vs 9%; $P < .001$) and ASAS40 (23% vs 3%; $P < .001$) response criteria compared to the CG (Fig 4). Adjusted ANCOVA models showed significant group differences in favour of the intervention for global pain, PtGA, self-efficacy, and self-reported exercise adherence. No significant difference was observed for health literacy (Fig 5).

Adherence rates

In addition to self-reported adherence, participants' usage of *Axia* was objectively tracked: during the 12-week study period, the app was used on an average of 69 days (SD 18.3) of 90 days, and cumulatively, for an average of 1145 minutes (SD 937.6 minutes). A total of 77.9% of participants used the app on at least 5 days a week, and 29.7% used *Axia* daily during the study period. The app was used by 93% of participants on at least half of the days of the study period. A total of 98.9% of the participants of the IG stated that they would like to continue using *Axia*.

Safety

All AEs were assessed during the trial. In total, 55 AEs (29%) were observed, 4 of which were severe AEs (SAEs). AE incidence rates of the IG (22%, n = 21; 1% SAE, n = 1) were lower than in the CG (37%, n = 34; 3% SAE, n = 3). No device-related AEs were identified in the IG. Table 3 lists all observed AEs.

DISCUSSION

This RCT provided the first robust evidence that a medical app can achieve clinically meaningful improvements in patient-reported disease activity, functional status, and quality of life in patients with axSpA receiving stable pharmacotherapy. The

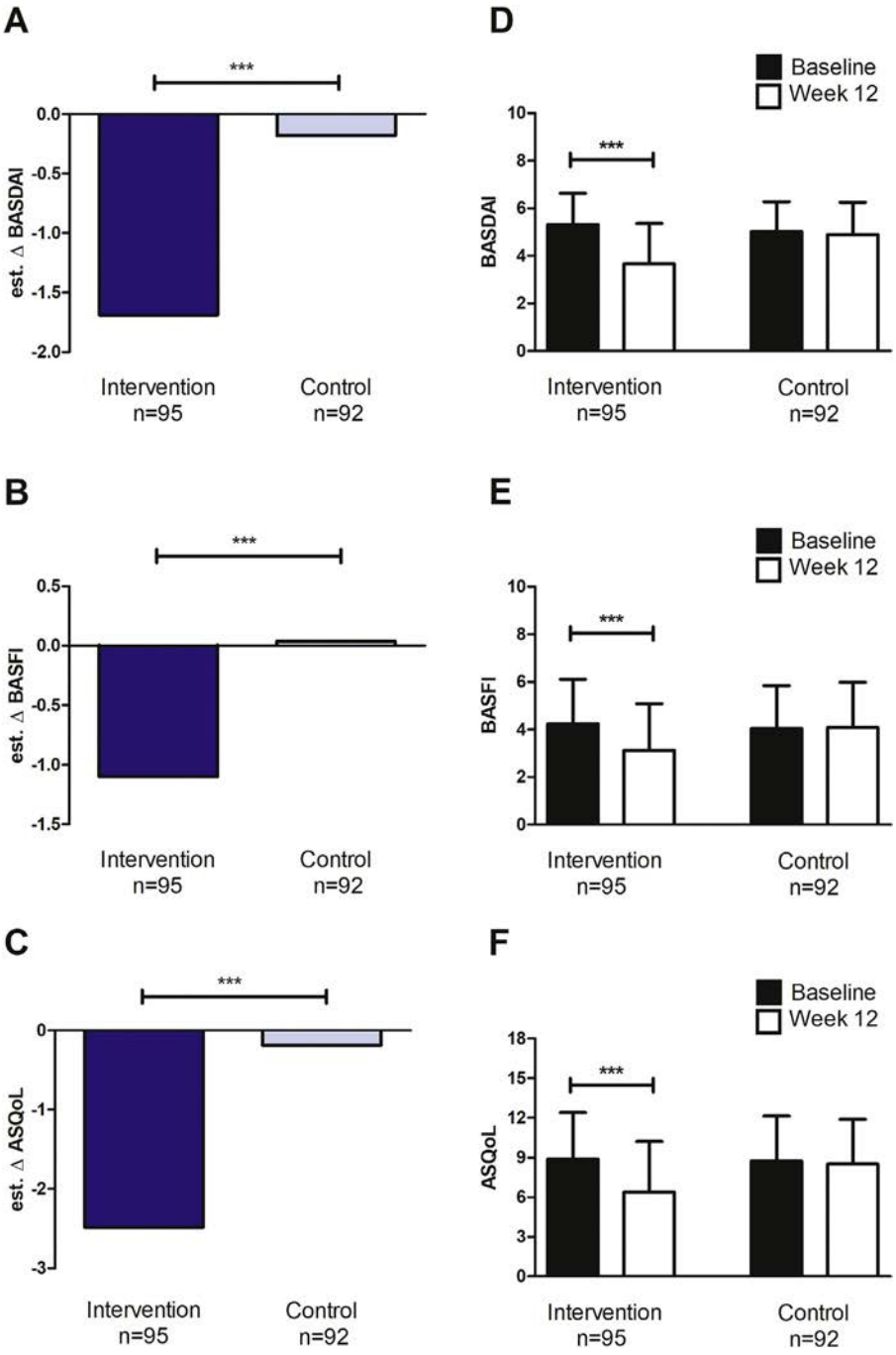

Figure 3. Results of the primary outcomes in the intention-to-treat population. (A-C) ANCOVA analyses, adjusted for baseline values and sex, confirmed significantly greater improvements for BASDAI (A), BASFI (B), and ASQoL (C) in the intervention group than in the control group. (D-F) The app intervention significantly improved mean BASDAI (D), BASFI (E), and ASQoL (F) compared to baseline, whereas no significant changes were observed in the control group. ***: $P < .001$. ANCOVA, analysis of covariance; ASQoL, Ankylosing Spondylitis Quality of Life Questionnaire; BASDAI, Bath Ankylosing Spondylitis Disease Activity Index; BASFI, Bath Ankylosing Spondylitis Functional Index; est., estimated.

Table 2
Association of HbE with the primary endpoints

Outcome	Delta HbE (min/wk)	n	Delta mean	SD	*P* value	Cohen's d
BASDAI	≥60	52	−1.94	1.47	.031	0.45
	<60	43	−1.32	1.27		
BASFI	≥60	52	−1.49	1.47	.004	0.60
	<60	43	−0.68	1.19		
ASQoL	≥60	52	−3.12	2.66	.008	0.55
	<60	43	−1.77	2.21		

ASQoL, Ankylosing Spondylitis Quality of Life; BASDAI, Bath Ankylosing Spondylitis Disease Activity Index; BASFI, Bath Ankylosing Spondylitis Functional Index; HbE, home-based exercise.

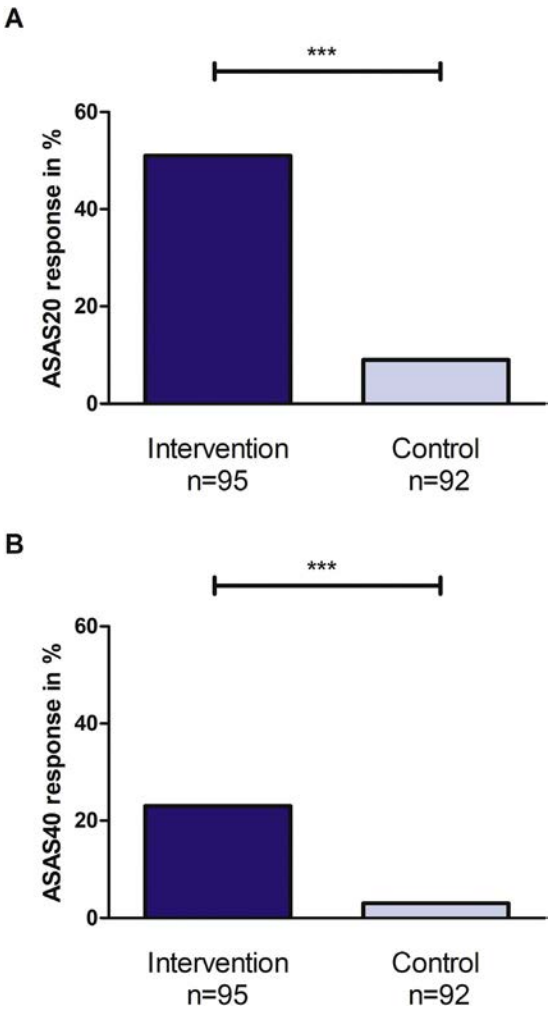

Figure 4. Higher ASAS20 and ASAS40 response rates in the Axia group after 12 weeks. The proportion of participants achieving ASAS20 (A) and ASAS40 responses (B) was significantly higher in the intervention group. ***: $P < .001$. ASAS, Assessment of Spondyloarthritis International Society.

Bechterew-App Trial met all 3 coprimary endpoints, demonstrating that *Axia* may serve as a new, scalable, nonpharmacological treatment modality for axSpA. To our knowledge, for a digital intervention, this is the first large-scale and methodologically rigorous RCT to show that an app-based intervention can significantly reduce disease activity in an iRMD.

The efficacy observed with *Axia* represents a marked advance over previous digital health studies in rheumatology. The positive effects of nonpharmacological therapies for axSpA are well-established, mostly from interventions delivered in traditional formats such as printed manuals or booklets [2,17,18]. In recent years, several app-based interventions have been explored [19,20]. However, these studies have often suffered from methodological limitations, including small sample sizes, non-disease-specific applications, or insufficient control designs. Crucially, none of these medical apps achieved significant or clinically relevant improvements in key outcomes such as disease activity, functional status, or quality of life [19,20]. In contrast, the Bechterew-App Trial provided high-quality evidence that an axSpA-specific medical app can achieve such outcomes.

The magnitude of the treatment effects observed in this trial is clinically noteworthy. The ASAS20 and ASAS40 response criteria are commonly used as primary or secondary endpoints in pharmacological trials for axSpA [21–24]. Historically, exercise interventions have shown only modest effects on disease activity [25], and consequently, robust comparable data on their impact on ASAS20 or ASAS40 responses are lacking. In this trial, the IG achieved ASAS20 and ASAS40 response rates of 51% and 23%, respectively, compared with 9% and 3% in the CG. For context, trials with tumour necrosis factor inhibitors (TNFi) typically report ASAS20 response rates of around 65% and ASAS40 rates between 39% and 48% [26]. A meta-analysis by Betts et al [27] found ASAS20 responses ranging from 50.5% to 71.7% for TNFi and interleukin-17 inhibitors, with placebo groups achieving around 27.9% for ASAS20 and 13.5% for ASAS40. While these figures offer a useful benchmark, differences in study design, blinding, and patient selection inevitably preclude direct head-to-head comparison and caution against interpreting the present results as evidence of equal or comparable efficacy to pharmacological treatments. Nevertheless, the magnitude of the ASAS20 and ASAS40 responses underscores the high therapeutic potential of Axia, and—more broadly—of app-based approaches in iRMDs.

The pronounced efficacy of Axia may be attributable to its low-threshold, location-independent accessibility as well as its multimodal, gamified design, which integrates physical activity, patient education, and behavioural support within a single digital platform. In addition, unlike generic exercise applications, Axia was developed exclusively for axSpA, integrating targeted exercise therapy tailored to the pathophysiology and movement limitations of this condition [14].

Another factor that may explain its superior effectiveness compared with conventional HbE approaches is the holistic physical activity concept deployed in this trial. *Axia* provides patients with a variety of options to increase physical activity, including patient-tailored axSpA-specific HbE of varying durations, cardiovascular-focused training sessions, and targeted HbE modules for acute pain and morning stiffness [14]. Furthermore, it directly promotes participation of sports alongside general activity enhancement through features such as daily step goals, a built-in step counter, and smartwatch integration [14]. Additionally, *Axia* especially encourages the integration of brief, highly accessible exercise habits into daily routines, such as linking 1 or 2 short exercises with a daily routine like getting out of bed or brewing coffee [14]. This contrasts with many other digital exercise interventions that focus primarily on longer, fixed sessions (eg, 20 minutes in the evening) [19,20]. Combining a wide range of exercise options and encouraging short, distributed bouts of activity embedded into everyday life may therefore represent a promising approach for exercise-based medical apps in iRMDs and other chronic diseases.

Sustaining long-term adherence is a recognised challenge in both exercise interventions and digital interventions, with low engagement and high attrition frequently cited as key barriers to efficacy [28,29]. As personal communication is known to enhance adherence to smartphone applications and interventions by motivating the user [29], the Bechterew-App Trial was deliberately designed to simulate real-world conditions by avoiding such interactions and to minimise potential adherence bias. After enrolment, interaction was limited to baseline allocation and postassessment follow-up, with no motivational prompts. Accordingly, no proactive contact was initiated with study participants during this period, and only channels for participant inquiries were made available. With a total of 77.9% of participants using the app on at least 5 days a week over a 12-week period, Axia still achieved adherence and usage rates far exceeding those reported in other axSpA trials with digital

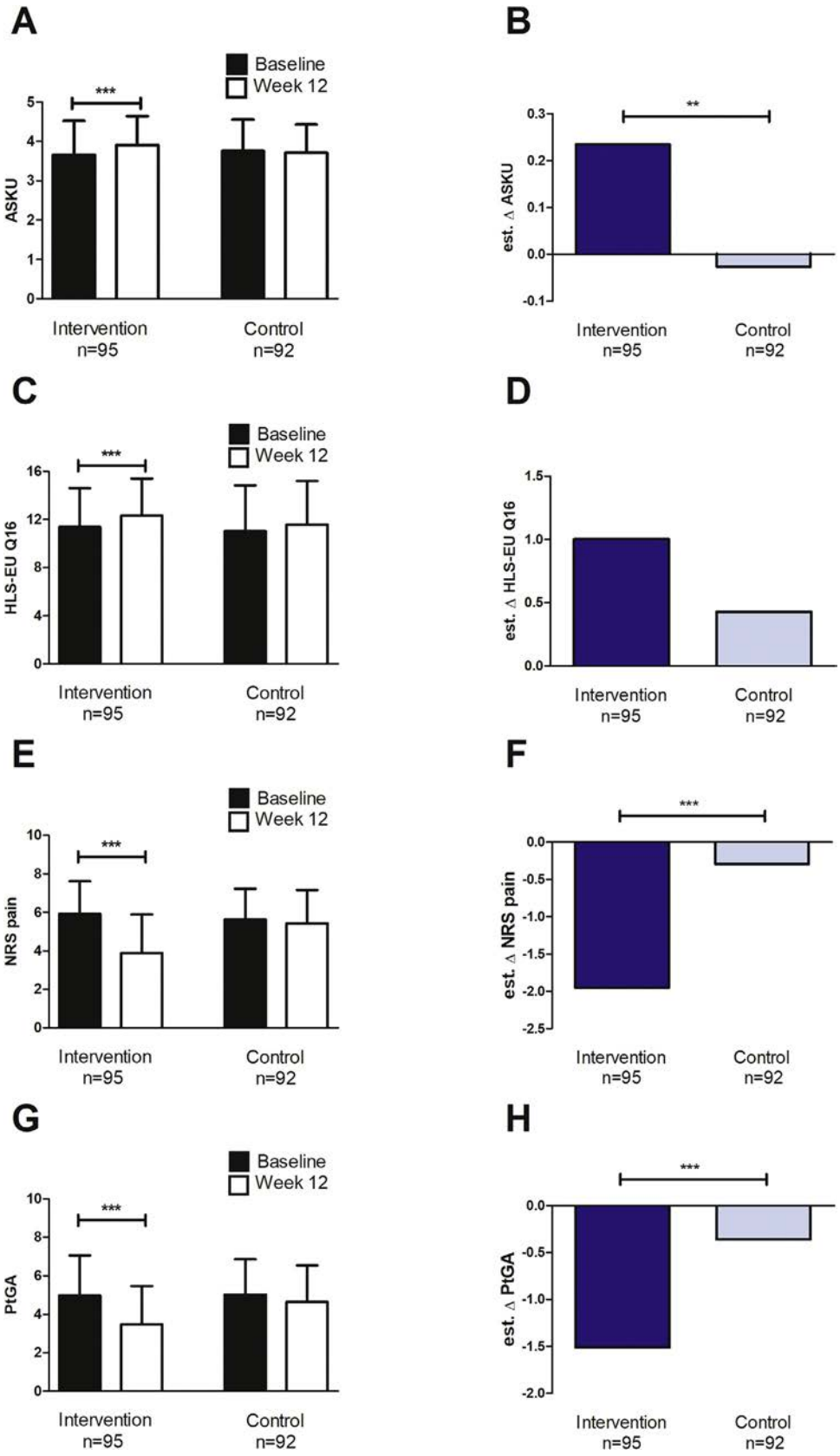

Figure 5. Results of further secondary outcomes in the intention-to-treat population. (A, C, E, G) The app intervention significantly improved the means of self-efficacy (ASKU), health literacy (HLS-EU Q16), pain (NRS pain), and patient global assessment (NRS PtGA) compared to baseline while no changes were observed in the control group. (B, D, F, H) ANCOVA analyses, adjusted for baseline values and sex, confirmed significantly greater improvements for ASKU, NRS pain, and NRS PtGA in the intervention group than in the control group. Differences in HLS-EU Q16 between intervention and control group were not significant in ANCOVA analysis. **: $P < .01$, ***: $P < .001$. ANCOVA, analysis of covariance; ASKU, Allgemeine Selbstwirksamkeit Kurzskala (German language questionnaire for self-efficacy); est., estimated; HLS-EU Q16, 16-Item European Health Literacy Survey Questionnaire; NRS, numeric rating scale; PtGA, patient global assessment.

Table 3
Safety during the 12-week treatment period

Adverse events	Control group (n = 92)	Intervention group (n = 95)	Total (n = 187)
Any adverse event n (%)	34 (37%)	21 (22%)	55 (29%)
Flare	7 (8%)	9 (9%)	16 (9%)
Uveitis	0 (0%)	1 (1%)	1 (1%)
Other MSK symptoms (not axSpA-related)	14 (15%)	6 (6%)	20 (11%)
Mild infectious disease	2 (2%)	2 (2%)	4 (2%)
Other	8 (9%)	2 (2%)	10 (5%)
Severe adverse events n (%)	3 (3%)	1 (1%)	4 (2%)
Death	0 (0%)	0 (0%)	0 (0%)
Seizure	0 (0%)	1 (1%)	1 (1%)
Prostate carcinoma	1 (1%)	0 (0%)	1 (1%)
Severe infection	1 (1%)	0 (0%)	1 (1%)
Hip replacement	1 (1%)	0 (0%)	1 (1%)
Device-related adverse events	n/a	0 (0%)	0 (0%)

axSpA, axial spondyloarthritis; MSK, musculoskeletal; n/a, not applicable.

interventions in real-world settings [28,29]. Gamification features—such as daily activity streaks, milestone tracking, and point rewards—may have contributed to sustained engagement and the observed treatment effects. Moreover, the possibility of perceiving early improvements in pain and mobility could have created a reinforcing feedback loop that further encouraged continued use. However, it remains uncertain whether such high adherence rates observed under trial conditions can be maintained in routine clinical practice, where external accountability and structured follow-up are often absent. Further pragmatic and longitudinal studies are needed to determine whether the observed engagement and clinical benefits are sustainable. Long-term follow-up studies of the Bechterew-App Trial are currently underway to address these questions.

The findings of this trial also have relevance beyond axSpA. In Germany, *Axia* has been submitted for approval as a reimbursable digital health application (DiGA) under the national fast-track pathway for prescription medical apps. If approved, *Axia* could be made available to all eligible patients nationwide, providing a scalable, low-barrier treatment option that complements existing pharmacological and nonpharmacological therapies [30]. Planned translations into additional languages and implementation in other European countries, as well as the United States, may also enable broader access to structured, evidence-based exercise therapy for axSpA in health systems where such programmes are limited or inconsistently provided. The underlying therapeutic approach—disease-specific, adaptive exercise combined with patient education, behavioural support, and gamification elements—represents a framework that could be adapted for other iRMDs in which exercise and self-management are integral to care, but long-term adherence is suboptimal.

Regarding safety, no concerning safety signals were observed, especially no device-related AEs.

The main limitation of this study is the absence of a double-blinded design and a placebo group. This is a common challenge in RCTs involving digital or app-based interventions, as participants can often easily unblind themselves by reviewing the internet on the content and function of the verum app.

Blinding of the study personnel was also not implemented; however, as per protocol, no direct contact occurred after group allocation, and all questionnaires were self-reported and completed by participants at home via eCRFs, minimising the potential for investigator-induced bias. A further limitation is the exclusive reliance on PROMs without objective clinical or biomarker-based endpoints. Due to the remote design, we did not screen for objective inflammatory markers (ie CRP) and relied solely on BASDAI to assess disease activity. Participant expectations might therefore have influenced the outcome of the PROMs, which are particularly prone to expectation and reporting bias. These effects are non-negligible, especially for subjective measures such as pain and PtGA. Although contact with investigators was minimised to reduce these biases, future studies must incorporate objective or clinician-assessed endpoints to validate the observed effects.

Chronic pain syndromes, including fibromyalgia, are frequent comorbidities of axSpA, which, however, were not systematically documented due to the remote nature of our trial and the structure of the screening assessment [31]. Therefore, we cannot report their exact prevalence in our cohort. This represents a relevant limitation, particularly because PROM-based endpoints cannot fully distinguish between improvements in inflammatory vs noninflammatory pain mechanisms, and app-based interventions have been shown to effectively improve chronic pain syndromes as well [32].

Our trial deliberately evaluated Axia as a whole under real-world conditions for digital health application (DHA/German "DiGA") approval. Accordingly, no firm conclusions can be drawn as to which specific components or usage patterns drove the effect, nor whether the observed benefits reflect changes in inflammatory activity or noninflammatory mechanisms. To conclusively address this relevant question, further studies with more differentiated designs are required.

In a small number of cases (5 participants in the IG and 8 participants in the CG), baseline data had to be deleted in accordance with data protection regulations, as consent to participate in the study was withdrawn. While this is a limitation, all withdrawals occurred prior to the 12-week assessment, and the small number of cases reduces the likelihood of systematic bias.

Key strengths of this trial include the large sample size for an RCT with a digital intervention and the high proportion of complete datasets, both of which enhance statistical power and minimise attrition bias. Moreover, the demographic and treatment characteristics of the study population—including the frequency of bDMARD and nonsteroidal anti-inflammatory drugs use, physiotherapy treatment, and levels of HbE and other sports activities—were closely aligned with those reported in recent national real-world observational studies [33,34], supporting representativeness. The higher mean BASDAI in our trial (5.17 vs 3.9 in the ATTENTUS study [33]) reflects the inclusion

criterion of BASDAI ≥3.5, which was applied to reduce heterogeneity and ensured that treatment effects were evaluated in patients with at least moderate disease activity. On the other hand, preselection of a study population with either low or moderate physical activity and a BASDAI ≥3.5, reflects a selection bias. This was intentional, as our aim was to detect a clear effect on BASDAI due to the app-driven increase in exercise therapy. Women were overrepresented, likely reflecting the higher uptake of DiGA among women, who account for approximately 73% of DHA users according to national health insurance data [35]. The lack of differentiation between difficult-to-manage and treatment-naïve patients with axSpA introduced clinical heterogeneity and may have influenced the outcomes, particularly if a substantial proportion had difficult-to-treat disease. Conversely, the low-threshold remote design enabled nationwide inclusion without on-site visits, resulting in a representative real-world axSpA cohort rather than a highly selected, homogeneous study population.

In conclusion, the Bechterew-App Trial provides the first methodologically rigorous evidence that a disease-specific, app-based multimodal intervention can achieve significant and clinically meaningful improvements in patient-reported disease activity, functional status, and quality of life in patients with axSpA receiving stable pharmacotherapy. These findings support the potential of mobile healthcare apps to complement existing pharmacological and nonpharmacological treatments and help close the gap between guideline-based exercise recommendations and their limited implementation in routine care. This is in line with the European Alliance of Associations for Rheumatology (EULAR) recommendations for remote care and mobile health applications [9,36], While the absence of blinding, reliance on PROMs, and the short intervention period warrant cautious interpretation, the magnitude of the observed effects and high adherence rates under real-world-like conditions justify further pragmatic and long-term evaluations. The *Axia* approach could also serve as a model for other iRMDs, where structured exercise and self-management are central to care but long-term adherence remains a challenge.

Acknowledgements

The abstract of this study was presented as oral presentation at the EULAR congress 2025 in Barcelona (LB0002). We would like to thank all the patients who participated in the trial. Furthermore, we also would like to thank the German patient self-help association (Deutsche Vereinigung Morbus Bechterew) for supporting us. We are also grateful to our statisticians Dr Victoria Rücker and Dr Uwe Malzahn for performing the sample size calculation. Applimeda is the developer and rights holder of Axia. MlM, TH, and RL are shareholders, partners, or employees of Applimeda. All other authors are not financially dependent on Applimeda.

Contributors

P-PS, MF, and MS contributed to conceptualisation and drafted the original manuscript. P-PS contributed to data curation. P-PS, MF, and MS performed the formal analysis and contributed to methodology together with AF, KSL, HL, AS, and BS. Investigation was carried out by P-PS, MF, MS, and PP. P-PS, MF, TH, MlM, AF, KSL, PP, MG, HL, OG, RL, AS, LH, BS, HE, and MS contributed to writing—review and editing. All authors reviewed and approved the final manuscript. P-PS and MS are the guarantors and attest that all authors meet the authorship criteria.

Funding

This research did not receive any specific grant from funding agencies in the public, commercial, or not-for-profit sectors. Axia was made available to participants free of charge for the study period. The corresponding author had full access to all of the data and had final responsibility for the decision to submit the manuscript for publication.

Competing interests

P-PS received speaker's fees and travel grants from Janssen-Cilag, UCB and AbbVie (less than US$10,000 each) as well as research funding from Chugai (US$25,000), Novartis (US $150,000) and AbbVie (US$ 12,000). MlM. reported to be Chief Executive Officer of Applimeda, Co-Founder and shareholder of Applimeda GmbH. TH reported to be Chief Regulatory & Medical Officer of Applimeda, Co-Founder and shareholder of Applimeda GmbH. HL received travel grants from UCB, Boehringer Ingelheim, Pfizer and AbbVie as well as compensation for consulting activity from Pfizer and for lecturing activities from Janssen. AF, KSL, PP, OG, HE, and AS declared no conflict of interest. MG received travel grants, compensation for advisory boards or speaker's fees from AbbVie, Chugai, Eli Lilly, Hexal, Janssen, Novartis, Pfizer and Takeda and research funding from Novartis (US$150,000). RL declared to be Chief Technology Officer of Applimeda, Co-Founder and shareholder of Applimeda GmbH. LH declared to be Former Chief Executive Officer of Deutsche Vereinigung Morbus Bechterew (DVMB). BS declared no conflict of interest. MF received speaker's fees, travel grants or compensation for board memberships from AbbVie, Novartis, Janssen and Eli Lilly. MS received speaker's fees, travel grants, research funding or compensation for consultancies or board memberships from AbbVie, Actelion, AstraZeneca, BMS, Boehringer/Ingelheim, Celgene, Chugai/Roche, Eli Lilly, Genzyme, Gilead, Hexal/Sandoz, Janssen-Cilag, MSD, Novartis, Pfizer, Sanofi Pasteur, Takeda (Shire) and UCB (less than US$10,000 each) and research funding from Novartis (US$150,000).

Patient consent for publication

Not applicable.

Ethics approval

The study was conducted in accordance with the Declaration of Helsinki and Good Clinical Practice guidelines. The study was approved by the ethics committee of the medical faculty of the University of Wuerzburg, Wuerzburg (DE/EKBY13) (Date July 31, 2023, No 92/23-am). The trial was prospectively registered at the German Clinical Trials Register (DRKS), DRKS-ID: DRKS00033783), date of first registry March 1st March 2024. All participants provided written informed consent before enrolment.

Provenance and peer review

Not commissioned; externally peer reviewed.

Data availability statement

The data underlying the results of this clinical trial are included in the article and its supplementary materials. To protect participant confidentiality and proprietary content, deidentified individual-level data are available upon reasonable request and subject to restricted access. Requests should be directed to the corresponding author P.-P. Strunz and must include a brief research proposal specifying the intended use.

Supplementary materials

Supplementary material associated with this article can be found in the online version at doi:10.1016/j.ard.2026.02.016.

Orcid

Patrick-Pascal Strunz: http://orcid.org/0000-0002-3168-7074

REFERENCES

[1] Sieper J, Braun J, Dougados M, Baeten D. Axial spondyloarthritis. Nat Rev Dis Primers 2015 Jul;1:15013. doi: 10.1038/nrdp.2015.13.

[2] Aytekin E, Caglar NS, Ozgonenel L, Tutun S, Demiryontar DY, Demir SE. Home-based exercise therapy in patients with ankylosing spondylitis: effects on pain, mobility, disease activity, quality of life, and respiratory functions. Clin Rheumatol 2012 Jan;31(1):91–7. doi: 10.1007/s10067-011-1791-5.

[3] Ortolan A, Webers C, Sepriano A, Falzon L, Baraliakos X, Landewé RB, et al. Efficacy and safety of non-pharmacological and non-biological interventions: a systematic literature review informing the 2022 update of the ASAS/EULAR recommendations for the management of axial spondyloarthritis. Ann Rheum Dis 2023 Jan;82(1):142–52. doi: 10.1136/ard-2022-223297.

[4] Ramiro S, Nikiphorou E, Sepriano A, Ortolan A, Webers C, Baraliakos X, et al. ASAS-EULAR recommendations for the management of axial spondyloarthritis: 2022 update. Ann Rheum Dis 2023 Jan;82(1):19–34. doi: 10.1136/ard-2022-223296.

[5] Kiltz U, Braun DGRh J, Becker DEGAM A, Chenot JF, et al. Langfassung zur S3-Leitlinie Axiale Spondyloarthritis inklusive Morbus Bechterew und Frühformen, Update 2019 : Evidenzbasierte Leitlinie der Deutschen Gesellschaft für Rheumatologie (DGRh) und der beteiligten medizinisch-wissenschaftlichen Fachgesellschaften und weiterer Organisationen [Long version on the S3 guidelines for axial spondyloarthritis including Bechterew's disease and early forms, update 2019: evidence-based guidelines of the German Society for Rheumatology (DGRh) and participating medical scientific specialist societies and other organizations]. Z Rheumatol 2019 Dec;78(Suppl 1):3–64 German. doi: 10.1007/s00393-019-0670-3.

[6] Ward MM, Deodhar A, Gensler LS, Dubreuil M, Yu D, Khan MA, et al. 2019 Update of the American College of Rheumatology/Spondylitis Association of America/Spondyloarthritis Research and Treatment Network Recommendations for the treatment of ankylosing spondylitis and nonradiographic axial spondyloarthritis. Arthritis Rheumatol 2019 Oct;71(10):1599–613. doi: 10.1002/art.41042.

[7] Strunz PP, Maire ML, Heusinger T, Hammel L, Gernert M, Schwaneck EC, et al. Apps in der rheumatologie: bedarf es einer app in der therapie der axialen spondyloarthritis? [Apps in rheumatology: is there a need for an app in therapy for axial spondyloarthritis?]. Z Rheumatol. 2023 Apr;82(3):256-61. German. doi:10.1007/s00393-021-01104-1 [Erratum: Z Rheumatol. 2021 Dec;80(Suppl 2):76. doi:10.1007/s00393-021-01121-0]

[8] Carbo M, Hilberdink B, Paap D, Wink F, Vlieland TV, van Weely S, et al. Physical activity in relation to health status, quality of life and compliance with World Health Organization recommendations in patients with axial spondyloarthritis. Arthritis Res Ther 2025;27:112. doi: 10.1186/s13075-025-03575-y.

[9] Najm A, Nikiphorou E, Kostine M, Richez C, Pauling JD, Finckh A, et al. EULAR points to consider for the development, evaluation and implementation of mobile health applications aiding self-management in people living with rheumatic and musculoskeletal diseases. RMD Open 2019 Sep;5(2):e001014. doi: 10.1136/rmdopen-2019-001014.

[10] Knitza J, Gupta L, Hügle T. Rheumatology in the digital health era: status quo and quo vadis? Nat Rev Rheumatol 2024;20:747–59. doi: 10.1038/s41584-024-01177-7.

[11] Lee AZY, Woon TH, Wang CTM, Kwan YH, Fong W. Facilitators and barriers to physical activity for patients with rheumatoid arthritis and axial spondyloarthritis. Int J Rheum Dis 2025 Feb;28(2):e70109. doi: 10.1111/1756-185X.70109.

[12] Iken A, Gademan MGJ, Nutma A, Poolman RW, Vliet Vlieland TPM, van Bodegom-Vos L. OP0358-PARE Barriers and facilitators for implementing long-standing, personalized exercise therapy in people with rheumatoid arthritis or axial spondyloarthritis and severe functional limitations. Ann Rheum Dis 2025;84(Suppl 1):291. doi: 10.1016/j.ard.2025.05.360.

[13] Strunz PP, Kiltz U, Kiefer D, Schmalzing M. Digitale Gesundheitsanwendungen und axiale Spondyloarthritis [Digital health applications and axial spondyloarthritis]. Z Rheumatol 2025 Dec;84(10):805–10 German. doi: 10.1007/s00393-025-01731-y.

[14] Strunz PP, Le Maire M, Heusinger T, Klein J, Labinsky H, Fleischer A, et al. The exercise-app Axia for axial spondyloarthritis enhances the home-based exercise frequency in axial spondyloarthritis patients - a cross-sectional survey. Rheumatol Int 2024 Jun;44(6):1143–54. doi: 10.1007/s00296-024-05600-w.

[15] Pavy S, Brophy S, Calin A. Establishment of the minimum clinically important difference for the Bath Ankylosing Spondylitis Indices: a prospective study. J Rheumatol 2005 Jan;32(1):80–5.

[16] Haywood KL, M Garratt A, Jordan K, Dziedzic K, Dawes PT. Disease-specific, patient-assessed measures of health outcome in ankylosing spondylitis: reliability, validity and responsiveness. Rheumatology (Oxford) 2002 Nov;41(11):1295–302. doi: 10.1093/rheumatology/41.11.1295.

[17] Durmus D, Alayli G, Cil E, Canturk F. Effects of a home-based exercise program on quality of life, fatigue, and depression in patients with ankylosing spondylitis. Rheumatol Int 2009 Apr;29(6):673–7. doi: 10.1007/s00296-008-0756-8.

[18] Kasapoglu Aksoy M, Birtane M, Taştekin N, Ekuklu G. The effectiveness of structured group education on ankylosing spondylitis patients. J Clin Rheumatol 2017 Apr;23(3):138–43. doi: 10.1097/RHU.0000000000000499.

[19] Song Y, Reifsnider E, Chen Y, Wang Y, Chen H. The impact of a theory-based mHealth intervention on disease knowledge, self-efficacy, and exercise adherence among ankylosing spondylitis patients: randomized controlled trial. J Med Internet Res 2022 Oct 20;24(10):e38501. doi: 10.2196/38501.

[20] Blaskowitz PPVA, Liphardt AM, Bouzas C, Coppers B, Petit P, Vuillerme N, et al. Impact of the digital health application ViViRA on spinal mobility, physical function, quality of life and pain perception in spondyloarthritides patients: a randomized controlled trial. Arthritis Res Ther 2024 Dec 3;26(1):208. doi: 10.1186/s13075-024-03443-1.

[21] Sieper J, Rudwaleit M, Baraliakos X, Brandt J, Braun J, Burgos-Vargas R, et al. The Assessment of SpondyloArthritis international Society (ASAS) handbook: a guide to assess spondyloarthritis. Ann Rheum Dis 2009 Jun;68(Suppl 2):ii1–44. doi: 10.1136/ard.2008.104018.

[22] van der Heijde D, Song IH, Pangan AL, Deodhar A, van den Bosch F, Maksymowych WP, et al. Efficacy and safety of upadacitinib in patients with active ankylosing spondylitis (SELECT-AXIS 1): a multicentre, randomised, double-blind, placebo-controlled, phase 2/3 trial. Lancet 2019 Dec 7;394(10214):2108–17. doi: 10.1016/S0140-6736(19)32534-6.

[23] van der Heijde D, Schiff MH, Sieper J, Kivitz AJ, Wong RL, Kupper H, et al. Adalimumab effectiveness for the treatment of ankylosing spondylitis is maintained for up to 2 years: long-term results from the ATLAS trial. Ann Rheum Dis 2009 Jun;68(6):922–9. doi: 10.1136/ard.2007.087270.

[24] Deodhar A, Supronik J, Kivitz A, Valenzuela G, Kapur K, Rohrer S, et al. Efficacy and safety of intravenous secukinumab in patients with active axial spondyloarthritis: results from a randomized, placebo-controlled, phase 3 study. Arthritis Rheumatol 2025 Feb;77(2):163–70. doi: 10.1002/art.42993.

[25] Martins NA, Furtado GE, Campos MJ, Leitão JC, Filaire E, Ferreira JP. Exercise and ankylosing spondylitis with New York modified criteria: a systematic review of controlled trials with meta-analysis. Acta Reumatol Port 2014 Oct-Dec;39(4):298–308.

[26] Kiltz U, Tsiami S, Kiefer D, Baraliakos X, Bühring B, Braun J. Assessments und outcome-parameter bei axialer Spondyloarthritis. Akt Rheumatol 2019;44(05):332–8. doi: 10.1055/a-0982-3633.

[27] Betts KA, Griffith J, Song Y, Mittal M, Joshi A, Wu EQ, et al. Network meta-analysis and cost per responder of tumor necrosis factor-α and interleukin inhibitors in the treatment of active ankylosing spondylitis. Rheumatol Ther 2016 Dec;3(2):323–36. doi: 10.1007/s40744-016-0038-y.

[28] Labinsky H, Gupta L, Raimondo MG, Schett G, Knitza J. Real-world usage of digital health applications (DiGA) in rheumatology: results from a German patient survey. Rheumatol Int 2023 Apr;43(4):713–9. doi: 10.1007/s00296-022-05261-7.

[29] Druce KL, Dixon WG, McBeth J. Maximizing engagement in mobile health studies: lessons learned and future directions. Rheum Dis Clin North Am 2019 May;45(2):159–72. doi: 10.1016/j.rdc.2019.01.004.

[30] Dittrich F, Mielitz A, Pustozerov E, Lawin D, von Jan U, Albrecht UV. Digital health applications from a government-regulated directory of reimbursable health apps in Germany-a systematic review for evidence and bias. Mhealth 2023 Jul 24;9:35. doi: 10.21037/mhealth-23-17.

[31] Jones GT, Mallawaarachchi B, Shim J, Lock J, Macfarlane GJ. The prevalence of fibromyalgia in axial spondyloarthritis. Rheumatol Int 2020 Oct;40 (10):1581–91. doi: 10.1007/s00296-020-04621-5.

[32] Gendreau RM, McCracken LM, Williams DA, Luciano JV, Dai Y, Vega N, et al. Self-guided digital behavioural therapy versus active control for fibromyalgia (PROSPER-FM): a phase 3, multicentre, randomised controlled trial. Lancet 2024 Jul 27;404(10450):364–74. doi: 10.1016/S0140-6736(24)00909-7.

[33] Meyer-Olson D, Hoeper K, Hammel L, Lieb S, Haehle A, Kiltz U. Nichtmedikamentöse Therapiemaßnahmen, Rehabilitationsleistungen und Mitgliedschaft in Selbsthilfeorganisationen bei axialer Spondyloarthritis (Die ATTENTUS axSpA-Studie) [Nonpharmacological treatment measures, rehabilitation services and membership in patient support groups in axial spondylarthritis (The ATTENTUS axSpA study)]. Z Rheumatol 2024 Aug;83 (6):500–9 German. doi: 10.1007/s00393-023-01410-w.

[34] Albrecht K, Thiele K, Alexander T, Aringer M, Eidner T, Henes J, et al. Aktuelle Zahlen zur rheumatologischen Versorgung – Jahresbericht aus der Kerndokumentation der regionalen kooperativen Rheumazentren [Current data on rheumatological care: annual report from the National database (NDB) of the regional collaborative arthritis centres in Germany]. Z Rheumatol 2024 Oct;83(8):666–74 German. doi: 10.1007/s00393-024-01497-9.

[35] GKV-Spitzenverband. DiGA-Bericht 2024. Berlin: GKV-Spitzenverband; 2025. Available from: https://www.gkv-spitzenverband.de/media/dokumente/krankenversicherung_1/telematik/digitales/2024_DiGA-Bericht_final.pdf. Accessed 14 July 14, 2025.

[36] de Thurah A, Bosch P, Marques A, Meissner Y, Mukhtyar CB, Knitza J, et al. 2022 EULAR points to consider for remote care in rheumatic and musculoskeletal diseases. Ann Rheum Dis 2022 Aug;81(8):1065–71. doi: 10.1136/annrheumdis-2022-222341.

Ann Rheum Dis 85 (2026) 1556–1569

Contents lists available at ScienceDirect

Annals of the Rheumatic Diseases

journal homepage: https://www.sciencedirect.com/journal/annals-of-the-rheumatic-diseases

Axial spondyloarthritis

Transmembrane TNF-α signalling of macrophages drives pathological osteogenesis in radiographic axial spondyloarthritis

Pengfei Ji[1,2,3,†,‡], Peitao Xu[1,2,†,‡], Jianan Jiang[1,2,3,†,‡], Mingxi Cai[1,2,3,†], Zihao Yuan[1,2,†], Qian Cao[2,4,†], Zhidong Liu[1,2,3,†], Wenjie Liu[1,2,†], Zhongyu Xie[1,2,4,†,**], Peng Wang[1,2,†,*]

[1] *Department of Orthopedics, The Eighth Affiliated Hospital of Sun Yat-Sen University, Shenzhen, PR China*
[2] *Guangdong Provincial Clinical Research Center for Orthopedic Diseases, The Eighth Affiliated Hospital, Sun Yat-sen University, Shenzhen, PR China*
[3] *Biological Laboratory of Hetao Cooperation Zone, the Eighth Affiliated Hospital of Sun Yat-sen University, Shenzhen, PR China*
[4] *Center for Biotherapy, The Eighth Affiliated Hospital of Sun Yat-Sen University, Shenzhen, PR China*

A R T I C L E I N F O

Article history:
Received 12 January 2026
Received in revised form 18 March 2026
Accepted 21 March 2026

A B S T R A C T

Objectives: This study aimed to elucidate the molecular mechanism uncoupling inflammation from pathological osteogenesis in radiographic axial spondyloarthritis (r-axSpA), specifically investigating the role of transmembrane TNF (tmTNF) reverse signalling.

Methods: We established a tmTNF-overexpressing transgenic mouse model that spontaneously recapitulates spinal ankylosis characteristic of r-axSpA. Single-cell RNA sequencing, genetic knockout (TNFR1/2), and macrophage depletion strategies were employed to identify cellular effectors. A mannose-modified nanoparticle system delivering Ikbkb siRNA was developed to assess targeted therapeutic intervention.

Results: Macrophages were identified as the core drivers of osteogenesis, promoting bone formation via TGF-β3 (transforming growth factor beta 3) and BMP2 (bone morphogenetic protein 2) upregulation. Mechanistically, we discovered a novel reverse signalling axis wherein soluble TNFR1 binds to tmTNF, inducing the interaction of the tmTNF intracellular domain with the proteasome subunit alpha type-1 (PSMA1). This interaction activates the IKKβ/NF-κB (inhibitor of nuclear factor kappa B kinase subunit beta / nuclear factor kappa B) pathway to upregulate TGF-β3 and BMP2, instructing macrophages to drive mesenchymal stem cell ossification. Crucially, targeted silencing of Ikbkb in macrophages significantly inhibited new bone formation.

Conclusions: This study reveals a distinct sTNFR1-tmTNF-PSMA1-NF-κB reverse signalling axis that empowers macrophages to drive pathological osteogenesis in r-axSpA. Targeting this axis offers a precise therapeutic strategy to arrest structural damage beyond solely controlling systemic inflammation.

*Correspondence to Dr. Peng Wang, Dr. Wenjie Liu, Department of Orthopedics, The Eighth Affiliated Hospital of Sun Yat-Sen University, Shenzhen, P.R. China.
**Correspondence to Dr. Zhongyu Xie, Center for Biotherapy, The Eighth Affiliated Hospital of Sun Yat-Sen University, Shenzhen, P.R. China.
E-mail addresses: liuwj76@mail.sysu.edu.cn (W. Liu), xiezhy23@mail.sysu.edu.cn (Z. Xie), wangp57@mail.sysu.edu.cn (P. Wang).
Handling editor Josef Smolen.
† Present address: 3025# Shennan Road, Shenzhen, 518033, PR China.
‡ Pengfei Ji, Peitao Xu, and Jianan Jiang contributed equally to this work.

https://doi.org/10.1016/j.ard.2026.03.023

WHAT IS ALREADY KNOWN ON THIS TOPIC

- Pathological bone formation in radiographic axial spondyloarthritis often progresses even when systemic inflammation is controlled by biologic therapies.
- The molecular mechanisms driving this structural damage—specifically the potential role of transmembrane TNF (tmTNF) reverse signalling—are poorly understood.

WHAT THIS STUDY ADDS

- We identified a novel 'reverse signalling' axis where tmTNF recruits proteasome subunit alpha type-1 (PSMA1) to activate NF-κB in macrophages, stimulating the secretion of osteogenic factors (TGF-β3/BMP2).
- Targeted silencing of this axis arrested bone formation in mice despite persistent inflammation, confirming that pathological ossification is a distinct downstream consequence of this pathway.

HOW THIS STUDY MIGHT AFFECT RESEARCH, PRACTICE OR POLICY

- These findings explain the clinical paradox of why bone progression dissociates from inflammatory activity.
- Targeting the tmTNF-PSMA1-NF-κB axis offers a precision strategy to halt the 'inflammation-osteogenesis transition' and prevent structural disability.

INTRODUCTION

Radiographic axial spondyloarthritis (r-axSpA), traditionally termed ankylosing spondylitis (AS), is a chronic autoimmune disorder characterised by the interplay of persistent inflammation and pathological new bone formation (syndesmophytes), leading to structural damage and functional loss [1,2]. In recent years, the clinical introduction of biological agents has marked a milestone breakthrough in the management of axial spondyloarthritis (axSpA). These therapies effectively inhibit articular inflammation and provide rapid relief from clinical symptoms such as back pain and morning stiffness; moreover, they retard radiographic progression to a certain extent. Multiple randomised controlled trials and long-term follow-up studies have confirmed that TNF inhibitors (TNFis) such as infliximab [3,4] and adalimumab [5,6], as well as IL-17 (interleukin 17)-targeting biologics such as secukinumab [7], can significantly reduce disease activity indices and inflammatory markers in patients. However, reliance solely on acute phase reactants such as C-reactive protein and erythrocyte sedimentation rate has limitations. As emphasised by the Assessment of SpondyloArthritis international Society guidelines [8], magnetic resonance imaging (MRI) is indispensable for determining disease activity, particularly by detecting bone marrow oedema—a critical predictor of future structural progression that can persist even when serologic markers are normalised [9,10]. This highlights a clinical paradox: radiographic progression often continues despite apparent clinical remission and normal inflammatory indices. This phenomenon suggests that the relationship between inflammation and ossification is far more intricate than previously understood. It implies that residual local inflammation detected by MRI, or specific local inflammatory mediators and immune microenvironments, may play a pivotal, direct role in driving the osteogenic programme [11,12]. Therefore, elucidating the specific cellular and molecular mechanisms by which inflammatory effectors trigger and sustain pathological ossification represents both a profound scientific challenge and an urgent, unmet clinical need.

As core effector cells of the innate immune system, macrophages serve as critical nodal points bridging chronic inflammation and aberrant bone repair in r-axSpA. Their infiltration at sites of pathology, such as entheses, correlates positively with radiographic progression [13,14]. Beyond driving inflammation, macrophages possess high plasticity, actively modulating the osteoblast/osteoclast balance and directly promoting ossification through the secretion of osteogenic factors [15–19]. It is well established that activation of bone morphogenetic protein (BMP) signalling is a requisite driver of ankylosis in murine models of SpA, as elegantly demonstrated by Lories et al. [20]. Furthermore, in the context of joint inflammation, proinflammatory cytokines such as TNF-α (tumor necrosis factor-α) have been shown to upregulate BMP2 (bone morphogenetic protein 2) expression in synovial fibroblasts via NF-κB signalling [21,22]. However, whether macrophages use similar mechanisms to trigger this osteogenic cascade remains to be elucidated.

TNF-α, primarily produced by macrophages, exists in soluble (sTNF) and transmembrane (tmTNF) forms. Crucially, unlike sTNF, tmTNF is disproportionately upregulated in axSpA tissues and acts as a unique membrane-anchored receptor capable of initiating 'reverse signalling' [23,24]. Clinical evidence indicates that high tmTNF expression is strongly associated with osteophyte formation [25], and tmTNF transgenic mice spontaneously develop spinal ankylosis characteristic of r-axSpA [26,27]. Given that macrophages are the primary carriers of tmTNF [28], we hypothesise that tmTNF reverse signalling may act as a specific molecular switch, activating NF-κB-dependent BMP pathways to reprogramme macrophages towards a pro-osteogenic phenotype. Despite these clues, the precise mechanisms by which this reverse signalling drives macrophage-mediated pathological ossification remain largely unexplored.

This study aims to unveil a novel signalling axis through which tmTNF regulates macrophage function via reverse signalling to drive pathological ossification in AS, thereby identifying a precise therapeutic target for intervening in osteophyte progression that transcends mere anti-inflammatory effects. We will first establish a transgenic mouse model with stable tmTNF expression to simulate the pathological synergy of 'inflammation-ossification' characteristic of AS, providing an ideal *in vivo* platform for mechanistic inquiry. Subsequently, by integrating this model with multiomics technologies, we seek to systematically identify the critical receptor molecules and downstream core signalling pathways of tmTNF reverse signalling, clarifying the central role of macrophages within this axis and identifying the key pro-osteogenic factors they secrete. Ultimately, through *in vivo* and *in vitro* functional validation, we will evaluate the therapeutic potential of targeting the tmTNF reverse signalling-macrophage axis, exploring the feasibility of novel strategies designed to specifically arrest the process of heterotopic ossification.

METHODS

Experimental animals and model construction

Founder mice for the tmTNF-overexpressing transgenic strain, as well as Tnfrsf1a knockout (*tmTNF*$^{+/+}$) and Tnfrsf1b knockout (*TNFRII*$^{-/+}$) strains, were generated with the assistance of Cyagen Biosciences. Independent breeding colonies and

genotyping protocols were subsequently established in-house. Initially, these founder mice were backcrossed with wild-type (WT) C57BL/6 mice to purify the genetic background. After multiple generations, homozygous mice were identified via polymerase chain reaction genotyping. Based on these colonies, further intercrossing was performed to generate homozygous *tmTNF*$^{+/+}$ mice, as well as *tmTNF*$^{+/+}$×*TNFRI*$^{-/-}$ and *tmTNF*$^{+/+}$×*TNFRII*$^{-/-}$ double-mutant mice. All animals were housed in a specific pathogen-free facility at the Laboratory Animal Center of Sun Yat-sen University. Mice were maintained under controlled conditions with a constant temperature of 22 ± 2°C, humidity of 55% ± 5%, and a 12-hour light/dark cycle, with *ad libitum* access to standard rodent chow and water. All animal experimental procedures were approved by the Institutional Animal Care and Use Committee (IACUC) of Sun Yat-sen University (Approval no. SYSU-IACUC-2024-0033GEM).

The severity of arthritis was evaluated in a double-blind manner using a semiquantitative clinical scoring system. The scoring criteria were as follows: 0, normal; 1, mild erythema or swelling of a single digit; 2, erythema or swelling of multiple digits; 3, obvious erythema or swelling of the entire paw; 4, severe deformity or ankylosis.

To deplete macrophages *in vivo*, 4-week-old *tmTNF*$^{+/+}$ mice received intravenous injections of clodronate liposomes (Clodronate Liposomes, Liposoma BV) or equal volumes of control liposomes once weekly for 4 weeks. To target the NF-κB pathway in macrophages, 6-week-old *tmTNF*$^{+/+}$ mice were intravenously injected with mannose-modified mesoporous silica nanoparticles loaded with *Ikbkb* siRNA, while the control group received non-targeting nanoparticles. Treatments were administered once weekly for 4 weeks. Following the final treatment, peripheral blood and joint tissues were collected for subsequent analysis.

CatWalk gait analysis and grip strength assessment

Gait analysis was performed using the CatWalk XT automated system (Noldus Information Technology). As mice voluntarily traversed a glass walkway in a dark tunnel, illuminated footprints were captured by a high-speed camera and transmitted to a computer for analysis. Key parameters, including footprint heatmaps, paw pressure intensity, regularity index, and mean paw print area, were quantified. In addition, muscle strength was evaluated using forelimb and all-limb grip strength tests. Multiple measurements were recorded for each mouse, and the mean value was calculated for statistical analysis.

Animal μCT scanning and histologic analysis

Twelve-week-old *tmTNF*$^{+/+}$ transgenic mice and WT control mice (n = 6 per group) were euthanised by CO_2 asphyxiation. The skin was incised along the ventral midline, internal organs were removed, and the entire carcass was immersed in 4% formaldehyde fixative and fixed at 4°C for 1 week. After fixation, the whole-mouse specimens were fitted in a cylindrical sample holder and scanned using a Scanco μCT40 system (Scanco Medical AG). The scanning parameters were set at 55 kVp and 70 μA. The acquired tomographic data were reconstructed into 3-dimensional images using MicroCT Ray V3.0 software (Scanco Medical). Following μCT scanning, target skeletal tissues, including the ankle joint and caudal vertebrae, were dissected. Bone samples were decalcified in 0.5 M ethylenediaminetetraacetic acid solution (Sigma-Aldrich) at 4°C until complete softening. After decalcification, tissues were washed, dehydrated through a graded ethanol series, embedded in paraffin, and sectioned at 5 μm thickness. The sections were stained with haematoxylin and eosin (H&E) to assess general tissue morphology and cellular architecture, and with Safranin O-fast green to evaluate the distribution and content of cartilage matrix (stained red by Safranin O) and bone tissue (stained green by Fast Green).

Statistical analysis

Statistical analyses were performed using GraphPad Prism 8.0 software (GraphPad Software, Inc.). All data are presented as mean ± SD. The assumption of normality was verified using the Shapiro-Wilk test. For data following a normal distribution, differences between 2 experimental groups were analysed using unpaired 2-tailed Student's *t*-tests, while comparisons among multiple groups were assessed using 1-way analysis of variance followed by Bonferroni's *post hoc* test to correct for multiple comparisons and control the false discovery rate. Sample sizes (n) representing biological replicates are explicitly stated in the corresponding figure legends. A P value of $<.05$ was considered statistically significant.

Detailed experimental procedures and specific materials are described in the Supporting Information.

RESULTS

Construction of a tmTNF transgenic mouse model mimicking the pathological features of radiographic axSpA

To elucidate the specific role of tmTNF in the pathogenesis of AS, particularly its contribution to pathological osteogenesis, we generated a tmTNF-overexpressing transgenic mouse model. Following the strategy established by the Kollias group (TgA86) [27], we engineered a construct containing the mouse *Tnf* genomic region with a cleavage-resistant mutation, stabilised by human HBB (hemoglobin subunit beta) regulatory elements to achieve specific high-level expression of tmTNF (Fig 1A; Supplementary Fig S1A). Through multiple generations of breeding, we established a homozygous line (*tmTNF*$^{+/+}$) with a stable phenotype. Genotyping and molecular characterisation confirmed the successful integration and predominant accumulation of the membrane-bound TNF form in target tissues (Supplementary Fig S1B-D).

These *tmTNF*$^{+/+}$ mice spontaneously developed progressive spinal kyphosis and rigid tail deformities (Fig 1B). Micro-CT 3-dimensional reconstruction revealed severe skeletal pathologies highly reminiscent of human AS, including bony fusion and ankylosis of the caudal vertebrae and an increased thoracic kyphosis angle. Notably, we observed distinct pathological changes in the sacroiliac joints, characterised by joint space narrowing and partial bony fusion on the ventral aspect (Fig 1E), alongside fusion of spinous processes in the pelvic region and osteophyte formation. Structural deformities were also evident in the hind limb ankle joints (Fig 1C-F).

Histologic analysis further corroborated the progressive nature of the disease. Commencing as early as 6 weeks of age, *tmTNF*$^{+/+}$ mice exhibited escalating cartilage destruction, inflammatory cell infiltration, and pannus formation in ankle joints and caudal vertebrae. Over time, these inflammatory changes culminated in the obliteration of joint spaces and substantial new bone formation (Fig 1G,H,L,M). Consistent with active aberrant ossification, immunohistochemical staining demonstrated markedly elevated expression of type I collagen (COL1) in the lesion sites (Fig 1I). Functionally, these structural

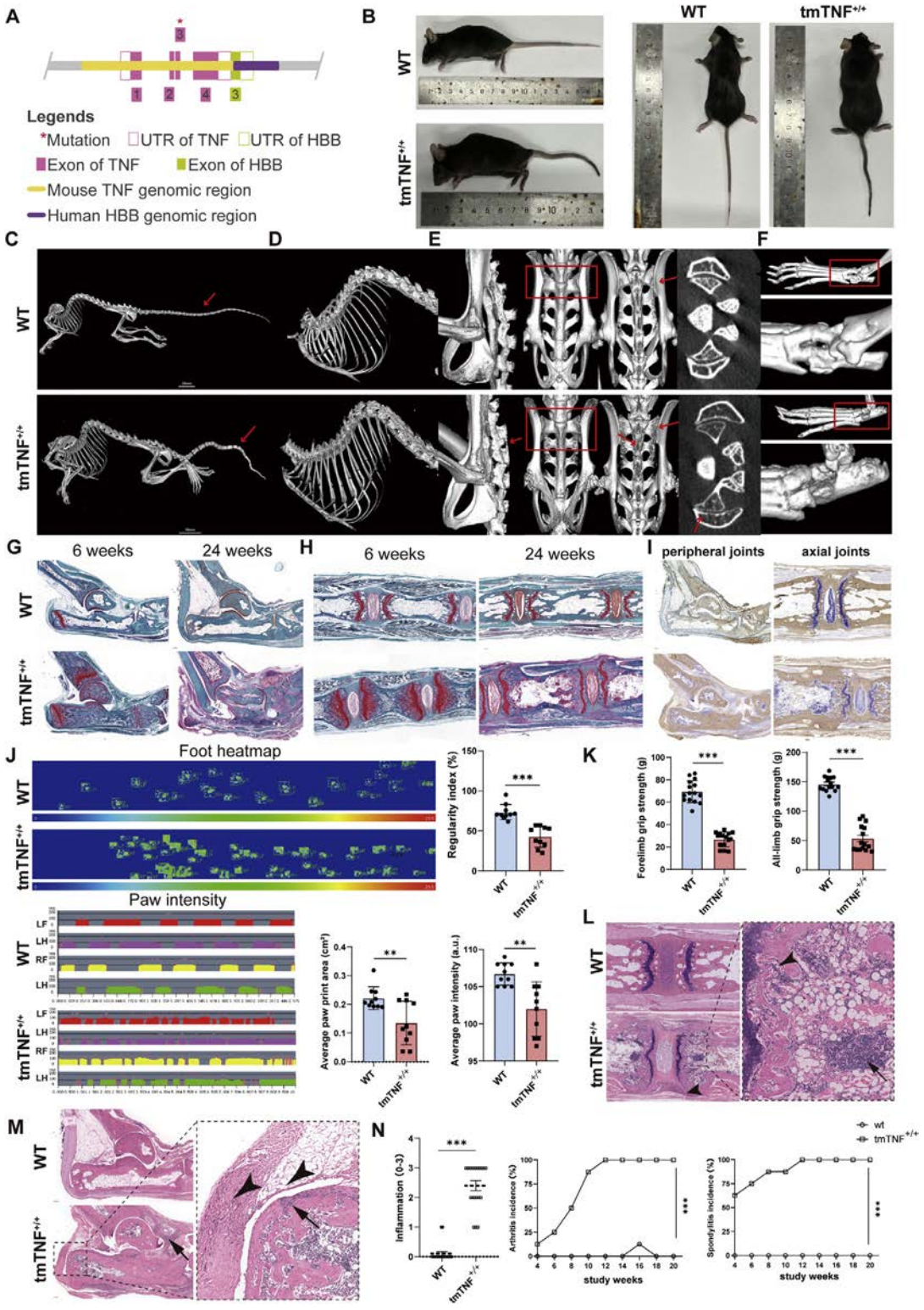

Figure 1. Phenotypic characterisation of tmTNF transgenic mice mimicking radiographic axSpA. (A) Schematic of the tmTNF transgene construct containing a cleavage-resistant mutation (asterisk). (B) Gross appearance of WT and *tmTNF*$^{+/+}$ mice showing kyphosis and tail deformity. (C-F) Micro-CT 3D reconstructions of the whole spine (C), thoracic spine (D), pelvis (E), and hind limb (F). In (E), red arrows indicate narrowing of the sacroiliac joint space and partial fusion on the ventral side. Red boxes indicate regions of spinal fusion and severe joint deformity (n = 6). (G,H) Safranin O-fast green staining of ankles (G) and caudal vertebrae (H) at 6 and 24 wk. (I) Immunohistochemistry for COL1 in ankle joints (left) and caudal vertebrae (right). (J) CatWalk gait analysis showing foot heatmaps and intensity traces (left), with quantification of regularity index, paw area, and intensity (right) (n = 15). (K) Forelimb and all-limb grip strength. (L,M) H&E staining of the spine (L) and ankle (M) showing inflammatory infiltration (arrows), pannus, and erosion (arrowheads). (N) Inflammation severity scores (left, n = 20) and cumulative incidence of arthritis (middle) and spondylitis (right). Data are mean ± SD. $^{*}P < .05$, $^{**}P < .01$, $^{***}P < .001$ (Student's *t*-test). Scale bars are as indicated. axSpA, axial spondyloarthritis; COL1, type I collagen; CT, Computed Tomography; HBB, Hemoglobin Subunit Beta (*β*-globin); H&E, haematoxylin and eosin; LF, Left Front paw; LH, Left Hind paw; RH, Right Hind paw; tmTNF, transmembrane TNF; TNF, Tumor Necrosis Factor; UTR, Untranslated Region; WT, wild-type.

damages translated into significant motor deficits, characterised by a disordered gait pattern with a reduced regularity index (Fig 1J) and a significant decline in limb grip strength (Fig 1K).

Collectively, these data demonstrate that the *tmTNF*$^{+/+}$ mouse model successfully recapitulates the core 'inflammation-ossification' pathological axis of AS, providing a robust *in vivo* platform for investigating the underlying mechanisms of structural progression.

Macrophages drive pathological osteogenesis via the TGF-β superfamily

To dissect the cellular heterogeneity driving the observed skeletal pathology and identify the specific immune cell subsets responsible for ossification, we performed single-cell RNA sequencing on ankle joint tissues. We observed a significant expansion of the monocyte/macrophage population in *tmTNF*$^{+/+}$ mice compared with WT controls (Fig 2A).

Crucially, bioinformatic interrogation revealed that these expanded macrophages are not merely inflammatory responders but are functionally reprogrammed. Their transcriptional profile was significantly enriched in pathways governing not only immune responses but also tissue repair and osteogenesis (Fig 2B-E; Supplementary Fig S2A). Gene Set Enrichment Analysis further confirmed this pathological dual function, highlighting the marked upregulation of gene sets associated with the early TGF-β1 response, Wnt signalling, and extracellular matrix organisation within the macrophage population (Fig 2F; Supplementary Fig S2B).

Subclustering analysis further resolved the heterogeneity of macrophages, identifying a distinct 'Fibrotic Mac' subset. This population was defined by the high expression of fibrotic and osteogenic markers, including *Fstl1, Col1a2, Col3a1, Bmp2*, and *Tgfb3* (Supplementary Fig S2C-G), a signature consistent with the 'fibrotic macrophage' state described in recent studies [29]. This suggests a direct transition from an inflammatory to a matrix-producing phenotype. Immunofluorescence staining of tissue sections confirmed the *in situ* colocalisation of TNF with F4/80$^+$ macrophages (Fig 2G). Crucially, in primary macrophages isolated from *tmTNF*$^{+/+}$ mice, members of the TGF-β superfamily—particularly *Tgfb3* and *Bmp2*—were significantly upregulated at both the mRNA and protein levels (Fig 2H-J).

To definitively establish the causative role of macrophages in this pathology, we depleted them *in vivo* using clodronate liposomes (Fig 2K). Flow cytometry analysis of the ankle joints and spinal tissues confirmed a high depletion efficiency, showing an approximately 85% reduction in the CD11b+F4/80+ macrophage population compared with the phosphate-buffered saline-liposome control group (Fig 2L). Following this successful reduction of the local macrophage burden, the mice exhibited significantly alleviated spinal kyphosis and reduced tail deformities (Fig 2M). Histologic assessment confirmed that macrophage depletion markedly inhibited heterotopic ossification (Fig 2N). Collectively, these results demonstrate that macrophages are the pivotal cellular drivers of pathological osteogenesis in *tmTNF*$^{+/+}$ mice, functioning through the upregulation of TGF-β superfamily signalling.

TNFR1 deficiency reverses the AS-like phenotype

To identify the specific receptor mediating the pathological effects of tmTNF, we crossed *tmTNF*$^{+/+}$ mice with *Tnfrsf1a* (TNFR1)- or *Tnfrsf1b* (TNFR2)-deficient mice (Fig 3A). The successful generation of double-mutant strains was confirmed by genotyping and immunoblot analysis, which verified the complete absence of TNFR1 or TNFR2 protein expression in the respective knockout lines (Supplementary Fig S3A-F).

Phenotypic assessment revealed that TNFR1 deficiency effectively reversed the gross pathological phenotypes of tmTNF *tmTNF*$^{+/+}$ mice, including spinal kyphosis and tail deformities. In contrast, TNFR2 deficiency conferred only limited amelioration (Fig 3B). Longitudinal histologic evaluation (at 6, 12, and 18 weeks) demonstrated that *tmTNF*$^{+/+}$×*TNFRI*$^{-/-}$ mice maintained intact joint architecture with negligible structural damage. Conversely, *tmTNF*$^{+/+}$×*TNFRII*$^{-/-}$ mice continued to exhibit progressive pathological osteogenesis comparable with the parental strain (Fig 3C,D).

At the molecular and cellular levels, the absence of TNFR1 significantly abrogated macrophage infiltration within articular tissues (Fig 3E). Immunohistochemistry and serum ELISA (Enzyme-Linked Immunosorbent Assay) analysis further indicated a marked downregulation of osteogenic factors, TGF-β3 (transforming growth factor beta 3) and BMP2, in both local tissues and systemic circulation of *tmTNF*$^{+/+}$×*TNFRI*$^{-/-}$ mice (Fig 3G,H,N). Consistently, immunoblot analysis of bone marrow-derived macrophages (BMDMs) confirmed that the tmTNF-driven upregulation of TGF-β3 and BMP2 proteins was normalised by TNFR1 deletion (Fig 3L, M). Functionally, *tmTNF*$^{+/+}$×*TNFRI*$^{-/-}$ mice exhibited a restoration of normal gait patterns and grip strength (Fig 3I,J), accompanied by a significant reduction in joint inflammation scores (Fig 3K). Collectively, these data indicate that the pathogenic efficacy of tmTNF—encompassing both inflammation and pathological ossification—is predominantly mediated via TNFR1 signalling.

tmTNF binding with sTNFR I in macrophage induced TGF-β3 and BMP2 expression to trigger osteogenesis

Immunofluorescence analysis of diseased joint sections revealed a striking spatial proximity between TNF$^+$F4/80$^+$ macrophages and CD90$^+$ mesenchymal stem cells (MSCs) (Fig 4A). This intimate physical association suggested a potential for direct intercellular communication. We hypothesised that tmTNF on macrophages might function as a receptor to receive signals from the microenvironment. To test this 'reverse signalling' hypothesis, we established an *in vitro* Transwell coculture system comprising primary macrophages and bone marrow-derived MSCs, using recombinant sTNFR proteins to specifically ligate and stimulate surface tmTNF on macrophages (Fig 4B).

Stimulation of *tmTNF*$^{+/+}$ macrophages with sTNFR I significantly enhanced the osteogenic differentiation of cocultured MSCs. This was evidenced by intensified Alizarin Red S staining (calcium deposition) and elevated alkaline phosphatase activity (Fig 4C,D). At the molecular level, the expression of key osteogenic markers, COL1 and RUNX2 (runt-related transcription factor 2), was markedly upregulated in MSCs (Fig 4E,F). Crucially, we investigated the intrinsic response of macrophages to this stimulation. Immunofluorescence and immunoblot analyses revealed that sTNFR I treatment induced high expression of TGF-β3 and BMP2 in *tmTNF*$^{+/+}$ macrophages in a dose-dependent manner (Fig 4G-J). Furthermore, comparative analysis demonstrated that sTNFR I was significantly more potent than sTNFR II in triggering this signalling cascade (Fig 4K), identifying sTNFR I as the predominant physiological ligand driving this process.

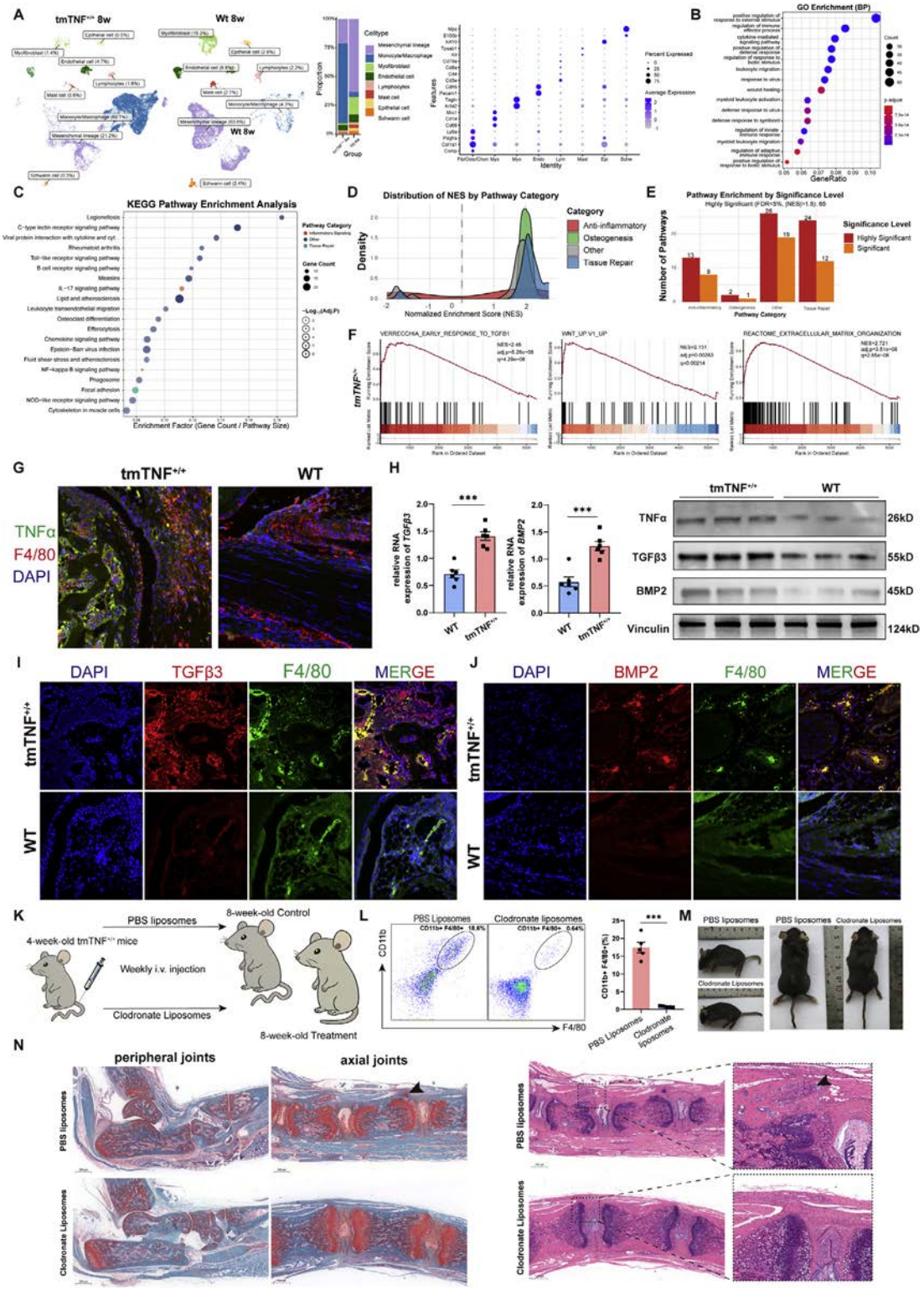

Figure 2. Macrophages drive pathological osteogenesis via the TGF superfamily in tmTNF transgenic mice. (A) scRNA-seq analysis of spine and sacroiliac joints from 8-wk-old mice. Shown are UMAP visualisation (left), cell type proportions (middle), and marker gene expression (right). (B,C) GO biological process (B) and KEGG pathway (C) enrichment analysis of differentially expressed genes in macrophages. (D-F) GSEA of macrophage transcriptomes showing NES distribution (D), pathway classification (E), and enrichment plots (F) for osteogenesis, repair, and Wnt/TGF-β signatures. (G) Immunofluorescence (IF) staining of TNF (green) and F4/80 (red) in ankle tissues. (H) qPCR (left, n = 6) and immunoblot (right) analysis of *Tgfb3* and *Bmp2* in sorted macrophages. (I,J) IF staining of F4/80 (green) with TGF-β3 (I) or BMP2 (J) (red) in tmTNF$^{+/+}$ tissues. (K) Schematic diagram of macrophage depletion using clodronate liposomes (4 wk). (L) Flow cytometry quantification of CD11b+ F4/80+ macrophage depletion in ankles **(n = 5). Data represent mean ± SD. $^{*}P < .001$. (M) Gross appearance showing reduced kyphosis and tail deformity in clodronate-treated mice compared with liposome controls. (N) Histologic analysis via Safranin O-fast green and H&E staining of ankle and spine sections demonstrated the suppression of ectopic ossification upon macrophage depletion. Data are mean ± SD. $^{*}P < .05$, $^{**}P < .01$, $^{***}P < .001$ (Student's *t*-test). Scale bars are as indicated. BMP2, Bone Morphogenetic Protein 2; DAPI, 4',6-diamidino-2-phenylindole; FDR, False Discovery Rate; GO, Gene Ontology; IL-17, Interleukin-17; KEGG, Kyoto Encyclopedia of Genes and Genomes; MERGE, merged fluorescence image; PBS, Phosphate-Buffered Saline; qPCR, quantitative real-time polymerase chain reaction; TGF, Transforming Growth Factor; TNF, Tumor Necrosis Factor; UMAP, Uniform Manifold Approximation and Projection; WT, wild-type.

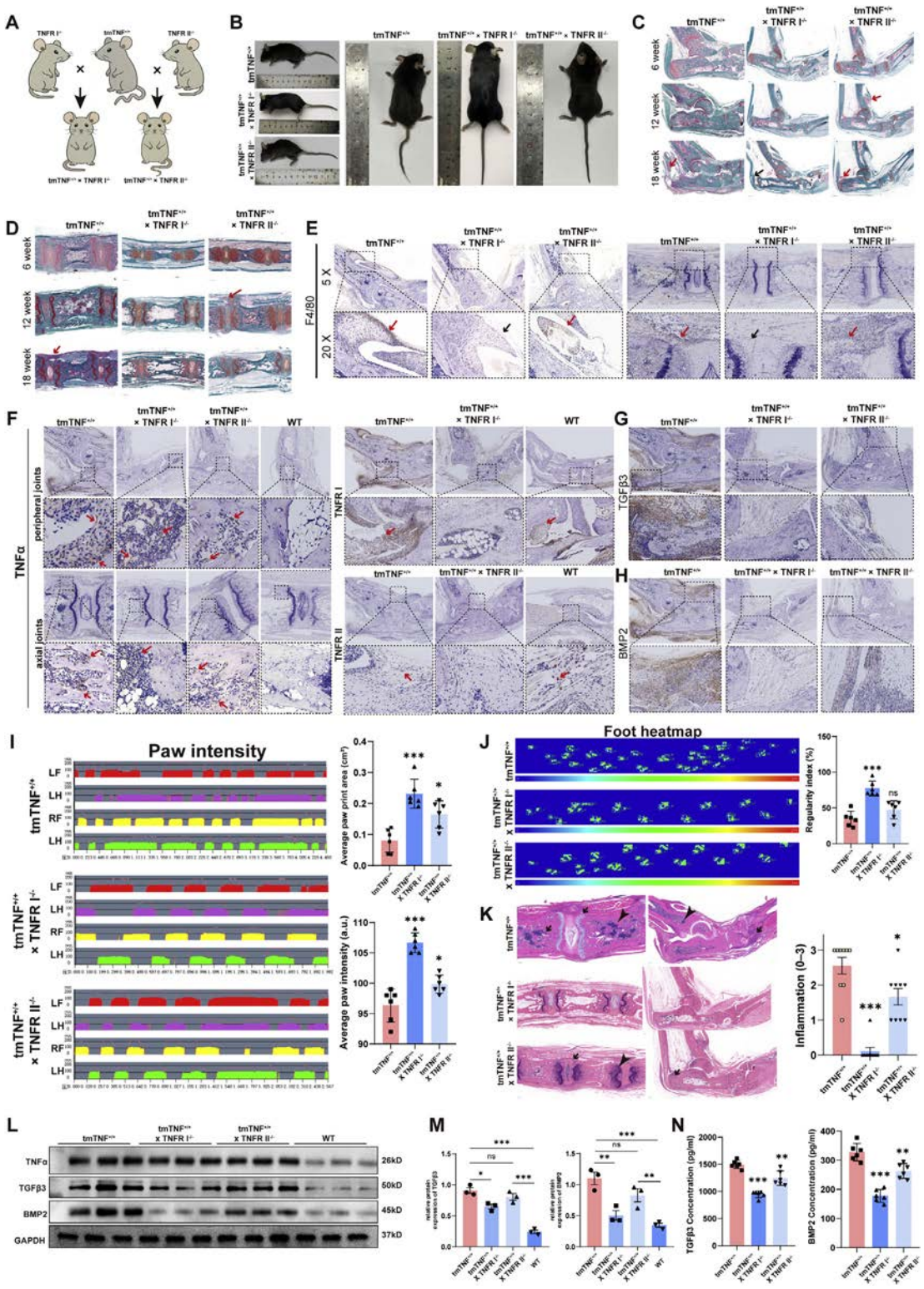

Figure 3. TNFR1 deficiency reverses pathological osteogenesis and inflammation in tmTNF transgenic mice. (A,B) Schematic of the breeding strategy (A) and representative gross appearance of indicated genotypes (B). (C,D) Time-course Safranin O-fast green staining of ankle joints (C) and spines (D) at 6, 12, and 18 wk. (E-H) Immunohistochemical staining of ankle and spine sections. Shown are macrophage infiltration (F4/80) (E), verification of TNFα and receptor expression (F), and levels of osteogenic factors TGF-β3 (G) and BMP2 (H). (I,J) CatWalk gait analysis showing paw intensity traces with average paw print area, and intensity quantification (I), and foot heatmaps with regularity index quantification (J) (n = 6). (K) Representative H&E staining and inflammation scoring (n = 9). (L,M) Immunoblot analysis (L) and quantification (M) of TGF-β3 and BMP2 in bone marrow-derived macrophages. (N) Serum TGF-β3 and BMP2 levels measured by ELISA (n = 6). Data are mean ± SD. $^{*}P < .05$, $^{**}P < .01$, $^{***}P < .001$ (Student's *t*-test or ANOVA). ANOVA, analysis of variance; BMP2, Bone Morphogenetic Protein 2; ELISA, Enzyme-Linked Immunosorbent Assay; GAPDH, Glyceraldehyde-3-Phosphate Dehydrogenase; H&E, haematoxylin and eosin; LF, left front paw; LH, left hind paw; ns, not significant; RH, right hind paw; TGF-β3, Transforming Growth Factor-β3; TNFR1, Tumor Necrosis Factor Receptor 1; tmTNF, transmembrane TNF; TNF, Tumor Necrosis Factor; WT, wild-type.

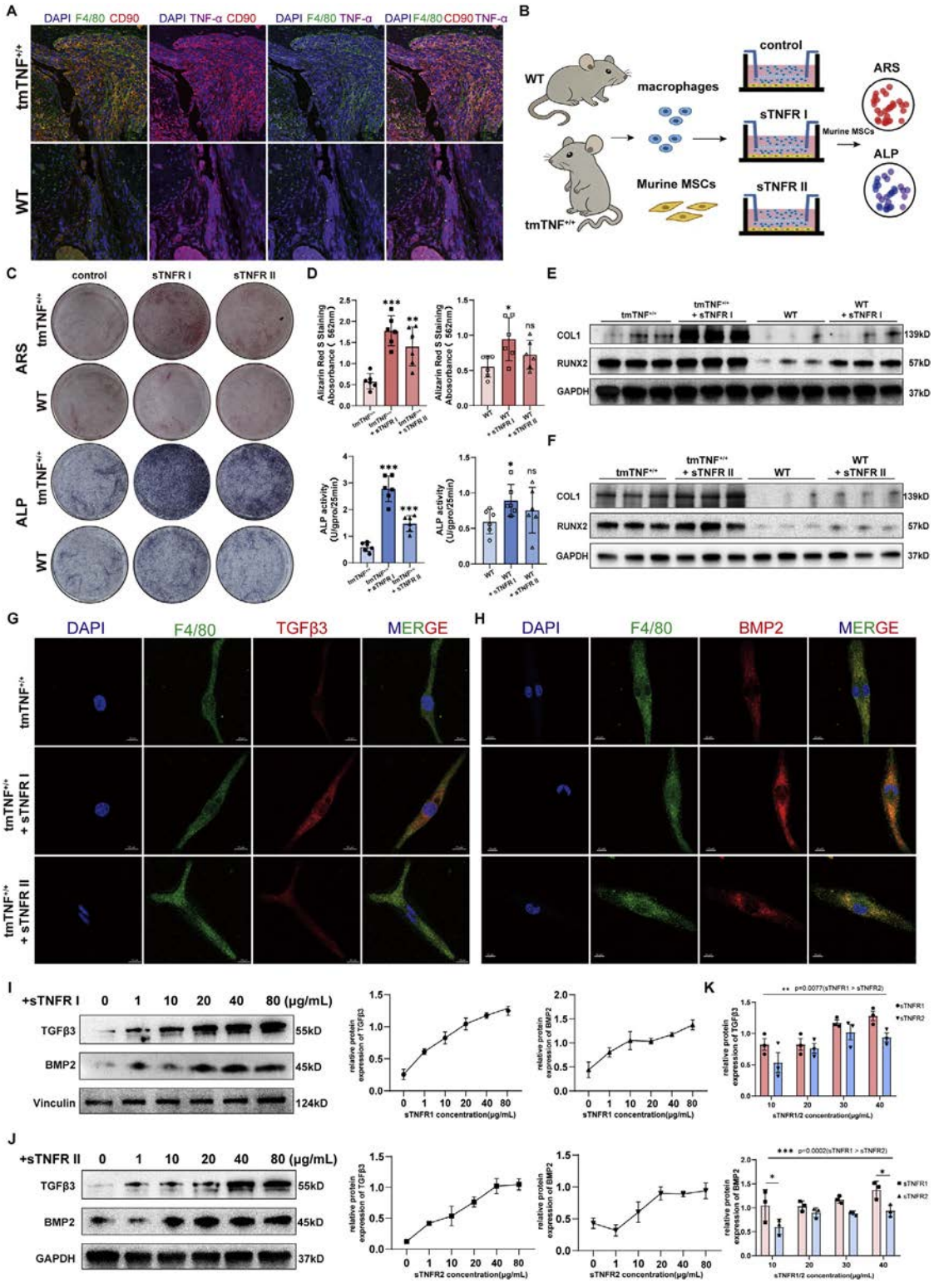

Figure 4. tmTNF functions as a receptor for sTNFR signalling to promote MSC osteogenesis by upregulating macrophage TGF superfamily expression. (A) Immunofluorescence showing the spatial proximity of F4/80 + TNF- macrophages and CD90$^+$ MSCs in *tmTNF*$^{+/+}$ ankle sections. (B) Schematic of the macrophage-MSC coculture and sTNFR stimulation assay. (C,D) ARS staining and ALP activity assays (C) with quantification (D) assessing MSC osteogenic differentiation (n = 6). (E,F) Immunoblot analysis of COL1 and RUNX2 in MSCs cocultured with macrophages upon sTNFR I (E) or sTNFR II (F) stimulation. (G,H) Immunofluorescence of TGF-β3 (G) and BMP2 (H) (red) in F4/80$^+$ macrophages (green) following sTNFR stimulation. (I,J) Immunoblots and dose-response curves of TGF-β3 and BMP2 expression in macrophages treated with indicated concentrations of sTNFR I (I) or sTNFR II (J). (K) Statistical comparison of TGF-β3 and BMP2 induction efficacy between sTNFR I and sTNFR II. Data are mean ± SD. $^*P < .05$, $^{**}P < .01$, $^{***}P < .001$ (Student's *t*-test or ANOVA) ANOVA, analysis of variance; ALP, Alkaline Phosphatase; ARS, Alizarin Red S; BMP2, Bone Morphogenetic Protein 2; COL1, type I collagen; DAPI, 4',6-diamidino-2-phenylindole; GAPDH, Glyceraldehyde-3-Phosphate Dehydrogenase; MSC, mesenchymal stem cell; MERGE, merged fluorescence image; ns, not significant; RUNX2, Runt-Related Transcription Factor 2; sTNFR, soluble Tumor Necrosis Factor Receptor; TGF, Transforming Growth Factor; tmTNF, transmembrane TNF; WT, wild-type.

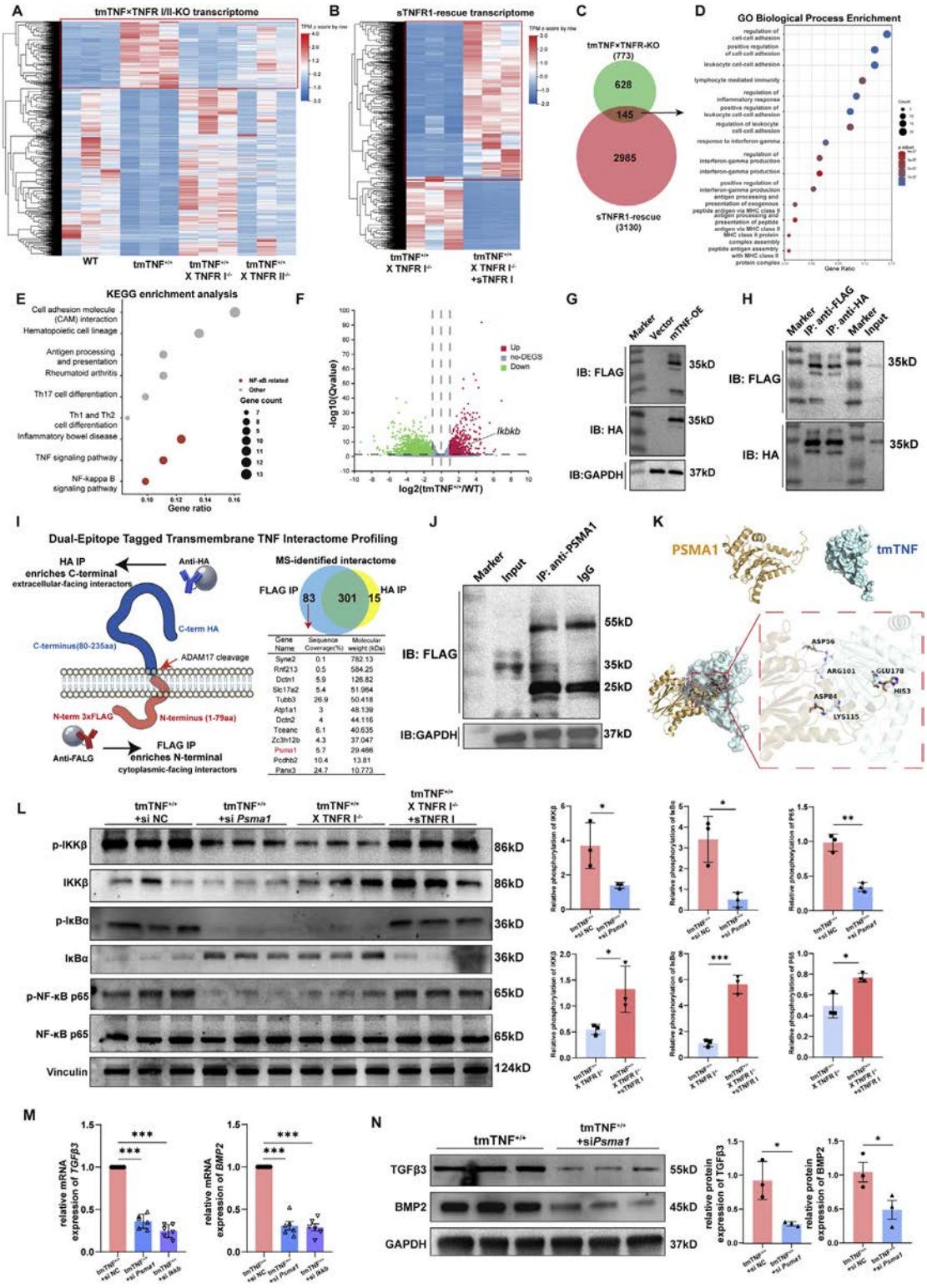

Figure 5. tmTNF activates NF-κB signalling by binding to PSMA1 to regulate TGF superfamily expression. (A-C) Transcriptomic analysis of macrophages. Heatmaps of indicated mouse genotypes (A) and sTNFR I-rescue experiments (B) are shown, along with the intersection of differentially expressed genes (C). (D-F) GO (D) and KEGG (E) enrichment analyses of intersecting genes, and a volcano plot (F) highlighting *Ikbkb*, implicating the NF-κB pathway. (G-I) Interactome profiling of tmTNF using a dual-tag (intracellular-flag/extracellular HA) IP-MS strategy. Shown are validation blots (G,H) and the identification of PSMA1 as a cytoplasmic interactor (I). (J,K) Validation of the tmTNF-PSMA1 interaction by Co-IP (J) and molecular docking simulation (K). Right: overall view of the docked complex; tmTNF is coloured in pale cyan, and PSMA1 is in sandy brown. The binding interface is highlighted by a red dashed box. Left: zoomed-in view of the interaction interface. Key amino acid residues contributing to the binding affinity are shown as sticks. Intermolecular interactions are colour-coded by dashed lines: magenta for salt bridges, yellow for hydrogen bonds, and grey for van der Waals forces. The accompanying table lists the HADDOCK energy scores and parameters for the top-ranked cluster. (L) Immunoblot analysis of NF-κB pathway phosphorylation. Activation is inhibited by si*Psma1* in tmTNF$^{+/+}$ macrophages (left) and induced by sTNFR I in *tmTNF*$^{+/+}$ × *TNFR I*$^{-/-}$ macrophages (right). (M,N) Expression of TGF-β3 and BMP2 at mRNA (M) (n = 6) and protein (N) levels following *Psma1* or *Ikbkb* knockdown. Data are mean ± SD. $^{*}P < .05$, $^{**}P < .01$, $^{***}P < .001$ (Student's *t*-test or ANOVA). ANOVA, analysis of variance; BMP2, Bone Morphogenetic Protein 2; Co-IP, co-immunoprecipitation; DEGS, Differentially Expressed Genes; FLAG, FLAG tag; GAPDH, Glyceraldehyde-3-Phosphate Dehydrogenase; GO, Gene Ontology; HA, Hemagglutinin tag; HADDOCK, High-Ambiguity-Driven Docking; IP-MS, immunoprecipitation-mass spectrometry; KEGG, Kyoto Encyclopedia of Genes and Genomes; KO, Knockout; MHC, Major Histocompatibility Complex; NF-κB, Nuclear Factor-kappa B; ns, not significant; PSMA1, proteasome subunit alpha type-1; sTNFR, soluble Tumor Necrosis Factor Receptor; TGF, Transforming Growth Factor; tmTNF, transmembrane TNF; TNF, Tumor Necrosis Factor.

Collectively, these findings unveil a novel reverse signalling axis—sTNFR I (ligand) →tmTNF (receptor) → TGF-β superfamily (downstream effectors)—through which macrophages are instructed to promote pathological osteogenesis.

tmTNF activates the NF-κB pathway to induce Tgfb3 and Bmp2 expression via direct interaction with PSMA1

To elucidate the downstream molecular mechanisms governing tmTNF reverse signalling, we performed a series of transcriptomic analyses. Initially, we compared the transcriptomes of articular macrophages from *tmTNF*$^{+/+}$ mice vs WT controls, identifying a set of tmTNF-dependent upregulated genes. Notably, the expression of these genes was normalised in *tmTNF*$^{+/+}$ ×*TNFRI*$^{-/-}$ mice (Fig 5A,B). Subsequently, we conducted a 'rescue' experiment by treating BMDMs from *tmTNF*$^{+/+}$×*TNFRI*$^{-/-}$ mice with exogenous sTNFR I to induce reverse signalling. Intersection analysis of the differentially expressed genes from both datasets identified a core signature of 145 genes (Fig 5C). Pathway enrichment analysis of this core set prominently highlighted the activation of the NF-κB signalling pathway, with *Ikbkb* (encoding IKKβ) emerging as a critical upregulated node (Fig 5D-F).

To identify the signal transducer directly interacting with the intracellular domain of tmTNF, we engineered a dual-tagged tmTNF lentiviral construct (N-terminal intracellular-Flag tag; C-terminal extracellular HA tag). Following transduction into RAW264.7 cells, we performed coimmunoprecipitation coupled with mass spectrometry (Co-IP/MS) (Fig 5G,H). This proteomic screen, validated by subsequent Co-IP assays, identified the proteasome subunit alpha type-1 (PSMA1) as a specific binding partner of the tmTNF intracellular domain (Fig 5I,J).

To further clarify the structural basis of this interaction, we performed molecular docking simulations. The results revealed a high binding affinity between PSMA1 and tmTNF, with the top-ranked complex model achieving a HADDOCK (high-ambiguity-driven docking) score of −44.7 ± 13.3 and a Z-score of −1.9, indicating a highly reliable prediction. Energy decomposition analysis suggested that electrostatic interactions (−410.3 ± 34.4 kcal/mol) and van der Waals forces (−95.5 ± 9.6 kcal/mol) were the primary drivers stabilising the complex. Detailed interface analysis identified critical interacting residues, specifically revealing a stable salt bridge formed between Asp56 in the intracellular domain of tmTNF and Arg101 of PSMA1 (Fig 5K).

Functional validation demonstrated that silencing Psma1 in *tmTNF*$^{+/+}$ macrophages significantly inhibited the phosphorylation of IKKβ, IκBα, and p65. Conversely, in a *TNFRI*$^{-/-}$ background, sTNFR I stimulation restored NF-κB pathway activation (Fig 5L). Furthermore, knockdown of either Psma1 or Ikbkb markedly suppressed the expression of *Tgfb3* and *Bmp2* (Fig 5M, N). Collectively, these findings prove that tmTNF directly interacts with PSMA1 to activate the downstream IKKβ/NF-κB (inhibitor of nuclear factor kappa B kinase subunit beta / nuclear factor kappa B) pathway, thereby upregulating TGF-β superfamily expression to drive pathological osteogenesis.

Macrophage-targeted Ikbkb-silencing selectively blocks the inflammation-driven osteogenic programme

Building upon our mechanistic insights and adapting the delivery strategy described by the Janak Lal Pathak group, we developed a macrophage-targeted nanomedicine designed to specifically interrupt the tmTNF-driven signalling axis. We engineered mannose-modified mesoporous silica nanoparticles (Man-MSN) to deliver *Ikbkb* siRNA (inhibitor of nuclear factor kappa B kinase subunit beta small interfering RNA) (si*Ikbkb*/Cy5.5@Man-MSN) specifically to macrophages (Fig 6A). Physicochemical characterisation via transmission electron microscopy and scanning electron microscopy confirmed a uniform spherical mesoporous morphology (Fig 6B). Upon cargo loading, the hydrodynamic diameter increased from ~114 nm to ~139 nm, and the Zeta potential shifted from +32.7 mV to +17.6 mV, confirming successful siRNA encapsulation. UV-Vis (ultraviolet−visible spectroscopy) and fluorescence spectra further verified Cy5.5 loading (Fig 6B). High encapsulation efficiencies were achieved for siRNA (92.16%) and Cy5.5 (68.57%), with drug-loading contents of 1.82% and 3.43%, respectively. *In vivo* imaging subsequently confirmed efficient nanoparticle accumulation within inflamed articular regions (Fig 6C).

At the molecular level, therapeutic administration significantly suppressed IKKβ protein levels and attenuated NF-κB pathway activity in macrophages (Fig 6D). Concurrently, this blockade led to a marked downregulation of TGF-β3 and BMP2 levels, both systemically in the serum and locally within macrophages (Fig 6E,F).

Phenotypically, the treatment notably ameliorated spinal kyphosis and tail deformities in the transgenic mice (Fig 6G). Histologic quantification revealed a significant inhibition of heterotopic ossification and ectopic chondrogenesis. Strikingly, however, inflammatory cell infiltration at the lesion sites remained largely unchanged in the treated group, and inflammation scores showed no significant difference compared with controls (Fig 6H,I). To further profile the systemic inflammatory status, we quantified key proinflammatory cytokines in the serum. Interestingly, the response was heterogeneous: while IL-12β and IL-17A levels were reduced, TNF and IL-1β levels remained unchanged, and IL-6 levels were conversely elevated (Fig 6J). This lack of uniform suppression of proinflammatory mediators contrasts with the profound inhibition of osteogenic factors, confirming that the treatment did not induce broad immunosuppression. Furthermore, the treatment regimen demonstrated a favourable safety profile, with no significant body weight loss (Fig 6K) or organ toxicity observed (Fig 6L). Collectively, these findings demonstrate that targeting the tmTNF-PSMA1-NF-κB axis does not broadly suppress the inflammatory response but selectively arrests its downstream osteogenic programme. This identifies this signalling axis as a specific therapeutic target to intervene in structural progression.

DISCUSSION

In this study, we delineate a previously unrecognised reverse signalling axis composed of sTNFR1-tmTNF-PSMA1-IKKβ/NF-κB. Within the pathological landscape of r-axSpA, this axis specifically instructs macrophages—the core effector cells of inflammation—to acquire and execute a pro-osteogenic function. By integrating genetic manipulation with pharmacological intervention, we verified that tmTNF acts not merely as a precursor to soluble TNF, but as a critical membrane-bound switch that drives pathological osteophyte formation. These findings clarify that pathological ossification in axSpA is driven by a specific, molecularly distinct signalling branch embedded within the broader inflammatory cascade.

Our results provide a molecular explanation for the clinical observation that radiographic progression can proceed even when systemic inflammatory markers are normalised [9,11]. The tmTNF transgenic mice utilised in this study spontaneously recapitulate this progressive ankylosis. Strikingly, targeting

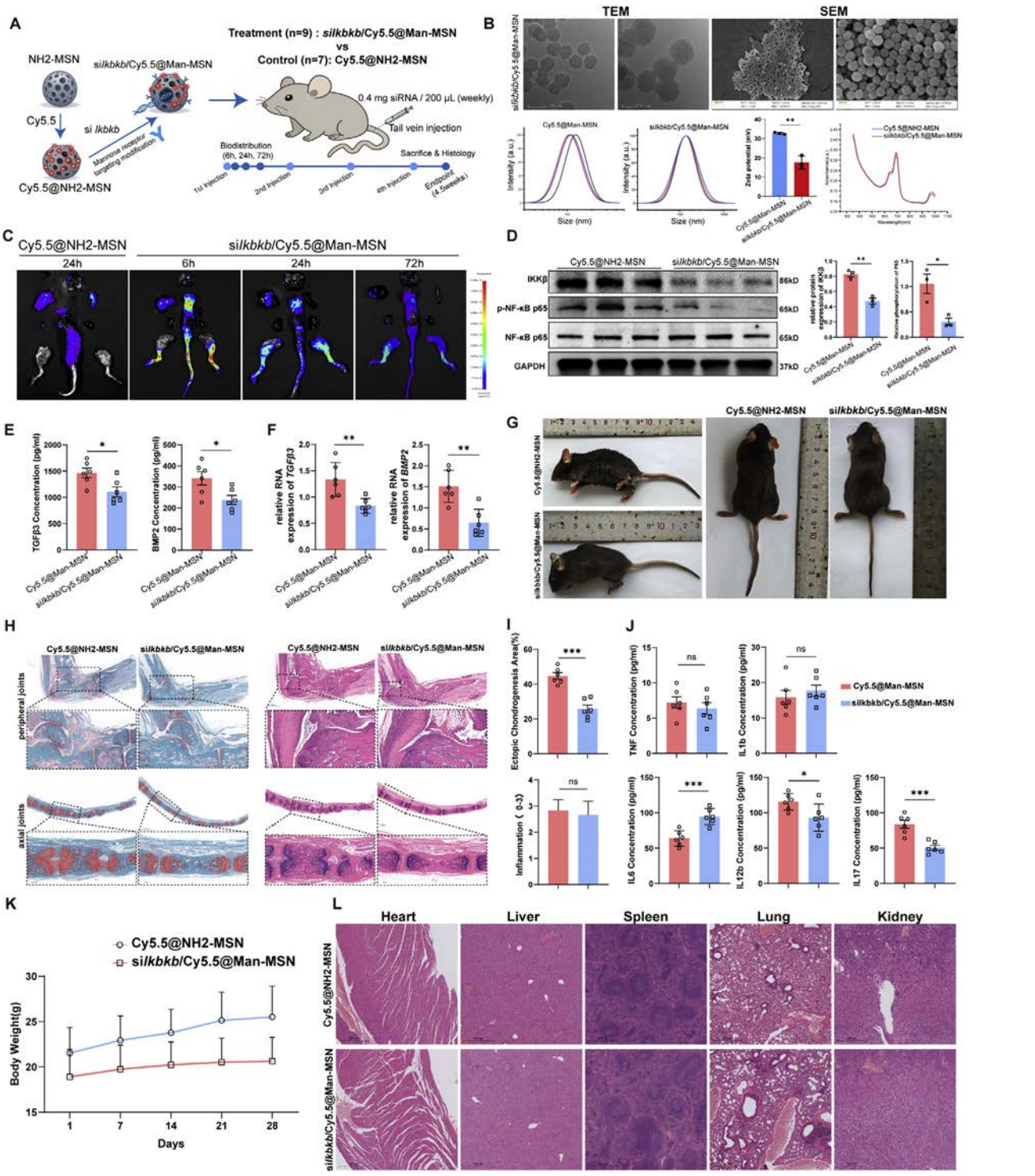

Figure 6. Macrophage-targeted delivery of *Ikbkb* siRNA inhibits pathological osteogenesis in tmTNF-overexpressing mice. (A) Schematic of the mannose-modified, siRNA-loaded mesoporous silica nanoparticle (si*Ikbkb*/Cy5.5@Man-MSN) synthesis and treatment protocol. (B) Characterisation of nanoparticles. Top: representative TEM (left) and SEM (right) images showing spherical morphology and mesoporous structure. Scale bars: 50 nm (TEM), 100 nm (SEM). Bottom: table summarising the hydrodynamic size (DLS), Polydispersity Index (PDI), and Zeta potential changes upon drug loading. UV-Vis absorption spectra and Fluorescence emission spectra confirming the successful coloading of siRNA and Cy5.5. (C) *In vivo* fluorescence imaging showing enhanced accumulation of targeted nanoparticles in affected areas. (D) Immunoblot analysis of IKKβ and NF-κB pathway activation in macrophages post-treatment. (E,F) Downregulation of TGF-β3 and BMP2 demonstrated by serum ELISA (E) and macrophage qPCR (F) (n = 6). (G) Gross appearance showing alleviated kyphosis and tail folding in treated mice. (H) Representative Safranin O-fast green and H&E staining of ankle and spine sections. Note the reduced ossification but persistent inflammation in the treated group. (I) Quantification of ectopic chondrogenesis area (top) and inflammation score (bottom), confirming specific inhibition of osteogenesis without altering inflammation. (J) Serum concentrations of proinflammatory cytokines (TNF, IL-1β, IL-6, IL-12β, and IL-17A) were assessed by ELISA, showing a heterogeneous inflammatory profile post-treatment. (K,L) Safety assessment via body weight (K) and H&E staining of major organs (L). Data are mean ± SD. $^{*}P < .05$, $^{**}P < .01$, $^{***}P < .001$, (Student's *t*-test). BMP2, Bone Morphogenetic Protein 2; ELISA, Bone Morphogenetic Protein 2; GAPDH, Glyceraldehyde-3-Phosphate Dehydrogenase; H&E, haematoxylin and eosin; IKKβ, Inhibitor of Nuclear Factor Kappa B Kinase Subunit Beta; IL, Interleukin; NF-κB, Nuclear Factor-kappa B; NH2-MSN, Amino-functionalized Mesoporous Silica Nanoparticles; ns, not significant; qPCR, Quantitative Real-Time Polymerase Chain Reaction; SEM, Scanning Electron Microscopy; siRNA, Small Interfering RNA; TEM, Transmission Electron Microscopy; TGF-β3, Transforming Growth Factor Beta 3; tmTNF, transmembrane TNF; TNF, Tumor Necrosis Factor; UV-Vi, Ultraviolet−Visible Spectroscopy.

macrophages with Ikbkb-silencing nanoparticles significantly inhibited heterotopic ossification without broadly suppressing inflammatory infiltration. This observation is consistent with the established concept of 'uncoupling' described in previous experimental models of SpA [30], where inflammation and remodelling can be dissociated. Our study advances this concept by identifying the tmTNF-PSMA1 axis as a specific molecular driver of this phenomenon. By precisely blocking the tmTNF-PSMA1-NF-κB axis, we effectively severed the link between chronic inflammation and aberrant bone formation, preventing the 'inflammation-osteogenesis transition'.

Mechanistically, this study advances the field on 2 interconnected fronts. First, we identified sTNFR1 as the primary physiological ligand triggering this pro-osteogenic reverse signal. This finding elucidates how osteogenic signals are specifically initiated within a complex microenvironment replete with various TNF forms and partially explains why drugs targeting different TNF pathways may yield disparate clinical outcomes [31]. Second—and representing a significant conceptual breakthrough—we identified the proteasome subunit PSMA1 [32,33] as the intracellular signal transducer for tmTNF. This interaction directly bridges membrane-bound tmTNF with the canonical intracellular IKKβ/NF-κB signalling pathway [34,35], revealing a mode of reverse signal transduction that was previously underappreciated. Unlike traditional signalling mechanisms that rely on the recruitment of adaptor proteins to receptor domains [36,37], this mechanism engages nonclassical signalling molecules to initiate a specific transcriptional programme, thereby establishing a new molecular paradigm for the functional diversity of cytokine reverse signalling.

Building on these mechanistic insights, our findings fundamentally reshape the understanding of macrophage function in r-axSpA pathology. While previous studies have identified synovial fibroblasts as a source of BMPs under inflammatory conditions [22], our data demonstrate that macrophages, under the instruction of tmTNF reverse signalling, also transition into a specialised pro-osteogenic phenotype. Importantly, this macrophage-driven mechanism does not negate the established central role of the HLA-B27/IL-23/Th17 axis in axSpA pathogenesis. Instead, we propose that these pathways likely operate synergistically: while HLA-B27 (human leukocyte antigen B27) misfolding and Th17-derived cytokines (IL-17, TNF) drive the upstream inflammatory cascade and immune activation [38], macrophages may function as downstream local 'executioners' of structural damage. Under the influence of this inflammatory milieu, the tmTNF reverse signalling axis acts as a specific switch, reprogramming macrophages to upregulate TGF-β3 and BMP2. These cells then directly propel MSCs toward aberrant osteogenic differentiation. This unique activation state, dictated by a specific signalling axis, transcends the classical M1/M2 dichotomy [39,40] and represents a functionally specialised macrophage subtype dedicated to pathological tissue remodelling.

From a translational perspective, these findings suggest that optimal axSpA management might benefit from addressing both the 'inflammatory' and 'remodelling' axes. Current TNFi primarily neutralise soluble TNF or block receptor binding [41]; while effective for symptoms, they may not fully silence the intracellular reverse signalling events triggered by tmTNF, particularly in deep tissue microenvironments. Therefore, targeting the tmTNF-PSMA1 interaction or macrophage-specific IKKβ represents a potential precision strategy. By specifically arresting the osteogenic programme embedded within the inflammatory response, such approaches could potentially complement existing therapies to halt structural progression.

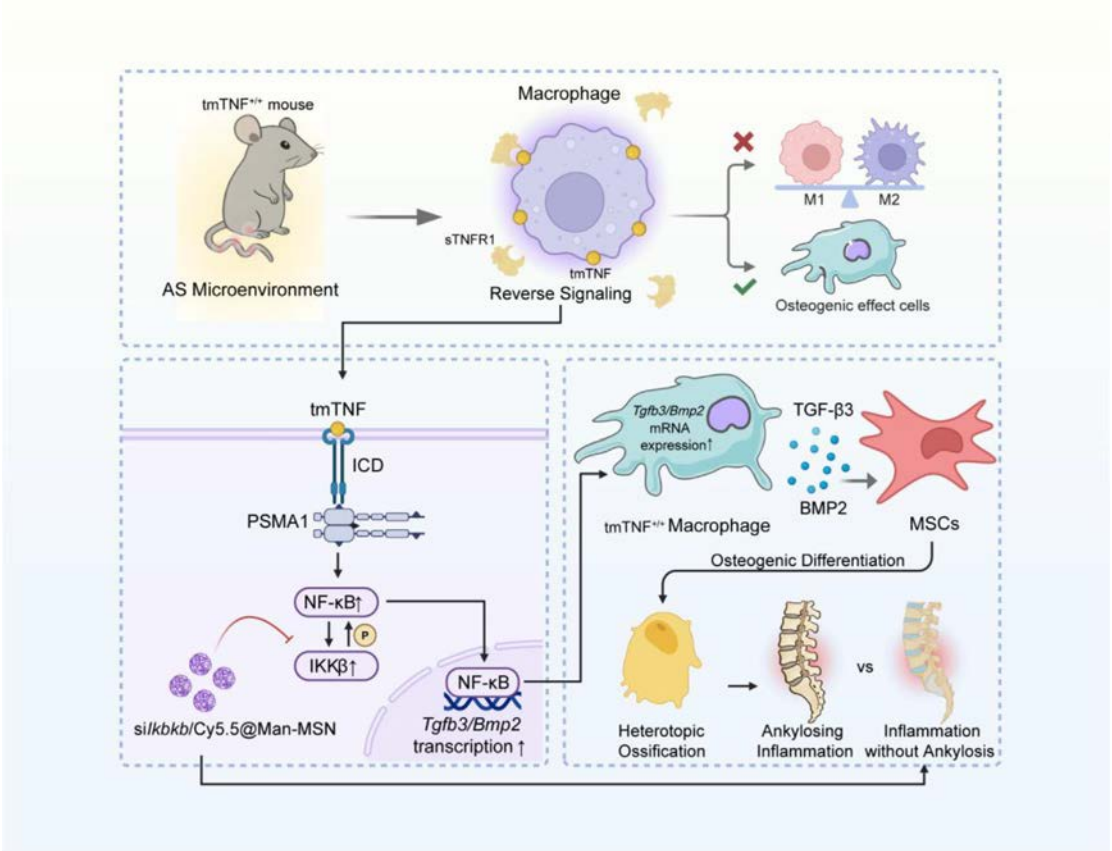

However, clear boundaries to this study exist. First, regarding the macrophage depletion strategy, we acknowledge that clodronate liposomes, while highly effective for macrophages, may also deplete a subset of phagocytic dendritic cells [42]. Nevertheless, the corroborating results obtained from our macrophage-specific mannose-targeted siRNA experiments strongly support macrophages as the primary effector cells in this axis. Second, this study relies on a transgenic mouse model driven by tmTNF overexpression. While this model recapitulates the ossification phenotype, it does not fully capture the complex human genetic background involving HLA-B27 [43] and ERAP1 (endoplasmic reticulum aminopeptidase 1), nor the diverse T-cell repertoires seen in patients [44]. Consequently, the interaction between HLA-B27-driven stress and the tmTNF axis remains to be elucidated. Furthermore, the potential impact of long-term suppression of this specific macrophage pathway on systemic immune homeostasis requires rigorous, longitudinal assessment. Most importantly, as no human validation was presented in this study, future research is critically needed to directly validate the activity of this signalling axis in lesions from patients with r-axSpA and correlate it with clinical progression.

Schematic diagram of tmTNF reverse signaling in osteogenic differentiation

Schematic overview of tmTNF reverse signaling through TNFR1. Activation of IKKβ/NF-κB by tmTNF induces the expression of TGF-β3 and BMP2, which synergistically promote osteogenic differentiation of MSCs and macrophages. This process results in heterotopic ossification and spinal ankylosis, a hallmark of AS.

CONCLUSION

In summary, this study systematically elucidates the cellular and molecular mechanisms by which tmTNF drives pathological osteogenesis in AS via a unique reverse signalling axis. This work not only expands our cognitive horizon regarding the biological diversity of TNF and the functional plasticity of macrophages but also provides a critical theoretical basis and potential novel targets for elevating the therapeutic goal in AS from ‘symptom control’ to ‘blockade of structural damage.’

Competing interests

All authors declare they have no competing interests.

Contributors

PJ and PX contributed to the conceptualisation and wrote the original draft. PJ was responsible for formal analysis and visualisation, and worked with JJ on data curation. PX supervised the study. MC, ZY, and ZL performed validation, and QC provided software support. PW, ZX, and WL acquired funding. PW and WL were responsible for project administration, and ZX provided resources. ZX and PW reviewed and edited the manuscript. All authors read and approved the final manuscript.

Funding

This study was supported by the Shenzhen Science and Technology Program (KCXFZ20230731092959001), the Guangdong Provincial Clinical Research Center for Orthopedic Diseases (2023B110001), and the National Natural Science Foundation of China (82372372, 82302661, and 82572703).

Patient consent for publication

Not applicable. This study did not involve human participants or identifiable patient data, so no patient consent was required.

Ethics approval

All animal experiments were conducted in strict accordance with the Guide for the Care and Use of Laboratory Animals and were approved by the Institutional Animal Care and Use Committee (IACUC) of Sun Yat-sen University (Approval nos. SYSU-IACUC-2024-0033GEM for breeding; SYSU-IACUC-2025-0622GEM and SYSU-IACUC-2025-0191GEM for interventional experiments). Parental strains of genetically engineered mice (C57BL/6 background) were obtained from Cyagen Biosciences (China), while wild-type C57BL/6 mice were purchased from the Production Department of the Laboratory Animal Center, Sun Yat-sen University. All subsequent breeding and housing were performed at the Laboratory Animal Center of Sun Yat-sen University (Shenzhen Campus). Mice in poor health were excluded from the study.

Provenance and peer review

Not commissioned; externally peer reviewed.

Data availability statement

The analysed data sets generated during the study are available from the corresponding author on reasonable request.

Declaration of generative AI and AI-assisted technologies in the writing process

The authors declare that they have not used Artificial Intelligence in this study.

Supplementary materials

Supplementary material associated with this article can be found in the online version at doi:10.1016/j.ard.2026.03.023.

Orcid

Peng Wang: http://orcid.org/0000-0002-5592-6842

REFERENCES

[1] Machado P, Landewé R, Braun J, Hermann KG, Baker D, van der Heijde D. Both structural damage and inflammation of the spine contribute to impairment of spinal mobility in patients with ankylosing spondylitis. Ann Rheum Dis 2010;69(8):1465–70.
[2] Braun J, Sieper J. Ankylosing spondylitis. Lancet 2007;369(9570):1379–90.
[3] Baraliakos X, Listing J, Rudwaleit M, Brandt J, Sieper J, Braun J. Radiographic progression in patients with ankylosing spondylitis after 2 years of treatment with the tumour necrosis factor alpha antibody infliximab. Ann Rheum Dis 2005;64(10):1462–6.
[4] Robinson DM, Keating GM. Infliximab: in ankylosing spondylitis. Drugs 2005;65(9):1283–91 [discussion 92–4].
[5] van der Heijde D, Salonen D, Weissman BN, Landewé R, Maksymowych WP, Kupper H, et al. Assessment of radiographic progression in the spines of

patients with ankylosing spondylitis treated with adalimumab for up to 2 years. Arthritis Res Ther 2009;11(4):R127.
[6] van der Heijde D, Breban M, Halter D, DiVittorio G, Bratt J, Cantini F, et al. Maintenance of improvement in spinal mobility, physical function and quality of life in patients with ankylosing spondylitis after 5 years in a clinical trial of adalimumab. Rheumatology (Oxford) 2015;54(7):1210–9.
[7] Braun J, Baraliakos X, Deodhar A, Poddubnyy D, Emery P, Delicha EM, et al. Secukinumab shows sustained efficacy and low structural progression in ankylosing spondylitis: 4-year results from the MEASURE 1 study. Rheumatology (Oxford) 2019;58(5):859–68.
[8] Sieper J, Rudwaleit M, Baraliakos X, Brandt J, Braun J, Burgos-Vargas R, et al. The Assessment of SpondyloArthritis international Society (ASAS) handbook: a guide to assess spondyloarthritis. Ann Rheum Dis 2009;68(Suppl 2) ii1–44.
[9] van der Heijde D, Landewé R, Einstein S, Ory P, Vosse D, Ni L, et al. Radiographic progression of ankylosing spondylitis after up to two years of treatment with etanercept. Arthritis Rheum 2008;58(5):1324–31.
[10] Lambert RG, Bakker PA, van der Heijde D, Weber U, Rudwaleit M, Hermann KG, et al. Defining active sacroiliitis on MRI for classification of axial spondyloarthritis: update by the ASAS MRI working group. Ann Rheum Dis 2016;75 (11):1958–63.
[11] Lories RJ, Derese I, de Bari C, Luyten FP. Evidence for uncoupling of inflammation and joint remodeling in a mouse model of spondylarthritis. Arthritis Rheum 2007;56(2):489–97.
[12] Lories RJ, Schett G. Pathophysiology of new bone formation and ankylosis in spondyloarthritis. Rheum Dis Clin North Am 2012;38(3):555–67.
[13] Braun J, Bollow M, Neure L, Seipelt E, Seyrekbasan F, Herbst H, et al. Use of immunohistologic and in situ hybridization techniques in the examination of sacroiliac joint biopsy specimens from patients with ankylosing spondylitis. Arthritis Rheum 1995;38(4):499–505.
[14] Bollow M, Fischer T, Reisshauer H, Backhaus M, Sieper J, Hamm B, et al. Quantitative analyses of sacroiliac biopsies in spondyloarthropathies: T cells and macrophages predominate in early and active sacroiliitis—cellularity correlates with the degree of enhancement detected by magnetic resonance imaging. Ann Rheum Dis 2000;59(2):135–40.
[15] Fuentelsaz-Romero S, Cuervo A, Estrada-Capetillo L, Celis R, García-Campos R, Ramírez J, et al. GM-CSF expression and macrophage polarization in joints of undifferentiated arthritis patients evolving to rheumatoid arthritis or psoriatic arthritis. Front Immunol 2020;11:613975.
[16] Vandooren B, Noordenbos T, Ambarus C, Krausz S, Cantaert T, Yeremenko N, et al. Absence of a classically activated macrophage cytokine signature in peripheral spondylarthritis, including psoriatic arthritis. Arthritis Rheum 2009;60(4):966–75.
[17] Franco GC, Kajiya M, Nakanishi T, Ohta K, Rosalen PL, Groppo FC, et al. Inhibition of matrix metalloproteinase-9 activity by doxycycline ameliorates RANK ligand-induced osteoclast differentiation in vitro and in vivo. Exp Cell Res 2011;317(10):1454–64.
[18] Blom AB, van Lent PL, Holthuysen AE, van der Kraan PM, Roth J, van Rooijen N, et al. Synovial lining macrophages mediate osteophyte formation during experimental osteoarthritis. Osteoarthritis Cartilage 2004;12 (8):627–35.
[19] Raggatt LJ, Partridge NC. Cellular and molecular mechanisms of bone remodeling. J Biol Chem 2010;285(33):25103–8.
[20] Lories RJ, Derese I, Luyten FP. Modulation of bone morphogenetic protein signaling inhibits the onset and progression of ankylosing enthesitis. J Clin Invest 2005;115(6):1571–9.
[21] Lories RJ, Derese I, Ceuppens JL, Luyten FP. Bone morphogenetic proteins 2 and 6, expressed in arthritic synovium, are regulated by proinflammatory cytokines and differentially modulate fibroblast-like synoviocyte apoptosis. Arthritis Rheum 2003;48(10):2807–18.
[22] Fukui N, Zhu Y, Maloney WJ, Clohisy J, Sandell LJ. Stimulation of BMP-2 expression by pro-inflammatory cytokines IL-1 and TNF-alpha in normal and osteoarthritic chondrocytes. J Bone Joint Surg Am 2003;85-A(Suppl 3): 59–66.
[23] Kaaij MH, van Tok MN, Blijdorp IC, Ambarus CA, Stock M, Pots D, et al. Transmembrane TNF drives osteoproliferative joint inflammation reminiscent of human spondyloarthritis. J Exp Med 2020;217(10): e20200288.
[24] Horiuchi T, Mitoma H, Harashima S, Tsukamoto H, Shimoda T. Transmembrane TNF-alpha: structure, function and interaction with anti-TNF agents. Rheumatology (Oxford) 2010;49(7):1215–28.
[25] Ishii S, Isozaki T, Furuya H, Takeuchi H, Tsubokura Y, Inagaki K, et al. ADAM-17 is expressed on rheumatoid arthritis fibroblast-like synoviocytes and regulates proinflammatory mediator expression and monocyte adhesion. Arthritis Res Ther 2018;20(1):159.
[26] Christodoulou-Vafeiadou E, Geka C, Ntari L, Kranidioti K, Argyropoulou E, Meier F, et al. Ectopic bone formation and systemic bone loss in a transmembrane TNF-driven model of human spondyloarthritis. Arthritis Res Ther 2020;22(1):232.
[27] Georgopoulos S, Plows D, Kollias G. Transmembrane TNF is sufficient to induce localized tissue toxicity and chronic inflammatory arthritis in transgenic mice. J Inflamm 1996;46(2):86–97.
[28] Watts AD, Hunt NH, Madigan MC, Chaudhri G. Soluble TNF-alpha receptors bind and neutralize over-expressed transmembrane TNF-alpha on macrophages, but do not inhibit its processing. J Leukoc Biol 1999;66 (6):1005–13.
[29] Sanin DE, Ge Y, Marinkovic E, Kabat AM, Castoldi A, Caputa G, et al. A common framework of monocyte-derived macrophage activation. Sci Immunol 2022;7(70):eabl7482.
[30] Schett G, Lories RJ, D'Agostino MA, Elewaut D, Kirkham B, Soriano ER, et al. Enthesitis: from pathophysiology to treatment. Nat Rev Rheumatol 2017;13 (12):731–41.
[31] Zhang JR, Liu XJ, Xu WD, Dai SM. Effects of tumor necrosis factor-α inhibitors on new bone formation in ankylosing spondylitis. Joint Bone Spine 2016;83(3):257–64.
[32] Cron KR, Zhu K, Kushwaha DS, Hsieh G, Merzon D, Rameseder J, et al. Proteasome inhibitors block DNA repair and radiosensitize non-small cell lung cancer. PLOS ONE 2013;8(9):e73710.
[33] Dai Q, Wang H, Li F, Huang R, Jiang C, Yuan L, et al. Tumor associated neutrophils promote prostate cancer progression by mediating neutrophil trap secretion through PSMA1- NF-κB-HIF-1α signaling axis. Front Immunol 2025;16:1467357.
[34] Brummelkamp TR, Nijman SM, Dirac AM, Bernards R. Loss of the cylindromatosis tumour suppressor inhibits apoptosis by activating NF-kappaB. Nature 2003;424(6950):797–801.
[35] Mercurio F, Zhu H, Murray BW, Shevchenko A, Bennett BL, Li J, et al. IKK-1 and IKK-2: cytokine-activated IkappaB kinases essential for NF-kappaB activation. Science 1997;278(5339):860–6.
[36] Webster JD, Vucic D. The balance of TNF mediated pathways regulates inflammatory cell death signaling in healthy and diseased tissues. Front Cell Dev Biol 2020;8:365.
[37] Haas TL, Emmerich CH, Gerlach B, Schmukle AC, Cordier SM, Rieser E, et al. Recruitment of the linear ubiquitin chain assembly complex stabilizes the TNF-R1 signaling complex and is required for TNF-mediated gene induction. Mol Cell 2009;36(5):831–44.
[38] Sieper J, Poddubnyy D. Axial spondyloarthritis. Lancet 2017;390 (10089):73–84.
[39] Cutolo M, Campitiello R, Gotelli E, Soldano S. The role of M1/M2 macrophage polarization in rheumatoid arthritis synovitis. Front Immunol 2022;13:867260.
[40] Sica A, Mantovani A. Macrophage plasticity and polarization: in vivo veritas. J Clin Invest 2012;122(3):787–95.
[41] Menegatti S, Guillemot V, Latis E, Yahia-Cherbal H, Mittermüller D, Rouilly V, et al. Immune response profiling of patients with spondyloarthritis reveals signalling networks mediating TNF-blocker function in vivo. Ann Rheum Dis 2021;80(4):475–86.
[42] Van Rooijen N, Sanders A. Liposome mediated depletion of macrophages: mechanism of action, preparation of liposomes and applications. J Immunol Methods 1994;174(1–2):83–93.
[43] Jaakkola E, Herzberg I, Laiho K, Barnardo MC, Pointon JJ, Kauppi M, et al. Finnish HLA studies confirm the increased risk conferred by HLA-B27 homozygosity in ankylosing spondylitis. Ann Rheum Dis 2006;65(6):775–80.
[44] Braun J, Märker-Hermann E, Rudwaleit M, Sieper J. HLA-B27 and the role of specific T cell receptors in the pathogenesis of spondyloarthritis. Ann Rheum Dis 2024;83(11):1406–8.

Ann Rheum Dis 85 (2026) 1570–1581

Contents lists available at ScienceDirect

Annals of the Rheumatic Diseases

journal homepage: https://www.sciencedirect.com/journal/annals-of-the-rheumatic-diseases

Systemic lupus erythematosus

Neutrophil transcriptomics in SLE reveals intrinsic disease signatures, shared *ex vivo* adaptation, and transcriptional reset after CAR T-cell therapy

Ehsan Dehdashtian[1], Guangnan Hu[1], Leah Whiteman[2], Md Tanimul Islam[1], Stefania Gallucci[2], Manuel Garber[3], Dominic Borie[4], Georg Schett[5], Roberto Caricchio[1,*]

[1] *Division of Rheumatology, Department of Medicine, UMass Chan Medical School, Worcester, MA, USA*
[2] *Lab of Dendritic Cell Biology, Division of Innate Immunity, Department of Medicine, UMass Chan Medical School, Worcester, MA, USA*
[3] *Department of Genomics and Computational Biology, UMass Chan Medical School, Worcester, MA, USA*
[4] *Kyverna Therapeutics, Emeryville, CA, USA*
[5] *Department of Medicine 3, Rheumatology and Immunology, Friedrich-Alexander University, Erlangen, Germany*

ARTICLE INFO

Article history:
Received 30 October 2025
Received in revised form 2 February 2026
Accepted 14 February 2026

ABSTRACT

Objectives: Systemic lupus erythematosus (SLE) is an autoimmune disease characterised by dysregulation of the adaptive and innate immunity. This study aimed to identify transcriptomic differences in neutrophils from patients with SLE and healthy individuals, analyse *ex vivo* adaptation dynamics, and evaluate the impact of chimeric antigen receptor (CAR) T-cell therapy on neutrophil transcriptomic profiles.

Methods: Neutrophils were isolated via negative selection from 7 patients with SLE and 7 healthy individuals. RNA sequencing was performed to assess transcriptomic differences, *ex vivo* dynamics over 60 minutes, and responses to lipopolysaccharide (LPS) stimulation. In addition, longitudinal transcriptomic data from a patient with SLE undergoing KYV-101 anti-CD19 CAR T-cell therapy were evaluated.

Results: We identified 258 differentially expressed genes consistently distinguishing SLE from healthy neutrophils; they spanned multiple clusters, enriched in interferon-related and DNA damage repair genes (upregulated), and ribosomal protein genes (downregulated). *Ex vivo* adaptation revealed shared activation pathways, such as NF-κB (Nuclear factor kappa-light-chain-enhancer of activated B cells) and apoptosis, in both groups. LPS stimulation highlighted overlapping inflammatory responses, demonstrating retained functional capacities in SLE neutrophils. Following CAR T-cell therapy of a patient with SLE, neutrophil transcriptomic profiles were realigned with healthy controls by 3 months posttreatment.

Conclusions: Neutrophils in SLE exhibit intrinsic, disease-specific transcriptomic alterations while sharing *ex vivo* adaptation dynamics with healthy individuals. The disease-specific alterations appear to be modifiable through targeted therapeutic intervention, as anti-CD19 CAR T-cell therapy resets neutrophil gene expression towards healthy patterns despite targeting B cells rather than neutrophils directly. These findings provide insights into SLE pathogenesis and highlight potential therapeutic strategies targeting both adaptive and innate immunity.

*Correspondence to Dr. Roberto Caricchio, Division of Rheumatology, Department of Medicine, UMass Chan Medical School, Worcester, MA, USA.
E-mail address: lupus.caricchio@umassmed.edu (R. Caricchio).
Handling editor Josef S. Smolen.

https://doi.org/10.1016/j.ard.2026.02.013

WHAT IS ALREADY KNOWN ON THIS TOPIC

- Neutrophils play a critical role in systemic lupus erythematosus (SLE) pathogenesis through dysregulated functions including enhanced NETosis, accelerated cell death, and elevated proinflammatory cytokine secretion.
- Transcriptomic studies have revealed aberrant interferon signatures in neutrophils from patients with SLE that contribute to chronic inflammation.

WHAT THIS STUDY ADDS

- We identify 258 intrinsically differentially expressed genes that consistently distinguish SLE neutrophils from healthy controls regardless of *ex vivo* culture duration, demonstrating persistent disease-specific transcriptomic alterations.
- Despite intrinsic differences, neutrophils from both patients with SLE and healthy individuals undergo similar *ex vivo* transcriptional adaptations over time, with shared activation of NF-κB and apoptosis pathways.
- Anti-CD19 chimeric antigen receptor T-cell therapy demonstrates the ability to reset neutrophil gene expression towards healthy patterns by 3 months posttreatment, despite targeting B cells rather than neutrophils directly.

HOW THIS STUDY MIGHT AFFECT RESEARCH, PRACTICE OR POLICY

- These findings highlight the interconnectedness of adaptive and innate immune dysfunction in SLE, suggesting that B cell-targeted therapies may have broader immunomodulatory effects than previously recognised.
- The identification of intrinsic, stable transcriptomic alterations in SLE neutrophils provides potential biomarkers for disease monitoring and therapeutic response assessment.
- Our results support the development of therapeutic strategies targeting both adaptive and innate immunity.

INTRODUCTION

Systemic lupus erythematosus (SLE) is a complex autoimmune disorder that disproportionately affects women of reproductive age. It is marked by the production of autoantibodies, immune complex (IC) deposition, and a profound inflammatory response that can affect nearly every organ in the body. [1]. Traditionally, SLE pathogenesis is attributed to dysfunctions in the adaptive immune system. However, emerging evidence underscores the role of the innate immune system in both the initiation and progression of the disease [2].

Neutrophils, as key players of the innate immune system, have gained significant attention in recent years for their role in SLE. Neutrophils from patients with SLE exhibit dysregulated functions, including enhanced NETosis, accelerated cell death, increased reactive oxygen species (ROS) production, and elevated secretion of proinflammatory cytokines such as tumour necrosis factor (TNF)-α, interferon (IFN)-α, and IFN-γ [2–5]. These aberrant neutrophil activities directly contribute to tissue damage, IC formation, and sustained inflammatory responses characteristic of SLE pathogenesis [2]. In addition, transcriptomic studies of neutrophils have provided critical insights into SLE pathogenesis, revealing aberrant IFN signatures, dysregulated apoptotic pathways, and enhanced neutrophil activation states that contribute to chronic inflammation and tissue damage [6].

Neutrophils play a critical role in SLE pathogenesis, yet it remains unclear to what extent their dysregulated phenotype is driven by the lupus environment vs intrinsic abnormalities. This study investigated the persistence of disease-specific transcriptional signatures in neutrophils from patients with SLE after their removal from the inflammatory milieu. By analysing *ex vivo* transcriptional adaptations in neutrophils maintained in stimulant-free conditions, we aim to distinguish intrinsic neutrophil dysfunction from that induced by the SLE inflammatory milieu. In addition, we examined neutrophil responses to lipopolysaccharide (LPS) stimulation to assess functional differences between SLE and healthy controls.

In recent years, chimeric antigen receptor (CAR) T-cell therapy has demonstrated promising results in patients with SLE who are refractory to conventional treatments [7,8]. Since both arms of the innate and adaptive immune systems are involved in SLE pathogenesis, we aimed to investigate the impact of this therapy on the gene expression profile of neutrophils from a patient with SLE undergoing CD19 CAR T-cell therapy.

METHODS

Patients and public involvement

Patients and/or the public were not involved in the design, conduction, reporting, or dissemination of this research.

Patients and blood collection

Seven patients with SLE were selected from the UMass Chan Lupus Center, a prospective cohort approved by the local institutional review board. All the patients met at least 4 criteria of the 2019 European League Against Rheumatism/American College of Rheumatology classification criteria [9]. Seven healthy controls were also included. Demographic data are shown in the Table. After informed consent, whole blood was collected in K_2 EDTA-coated tubes (BD Vacutainer, BD, USA, 366643). In addition to the 7 patients, a 28-year-old woman with refractory SLE, who underwent lymphodepletion and subsequent CD19 CAR T-cell therapy with KYV-101 (Kyverna Therapeutics, Inc) via expanded access through a Single-Patient Investigational New Drug application, was also included. Blood samples from this patient were collected at 10 time points: twice before CD19 CAR T-cell infusion and 8 times afterwards.

Neutrophil purification and culture

Blood samples were incubated at room temperature for 1 hour and then centrifuged at 1500 × *g* for 15 minutes. The buffy coat was collected, and neutrophils were isolated by negative selection using the EasySep Direct Human Neutrophil Isolation Kit (STEMCELL Technologies, Canada, 19666), according to the manufacturer's instructions. For the patient undergoing CAR T-cell therapy, neutrophils were purified directly from whole blood without prior centrifugation or buffy coat separation, using the same kit. This modified approach was implemented due to the limited blood sample volume. Following isolation, purity was confirmed via flow cytometry using CD45 (BioLegend, USA, 304050), CD16 (Biosciences, BD, USA, 562293), and CD66b (BioLegend, USA, 305104) as neutrophil markers (Supplementary Fig S1).

After isolation and cell counting, neutrophils were centrifuged at 400 × *g* for 10 minutes with the acceleration and brake set to 4. The cell pellet was resuspended at 2×10^6 cells/mL in RPMI 1640 medium (phenol red–free) (Gibco, USA, 11835-030) supplemented with 1% L-glutamine (Gibco, USA, 25-030-081), then seeded at 1×10^6 cells/well in 24-well tissue culture-treated plates (Corning Costar, USA, 3526). Neutrophils were either stimulated with LPS (100 ng/mL) (Sigma-Aldrich, USA, L3755) or left

Table
Demographic and clinical characteristics of study participants

Demographics	Healthy	SLE
Age, median (Q1, Q3), y	36 (23, 40)	34 (31, 57)
Sex, % female	100	71.4
Race/ethnicity, no.		
African American	2	2
White	4	3
Other	1	2
Disease duration median (Q1, Q3)	-	7 (2, 9)
Medication usage, %		
Hydroxychloroquine	-	86
Mycophenolate mofetil	-	57
Prednisone	-	43
SLEDAI, median (Q1, Q3)	-	0 (0, 6)

SLE, systemic lupus erythematosus; SLEDAI, SLE Disease Activity Index.
Demographic data, disease characteristics, medication usage of healthy controls (n = 7), and patients with SLE (n = 7) included in the study. Age, disease duration, and SLEDAI are presented as median with first (Q1) and third (Q3) quartiles. Medication usage is shown as a percentage of patients with SLE receiving each treatment. Race/ethnicity is presented as absolute numbers.

unstimulated and incubated at 37°C with 5% CO_2. Unstimulated cells were pelleted at 0, 30, and 60 minutes, whereas LPS-stimulated neutrophils were pelleted at 60 minutes to capture early transcriptional changes while avoiding spontaneous neutrophil activation and NETosis that occurs rapidly in *ex vivo* conditions [10]. The full time-course analysis (0, 30, and 60 minutes) was performed on all patients with SLE and 3 healthy controls. For the CAR T-cell therapy patient, neutrophils were pelleted only at time 0, without incubation. Four additional healthy controls were also processed at time 0 only for validation purposes. All pelleting steps were performed at 400 × *g* for 10 minutes. Pellets were then resuspended in 500 µL Tri-Reagent (Zymo Research, USA, R2050-1-200) and stored at −80°C.

RNA extraction and RNA sequencing library preparation

The RNA from neutrophils was extracted using the TRI Reagent Solution protocol (ThermoFisher Scientific, USA, AM9738). Purity and integrity were confirmed using the TapeStation system (Agilent Technologies). mRNA was purified using the NEBNext Poly(A) mRNA Magnetic Isolation module (NewEngland Biolabs, USA, E7490S/L). Subsequently, libraries were prepared using the xGEN Broad-Range RNA Library Prep Kit (Integrated DNA Technologies, USA, 10009813) and xGen Normalase UDI Primers (Integrated DNA Technologies, USA, 10009796). The prepared libraries were enzymatically pooled using the xGen Normalase Module (Integrated DNA Technologies, USA, 10009793) and sequenced, generating 150 bp paired-end reads (Azenta Life Sciences).

Quantitative real-time polymerase chain reaction validation

To validate RNA sequencing findings, quantitative real-time polymerase chain reaction (qPCR) was performed for select genes (ABCA1, GRAMD1B, MDK, IL8, IL1B, and TNF) using standard protocols. Relative expression was calculated using the $2^{-\Delta\Delta Ct}$ method with RPLP0 as the housekeeping gene.

B cell activating factor ELISA

Plasma B cell activating factor (BAFF) concentrations were measured in samples from healthy controls (n = 3) and patients with SLE (n = 7) using the Human BAFF DuoSet ELISA kit (R&D Systems, USA, DY124-05). For neutrophil secretion studies, neutrophils were isolated from an independent pool of healthy controls (n = 3) and patients with SLE (n = 12), cultured at 2 × 10^6 cells/mL in *X-VIVO* 15 medium (Lonza, USA, 04-418Q), and stimulated with PBS (Gibco, USA, 14190-144) or LPS (100 ng/mL) for 18 hours. Supernatants were collected, and BAFF concentrations were measured by ELISA (enzyme-linked immunosorbent assay).

Statistical analysis

We generated FASTQ files from RNA sequencing and assessed their quality using FastQC. We mapped the reads to the GRCh38 reference human genome using RSEM v1.3.3 to quantify the number of reads per gene. We analysed the resulting count matrix with the R package DESeq2 (v1.44.0) [11] and identified differentially expressed genes (DEGs) using thresholds of fold change > 1.5 and an adjusted *P* value <.05. We generated principal component analysis (PCA) plots using the plotPCA function in DESeq2 based on the top 2000 most variable genes, and heatmaps using data normalised with the EdgeR function, log2(CPM + 4). To assess whether disease status (SLE vs healthy) affected the pattern of time-dependent gene expression changes, we incorporated DESeq2 interaction term analysis. We used the design formula: design = ~ SLE_Health + Time_point + SLE_Health:Time_point. To assess whether including the interaction term improved the model, we performed a likelihood ratio test comparing this full model to a reduced model (design = ~ SLE_Health + Time_point). Gene expression with an adjusted *P* value ≤.05 in this test was considered to be significant based on both the time factor and the disease status. We identified enriched pathways through hypergeometric testing with the Kyoto Encyclopedia of Genes and Genomes (KEGG) database and defined significantly enriched pathways using a false discovery rate cutoff of < 0.05. We conducted data analysis using GraphPad Prism 10 software. We generated heatmaps with the ComplexHeatmap package in R, and created all other plots using either the ggplot2 package in R or GraphPad Prism 10 software. To validate our findings against external datasets, we generated a combined heatmap incorporating data from the GSE139360 dataset by Mistry et al [6]. Gene Set Variation Analysis (GSVA) scores were calculated for each intrinsic DEG cluster to assess functional implications across datasets. Two-way analysis of variance tests were performed on the GSVA scores to identify significant variations.

RESULTS

Neutrophils from healthy individuals and patients with SLE display different intrinsic transcriptomic profiles at baseline which, however, undergo similar changes over time

We conducted a PCA to characterise the overall transcriptomic profiles of neutrophils from healthy individuals and individuals with SLE following 0, 30, and 60 minutes of *ex vivo* culture. The PCA plot shows a distinct separation between healthy and SLE neutrophils primarily along the PC1 axis, highlighting intrinsic differences in their transcriptomic profiles. However, both groups follow similar trajectories over time along the PC2 axis (Fig 1).

This parallel progression suggests that, despite inherent differences, neutrophils from healthy individuals and individuals with SLE undergo comparable transcriptomic shifts over time. Guided by this observation, we used DESeq2 to identify DEGs,

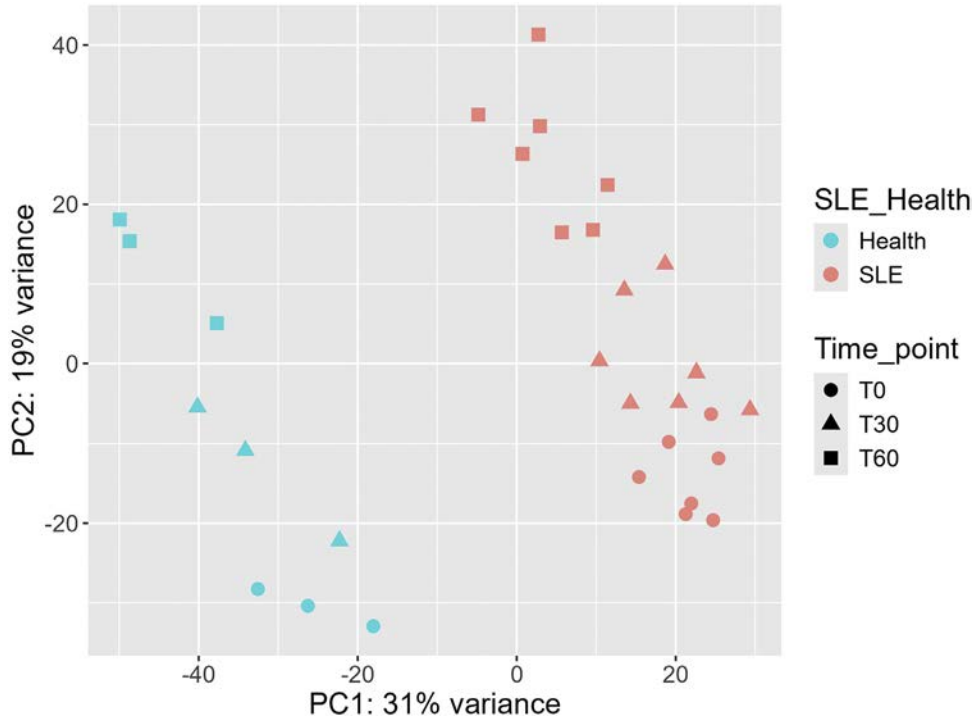

Figure 1. Principal component analysis (PCA). PCA was conducted on neutrophils from healthy individuals and individuals with SLE at 3 time points (0, 30, and 60 minutes). The PCA plot shows a clear separation between healthy and SLE samples along the PC1 axis, indicating intrinsic differences, and a progression along the PC2 axis representing longitudinal transcriptomic shifts. PC1, principal component 1; PC2, Principal component 2; SLE, systemic lupus erythematosus.

confirming that the time factor had no significant interaction with disease status. These findings indicate that the observed time-dependent changes in gene expression are independent of SLE, with both groups displaying similar patterns of transcriptional adaptation during *ex vivo* culture.

Intrinsic differences in neutrophil transcriptomics of healthy individuals and individuals with SLE

A Venn diagram was generated to illustrate the DEG patterns between neutrophils from healthy individuals and individuals with SLE across 3 time points: 0, 30, and 60 minutes (Supplementary Fig S2). The DEGs were identified using the thresholds of fold change > 2 and an adjusted *P* value <.01. This diagram reveals the overlapping and unique gene sets for each comparison. Notably, 262 DEGs were identified as common across all 3 time points, suggesting stable intrinsic differences in transcriptomic profiles between neutrophils from healthy individuals and individuals with SLE, regardless of *ex vivo* culture duration. Of these 262 DEGs, 4 genes were related to the Y chromosome and were excluded from future analyses, and the rest were referred to as intrinsic DEGs. To validate these findings, we compared SLE neutrophils (n = 7) to a group of healthy individuals (n = 7) at time 0, confirming that intrinsic DEG expression patterns remained consistent (Supplementary Fig S3).

To assess whether these intrinsic differences vary with disease activity, we examined their relationship with clinical parameters. Disease activity was measured using the SLE Disease Activity Index (SLEDAI) score for all patients. When patients were stratified into groups based on their SLEDAI scores, comparative analysis revealed no significant differences in neutrophil gene expression patterns between these groups (not shown). Similarly, when patients were grouped according to their medication regimens, no significant differences in transcriptomic profiles were observed between treatment groups (not shown). These findings further support that the observed transcriptomic differences reflect intrinsic disease-specific characteristics that remain stable regardless of clinical disease activity or therapeutic intervention.

We categorised the intrinsic DEGs into several clusters based on information from KEGG, Reactome, WikiPathways, Hallmark, and Gene Ontology (GO) databases. Our first 5 clusters included genes related to IFN signalling, Rho GTPase activity, cytoskeleton organisation, DNA damage repair, and ribosome function. We formed a sixth cluster from long noncoding RNAs (lncRNAs) and grouped the less well-characterised DEGs into a final cluster labelled 'other'. We generated heatmaps to display the expression patterns of these gene clusters across the 3 time points (Fig 2).

The first cluster (IFN-related genes) shows significant upregulation in patients with SLE compared with healthy individuals. The second and third clusters contain genes from the Rho GTPase and cytoskeleton gene sets, which regulate intracellular trafficking, cell migration, cell polarity, gene expression, and cell proliferation. These biological processes underpin essential immune functions such as cellular trafficking, phagocytosis, and antigen recognition [12,13]. The DNA damage repair gene set, which forms the next cluster, also exhibits upregulation in SLE samples, whereas the ribosome gene cluster shows downregulation in SLE neutrophils relative to healthy controls. In addition, the lncRNA cluster—which includes, among others, *JPX*, *FTX*, *NRIR*, *LINC02574*, and *IRF1-AS1*—displays higher expression in SLE samples. The 'other' cluster contains DEGs upregulated in SLE neutrophils that lack significant enrichment information in the databases we used. Based on a literature review, we further categorised several well-characterised genes from the 'other' cluster into 6 groups (Supplementary Fig S4 and Supplementary Table).

Comparison with an independent dataset [6] confirmed that the intrinsic transcriptomic differences we identified between healthy and SLE neutrophils are consistent with previous findings (Supplementary Fig S5). In addition, analysis of pathway

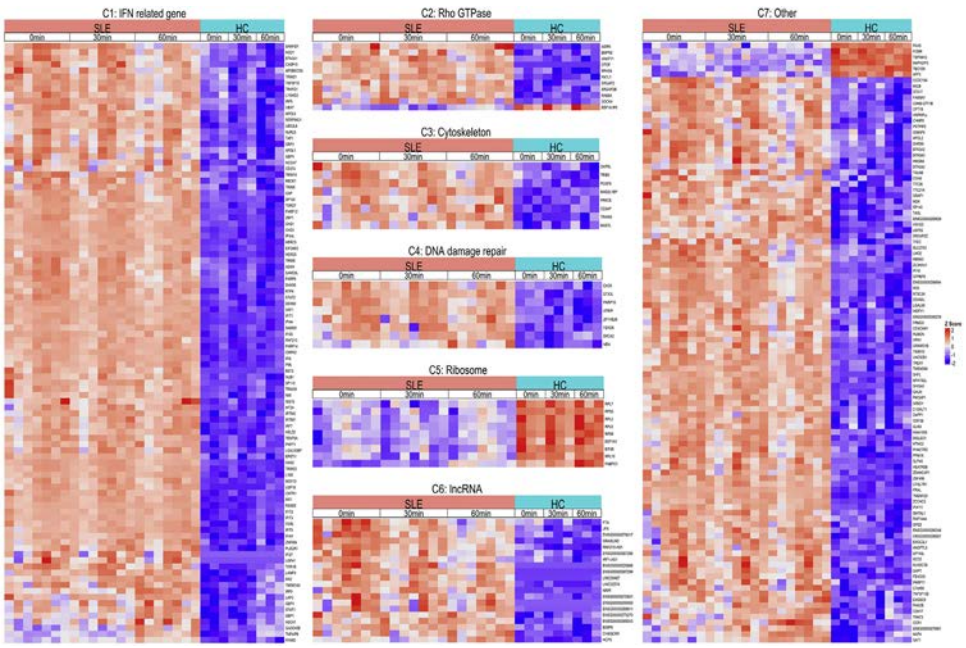

Figure 2. Clustered heatmap of intrinsic DEGs. Heatmap showing expression patterns of intrinsic DEGs categorised into 7 clusters including interferon-related, Rho GTPase, cytoskeleton, DNA damage repair, ribosome, and long noncoding RNA (lncRNA). The 'other' cluster includes genes with

activity through GSVA scores (Fig 3) revealed significant variations in functional pathways between healthy and SLE neutrophils. Notably, the IFN-related genes, along with other intrinsic gene clusters, maintained their differential expression patterns in SLE neutrophils throughout the culture adaptation period, suggesting that these transcriptomic alterations are long-lived and intrinsic to SLE neutrophils rather than simply reflecting their immediate inflammatory milieu.

Impact of time progression on transcriptomic profiles of neutrophils

We performed differential gene expression analyses on neutrophils from both healthy individuals and patients with SLE at 3 time points (0, 30, and 60 minutes) following *ex vivo* culture. Volcano plots (Supplementary Fig S6A) illustrate the DEGs for each pairwise comparison in both groups. These plots highlight genes that were significantly upregulated or downregulated over time in neutrophils from both healthy and SLE donors.

Venn diagrams further clarify the relationships among DEGs across the 3 time-point comparisons (Supplementary Fig S6B). In the first Venn diagram, each set (circle) represents the following comparisons of DEGs combining both healthy and SLE samples: (i) 0 vs 30, (ii) 0 vs 60 minutes, and (iii) 30 vs 60 minutes. The second and third Venn diagrams show these *ex vivo* time-dependent DEG patterns separately for healthy controls and patients with SLE. Although these latter diagrams appear to show different numbers of DEGs between healthy and SLE neutrophils over time, our statistical analysis revealed that, despite having different baseline transcriptional profiles, neutrophils from both groups undergo similar *ex vivo* adaptations in gene expression over time (except for the 3 genes of *BTG2*, *SEPTIN4*, and *GSTO2*).

We used heatmaps to visualise the DEGs that are common across groups (Fig 4A). Based on these heatmaps and Venn diagrams, we observed 3 main groups of gene expression changes: (i) genes that downregulate significantly from 0 to 30 minutes and continue in the same direction through 60 minutes, (ii) genes that upregulate significantly from 0 to 30 minutes and continue in the same direction through 60 minutes, and (iii) genes that mainly show significant changes in expression only between 30 and 60 minutes (Fig 4B).

To identify the biological processes affected by these changes, we performed KEGG pathway enrichment analysis on DEGs from each comparison group (Fig 4C). The first group showed no enrichment. The second group showed enrichment in multiple inflammatory pathways, including NF-κB, TNF, IL-17 signalling, and apoptosis. In the third group, while NF-κB signalling persisted, we observed a shift towards cell death-related processes, with significant enrichment in apoptosis, mitogen-activated protein kinase signalling, and longevity regulating pathways. A common feature is that neutrophils undergo activation and cell death over time following isolation, as indicated by the consistent activation of the NF-κB and apoptosis pathways [14]. This time-dependent progression from broad inflammatory response to focused activation and ultimately cell death pathways provides insights into neutrophil behaviour under *ex vivo* conditions, though we acknowledge these changes may partly reflect artificial activation due to isolation procedures and culture conditions.

Distinct DEGs in SLE neutrophils: cholesterol handling and immune function

Apart from the enrichment tests, some of the differences in intrinsic DEGs between healthy and SLE neutrophils are of particular interest. Among these, *ABCA1*, *MDK*, and *GRAMD1B*, which are involved in cholesterol metabolism, are worth mentioning. *GRAMD1B* is an IFN-I inducible gene that codes for a protein involved in the transport of high-density lipoprotein and low-density lipoprotein-derived cholesterol from the plasma membrane to the endoplasmic reticulum [15,16]. Conversely, ABCA1 is an integral plasma membrane protein that plays a major role in exporting excess cholesterol out of the cell [17]. MDK is involved in decreasing *ABCA1* expression, thus inhibiting the cholesterol efflux out of the cell [18]. Although all these

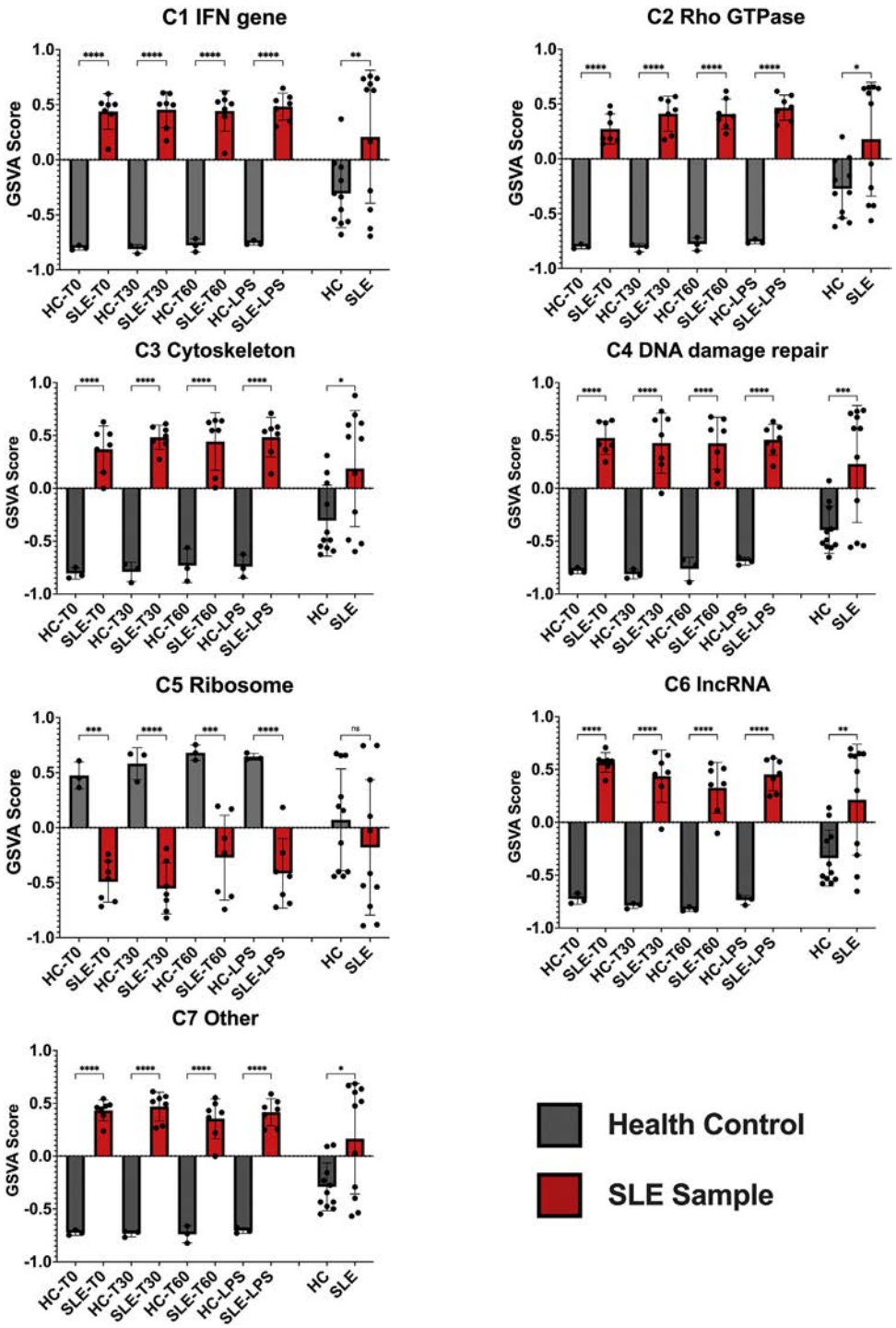

Figure 3. GSVA scores of intrinsic DEG clusters across datasets. GSVA scores calculated for each intrinsic DEG cluster, comparing pathway activities in neutrophils from healthy individuals and patients with SLE. Data from this study are displayed alongside corresponding GSVA scores from the GSE139360 dataset. Two-way ANOVA tests were used to compare the scores, revealing significant differences in clusters associated with intrinsic transcriptomic alterations in SLE neutrophils. ANOVA, analysis of variance; DEG, differentially expressed gene; GSVA, Gene Set Variation Analysis; GTPase, Guanosine Triphosphatases; HC, healthy control; lncRNA, long noncoding RNA; LPS, lipopolysaccharide; SLE, systemic lupus erythematosus.

genes are upregulated in neutrophils from patients with SLE compared with healthy individuals, *ABCA1* shows a markedly lower fold change than the other 2 genes, suggesting potential abnormalities in cholesterol metabolism of neutrophils from patients with SLE (Supplementary Fig S7). Further evidence suggesting altered cholesterol metabolism in patients with SLE neutrophils is the upregulation of *C7orf50*, which encodes the hormone Cholesin that functions to inhibit cholesterol synthesis in the liver [19].

To validate these transcriptomic findings, we performed qPCR analysis of *ABCA1*, *GRAMD1B*, and *MDK* expression in neutrophils from healthy controls and patients with SLE (Supplementary Fig S8A,B). At time 0, all 3 genes showed significantly higher expression in SLE neutrophils compared with healthy controls. This differential expression pattern persisted at 60 minutes of *ex vivo* culture, confirming the stability of these intrinsic transcriptomic differences.

Another gene of interest from the 'other' cluster is *TNFSF13B*, which encodes BAFF, a key player in SLE pathogenesis [20]. Quantitative analysis revealed significant upregulation of *TNFSF13B* (more than 2-fold) in neutrophils from patients with SLE compared with healthy individuals. Notably, this

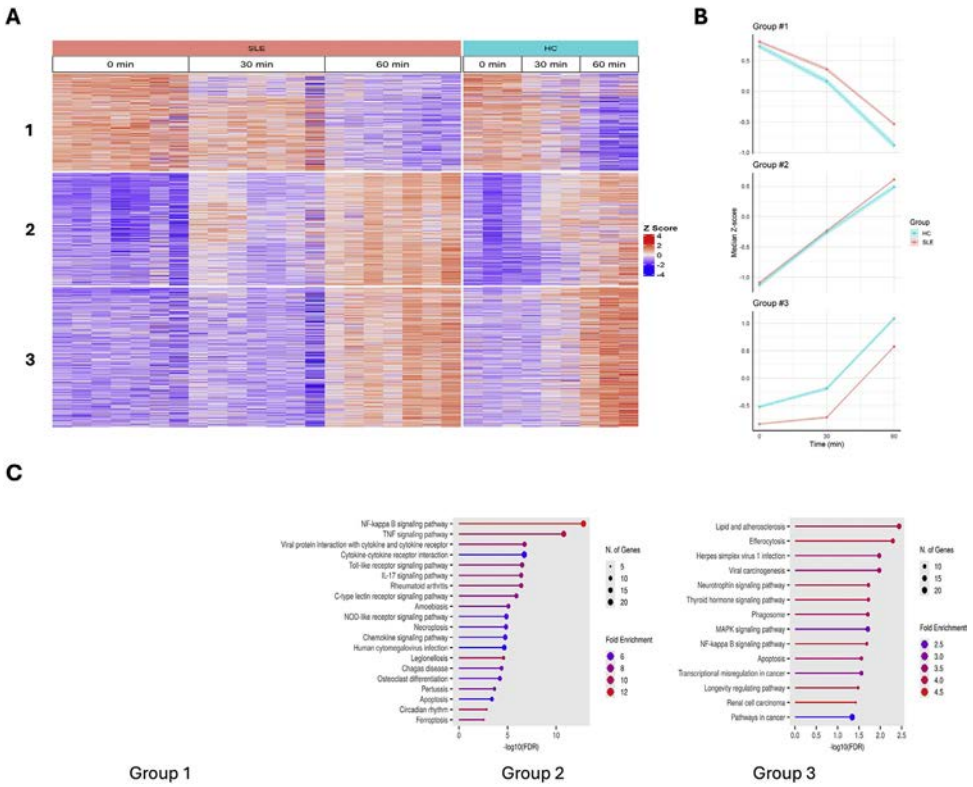

Figure 4. Heatmap of temporal transcriptomics in neutrophils and pathway enrichment analysis. (A) Heatmap displaying temporal transcriptomics of neutrophils categorised into 3 groups: (i) sustained downregulation from time 0 to 60 minutes, (ii) sustained upregulation from time 0 to 60 minutes, and (iii) changes only between 30 and 60 minutes. (B) Graphic conceptualisation of the 3 groups. (C) KEGG pathway enrichment analysis identifies key pathways impacted by time progression, including NF-κB activation, TNF signalling, and apoptosis, in neutrophils from both groups. HC, healthy control; KEGG, Kyoto Encyclopedia of Genes and Genomes; NF-κB, Nuclear Factor kappa-light-chain-enhancer of activated B cells; SLE, systemic lupus erythematosus; TNF, tumour necrosis factor.

upregulation was consistently maintained across all 3 time points examined, suggesting that it represents a stable intrinsic feature of SLE neutrophils.

To validate the *TNFSF13B* transcriptomic findings at the protein level, we measured BAFF concentrations in plasma from healthy controls (n = 3) and patients with SLE (n = 7). Plasma BAFF levels showed a trend towards elevation in patients with SLE compared with healthy controls (P = .0667; Supplementary Fig S9), consistent with a previous report demonstrating significantly elevated serum BAFF in patients with SLE [21]. To determine whether neutrophils directly contribute to BAFF secretion, we cultured neutrophils from an independent pool of healthy controls (n = 3) and patients with SLE (n = 12) for 18 hours with or without LPS stimulation. Both healthy and SLE neutrophils significantly increased BAFF secretion following LPS stimulation (Supplementary Fig S10), consistent with evidence that neutrophil activation promotes BAFF release [21]. However, baseline and LPS-stimulated BAFF secretion did not differ significantly between groups, despite the observed transcriptional upregulation in SLE neutrophils. This discordance between mRNA and secreted protein levels suggests post-transcriptional regulation of BAFF production, potentially involving retention of membrane-bound BAFF or differences in protein processing and release. In addition, the elevated plasma BAFF observed in SLE likely reflects contributions from multiple cellular sources beyond neutrophils.

MICB is another upregulated gene in neutrophils of patients with SLE. It is upregulated under cellular stress and DNA damage and can tag cells for elimination by natural killer cells [22]. This suggests that neutrophil elimination and the release of their cellular contents may continuously occur in SLE. Among the IFN-related gene cluster, *MOV10*, which can act as an autoantigen in SLE [23], is upregulated in neutrophils of patients with SLE compared with healthy individuals.

LPS induces a common inflammatory response in neutrophils while preserving SLE-specific transcriptional differences

Given the elevated interferon signature in SLE neutrophils, we hypothesised that these cells might exhibit an altered response to pathogen-associated molecular patterns compared with healthy controls. To test this hypothesis, neutrophils from both healthy donors and patients with SLE were stimulated with LPS, followed by transcriptomic analysis to detect LPS-induced gene expression changes. Surprisingly, the analysis revealed that both groups shared a common set of DEGs in response to LPS, including classic inflammatory genes such as *IL1B*, *CXCL2*, *TNF*, and *CCL20*.[24–27]. To visualise these transcriptional changes, we generated a heatmap incorporating both the LPS-induced DEGs and the SLE-specific DEGs, illustrating the common inflammatory response as well as the persistence of disease-specific transcriptional signatures (Fig 5A).

To further investigate the pathways activated by LPS, we performed KEGG and GO enrichment analyses on the DEGs identified in both healthy and SLE neutrophils in response to LPS (Fig 5B,C). KEGG pathway analysis revealed significant enrichment of inflammatory and immune-related pathways, including TNF signalling, NF-κB activation, and IL-17 signalling, consistent with a robust inflammatory response to LPS. Similarly, GO biological process (GO:BP) analysis highlighted inflammatory

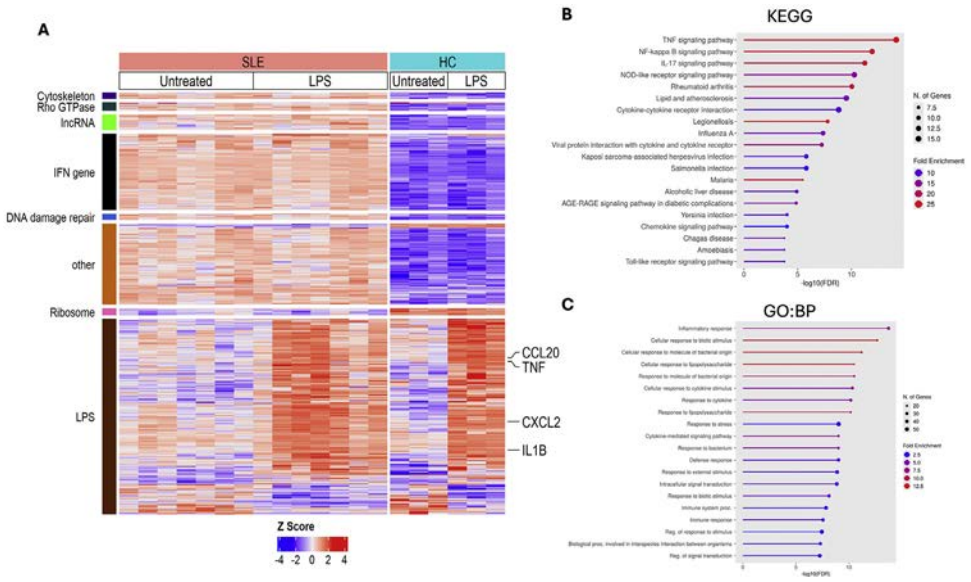

Figure 5. Impact of LPS stimulation on neutrophil transcriptomics. (A) Heatmap displaying shared inflammatory response genes induced by LPS stimulation in neutrophils from both healthy individuals and individuals with SLE (labelled as 'LPS'), along with the persistence of intrinsic transcriptional differences between neutrophils from both groups (organised in clusters: cytoskeleton, Rho GTPase, lncRNA, IFN genes, DNA damage repair, other, and ribosome) despite LPS treatment. (B) KEGG pathway analysis of LPS-induced DEGs, showing enrichment of key inflammatory pathways such as TNF and NF-κB signalling. (C) GO biological process (GO:BP) analysis reveals significant enrichment of inflammatory and immune response pathways following LPS stimulation. CCL2, C-C motif chemokine ligand 2; DEG, differentially expressed gene; FDR, false discovery rate; GTPase, Guanosine Triphosphatases; HC, healthy control; IFN, interferon; IL, Interleukin; IL-17, Interleukin-17; IL1B, Interleukin-1β; KEGG, Kyoto Encyclopedia of Genes and Genomes; lncRNA, long noncoding RNA; NF-κB, Nuclear Factor kappa-light-chain-enhancer of activated B cells; NOD, Nucleotide-binding Oligomerization Domain; LPS, lipopolysaccharide; SLE, systemic lupus erythematosus; TNF, tumour necrosis factor.

response, cellular response to biotic stimulus, and LPS as key processes induced by LPS in both groups. These findings indicate that LPS elicits a shared proinflammatory transcriptional programme in neutrophils, regardless of disease status.

Despite this common response to LPS, we observed that the intrinsic transcriptional differences that distinguish SLE from healthy neutrophils remained intact with minimal response to LPS, further supporting the idea that lupus-associated transcriptional alterations persist even in the presence of external inflammatory stimuli. qPCR validation of key inflammatory genes (*IL8*, *IL1B*, and *TNF*) following LPS stimulation confirmed comparable expression levels between healthy and SLE neutrophils, with no significant differences observed between groups (Supplementary Fig S8C). These results corroborate our transcriptomic findings demonstrating preserved inflammatory responsiveness in SLE neutrophils.

Longitudinal impact of CAR T-cell therapy on intrinsic transcriptomic profiles in neutrophils of patient with SLE

To investigate the longitudinal impact of CD19 CAR T-cell therapy on intrinsic DEGs in neutrophils, we analysed data from a patient with SLE undergoing this treatment. The patient, who had a SLEDAI score of 17 before treatment, received CD19 CAR T-cell therapy in 2024 (day 0). Notably, by 4 months posttreatment, the patient's SLEDAI score had decreased to 4, indicating significant clinical improvement. Moreover, by month 5 postinfusion, the patient was off any immunosuppressive therapy (Supplementary Fig S11A).

A heatmap was generated to visualise the expression patterns of the previously identified intrinsic DEGs in the patient's neutrophils at baseline (pretreatment) and multiple time points posttreatment: day 3, day 7, day 14, day 21, day 28, day 56, month 3, and month 5. For reference, neutrophil samples from 3 healthy individuals were included, allowing for a direct comparison between healthy controls and the patient at various stages posttreatment (Fig 6A).

The heatmap clusters genes according to the same pathway-based enrichment categories identified earlier in our analysis, providing insight into how those intrinsic DEGs evolve over time in response to CD19 CAR T-cell therapy. At baseline, the patient's neutrophil transcriptome differed markedly from healthy controls, with upregulation of interferon, DNA damage repair, Rho GTPase, cytoskeleton, lncRNA, and other gene clusters, whereas ribosomal structural protein genes were downregulated. Following therapy, we observed modest changes in gene expression during the first 2 months, but a substantial transition began around 3 months, with the neutrophil expression profile at month 3 and month 5 closely resembling that of healthy controls across most gene clusters.

To provide a more quantitative assessment of these longitudinal changes, GSVA scores were calculated for each time point in the CD19 CAR T-cell therapy patient, based on the same gene clusters used in previous analyses (Fig 6B). The GSVA plot provides a quantitative view of pathway activity changes over time. As shown in the figure, following initial CAR T-cell therapy, we observed some fluctuation in pathway scores during the first month, followed by a consistent trend towards healthy control values across most gene clusters by month 3. This gradual normalisation timeline is consistent with a progressive immune reset process. Except for the ribosome cluster, the gene expression levels in all other clusters resembled those of healthy controls by 3 months posttherapy.

To complement these findings, further analysis confirmed profound B cell depletion following therapy, with CD19+ B cell counts dropping from approximately 2000 cells/μL pretreatment to near-undetectable levels postinfusion and remaining depleted throughout the follow-up period (Supplementary Fig S11B). Notably, the timeline of neutrophil transcriptomic normalisation—becoming evident by month 3—occurred well after

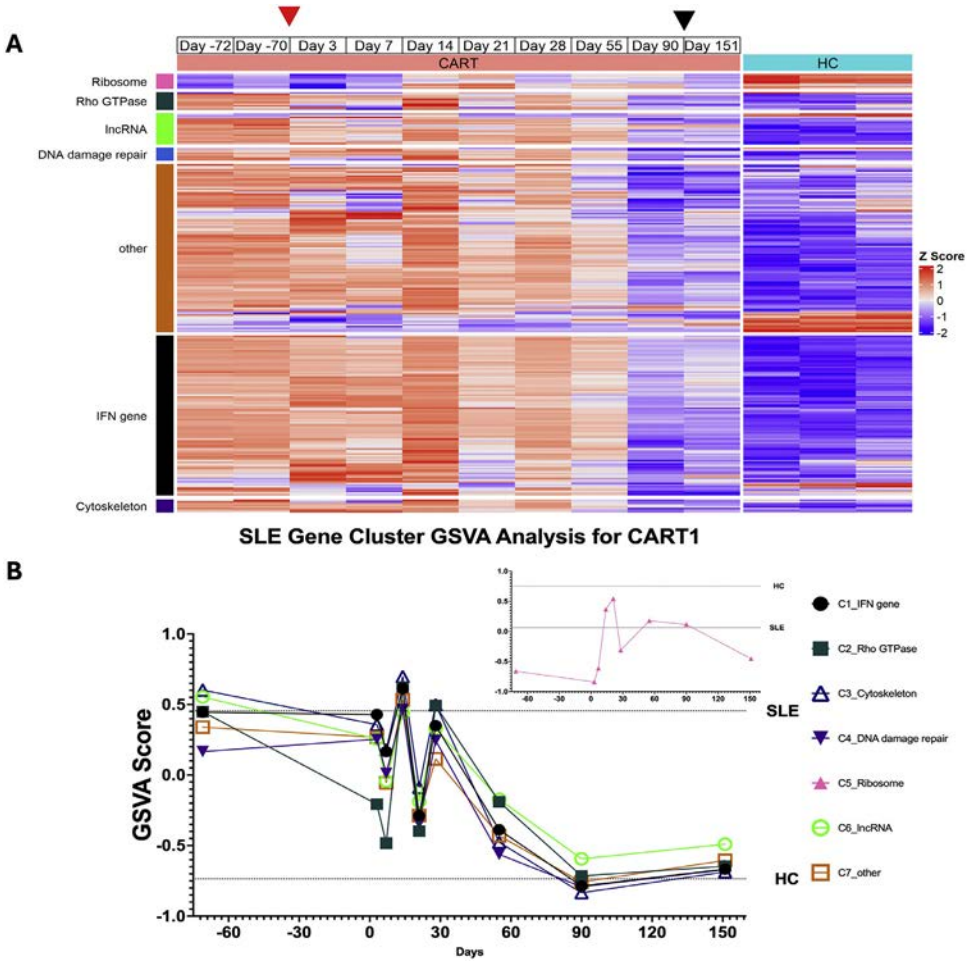

Figure 6. Longitudinal transcriptomic and GSVA score analysis post-CAR-T-cell therapy. (A) Heatmap visualising intrinsic DEG expression in a patient with SLE undergoing CAR T-cell therapy across baseline (2 pretreatment time points) and 8 posttreatment time points. Samples from 3 healthy individuals serve as controls. Red arrowhead indicates day 0 (CAR T-cell infusion) and black arrowhead marks when the patient discontinued all immunosuppressive medications. (B) GSVA plots showing pathway activity for intrinsic DEG clusters across time points in the CAR T-cell therapy patient. The analysis reveals dynamic transcriptomic reprogramming, with most clusters approaching healthy transcriptomic profiles by 3 months posttreatment. CAR, chimeric antigen receptor; DEG, differentially expressed gene; GSVA, Gene Set Variation Analysis; GTPase, Guanosine Triphosphatases; HC, healthy control; IFN, interferon; lncRNA, long noncoding RNA; SLE, systemic lupus erythematosus.

B cell depletion was established. qPCR analysis of select intrinsic DEGs (*ABCA1*, *GRAMD1B*, and *MDK*) in the CAR T-cell therapy patient revealed decreased expression at 3 to 5 months postinfusion compared with pretreatment levels (Supplementary Fig S8D). These findings provide additional validation for the transcriptomic reset observed following therapy.

DISCUSSION

This study provides a comprehensive investigation into the transcriptomic landscape of neutrophils in SLE, offering several novel insights that extend beyond previous work in this field.

By employing a refined neutrophil isolation technique and examining *ex vivo* transcriptomic adaptations over time, we have introduced an approach that, to the best of our knowledge, has not been previously utilised in SLE neutrophil research. Although previous studies have examined neutrophil transcriptomics in SLE [2,6], our work presents 3 key innovations: (i) the assessment of transcriptomic stability during *ex vivo* adaptation, allowing discrimination between intrinsic versus microenvironment-induced differences; (ii) the evaluation of functional responses to LPS stimulation alongside disease-specific signatures; and (iii) the first longitudinal analysis of neutrophil transcriptomic changes following CD19 CAR T-cell therapy in a patient with SLE.

Our findings revealed that neutrophils from both healthy and SLE groups exhibited remarkably similar and rapid transcriptional adaptation patterns during culture. This parallel behaviour in response to *ex vivo* conditions suggests that, despite disease status and ongoing therapy, SLE neutrophils retain many core functional capabilities similar to healthy controls. Both populations showed coordinated activation of key pathways including NF-κB signalling, inflammatory responses, and regulated progression towards apoptosis. Although these shared responses demonstrate the preservation of essential neutrophil functions in SLE despite disease-specific differences, they also highlight the challenges of maintaining neutrophil stability *ex vivo* and underscore the importance of rapid processing in transcriptomic studies [28].

Our findings also revealed that while healthy and SLE neutrophils can exhibit similar transcriptomic changes in response to time, there are intrinsic DEGs between the 2 groups that remain consistently different regardless of the *in vitro* culture duration. These persistent DEGs likely reflect fundamental differences in the baseline biology of neutrophils from healthy individuals and individuals with SLE and possibly also reflect the disease vs health status, irrespective of the disease activity. These genes

were categorised into several clusters, each providing unique insights into SLE pathogenesis. The upregulation of interferon-related genes in SLE neutrophils aligns with the established role of interferons in SLE pathogenesis [29]. This finding reinforces the critical importance of interferon signalling in the molecular mechanism of the disease.

Apart from interferon-related genes, differences in other functional gene clusters were observed between neutrophils from patients with SLE and controls. The upregulation of most Rho GTPase and cytoskeleton gene sets in SLE neutrophils may be due to the aberrant neutrophil activation in patients with SLE [30]. Increased expression of DNA damage repair genes in neutrophils from patients with SLE may reflect efforts by the cells to repair DNA damage caused by various factors, such as elevated levels of ROS [30−32]. The downregulation of ribosomal structural protein gene expression may result from the metabolic reprogramming of cells under immunological stress, which redirects their transcriptomic machinery towards the production of inflammatory genes rather than housekeeping ones [33−35].

JPX and *FTX* are 2 of the lncRNAs involved in X chromosome inactivation by upregulating the expression of *Xist* [36]. Despite the increased expression of *JPX* and *FTX* in our dataset, the level of *Xist* does not show a significant difference between neutrophils from healthy individuals and those with SLE. However, *Tasl* (categorised in 'other' cluster), an X-linked member of the TLR7-9 pathway, is consistently upregulated in SLE neutrophils compared with healthy individuals, suggesting abnormal X chromosome inactivation in neutrophils of patients with SLE similar to their T cells and B cells, as shown by previous studies [37−39]. *NRIR*, *LINC02574* and *IRF1-AS1* are also among the lncRNA cluster and are considered interferon-stimulated genes, which are expected to be upregulated in SLE [29,40−42]. Interestingly, *IRF1-AS1* depletion in HeLa cells resulted in increased expression of *Xist* [42]. Thus, the overexpression of this gene in neutrophils from patients with SLE might contribute to altered X chromosome inactivation and may explain why *Xist* is not upregulated despite the increased expression of *JPX* and *FTX* lncRNAs.

Comparing our intrinsic DEGs with the previous study by Mistry et al [6] (Fig 3 and Supplementary Fig S5) confirms the presence of most of the intrinsic DEGs between healthy and patient neutrophils in their dataset as well. However, the GSVA score difference between healthy individuals and individuals with SLE regarding intrinsic DEGs clusters is less in their dataset, which may be attributed to the neutrophil purification method using density gradient medium, which inadvertently results in more neutrophil activation compared with using negative selection by magnetic beads [28]. The GSVA scores of ribosome cluster in Mistry et al [6] datasets did not show a significant difference between healthy individuals and individuals with SLE, possibly due to patients' heterogenicity.

Correlation analysis between GSVA scores for our intrinsic DEG clusters and previously identified interferon-stimulated gene (ISG) [43] GSVA scores in SLE samples revealed a fundamental distinction between neutrophils and other immune cells (Supplementary Fig S12). Although the IFN-related cluster (C1) showed significant ISG correlation in neutrophils, clusters C2-C6—representing Rho GTPase, ribosome, cytoskeleton, DNA damage repair, and lncRNA—showed no significant ISG correlation in our neutrophil dataset. In contrast, these same clusters exhibited highly significant ISG correlations across peripheral blood mononuclear cells (GSE50772) [44], whole blood (SRP136102) [45], and B cells (SRP156583) [46]. This IFN-independent pattern of dysregulation in multiple functional pathways distinguishes neutrophil contributions to SLE pathogenesis from the predominantly IFN-driven dysfunction observed in other immune cells, suggesting unique neutrophil-specific mechanisms.

An important consideration in SLE neutrophil research is the role of low-density granulocytes (LDGs), a distinct proinflammatory neutrophil subset that colocalises with peripheral blood mononuclear cells after density gradient centrifugation [47,48]. LDGs in SLE display prominent type I interferon signatures, enhanced spontaneous NETosis, increased production of proinflammatory cytokines, and impaired phagocytic capacity [5,6,47]. Given that LDGs represent a significant proportion of circulating neutrophils in patients with SLE, particularly those with active disease [6,48], the intrinsic transcriptomic differences we identified likely reflect contributions from both LDG and normal-density neutrophil populations.

Our LPS stimulation experiment revealed that both healthy and SLE neutrophils demonstrated overlapping inflammatory responses, as evidenced by the upregulation of common inflammatory genes. Importantly, while LPS induced substantial transcriptional changes in both groups, the intrinsic disease-specific signatures that distinguish SLE neutrophils remained intact. This indicates that the mechanisms controlling the SLE-specific gene expression operate independently from pathways responding to infectious stimuli. The coexistence of these parallel inflammatory mechanisms could potentially lead to enhanced tissue damage during infectious challenges, which may help explain the increased risk of complications that patients with SLE face during infections [49].

The longitudinal analysis of a patient with SLE undergoing CD19 CAR T-cell therapy provided unique insights into neutrophil transcriptomic recovery. The gene expression patterns did not immediately normalise after treatment, indicating that neutrophil transcriptomes may require some time to realign with healthy profiles, highlighting the importance of lupus epigenetics [6,50]. By 3 months posttherapy, most gene clusters approached healthy neutrophil characteristics, suggesting a gradual immunological reset. The temporal dissociation between rapid B cell depletion and gradual neutrophil transcriptomic normalisation suggests that the resetting of innate immune gene expression requires time for systemic immunological recalibration following elimination of autoreactive B cells. Notably, this therapeutic approach highlights the interconnectedness of adaptive and innate immune dysfunction in SLE, as evidenced by changes in neutrophil gene expression following CD19-targeted intervention. This study, while only in a single patient, also reveals how anti-CD19 CAR T-cell therapy can drive durable remission through deep B cell depletion to broadly reset the immune system to patterns seen in healthy individuals.

Our study introduces several methodological advances. By utilising negative selection for neutrophil isolation, we minimised potential activation artefacts common in traditional isolation techniques. This approach also enabled the uniform isolation of all neutrophils, regardless of their density. Furthermore, the examination of transcriptomic patterns during *ex vivo* adaptation, complemented by LPS stimulation experiments, offers a more comprehensive and dynamic understanding of neutrophil behaviour in SLE.

While our study offers valuable insights, several limitations should be acknowledged. The relatively small sample size and focus on a single CD19 CAR T-cell therapy patient suggest the need for larger and more comprehensive studies. In addition, while our transcriptomic analysis identified differential expression of cholesterol metabolism genes (*ABCA1*, *MDK*, and

GRAMD1B), functional validation through direct cholesterol measurements was not performed. Future research could explore the functional implications of the identified transcriptomic differences and investigate potential therapeutic interventions targeting these molecular pathways.

CONCLUSION

This comprehensive transcriptomic analysis of neutrophils in SLE unveils complex molecular alterations that contribute to our understanding of the disease's pathogenesis. By highlighting intrinsic differences, time-dependent shifts, and inflammatory responses, our study provides a foundation for a deeper understanding of neutrophil involvement in SLE pathogenesis and highlights potential avenues for therapeutic intervention. Finally, our longitudinal analysis of neutrophil transcriptomes following anti-CD19 CAR T-cell therapy, though limited to a single patient, provides compelling evidence of immune reset beyond the targeted B cell compartment, with neutrophil gene expression profiles normalising towards healthy patterns by 3 months posttreatment. This finding suggests that targeted immunotherapy can induce systemic immune reprogramming and restore normal gene expression in innate immune cells, offering a potential explanation for the durable remissions observed with CAR T-cell therapy in SLE.

Acknowledgements

We thank Ricardo Grieshaber-Bouyer for the constructive criticisms. We also sincerely thank the patients and their families who generously contributed to the study and allowed us to use samples and data for this work.

Contributors

ED contributed to methodology, investigation, analysis, data curation, and manuscript drafting. GH and MTI contributed to methodology, investigation, and data curation. LW contributed to data curation and manuscript editing. SG, DB, MG, and GS reviewed and edited the manuscript. SG and RC supervised the study. RC conceptualised the project, secured funding, and oversaw the project. All authors reviewed and approved the final manuscript for submission.

Funding

The work of GS is supported by the Lupus Insight Award from the Lupus Research Alliance and the Deutsche Forschungsgemeinschaft (DFG) through the Leibniz Award (GS) and the CRC1755 (CASCAID 550296805).

Competing interests

All authors declare that they have no competing interests.

Patient consent for publication

Not applicable.

Ethics approval

Written informed consent was obtained from all participants with approval from the research ethics committee of the institutional review board at UMass Chan Medical School.

Provenance and peer review

Not commissioned; externally peer reviewed.

Declaration of generative AI and AI-assisted technologies in the writing process

During the preparation of this work, the authors used Claude AI in order to improve the readability of the text. After using this tool/service, the authors reviewed and edited the content as needed and take full responsibility for the content of the publication.

ORCID iDs

Ehsan Dehdashtian http://orcid.org/0009-0001-2956-6820
Guangnan Hu http://orcid.org/0000-0003-1570-6770
Leah Whiteman http://orcid.org/0009-0001-2297-5998
Stefania Gallucci http://orcid.org/0000-0003-4737-8003
Manuel Garber http://orcid.org/0000-0001-8732-1293
Dominic Borie http://orcid.org/0009-0008-3569-2576
Georg Schett http://orcid.org/0000-0001-8740-9615
Roberto Caricchio http://orcid.org/0000-0002-1379-1118

Supplementary materials

Supplementary material associated with this article can be found in the online version at doi:10.1016/j.ard.2026.02.013.

REFERENCES

[1] Jung J-Y, Suh C-H. Infection in systemic lupus erythematosus, similarities, and differences with lupus flare. Korean J Intern Med 2017;32(3):429–38.
[2] Gupta S, Kaplan MJ. Bite of the wolf: innate immune responses propagate autoimmunity in lupus. J Clin Invest 2021;131(3):e144918.
[3] Villanueva E, Yalavarthi S, Berthier CC, Hodgin JB, Khandpur R, Lin AM, et al. Netting neutrophils induce endothelial damage, infiltrate tissues, and expose immunostimulatory molecules in systemic lupus erythematosus. J Immunol 2011;187(1):538–52.
[4] Palanichamy A, Bauer JW, Yalavarthi S, Meednu N, Barnard J, Owen T, et al. Neutrophil-mediated IFN activation in the bone marrow alters B cell development in human and murine systemic lupus erythematosus. J Immunol 2014;192(3):906–18.
[5] Denny MF, Yalavarthi S, Zhao W, Thacker SG, Anderson M, Sandy AR, et al. A distinct subset of proinflammatory neutrophils isolated from patients with systemic lupus erythematosus induces vascular damage and synthesizes type I IFNs. J Immunol 2010;184(6):3284–97.
[6] Mistry P, Nakabo S, O'Neil L, Goel RR, Jiang K, Carmona-Rivera C, et al. Transcriptomic, epigenetic, and functional analyses implicate neutrophil diversity in the pathogenesis of systemic lupus erythematosus. Proc Natl Acad Sci U S A 2019;116(50):25222–8.
[7] Schett G, Müller F, Taubmann J, Mackensen A, Wang W, Furie RA, et al. Advancements and challenges in CAR T cell therapy in autoimmune diseases. Nat Rev Rheumatol 2024;20(9):531–44.
[8] Müller F, Hagen M, Wirsching A, Kharboutli S, Aigner M, Völkl S, et al. CD19 CAR-T cells for treatment-refractory autoimmune diseases: the phase 1/2 CASTLE basket trial. Nat Med 2026.
[9] Aringer M, Costenbader K, Daikh D, Brinks R, Mosca M, Ramsey-Goldman R, et al. 2019 European League Against Rheumatism/American College of Rheumatology classification criteria for systemic lupus erythematosus. Arthritis Rheumatol 2019;71(9):1400–12.
[10] Kamoshida G, Kikuchi-Ueda T, Nishida S, Tansho-Nagakawa S, Kikuchi H, Ubagai T, et al. Spontaneous formation of neutrophil extracellular traps in serum-free culture conditions. FEBS Open Bio 2017;7(6):877–86.
[11] Love MI, Huber W, Anders S. Moderated estimation of fold change and dispersion for RNA-seq data with DESeq2. Genome Biol 2014;15(12):550.
[12] El Masri R, Delon J. RHO GTPases: from new partners to complex immune syndromes. Nat Rev Immunol 2021;21(8):499–513.
[13] Shih Y-L, Rothfield L. The bacterial cytoskeleton. Microbiol Mol Biol Rev 2006;70(3):729–54.

[14] Su VY-F, Lin C-S, Hung S-C, Yang K-Y. Mesenchymal stem cell-conditioned medium induces neutrophil apoptosis associated with inhibition of the NF-κB pathway in endotoxin-induced acute lung injury. Int J Mol Sci 2019;20 (9):2208.
[15] Esposito F, Osiceanu AM, Sorosina M, Ottoboni L, Bollman B, Santoro S, et al. A Whole-Genome Sequencing Study Implicates GRAMD1B in multiple sclerosis susceptibility. Genes (Basel) 2022;13(12):2392.
[16] Jonas K, Prinz F, Ferracin M, Krajina K, Deutsch A, Madl T, et al. MiR-4646-5p acts as a tumor-suppressive factor in triple negative breast cancer and targets the cholesterol transport protein GRAMD1B. Noncoding RNA 2023;10(1):2.
[17] Liu Y, Tang C. Regulation of ABCA1 functions by signaling pathways. Biochim Biophys Acta 2012;1821(3):522–9.
[18] Ou HX, Huang Q, Liu CH, Xiao J, Lv YC, Li X, et al. Midkine inhibits cholesterol efflux by decreasing ATP-binding membrane cassette transport protein A1 via adenosine monophosphate-activated protein kinase/mammalian target of rapamycin signaling in macrophages. Circ J 2020;84(2):217–25.
[19] Hu X, Chen F, Jia L, Long A, Peng Y, Li X, et al. A gut-derived hormone regulates cholesterol metabolism. Cell 2024;187(7):1685–700 e18.
[20] Möckel T, Basta F, Weinmann-Menke J, Schwarting A. B cell activating factor (BAFF): structure, functions, autoimmunity and clinical implications in systemic lupus erythematosus (SLE). Autoimmun Rev 2021;20 (2):102736.
[21] Wang T, Vasconcellos A, Marken J, Skopelja-Gardner S, Lood C, Giltiay NV. Immune complex-driven neutrophil activation and BAFF release: a link to B cell responses in SLE. Lupus Sci Med 2022;9(1):e000709.
[22] Ferrari de Andrade L, Tay RE, Pan D, Luoma AM, Ito Y, Badrinath S, et al. Antibody-mediated inhibition of MICA and MICB shedding promotes NK cell–driven tumor immunity. Science 2018;359(6383):1537–42.
[23] Ukadike KC, Colyer AN, Duvvuri B, Bengtsson AA, Taylor MS, LaCava J, et al. Multiple RNA-binding proteins associated with long interspersed element-1 encoded ORF1p are targeted by the autoimmune response in systemic lupus erythematosus. J Cell Mol Immunol 2023;2(1):35–44.
[24] Scapini P, Laudanna C, Pinardi C, Allavena P, Mantovani A, Sozzani S, et al. Neutrophils produce biologically active macrophage inflammatory protein-3alpha (MIP-3alpha)/CCL20 and MIP-3beta/CCL19. Eur J Immunol 2001;31 (7):1981–8.
[25] Chen KW, Groß CJ, Sotomayor FV, Stacey KJ, Tschopp J, Sweet MJ, et al. The neutrophil NLRC4 inflammasome selectively promotes IL-1β maturation without pyroptosis during acute Salmonella challenge. Cell Rep 2014;8 (2):570–82.
[26] Sawant KV, Sepuru KM, Lowry E, Penaranda B, Frevert CW, Garofalo RP, et al. Neutrophil recruitment by chemokines Cxcl1/KC and Cxcl2/MIP2: role of Cxcr2 activation and glycosaminoglycan interactions. J Leukoc Biol 2021;109(4):777–91.
[27] Xing Z, Kirpalani H, Torry D, Jordana M, Gauldie J. Polymorphonuclear leukocytes as a significant source of tumor necrosis factor-alpha in endotoxin-challenged lung tissue. Am J Pathol 1993;143(4):1009–15.
[28] Blanter M, Cambier S, De Bondt M, Vanbrabant L, Pörtner N, Abouelasrar Salama S, et al. Method matters: effect of purification technology on neutrophil phenotype and function. Front Immunol 2022;13:820058.
[29] Caielli S, Wan Z, Pascual V. Systemic lupus erythematosus pathogenesis: interferon and beyond. Annu Rev Immunol 2023;41(1):533–60.
[30] Fresneda Alarcon M, McLaren Z, Wright HL. Neutrophils in the pathogenesis of rheumatoid arthritis and systemic lupus erythematosus: same foe different M.O. Front Immunol 2021;12:649693.
[31] Elloumi N, Ben Mansour R, Marzouk S, Mseddi M, Fakhfakh R, Gargouri B, et al. Differential reactive oxygen species production of neutrophils and their oxidative damage in patients with active and inactive systemic lupus erythematosus. Immunol Lett 2017;184:1–6.
[32] Hemnani T, Parihar MS. Reactive oxygen species and oxidative DNA damage. Indian J Physiol Pharmacol 1998;42(4):440–52.
[33] McCormick C, Khaperskyy DA. Translation inhibition and stress granules in the antiviral immune response. Nat Rev Immunol 2017;17(10):647–60.
[34] Sun L, Yang X, Yuan Z, Wang H. Metabolic reprogramming in immune response and tissue inflammation. Arterioscler Thromb Vasc Biol 2020;40 (9):1990–2001.
[35] Thorrez L, Van Deun K, Tranchevent LC, Van Lommel L, Engelen K, Marchal K, et al. Using ribosomal protein genes as reference: a tale of caution. PLoS One 2008;3(3):e1854.
[36] Soma M, Fujihara Y, Okabe M, Ishino F, Kobayashi S. Ftx is dispensable for imprinted X-chromosome inactivation in preimplantation mouse embryos. Sci Rep 2014;4(1):5181.
[37] Lovell CD, Jiwrajka N, Amerman HK, Cancro MP, Anguera M. Xist deletion in B cells results in systemic lupus erythematosus phenotypes. bioRxiv:2024.05.15.594175 [cited 2025 Aug 10]. 2024. Available from: https://www.biorxiv.org/content/10.1101/2024.05.15.594175v1
[38] Syrett CM, Paneru B, Sandoval-Heglund D, Wang J, Banerjee S, Sindhava V, et al. Altered X-chromosome inactivation in T cells may promote sex-biased autoimmune diseases. JCI insight 2019;4(7):e126751.
[39] Heinz LX, Lee J, Kapoor U, Kartnig F, Sedlyarov V, Papakostas K, et al. TASL is the SLC15A4-associated adaptor for IRF5 activation by TLR7–9. Nature 2020;581(7808):316–22.
[40] Shen M, Duan C, Xie C, Wang H, Li Z, Li B, et al. Identification of key interferon-stimulated genes for indicating the condition of patients with systemic lupus erythematosus. Front Immunol 2022;13:962393.
[41] Zhang Y, Chi X, Hu J, Wang S, Zhao S, Mao Y, et al. LncRNA LINC02574 inhibits influenza A virus replication by positively regulating the innate immune response. Int J Mol Sci 2023;24(8):7248.
[42] Barriocanal M, Prats-Mari L, Razquin N, Prior C, Unfried JP, Fortes P. ISR8/IRF1-AS1 is relevant for IFNα and NF-κB responses. Front Immunol 2022;13:829335.
[43] Yao Y, Higgs BW, Morehouse C, de Los, Reyes M, Trigona W, Brohawn P, et al. Development of potential pharmacodynamic and diagnostic markers for anti-IFN-α monoclonal antibody trials in systemic lupus erythematosus. Hum Genomics Proteomics 2009:374312 2009.
[44] Kennedy WP, Maciuca R, Wolslegel K, Tew W, Abbas AR, Chaivorapol C, et al. Association of the interferon signature metric with serological disease manifestations but not global activity scores in multiple cohorts of patients with SLE. Lupus Sci Med 2015;2(1):e000080.
[45] Oon S, Monaghan K, Ng M, Hoi A, Morand E, Vairo G, et al. A potential association between IL-3 and type I and III interferons in systemic lupus erythematosus. Clin Transl Immunology 2019;8(12):e01097.
[46] Scharer CD, Blalock EL, Mi T, Barwick BG, Jenks SA, Deguchi T, et al. Epigenetic programming underpins B cell dysfunction in human SLE. Nat Immunol 2019;20(8):1071–82.
[47] Carmona-Rivera C, Kaplan MJ. Low-density granulocytes: a distinct class of neutrophils in systemic autoimmunity. Sem immunopathol 2013;35(4):455–63.
[48] Tay SH, Celhar T, Fairhurst AM. Low-density neutrophils in systemic lupus erythematosus. Arthritis Rheumatol 2020;72(10):1587–95.
[49] Danza A, Ruiz-Irastorza G. Infection risk in systemic lupus erythematosus patients: susceptibility factors and preventive strategies. Lupus 2013;22 (12):1286–94.
[50] Ostuni R, Natoli G, Cassatella MA, Tamassia N. Epigenetic regulation of neutrophil development and function. Sem immunol 2016;28(2):83–93.

Ann Rheum Dis 85 (2026) 1582–1595

Contents lists available at ScienceDirect

Annals of the Rheumatic Diseases

journal homepage: https://www.sciencedirect.com/journal/annals-of-the-rheumatic-diseases

Systemic lupus erythematosus

A pathogenic gut lipoglycan drives systemic thromboinflammation in lupus nephritis

Abhimanyu Amarnani[1], Cristobal F. Rivera[2], Macintosh Cornwell[3], Tyler Weinstein[1], Zakia Azad[1], Susan R.S. Gottesman[2], Cynthia Loomis[4], Andy Lee[1], Nimat Ullah[1], Joshua Prasad[1], Mingyang Yi[1], Laura Cooney[5], Betsy J. Barnes[6], Nicolas Gisch[7], Kelly V. Ruggles[3], Bhama Ramkhelawon[2], Gregg J. Silverman[1,*]

[1] *Division of Rheumatology, Department of Medicine, NYU Grossman School of Medicine, New York, NY, USA*
[2] *Department of Cell Biology, NYU Grossman School of Medicine, New York, NY, USA*
[3] *Division of Precision Medicine, Department of Medicine, NYU Grossman School of Medicine, New York, NY, USA*
[4] *Department of Pathology, NYU Grossman School of Medicine, New York, NY, USA*
[5] *University of Michigan and Immune Tolerance Network, Ann Arbor, MI, USA*
[6] *Institute for Molecular Medicine, Feinstein Institutes, New York, NY, USA*
[7] *Division of Bioanalytical Chemistry, Research Center Borstel, Leibniz Lung Center, Borstel, Germany*

ARTICLE INFO

Article history:
Received 24 October 2025
Received in revised form 12 February 2026
Accepted 4 March 2026

ABSTRACT

Objectives: The gut microbiome plays a crucial role in regulating systemic immunity and has been implicated in several chronic inflammatory diseases. Intestinal expansions of *Ruminococcus gnavus* (RG), a dominant gut commensal, correlate with disease flares in lupus nephritis (LN), but the underlying mechanism remains unknown.

Methods: In a Pilot cohort of patients with biopsy-proven LN, subsetted by gut microbiota community, immune status was characterised using bulk-blood RNA sequencing libraries, serum levels of representative host proteins, and levels of immunoglobulin (Ig)G antibodies to the novel lipoglycan (LG) produced by pathogenic RG strains. A Validation LN cohort was evaluated for blood transcriptomic profiles and levels of anti-LG antibodies. In murine models, mechanistic hypotheses were tested after RG gut colonisation or after intraperitoneal injection with an LG preparation, with outcomes determined by transcriptomic analyses, platelet functional readouts, and tissue histology.

Results: In a Pilot cohort of patients with LN, RG gut expansions were associated with high-level platelet, neutrophil, and monocyte activation. Serum levels of platelet factor 4 and release of neutrophil extracellular traps (NETs) were significantly higher in patients with high serum IgG antibody against the novel RG-specific LG, a marker of *in vivo* immune exposure. An LN Validation cohort confirmed these correlates and showed that anti-LG antibodies serve as a surrogate for thromboinflammatory profile in this LN-associated endotype. In mice, gut colonisation with LG-producing RG strains or a single LG injection caused megakaryocytosis and platelet activation; RG colonisation with LG-producing strains induced tubulointerstitial injury with NETosis. *In vivo* responses to LG toxin were Toll-like receptor 2-dependent.

Conclusions: Gut expansions of the RG pathobiont may contribute to autoimmune pathogenesis through the LG toxin and cause LN flares through thromboinflammatory mechanisms in this previously unrecognised LN endotype.

*Correspondence to Dr. Gregg J. Silverman.
E-mail address: Gregg.Silverman@nyulangone.org (G.J. Silverman).
Handling editor Josef S. Smolen.

https://doi.org/10.1016/j.ard.2026.03.002

WHAT IS ALREADY KNOWN ON THIS TOPIC

- The gut microbiome has been recognized as a regulator of systemic immunity.
- Lupus nephritis (LN) is a serious illness, yet despite improvements in therapeutic interventions, many patients progress to renal failure.
- Intestinal blooms of Ruminococcus gnavus (RG)(renamed Mediterraneibacter gnavus) are associated with higher lupus disease activity.
- Strains isolated from lupus patients have been shown to produce a cell wall-associated novel lipoglycan (LG); however, the roles of this lipoglycan in the pathogenesis of lupus and disease progression remain unclear.

WHAT THIS STUDY ADDS

- We identify a distinct LN endotype in which systemic innate immune thromboinflammation is linked to RG gut blooms and the immune response to a novel RG-associated LG.
- In the Pilot and Validation cohorts, the serum level of anti-LG antibody was shown to be a reliable surrogate biomarker for this inflammatory profile (endotype), based on transcriptomic profiles of platelet activation and neutrophil degranulation, as well as immunoassay measures of Platelet Factor 4 levels (PF4) and neutrophil extracellular trap (NET) release.
- Murine gut colonization demonstrated that only RG strains that produce the novel immunogenic surface LG toxin, or injection of an LG preparation from RG alone, induced increased megakaryocytosis, platelet activation, and renal injury, remarkably mirroring findings in LN patients with RG intestinal blooms.

HOW THIS STUDY MIGHT AFFECT RESEARCH, PRACTICE OR POLICY

- This study identified a previously unsuspected, yet common, LN endotype in which renal flares are driven by gut bacterial blooms.
- Anti-LG antibody testing may help identify LN patients with this unique endotype, and therefore those most at risk for microbiome-driven thromboinflammation and renal involvement, with implications for disease presentation, therapeutic decision-making, and subsequent personalized treatment.
- This work opens the door to new therapeutic directions, including newly characterized RG-induced pathogenic pathways, TLR2 blockade, and the therapeutic targeting of intestinal blooms of pathobiont strains.
- Taken together, our findings may provide a means to treat a common driver of LN flares without the immunosuppression inherent to current treatments.

INTRODUCTION

The gut microbiome is a key regulator of systemic health and is implicated as a significant driver in chronic autoimmune and inflammatory diseases [1,2]. We investigated the importance of this connection in systemic lupus erythematosus (SLE), an autoimmune disease characterised by considerable clinical heterogeneity in which recurrent flares often cause severe multiorgan damage. A fundamental quandary in SLE is how clinical and immunologic diversity arises and whether there are distinct patient subsets that each reflect unique underlying pathogenic mechanisms. This question may be fundamental to understanding the causes of lupus nephritis (LN), which affects half of SLE patients and is a major contributor to morbidity and mortality.

Despite recent therapeutic advancements, within 10 years of diagnosis, 1 in 5 patients progresses to end-stage renal disease [3]. In genetically predisposed individuals, environmental factors, including the gut microbiome, are suspected to play a role in the development of SLE and the subsequent triggering of disease flares; however, their contributions remain poorly understood. We hypothesise that a shift in the balance of intestinal commensals, leading to the release of microbial factors through a compromised gut barrier, is a key driver of disease flares [4,5]. This hypothesis underscores the significance of a comprehensive understanding of the interplay between disease predisposition, shifts in the gut microbiome, and the immunopathogenesis of SLE.

The gut microbiota plays a crucial role in immune development and homeostasis. Dysbiosis, or an imbalance in the gut microbiota, can increase gut permeability, contributing to the development of inflammatory and autoimmune diseases. In female patients with SLE, renal involvement is associated with expansions of specific strains of the pathobiont species that was recently renamed *Mediterraneibacter gnavus* [6]. Earlier work, to which we refer here, used the species name *Ruminococcus gnavus* (RG) [7–9]. RG, a member of the *Lachnospiraceae* family of obligate anaerobes, is a key species in the human gut microbiome [10,11]. Strains of RG generally first colonise humans during infancy [11]. In adults, several chronic inflammatory diseases have been associated with RG gut expansions [4,10]. In addition, substantial genomic diversity has been documented among RG strains [9,12], suggesting that not all strains may have pathogenic potential, and the pathways triggered by RG colonisation remain undefined.

In cross-sectional studies of cohorts of patients with SLE from diverse ethnic and racial backgrounds across 3 continents [7,13–15], RG gut expansions directly correlated with higher disease activity. Longitudinal studies have shown that, in individual patients, RG blooms are temporally associated with LN disease flares [9]. RG strains isolated from patients with active LN produce a novel form of lipoglycan (LG) [9], which has been characterised by mass spectrometry and nuclear magnetic resonance. This LG is a complex glycan with a unique structure featuring prominent mannoses and lipid anchors that attach it to the bacterial cell membrane. LGs produced by different RG strains share a conserved structure recognised by post-immunisation monoclonal antibodies [9] and also by spontaneously arising serum immunoglobulin (Ig)G2 anti-LG antibodies, which are found at high levels in approximately one-third or more of patients with active LN [7,9]. Evidence suggests a pathogenic role: murine colonisation RG strains, which produce the LG toxin and were isolated from lupus patients, translocate out of the gut and modulate the systemic immune response. LG-producing strains also accelerate the progression of lupus-like autoimmune disease, but the mechanisms underlying this effect remain undefined [16].

In this study, we investigated the mechanism(s) by which intestinal RG may directly influence autoimmune pathogenesis in LN patients. We specifically tested the hypothesis that gut colonisation with certain RG strains that produce the novel LG drives disease progression. Using patient cohorts with LN and relevant murine models, we aimed to elucidate the underlying pathogenic mechanisms. Our studies identified a significant subset of LN patients characterised by immune responses to LG. We delineate herein the role of this LG in activating platelets and neutrophils, which contribute to inflammatory renal injury.

RESULTS

LN patients in a Pilot cohort can be dichotomised based on the presence of RG intestinal blooms

In recent studies, we reported a significant correlation between high lupus disease activity and expansions of the gut

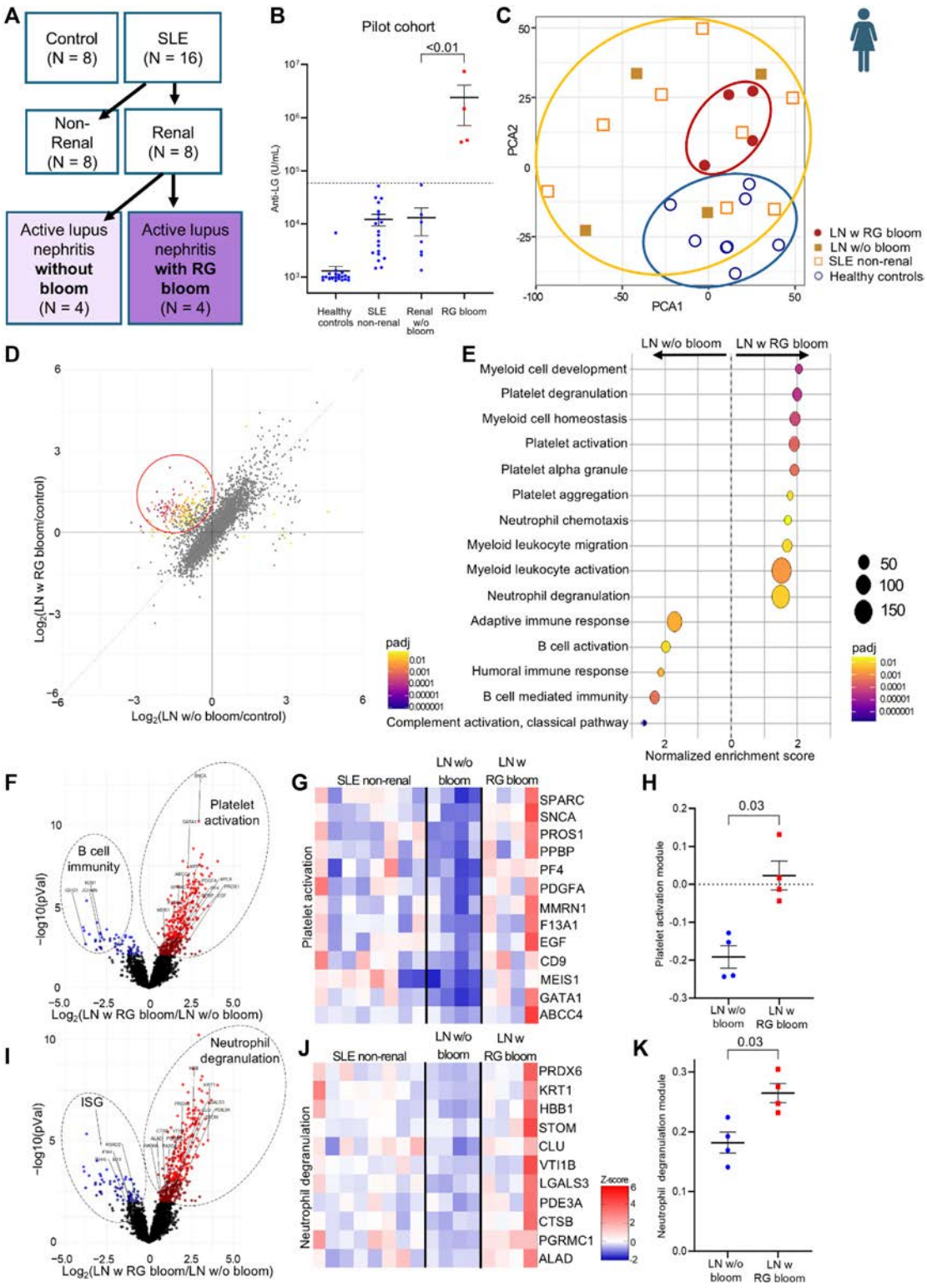

Figure 1. Whole-blood RNA sequence analysis of patients with lupus nephritis (LN) demonstrates increased platelet activation in patients with *Ruminococcus gnavus* (RG) intestinal blooms. (A) In the Pilot cohort, patients with LN (class III or IV based on renal biopsy) were dichotomised by serum levels of RG anti-lipoglycan (LG) immunoglobulin (Ig)G for RNA sequencing. (B) Antibody levels reactive with the RG LG in the sera of healthy controls (n = 20), nonrenal (systemic lupus erythematosus [SLE]) patients (n = 20), LN patients without gut blooms (n = 8), and LN patients with RG gut blooms (n = 4) in the Pilot New York University (NYU) cohort [7,9]. (C) Principal component analysis (PCA) of gene expression in whole-blood RNA sequencing libraries with top 25% variance between control, SLE without LN (SLE nonrenal), LN without RG bloom, and LN with RG gut bloom. In the prior study [9], a gut RG bloom was defined as >1% RG abundance (LN with RG bloom), which was ~10-fold higher than the mean abundance in healthy participants. PC1 40.9%, PC2 19.1%, and PC3 7.8%. (D) Scatter plot of Log2-fold change in gene expression comparing LN patients with RG blooms (LN with RG bloom) vs controls to LN patients without bloom vs healthy controls. Two hundred seventeen genes are significantly differentially expressed between the LN with RG bloom and the LN without bloom (adjusted $P < .05$), with 202 upregulated and 15 downregulated. Colour scheme adjusted P value of LN with RG bloom vs LN without bloom. (E) Gene set enrichment analysis results of ranked genes based on LN with RG bloom vs LN without bloom, showing significantly overrepresented pathways from genes increased in LN with RG bloom (right) or instead, increased in LN without bloom (left). The absolute value of the normalised enrichment score (NES) is shown. NES and P_{adj} values are listed in Supplementary Table S2. (F) LN with RG bloom is devoid of B-cell activation and the classical complement pathway; instead, these pathways are associated with LN without

commensal anaerobe, RG [7,9,14]. A longitudinal study of a cohort of female patients with SLE, as defined by the European League Against Rheumatism/American College of Rheumatology 2019 criteria [17], here termed the Pilot cohort, included 8 patients without evidence of renal disease and 8 who fulfilled the clinical criteria for LN (Fig 1A) [7,9] at the time of high disease activity. These LN patients all had elevated serum anti-double-stranded DNA (dsDNA) autoantibodies and hypocomplementemia [9], with renal biopsies documenting International Society of Nephrology/Renal Pathology Society histopathologic class III or IV proliferative glomerulonephritis [9] (Supplementary Table S1). All patients in our Pilot cohort had normal platelet counts and lacked antiphospholipid autoantibodies. Four LN patients had RG expansions, which we have termed 'blooms' when they represent >1% of the community [9]. This subset of LN patients with RG blooms also developed robust antibody responses against a structurally unique, membrane-associated LG produced by RG strains isolated from patients with active LN [7,9] (Fig 1B; Supplementary Data S1). Faecal RG abundance significantly correlated with the serum level of anti-LG IgG antibodies [7]. Within this Pilot cohort, LN patients with RG intestinal blooms displayed among the highest levels of serum IgG antibodies to this pathobiont species-associated LG, whereas the remaining LN patients showed neither expansions of RG nor identifiable antimicrobial antibody elevations compared to healthy subjects [7,9] (Fig 1B). LN patients with RG blooms also had evidence of increased systemic inflammation and immune activation, with significantly higher levels of the host acute phase reactant, lipopolysaccharide-binding protein (Supplementary Data S2), indicating increased intestinal permeability, microbial translocation, and a strong host innate immune response to circulating microbial components, including lipopolysaccharide [18].

Differential blood transcript expression in patients with LN and RG blooms

To provide an unbiased global snapshot of a patient's immune system, RNA sequencing (RNA-seq) libraries were prepared from whole blood and then analysed using unsupervised principal component analysis (PCA). As expected [19,20], in the Pilot cohort, we found a clear separation between the SLE patients and the control subjects (Fig 1C). As further anticipated based on earlier reports [21–23], there were features shared between patients with nonrenal and renal disease (Fig 1C; Supplementary Data S3). Surprisingly, LN patients with RG gut blooms formed a distinct cluster that was separate from those with LN and no blooms (Fig 1C). Although there was no significant difference in the steroid dose received (Supplementary Table S1), compared with the other LN patients, in the LN patients with RG blooms, 202 genes were upregulated and 15 were underexpressed (Fig 1D), which represented a tractable gene set amenable to meaningful interrogation.

In female LN patients with RG blooms in the Pilot cohort, gene set enrichment analysis (GSEA) [24] revealed that 5 of the top 20 most overexpressed pathways were associated with platelet activation and neutrophil degranulation compared with patients without blooms (Fig 1E; Supplementary Tables S2 and S3). Unlike the heterogeneous patterns found in SLE patients without prominent renal involvement, those with LN and gut RG blooms exhibited distinctly enhanced expression of platelet activation [25] (Fig 1F). These included transcripts for α-granule-related factors, such as platelet factor 4 (PF4), a chemokine that attracts immune cells and modulates platelet–immune cell interactions [26], and protein S (*Pros1*), which is crucial for clotting, apoptotic cell clearance, and immune modulation [27]. The LN patients with RG blooms also exhibited upregulation of transcripts for key platelet activation factors, including alpha-synuclein and platelet-derived growth factor A (Fig 1G,H). As expected [21,23], based on module analysis, some nonrenal patients showed elevated transcripts associated with platelet and neutrophil activation (Supplementary Data S3). However, anti-LG antibody levels were not increased in these patients (Supplementary Data S1A).

Patients with RG blooms also showed enhanced representation of pathways involved in neutrophil migration, chemotaxis, and degranulation, indicating broader immune activation. Furthermore, LN patients with RG blooms also showed transcript overexpression of specific genes, including *LGALS3* and *PRDX6* (Fig 1J, K), which are involved in neutrophil degranulation. In many cases, overexpression of genes involved in platelet activation correlated with expression of genes reflecting neutrophil degranulation (Supplementary Data S4A,B). However, these patients did not exhibit significantly elevated expression of interferon-stimulated genes (ISGs) (Supplementary Data S4A,B). Furthermore, LN patients without blooms instead had an overrepresentation of genes related to B-cell activation, humoral responses, and complement activation, which have been shown to play classical roles in LN disease development [19,28] (Fig 1E).

Although the number of longitudinal samples available for our study was limited, during intestinal RG blooms during disease flares, transcriptomic analyses showed that these LN patients had higher expression of the platelet activation module (Supplementary Data S5-S7). Furthermore, although it did not attain significance, the level of platelet gene activation was directly associated with that of neutrophil gene activation (r_{rm} = 0.86, P = .062, Supplementary Data S6), which further supported a coordinated immune response involving platelets and neutrophils. Conversely, the expression level of platelet activation showed an inverse correlation trend with ISG modules (r_{rm} = −0.88, P = .05, Supplementary Data S6), suggesting a reciprocal relationship during overall disease flares. Longitudinal evaluation of transcript modules showed a significant positive correlation between increased SLE disease activity (measured by the Systemic Lupus Erythematosus Disease Activity Index [SLEDAI]) and neutrophil module expression (r_{rm} = 0.99, P = .001), while there was coordinated negative correlation of B-cell (r_{rm} = −0.97, P = .006) and ISG modules (r_{rm} = −0.96, P = .01) (Supplementary Data S7).

Serum anti-LG IgG antibody levels are markers of gut dysbiosis associated with RG blooms

In our earlier studies of SLE patients, higher levels of antibodies that bind to the LG produced by RG strains were correlated

bloom. Gene expression of LN with RG bloom vs LN without bloom, with genes related to platelet activation (right) and B-cell activation (left), noted. (G) Heatmap of gene expression involved in platelet activation in nonrenal SLE patients, LN patients without bloom, and LN patients with RG bloom. (H) Singscore modules assessing platelet activation pathway in LN patients with RG bloom vs those without RG bloom. (I) Expression of genes related to neutrophil degranulation (right) and interferon-stimulated genes (ISGs) (left), with (J) heatmap of gene expression in nonrenal SLE, LN without bloom, and LN with RG bloom patients, and (K) Singscore module of neutrophil degranulation genes in LN patients with RG bloom and without gut bloom; unpaired nonparametric *t*-test.

with higher lupus disease activity, as measured by the SLEDAI [29], and with serum IgG autoantibodies to native DNA [7]. Elevated levels of serum IgG antibodies against the novel surface LG from RG strains also significantly correlated with the faecal abundance of the RG species [4], a pattern here reproduced in a smaller cohort (Supplementary Data S1). To further investigate the immunobiologic implications of this specific host immune response, in patients of the Pilot cohort, we assessed levels of serum IgG to the RG-specific LG product [9] (Supplementary Data S1). We also studied a Validation cohort of patients with active biopsy-proven class III or IV LN from the standard-of-care control arm of the previously reported randomised multisite Abatacept and Cyclophosphamide Combination Therapy for Lupus Nephritis (ACCESS) trial (NCT00774852) [30] (Supplementary Table S4). Specifically, we sought to determine whether serum anti-LG IgG levels, which reflect the host response to RG colonisation and blooms [7,9], also correlated with systemic transcriptomic profiles at the time of LN flares (Supplementary Table S5).

Serum IgG antibody levels against the novel surface LG of the RG2 strain [4] were quantified with a previously reported immunoassay [9], and patient sera were stratified based on an anti-LG antibody cutoff value (59,000 U/mL). In the Pilot cohort, anti-LG IgG antibody levels were increased in the patients with LN with RG blooms compared with the patients with LN without RG bloom and the nonrenal patients (Supplementary Data S1A). In the Validation cohort, we found that 12 of these 20 active LN patients had anti-LG IgG antibody levels that exceeded the cutoff value (Supplementary Data S1).

These LN patients had been recruited from 11 of the 21 clinical sites in the ACCESS trial (Supplementary Data S8), geographically dispersed throughout the United States. Otherwise, these patients showed no associations between anti-LG antibody levels and patient demographics, antiphospholipid antibody positivity, anti-dsDNA autoantibody levels, complement levels, urinary protein-to-creatinine ratio, white and red blood cell counts, platelet counts, estimated glomerular filtration rate, or serum albumin level (Supplementary Table S3). Anti-LG antibody levels were unaffected by medications or corticosteroid exposure; however, the LN patients with elevated anti-LG antibodies were older ($P = .02$). In this cohort, each LN patient generally maintained a stable anti-LG antibody level over a 2-year follow-up period, with few exceptions [9] (Supplementary Data S1B).

Anti-LG antibody levels are correlated with platelet activation and neutrophil degranulation gene signatures

In the Pilot cohort, the LN subset with RG blooms had significantly higher expression of transcripts for platelet activation and neutrophil degranulation ($P = .03$) (Fig 1). However, there was no correlation with differences in the levels of specific cell types (eg, platelets or neutrophils) in the blood (Supplementary Data S9). In the Validation LN cohort, PCA of bulk-blood RNA-seq libraries, based on anti-LG antibody positivity, did not distinguish patients with global gene representation (Supplementary Data S10A). In contrast, anti-LG antibody positive and negative subsets significantly distinguished those with platelet module-specific gene expression, which was consistent with the findings that elevated anti-LG antibody levels correlated with significantly higher expression of platelet activation genes ($P = .04$) (Fig 2A-D [31]; Supplementary Tables S2 and S3; Supplementary Data S10B,C). Hence the multiscale approach validated both the biological specificity and the reproducibility of the platelet activation signature as a pathway-level biomarker in LN. Furthermore, in the Validation cohort, the levels of anti-LG antibodies also significantly directly correlated with platelet activation ($r = 0.47$, $P < .05$), with neutrophil extracellular trap (NET) fragmentation ($r = 0.45$, $P < .05$), and with a positive numerical trend with the neutrophil degranulation transcript module ($r = 0.43$, $P = .06$) (Supplementary Data S11 and S12; Supplementary Table S5).

Hierarchical clustering of these overexpressed pathways in the anti-LG positive patients in the Validation cohort mirrored the patterns found in patients with RG blooms in the Pilot cohort (Supplementary Data S13). In contrast, there was no direct or indirect significant association with ISG expression (Supplementary Table S5). However, we also identified an exception—an LN patient with elevated platelet activation gene expression despite negative anti-LG antibody levels. This patient had a significantly elevated pathologic-range protein-to-creatinine ratio (>20 g/g) (Fig 2B; Supplementary Data S13), suggesting that serum antibody loss may have resulted from pathologic urinary excretion.

To assess these profiles in independent SLE cohorts, we analysed transcriptomic data from published reports on 390 patients with active LN [19,20,32,33]. We found inverse relationships between platelet activation/neutrophil degranulation genes with both ISG and B-cell activation/differentiation genes (Supplementary Data S4C,D), and the same relationships seen for modules for ISG and B-cell activation. However, in this composite of datasets from several reports, there was no identifiable relationship between platelets and neutrophil modules, and this was expected as there was no means to dichotomise this heterogeneous lupus dataset based on gut RG representation or circulating anti-LG antibody levels. Hence, RNA-seq analyses across cohorts provided circumstantial evidence for a distinct pathway of platelet activation and neutrophil degranulation that was first identified in LN patients with RG blooms, distinguishing this patient flare endotype, from flares involving previously implicated pathways, which are characterised by overexpression of B-cell activation and interferon-related genes [19].

Peripheral transcript profiles of platelet and neutrophil activation are associated with elevated serum PF4 and NETosis proteins

To further investigate the mechanisms underlying the observed platelet and neutrophil activation, we assessed for correlations between gene expression and serum levels of relevant self-proteins. Validation cohort patients with positive anti-LG antibody levels showed increased platelet activation gene scores and higher serum PF4 protein levels, confirming *in vivo* platelet activation (Fig 2C,D,F). These patients also exhibited gene signatures of increased neutrophil degranulation, as well as higher serum levels of NET fragments, including myeloperoxidase, citrulline-modified histone 3, and dsDNA, compared with anti-LG antibody-negative patients (Fig 2C,E,G). Significant correlations were found between levels of serum PF4 protein and platelet-related transcripts, including *PROS1* ($r = 0.52$, $P = .02$), *PPBP* ($r = 0.48$, $P = .03$), and *TREML1* ($r = 0.48$, $P = .03$), indicating coordinated platelet degranulation (Supplementary Data S14). Similarly, correlations between serum NET fragments, a hallmark of NETosis, and transcripts related to neutrophil degranulation and epithelial damage (*KRT1*: $r = 0.58$, $P = .02$; *EGF*: $r = 0.53$, $P = .04$) were observed (Supplementary Data S15). These direct transcript-protein relationships provide robust evidence for coordinated platelet, neutrophil activation, and NETosis as contributors to disease activity.

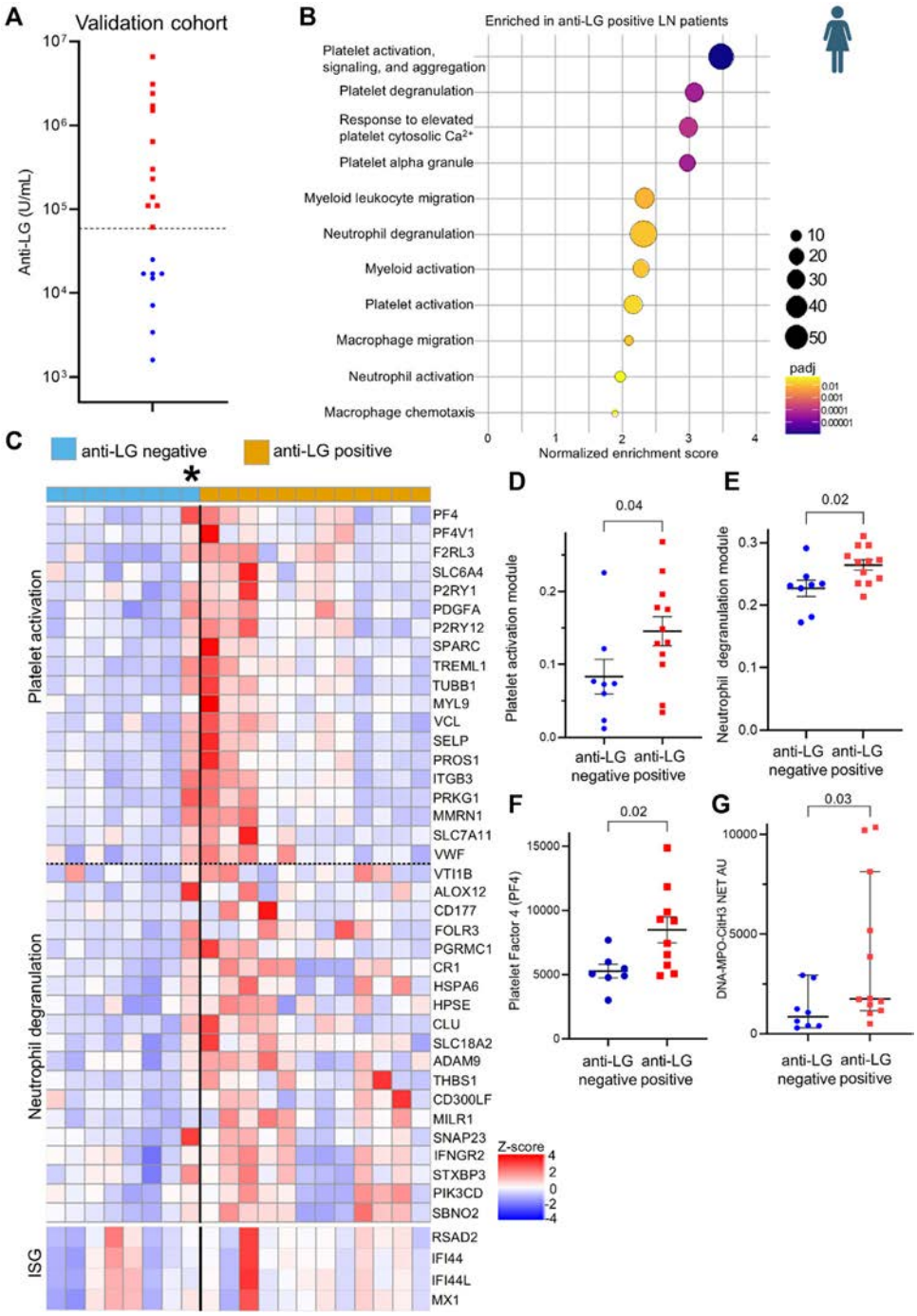

Figure 2. Patients with anti-lipoglycan (LG) positive antibody levels in the Validation cohort displayed transcript profile evidence of platelet activation. (A) Using a quantitative Luminex-based assay, lupus nephritis (LN) patients were dichotomised based on a cutoff for immunoglobulin (Ig)G anti-LG reactivity (horizontal dashed line), distinguishing those with negative (n = 8) vs positive (≥5.9×10^4 U/mL; n = 12) antibody levels. Validation cohort LN samples were from the ITN034AI trial (NCT00774852) (see methods in the Supplementary Materials). (B) Pathways and (C) genes related to platelet and neutrophil activation were increased in anti-LG-positive patients. Pathway normalised enrichment score (NES) values and statistics are listed in Supplementary Table S2. *Indicates an unusual patient with a negative anti-LG antibody level who had a significantly elevated urine protein/creatine ratio of >20 g/g (see text and Supplementary Data S4). (D) Platelet gene expression module and (E) Neutrophil degranulation gene module scores in the anti-LG negative patients (n = 8) vs anti-LG-positive patients (n = 12) in the Validation cohort. (F) Platelet factor 4 (PF4) protein levels in the serum of patients with class III or class IV LN in the Validation cohort (n = 17). (G) Serum neutrophil extracellular trap (NET) fragment detection by enzyme-linked immunosorbent assay for citrullinated histone 3 (CitH3), myeloperoxidase (MPO), and DNA, which are serum markers for NETosis in the patients in the Validation cohort (n = 20). NET fragment detection utilised a published methodology for simultaneous detection of MPO-CitH3 and DNA fragments [31]. Statistics represent an unpaired, nonparametric *t*-test. AU, arbitrary units.

Intestinal colonisation of mice with LG-producing RG strains induces platelet activation

We next sought to survey for potential causal relationships between the influences of RG strains from LN patients and *in vivo* platelet activation [8,16] (Fig 3A). To assess the gut presence of RG akin to the RG-colonized LN subset, RG-specific quantitative polymerase chain reaction assays of faecal samples documented high-level colonisation in mice given RG strains isolated from LN patients, at 2 weeks post-gavage, but not in the controls (Fig 3B). Notably, after challenge, the rapid appearance of high serum fluorescein isothiocyanate-dextran

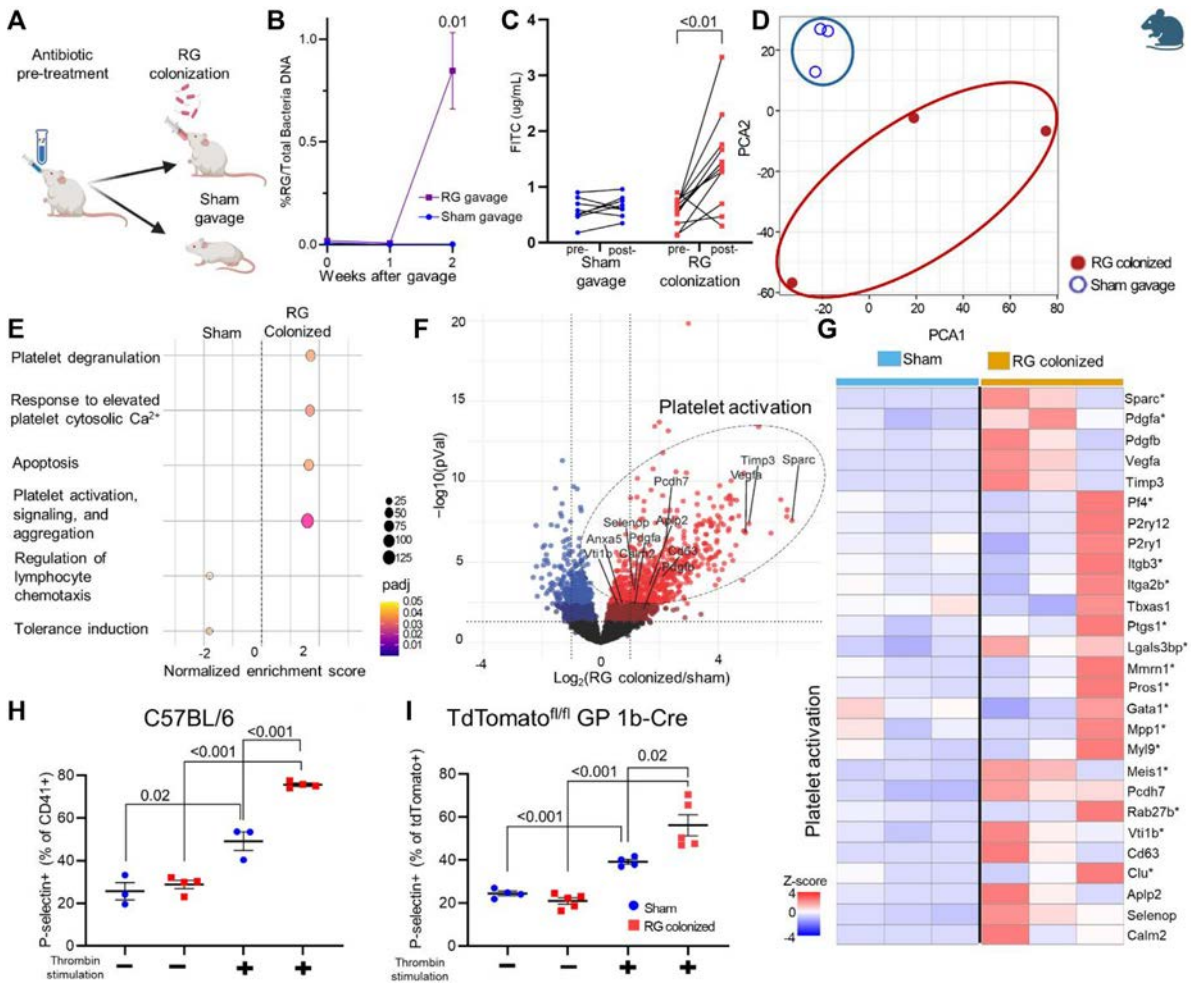

Figure 3. *Ruminococcus gnavus* (RG) gut gavage induces platelet-targeted transcriptomic changes and activates peripheral platelets. (A) The experimental model used antibiotic pretreatment, then subsequent murine gavage of RG or sham, and sample collection. (B) Polymerase chain reaction assessment of stool samples throughout the experiment identified peak RG colonisation of C57BL/6 mice at 2 weeks after the last gavage. Mice were pretreated for 2 weeks with an antibiotic cocktail of enrofloxacin, ampicillin, and metronidazole. Mice were then gavaged with either sham or RG every other day for a total of 5 administrations over 2 weeks. Timepoint 0 represents the end of this gavage period (n = 3 per group). (C) FITC-dextran levels in serum pre- and post-oral gavage of sham vs RG gavage-treated (RG-colonised) mice. n > 7 mice per group. (D) Principal component analysis of the top 25% varied genes in C57BL/6 mice at 2 weeks, and 4 weeks post-gavage, with either sham or RG. PC1 48.7%, PC2 28.3%. n = 3 per group. (E) Gene set enrichment analysis detected genes overexpressed in RG compared with sham at 2 weeks post-gavage. Pathway normalised enrichment scores are listed in Supplementary Table S2. (F) Expression at 2 weeks post-gavage of genes related to platelet activation. (G) Heatmap of whole-blood RNA sequencing (RNA-seq) genes related to platelet activation, in sham gavage (left) and RG-colonised (right) mice. *Indicates transcripts overrepresented in pathway analyses for platelet activation and/or degranulation in both murine RG colonisation model and human whole-blood RNA-seq studies (Figs 1, 2). (H, I) P-selectin^{+} platelets (relative to CD41^{+} FSC^{low}) in C57BL/6 mice (H) and GP1b-Cre^{+} platelets in tdTomato-GP1bCre mice (I) with or without thrombin stimulation detected by flow cytometry. n > 3 mice per group. FITC, fluorescein isothiocyanate, FSC, forward scatter; GP1b, glycoprotein Ib.

levels documented impaired intestinal barrier functional integrity in RG-colonised mice (Fig 3C), akin to findings in LN patients with RG intestinal blooms (Supplementary Data S1). Overall, in RG gut colonisation studies, there was no evidence of sepsis, infection, changes in body temperature, or weight loss in treated mice. Colonisation with LG-producing RG induced significant global changes in the transcriptome, affecting over 700 enriched pathways (Supplementary Table S2). As shown by PCA, whole-blood RNA-seq libraries from peak RG colonisation revealed distinct gene expression profiles (Fig 3D). In RG-gavaged mice, there was significant overrepresentation of pathways for platelet activation and degranulation (Fig 3E; Supplementary Tables S2 and S3), mirroring findings in LN patients with RG blooms (Figs 1 and 2). Key genes involved in platelet activation and aggregation, such as *Pros1, Pdgfa, Pf4*, and *Sparc*, were notably overrepresented (Fig 3F, G). Although RG colonisation did not affect total white blood cell, lymphocyte, or platelet counts, mean platelet volume, or haemoglobin levels (Supplementary Data S16), RG-colonised mice did have significantly lower circulating neutrophil levels (P = .02), suggesting that RG-induced platelet activation may accelerate peripheral neutrophil consumption.

To understand RG-driven platelet activation in thromboinflammatory conditions, we used a standard set of experimental agonists to assess *ex vivo* platelet responsiveness in RG-colonised mice. During thrombogenesis, P-selectin is packaged into platelet cytoplasmic α-granule organelles. Using flow cytometry, we quantified P-selectin levels expressed on platelet membranes. We found that, upon *ex vivo* activation with thrombin, P-selectin rapidly translocated to the platelet surface in RG-gavaged mice, but not in sham-treated mice (Fig 3H; Supplementary Data S17), where it is accessible for cell-cell interactions, including those with neutrophils. Using RG-colonised *tdTomato-GP1b* transgenic mice (Supplementary Data S18), we found no differences in basal P-selectin expression. However, after *in vitro* challenge with thrombin, we documented enhanced P-selectin responses

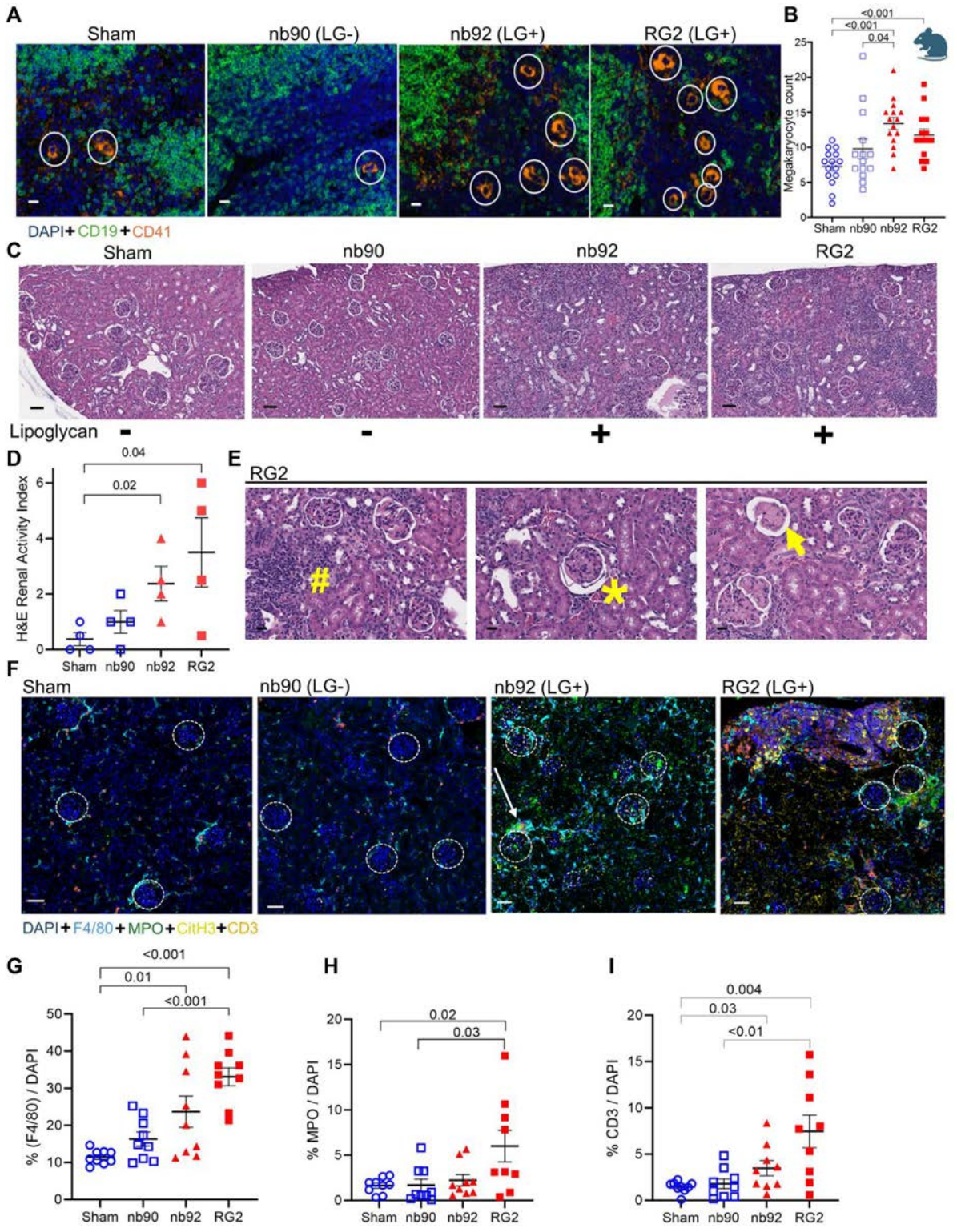

Figure 4. Colonisation of lupus-prone mice causes splenic megakaryocytosis and increased renal cellular infiltration by macrophage/monocytes and lymphocytes with increased local NETosis. (A, B) Splenic immunohistochemistry shows an increased number of megakaryocytes, representing megakaryocytosis, after gut colonisation with the *Ruminococcus gnavus* RG2 strain and the nb92 subclone that produces lipoglycan (LG), but not after sham or colonisation with the nb90 subclone that does not produce LG. See Supplementary Data S32. Immunofluorescence of splenic megakaryocytes in 12-month-old, female, *FcγRIIb*$^{-/-}$ mice (as defined by CD41^{+} cells) after gavage with LG-positive RG subclone or strain (nb92, RG2) versus a subclone that does not produce LG (nb90). The cell counts represent the number of cells per low-power field (n > 3 mice per group). (C) Representative kidney sections (hematoxylin and eosin stained) after colonisation of *FcγRIIb*$^{-/-}$ mice with LG-producing RG strains (nb92, RG2), and LG-non-producing strain (nb90), 10 days after the last gavage. Bar = 50 μm. (D) Quantification of the renal activity index evaluated a blinded reviewer for the presence (score 0-3) of mononuclear tubulointerstitial cells, glomerular leukocyte infiltration, hyalinisation of glomeruli, closed capillary loops, or early crescent formation/fibrotic ring (see Supplementary Table S6). Statistics represent an unpaired *t*-test. (E) Example of glomeruli of RG2 (LG-producing RG strain)-colonised *FcγRIIb*$^{-/-}$ lupus-prone female mice, showing mononuclear interstitial cellular infiltrations (#), early crescent formation (*) and hyalinisation (arrow) (original magnification, 40×). Bar = 20 µm. (F) Representative images of merged immunofluorescence of macrophage/monocytes (F4/80), neutrophils (MPO), with evidence of NETosis (CitH3), and T cells (CD3). Bar = 50 µm. Regions of interest with glomeruli and surrounding macrophages are encircled with dashed lines. Arrow highlights area of NETosis adjacent to a glomerulus, based on MPO, CitH3, and F4/80 detection.

(Fig 3I). In contrast, no functional differences were observed with either type I collagen or adenosine diphosphate (ADP), which act via receptors distinct from those activated by thrombin (Supplementary Data S19).

RG colonisation leads to a robust local intestinal immune response

After gavage with an LG-producing RG strain, but not in sham-gavaged control mice, RG colonisation led to large lymphoid aggregates in the ileal lamina propria. These contained IgA^+CD45^+ lymphocytes (Supplementary Data S20A-D). Additionally, RG-colonised mice showed reduced epithelial expression of claudin-1, a protein essential for maintaining intestinal barrier integrity (Supplementary Data S20E,F). These findings suggest that certain RG strains can compromise gut barrier function, potentially allowing systemic exposure to numerous microbial factors.

Intestinal colonisation increases the number of megakaryocytes in the bone marrow and spleen

Platelets, formed from the fragmentation of megakaryocyte cytoplasm in the bone marrow, lack nuclei and mitochondria. In *GP1b-td*Tomato platelet reporter mice, we examined the effect of RG gut colonisation on megakaryocytes. After colonisation with LG-producing RG, megakaryocyte numbers significantly increased in the bone marrow (Supplementary Data S21A). We also assessed the impact on the spleen, a key site for platelet storage and extramedullary production during periods of increased demand, such as in sepsis [34]. RG gavage resulted in significantly higher megakaryocyte numbers in the spleen compared with sham-treated mice (Supplementary Data S21B) (Supplementary Data S33).

Pathogenic LG-producing RG strains induce renal injury in lupus-prone mice

To assess the influence of LG production, we used bacterial strains with or without the capacity to produce LG *in vitro* [7]. These included newly isolated RG subclones obtained by subculture and colony isolation from the previously described S107-48 RG strain recovered from an LN patient [9]. For these studies, we used the nb90 subclone, which lacks LG production, and the nb92 subclone, which consistently produces LG. In wild-type mice, colonisation with LG-producing strains did not lead to renal pathology (Supplementary Data S22).

To consider potential effects on autoimmune pathogenesis and end-organ effects, we studied the effect of RG colonisation in lupus-prone *FcγRIIb*$^{-/-}$ mice, which are at risk of autoimmune renal injury [35,36]. *FcγRIIb*$^{-/-}$ mice were gut-colonised with the control RG1 (also called the ATCC 29149) strain (an LG-non-producing RG strain [7] from a healthy donor) or with the LG-producing nb92, or RG2 (also called CC55_001C) strains (Supplementary Data S32). The LG-producing strains significantly increased spleen megakaryocyte numbers, whereas the LG-non-producing strain did not (Fig 4A,B). In lupus-prone mice, colonisation with LG-producing RG strains (nb92 or RG2) in *FcγRIIb*$^{-/-}$ mice induced significant renal cellular infiltration, marked by tubulointerstitial lymphocytic infiltrates (Fig 4C,D,E) with prominent T-cell and macrophage populations identified by immunofluorescence (Fig 4F) (Supplementary Tables S6 and S7). Furthermore, in mice colonised with LG-producing RG strains, there was deposition of myeloperoxidase and citrullinated histone 3 markers consistent with neutrophil degranulation and death by NETosis (Fig 4F-I; Supplementary Data S23). This renal pathology was not present in sham-gavaged mice or in mice colonised with the control LG-nonproducing strain. Hence, in genetically lupus-prone female mice, LG-producing *RG* strains drive both NETosis and renal injury.

Intraperitoneal injection of LG alone drives platelet activation and in vivo megakaryocytosis

We next sought to determine whether the LG glycan moiety alone is sufficient to drive these features *in vivo,* and we therefore administered a purified LG preparation via intraperitoneal injection. As with our findings after RG colonisation (Fig 3), in LG-injected mice RNA library analysis revealed overexpression of genes associated with platelet activation compared with vehicle-injected mice (Fig 5A-C; Supplementary Tables S2 and S3; Supplementary Data S24). In both wild-type and lupus-prone mice, LG treatment significantly increased functional platelet responses to *ex vivo* thrombin stimulation (Fig 5D,E), without associated alterations in total white blood cell count, lymphocytes, neutrophils, haemoglobin, platelet count, or mean platelet volume compared with vehicle controls (Supplementary Data S25, S26). LG injection induced enhanced *ex vivo* platelet responses at 6 days post-injection, but not at earlier time points (8 hours or 2 days; Supplementary Data S27). Given the ~4-day platelet lifespan in mice [37], this suggests that the influence of LG is mediated by sensitisation of newly formed platelets to thrombin stimulation, which then mature, rather than by direct effects of the lipoglycan on mature platelets.

LG-injected mice also exhibited splenic megakaryocytosis (Fig 5F), indicating that LG affects platelet progenitors and subsequent platelet activation functions. However, there was no increase in functional aggregation rates after thrombin or ADP stimulation compared with vehicle-injected mice (Supplementary Data S28). Hence, LG specifically drives platelet activation but not the platelet aggregation that leads to clot formation.

RG drives platelet activation and immune modulation in both lupus patients and murine models

As described above, in both human and murine studies, we found consistent evidence of RG-driven platelet activation and innate immune modulation. Indeed, in RG-colonised mice, the pathways for platelet activation, degranulation, and NETosis closely matched those in RG-exposed LN patients. Under the influence of LG-producing strains, the shared overexpression pattern was also seen at the level of individual genes crucial for regulating platelet activation, degranulation, and NET formation in a pathway-dependent manner (Supplementary Data S29).

(G) Cell percentage of $F4/80^+$ cells (macrophages), (H) MPO^+ cells (neutrophils), and (I) $CD3^+$ cells (T cells) relative to all cells (DAPI) in low-power fields, with >3 fields evaluated per mouse (n = 3 mice per group). Statistics represent an unpaired *t*-test. CitH3, citrullinated histone 3; DAPI, 4′,6-diamidino-2-phenylindole; FcγRIIb, Fc gamma receptor IIb; MPO, myeloperoxidase; NET, neutrophil extracellular trap.

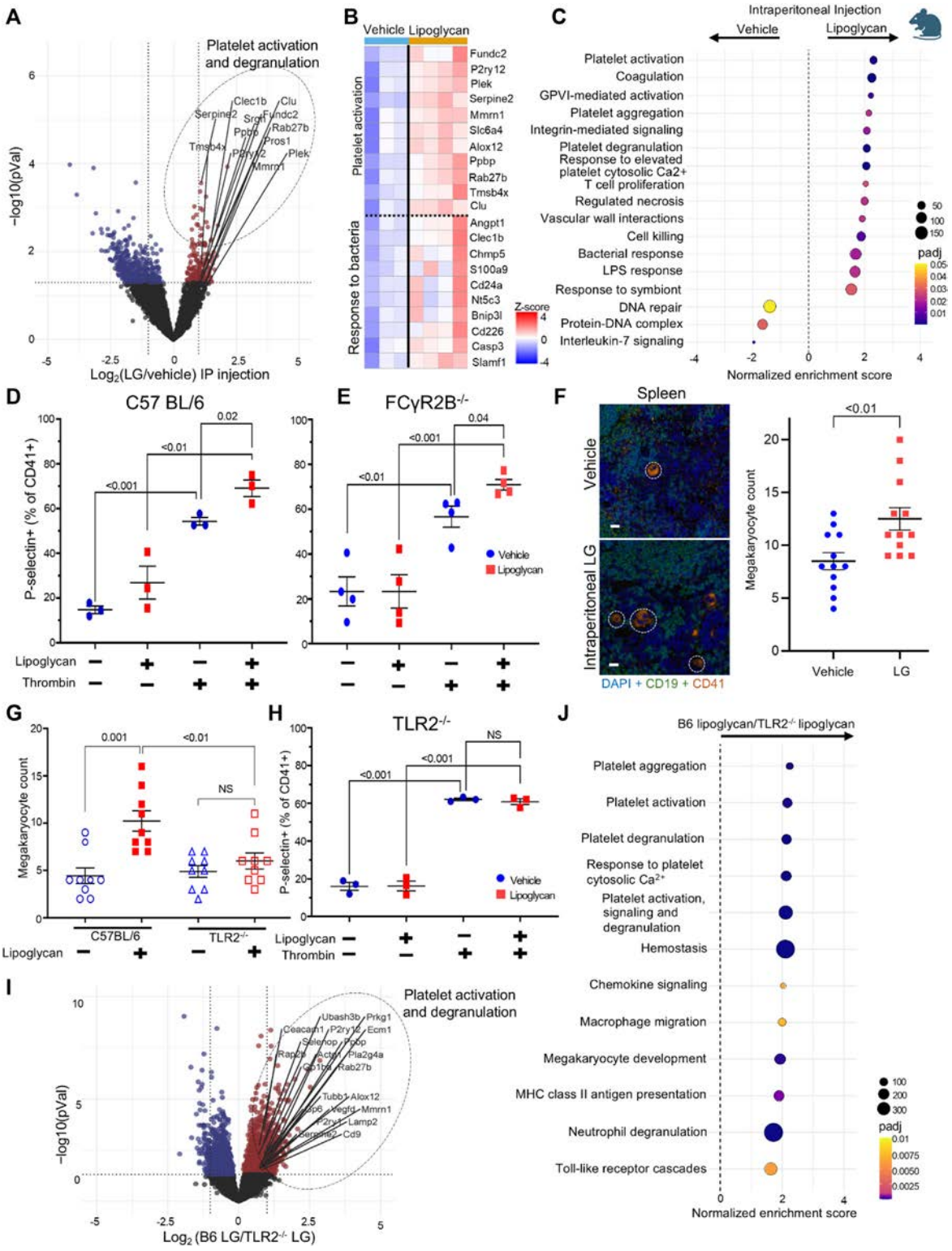

Figure 5. Intraperitoneal (IP) administration of lipoglycan (LG) preparation in C57BL/6, *FcγRIIb*$^{-/-}$ and *TLR2*$^{-/-}$ mice increases splenic megakaryocyte numbers, peripheral blood platelet activation, and P-selectin externalisation. (A) Platelet activation genes were increased in whole-blood RNA sequencing (RNA-seq) studies 6 days after a single IP injection of an LG preparation (1.5 μg/g), isolated from the RG2 strain, into *FcγRIIb*$^{-/-}$ mice. n greater than or equal to 3 mice per group. (B) Heatmap visualisation of genes related to platelet activation and degranulation and the associated immune activation pathways induced by RG bacterial products. (C) Gene set enrichment analysis (GSEA) detects pathways overrepresented in mice after LG injection. Pathway normalised enrichment scores (NES) are listed in Supplementary Table S2. (D, E) Functional platelet activation 6 days after IP LG injection was evaluated by flow cytometric monitoring of the percentage of surface P-selectin expressing cells after *ex vivo* thrombin stimulation in (D) C57BL/6 and (E) *FcγRIIb*$^{-/-}$ mice. n > 3 mice per group. (F) Immunofluorescence megakaryocyte quantification in the spleen of 5- to 8-month-old lupus-prone, female, *FcγRIIb*$^{-/-}$ mice 6 days after one-time LG IP injection. Bar = 50 μm. Cell counts are the number of cells per low-power field (n > 3 mice per group). (G-I) TLR2-dependence of RG LG preparation-mediated activities. (G) Increased megakaryocyte numbers in the spleen were observed in wild-type LG-injected mice, but not LG-injected *TLR2*$^{-/-}$ mice. Cell counts are the number of cells per low-power field (n = 3-4 fields per mouse, n > 3 mice per group). (H) Percentage of surface P-selectin-expressing cells, functional platelet activation 6 days after IP LG injection, in response to *ex vivo* thrombin stimulation in *TLR2*$^{-/-}$ mice (n > 3 mice per group). (I) Platelet activation genes were increased in RNA-seq studies of whole blood collected 6 days after LG injection in both C57BL/6 (B6) and *TLR2*$^{-/-}$ mice (n > 3 mice per group). (J) GSEA showed increased expression

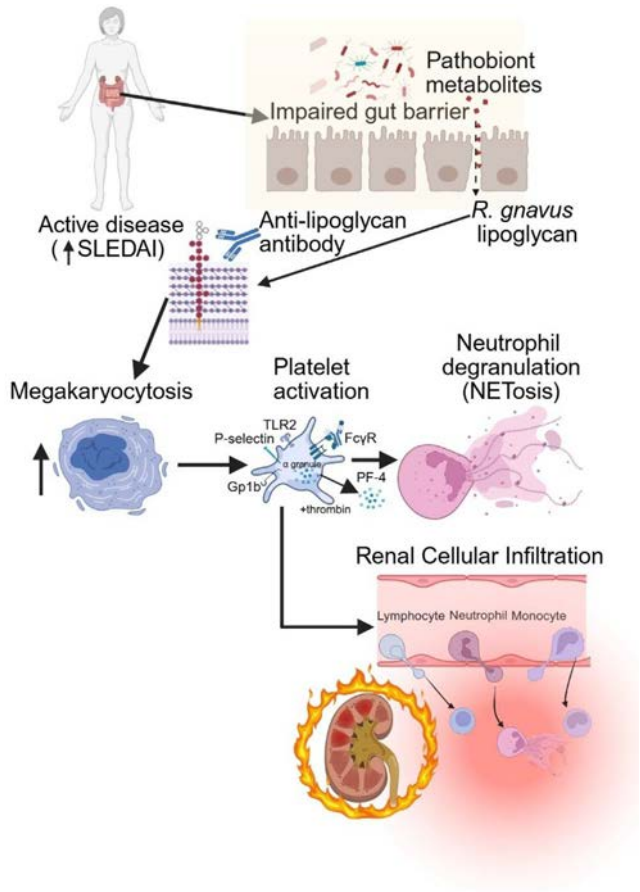

Figure 6. A mechanistic hypothesis of the influence of RG on systemic lupus erythematosus pathogenesis. Impaired gut barrier function allows microbial products to translocate, exposing the immune system to RG surface lipoglycan (LG). RG can activate platelets via Toll-like receptor 2 (TLR2), and, potentially, via immune complexes acting through FcγR and complement/mannose-binding lectin, promoting platelet–immune cell interactions. This leads to lupus nephritis injury via P-selectin-mediated neutrophil priming, resulting in the release of neutrophil extracellular traps (NETs) that contain inflammatory factors and active neutrophil proteases. Activated platelets also release soluble factors, such as platelet factor 4 (PF-4), which drive granulocyte maturation and further sustain inflammation. NET, neutrophil extracellular trap; RG, *Ruminococcus gnavus*; SLEDAI, Systemic Lupus Erythematosus Disease Activity Index. Adapted from [4,39].

Megakaryocytosis, altered platelet function, and transcriptomic activation mediated by LG preparations in vivo are Toll-like receptor 2-dependent

Prior studies using a reporter cell line implicated Toll-like receptor (TLR)2 in the immune activation induced by an LG preparation isolated from RG by chromatography (see Methods [7]). As TLR2 is expressed on megakaryocytes and platelets [38], we therefore tested the *in vivo* responses to such LG preparations. In wild-type mice, a single LG injection induced megakaryocytosis expansion of these platelet precursors (Fig 5G), as well as platelet activation and TLR-mediated cascade pathways, whereas neither was observed in *TLR2*$^{-/-}$ mice (Fig 5H,I; Supplementary Data S30). In LG-injected wild-type mice, GSEA confirmed overrepresentation of pathways associated with platelet activation, degranulation, macrophage migration, and neutrophil degranulation, which was not observed in LG-injected *TLR2*$^{-/-}$ mice (Fig 5J; Supplementary Tables S2 and S3; Supplementary Data S31). These findings highlight the crucial *in vivo* role of the TLR2 cascade in mediating the thromboinflammatory response triggered by LG preparations (Fig 6 [4,39]).

DISCUSSION

In this study, we identified a distinct pathophysiologic endotype in patients with LN characterised by gut expansion of the pathobiont RG and the release of a proinflammatory LG toxin. In 2 independent cohorts, unbiased whole-blood RNA-seq (Figs 1 and 2) provided a comprehensive view of the immune landscape. LN patients with RG blooms exhibited a gene expression profile indicative of platelet activation and neutrophil degranulation. In contrast, LN patients without gut bloom displayed distinct transcriptional patterns associated with B-cell and complement activation [19,20]. In support of this, analysis of publicly available whole-blood gene expression datasets underscored the clear separation of these molecular pathologic endotypes among patients with active LN, especially the inverse correlation between platelet activation and B-cell activation modules.

To further investigate the causative roles in lupus-like disease, we conducted animal studies. Our murine gut colonisation experiments demonstrated that only RG strains that produced the unique immunogenic surface LG toxin, or injection of an LG preparation from RG alone, induced increased tissue levels of megakaryocytes, platelet activation, and renal injury (Figs 3 and 4). Indeed, megakaryocytes and platelets express innate immune receptors, including TLRs, which can stimulate proliferation and differentiation, particularly in the context of inflammation, infection, or sepsis [38]. Transcript profiles were induced by LG injection that reiterated findings after colonisation with LG-producing RG strains (Fig 5A-C), as well as induced functional activation in platelets (Fig 5D, E). However, responses induced by an LG preparation from RG were not observed in *TLR2*-deficient mice (Fig 5). Notably, to induce platelet activation via specific signalling pathways, TLR2 functions as a heterodimer [40]. Our RNA-seq data demonstrated implicated activation via the TLR2 and the TLR1 signalling subunit. These findings align with a report that synthetic TLR2 agonists can activate platelets [41] and contribute to thromboinflammatory responses and NETosis [42]. However, it remains possible that other host innate immune receptors, such as C-type lectins, also contribute to RG-driven immune activation.

Beyond platelet effects, which included increased serum P-selectin expression, RG blooms in LN patients enhanced the expression of genes associated with NET formation (eg, myeloperoxidase, citrullinated histone H3, dsDNA) [31,43], features of the thromboinflammatory innate pathway also observed in sepsis [44]. In our patients with RG intestinal expansions, we observed no episodes of bacteraemia, epithelial barrier invasion, or associated tissue injury. Furthermore, unlike in sepsis, neither thrombosis nor vascular clotting was prominent, and these patients showed no signs of disseminated intravascular

of genes related to platelet activation and degranulation pathways in B6 mice, but not in *TLR2*$^{-/-}$ mice, after IP injection of LG preparation. Pathway NES listed in Supplementary Table S2. In panels A and I, vertical dashed lines indicate $\log_2$(Fold Change) ±1, representing a 2-fold change in gene expression. Unpaired, nonparametric *t*-test. DAPI, 4′,6-diamidino-2-phenylindole; FcγRIIb, Fc gamma receptor IIb; TLR2, Toll-like receptor 2.

coagulation or thrombocytopenia. To better define the central features shared by patients with this LN endotype, we intentionally excluded patients with clinical antiphospholipid syndrome, thereby clarifying that these autoimmune features are not integral to this LG toxin-driven thromboinflammatory endotype.

Supporting the translational relevance of our murine models, comparative analysis of patient and murine RNA-seq libraries revealed conserved pathway overexpression (Supplementary Data S29). Hence, despite species-specific differences between mice and humans, and significant differences in LG exposure timelines (short-term in murine models vs years in LN patients), the transcriptomic profiles induced by murine RG gut colonisation remarkably mirrored those observed in LN patients with RG intestinal blooms.

In the kidneys of lupus-prone mice, within weeks of RG colonisation, a profound cellular infiltration by neutrophils, macrophages, and T cells was observed. This provided a novel model of early-stage immune cell infiltration driven by gut dysbiosis. In contrast, glomerulonephritis in patients with SLE typically develops over a longer period. Murine studies confirmed that these LG preparations alone can induce the central features of an early step in autoimmune renal pathogenesis.

In mice, we observed neutrophil infiltration and degranulation, as well as macrophage and T-cell entry into the kidneys of RG-colonised lupus-prone mice. Just weeks after murine RG gut colonisation, we observed immune cell infiltration, representing an early-stage model of dysbiosis-driven inflammation. However, refinements in experimental design can address the consequences of prolonged intestinal RG persistence and its impact on long-term renal pathology that is more typical in human LN pathogenesis. Overall, our findings from human and murine studies support the hypothesis that gut expansion of pathogenic RG strains in LN patients drives platelet and immune activation, as well as renal disease (Fig 6).

Among the limitations that warrant consideration, the Pilot cohort size was modest and from a single site. Because women are most affected by LN, the Pilot cohort comprised female patients, and the 20 LN patients in the Validation cohort included only one male patient. Although gut microbiota data were unavailable for the Validation cohort, the number of significant cross-data correlations in this cohort demonstrated that anti-LG IgG antibody levels served as a powerful surrogate for identifying patients with the thromboinflammatory endotype. The LG from RG strains is specifically recognised by a well-characterised recombinant antibody, although future studies will be needed to extend testing to additional strains and other glycan molecules. In addition, we appreciate that a copurified minor component may influence the host response to LG [7]. It remains possible that, at the molecular level, TLR2 dependence does not rely on a direct interaction with the LG itself but rather with a copurified factor [45−48].

The initial renal injury from RG colonisation and LG exposure mirrors aspects of early cellular infiltration seen in sepsis-driven acute kidney injury [49,50]. However, this RG-associated early inflammatory renal injury occurs without overt infection or widespread thromboses. We hypothesise that such repeated or prolonged insults are necessary for the development of all the features of classical LN in susceptible individuals.

Taken together, our findings define an LN endotype associated with blooms of LG-producing RG strains and the underlying mechanisms. In patients with LN, platelet activation has previously been linked to leukocyte recruitment and end-organ injury [22,51−53], roles central to this endotype. Unlike other LN endotypes, which include B-cell activation or interferon pathways, our findings suggest that a pathogenic subset of LN patients can be identified using the anti-LG antibody biomarker, reflecting the *in vivo* influence of a gut pathobiont that acts via specific disease mechanisms. Overall, this previously unknown LN endotype is triggered by systemic platelet activation—beyond their traditional roles in thrombosis—as immune sentinels that drive inflammation. As a result, our studies are reshaping our understanding of LN pathogenesis in lupus patients with RG blooms.

In-depth studies are now needed to investigate the relationship between elevated anti-LG antibody levels and the risk of renal failure, as well as the potential for impairment of clinical responses to therapy due to overwhelming microbiome-induced innate immune activation in the lupus host. Similarly, our understanding of RG ecobiology, particularly the relationship with time-dependent shifts in pathogenic strains and overall disease activity, is currently limited. We documented remarkably high antibody levels against the LG toxin in many patients with LN. The direct pathogenic properties of such antibodies, and/or their IgG immune complexes with the lipoglycan, need to be characterised in patients with this endotype. The effects on platelet biology and functionality, including transcript levels in isolated platelets from affected individuals, should also be investigated. The induced B-cell/antibody clones should also be evaluated for their potential contribution to pathogenesis through cross-reactivity with self- or renal antigens and by forming complexes *in vivo*. We found a significant difference in the mean age of the patients in the Validation cohort in anti-LG antibody high versus anti-LG antibody low subsets (Supplementary Table S3; $P = .02$), although for the categorical age distributions (18-24, 25-39, >40 years) there were no significant differences ($P = .25$). It currently appears unlikely that RG intestinal expansions occur only late in the course of LN pathogenesis, as we have detected high anti-LG antibody levels in individual patients on the day of LN biopsy and diagnosis [13]. However, to address this question, longitudinal studies of patients with LN enrolment at disease onset may be necessary.

In summary, our study highlights the unique pathophysiology underlying RG blooms in a subset of LN patients. Our findings reveal many parallels with poststreptococcal autoimmune syndromes, such as rheumatic fever and poststreptococcal glomerulonephritis, as recently discussed [4]. However, in the absence of overt infections and associated tissue barrier destruction, RG blooms provoke host immune responses that disrupt gut barrier function [4,5]. The detection of RG blooms and related systemic anti-LG antibody responses should serve as a biomarker to identify patients at higher risk for this endotype of disease flare and tissue damage, particularly in genetically susceptible individuals. Future work in SLE inception cohorts will therefore also be needed to assess the dynamics of RG strain expansion, competition, and persistence.

Early clinical testing of anti-LG antibody as a biomarker may help stratify patients by risk of microbiome-induced disease flares, potentially as early as their first clinical presentation. Detection of this pronounced platelet-driven immune response in an LN patient may inform therapy decisions more effectively, facilitating a personalised medicine approach [38]. These findings highlight the potential clinical opportunities to target RG-induced pathways, including through TLR2 blockade or selective antibiotic treatment, which may spare some patients the broad immunosuppressive effects and associated adverse events of current standard-of-care therapies for lupus.

METHODS

This study was conducted in accordance with the principles outlined in the Declaration of Helsinki. Written informed consent, approved by the New York University (NYU) Institutional Review Board, was obtained from all subjects before their enrolment in the study for research use and publication of their data. Detailed methods are provided in the Supplementary Material.

Acknowledgements

We are grateful to Parthiban Rajasekaran and Sanofi for advice, and to Sharon Chung and the Immune Tolerance Network for biosamples used in the Validation cohort. Histological analyses were aided by Mark Alu and Gyles Ward, as well as the NYU GSOM Experimental Pathology Core. RNA sequencing studies were conducted at the NYU Genome Technology Center, with contributions from Gael Westby, Emily Guzman, Shyanon Rai, and Paul Zappile, under the supervision of Adriana Heguy. Flow cytometry studies were completed through the NYU Cytometry and Cell Sorting Laboratory, with guidance from Catherine Rapelje, Florenal Joseph, and Jiangwei Li. These NYU facilities are funded in part by the Cancer Center Support Grant NIH/NCI 5 P30CA16087 at the Laura and Isaac Perlmutter Cancer Center. We are grateful to Kate Trujillo, Uzair Chaudhary, Steven Medvedovsky, Sophia DelGiudice, and Heiko Käßner for their technical assistance. We also appreciate the advice and assistance of Bharati Matta and Tatiana Borja with neutrophil assays and platelet activation flow cytometry assays. We are grateful to Jason Knight, Marc Scherlinger, Patrick Blanco, Eric Morand, Diance, Kamen, Karen Costenbader, Laurence Morel and Brad Rovin for key discussions. We thank Peter Izmirly and Jill Buyon for clinical support. We thank the clinical coordinators of this study and all our patients for their participation.

Contributors

Study design: GJS and AA. Flow cytometric analysis: AA, CFR. RNA sequencing: AA, MC, LC, KR. Platelet and neutrophil immunoassay methodology and analyses: AA, AL, TW, BB. Histology analysis: AA, SRSG, CL. Murine colony management and colonisation studies: AL, ZA, MY, CFR, AA, GJS. *Ruminococcus gnavus* characterisation, maintenance, and bacterial pellet analysis: NG, GJS. Lipoglycan isolation: NG. Platelet activation studies: AA, CFR, MC, JP, BR, KR. Illustrations: AA and GJS. Manuscript writing: AA, GJS. Manuscript editing: GJS, AA, CFR, NG, AL, BJB, SRSG, TW, LC, ZA, BR, KR.

Funding

This study was in part funded by NIH P50-AR070591, R01 AI143313, R21AI180737, the Lupus Foundation of America Gilkeson Career Development Award (AA), NIH 5T32AR069515-07 (AA), and the Department of Defense CDMRP LRP W81XWH-18-1-0674 (BJ), and by Sanofi, Lyon, France. Prior studies were funded in part by the Lupus Research Alliance (GJS) and the Colton Center (GJS).

Competing interests

GJS reports financial support was provided by Sanofi and National Institutes of Health. GJS has patent pending to NYU. Grant support from Novartis and Genentech. No direct relationship to this project. All the other authors declare they have no competing interests.

Patient consent for publication

Written informed consent was obtained.

Ethics approval

Supervised by the NYU IRB.

Provenance and peer review

Not commissioned; externally peer reviewed.

Data availability statement

Clinical data for patients in our Pilot cohort are available in our prior publications [7,9], and for the 35 Validation cohort included in the Supplementary data, from the Immune Tolerance Network [26] (itntrialshare.org) of the NIAID. Datasets for RNA sequence data will be made available to online repositories. Additional primary data are available to qualified parties on request.

Supplementary materials

Supplementary material associated with this article can be found in the online version at doi:10.1016/j.ard.2026.03.002.

Orcid

Nicolas Gisch: http://orcid.org/0000-0003-3260-5269
Gregg J. Silverman: http://orcid.org/0000-0001-9480-9457

REFERENCES

[1] Meadows V, Antonio JM, Ferraris RP, Gao N. *Ruminococcus gnavus* in the gut: driver, contributor, or innocent bystander in steatotic liver disease? FEBS J 2025;292(6):1252–64.
[2] Miyauchi E, Shimokawa C, Steimle A, Desai MS, Ohno H. The impact of the gut microbiome on extra-intestinal autoimmune diseases. Nat Rev Immunol 2023;23(1):9–23.
[3] Anders HJ, Saxena R, Zhao MH, Parodis I, Salmon JE, Mohan C. Lupus nephritis. Nat Rev Dis Primers 2020;6(1):7.
[4] Silverman GJ, Azzouz DF, Gisch N, Amarnani A. The gut microbiome in systemic lupus erythematosus: lessons from rheumatic fever. Nat Rev Rheumatol 2024;20:143–57.
[5] Amarnani A, Silverman GJ. Understanding the roles of the microbiome in autoimmune rheumatic diseases. Rheumatol Immunol Res 2023;4(4):177–87.
[6] Togo AH, Diop A, Bittar F, Maraninchi M, Valero R, Armstrong N, et al. Description of *Mediterraneibacter massiliensis*, gen. nov., sp. nov., a new genus isolated from the gut microbiota of an obese patient and reclassification of *Ruminococcus faecis, Ruminococcus lactaris, Ruminococcus torques, Ruminococcus gnavus* and *Clostridium glycyrrhizinilyticum* as *Mediterraneibacter faecis* comb. nov., *Mediterraneibacter lactaris* comb. nov., *Mediterraneibacter torques* comb. nov., *Mediterraneibacter gnavus* comb. nov. and *Mediterraneibacter glycyrrhizinilyticus* comb. nov. Antonie Van Leeuwenhoek. 2018;111:2107-28.
[7] Azzouz D, Omarbekova A, Heguy A, Schwudke D, Gisch N, Rovin BH, et al. Lupus nephritis is linked to disease-activity associated expansions and immunity to a gut commensal. Ann Rheum Dis 2019;78(7):947–56.
[8] Silverman GJ, Deng J, Azzouz DF. Sex-dependent Lupus *Blautia* (*Ruminococcus*) *gnavus* strain induction of zonulin-mediated intestinal permeability and autoimmunity. Front Immunol 2022;13:897971.
[9] Azzouz DF, Chen Z, Izmirly PM, Chen LA, Li Z, Zhang C, et al. Longitudinal gut microbiome analyses and blooms of pathogenic strains during lupus disease flares. Ann Rheum Dis 2023;82(10):1315–27.
[10] Juge N. Microbe profile: *Ruminococcus gnavus*: the yin and yang of human gut symbionts. Microbiology (Reading) 2023;169(8):001383.

[11] Sagheddu V, Patrone V, Miragoli F, Puglisi E, Morelli L. Infant early gut colonization by *Lachnospiraceae*: high frequency of *Ruminococcus gnavus*. Front Pediatr 2016;4:57.
[12] Nooij S, Plomp N, Sanders IMJG, Schout L, van der Meulen AE, Terveer EM, et al. Metagenomic global survey and in-depth genomic analyses of *Ruminococcus gnavus* reveal differences across host lifestyle and health status. Nat Commun 2025;16(1):1182.
[13] Silverman G, Azzouz D, Grönwal C, Gunnarsson I, Svenungsson E. Validation of a serologic antibody biomarker against a candidate gut pathobiont for the diagnosis of lupus nephritis [Abstract]. Arthritis Rheumatol 2019;71(Suppl 10):1915.
[14] Chen BD, Jia XM, Xu JY, Zhao LD, Ji JY, Wu BX, et al. An autoimmunogenic and proinflammatory profile defined by the gut microbiota of patients with untreated systemic lupus erythematosus. Arthritis Rheumatol 2021;73(2):232–43.
[15] Toumi E, Goutorbe B, Plauzolles A, Bonnet M, Mezouar S, Militello M, et al. Gut microbiota in systemic lupus erythematosus patients and lupus mouse model: a cross species comparative analysis for biomarker discovery. Front Immunol 2022;13:943241.
[16] Ma L, Ge Y, Six N, Choi SC, Brown J, Castellanos Garcia A, et al. Gut expansion of a human lupus pathobiont is associated with autoantibody production and T cell dysregulation. ACR Open Rheumatol 2025;7(5):e70033.
[17] Aringer M, Costenbader K, Daikh D, Brinks R, Mosca M, Ramsey-Goldman R, et al. 2019 European League Against Rheumatism/American College of Rheumatology classification criteria for systemic lupus erythematosus. Arthritis Rheumatol 2019;71(9):1400–12.
[18] Fasano A. All disease begins in the (leaky) gut: role of zonulin-mediated gut permeability in the pathogenesis of some chronic inflammatory diseases. F1000Res. 2020;9:F1000 Faculty Rev-69.
[19] Banchereau R, Hong S, Cantarel B, Baldwin N, Baisch J, Edens M, et al. Personalized immunomonitoring uncovers molecular networks that stratify lupus patients. Cell 2016;165(3):551–65.
[20] Figgett WA, Monaghan K, Ng M, Alhamdoosh M, Maraskovsky E, Wilson NJ, et al. Machine learning applied to whole-blood RNA-sequencing data uncovers distinct subsets of patients with systemic lupus erythematosus. Clin Transl Immunol 2019;8(12):e01093.
[21] Muller MA, Luttrell-Williams E, Bash H, Cornwell MG, Belmont HM, Izmirly P, et al. Platelet gene expression in systemic lupus erythematosus and cardiovascular health. JACC Basic Transl Sci 2025;10(12):101395.
[22] Berger JS, Cornwell MG, Xia Y, Muller MA, Smilowitz NR, Newman JD, et al. A Platelet Reactivity Expression Score derived from patients with peripheral artery disease predicts cardiovascular risk. Nat Commun 2024;15(1):6902.
[23] Lood C, Amisten S, Gullstrand B, Jönsen A, Allhorn M, Truedsson L, et al. Platelet transcriptional profile and protein expression in patients with systemic lupus erythematosus: up-regulation of the type I interferon system is strongly associated with vascular disease. Blood 2010;116(11):1951–7.
[24] Subramanian A, Tamayo P, Mootha VK, Mukherjee S, Ebert BL, Gillette MA, et al. Gene set enrichment analysis: a knowledge-based approach for interpreting genome-wide expression profiles. Proc Natl Acad Sci U S A 2005;102(43):15545–50.
[25] Foroutan M, Bhuva DD, Lyu R, Horan K, Cursons J, Davis MJ. Single sample scoring of molecular phenotypes. BMC Bioinformatics 2018;19(1):404.
[26] Liu Q, Zhu W, Wen X, Da Y. The role of platelet–neutrophil interactions in driving autoimmune diseases. Immunology 2025;175(1):1–15.
[27] Lemke G. How macrophages deal with death. Nat Rev Immunol 2019;19(9):539–49.
[28] Dai X, Fan Y, Zhao X. Systemic lupus erythematosus: updated insights on the pathogenesis, diagnosis, prevention and therapeutics. Signal Transduct Target Ther 2025;10(1):102.
[29] Gladman DD, Ibañez D, Urowitz MB. Systemic lupus erythematosus disease activity index 2000. J Rheumatol 2002;29(2):288–91.
[30] ACCESS Trial Group. Treatment of lupus nephritis with abatacept: the abatacept and cyclophosphamide combination efficacy and safety study. Arthritis Rheumatol 2014;66(11):3096–104.
[31] Matta B, Battaglia J, Barnes BJ. Detection of neutrophil extracellular traps in patient plasma: method development and validation in systemic lupus erythematosus and healthy donors that carry *IRF5* genetic risk. Front Immunol 2022;13:951254.
[32] Wither JE, Prokopec SD, Noamani B, Chang N-H, Bonilla D, Touma Z, et al. Identification of a neutrophil-related gene expression signature that is enriched in adult systemic lupus erythematosus patients with active nephritis: clinical/pathologic associations and etiologic mechanisms. PLoS One 2018;13(5):e0196117.
[33] Chiche L, Jourde-Chiche N, Whalen E, Presnell S, Gersuk V, Dang K, et al. Modular transcriptional repertoire analyses of adults with systemic lupus erythematosus reveal distinct type I and type II interferon signatures. Arthritis Rheumatol 2014;66(6):1583–95.
[34] Puhm F, Laroche A, Boilard E. Diversity of megakaryocytes. Arterioscler Thromb Vasc Biol 2023;43(11):2088–98.
[35] Horvei KD, Pedersen HL, Fismen S, Thiyagarajan D, Schneider A, Rekvig OP, et al. Lupus nephritis progression in FcγRIIB$^{-/-}$yaa mice is associated with early development of glomerular electron dense deposits and loss of renal DNase I in severe disease. PLoS One 2017;12(11):e0188863.
[36] Thim-Uam A, Surawut S, Issara-Amphorn J, Jaroonwitchawan T, Hiengrach P, Chatthanathon P, et al. Leaky-gut enhanced lupus progression in the Fc gamma receptor-IIb deficient and pristane-induced mouse models of lupus. Sci Rep 2020;10(1):777.
[37] Armstrong PC, Allan HE, Kirkby NS, Gutmann C, Joshi A, Crescente M, et al. Temporal in vivo platelet labeling in mice reveals age-dependent receptor expression and conservation of specific mRNAs. Blood Adv 2022;6(23):6028–38.
[38] Beaulieu LM, Lin E, Morin KM, Tanriverdi K, Freedman JE. Regulatory effects of TLR2 on megakaryocytic cell function. Blood 2011;117(22):5963–74.
[39] Scherlinger M, Richez C, Tsokos GC, Boilard E, Blanco P. The role of platelets in immune-mediated inflammatory diseases. Nat Rev Immunol 2023;23(8):495–510.
[40] Blair P, Rex S, Vitseva O, Beaulieu L, Tanriverdi K, Chakrabarti S, et al. Stimulation of Toll-like receptor 2 in human platelets induces a thromboinflammatory response through activation of phosphoinositide 3-kinase. Circ Res 2009;104(3):346–54.
[41] Cognasse F, Nguyen KA, Damien P, McNicol A, Pozzetto B, Hamzeh-Cognasse H, et al. The inflammatory role of platelets via their TLRs and Siglec receptors. Front Immunol 2015;6:83.
[42] Clark SR, Ma AC, Tavener SA, McDonald B, Goodarzi Z, Kelly MM, et al. Platelet TLR4 activates neutrophil extracellular traps to ensnare bacteria in septic blood. Nat Med 2007;13(4):463–9.
[43] Etulain J, Martinod K, Wong SL, Cifuni SM, Schattner M, Wagner DD. P-selectin promotes neutrophil extracellular trap formation in mice. Blood 2015;126(2):242–6.
[44] Sun R, Huang J, Yang Y, Liu L, Shao Y, Li L, et al. Dysfunction of low-density neutrophils in peripheral circulation in patients with sepsis. Sci Rep 2022;12(1):685.
[45] Gisch N, Kohler T, Ulmer AJ, Müthing J, Pribyl T, Fischer K, et al. Structural reevaluation of *Streptococcus pneumoniae* lipoteichoic acid and new insights into its immunostimulatory potency. J Biol Chem 2013;288(22):15654–67.
[46] Zähringer U, Lindner B, Inamura S, Heine H, Alexander C. TLR2 - promiscuous or specific? A critical re-evaluation of a receptor expressing apparent broad specificity. Immunobiology 2008;213(3-4):205–24.
[47] Kang JY, Nan X, Jin MS, Youn S-J, Ryu YH, Mah S, et al. Recognition of lipopeptide patterns by Toll-like receptor 2-Toll-like receptor 6 heterodimer. Immunity 2009;31(6):873–84.
[48] Lavagna A, Auger J-P, Dumesnil A, Roy D, Girardin SE, Gisch N, et al. Interleukin-1 signaling induced by Streptococcus suis serotype 2 is strain-dependent and contributes to bacterial clearance and inflammation during systemic disease in a mouse model of infection. Vet Res 2019;50(1):52.
[49] Deng B, Wang S, Zhou P, Ding F. New insights into immune cell diversity in acute kidney injury. Cell Mol Immunol 2023;20(6):680–2.
[50] Dellepiane S, Leventhal JS, Cravedi P. T cells and acute kidney injury: a two-way relationship. Front Immunol 2020;11:1546.
[51] El Bannoudi H, Cornwell M, Luttrell-Williams E, Engel A, Rolling C, Barrett TJ, et al. Platelet LGALS3BP as a mediator of myeloid inflammation in systemic lupus erythematosus. Arthritis Rheumatol 2023;75(5):711–22.
[52] Morrell CN, Pariser DN, Hilt ZT, Vega Ocasio D. The platelet Napoleon complex-small cells, but big immune regulatory functions. Ann Rev Immunol 2019;37(1):125–44.
[53] Liu Z, Li L, Zhang H, Pang X, Qiu Z, Xiang Q, et al. Platelet factor 4(PF4) and its multiple roles in diseases. Blood Rev 2024;64:101155.

Ann Rheum Dis 85 (2026) 1596–1609

Contents lists available at ScienceDirect

Annals of the Rheumatic Diseases

journal homepage: https://www.sciencedirect.com/journal/annals-of-the-rheumatic-diseases

Systemic lupus erythematosus

An immunometabolic signature of major depressive disorder in systemic lupus erythematosus

Pierre Ellul[1,2], Nicolas Tchitchek[1], Grete Kvedaraviciute[1], Roberta Lorenzon[1,3], Isabelle Melki[4], Richard Delorme[2], Michelle Rosenzwajg[1,3], David Klatzmann[1,3,*]

[1] *Immunology-Immunopathology- Immunotherapy (i3), INSERM, UMR_S 959, Sorbonne Université, Paris, France*
[2] *Child and Adolescent Psychiatry Department, Robert Debré Hospital, Université Paris Cité, Paris, France*
[3] *Biotherapy (CIC-BTi) and Inflammation-Immunopathology-Biotherapy Department (i2B), Pitié-Salpêtrière Hospital, AP-HP, Paris, France*
[4] *Department of General Pediatrics, Trousseau Hospital, Sorbonne Université, Assistance Publique-Hôpitaux de Paris (AP-HP), Paris, France*

A R T I C L E I N F O

Article history:
Received 10 December 2025
Received in revised form 2 February 2026
Accepted 19 February 2026

Handling editor Josef S. Smolen

A B S T R A C T

Objectives: Systemic lupus erythematosus (SLE) frequently affects the central nervous system, leading to neuropsychiatric SLE (NPSLE). Major depressive disorder in SLE (SLE_{MDD}) is the most frequent manifestation of NPSLE and is believed to arise from an immune-mediated process. However, biomarkers for SLE_{MDD} remain lacking. The aim of this study was to identify candidate immunometabolic biomarkers associated with SLE_{MDD}.

Methods: We analysed deep flow cytometry immune phenotyping, gut microbiota profiling, and targeted mass spectrometry–based metabolomics from 99 patients from the LUPIL-2 study (NCT02955615). Biological signatures were identified using unsupervised principal component analysis and supervised decision tree classification. They were then validated in an independent cohort from the TRANSIMMUNOM study (NCT02466217).

Results: SLE_{MDD} patients exhibited a distinct immune profile with decreased naïve $CD4^+$ T cells and naïve regulatory T cells (Tregs), alongside increased $ICOS^+$ effector memory Tregs (94% classification accuracy). Gut microbiota diversity was reduced with depletion of *Akkermansia muciniphila* and enrichment of *Faecalibacterium prausnitzii*. Metabolomic analyses revealed disruptions in kynurenine and short-chain fatty acid pathways, including decreased butyrate levels. Integrative analyses demonstrated coordinated alterations linking Treg activation, microbial metabolites, and immune pathways, distinguishing SLE_{MDD} from $SLE_{non\text{-}MDD}$ with up to 85% accuracy.

Conclusions: SLE_{MDD} is associated with an immunometabolic signature involving alterations in Treg phenotype, gut microbiota composition, and metabolic pathways. These findings provide a rationale for future immunoregulatory or microbiota-targeted therapeutic strategies in SLE_{MDD}.

INTRODUCTION

Systemic lupus erythematosus (SLE) is a chronic systemic autoimmune disease with heterogeneous clinical manifestations. Its incidence ranges from 1 to 10 per 100,000 individuals, with a prevalence estimated between 20 and 150 per 100,000 [1]. Compared to other systemic autoimmune diseases, such as systemic sclerosis, Sjögren's syndrome, connective tissue diseases,

*Correspondence to Prof David Klatzmann, Clinical Investigation Center for Biotherapies and Immunology-Immunopathology-Immunotherapy department, Hôpital Pitié-Salpêtrière, 83 Bd de l 'Hôpital, Paris F-75013, France.

E-mail address: david.klatzmann@sorbonne-universite.fr (D. Klatzmann).

Pierre Ellul and Nicolas Tchitchek contributed equally.

https://doi.org/10.1016/j.ard.2026.02.019

WHAT IS ALREADY KNOWN ON THIS TOPIC

- We searched PubMed from inception to September 2025 for articles published in English, using search terms related to systemic lupus erythematosus (SLE) and major depressive disorder (MDD) (for example, "depression" OR "MDD" OR "major depressive disorder") AND ("lupus" OR "systemic lupus erythematosus" OR "SLE"). Several studies examined the comorbidity between SLE and MDD-related symptoms (SLE_{MDD}). Despite the heterogeneity of the studies, the prevalence was never less than 20%, and all reported that MDD affects the prognosis of SLE in terms of quality of life, morbidity, and mortality. Others have investigated the mechanistic links between depressive symptoms and SLE. Despite the weakness of the level of evidence, this association seems to be underpinned not by genetic factors but by complex immunometabolic pathways. Indeed, an increase in inflammatory mediators was associated with an increase in MDD associated with SLE (SLE_{MDD}). Unfortunately, each study has focused on limited immunological and/or metabolic components, making it difficult to formulate pathophysiological hypotheses.

WHAT THIS STUDY ADDS

- We used an international multicentre cohort of SLE patients for discovery and an independent French cohort for validation. We performed deep cell immunophenotyping, gut microbiome, and target metabolomic profiling. We identified an immunometabolic signature of SLE_{MDD} with a classification prediction performance of 94%. This signature includes ICOS+ effector memory regulatory T cell (Treg), depletion of *Akkermansia muciniphila*, and enrichment of *Faecalibacterium prausnitzii* and metabolomic disruptions in kynurenine and short-chain fatty acid pathways, including decreased butyrate levels.

HOW THIS STUDY MIGHT AFFECT RESEARCH, PRACTICE OR POLICY

- A substantial body of evidence suggests that SLE_{MDD} may specifically result from an immunometabolic dysregulation. Our findings provide further support for an immunometabolic involvement in SLE_{MDD} and identify Treg insufficiency and serotonin deficiency as key predictors of SLE_{MDD}. These findings should lead to the investigation of the use of these factors as biomarkers for SLE_{MDD} and may open new avenues in the development of immunotherapy for SLE_{MDD}.

or vasculitis, SLE carries higher mortality [1], driven primarily by infections, renal complications, and neuropsychiatric involvement. Neuropsychiatric SLE (NPSLE) affects 25% to 50% of patients and remains one of the most debilitating and diagnostically challenging aspects of the disease [2].

NPSLE encompasses a broad spectrum of neurological and psychiatric manifestations, many of which lack specific biomarkers and can mimic primary psychiatric disorders. Among these, major depressive disorder in SLE (SLE_{MDD}) is the most frequent condition directly attributable to lupus—that is, resulting from a primary immune-mediated pathogenic mechanism [2]. SLE_{MDD} affects up to 30% of patients and substantially worsens prognosis, disability, and quality of life (QoL) [3,4].

Major depressive disorder (MDD) is defined clinically by at least 2 weeks of persistent affective, cognitive, and somatic symptoms, including depressed mood, anhedonia, impaired concentration, and recurrent thoughts of death [5]. Its pathophysiology involves complex alterations in neurobiological stress-response systems [6], including chronic hyperactivity of the hypothalamic-pituitary-adrenal axis and low-grade systemic inflammation. The immune system is tightly integrated into these pathways through bidirectional interactions with neuroendocrine circuits [7].

A substantial body of evidence now supports inflammation as a causal contributor to MDD: (i) patients with MDD display elevated peripheral inflammatory markers; (ii) higher baseline inflammation predicts incident MDD in the general population [7]; (iii) proinflammatory therapies such as interferon-α frequently induce depressive symptoms; and (iv) anti-inflammatory treatments can alleviate depressive symptoms in inflammatory diseases [8]. Notably, murine models of SLE exhibit inflammation-driven depressive-like behaviours, reinforcing the link between immune dysregulation and SLE_{MDD} [9].

Beyond inflammation, gut microbiota dysbiosis and associated metabolic pathways have emerged as important regulators of mood and affect. Approximately 90% of peripheral serotonin is produced by enterochromaffin cells [10], and this production is tightly modulated by spore-forming commensals [11] and microbiota-derived short-chain fatty acids (SCFAs) [12]. Thus, profiling gut microbes and their metabolites provides key insight into the immunometabolic mechanisms linking dysbiosis to mood disorders, including SLE_{MDD}. Inflammation and gut microbiota converge at the interface of immune, metabolic, and neuroendocrine systems [13], and their study could enlighten the pathophysiology of SLE_{MDD}.

In this study, we applied an integrative immunometabolic approach combining deep flow cytometry immune phenotyping, gut microbiota metabolic pathway (GMMP) analysis, and targeted mass spectrometry–based metabolomics to identify candidate biomarkers associated with SLE_{MDD} in 2 independent SLE cohorts.

METHODS

The LUPIL-2 clinical trial

The LUPIL-2 clinical trial [14] (NCT02955615) is an international, multicentre, randomised, double-blind, placebo-controlled phase II study. Eligible participants were adults (≥18 years) with a confirmed diagnosis of SLE, according to either the revised 1997 American College of Rheumatology classification criteria or the 2012 Systemic Lupus International Collaborating Clinics criteria and presented with moderate to severe disease activity (Safety of Estrogens in Lupus Erythematosus National Assessment–Systemic Lupus Erythematosus Disease Activity Index [SELENA-SLEDAI] ≥6); 99/100 patients from the LUPIL-2 clinical trial were included in this study (1 patient had missing data for SELENA-SLEDAI).

Depressive status was assessed retrospectively using baseline responses from the study's QoL questionnaire. To approximate MDD symptoms as defined by the DSM-5, we selected 4 QoL subscores—intimate relationships, burden on others, emotional health, and fatigue—as proxies for the following DSM-5 symptoms: feelings of worthlessness or excessive/inappropriate guilt, depressed mood, markedly diminished interest or pleasure in activities, and fatigue, respectively [15] (Supplementary Fig S1).

Thresholds for each subscore were defined as the midpoint between the median and the third quartile, in order to approximate the expected MDD prevalence of 30% among SLE patients. To reduce misclassification due to arbitrary thresholds, participants were classified as having depression only if they met or exceeded the threshold on at least 3 of the 4 selected items. Using this approach, 30 out of 99 SLE patients (30%) were classified as depressed, in line with previously reported prevalence estimates [4].

The TRANSIMMUNOM clinical trial

The TRANSIMMUNOM study [16] (NCT02466217) was designed to identify and validate biomarkers and therapeutic targets in immune-mediated diseases using systems immunology approaches. Patients were recruited from multiple departments across Parisian hospitals, including the diabetology, ophthalmology, internal medicine, and clinical immunology departments of Pitié-Salpêtrière Hospital; the rheumatology and gastroenterology departments of Saint-Antoine Hospital; and the internal medicine department of Tenon Hospital. To ensure inclusion criteria comparable to those used for the LUPIL-2 patients, we restricted the analysis to active patients with a SELENA-SLEDAI score ≥6 (n = 12).

In contrast to LUPIL-2, depressive symptoms in SLE TRANSIMMUNOM participants were assessed using the Hospital Anxiety and Depression Scale (HADS) [17]. Following standard clinical cutoffs, participants were classified as not depressed if their total HADS score was ≤7 and depressed if the score was ≥11 [17]. For participants with intermediate scores (8–10), corresponding to ambiguous symptomatology, depression status was further evaluated using a self-report version of the QoL questionnaire. This version, distinct from that used in LUPIL-2, specifically assesses the presence of depressive symptoms. Participants who endorsed 2 or more items were classified as depressed.

Cytometry profiling

Flow cytometry was performed using 12 predefined panels, as previously described [18]. Among these, 3 panels were specifically designed to assess T cell activation, migration, and memory phenotypes; 1 panel was dedicated to characterising $CD4^+$ T cell polarisation using a combination of chemokine receptors, while 2 panels focused on the phenotypic profiling of regulatory T cells (Tregs). The remaining panels were used to analyse a broad range of immune cell subsets, including B cells, natural killer cells, monocytes, dendritic cells, mucosal-associated invariant T cells, and myeloid-derived suppressor cells. A panel was also developed for the enumeration of major immune cell populations, incorporating counting beads to allow for the absolute quantification of these subsets. These absolute counts were subsequently used as reference values to extrapolate absolute cell numbers across the other panels, based on overlapping populations. All the panels used were the same that have been described in [18] using exactly the same clones and methods. The panel used to quantify the abundance of the innate lymphoid cell is described in [19].

All cytometric acquisitions were carried out on a Gallios flow cytometer equipped with 3 lasers (violet: 405 nm, blue: 488 nm, violet: 638 nm), enabling the detection of 10 fluorescent parameters (Beckman Coulter), maintained daily according to the manufacturer's guidelines using Flow Check Pro and Flow Set Pro fluorospheres. Data acquisition was performed using Kaluza software (Beckman Coulter). Cell populations were defined using previously established gating strategies [18], and data were analysed by manual gating with Kaluza analysis 1.3 software (Beckman Coulter).

Unsupervised analysis of flow cytometry data

Cytometry profiles were visualised using Uniform Manifold Approximation and Projection (UMAP) based on the expression of all markers [16]. This dimensionality reduction technique preserves the global structure of the data while facilitating the visual identification of cellular subpopulations. To further explore population structure, the K-means clustering algorithm was applied to automatically partition cells into 100 clusters based on phenotypic similarity. Quality control procedures for these unsupervised analyses are detailed in Supplementary Figure S2.

Gut microbiome profiling

Patients were provided with a standardised stool collection kit (Metagenopolis, INRA) to ensure proper sample collection and preservation during transport prior to microbiota analysis. Total faecal DNA was extracted and subjected to shotgun metagenomic sequencing using Ion Proton technology (ThermoFisher), generating an average of 23.7 ± 0.8 million single-end short reads per sample (read length: 150 bp). Each sample yielded a minimum of 20 million single-end reads, with fragment sizes ranging from 45 to 370 bp.

Raw sequencing reads were processed using AlienTrimmer to remove residual sequencing adaptors and low-quality bases [20]. Reads were then filtered to exclude human and dietary contaminant DNA using genome assemblies of *Homo sapiens, Bos taurus*, and *Arabidopsis thaliana*, applying a 97% identity threshold. Reads shorter than 100 bp after trimming were discarded.

Microbial taxonomic composition and functional profiling were assessed using MetaPhlAn2 and HUMAnN2, respectively [21,22], allowing quantification of both microbial species and metabolic pathways. The Rényi taxonomic diversity profiles were evaluated using the vegan package (version 2.6.4).

Microbiome profiling was available for 69 patients from the LUPIL-2 trial.

Targeted mass spectrometry–based metabolomics analysis

Tryptophan metabolites were quantified using a targeted LC-MS/MS method, with analytical parameters described in reference [23] and the list of quantified metabolites provided in [24]. For SCFAs, a separate LC-MS/MS protocol was applied, as detailed in [25]. These 2 targeted assays were designed to quantify distinct classes of metabolites and do not aim to reconstruct complete upstream-downstream metabolic pathways. For both metabolite classes, quantification was performed using TargetLynx software (Waters), which was used to construct calibration curves and quantify analytes. Calibration curves were generated individually for each metabolite based on the intensity ratio (response) between the analyte and its corresponding internal standard. Each calibration curve defines a quantification range, from the lower limit of quantification to the upper limit of quantification. Quality control samples were used to validate the accuracy of each quantification batch. The %Diff formula was applied to assess the deviation between measured and theoretical concentrations, ensuring consistency and reliability of the results. Metabolomic profiling was available for 83 patients from the LUPIL-2 trial.

Statistical analyses

Prior to each analysis, the normality of variable distributions was assessed using the Shapiro-Wilk test. For continuous variables, either Student's *t* test or the Wilcoxon rank-sum test was applied, depending on the distribution. Categorical variables were compared using Fisher's exact test. To reduce the risk of false positives in univariate comparisons, a significance

threshold of $P < .01$ was adopted. To identify immune variables associated with depression in a multivariate framework, we employed classification decision trees, a type of supervised learning algorithm. These models enable intuitive interpretation of complex datasets by segmenting observations into branches based on hierarchical decision rules. Classification trees were generated using the 'partykit' R package [26]. Model performance was evaluated using the area under the receiver operating characteristic curve (AUC), as well as accuracy, sensitivity, and specificity metrics. Principal component analyses (PCAs) were performed using the FactoMineR R package, based on unscaled abundances of immune cell parameters, microbial taxa, and metabolic pathways [27]. Integrated analyses were performed on the subset of 33 patients for whom matched multiomics profiles were available.

Data availability

The datasets generated and/or analysed during the current study are available from the corresponding author upon reasonable request.

RESULTS

Among the 99 patients enrolled in the LUPIL-2 study, 30 patients (30.3%) were identified as having SLE_{MDD} at baseline. No significant differences in demographic or SLE-related clinical parameters were observed between SLE_{MDD} and $SLE_{non\text{-}MDD}$ patients (Table 1), notably for gender distribution and disease activity scores (assessed by both SELENA-SLEDAI and British Isles Lupus Assessment Group).

Table 1
Demographic and clinical characteristics of depressed and nondepressed patients with systemic lupus erythematosus in the LUPIL-2 study

	SLE_{MDD} (n = 30; 30.3%)	$SLE_{non\text{-}MDD}$ (n = 69; 69.7%)	*P* value
Demographics			
Age (y)	41.53 (±11.16)	40.58 (±12.5)	.70
Sex ratio (M/F)	2/28	7/62	.86
Geographic origin			.27
Bulgaria	12 (40%)	14 (20.3%)	
France	1 (3.3%)	8 (11.6%)	
Germany	2 (6.7%)	7 (10.1%)	
Mauritius	4 (13.3%)	16 (23.2)	
Mexico	3 (10%)	10 (14.5%)	
Portugal	0 (0%)	3 (4.3%)	
Romania	6 (20%)	8 (11.6%)	
Spain	2 (6.7%)	3 (4.34)	
Education level			.18
Bachelor's degree or less	20 (74.1%)	39 (75%)	
Advanced level	7 (25.9%)	13 (25%)	
Anthropometric information			
Weight (kg)	67.61 (±12.9)	66.24 (±14.8)	.40
BMI	24.7 (±4.5)	25.09 (±5.36)	.90
SLE clinical characteristics			
Duration of SLE (y)	12.7 (±10.2)	8.4 (±6.9)	.06
SELENA-SLEDAI	10.03 (±3.09)	10.7 (±3.7)	.50
BILAG index	16.13 (±5.2)	15.9 (±7.06)	.80

BILAG, British Isles Lupus Assessment Group; BMI, body mass index; SELENA-SLEDAI, Safety of Estrogens in Lupus Erythematosus National Assessment–Systemic Lupus Erythematosus Disease Activity Index; SLE, systemic lupus erythematosus; SLE_{MDD}, major depressive disorder in SLE. Sex refers to biological sex (female/male), and the sex ratio corresponds to the distribution of male and female participants.
Values are shown as mean ± SD or n (%), as appropriate. *P* values correspond to statistical comparisons performed between SLE_{MDD} and $SLE_{non\text{-}MDD}$ groups.

T cell phenotyping signature of SLE_{MDD}

Prior studies have consistently shown that Tregs are dysregulated in active SLE, with reduced percentages of naïve Tregs and increased frequencies of activated effector memory T cells associated with elevated disease activity, while ICOS Tregs undergo impaired differentiation during SLE disease progression [28,29]. Furthermore, T cell alterations in SLE, including increased PD-1^+ T cell expression and shifts from naïve to memory phenotypes, have been linked to organ involvement and, critically, to neuropsychiatric symptoms through mechanisms involving infiltrating T cells into the central nervous system [30].

Using deep immunophenotyping, we identified 18 lymphocyte subpopulations that were differentially abundant between SLE_{MDD} and $SLE_{non\text{-}MDD}$ patients (n = 52, Fig 1A). SLE_{MDD} patients exhibited a decrease in naïve $CD4^+$ T cells, along with an increase in $CD4^+$ and $CD8^+$ T cells displaying an effector/central memory phenotype. When comparing SLE_{MDD} and $SLE_{non\text{-}MDD}$ groups, SLE_{MDD} patients showed significantly lower frequencies of naïve $CD4^+$ T cells (P value = .001) and naïve Tregs (P value = .0008), and higher frequencies of PD-1^+ $CD4^+$ T cells (P value = .006) and $ICOS^+$ effector memory Tregs (P value = .007) (Fig 1C-F).

To assess the relevance of these observations, we analysed their power of classification. Using decision trees, $ICOS^+$ Tregs were the best discriminators of SLE_{MDD} vs $SLE_{non\text{-}MDD}$ with 94% accuracy, a sensitivity of 100%, a specificity of 92%, and an AUC of 0.98 (Fig 1B).

To further refine the phenotypic characterisation of SLE_{MDD}-associated lymphocyte subsets, we performed unsupervised clustering of cytometry data. Cells were embedded using UMAP based on surface marker expression and grouped into clusters using the K-means algorithm (Fig 1G). These clusters were then assigned a label based on their defining phenotype. SLE_{MDD} was associated with a notable shift in T cell phenotypes, characterised by a reduction in several $CD4^+$ T cell subsets, including naïve $CD4^+$ T cells ($CD45RA^+$, $CCR7^+$, $CD103^-$- Cluster 79 and M1), tissue-resident naïve $CD4^+$ T cells ($CD45RA^+$, $CCR7^+$, $CD103^+$- Cluster 97), as well as tissue-resident memory $CD4^+$ T cells ($CD45RA^-$, $CCR7^+$, $CD103^+$- Cluster 83 and M3). In contrast, an increase was observed in TEMRA $CD8^+$ T cells ($CD45RA^+$, $CCR7^+$, $CD103^+$- Cluster M4) and in a population of resident effector memory $CD4^+$ and $CD8^+$ T cells ($CD45RA^-$, $CCR7^-$, $CD103^+$ - Cluster 57, 59 and M5) (Fig 1H,I).

While these markers reflect phenotypic activation and differentiation states of Tregs rather than direct measures of suppressive function, our findings highlight a reshaping of the T cell compartment in SLE_{MDD}, involving both regulatory and effector subsets.

Validation of the immunometabolic signature of SLE_{MDD}

As no suitable external cohort with comparable data was available, we could not directly validate the combined immunometabolic signature in an independent dataset. However, since flow cytometry immunophenotyping alone demonstrates good classification performance, we applied the immunological signature identified in LUPIL-2 to an independent cohort derived from the TRANSIMMUNOM study, for which we had performed identical deep flow cytometry immunophenotyping (n = 10). This cohort included 23 patients with SLE (13 SLE_{MDD} (56.5%)

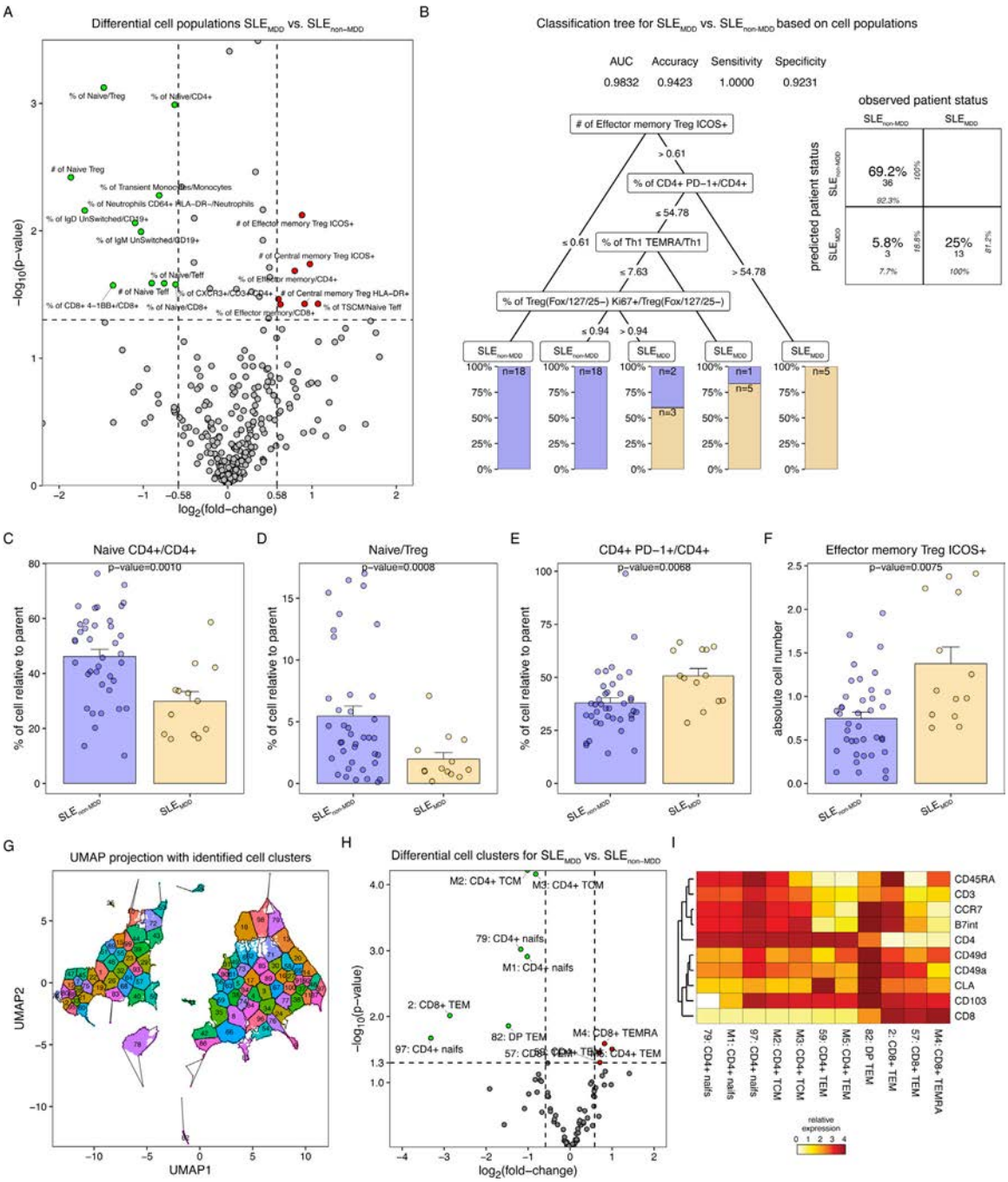

Figure 1. Immunophenotypic differences between SLE patients with and without major depressive disorder. (A) Volcano plot showing immune cell populations differentially abundant between SLE_{MDD} and $SLE_{non\text{-}MDD}$ patients. (B) Decision tree model based on flow cytometry variables used to classify patients by depression status. The tree illustrates hierarchical rules derived from cell subset abundances. (C-F) Distribution of selected T cell subsets in SLE_{MDD} and $SLE_{non\text{-}MDD}$ patients, including naïve $CD4^+$ T cells, naïve regulatory T cells (Tregs), PD-1^+ $CD4^+$ T cells, and $ICOS^+$ effector memory Tregs. (G) UMAP projection of flow cytometry data showing clustering of lymphocyte populations based on marker expression. (H) Volcano plot showing clusters differentially abundant between SLE_{MDD} and $SLE_{non\text{-}MDD}$ groups, as identified by unsupervised clustering. (I) Heatmap showing the relative expression levels of selected surface markers across representative T cell clusters. A total of 52 patients were included in these cytometry analyses. AUC, area under the receiver operating characteristic curve; SLE, systemic lupus erythematosus; $SLE_{MDD,}$ major depressive disorder in SLE; UMAP, Uniform Manifold Approximation and Projection.

and 10 $SLE_{non\text{-}MDD}$ (43.5%)). In order to have similar inclusion criteria to those for LUPIL-2 patients, we only included active patients from TRANSIMMUNOM (with a SELENA-SLEDAI score ≥6) (Table 2).

To first explore group separation in a nonsupervised framework, we performed a PCA. This analysis revealed a partial separation between SLE_{MDD} and $SLE_{non\text{-}MDD}$ patients along the first principal component (PC1), which accounted for 60.32% of the total variance (Fig 2A). Inspection of the PCA correlation circle (Fig 2B) indicated that PC1 was mainly driven by opposing contributions of naïve Teffs and central memory Tregs, highlighting these populations as major sources of variance in the dataset. In contrast, PC2 (23.31% of the variance) captured additional variability across samples but was not associated with specific variables and was not relevant for the group discrimination. Some overlap between groups was observed, reflecting interindividual heterogeneity within each clinical category rather than a strict separation.

Table 2
Demographic, clinical, and biological characteristics of SLE_{MDD}, $SLE_{non-MDD}$ patients in TRANSIMMUNOM

	SLE_{MDD} (n = 7; 58%)	$SLE_{non-MDD}$ (n = 5; 42%)	*P* value
Demographic			
Age (y)	40.71 (±7.5)	49.6 (±8.08)	.12
Sex ratio (M/F)	0/7	1/4	.15
Education level			.20
Bachelor's degree or less	4 (57%)	2 (40%)	
Advanced level	3 (43%)	3 (60%)	
Anthropometric information			
Weight (kg)	62.7 (±10.1)	55.98 (±4.01)	.14
BMI	22.07 (±3.43)	21.07 (±2.1)	.75
SLE clinical characteristics			
Duration of SLE (mo)	104 (±101.1)	90.8 (±66.6)	.87
SELENA-SLEDAI	13.1 (±7.1)	9.5 (±3.0)	.27
HAD	20.29 (±4.4)	5.8 (±3.42)	.005

BMI, body mass index; HAD, Hospital Anxiety and Depression Scale; SELENA-SLEDAI, Safety of Estrogens in Lupus Erythematosus National Assessment −Systemic Lupus Erythematosus Disease Activity Index; SLE, systemic lupus erythematosus; SLE_{MDD}, major depressive disorder in SLE.

We then assessed the discriminative power of this signature using a supervised classification approach based on a random forest model. In this context, increased proportions of central memory Tregs together with decreased proportions of naïve Teffs emerged again as the most important features contributing to the classification of SLE_{MDD} vs $SLE_{non-MDD}$ patients (Fig 2C). The random forest model achieved an overall accuracy of 100%, with both sensitivity and specificity reaching 100%, as summarised by the confusion matrix (Fig 2D).

Gut microbiota signature of SLE_{MDD}

Given the well-established interactions between the gut microbiome and immune responses, we next investigated gut microbiota composition. Indeed, accumulating evidence demonstrates that SLE patients exhibit gut microbiota dysbiosis characterised by reduced microbial diversity and richness, decreased Firmicutes/Bacteroidetes ratio, and alterations in specific bacterial taxa, including depletion of *Akkermansia muciniphila* and *Faecalibacterium prausnitzii* [31,32].

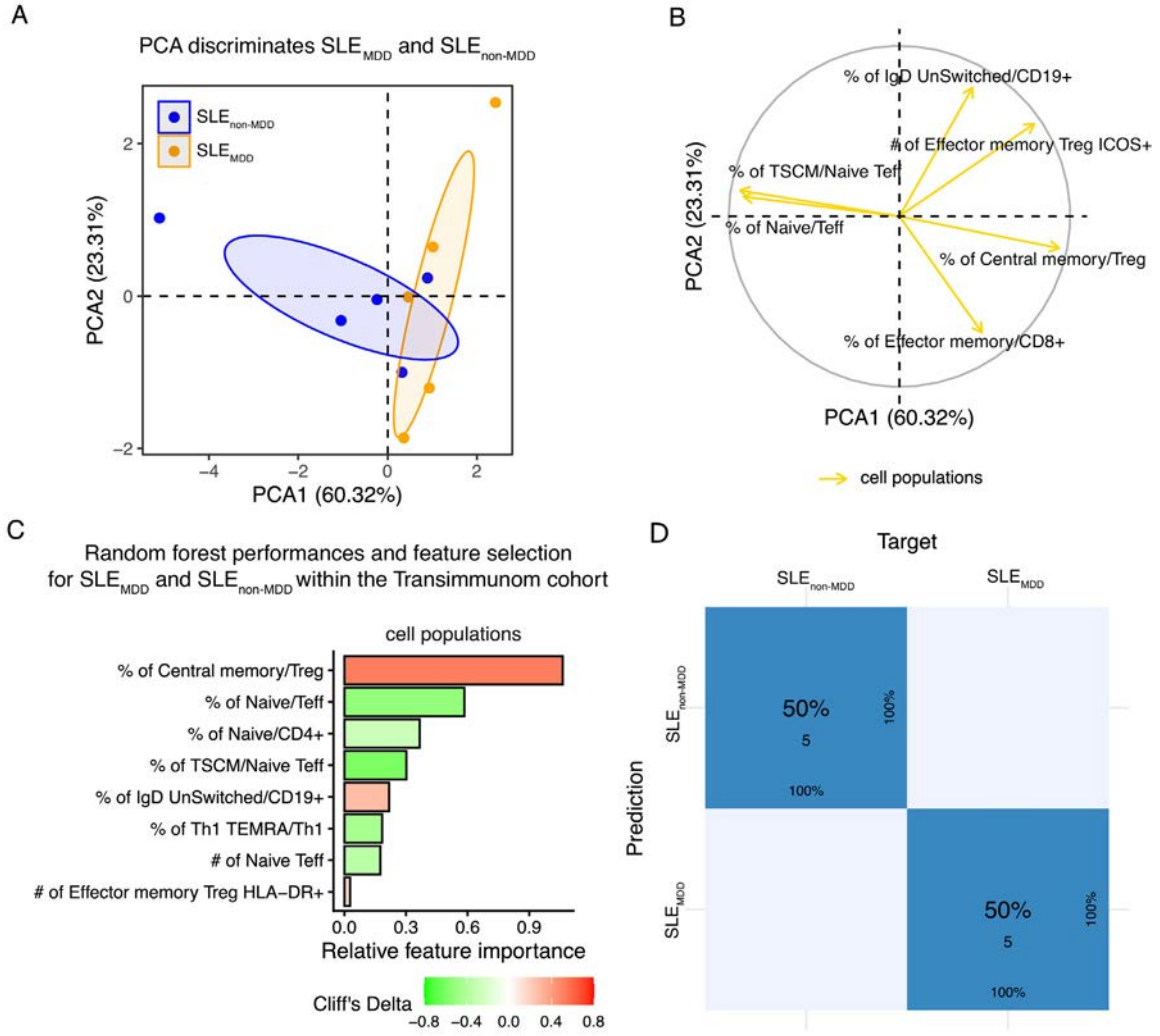

Figure 2. Validation of the lymphocyte-based signature in the independent TRANSIMMUNOM cohort. (A) Principal component analysis (PCA) of flow cytometry variables distinguishes SLE_{MDD} from $SLE_{non-MDD}$ patients. (B) PCA correlation circle showing the contribution of individual cell population variables to the principal components. (C) Random forest classifier built on the same variables, with a ranked list of the most informative features. (D) Confusion matrix based on random forest model performance. A total of 10 patients were included in these cytometry analyses. SLE, systemic lupus erythematosus; SLE_{MDD}, major depressive disorder in SLE.

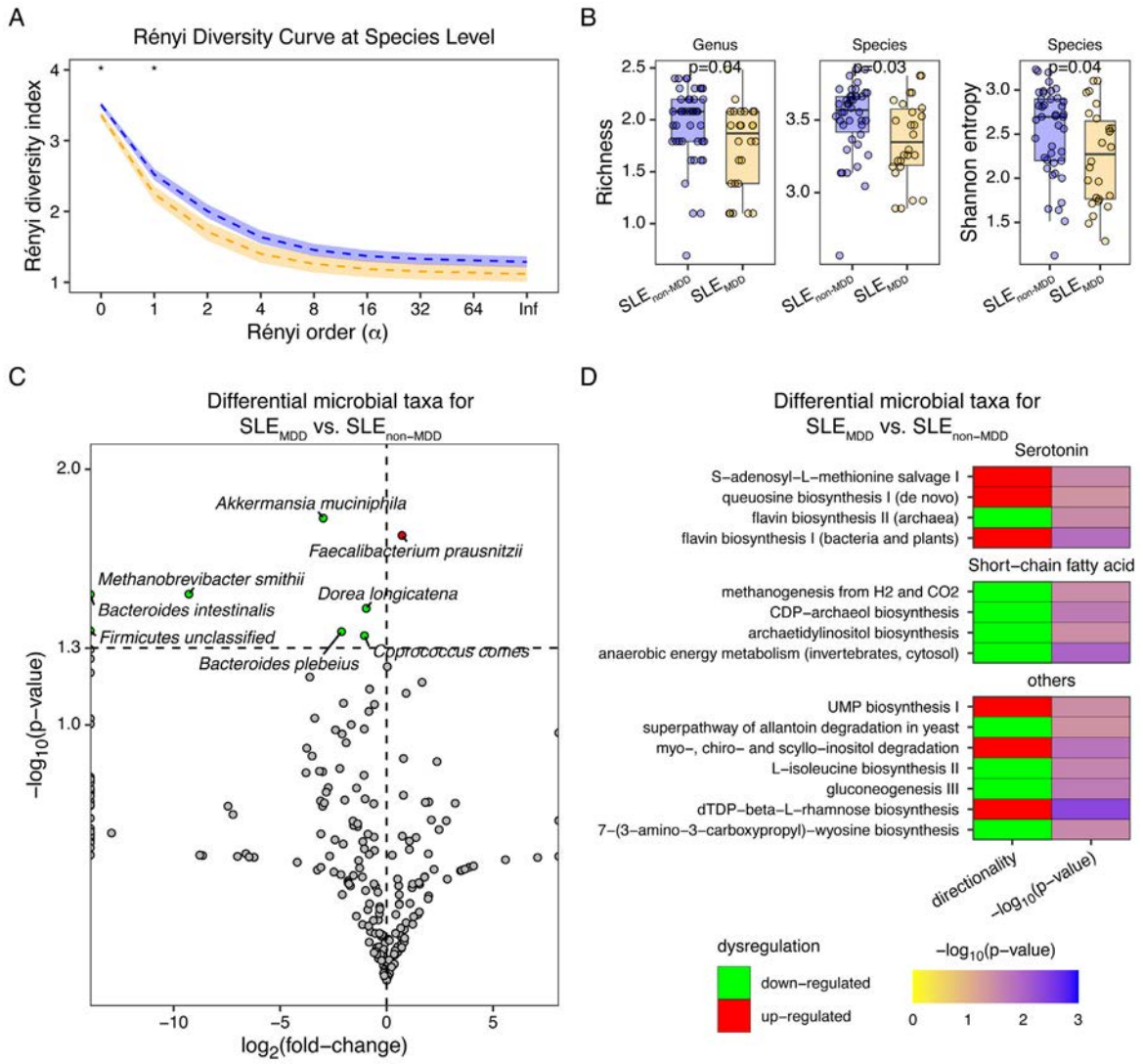

Figure 3. Differences in gut microbiota composition and microbial metabolic pathways between SLE_{MDD} and $SLE_{non\text{-}MDD}$ patients. (A) Rényi diversity curves at the species level comparing gut microbial diversity across groups. (B) Box plots showing species richness and Shannon entropy. (C) Volcano plot of microbial taxa displaying differential abundance between groups, with selected species highlighted. (D) Differential analysis of microbial metabolic pathways inferred from metagenomic data. Each bar represents a pathway annotated by directionality and functional category, including associations with short-chain fatty acids and serotonin-related metabolism. A total of 69 patients were included in these microbiome analyses. AUC, area under the receiver operating characteristic curve; 5-HIAA, 5-hydroxyindoleacetic acid; IPA, indole-3-propionic acid; SLE, systemic lupus erythematosus; SLE_{MDD}, major depressive disorder in SLE.

Firstly, compared with $SLE_{non\text{-}MDD}$ patients, we found that patients with SLE_{MDD} exhibit lower microbial diversity, as evidenced by the Rényi diversity index (Fig 3A), as well as lower genus richness (*P* value = .04), species richness (*P* value = .03), and Shannon entropy (*P* value = .04) (Fig 3B). Differential analysis of gut microbiota taxa revealed a significant decrease in several bacteria, including *A. muciniphila* and Firmicutes, as well as a notable increase in *F. prausnitzii* (Fig 3C). Secondly, differential analysis of GMMP revealed that SLE_{MDD} patients exhibited a remarkable overexpression of GMMPs related to the tryptophan/serotonin pathway, as well as a reduction in GMMPs related to fatty acid biosynthesis (Fig 3D). Additionally, there were also disruptions of other GMMP, notably related to sugar and amino acid biosynthesis (Fig 3D).

Serum metabolomic signature of SLE_{MDD}

Emerging evidence indicates that the gut microbiota might influence tryptophan metabolism in SLE, although this relationship remains to be fully elucidated [33]. Given the relationship between tryptophan and SCFA with Tregs homeostasis, we next performed targeted mass spectrometry–based metabolomics to directly quantify metabolites involved in serotonin-related tryptophan and SCFA pathways (n = 83).

Targeted metabolomic profiling of the serotonin and kynurenine pathways revealed selective alterations in SLE_{MDD} patients compared to $SLE_{non\text{-}MDD}$ patients. The central serotonergic pathway—including tryptophan availability, conversion to serotonin, and serotonin degradation—appeared largely preserved. No significant difference in plasma tryptophan levels was observed between the groups, indicating that systemic tryptophan availability per se is not altered in SLE_{MDD}; similarly, no significant changes were observed in serotonin (5-HT), its main degradation product 5-hydroxyindoleacetic acid (5-HIAA), or the indole-3-propionic acid (IPA)/5-HIAA ratio.

In contrast, compared with $SLE_{non\text{-}MDD}$ patients, SLE_{MDD} patients showed significant changes in the kynurenine pathway. Quinolinic acid (QA), a neurotoxic product of the kynurenine

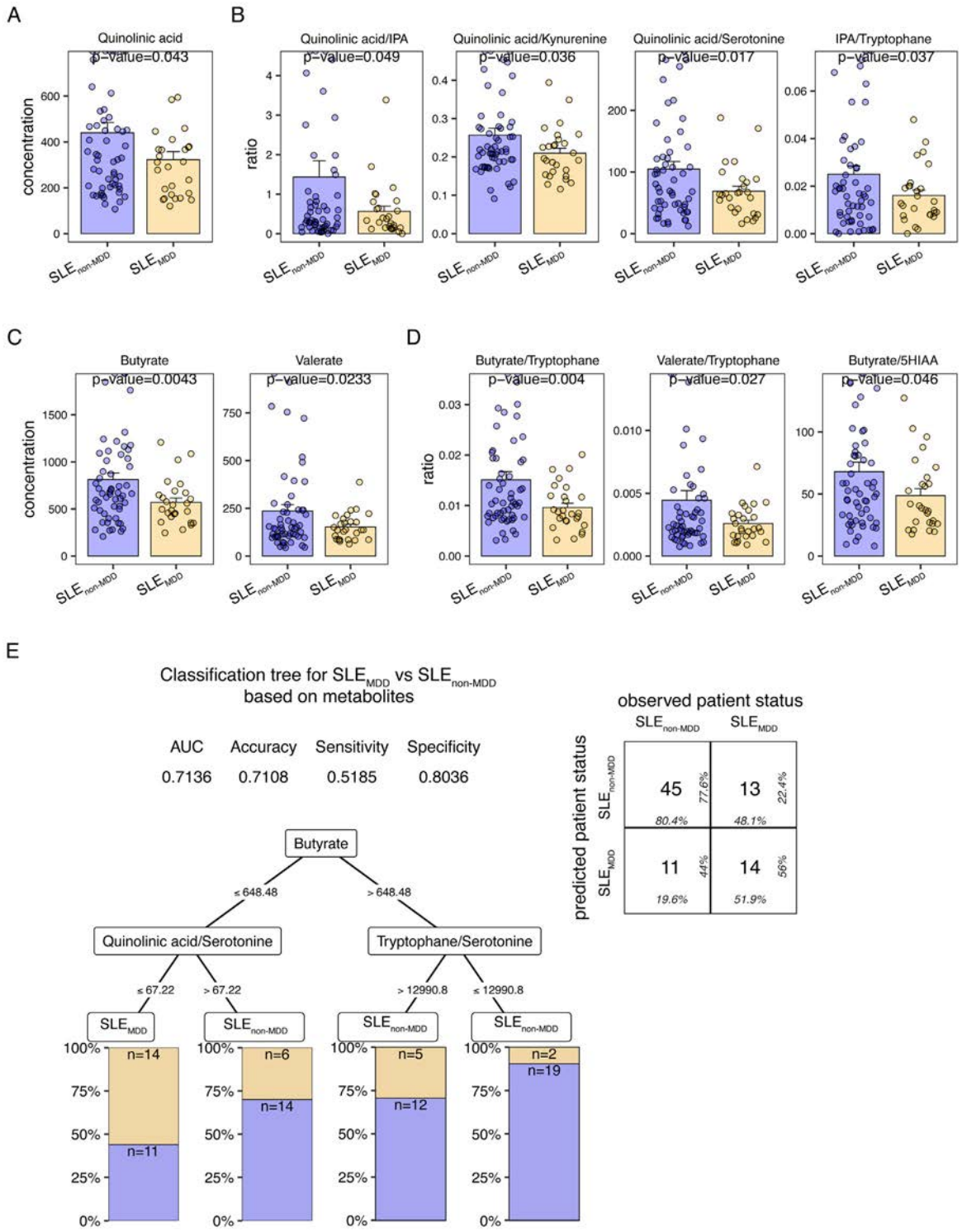

Figure 4. Targeted plasma metabolomics in SLE patients with and without major depressive disorder. (A) Concentration of quinolinic acid, a metabolite produced in the kynurenine branch of tryptophan metabolism. (B) Ratios derived from indole-3-propionic acid, kynurenine, quinolinic acid, and serotonin that summarise relative fluxes within the tryptophan-serotonin and tryptophan−kynurenine pathways. (C) Concentrations of the short-chain fatty acids butyrate and valerate. (D) Ratios combining butyrate or valerate with either tryptophan or the serotonin catabolite 5-hydroxyindoleacetic acid, illustrating integration between short-chain-fatty-acid production and serotonin metabolism. (E) Classification tree built from the metabolite variables, showing the hierarchical rules that separate patients according to depression status. A total of 83 patients were included in these metabolomic analyses. AUC, area under the receiver operating characteristic curve; Ig, immunoglobulin; PCA, principal component analysis; SLE, systemic lupus erythematosus; $SLE_{MDD,}$ major depressive disorder in SLE; Treg, regulatory T cell.

pathway, was significantly lower in SLE_{MDD} patients (P = .04) (Fig 4A), together with lower QA/IPA (P value = .04), QA/kynurenine (P value = .03), and QA/5-HT (P value = .01) ratios (Fig 4B). While absolute levels of IPA, a neuroprotective microbial metabolite of tryptophan, did not differ significantly between SLE_{MDD} and $SLE_{non\text{-}MDD}$ patients, the IPA/tryptophan ratio was significantly lower in SLE_{MDD} patients (P value = .03) (Fig 4B).

Compared with $SLE_{non\text{-}MDD}$ patients, SLE_{MDD} patients showed lower plasma levels of butyrate (*P* value = .004) and valerate (*P* value = .02) (Fig 4C). In addition, acetate and propionic acid levels were not significantly different. Those results suggest a selective disruption rather than a global SCFA depletion. The branched chain/straight chain ratio is also nonsignificantly different, indicating that the global balance between carbohydrate and protein fermentation pathways is conserved and further confirming the specificity of the disruption in butyrate/valerate pathways.

To explore potential interactions between SCFA metabolism and the tryptophan-serotonin axis, several cross-pathway ratios were examined. Compared with $SLE_{non\text{-}MDD}$ patients, SLE_{MDD} patients showed lower butyrate/tryptophan (*P* value = .003) and valerate/tryptophan (*P* value = .02) ratios, indicating a relative reduction in SCFA production with respect to tryptophan availability (Fig 4D). Moreover, compared with $SLE_{non\text{-}MDD}$ patients, SLE_{MDD} patients showed a lower butyrate/5-HIAA ratio (*P* value = .04), while serotonin-related metabolites did not differ between groups. Notably, the butyrate/5-HT ratio is not significantly different, further supporting that primary serotonergic metabolism is preserved, while secondary interactions involving serotonin catabolism and microbial activity may be altered. The importance of butyrate and QA/5HT in particular was further supported by a classification tree, which achieved a receiver operating characteristic (ROC) area under the curve (AUC) of 0.71 with an 71% accuracy, with a sensitivity of 51%, specificity of 80% (Fig 4E).

Coexpression network analysis of immunophenotyping and metabolomics

To further explore our hypothesis of a complex interaction between immune cell populations, GMMP, and targeted metabolites, we assessed the discriminatory capacity of an integrated immunometabolic feature to distinguish between SLE_{MDD} and $SLE_{non\text{-}MDD}$ patients using PCA (n = 33).

Using the features that we had previously found to be different between the groups, PCA revealed distinct separation between the 2 groups (Fig 5A). The PC1, which accounted for 16.1% of the variance, was driven by a combination of immune cell populations, metabolites, and pathway variables. In contrast, the second component (PC2), which captured approximately 12.8% of the variance, was influenced by SCFA/serotonin metabolites (see Fig 5B and Supplementary Fig S3).

Secondly, random forest classification analysis showed that the immunometabolic signature could accurately distinguish between SLE_{MDD} patients with 85% accuracy, 70% sensitivity, and 100% specificity (AUC = 0.98; Fig 5C). The most informative variables contributing to the classification were (i) microbial pathways related to sugar and amino acid biosynthesis; (ii) the metabolome, which confirmed the importance of SCFA and its interaction with serotonin; and (iii) the lymphocyte population, which showed an increase in central/effector memory Tregs and Teff, and a decrease in naïve CD4+ (Fig 5C).

Lastly, to better analyse the interconnection between the different components of the SLE_{MDD} signature, we used coexpression network analysis (Fig 5D). Specifically, we identified all significant correlations between variable pairs across these 3 data layers. Firstly, we confirmed that the immune cell populations (brown circles) are highly interconnected (Fig 5D). Second, we found that activated Treg–related variables exhibited high centrality within the correlation network connecting immune cell populations, microbial pathways, and circulating metabolites. Specifically, we highlighted that effector memory Treg ICOS+ are highly connected with serotonin synthesis and degradation (tryptophan/serotonin, serotonin/5-HIAA, 3-OH-anthranilic acid) pathways, as well as with $CR45RA^+$ Tregs and CD95+ central memory Tregs, specifically with the kynurenine pathway of serotonin degradation (QA/serotonin, QA/kynurenine, serotonin/kynurenine and kynurenine) (Fig 5D). Thirdly, SCFA and serotonin-related metabolites were interconnected and also linked to GMMP features (Fig 5D).

DISCUSSION

In this study, we identified candidate immunometabolic biomarkers associated with SLE_{MDD}, a frequent and clinically heterogeneous manifestation for which objective biological markers remain limited. This signature integrates coordinated alterations across immune phenotypes, microbial metabolic pathways, and circulating metabolites, consistent with a systems-level immunometabolic state rather than isolated abnormalities. While not establishing causality, these findings propose a coherent set of candidate biological markers—validated in part across independent cohorts—that support the view that SLE_{MDD} reflects a distinct, immune-associated biological context beyond nonspecific psychological or reactive mechanisms.

Treg abnormalities as a central feature of SLE_{MDD}

The most prominent immunological feature associated with SLE_{MDD} was a shift in the phenotypic composition of the Treg compartment. SLE_{MDD} patients displayed a marked reduction in naïve Tregs together with a significant increase in $ICOS^+$ effector memory Tregs. The strong discriminative performance of $ICOS^+$ Tregs—achieving 94% accuracy—supports their role as a core component of the SLE_{MDD} immune signature. Furthermore, unsupervised clustering confirmed a broader reconfiguration of the T cell landscape, including a loss of naïve $CD4^+$ T cells and an expansion of memory and tissue-resident effector populations. This phenotype indicates chronic activation and accelerated differentiation, a pattern consistent with a Treg response to sustained immune stimulation.

Naïve Tregs are particularly reduced in active SLE, while effector memory T cell populations accumulate due to chronic immune stimulation. $ICOS^+$ Tregs represent a functionally distinct subset with superior suppressive capacity mediated primarily by IL-10 production [28]. Notably, impaired differentiation of $ICOS^+$ Tregs has been documented during the transition from low to high disease activity in SLE patients. In line with previous reports of impaired Treg function in SLE, the increased frequency of $ICOS^+$ effector memory Tregs in SLE_{MDD} is more likely to reflect a phenotypic shift within the Treg compartment rather than restored regulatory competence. Thus, the observed expansion of $ICOS^+$ effector memory Tregs may reflect a compensatory or dysregulated activation state rather than effective immune regulation.

Together, these data position Treg imbalance within a broader context of immune activation and impaired homeostatic regulation. However, they do not establish whether the observed Treg alterations represent a primary driver of this immune state or a secondary response. Consistently, this expansion of $ICOS^+$ Tregs was accompanied by increased frequencies of activated $CD4^+$ and $CD8^+$ T cells, further supporting the

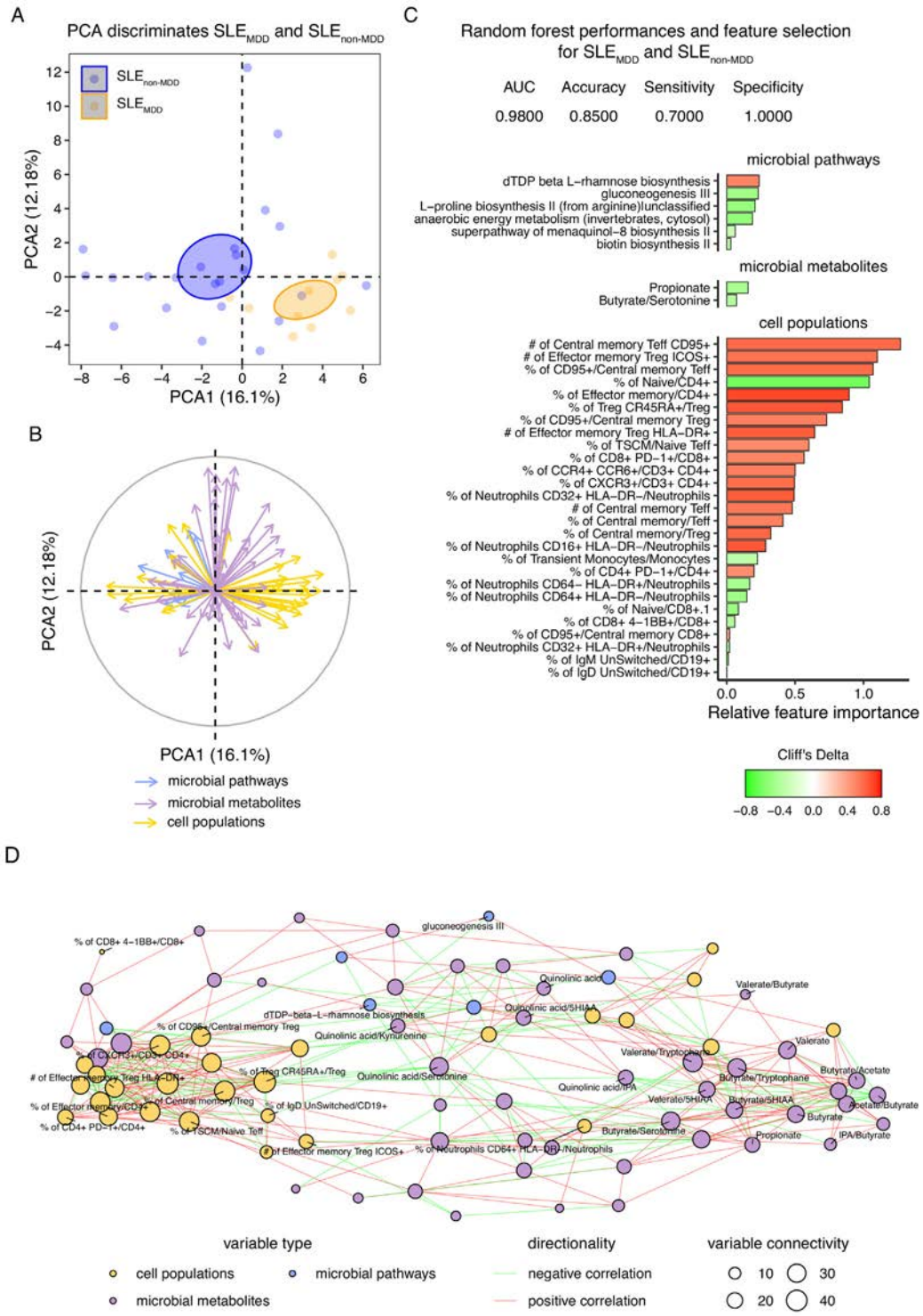

Figure 5. Multilayer immunometabolic signature separating SLE$_{MDD}$ from SLE$_{non-MDD}$ patients. (A) Principal component analysis (PCA) based on immune cell phenotypes, microbial metabolic pathways, and targeted metabolites; each point represents 1 patient. (B) Correlation circle of the same PCA; vectors are coloured by data layer (cell populations, microbial metabolites, microbial pathways). (C) Random forest model trained on the integrated dataset, showing overall performance metrics and ranked variable importance. (D) Network of significant pairwise correlations among variables retained in the signature; node colour indicates data layer and edge colour indicates correlation sign. A total of 33 patients were included in these integrated omics analyses. Ig, immunoglobulin; SLE, systemic lupus erythematosus; SLE$_{MDD}$, major depressive disorder in SLE.

notion of a globally activated immune environment rather than effective immune regulation. This hypothesis is further supported by the tendency of SLE$_{MDD}$ patients to exhibit a longer disease duration (trend in the LUPIL-2 cohort, $P < .06$), which is compatible with sustained immune stimulation and chronic T cell activation driving progressive phenotypic remodelling of the Treg compartment. This hypothesis would require dedicated functional assays to be formally tested.

Integration of Treg changes with microbial and metabolic alterations

Beyond immune cell abnormalities, SLE$_{MDD}$ exhibited coordinated changes in gut microbial composition and metabolic output. We observed a general reduction in microbial diversity in SLE$_{MDD}$ patients, an anomaly that has been described independently in MDD and SLE [34]. Here, our results highlight that

this is even more pronounced in SLE_{MDD}. Similarly, we observed a specific depletion of *A. muciniphila* which has also been observed in both conditions separately [35,36] and which thus appears also more pronounced in patients with SLE_{MDD}. Of note, interventional approaches that aim to increase levels of *A. muciniphila* are ongoing for both mood disorders and autoimmune disorders, with preliminary data suggesting a beneficial impact on inflammation, gut integrity, and neuroimmune signalling [37−39]. In contrast, we also found that *F. prausnitzii* levels increased in SLE_{MDD}, despite them generally decreasing in SLE and primary MDD [40,41]. *F. prausnitzii* abundance is negatively correlated with inflammatory markers, and augmenting this bacterium in animal models demonstrates anti-inflammatory and neuroprotective effects [42,43]. As *F. prausnitzii* is a major butyrate producer, and we found low butyrate levels in SLE_{MDD}, we hypothesised that its increase could reflect an attempt at combating inflammation.

Altogether, coordinated changes in gut microbial composition and metabolic output, with reduced alpha diversity and depletion of *A. muciniphila* indicated a disrupted gut ecosystem, with immunometabolic consequences.

The metabolomic alterations observed in this study suggest a disruption of immune−microbial−neurotransmitter crosstalk in SLE_{MDD}. Although tryptophan and serotonin levels remained unchanged, key shifts in the downstream metabolism of tryptophan, specifically a reduction in QA (known to play a central role in the pathophysiology of MDD [44]) and lower QA/kynurenine and QA/IPA ratios, point towards altered activity of the indoleamine 2,3-dioxygenase (IDO) pathway. As IDO expression is typically upregulated in proinflammatory contexts such as SLE [45], this points to impaired regulatory mechanisms with a potential defect in Tregs which function and stability depend on both IDO signalling [46] and butyrate [47].

Importantly, these metabolomic changes differ from the classical model of inflammation-driven activation of the tryptophan −kynurenine pathway described in SLE and MDD. Although tryptophan is a common upstream substrate, its metabolism can diverge towards either the kynurenine pathway, mainly regulated by IDO, or the serotonin pathway, which depends on tryptophan hydroxylase activity [48]. In our study, the absence of increased kynurenine levels together with reduced QA and altered QA-based ratios does not support a global activation of the kynurenine pathway. Instead, combined with the gut microbiota functional analyses, these findings suggest a preferential shift of tryptophan metabolism towards microbiota-associated serotonin-related pathways. This points to an alteration of immune−microbial−neurotransmitter interactions in SLE_{MDD}, rather than a simple increase in inflammation-driven IDO activity.

The observed metabolomic changes thus likely confirm the breakdown in this regulatory mechanism, rather than a true absence of inflammation. Consistent with this, we observed a pronounced decrease in butyrate and valerate—2 SCFAs known to promote Treg differentiation and stability. Butyrate modulates immune homeostasis through epigenetic regulation (notably histone deacetylase inhibition) and gut-brain axis communication by modulating blood-brain barrier permeability and suppressing neuroinflammation [49]. Butyrates are also essential components of neuronal phospholipid membranes that regulate brain homeostasis [50]. Reduction in butyrate is also associated with MDD, and its supplementation is an effective treatment [51−53].

Coexpression network analysis enabled an innovative integrative approach that simultaneously captured multiple layers of biological interaction, providing systems-level insights substantially more comprehensive than conventional single-modality analyses. $ICOS^+$ Treg−related variables occupied a highly connected position within the correlation network, linking T cell subsets, SCFAs, serotonin-related metabolites, and microbial metabolic pathways. This pattern reflects network convergence across immune, microbial, and metabolic data layers rather than dominance in disease mechanisms. Importantly, this integrative architecture supports testable, hypothesis-generating models in which alterations in microbial SCFA production, particularly butyrate, and in tryptophan catabolism via the IDO-kynurenine pathway are associated with shifts in Treg differentiation and activation states. Overall, these findings indicate that SLE_{MDD} is characterised by coordinated immunometabolic alterations spanning multiple biological compartments, providing a structured framework for future mechanistic and interventional studies rather than definitive causal conclusions.

Although direct experimental evidence simultaneously linking lupus, gut microbiota alterations, and depressive-like behaviour remains limited in animal models, preclinical studies provide strong biological plausibility for the immunometabolic pathways highlighted here. Lupus-prone MRL/lpr mice spontaneously develop depression-like behaviours early in the disease course, preceding major systemic pathology [9]. In parallel, gut microbiota composition has been shown to shape lupus severity through microbiota-dependent modulation of tryptophan metabolism and downstream immune activation, implicating the IDO-kynurenine axis as a key interface between microbial metabolism and immune regulation [33]. Together, these data support the plausibility of a microbiota-tryptophan/IDO-immune axis contributing to mood symptoms in SLE and motivate future causal investigations.

Our study has some limitations. First, we used a general QoL scale to identify SLE_{MDD} patients in LUPIL-2 rather than a MDD specific scale. However, the score we used appears to have validity as it allowed to discover an immunometabolic signature in line with well-validated central pathways in the pathophysiology of MDD. It also has an external validity as the SLE_{MDD} signature discovered based on this classification is valid in an independent cohort for which patients could be assigned to MDD using a classical scale. Secondly, the number of patients included is limited, but this limitation must be balanced against the fact that (i) SLE is a rare disease, (ii) we isolated a signature from an international multicentre study and replicated it on a different study including healthy controls, allowing us to better discriminate SLE_{MDD} patients from controls and $SLE_{non\text{-}MDD}$, (iii) we used several supervised and unsupervised classification algorithms allowing us to overcome this small number of patients and obtain similar results, and (iv) while flow cytometry, microbiome profiling, and metabolomics were not available for exactly the same set of patients, we did not observe significant differences in key clinical variables between the subsets analysed in each modality, supporting that these subsets were representative of the overall cohort. Third, given the cross-sectional and observational nature of the data, our findings describe associations and therefore preclude any inference regarding causality between depressive symptoms and immune, microbial, or metabolic alterations. Importantly, the present analyses do not support a unique initiating role for any single biological compartment. Several causal models could account for the observed immunometabolic patterns, including microbiota-driven effects on immune regulation and metabolite availability (eg, SCFAs), immune-driven alterations of microbial composition and metabolism, or bidirectional feedback loops between these systems. In

this framework, Treg–related phenotypic changes should be viewed as integrative components of a broader immunometabolic state rather than as primary drivers of depressive symptoms. This latter possibility is supported by the improved clinical outcome observed in the 2 clinical studies of IL-2_{LD} in depression [54,55].

Perspectives

While this study delineates a reproducible immunometabolic profile associated with depressive symptoms in SLE, the reasons why such alterations arise in a subset of patients remain unknown. Addressing these questions will require longitudinal and experimental studies designed to disentangle causal relationships between immune regulation, microbiota-derived metabolites, and neuropsychiatric manifestations, as well as clinical trials testing Treg stimulation by IL-2 or faecal microbiota transplantation to identify causal defects.

These data collectively support a model in which SLE_{MDD} arises from a convergent immunometabolic mechanism involving (i) chronic Treg activation and loss of naïve Tregs, (ii) gut microbiota dysbiosis with depletion of SCFA-producing bacteria, and (iii) disruption of tryptophan and SCFA pathways, highlighting a cross talk between microbial metabolites and immune regulatory circuits. This integrated signature highlights new avenues for therapeutic intervention. Interventions aimed at restoring Treg homeostasis—such as low-dose IL-2 therapy—may be particularly relevant, as could microbiota-directed therapies (dietary modulation, probiotics, or SCFA supplementation). In this line, 2 studies recently reported promising results for the treatment of MDD by low-dose IL-2 [54,55].

Future studies should explore longitudinal dynamics, causality, and the mechanistic interplay between microbial metabolites, peripheral immune regulation, and central nervous system involvement. Importantly, interventional trials targeting these pathways will be essential to translate this immunometabolic signature into clinically actionable strategies.

Competing interests

MR, RL, and DK are inventors for patent applications related to the therapeutic use of IL-2_{LD}, which belongs to their academic institutions and has been licensed to ILTOO Pharma. MR and DK hold shares in ILTOO Pharma. All other authors declare they have no competing interests.

Acknowledgements

We thank the patients and all the contributors to the LUPIL-2 and TRANSIMMUNOM studies.

Contributors

DK conceived and supervised the LUPIL-2 and TRANSIMMUNOM studies. RL and PE analysed MDD of LUPIL-2 and TRANSIMMUNOM patients, validated by IM and RD. MR supervised the immunomonitoring of LUPIL-2 and TRANSIMMUNOM patients. PE, NT, and DK analysed the results. PE, NT, and DK wrote the first draft of the manuscript that was edited by all authors.

Funding

The study was sponsored by Assistance Publique-Hôpitaux de Paris. Funding was provided by the French National Research Agency (ANR-11-IDEX-0004-02, LabEx TRANSIMMUNOM and ANR-16-RHUS-0001, RHU IMAP to DK), the clinical study sponsor, ILTOO Pharma, and the INSERM (Contrat "Postes d'accueil" to PE). ILTOO Pharma provided the investigational drug and the placebo. Immune investigations were supported by an ANR grant iMAP (ANR-16-RHUS-0001). For this analysis of MDD in SLE, the funders of the study provided access to raw data but had no role in data analysis, data interpretation, or writing of the report.

Patient consent for publication

Written informed consent was obtained from all participants for participation in the study and for publication of the data.

Ethics approval

All procedures were conducted in accordance with the Declaration of Helsinki and Good Clinical Practice guidelines. The study protocol was approved by the Institutional Review Board of Pitié-Salpêtrière Hospital (Ethics Committee Ile-de-France, reference 48-15). Written informed consent was obtained from all participants prior to enrolment.

Provenance and peer review

Not commissioned; externally peer reviewed.

Data availability statement

The data required for this article is available on request.

Supplementary materials

Supplementary material associated with this article can be found in the online version at doi:10.1016/j.ard.2026.02.019.

Orcid

Pierre Ellul: http://orcid.org/0000-0003-1862-6952

REFERENCES

[1] Barber MRW, Drenkard C, Falasinnu T, Hoi A, Mak A, Kow NY, et al. Global epidemiology of systemic lupus erythematosus. Nat Rev Rheumatol 2021;17:515–32. doi: 10.1038/s41584-021-00668-1.
[2] Legge AC, Hanly JG. Recent advances in the diagnosis and management of neuropsychiatric lupus. Nat Rev Rheumatol 2024;20:712–28. doi: 10.1038/s41584-024-01163-z.
[3] Gold SM, Köhler-Forsberg O, Moss-Morris R, Mehnert A, Miranda JJ, Bullinger M, et al. Comorbid depression in medical diseases. Nat Rev Dis Primers 2020;6:69. doi: 10.1038/s41572-020-0200-2.
[4] Moustafa AT, Moazzami M, Engel L, Bangert E, Hassanein M, Marzouk S, et al. Prevalence and metric of depression and anxiety in systemic lupus erythematosus: a systematic review and meta-analysis. Semin Arthritis Rheum 2020;50:84–94. doi: 10.1016/j.semarthrit.2019.06.017.
[5] Otte C, Gold SM, Penninx BW, Pariante CM, Etkin A, Fava M, et al. Major depressive disorder. Nat Rev Dis Primers 2016;2:16065. doi: 10.1038/nrdp.2016.65.
[6] Marx W, Penninx BWJH, Solmi M, Furukawa TA, Firth J, Carvalho AF, et al. Major depressive disorder. Nat Rev Dis Primers 2023;9:44. doi: 10.1038/s41572-023-00454-1.
[7] Miller AH, Raison CL. The role of inflammation in depression: from evolutionary imperative to modern treatment target. Nat Rev Immunol 2016;16:22–34. doi: 10.1038/nri.2015.5.
[8] Drevets WC, Wittenberg GM, Bullmore ET, Manji HK. Immune targets for therapeutic development in depression: towards precision medicine. Nat Rev Drug Discov 2022;21:224–44. doi: 10.1038/s41573-021-00368-1.

[9] Gao H-X, Campbell SR, Cui M-H, Zong P, Hee-Hwang J, Gulinello M, et al. Depression is an early disease manifestation in lupus-prone MRL/lpr mice. J Neuroimmunol 2009;207:45–56. doi: 10.1016/j.jneuroim.2008.11.009.
[10] Gao K, Mu C-L, Farzi A, Zhu WY. Tryptophan metabolism: a link between the gut microbiota and brain. Adv Nutr 2020;11:709–23. doi: 10.1093/advances/nmz127.
[11] Yano JM, Yu K, Donaldson GP, Shastri GG, Ann P, Ma L, et al. Indigenous bacteria from the gut microbiota regulate host serotonin biosynthesis. Cell 2015;161:264–76. doi: 10.1016/j.cell.2015.02.047.
[12] Reigstad CS, Salmonson CE, Rainey 3rd JF, Szurszewski JH, Linden DR, Sonnenburg JL, et al. Gut microbes promote colonic serotonin production through an effect of short-chain fatty acids on enterochromaffin cells. FASEB J 2015;29:1395–403. doi: 10.1096/fj.14-259598.
[13] Liu L, Wang H, Chen X, Zhang Y, Zhang H, Xie P. Gut microbiota and its metabolites in depression: from pathogenesis to treatment. EBioMedicine 2023;90:104527. doi: 10.1016/j.ebiom.2023.104527.
[14] Humrich JY, Cacoub P, Rosenzwajg M, Pitoiset F, Pham HP, Guidoux J, et al. Low-dose interleukin-2 therapy in active systemic lupus erythematosus (LUPIL-2): a multicentre, double-blind, randomised and placebo-controlled phase II trial. Ann Rheum Dis 2022;81:1685–94. doi: 10.1136/ard-2022-222501.
[15] American Psychiatric Association. Diagnostic and statistical manual of mental disorders: DSM-5. 5th ed. Washington: American Psychiatric Association; 2013.
[16] Lorenzon R, Mariotti-Ferrandiz E, Aheng C, Ribet C, Toumi F, Pitoiset F, et al. Clinical and multi-omics cross-phenotyping of patients with autoimmune and autoinflammatory diseases: the observational TRANSIMMUNOM protocol. BMJ Open 2018;8:e021037. doi: 10.1136/bmjopen-2017-021037.
[17] Zigmond AS, Snaith RP. The hospital anxiety and depression scale. Acta Psychiatr Scand 1983;67:361–70. doi: 10.1111/j.1600-0447.1983.tb09716.x.
[18] Pitoiset F, Cassard L, El Soufi K, Boselli L, Grivel J, Roux A, et al. Deep phenotyping of immune cell populations by optimized and standardized flow cytometry analyses. Cytometry A 2018;93:793–802. doi: 10.1002/cyto.a.23570.
[19] Tchitchek N, Binvignat M, Roux A, Pitoiset F, Dubois J, Marguerit G, et al. Deep immunophenotyping reveals that autoimmune and autoinflammatory disorders are spread along two immunological axes capturing disease inflammation levels and types. Ann Rheum Dis 2024;83:638–50. doi: 10.1136/ard-2023-225179.
[20] Criscuolo A, Brisse S. AlienTrimmer: a tool to quickly and accurately trim off multiple short contaminant sequences from high-throughput sequencing reads. Genomics 2013;102:500–6. doi: 10.1016/j.ygeno.2013.07.011.
[21] Truong DT, Franzosa EA, Tickle TL, Scholz M, Weingart G, Pasolli E, et al. MetaPhlAn2 for enhanced metagenomic taxonomic profiling. Nat Methods 2015;12:902–3. doi: 10.1038/nmeth.3589.
[22] Franzosa EA, McIver LJ, Rahnavard G, Thompson LR, Schirmer M, Weingart G, et al. Species-level functional profiling of metagenomes and metatranscriptomes. Nat Methods 2018;15:962–8. doi: 10.1038/s41592-018-0176-y.
[23] Alarcan H, Chaumond R, Emond P, Benz-De Bretagne I, Lefèvre A, Bakkouche SE, et al. Some CSF kynurenine pathway intermediates associated with disease evolution in amyotrophic lateral sclerosis. Biomolecules 2021;11:691. doi: 10.3390/biom11050691.
[24] Lefèvre A, Mavel S, Nadal-Desbarats L, Galineau L, Attucci S, Dufour D, et al. Validation of a global quantitative analysis methodology of tryptophan metabolites in mice using LC-MS. Talanta 2019;195:593–8. doi: 10.1016/j.talanta.2018.11.094.
[25] Monteiro J, Lefèvre A, Dufour-Rainfray D, Oury A, Chicheri G, Galineau L, et al. Multi-compartment SCFA quantification in human. AJAC 2024;15:177–200. doi: 10.4236/ajac.2024.156012.
[26] Hothorn T, Zeileis A. partykit: A modular toolkit for recursive partitioning in R. J Mach Learn Res 2015;16:3905–9.
[27] Le S, Josse J, Husson F. FactoMineR: an R package for multivariate analysis. J Stat Softw 2008;25:1–18.
[28] Kälble F, Wu L, Lorenz H-M, eier M, Schaier M, Steinborn A. Impaired differentiation of highly proliferative ICOS+-Tregs is involved in the transition from low to high disease activity in systemic lupus erythematosus (SLE) patients. Int J Mol Sci 2021;22:9501. doi: 10.3390/ijms22179501.
[29] Ohmes J, Comdühr S, Akbarzadeh R, Riemekasten G, Humrich JY. Dysregulation and chronicity of pathogenic T cell responses in the pre-diseased stage of lupus. Front Immunol 2022;13:1007078. doi: 10.3389/fimmu.2022.1007078.
[30] Moore E, Huang MW, Reynolds CA, Macian F, Putterman C. Choroid plexus-infiltrating T cells as drivers of murine neuropsychiatric lupus. Arthritis Rheumatol 2022;74:1796–807. doi: 10.1002/art.42252.
[31] Parodi E, Novi M, Bottino P, La Porta E, Merlotti G, Castello LM, et al. The complex role of gut microbiota in systemic lupus erythematosus and lupus nephritis: from pathogenetic factor to therapeutic target. Microorganisms 2025;13:445. doi: 10.3390/microorganisms13020445.
[32] Pan Q, Guo F, Huang Y, Li A, Chen S, Chen J, et al. Gut microbiota dysbiosis in systemic lupus erythematosus: novel insights into mechanisms and promising therapeutic strategies. Front Immunol 2021;12:799788. doi: 10.3389/fimmu.2021.799788.
[33] Choi S-C, Brown J, Gong M, Ge Y, Zadeh M, Li W, et al. Gut microbiota dysbiosis and altered tryptophan catabolism contribute to autoimmunity in lupus-susceptible mice. Sci Transl Med 2020;12:eaax2220. doi: 10.1126/scitranslmed.aax2220.
[34] Yao H, Yang H, Wang Y, Xing Q, Yan L, Chai Y. Gut microbiome and fecal metabolic alteration in systemic lupus erythematosus patients with depression. Front Cell Infect Microbiol 2022;12:1040211. doi: 10.3389/fcimb.2022.1040211.
[35] McGaughey KD, Yilmaz-Swenson T, Elsayed NM, Cruz DA, Rodriguiz RM, Kritzer MD, et al. Relative abundance of Akkermansia spp. and other bacterial phylotypes correlates with anxiety- and depressive-like behavior following social defeat in mice. Sci Rep 2019;9:3281. doi: 10.1038/s41598-019-40140-5.
[36] Lei W, Cheng Y, Gao J, Liu X, Shao L, Kong Q, et al. Akkermansia muciniphila in neuropsychiatric disorders: friend or foe? Front Cell Infect Microbiol 2023;13:1224155. doi: 10.3389/fcimb.2023.1224155.
[37] Guo D, Park C, Li Y, Li B, Yang Q, Deng Y, et al. Akkermansia muciniphila ameliorates depressive disorders in a murine alcohol-LPS (mALPS) model. Food Funct 2022;13:12766–76. doi: 10.1039/d2fo01478e.
[38] Guo H, Liu X, Chen T, Wang X, Zhang X. Akkermansia muciniphila improves depressive-like symptoms by modulating the level of 5-HT neurotransmitters in the gut and brain of mice. Mol Neurobiol 2024;61:821–34. doi: 10.1007/s12035-023-03602-6.
[39] Guo M, Lu M, Chen K, Xu R, Xia Y, Liu X, et al. Akkermansia muciniphila and Lactobacillus plantarum ameliorate systemic lupus erythematosus by possibly regulating immune response and remodeling gut microbiota. mSphere 2023;8:e0007023. doi: 10.1128/msphere.00070-23.
[40] Effendi RMRA, Anshory M, Kalim H, Dwiyana RF, Suwarsa O, Pardo LM, et al. Akkermansia muciniphila and Faecalibacterium prausnitzii in immune-related diseases. Microorganisms 2022;10:2382. doi: 10.3390/microorganisms10122382.
[41] Hao Z, Wang W, Guo R, Liu H. Faecalibacterium prausnitzii (ATCC 27766) has preventive and therapeutic effects on chronic unpredictable mild stress-induced depression-like and anxiety-like behavior in rats. Psychoneuroendocrinology 2019;104:132–42. doi: 10.1016/j.psyneuen.2019.02.025.
[42] Zhang J, Huang Y-J, Trapecar M, Wright C, Schneider K, Kemmitt J, et al. An immune-competent human gut microphysiological system enables inflammation-modulation by Faecalibacterium prausnitzii. npj Biofilms Microbiomes 2024;10:31. doi: 10.1038/s41522-024-00501-z.
[43] Martín R, Miquel S, Chain F, Natividad JM, Jury J, Lu J, et al. Faecalibacterium prausnitzii prevents physiological damages in a chronic low-grade inflammation murine model. BMC Microbiol 2015;15:67. doi: 10.1186/s12866-015-0400-1.
[44] Savitz J, Drevets WC, Wurfel BE, Ford BN, Bellgowan PS, Victor TA, et al. Reduction of kynurenic acid to quinolinic acid ratio in both the depressed and remitted phases of major depressive disorder. Brain Behav Immun 2015;46:55–9. doi: 10.1016/j.bbi.2015.02.007.
[45] Lood C, Tydén H, Gullstrand B, Klint C, Wenglén C, Nielsen CT, et al. Type I interferon-mediated skewing of the serotonin synthesis is associated with severe disease in systemic lupus erythematosus. PLoS One 2015;10:e0125109. doi: 10.1371/journal.pone.0125109.
[46] Baban B, Chandler PR, Sharma MD, Pihkala J, Koni PA, Munn DH, et al. IDO activates regulatory T cells and blocks their conversion into Th17-like T cells. J Immunol 2009;183:2475–83. doi: 10.4049/jimmunol.0900986.
[47] Furusawa Y, Obata Y, Fukuda S, Endo TA, Nakato G, Takahashi D, et al. Commensal microbe-derived butyrate induces the differentiation of colonic regulatory T cells. Nature 2013;504:446–50. doi: 10.1038/nature12721.
[48] Chen Y, Guillemin GJ. Kynurenine pathway metabolites in humans: disease and healthy States. Int J Tryptophan Res 2009;2:1–19. doi: 10.4137/ijtr.s2097.
[49] Caspani G, Kennedy S, Foster JA, Swann J. Gut microbial metabolites in depression: understanding the biochemical mechanisms. Microb Cell 2019;6:454–81. doi: 10.15698/mic2019.10.693.
[50] Chen CT, Domenichiello AF, Trépanier M-O, Liu Z, Masoodi M, Bazinet RP. The low levels of eicosapentaenoic acid in rat brain phospholipids are maintained via multiple redundant mechanisms. J Lipid Res 2013;54:2410–22. doi: 10.1194/jlr.M038505.

[51] Liao Y, Xie B, Zhang H, He Q, Guo L, Subramanieapillai M, et al. Efficacy of omega-3 PUFAs in depression: a meta-analysis. Transl Psychiatry 2019;9:190. doi: 10.1038/s41398-019-0515-5.

[52] Sun J, Wang F, Hong G, Pang M, Xu H, Li H, et al. Antidepressant-like effects of sodium butyrate and its possible mechanisms of action in mice exposed to chronic unpredictable mild stress. Neurosci Lett 2016;618:159–66. doi: 10.1016/j.neulet.2016.03.003.

[53] Valvassori SS, Varela RB, Arent CO, Dal-Pont GC, Bobsin TS, Budni J, et al. Sodium butyrate functions as an antidepressant and improves cognition with enhanced neurotrophic expression in models of maternal deprivation and chronic mild stress. Curr Neurovasc Res 2014;11:359–66. doi: 10.2174/1567202611666140829162158.

[54] Poletti S, Zanardi R, Mandelli A, Aggio V, Finardi A, Lorenzi C, et al. Low-dose interleukin 2 antidepressant potentiation in unipolar and bipolar depression: safety, efficacy, and immunological biomarkers. Brain Behav Immun 2024;118:52–68. doi: 10.1016/j.bbi.2024.02.019.

[55] Leboyer M, Foiselle M, Tchitchek N, Tamouza R, Lorenzon R, Richard JR, et al. Low-dose interleukin-2 in patients with bipolar depression: A phase 2 randomised double-blind placebo-controlled trial. Brain Behav Immun 2025;123:177–84. doi: 10.1016/j.bbi.2024.09.005.

Ann Rheum Dis 85 (2026) 1610–1624

Contents lists available at ScienceDirect

Annals of the Rheumatic Diseases

journal homepage: https://www.sciencedirect.com/journal/annals-of-the-rheumatic-diseases

Sjögren's disease

Human hypofunctional *NCF1* variant aggravates salivary gland immunopathology in Sjögren's disease by promoting switched memory B-cell recruitment and long-lived plasma cell differentiation

Xinran Yuan[1,2,#], Xiaodong Qin[3,#,*], Xinjie Wu[3,#], Yi Chen[3,#], Yujiao Wang[1], Yulu Zhang[1], Dong Xie[3], Yao Liu[4], Jian Zhao[2], Joel M. Guthridge[5], Judith A. James[5], Christopher J. Lessard[6,7], Nan Shen[8], Lingyun Sun[1,*], Betty P. Tsao[2,*]

[1] *Department of Rheumatology and Immunology, Nanjing Drum Tower Hospital, Affiliated Hospital of Medical School, Nanjing University, Nanjing, Jiangsu, PR China*
[2] *Division of Rheumatology and Immunology, Department of Medicine, Medical University of South Carolina, Charleston, South Carolina, USA*
[3] *Department of Orthopedic Surgery, Nanjing Drum Tower Hospital, Affiliated Hospital of Medical School, Nanjing University, Nanjing, Jiangsu, PR China*
[4] *Department of Pathology, Nanjing Drum Tower Hospital, Affiliated Hospital of Medical School, Nanjing University, Nanjing, Jiangsu, PR China*
[5] *Arthritis and Clinical Immunology, Oklahoma Medical Research Foundation, Oklahoma City, Oklahoma, USA*
[6] *Genes and Human Disease Research Program, Oklahoma Medical Research Foundation, Oklahoma City, Oklahoma, USA*
[7] *Department of Pathology, University of Oklahoma Health Sciences Center, Oklahoma City, Oklahoma, USA*
[8] *Department of Rheumatology, Renji Hospital, Shanghai Jiao Tong University School of Medicine, Shanghai, PR China*

ARTICLE INFO

Article history:
Received 5 November 2025
Received in revised form 27 February 2026
Accepted 23 March 2026

ABSTRACT

Objectives: We assessed the role of a systemic lupus erythematosus causal, hypofunctional variant, neutrophil cytosolic factor 1 (*NCF1*)-p.Arg90His (p.R90H) substitution, in Sjögren's disease (SjD).
Methods: Association between *NCF1*-H90 and SjD was assessed in case-control cohorts. Peripheral blood mononuclear cells (PBMCs) and minor salivary gland (MSG) from patients with Sjögren's Syndrome type A antigen (SSA)+ SjD were assessed using cytometry by time-of-flight and single-cell RNA sequencing, respectively.
Results: The *NCF1*-H90 allele was associated with increased risk for SjD in Chinese and European Americans (P_{meta} = 1.15E-55, odds ratio [OR] = 2.58), exhibiting a more robust association in patients with SSA+ SjD (OR = 3.37 in Chinese and OR = 2.60 in European Americans). In a longitudinal observational cohort, patients with homozygous H90 SjD at baseline had lower levels of complement C4 and higher scores on labial salivary gland biopsy, European Alliance of Associations for Rheumatology (EULAR) Sjögren's Syndrome Disease Activity Index (ESSDAI), and EULAR Sjögren's Syndrome Patient Reported Index (ESSPRI). These patients with H90 SjD

*Correspondence to Dr. Betty P Tsao, Division of Rheumatology & Immunology, Department of Medicine, Medical University of South Carolina, Charleston, SC, USA; Dr. Lingyun Sun, Nanjing Drum Tower Hospital, Affiliated Hospital of Medical School, Nanjing University, Nanjing, China; and Xiaodong Qin, Nanjing Drum Tower Hospital, Affiliated Hospital of Medical School, Nanjing University, Nanjing, China.
E-mail addresses: qinxd_njumed@163.com (X. Qin), lingyunsun@nju.edu.cn (L. Sun), tsaob@musc.edu (B.P. Tsao).
Handling editor Josef S. Smolen.
[1] Xinran Yuan, Xiaodong Qin, Xinjie Wu, and Yi Chen contributed equally.

https://doi.org/10.1016/j.ard.2026.03.026

sustained elevated ESSDAI and ESSPRI scores during follow-up years with decreased survival. The 0, 1, and 2 copies of H90 carriage in SjD PBMCs exhibited dose-dependent decreases in switched memory B cells, which might be recruited by fibroblasts into MSG, and further differentiated into long-lived Immunoglobulin G (IgG+) plasma cells, resulting in elevated serum SSA+ IgG levels and greater disease severity. In a retrospective belimumab-treated SSA+ female cohort, homozygous H90 patients showed significantly greater improvement in ESSDAI, C4 levels, and serum SSA+ IgG levels, supporting the role of *NCF1*-H90 as a predictive biomarker for enhanced response to B-cell-targeted therapy.

Conclusions: Low *NCF1* activity increases the risk of severe SSA+ SjD by driving switched memory B-cell trafficking and IgG+ plasma cell differentiation, revealing targetable pathways in SSA+ SjD.

WHAT IS ALREADY KNOWN ON THIS TOPIC

- The hypofunctional p.Arg90His (p.R90H, rs201802880) substitution in neutrophil cytosolic factor 1 (*NCF1*), which reduces NADPH (Nicotinamide Adenine Dinucleotide Phosphate) oxidase 2 activity and induces a type I interferon (IFN-I) signature, strongly associates with the risk of multiple autoimmune diseases, including systemic lupus erythematosus (SLE) and systemic sclerosis (SSc). It is associated not only with the risk of developing autoimmune diseases but also with the progression to specific tissue damage, including renal involvement in SLE and pulmonary fibrosis in SSc.

WHAT THIS STUDY ADDS

- The hypofunctional *NCF1*-H90 variant is strongly associated with Sjögren's Syndrome type A antigen (SSA)+ SjD in Chinese and European Americans. The H90 variant was dose dependently associated with increased inflammatory infiltration in salivary glands, disease activity, and mortality in a longitudinal Chinese cohort.
- We put forth a coordinated pathogenic axis in patients with SSA+ SjD carrying the *NCF1*-H90 variant, wherein $CXCL12^+$ fibroblasts with heightened IFN signatures recruit peripheral switched memory B cells into salivary glands, supporting their differentiation into autoantibody-producing, long-lived Immunoglobulin G (IgG+) plasma cells.
- Homozygous H90 female patients with SSA+ SjD exhibit superior treatment responses to belimumab, suggesting its potential utility as a predictive biomarker for guiding B-cell-targeted therapy in SjD.

HOW THIS STUDY MIGHT AFFECT RESEARCH, PRACTICE OR POLICY

- Stratifying patients with SSA+ SjD by *NCF1* risk genotyping identifies responders to B-cell-targeted therapy, enabling more effective and personalised treatments.

INTRODUCTION

Sjögren's disease (SjD) is a chronic autoimmune disease characterised by lymphocytic infiltration and secretory gland dysfunction, resulting in dryness of the mouth and eyes [1,2]. Although the aetiology of SjD is not completely known, a genetic component is recognised. Genome-wide association studies (GWAS) and ImmunoChip analyses have identified nearly 30 SjD-associated risk loci [3]. A strong susceptibility locus, rs117026326 within the *GTF2I* intergenic region at 7q11.23, was first identified in a SjD GWAS of Chinese ancestry [4]. Subsequently, we identified the *NCF1*-R90H variant (p.R90H, rs201802880) at 7q11.23 associated with robust risk of multiple autoimmune diseases, including SjD, systemic lupus erythematosus (SLE), and rheumatoid arthritis [5]. The hypofunctional *NCF1*-R90H has been proven to be an established causal variant of SLE and systemic sclerosis (SSc) [6,7], causing defective efferocytosis in macrophages [6], endosomal Toll-like receptor (TLR)-signalling impairment in plasmacytoid cells and B cells [8–10], and upregulated type I interferon (IFN-I) stimulated gene expression [11].

Patients with SjD exhibit symptoms of B-cell activation, including production of autoantibodies to SSA (Ro) and Sjögren's Syndrome type B antigen (SSB) (La), hypergammaglobulinaemia, and mucosa-associated lymphoid tissue lymphoma [12]. The finding that antibodies to SSA and SSB can be detected years before disease diagnosis suggests an early key role of B cells in the development of SjD [13]. The observations that $CD27^+$ memory B cells decrease in peripheral blood mononuclear cells (PBMCs) while accumulating in salivary glands [14,15] suggest the migration or retention of memory B cells in the inflamed salivary glands; however, the underlying mechanism is unclear.

Here, we assessed *NCF1*-R90H variant-associated SjD characteristics and how this variant may affect pathogenic mechanisms, focusing on paired peripheral blood and salivary gland samples from newly diagnosed, untreated patients with SjD to delineate likely molecular and cellular pathogenic pathways. Specifically, we define the nomenclature for the *NCF1*-p.R90H locus: homozygous H90 is labelled as *NCF1*-H90 or H90, homozygous R90 is labelled as *NCF1*-R90 or R90, and heterozygous is labelled as *NCF1*-90R/H or 90R/H.

METHODS

All methods are provided in the Supplementary information.

RESULTS

Robust association of the hypofunctional NCF1-H90 variant with patient with SSA+ SjD subset in Han Chinese and European American ancestries

The association between the *NCF1*-H90 allele and risk for SjD was assessed in 1313 patients with SjD and 3210 controls (odds ratio [OR] = 2.58, P_{meta} = 1.15E-55). We observed an association between the H90 variant of *NCF1* and SjD in 2 independent Han Chinese cohorts (OR = 2.60, P = 2.52E-53 in total), with more robust association signals in the SSA+ subset (OR = 3.37, P = 9.63E-55 in total). The association between the *NCF1*-H90 variant and SjD was confirmed in European Americans (OR = 2.35, P = 9.70E-4), with a stronger association in patients with SSA+ (OR = 2.60, P = 1.05E-3). Moreover, patients with SSA+ exhibited a stronger association with the *NCF1*-H90 variant in Chinese patients (OR = 2.05, P = 8.14E-11) than patients with SSA− (Table, Supplementary Table S1). In both Chinese cohorts, patients with SjD carrying 1 or 2 copies of the H90 variant showed earlier age at diagnosis and higher SSA seropositivity (Supplementary Table S2). These findings

Table
Robust association of the *NCF1* variant with SjD in SSA+ subset of patients

SNP	Ancestry			Subject		MAF %		*P*	OR	(95% Cl)
				Case	Control	Case	Control			
rs201802880 (p.Arg90His, A/G)	Chinese	Cohort 1		565	190	33.9	18.4	5.76E-8	2.22	(1.67-2.97)
			SSA(+)	352		40.2		6.83E-12	2.99	(2.18-4.08)
			SSA(−)	213		23.5		8.50E-2	1.35	(0.96-1.89)
		Cohort 2		446[a]	2089[b]	37.8	16.8	2.00E-37	2.84	(2.42-3.32)
			SSA(+)[c]	171		43.9		6.78E-28	3.70	(2.93-4.68)
			SSA(−)[c]	110		27.7		5.09E-5	1.87	(1.38-2.53)
		Total		1011	2279	35.6	16.9	2.52E-53	2.60	(2.30-2.93)
			SSA(+)	523		41.4		9.63E-55	3.37	(2.90-3.93)
			SSA(−)	323		24.9		1.24E-6	1.61	(1.33-1.95)
	European			302[a]	931[a]	4.8	2.2	9.70E-04	2.35	(1.42-3.91)
	American		SSA(+)[d]	189		5.3		1.05E-03	2.60	(1.47-4.60)
			SSA(−)[d]	109		3.7		1.34E-01	1.84	(0.83-4.09)
	Meta-analysis			1313	3210	28.5	12.6	1.15E-55	2.58	
				SSA(+)	SSA(−)	SSA(+)	SSA(−)			
	Chinese Total			523	323	41.4	24.9	8.14E-11	2.05	(1.65-2.54)
	European American			189	109	5.3	3.7	0.382	1.45	(0.63-3.33)
	Meta-analysis			712	432	31.8	19.6	7.51E-11	2.00	

MAF, minor allele frequency; *NCF1*, neutrophil cytosolic factor 1; SSA, Sjögren's Syndrome type A antigen; SNP, Single Nucleotide Polymorphism; SjD, Sjögren's disease; OR, odds ratio.
[a] Data from our previous study [5].
[b] Data from our previous study [7].
[c] Of 446 patients, 281 in Chinese Cohort 2 have the SSA antibody data.

supported the notion that abnormally low NADPH (Nicotinamide Adenine Dinucleotide Phosphate) oxidase 2 (NOX2) activity, due to the hypofunctional *NCF1*-H90 variant, predisposed to SjD, especially in the subset of patient with SSA+ of multiple ancestries.

Increased risk of salivary gland inflammatory infiltration, disease activity, and mortality in a longitudinal cohort of patients with SjD carrying the NCF1-H90 variant

We assessed the relationship between the carriage of the *NCF1*-H90 variant and clinical characteristics of 131 patients in a longitudinal observational cohort with at least 4-year follow-up from the Chinese cohort 1. Among them, 53 were homozygous for *NCF1*-R90 (40.5%), 63 were *NCF1*-90R/H (48.1%), and 15 were homozygous for *NCF1*-H90 (11.5%). The minor allele frequency of the H90 allele in this cohort was 35.5%, including 40.4% in the SSA+ group and 23.0% in the SSA− group, consistent with our cohort 1 findings (Table). The baseline demographics and clinical manifestations at diagnosis of the longitudinal cohort are depicted in Supplementary Table S3.

Although we observed no genotype-associated differences in sex or disease duration, those carrying the *NCF1*-H90 variant showed a trend towards an earlier age at diagnosis (P = .079). With respect to autoantibody profiles, the H90 group exhibited elevated Antinuclear Antibody titres (P = 1.50E-3) and SSA seropositivity (P = .024) as well as decreased complement C4 levels (P = 1.80E-5) compared with either the 90R/H or R90 group (Supplementary Table S3, Fig 1A). The salivary gland inflammatory infiltration assessed using labial salivary gland biopsy (LSGB) Score (Chisholm-Mason Score) was significantly higher in the H90 group than either the 90R/H or R90 group at baseline (Fig 1B). Importantly, the disease severity, evaluated using the EULAR Sjögren's Syndrome Disease Activity Index (ESSDAI) Score and the EULAR Sjögren's Syndrome Patient Reported Index (ESSPRI) Score, was significantly higher in the H90 group than in either the 90R/H or R90 group at baseline, and remained the highest at the last follow-up (LFU) (Fig 1C,D). The 0, 1, or 2 copies of H90 carriage dose dependently associated with decreased C4 level, elevated LSGB, ESSDAI, and ESSPRI Score, indicating contribution of *NCF1*-H90 variant in salivary gland inflammatory infiltration and disease severity for patients with SjD (Fig 1A-D). Although the overall survival rate of these 131 patients was 90.1% (118/131) during an average 5.6-year period, survival rate was 73.3% (11/15) in the H90 group, 90.5% (57/63) in the 90R/H group, and 94.3% (50/53) in the R90 group, respectively, indicating that H90 carriage in patients with SjD is associated with shorter survival (Fig 1E). All 13 recorded deaths were due to severe visceral complications of SjD (Supplementary Table S4).

Within the SSA+ subset, the *NCF1*-H90 genotype was associated with a trend towards earlier age at diagnosis (P = .078) and elevated Antinuclear Antibody titres (P = .037) (Supplementary Table S5). Moreover, patients with SSA+ carrying 2 copies of the H90 variant exhibited lower C4 levels and higher LSGB, ESSDAI, and ESSPRI scores at both baseline and LFU. There were dose-dependent associations between the 0, 1, or 2 copies of H90 and decreased C4 levels, elevated LSGB, ESSDAI, and ESSPRI scores (Fig 1A-D). The overall survival rate was 86.2% (81/94), and the H90 group (69.2%, 9/13) had a lower survival rate than the 90R/H group (88.0%, 44/50) and R90 group (90.3%, 28/31) (Fig 1E).

Proportions of $CD27^+CD19^+IgD^-$ switched memory B cells in PBMCs of patients with SjD correlated with NCF1-H90 dose and disease activity

To further explore the involvement of the NCF1-H90 variant in SjD disease progression, we comprehensively profiled PBMCs from 15 female patients with SSA+ in the 131 Chinese longitudinal cohort using cytometry by time-of-flight (CyTOF) (n = 5 per genotype). The demographics and clinical manifestations of these subjects at the time of blood draw are depicted in Supplementary Table S6. The H90 group had a significantly higher ESSDAI Score than the R90 or 90R/H group.

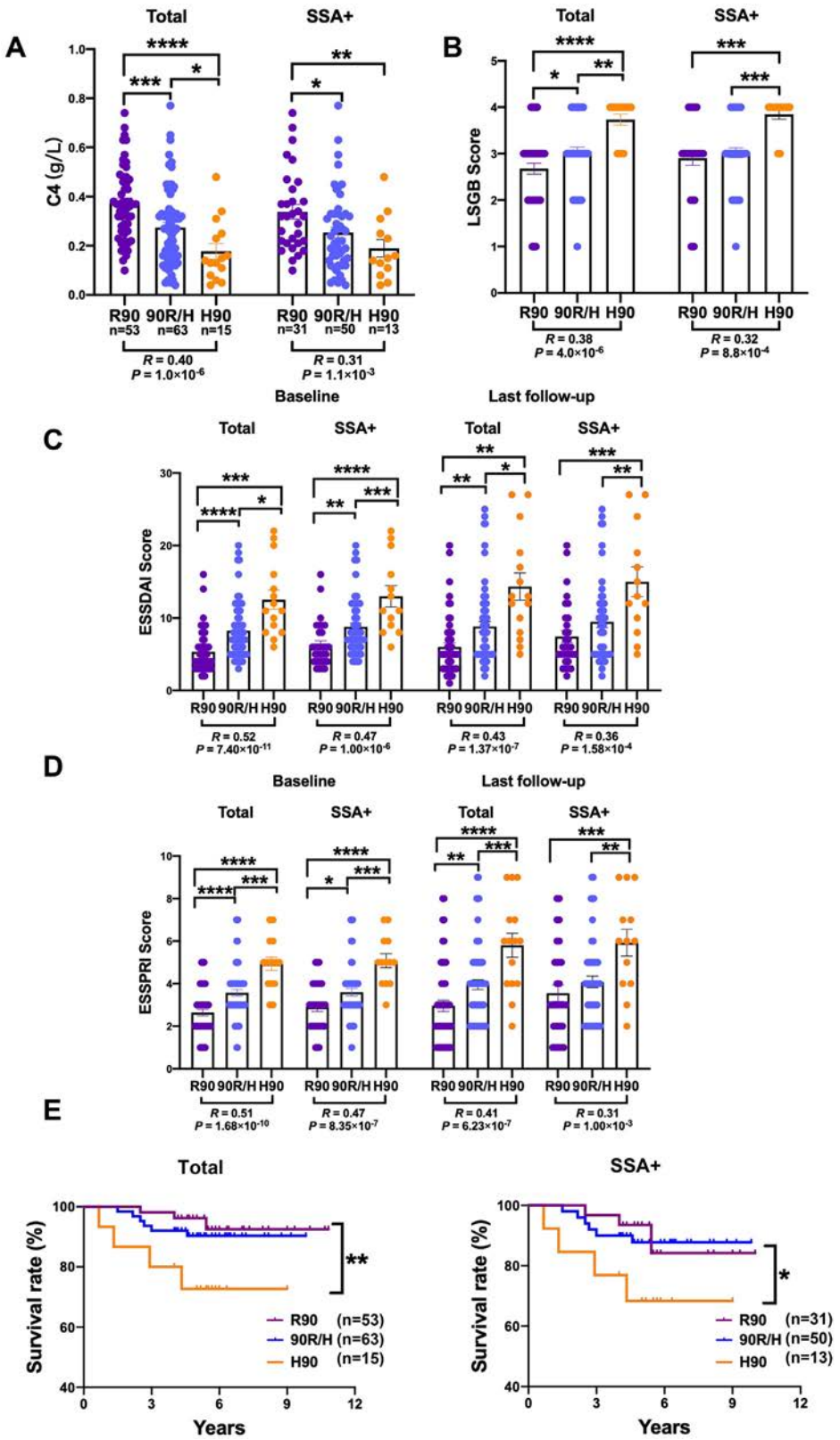

Figure 1. Dose-dependent association of the *NCF1*-H90 variant with decreased levels of complement C4 and increased inflammatory infiltrates in salivary glands, disease activity, and mortality in Chinese patients with SjD. A total of 131 patients with SjD (containing 94 patients with SSA+ from Chinese cohort 1 in the Table) were consecutively enrolled in a longitudinal observational cohort stratified by genotypes. (A,B) A dose-dependent association of the *NCF1*-H90 variant with decreased serum complement C4 level, elevated LSGB score of all patients/patients with SSA+ at enrolment. (C,D) A dose-dependent association of the *NCF1*-H90 variant with elevated ESSDAI and ESSPRI scores of all patients/patients with SSA+ at enrolment and last follow-up. (E) Kaplan-Meier survival curve of these 131 patients with SjD and 94 patients with SSA+. *$P < .05$; **$P < .01$; ***$P < .001$; ****$P < .0001$. *P* values among the 3 groups were determined using one-way ANOVA with Bonferroni's multiple-comparison test for continuous variables. The association of H90 copy numbers with C4 level, LSGB Score, ESSDAI Score, or ESSPRI Score was calculated using a linear regression test. Results were shown as mean ± SEM. 90R/H, heterozygous for *NCF1*-90R/H; ANOVA, Analysis of Variance; ESSDAI, EULAR Sjögren's Syndrome Disease Activity Index; ESSPRI, EULAR Sjögren's Syndrome Patient Reported Index; H90, homozygous for *NCF1*-H90; LSGB, labial salivary gland biopsy; *NCF1*, neutrophil cytosolic factor 1; R90, homozygous for *NCF1*-R90; SjD, Sjogren disease SEM, Standard Error of the Mean.

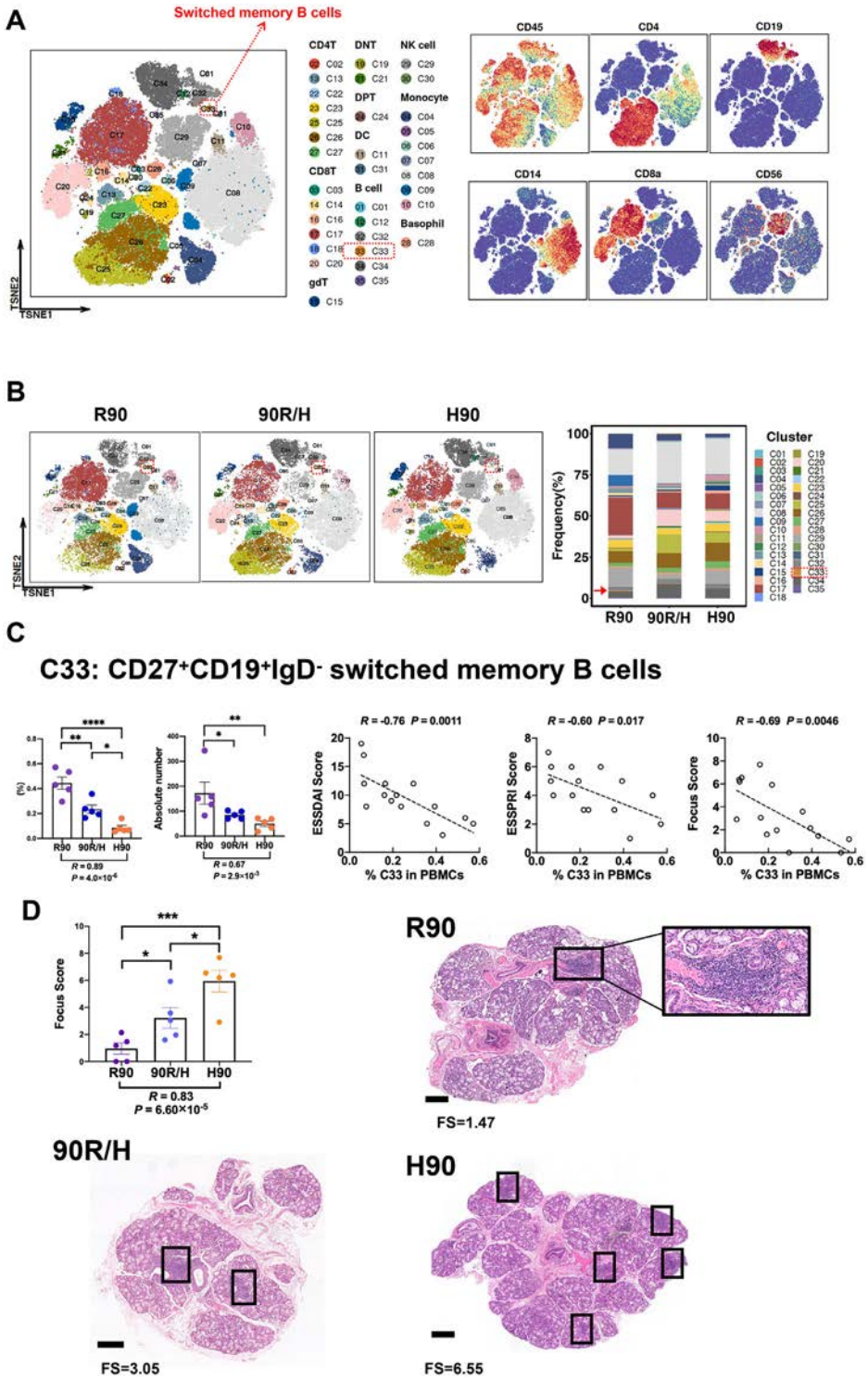

Figure 2. Proportions of $CD27^+CD19^+IgD^-$ switched memory B cells in PBMCs of patients with SjD correlated with *NCF1*-H90 dose and disease activity. (A) Left: tSNE plot of the CyTOF data of $CD45^+$ cells from PBMCs of 15 patients with SjD. A total of 35 clusters were identified, and each specific immune cell type was annotated using established marker gene expression. Right: tSNE plot of all $CD45^+$ cells coloured by the expression levels of CD45, CD4, CD19, CD14, CD8a, and CD56. (B) Left: tSNE plot of all $CD45^+$ cells from PBMCs of patients with R90 (n = 5), 90R/H (n = 5), and H90 (n = 5). Right: proportions of 35 cell clusters in the 3 groups. (C) Proportions and numbers of cluster 33 ($CD27^+CD19^+IgD^-$ switched memory B cells) associated with H90 copy numbers, ESSDAI Score, ESSPRI Score, and Focus Score. (D) A dose-dependent association of the *NCF1*-H90 variant with elevated Focus Score. Representative images of salivary gland stained with H&E from 1 patient of each genotype group representing the mean value of Focus Score. The box showed a focus of lymphocyte infiltration. * $P < .05$; ** $P < .01$; *** $P < .001$; **** $P < .0001$. *P* values among the 3 groups were determined using one-way ANOVA with Bonferroni's multiple-comparison test. The association of H90 copy numbers with the percentage and number of C33 or Focus Score was calculated using a linear regression test. The correlation was calculated using the Pearson correlation test. Results were shown as mean ± SEM. ANOVA, Analysis of Variance; CyTOF, cytometry by time-of-flight; DC, dendritic cell; DNT, double negative T cell; DPT, double positive T cell; ESSDAI, EULAR Sjögren's Syndrome Disease Activity Index; ESSPRI, EULAR Sjögren's Syndrome Patient Reported Index; FS, Focus Score; gDT, $\gamma\delta$ T cell; H90, homozygous for *NCF1*-H90; H&E, haematoxylin and eosin; IgD, Immunoglobulin D; *NCF1*, neutrophil cytosolic factor 1; NK, natural killer; PBMCs, peripheral blood mononuclear cells; SjD, Sjogren disease; tSNE, t-distributed stochastic neighbour embedding.

Based on expression levels of lineage-associated markers, PBMCs were partitioned into 35 cell clusters (Supplementary Fig S1 and Supplementary Table S7) visualised on a t-distributed stochastic neighbour embedding map (Fig 2A,B), which were annotated into 10 major immune cell lineages: $CD4^+$ T cells, $CD8^+$ T cells, $\gamma\delta$ T cells, double negative T cells, double positive T cells, dendritic cells (DC), B cells, natural killer (NK) cells, monocytes, and basophils. Both the frequency and absolute number of cluster 33 (cluster comprising predominantly $CD27^+CD19^+IgD^-$ switched memory B cells) were significantly decreased in the H90 group compared with the 90R/H or R90 groups (Fig 2C), exhibiting an H90 dose-dependent decrease in both percentage and absolute number of this cluster. The percentage of $CD27^+CD19^+IgD^-$ switched memory B cells was negatively correlated with ESSDAI, ESSPRI, and Focus Score (Fig 2C). The H90 group had significantly higher Focus Score than the R90 or 90R/H group, and the 0, 1, or 2 copies of H90 carriage dose dependently associated with increased Focus Score (Fig 2D and Supplementary Table S6).

Other significant changes in the PBMCs of H90 group compared with those from R90 group included $CX3CR1^+CD68^+CD86^+HLA\text{-}DR^+CD11b^+CD11c^+$ monocytes (cluster 10), $CD8^+CXCR3^+$ effector memory T cells (cluster 14), $CD3^+CD68^+CD127^+$ $\gamma\delta$ T cells (cluster 15), $CD8^+CD68^+$ effector T cells (cluster 17), $CD4^+CD25^+$ regulatory T cells (cluster 22) [16], and NK cells (cluster 30) (Supplementary Fig S2). However, no significant correlation was found between the proportion of these differentially expressed clusters and Focus Score, ESSDAI Score, or ESSPRI Score (Supplementary Fig S3).

NCF1-H90 variant drives increased proportions of CXCR4-enriched switched memory B cells and plasma cells, and elevated expression of ISGs of fibroblasts in MSG

To explore functional consequences of the decreased switched memory B-cell subset in PBMCs and its underlying mechanism in salivary glands, we collected minor salivary glands (MSGs) from 3 patients with H90 and 4 patients with R90. Detailed clinical characteristics were recorded at the time that paired blood (CyTOF study) and salivary gland samples were collected (Supplementary Table S6).

Single-cell suspensions of MSG tissues were subjected to single-cell RNA sequencing (scRNA-seq) using the MobiNova-100 Single Cell System. After quality control processing, a total of 68,496 high-quality single-cell transcriptomes were identified and visualised as 12 major cell subpopulations based on known cell type-specific marker gene expression using uniform manifold approximation and projection (Fig 3A,B, Supplementary Fig S4). The proportion of B cells (top 3 maker genes: *MS4A1, CD79A*, and *CXCR4*, defined as CXCR4-enriched switched memory B cells) was significantly elevated in the H90 group than the R90 group, and mucous acinar cells, plasma cells, and endothelial cells also showed significantly higher abundance in the H90 group (Fig 3C, Supplementary Fig S5A). Moreover, the percentage of switched memory B cells in the MSG was negatively correlated with that in the paired PBMCs (Fig 3D), suggesting that substantial switched memory B-cell migration from peripheral blood into salivary glands occurred in a patient with SjD carrying the *NCF1*-H90 genotype, thereby causing severe inflammatory infiltration in the MSG. Furthermore, the proportions of switched memory B cells in MSG were positively correlated with the proportions of plasma cells and the Focus Score. Similarly, proportions of plasma cells in MSG showed a positive correlation with the serum IgG levels, SSA+ IgG levels, and Focus Score (Fig 3D). In contrast, no significant correlations were observed between proportions of mucous acinar cells and switched memory B cells or plasma cells, nor between the proportions of mucous acinar cells and the Focus Score in MSG, and nor between the proportions of plasma cells and serum IgA levels (Supplementary Fig S5B-E).

The elevated differentially expressed genes (DEGs) of the H90 group in each of the cell types were dominated by interferon-stimulated genes (ISGs), and functional enrichment analysis showed that DEGs are mainly involved in the interferon-associated signalling (Supplementary Fig S6). Hence, we further calculated both type I and type II IFN scores using the scRNA-seq dataset (Supplementary Table S8). The H90 group exhibited significantly elevated IFN-I and IFN-II scores relative to the R90 group in most cell types. Among these, fibroblasts exhibited the greatest fold increase in IFN-I score in the H90 relative to the R90 group, whereas pericytes and fibroblasts showed the most pronounced fold increase in IFN-II Score (Fig 3E, Supplementary Fig S7). Moreover, the IFN-I and IFN-II Scores of MSG were significantly increased in patients with SjD compared with healthy controls, and fibroblasts also showed the greatest fold increase in IFN-I score in patients relative to controls in our analysis of published scRNA-seq data from Chinese subjects (Supplementary Fig S8) [17]. Because low reactive oxygen species (ROS) due to the *NCF1*-H90 variant is strongly associated with various autoimmune diseases [6,9], we calculated the ROS Score of MSG using the scRNA-seq dataset (Supplementary Table S8). Both overall ROS and NOX2-ROS Scores of MSG were significantly lower in the H90 group than the R90 group, in which both T cells and B cells exhibited a high fold decrease in NOX2-ROS scores in the H90 group (Supplementary Fig S9A-F). Moreover, the NOX2-ROS Score showed significant negative correlation with *CXCR4* expression in B cells, and the total ROS Score also showed significant negative correlations with *CXCL12* expression across multiple stromal cell types (Supplementary Fig S9G-H).

Further dissection of the B-cell compartment revealed that glandular B cells in the H90 group were enriched for a $ZEB2^+$ subset (1.54% vs 0.26%, $P = .032$) displaying an age-associated B cell (ABC)-like phenotype and elevated expression of ISGs [18]. This $ZEB2^+$ subset accounted for the elevated IFN-I signature and the reduced NOX2-ROS observed in total B cells (Supplementary Fig S10). Within the T/NK compartment, T peripheral helper (Tph) and $IL7R^+CD4^+$ T cells were significantly increased in the H90 group, whereas $CD8^+$ T-cell subsets were decreased and NK cells unchanged. Meanwhile, Tph and $IL7R^+CD4^+$ T cells exhibited high *CXCR4* levels comparable with those of B cells, whereas $CD8^+$ T cells and NK cells showed low *CXCR4* levels (Supplementary Fig S11A-D). By contrast, plasmacytoid dendritic cell (pDCs) and neutrophils were not detected in the myeloid compartment from our glandular scRNA-seq data (Supplementary Fig S11E-G).

NCF1-H90 variant promotes interaction between CXCR4-enriched memory B cells and $CXCL12^+$ fibroblasts with elevated IFN scores in MSG

Next, we subcategorised fibroblasts into 3 distinct subpopulations based on DEGs signatures: $THBS4^+$, $CXCL12^+$, and $TNXB^+$ fibroblasts. The proportion of $CXCL12^+$ fibroblasts was increased in the H90 group (Fig 4A), exhibiting the highest IFN-I and IFN-II scores among all subsets (Fig 4B,C). Functional enrichment analysis revealed that DEGs of $CXCL12^+$ fibroblast were mainly associated with interferon signalling and negative regulation of B-cell apoptosis (Supplementary Fig S12A). To

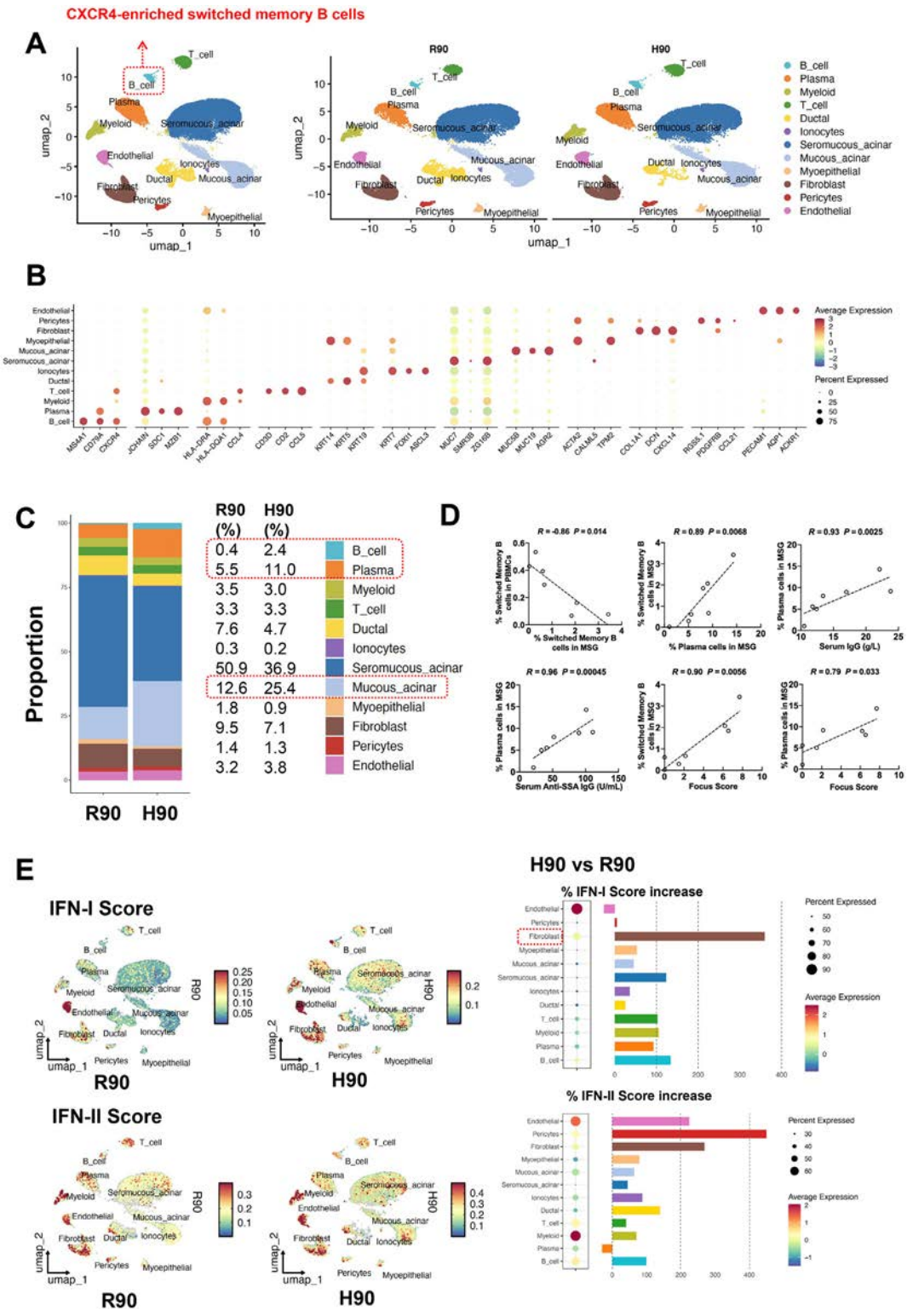

Figure 3. *NCF1*-H90 variant drives increased proportions of CXCR4-enriched switched memory B cells and plasma cells, and expression of ISGs in MSG fibroblasts from Chinese patients with SjD. (A) Left: UMAP visualisation of 68,496 single cells from MSG tissue, coloured by annotated cell subset and revealing 12 distinct cell clusters. Right: UMAP of cells from the R90 (n = 4) and H90 (n = 3) groups. All patients underwent concurrent salivary gland biopsy and PBMC collection; PBMC data were analysed by CyTOF in Figure 2. (B) Dot plots depict the expression of selected marker genes in each cell type. (C) Comparison of cell subset proportions between R90 and H90 groups, which was calculated in Supplementary Figure S5A. (D) The correlation among the percentages of switched memory B cells in MSG, switched memory B cells in PBMCs, plasma cells in MSG, serum IgG levels, serum SSA + IgG levels, and Focus Score. (E) Left: UMAP projection of IFN-I and IFN-II scores across cell subsets. Both scores were elevated in the H90 group compared to the R90 group. Right: fibroblasts exhibited the greatest fold increase in IFN-I score in the H90 relative to the R90 group, whereas pericytes and fibroblasts showed the most pronounced fold increase in IFN-II scores. The correlation was calculated using the Spearman correlation test. CyTOF, cytometry by time-of-flight; CXCR4, C-X-C motif chemokine receptor type 4; HLA, Human Leukocyte Antigen; H90, homozygous for *NCF1*-H90; IFN-I, interferon type I; IFN-II, interferon type II; IgG, Immunoglobulin G; ISGs, interferon-stimulated genes; MSG, minor salivary gland; *NCF1*, neutrophil cytosolic factor 1; PBMCs, peripheral blood mononuclear cells; PDGFRB, Platelet-Derived Growth Factor Receptor Beta; R90, homozygous for *NCF1*-R90; SSA, Sjögren's Syndrome type A antigen; SjD, Sjögren's disease; UMAP, Uniform Manifold Approximation and Projection.

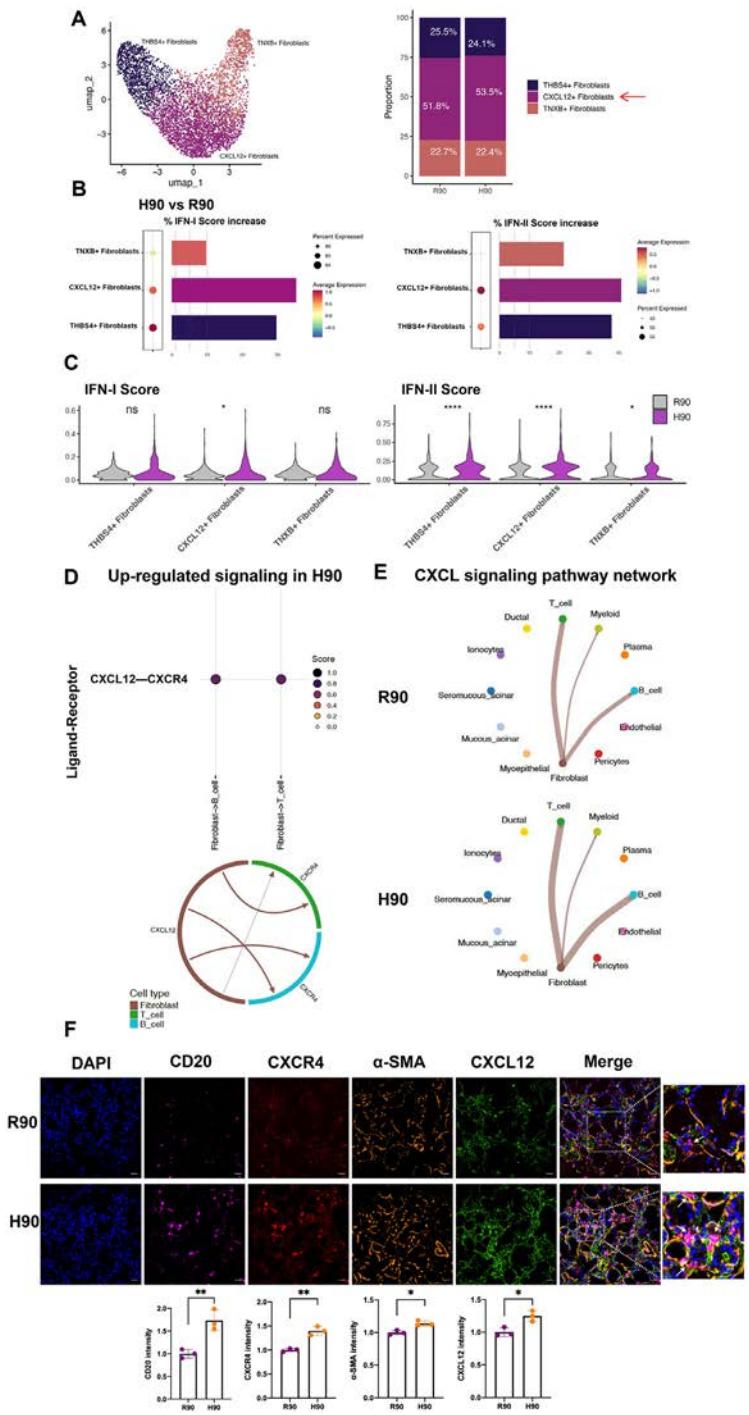

Figure 4. *NCF1*-H90 genotype promotes interaction between CXCR4-enriched memory B cells and CXCL12$^+$ fibroblasts with elevated IFN-I and IFN-II scores in MSG from Chinese patients with SjD. (A) UMAP plot of the distribution of fibroblasts in MSG coloured by cell subsets. The proportion of CXCL12$^+$ fibroblasts was elevated in the H90 group. (B,C) Both IFN-I and IFN-II scores in CXCL12$^+$ fibroblasts were significantly higher in the H90 group compared with the R90 group. (D) The most prominently upregulated fibroblast-specific signalling in the H90 group was the interaction between CXCL12$^+$ fibroblasts and CXCR4-enriched B/T cells. (E) The interaction strength within the CXCL signalling network between fibroblasts and switched memory B cells in MSG was enhanced in the H90 group. (F) Increased interaction between CXCR4-enriched B cells and CXCL12$^+$ fibroblasts in patients with SjD carrying *NCF1*-H90 genotype (n = 3 for each group). The arrow indicated the interaction between CXCR4$^+$ (red) B cell (magenta) and CXCL12$^+$ (green) fibroblast (orange). Scale bar: 20 μm. * $P < .05$; ** $P < .01$; **** $P < .0001$. *P* values between R90 and H90 groups were determined using 2-tailed Student's t-test. CXCL12, C-X-C motif chemokine ligand 12; CXCR4, C-X-C motif chemokine receptor type 4; DAPI, 4',6-diamidino-2-phenylindole; H90, homozygous for *NCF1*-H90; IFN-I, interferon type I; IFN-II, interferon type II; MSG, minor salivary gland; *NCF1*, neutrophil cytosolic factor 1; R90, homozygous for *NCF1*-R90; SjD, Sjogren disease; THBS, Thrombospondin; TNXB:,Tenascin XB; UMAP, Uniform Manifold Approximation and Projection α-SMA, α-smooth muscle actin.

further delineate dysregulated intercellular communication involving fibroblasts, we performed ligand-receptor interaction analysis using CellChat. The analysis identified CXCL12-CXCR4 as the most significantly upregulated signalling axis between fibroblasts and other cell types in the H90 group. Conversely, several interactions, including COL1A2-(ITGA2+ITGB1), HLA-B-CD8A, etc, were downregulated (Fig 4D and Supplementary Fig S12B,C). To gain deeper mechanistic insight into the functional consequences of this interaction, we employed NicheNet, a computational method that integrates prior knowledge of signalling and gene regulatory networks to predict ligand-target links [19]. This analysis predicted that signalling from CXCL12$^+$ fibroblasts via the CXCL12-CXCR4 axis specifically upregulates key genes in B cells, most notably the canonical ISG —*IFI44L* (Supplementary Fig S12D). Moreover, interaction strength within the CXCL signalling network between fibroblasts and switched memory B cells or T cells was enhanced in MSG of the H90 group (Fig 4E), suggesting that CXCL12$^+$ fibroblasts may recruit CXCR4$^+$ immune cells into MSG, thereby promoting glandular inflammation. Consistent with this mechanism, we observed significant accumulation of CXCR4-enriched switched memory B cells adjacent to CXCL12$^+$ fibroblasts in MSG for patients with H90 (Fig 4F).

NCF1-H90 genotype promotes elevated proportions of long-lived IgG+ plasma cells in MSG correlated with serum levels of SSA+IgG

Because plasma cells are the terminally differentiated B cells, we further explored the features of plasma cell subpopulations. We identified plasma cell subpopulations based on the secreted immunoglobulin class, and IgG+ plasma cells were significantly

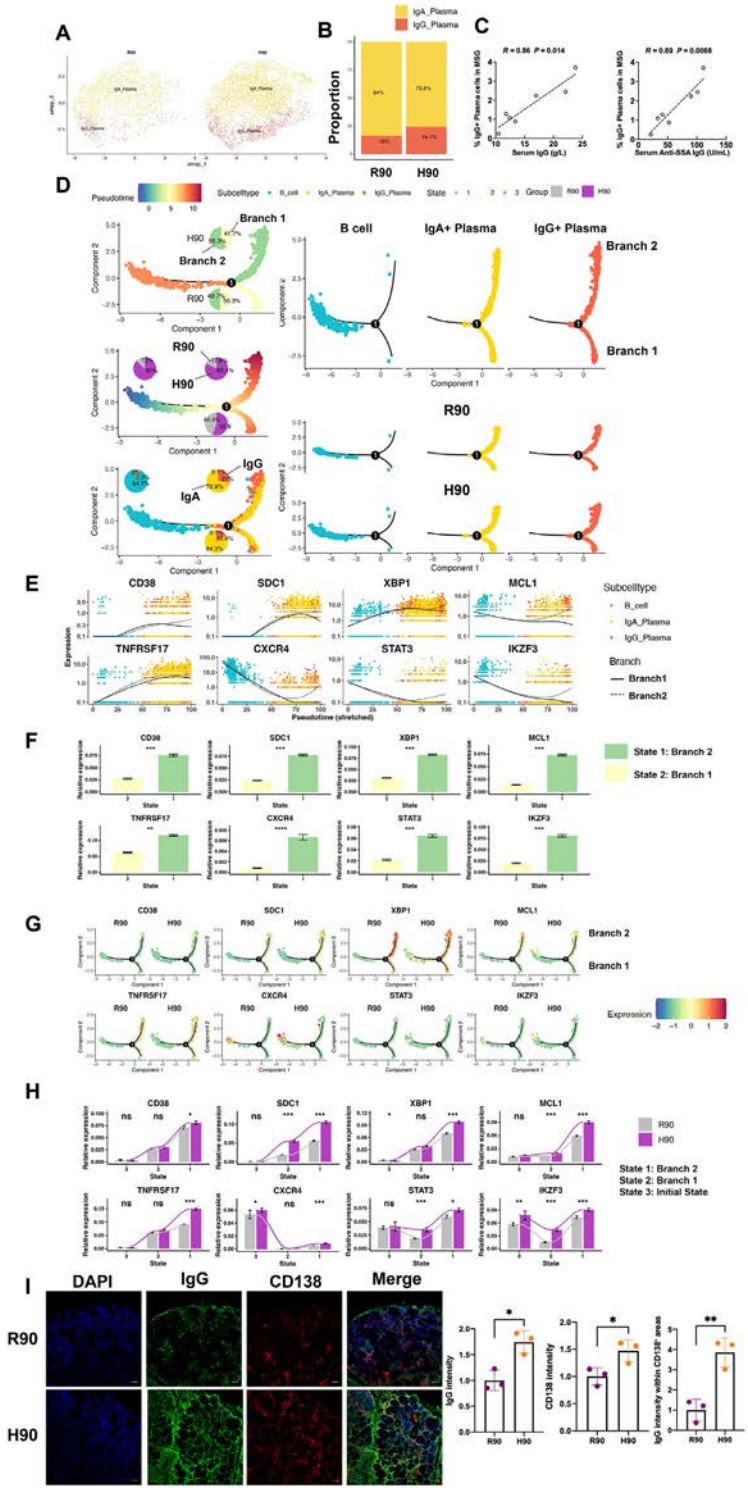

Figure 5. *NCF1*-H90 genotype promotes elevated proportions of long-lived IgG+ plasma cells in MSG correlated with serum levels of SSA+ IgG. (A) UMAP visualisation of plasma cells in MSG, coloured by cell subset. (B) Proportion of IgG+ and IgA+ plasma cells between the H90 and R90 groups, which was calculated in Supplementary Figure S11B. (C) Proportions of IgG+ plasma cells show a positive correlation with serum SSA+ IgG level. (D) Scatter plot of B cells and plasma cells, coloured by pseudotime, illustrating a bifurcated differentiation trajectory. The H90 group shows a higher proportion of cells in Branch 2, which contains elevated numbers of IgG+ plasma cells. (E,F) The markers related to LLPC survival increased significantly in branch 2 (dotted line) compared with branch 1 (full line). (F) A quantitative analysis of panel (E). (G,H) In branch 2, the markers related to LLPC survival significantly increased in the H90 group compared with the R90 group. (H) A quantitative analysis of panel (G). (I) Increased IgG+ plasma cells in patients with SjD carrying the *NCF1*-H90 genotype (n = 3 for each group). Scale bar: 20 μm. The correlation was calculated using the Spearman correlation test. * $P < .05$; ** $P < .01$; *** $P < .001$; **** $P < .0001$. *P* values between R90 and H90 groups or between branch 1 and branch 2 were determined using 2-tailed Student's t-test. DAPI, 4',6-diamidino-2-phenylindole, H90, homozygous for *NCF1*-H90; IgA, Immunoglobulin A; IgG, Immunoglobulin G; LLPC, long-lived plasma cell; ns, no significance; MSG, minor salivary gland; *NCF1*, neutrophil cytosolic factor 1; R90, homozygous for *NCF1*-R90; SjD, Sjogren's disease; SSA, Sjögren's Syndrome type A antigen, UMAP, Uniform Manifold Approximation and Projection.

elevated in the H90 group (Fig 5A,B, Supplementary Fig S13). This expansion correlated strongly with elevated serum IgG and SSA+ IgG levels (Fig 5C).

To elucidate the developmental trajectory linking switched memory B cells to plasma cells, we used monocle 2 to construct a model of the differentiation potential trajectory for all B cells and plasma cells collected from H90 and R90 groups. The analysis revealed 2 branching differentiation pathways towards the plasma cell fate. Both branches contained mixed IgA+ and IgG + plasma cells; however, the H90 group showed a pronounced enrichment in branch 2 (41.7% in branch 1 vs 58.3% in branch 2), which was also enriched for IgG+ plasma cells (15.6% in branch 1 vs 27.0% in branch 2) (Fig 5D). We then investigated trends in gene expression along pseudotime by the branch expression analysis model. gene ontology functional enrichment analysis of genes reclustered into 4 clusters, and the genes associated with the differentiation process from B cells to plasma cells were predominantly clustered in cluster 4 (Supplementary Fig S14). Gene expression dynamics along the pseudotime trajectory further demonstrated that expression markers related to long-lived plasma cell (LLPC) survival and maintenance, such as *SDC1, MCL1, TNFRSF17, CXCR4, STAT3*, and *IKZF3*, were

upregulated in branch 2 (Fig 5E,F), with significantly higher expression in the H90 group than in the R90 group (Fig 5G,H). Consistently, immunofluorescence staining confirmed an increase in IgG+ plasma cells accompanied by a reduction in IgA+ plasma cells in the salivary glands of patients with SjD carrying the *NCF1*-H90 variant (Fig 5I, Supplementary Fig S15).

To independently validate the LLPC characteristics of branch 2, we derived an LLPC-enriched gene signature from a published dataset (GSE180090) [20] and scored our salivary gland plasma cells. This analysis confirmed that cells within branch 2 exhibited significantly higher LLPC signature scores than those in branch 1 (Supplementary Fig S16), supporting their LLPC-like phenotype.

In summary, these findings indicated that the *NCF1*-H90 variant promoted the accumulation and local differentiation of IgG + plasma cells in the MSG, and the proportions of IgG+ plasma cells correlated with elevated circulating SSA+ IgG levels in Chinese patients affected with SjD.

NCF1-H90 variant predicts improved B-cell-targeted therapy outcomes

To evaluate the effect of the *NCF1*-H90 genotype on treatment response to B-cell-targeted therapy in patients with SjD, we retrospectively analysed an independent cohort of 19 female patients with SSA+ SjD treated at our centre. All patients had received belimumab for at least 1 year. Treatment consisted of intravenous belimumab at 10 mg/kg administered at weeks 0, 2, and 4, and every 4 weeks thereafter. Clinical and laboratory parameters, including ESSDAI, ESSPRI, serum IgG, and C4 levels, were assessed at baseline, week 24, week 48, and at the LFU (mean follow-up duration: 65.5 ± 8.5 weeks, range: 56-84 weeks) (Supplementary Table S9).

At the LFU, the H90 group showed a marked reduction in ESSDAI Score, with significantly greater improvement than the other groups. A dose-dependent association was observed between the copy number of H90 alleles and the change in ESSDAI Score at LFU. Similarly, serum IgG levels declined more substantially in the H90 group, also in a dose-dependent manner. Anti-SSA IgG levels were significantly reduced only in the H90 group. Furthermore, C4 levels increased most markedly in the H90 group with a clear dose-dependent relationship across H90 copy numbers (Fig 6A, Supplementary Fig S17A-D). Moreover, multivariate logistic regression showed that only the H90 genotype remained a significant, independent predictor of greater ESSDAI reduction after adjusting for baseline serum IgG and IFN-a levels (Supplementary Fig S17E). Consistent with these clinical improvements after belimumab treatment, immunofluorescence staining revealed a more pronounced reduction in CXCR4-enriched B cells within the salivary glands of the H90 group compared with those of the R90 group (Fig 6B).

DISCUSSION

Here, we show that the hypofunctional H90 *NCF1* allele is one of the strongest common risk variants for SjD in a case-control study and provide a detailed phenotypic characterisation linking this variant to specific cellular alterations in PBMCs and MSG using both CyTOF and scRNA-seq (Fig 7). The *NCF1* locus is complicated by the presence of pseudogenes (*NCF1B* and *NCF1C*), leading to frequent copy number variations, which is common in Europeans (>15%) but rare in East Asians (<2%) [5], explaining why initial European GWAS missed this variant. In the present study, we validated the association of the *NCF1*-H90 variant with SjD in both Chinese and European American populations, in which more robust association signals were observed in patients with SSA+ SjD (Table). Moreover, the *NCF1*-H90 variant was associated with an earlier age at diagnosis in both ancestral groups (Supplementary Table S2), consistent with earlier SLE onset linked to this variant [5,21].

Previous work links the *NCF1*-H90 variant to tissue-specific injury in various autoimmune diseases, including renal involvement in SLE and pulmonary fibrosis in SSc [6,7]. Our study now adds salivary gland immunopathology in SjD to this genetic effect, showing, in a longitudinal Chinese SjD cohort, that the H90 allele accelerates local inflammation and disease activity (Fig 1). This supports the model that the *NCF1*-R90H variant functions as a common amplifier of end-organ damage across different autoimmune contexts, rather than initiating any single disease. To our knowledge, this study is the first to report a dose-dependent association between the H90 allele and elevated ESSDAI and ESSPRI scores, both at baseline and after a median 5.6-year follow-up. Moreover, patients with SjD carrying 2 copies of the H90 allele exhibited lower C4 levels, higher LSGB scores, and increased disease morbidity. Given that anti-SSA antibody status is strongly linked with distinct genetic and clinical subtypes [22], we further analysed patients with SSA+ to minimise potential confounding effects. The persistence of the *NCF1*-H90 genotype effect within the SSA+ subgroup reinforces its role as a causal variant contributing to SjD severity.

B cells are critically involved in the pathogenesis of SjD [12,23], with peripheral blood studies consistently showing reduced $CD27^+$ memory B cells [14,15,24,25]. A high-dimensional CyTOF analysis of PBMCs from patients with SSA+ SjD revealed a significant decrease in both the frequency and absolute number of $CD27^+$ memory B cells, with inverse correlation with ESSDAI scores [26]. Our CyTOF study of PBMCs from patients with SSA+ SjD further demonstrated that the decreased proportion of $CD27^+CD19^+IgD^-$ switched memory B cells negatively correlated with the dose of the *NCF1*-H90 variant and disease activity measured using ESSDAI, ESSPRI, and Focus scores.

The observed reduction in circulating memory B cells in SjD may reflect their migration into inflamed salivary glands, although the precise mechanisms remain unclear. To explore this further, we performed scRNA-seq on salivary gland tissues from patients with SSA+ SjD whose paired PBMCs were studied using CyTOF. The only B-cell population in MSG, the CXCR4-enriched switched memory B-cell subset, showed a significant increase in the H90 group. Notably, the proportion of these CXCR4-enriched switched memory B cells in MSG was negatively correlated with the frequency of $CD27^+CD19^+IgD^-$ switched memory B cells in the PBMCs collected at the time of MSG biopsies. Given that elevated surface expression of CXCR4 (a chemokine receptor facilitating B-cell migration to lymphoid tissues) on peripheral blood B cells from patients with SjD compared with healthy controls [27], we deduced that the reduction in switched memory B cells in PBMCs and their concomitant accumulation in MSG within the H90 group represent the migration of this B-cell subset from the circulation into glandular tissues. Moreover, the selective enrichment of $ZEB2^+$ B cells with an ABC-like phenotype identifies this subset as a key driver of the heightened IFN-I signature and diminished NOX2-ROS observed in the H90 group, which is consistent with previous findings that ZEB2 emerges as a driver of B-cell autoimmunity and the ZEB2-JAK-STAT axis governs ABC differentiation [18]. Within the T-cell niche, the expansion of CXCR4-high Tph and $IL7R^+CD4^+$ T cells, and the paucity of CXCR4-low $CD8^+$ T cells, demonstrates that differential CXCR4 expression may

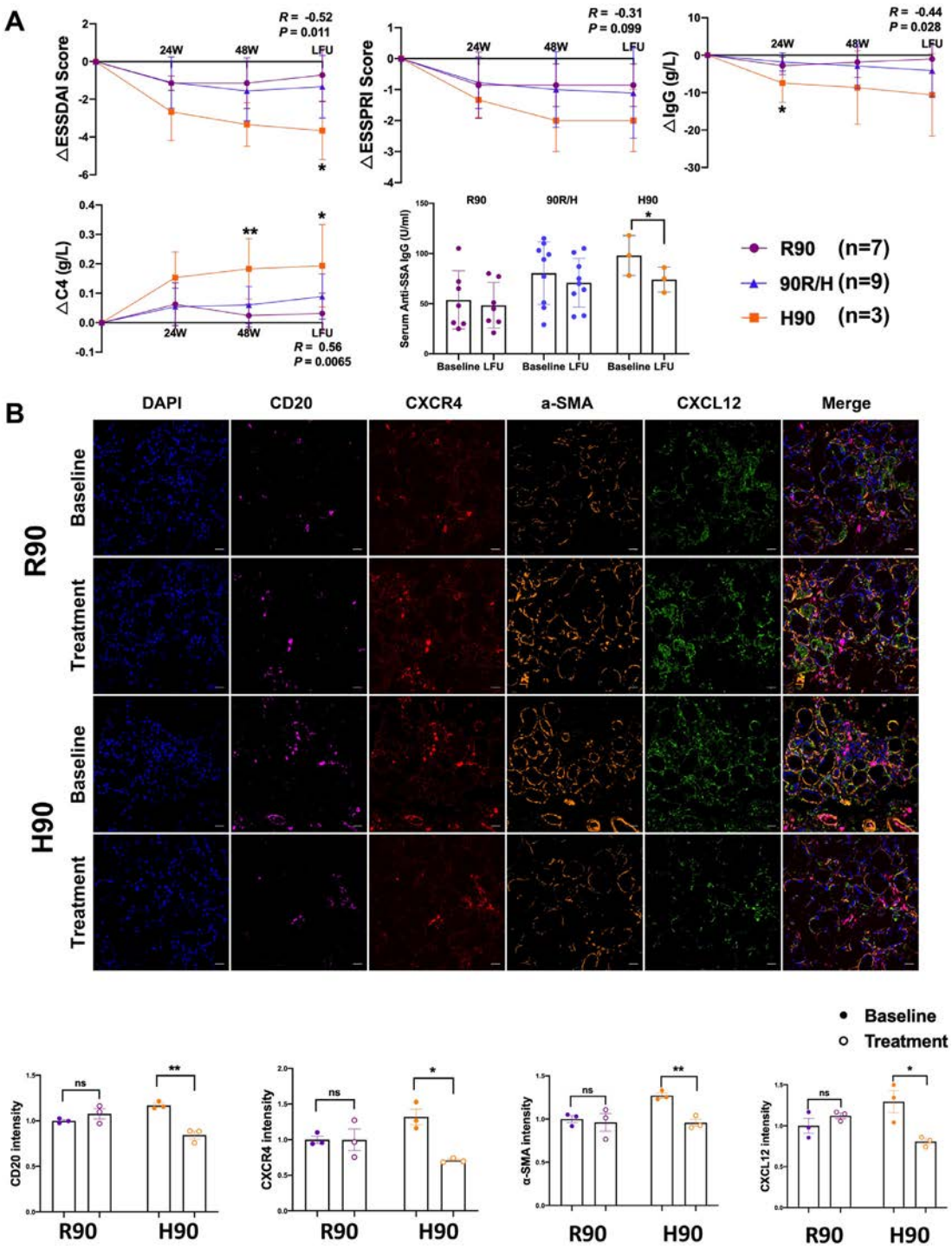

Figure 6. *NCF1*-H90 variant predicts improved B-cell-targeted therapy outcomes. (A) Comparison of changes in ESSDAI, ESSPRI, serum IgG, and C4 levels among the R90, 90R/H, and H90 groups at week 24, week 48, and the final follow-up. Comparison of serum SSA IgG level between baseline and LFU in each group. (B) Immunofluorescence staining shows a more pronounced reduction in CXCR4-enriched B cells in the salivary glands of H90 carriers compared with the R90 group after belimumab treatment (n = 3 for each group). Scale bar: 20 μm. The △ values were calculated as the follow-up value minus the baseline value for each parameter. * $P < .05$; ** $P < .01$. *P* values among the 3 groups were determined using one-way ANOVA. *P* values between baseline and LFU were determined using a paired t-test. The association between H90 copy numbers and changes in ESSDAI, ESSPRI, serum IgG, and C4 levels at the last follow-up was assessed using linear regression. Data are presented as mean ± SEM. ESSDAI, EULAR Sjögren's syndrome disease activity index; ANOVA, Analysis of Variance; DAPI, 4',6-diamidino-2-phenylindole; ESSPRI, EULAR Sjögren's Syndrome Patient Reported Index; H90, homozygous for *NCF1*-H90; IgG, Immunoglobulin G; LFU, last follow-up; ns, no significance; *NCF1*, neutrophil cytosolic factor

govern subset-specific recruitment of T cells via the CXCR4-CXCL12 axis. The absence of transcriptionally detectable pDCs and neutrophils in our MSG, consistent with recent SjD scRNA-seq studies [28–30], indicates that the prominent IFN-I signature originates from fibroblasts, B cells, and epithelial cells rather than infiltrating pDCs.

The strong expression of CXCL12 in the inflamed salivary glands of patients with SjD contributes to a supportive environment that attracts CXCR4-enriched switched memory B cells (via CXCR4-CXCL12 interactions) migrating into MSG and differentiating into plasma cells [31]. Plasma cells are often localised near CXCL12-expressing salivary gland epithelial cells and

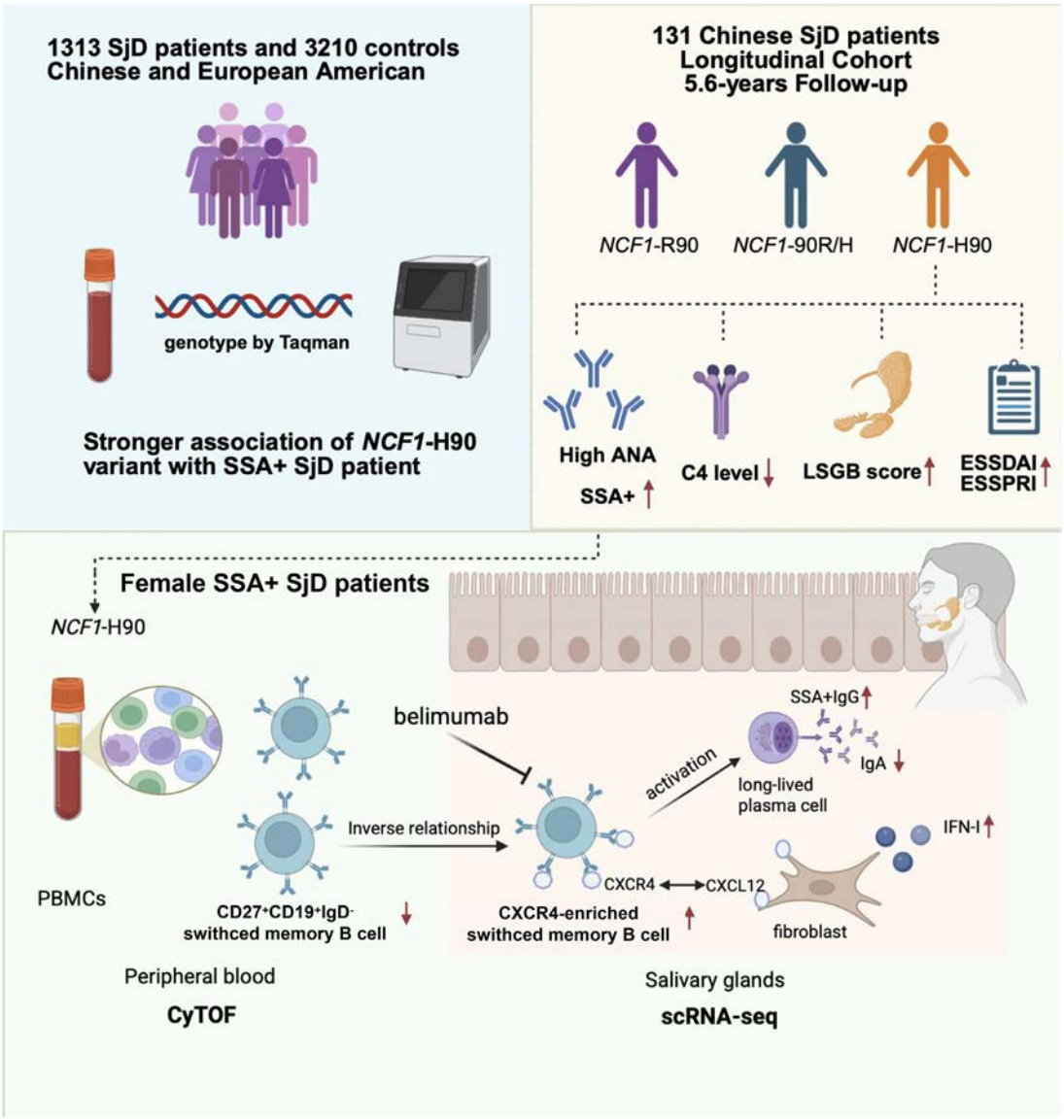

Figure 7. Overview of the experimental workflow. Our experiments could be summarised into 3 parts: 1. The *NCF1*-H90 allele is one of the strongest common risk variants for patients with SSA+ SjD in a case-control association study; 2. Analysis within a longitudinal cohort of Chinese patients with SjD confirms that the *NCF1*-H90 variant is associated with elevated ANA titres, anti-SSA seropositivity, decreased serum C4 levels, higher LSGB scores, and greater disease activity 3. Combined CyTOF profiling of PBMCs and scRNA-seq of salivary gland tissues from female patients with SSA+ SjD reveal that the *NCF1*-H90 variant promotes the infiltration of circulating switched memory B cells into salivary glands. These cells interact with $CXCL12^+$ fibroblasts with elevated IFN-I and IFN-II scores and subsequently differentiate into long-lived IgG+ plasma cells. The process is susceptible to inhibition by belimumab. 90R/H, heterozygous for *NCF1*-90R/H; ANA, Antinuclear Antibody; CyTOF, cytometry by time-of-flight; ESSDAI, EULAR Sjögren's syndrome disease activity index; ESSPRI, EULAR Sjögren's Syndrome Patient Reported Index; H90, homozygous for *NCF1*-H90; IFN-I, type I interferon; IgG, Immunoglobulin G; LSGB, labial salivary gland biopsy; *NCF1*, neutrophil cytosolic factor 1; PBMCs, peripheral blood mononuclear cells; R90, homozygous for *NCF1*-R90; scRNA-seq, single-cell RNA sequencing; SjD, Sjogren disease; SSA, Sjögren's Syndrome type A antigen.

adipocytes, suggesting a potential role for CXCL12 in supporting plasma cell survival [32]. Although the proportion of $CXCL12^+$ fibroblasts was only marginally increased in the H90 group, this subset exhibited the highest IFN-I and IFN-II scores among all fibroblast subpopulations (Fig 4B,C). This functional distinction made it a prime candidate for investigation. Moreover, the CXCR4-CXCL12 axis was the most markedly upregulated ligand-receptor pair between fibroblasts and immune cells (Fig 4D), and we observed accumulated CXCR4-enriched switched memory B cells in proximity to $CXCL12^+$ fibroblasts in MSG tissues from patients with H90 (Fig 4F). These findings support that $CXCL12^+$ fibroblasts, through their functional state and chemokine signalling, contribute to the recruitment of CXCR4-enriched switched memory B cells into the salivary glands, and constitute a key component of the inflammatory niche for B-cell differentiation, characterised by a high IFN-I signature.

Analysis of plasma cell phenotypes in salivary glands from patients with SjD has revealed the presence of both IgA+ and IgG+ plasma cells [32]. Previous studies demonstrated that patients with a Focus Score ≥ 2 exhibited upregulated IgG+ plasma cells but not IgA+ plasma cells [32]. Additionally, plasma cells within MSG could produce anti-SSA/Ro and anti-SSB/La autoantibodies, the levels of which correlated with those in sera [33]. We observed a significant increase in the proportion of plasma cells in the MSG of the H90 group, which positively correlated with serum IgG levels, SSA+ IgG levels, and Focus Score (Fig 3D). Specifically, IgG+ plasma cells—but not IgA+ plasma cells—were significantly expanded in H90

carriers, and this increase was strongly associated with elevated serum IgG and SSA+ IgG levels (Fig 5B,C). Moreover, these IgG + plasma cells in the H90 group exhibited higher expression of *SDC1, MCL1, TNFRSF17, CXCR4, STAT3*, and *IKZF3*—markers related to survival of LLPC (Fig 5E-H). These results suggested that the *NCF1*-H90 variant might promote long-lived IgG+ plasma cells within the salivary gland microenvironment. This finding aligns with earlier reports indicating that plasma cells in MSG of patients with SjD with high Focus Score display a long-lived phenotype [32]. It has been proposed that LLPC may occupy survival niches in salivary glands, and therapeutic strategies targeting these niches may hold clinical benefit [34].

Building on evidence from the BELISS (Efficacy and Safety of Belimumab in Subjects With Primary Sjögren's Syndrome) open-label phase II study, which reported symptomatic improvement in a subset of patients with SjD following belimumab treatment and called for future trials to identify responder subgroups [35,36], our retrospective analysis provides a potential genetic basis for such stratification. We observed that in female patients with SSA+ SjD, carriers of the homozygous *NCF1*-H90 genotype exhibited a superior treatment response, characterised by significantly greater reductions in ESSDAI Score, serum SSA+ IgG levels, and more pronounced increases in C4 levels. These findings strongly suggest that *NCF1*-H90 genotyping could help identify patients with SjD who are most likely to derive substantial benefit from B-cell-targeted therapies.

Hypofunctional *NCF1*-H90 variants, leading to reduced ROS production, are causal variants in multiple autoimmune diseases, as demonstrated in corresponding animal models [6,9,21,37]. In line with this, we calculated ROS scores from scRNA-seq data of MSG and found significantly lower overall ROS and NOX2-ROS in the H90 group, with T cells and B cells showing the greatest reductions of NOX2-ROS. Previous studies have established that NOXs serve as the primary source of ROS in B cells, and oxidase-deficient B cells from patients with chronic granulomatous disease exhibit hyperresponsiveness to TLR7/9 activation [38,39]. Similarly, global or B-cell-specific deletion of *Ncf1* in murine lupus models enhances endosomal TLR signalling, spontaneous germinal centre formation, and humoral autoimmunity [10]. Thus, diminished ROS levels in B cells within the salivary glands may aberrantly activate antibody-producing B cells to SSA antigens associated with RNA via nucleic acid-binding TLRs in homozygous H90 carriers.

Limitations of this study include the following: (1) although population admixture could not be corrected via principal component analysis, we strengthened the validity of findings by validating the association between the H90 variant and pathological features of SjD across both peripheral blood and salivary glands. (2) Despite being unable to isolate sufficient CXCR4-enriched switched memory B cells from MSG for *in vitro* differentiation into plasma cells to establish a direct relationship, the pseudotime trajectory analysis supported their developmental link, which was further corroborated by immunofluorescence staining. (3) Belimumab response was assessed in a small retrospective cohort; future prospective randomised controlled trials are warranted to definitively establish the association between the *NCF1*-R90H variant and belimumab efficacy. (4) A potential limitation in the interpretation of our 5.6-year-long-term retrospective clinical data is attrition bias. Patients who achieve sustained remission are less likely to remain engaged in regular specialist follow-up. A multicentre prospective investigation with scheduled follow-up is needed in the future. (5) The observed increase in mucous acinar cells within the salivary gland of the H90 group remains mechanistically unexplained, and its specific contribution to SjD pathogenesis warrants future investigation. (6) A limitation of our CyTOF analysis is the absence of CD38, which prevented us from definitively distinguishing between memory B cells and immature antibody-secreting cells. Future studies employing more targeted panels will be needed to resolve this.

In summary, the *NCF1*-R90H variant was associated with SjD susceptibility, particularly in patients with SSA+. The patients with SjD carrying the homozygous H90 genotype had an abnormally decreased switched memory B-cell subset in peripheral blood, which might be recruited by $CXCL12^+$ fibroblasts into MSG, and further differentiated into long-lived IgG+ plasma cells, resulting in elevated serum SSA+ IgG levels and greater disease severity. The B cells and the LLPCs are promising therapeutic targets in SjD, particularly in the patients with SSA+ carrying the H90 variant.

Competing interests

CJL received consulting fees from Johnson & Johnson Innovative Medicine Research Alliance. All other authors declare no competing interests.

Acknowledgements

We thank Dr Xiaojun Tang, Shu Liu, and Anning Wang for their excellent technical assistance, as well as the patients and healthy controls for their kind participation in this research.

Contributors

XY contributed to writing—original draft, investigation, methodology, formal analysis, conceptualisation, and funding acquisition. XQ contributed to writing—original draft, writing—review & editing, investigation, methodology, data curation, formal analysis, and funding acquisition. XW contributed to writing—review & editing, methodology, software, and data curation. YC contributed to investigation, data curation, and conceptualisation. YW contributed to investigation. YZ contributed to data curation. DX contributed to investigation and data curation. YL contributed to methodology and resources. JZ contributed to formal analysis and data curation. JMG contributed to resources. JAJ contributed to resources. CJL contributed to writing—review & editing and resources. NS contributed to writing—review & editing, resources, and data curation. LS contributed to writing—review & editing, project administration, supervision, validation, conceptualisation, and funding acquisition. BPT contributed to writing—review & editing, project administration, supervision, validation, resources, conceptualisation, and funding acquisition.

Funding

This work was supported by the National Natural Science Foundation of China (82572066, 81901649, and 82002260), the Natural Science Foundation of Jiangsu Province (BK20251723), Jiangsu Health International Exchange Program, Nanjing Health Science and Technology Development Special Fund Project for Outstanding Youth Science and Technology Talents (JQX25006), Scientific Research Project of Jiangsu Provincial Health Commission (MQ2025042), and Funding for Clinical Trials from Nanjing Drum Tower Hospital (2022-LCYJ-PY-39). BPT is supported by NIH grant (R21 AR081933-01A1 and RO1 AR085045) and the SmartState Endowment.

Patient consent for publication

Patients and/or the public were not involved in the design, or conduct, or reporting, or dissemination plans of this research.

Ethics approval

Study participants were recruited with informed consents approved by the Ethics Committee of the Affiliated Drum Tower Hospital of Nanjing University Medical School (no. 2009004), Shanghai Jiao Tong University School of Medicine (KY-2022-023-B), University of California, Los Angeles IRB (10-001489), and Oklahoma Medical Research Foundation (95-12 and 06-12).

Provenance and peer review

Not commissioned; externally peer reviewed.

Data availability statement

All data relevant to the study are included in the article or uploaded as supplementary information. Original data are available on reasonable request. The single-cell RNA sequencing data have been deposited in the Genome Sequence Archive for Human (GSA-Human, https://ngdc.cncb.ac.cn/gsa-human) under accession number HRA016053.

Supplementary materials

Supplementary material associated with this article can be found in the online version at doi:10.1016/j.ard.2026.03.026.

Orcid

Betty P. Tsao: http://orcid.org/0000-0001-7938-5975

REFERENCES

[1] Ramos-Casals M, Brito-Zerón P, Sisó-Almirall A, Bosch X. Primary Sjogren syndrome. BMJ 2012;344:e3821.
[2] Mariette X, Criswell LA. Primary Sjogren's syndrome. N Engl J Med 2018;378:931–9.
[3] Thorlacius GE, Bjork A, Wahren-Herlenius M. Genetics and epigenetics of primary Sjogren syndrome: implications for future therapies. Nat Rev Rheumatol 2023;19:288–306.
[4] Li Y, Zhang K, Chen H, Sun F, Xu J, Wu Z, et al. A genome-wide association study in Han Chinese identifies a susceptibility locus for primary Sjogren's syndrome at 7q11.23. Nat Genet 2013;45:1361–5.
[5] Zhao J, Ma J, Deng Y, Kelly JA, Kim K, Bang SY, et al. A missense variant in NCF1 is associated with susceptibility to multiple autoimmune diseases. Nat Genet 2017;49:433–7.
[6] Geng L, Zhao J, Deng Y, Molano I, Xu X, Xu L, et al. Human SLE variant NCF1-R90H promotes kidney damage and murine lupus through enhanced Tfh2 responses induced by defective efferocytosis of macrophages. Ann Rheum Dis 2022;81:255–67.
[7] Yuan X, Qin X, Takemoto K, Zhao J, Sanderson M, Xu X, et al. Human hypofunctional NCF1 variants promote pulmonary fibrosis in the bleomycin-induced mouse model and patients with systemic sclerosis via expansion of SPP1(+) monocytes-derived macrophages. Ann Rheum Dis 2025;84:294–306.
[8] Meng Y, Ma J, Yao C, Ye Z, Ding H, Liu C, et al. The NCF1 variant p.R90H aggravates autoimmunity by facilitating the activation of plasmacytoid dendritic cells. J Clin Invest 2022;132:e153619.
[9] Luo H, Urbonaviciute V, Saei AA, Lyu H, Gaetani M, Végvári Á, et al. NCF1-dependent production of ROS protects against lupus by regulating plasmacytoid dendritic cell development and functions. JCI Insight 2023;8:e164875.
[10] Liu S, Lagos J, Shumlak NM, Largent AD, Lewis STE, Holder U, et al. NADPH oxidase exerts a B cell-intrinsic contribution to lupus risk by modulating endosomal TLR signals. J Exp Med 2024;221:e20230774.
[11] Muskardin TLW, Niewold TB. Type I interferon in rheumatic diseases. Nat Rev Rheumatol 2018;14:214–28.
[12] Nocturne G, Mariette X. B cells in the pathogenesis of primary Sjogren syndrome. Nat Rev Rheumatol 2018;14:133–45.
[13] Jonsson R, Theander E, Sjöström B, Brokstad K, Henriksson G. Autoantibodies present before symptom onset in primary Sjogren syndrome. JAMA 2013;310:1854–5.
[14] Hansen A, Odendahl M, Reiter K, Jacobi AM, Feist E, Scholze J, et al. Diminished peripheral blood memory B cells and accumulation of memory B cells in the salivary glands of patients with Sjogren's syndrome. Arthritis Rheum 2002;46:2160–71.
[15] Roberts ME, Kaminski D, Jenks SA, Maguire C, Ching K, Burbelo PD, et al. Primary Sjogren's syndrome is characterized by distinct phenotypic and transcriptional profiles of IgD+ unswitched memory B cells. Arthritis Rheumatol 2014;66:2558–69.
[16] Gottenberg JE, Lavie F, Abbed K, Gasnault J, Le Nevot E, Delfraissy JF, et al. CD4 CD25high regulatory T cells are not impaired in patients with primary Sjogren's syndrome. J Autoimmun 2005;24:235–42.
[17] Xiang N, Xu H, Zhou Z, Wang J, Cai P, Wang L, et al. Single-cell transcriptome profiling reveals immune and stromal cell heterogeneity in primary Sjogren's syndrome. iScience 2023;26:107943.
[18] Dai D, Gu S, Han X, Ding H, Jiang Y, Zhang X, et al. The transcription factor ZEB2 drives the formation of age-associated B cells. Science 2024;383:413–21.
[19] Browaeys R, Saelens W, Saeys Y. NicheNet: modeling intercellular communication by linking ligands to target genes. Nat Methods 2020;17:159–62.
[20] Joyner CJ, Ley AM, Nguyen DC, Ali M, Corrado A, Tipton C, et al. Generation of human long-lived plasma cells by developmentally regulated epigenetic imprinting. Life Sci Alliance 2022;5:e202101285.
[21] Olsson LM, Johansson ÅC, Gullstrand B, Jönsen A, Saevarsdottir S, Rönnblom L, et al. A single nucleotide polymorphism in the NCF1 gene leading to reduced oxidative burst is associated with systemic lupus erythematosus. Ann Rheum Dis 2017;76:1607–13.
[22] Thorlacius GE, Hultin-Rosenberg L, Sandling JK, Bianchi M, Imgenberg-Kreuz J, Pucholt P, et al. Genetic and clinical basis for two distinct subtypes of primary Sjogren's syndrome. Rheumatology (Oxford) 2021;60:837–48.
[23] Hamza N, Bos NA, Kallenberg CG. B-cell populations and sub-populations in Sjogren's syndrome. Presse Med 2012;41:e475–83.
[24] Hansen A, Gosemann M, Pruss A, Reiter K, Ruzickova S, Lipsky PE, et al. Abnormalities in peripheral B cell memory of patients with primary Sjogren's syndrome. Arthritis Rheum 2004;50:1897–908.
[25] Bohnhorst JØ, Bjørgan MB, Thoen JE, Natvig JB, Thompson KM. Bm1-Bm5 classification of peripheral blood B cells reveals circulating germinal center founder cells in healthy individuals and disturbance in the B cell subpopulations in patients with primary Sjogren's syndrome. J Immunol 2001;167:3610–8.
[26] Mingueneau M, Boudaoud S, Haskett S, Reynolds TL, Nocturne G, Norton E, et al. Cytometry by time-of-flight immunophenotyping identifies a blood Sjogren's signature correlating with disease activity and glandular inflammation. J Allergy Clin Immunol 2016;137:1809–1821.e12.
[27] Hansen A, Reiter K, Ziprian T, Jacobi A, Hoffmann A, Gosemann M, et al. Dysregulation of chemokine receptor expression and function by B cells of patients with primary Sjogren's syndrome. Arthritis Rheum 2005;52:2109–19.
[28] Pranzatelli TJF, Perez P, Ku A, Matuck B, Huynh K, Sakai S, et al. GZMK(+) CD8(+) T cells target a specific acinar cell type in Sjogren's disease. Ann Rheum Dis 2025. doi: 10.1016/j.ard.2025.08.014.
[29] Nayar S, Turner JD, Asam S, Fennell E, Pugh M, Colafrancesco S, et al. Molecular and spatial analysis of tertiary lymphoid structures in Sjogren's syndrome. Nat Commun 2025;16:5.
[30] Wu G, Wu F, Wang L, Ying L, Lu W, Qian K, et al. Application of imaging mass cytometry for spatially profiling the microenvironment of salivary glands in primary Sjogren's syndrome. Cell Death Dis 2025;16:392.
[31] Amft N, Curnow SJ, Scheel-Toellner D, Devadas A, Oates J, Crocker J, et al. Ectopic expression of the B cell-attracting chemokine BCA-1 (CXCL13) on endothelial cells and within lymphoid follicles contributes to the establishment of germinal center-like structures in Sjogren's syndrome. Arthritis Rheum 2001;44:2633–41.
[32] Szyszko EA, Brokstad KA, Oijordsbakken G, Jonsson MV, Jonsson R, Skarstein K. Salivary glands of primary Sjogren's syndrome patients express factors vital for plasma cell survival. Arthritis Res Ther 2011;13:R2.
[33] Tengnér P, Halse AK, Haga HJ, Jonsson R, Wahren-Herlenius M. Detection of anti-Ro/SSA and anti-La/SSB autoantibody-producing cells in salivary glands from patients with Sjogren's syndrome. Arthritis Rheum 1998;41:2238–48.

[34] Leah E. Connective tissue diseases: Long-lived plasma cells in Sjogren's syndrome-a salivary survival niche? Nat Rev Rheumatol 2011;7:130.
[35] Mariette X, Seror R, Quartuccio L, Baron G, Salvin S, Fabris M, et al. Efficacy and safety of belimumab in primary Sjogren's syndrome: results of the BELISS open-label phase II study. Ann Rheum Dis 2015;74:526–31.
[36] Mariette X, Barone F, Baldini C, Bootsma H, Clark KL, De Vita S, et al. A randomized, phase II study of sequential belimumab and rituximab in primary Sjogren's syndrome. JCI Insight 2022;7:e163030.
[37] Chen T, Zhou Z, Liu Y, Xu J, Zhu C, Sun R, et al. Neutrophils with low production of reactive oxygen species are activated during immune priming and promote development of arthritis. Redox Biol 2024;78:103401.
[38] McLetchie S, Volpp BD, Dinauer MC, Blum JS. Hyper-responsive Toll-like receptor 7 and 9 activation in NADPH oxidase-deficient B lymphoblasts. Immunology 2015;146:595–606.
[39] Kovács I, Horváth M, Lányi Á, Petheő GL, Geiszt M. Reactive oxygen species-mediated bacterial killing by B lymphocytes. J Leukoc Biol 2015;97:1133–7.

Ann Rheum Dis 85 (2026) 1625–1636

Contents lists available at ScienceDirect

Annals of the Rheumatic Diseases

journal homepage: https://www.sciencedirect.com/journal/annals-of-the-rheumatic-diseases

Scleroderma

Topoisomerase 1-DNA complexes are preferentially recognised by a subset of anti-topoisomerase 1 autoantibodies and their corresponding B cell receptors in systemic sclerosis

Sam Neppelenbroek[1], Corrie M. Wortel[1], Danique M.H. van Rijswijck[2], Marjolein J.A.L. Wetzels[1], Robbert Q. Kim[3], Nikki M. Loof[1], Martina Erbì[4], E.W. Nivine Levarht[1], Bart Everts[4], Albert J.R. Heck[2], Jeska K. de Vries-Bouwstra[1], Cynthia M. Fehres[1], René E.M. Toes[1], Hans U. Scherer[1,*]

[1] *Department of Rheumatology, Leiden University Medical Center, Leiden, The Netherlands*
[2] *Biomolecular Mass Spectrometry and Proteomics, Bijvoet Center for Biomolecular Research and Utrecht Institute for Pharmaceutical Sciences, Utrecht University, Utrecht, The Netherlands*
[3] *Protein Facility, Department of Cell and Chemical Biology, Leiden University Medical Center, Leiden, The Netherlands*
[4] *Leiden University Center for Infectious Diseases (LU-CID), Leiden University Medical Center, Leiden, The Netherlands*

ARTICLE INFO

Article history:
Received 1 May 2025
Received in revised form 12 March 2026
Accepted 14 March 2026

ABSTRACT

Objectives: Systemic sclerosis (SSc) is a deleterious disease. Its clinical management is complicated by strong interpatient heterogeneity. Progressive organ fibrosis is linked to autoantibodies against topoisomerase 1 (TOP1). Here, we hypothesised that the interaction between anti-TOP1 autoantibodies (ATAs) and TOP1 could influence SSc pathogenesis. TOP1 is a DNA-binding enzyme. Therefore, we studied the effects and functional consequences of TOP1-DNA binding on ATA recognition.

Methods: ATA monoclonal antibodies (ATA mAbs) and ATA-expressing B cell lines were generated from patient-derived TOP1-reactive B cells. Reactivity of monoclonal and polyclonal ATAs towards TOP1 and TOP1-DNA cleavage complexes (TOP1cc) was determined by enzyme-linked immunosorbent assay and mass photometry. Immunostimulatory properties of ATA mAbs in complex with TOP1/TOP1cc were assessed on monocytic THP-1 cells and primary monocytes. The stimulatory effects of TOP1-DNA complexes were tested on ATA-expressing B cells.

Results: TOP1-DNA binding differentially affected TOP1 recognition by ATA mAbs. A subset of ATA mAbs showed enhanced binding to TOP1cc, whereas others recognised TOP1 and TOP1cc to a similar extent. ATAs with enhanced TOP1cc recognition were observed in ATA$^+$ patients and correlated with ATA levels and interstitial lung disease. These 'TOP1cc-enhanced ATAs' affected the enzymatic function of TOP1 and, in complex with TOP1cc, increased proinflammatory cytokine production by THP-1 cells and primary monocytes. B cells expressing 'TOP1cc-enhanced ATAs' responded strongly to stimulation with TOP1-DNA complexes, whereas additive effects were not observed for B cells expressing 'regular' ATAs.

*Correspondence to Dr. Hans Ulrich Scherer.
E-mail address: h.u.scherer@lumc.nl (H.U. Scherer).
Handling editor Josef S. Smolen.

https://doi.org/10.1016/j.ard.2026.03.016

Conclusions: The differential recognition of TOP1 upon DNA binding by ATAs demonstrates heterogeneity in the ATA B cell response, possibly impacting disease-relevant processes in severe SSc.

WHAT IS ALREADY KNOWN ON THIS TOPIC

- Autoantibodies targeting topoisomerase 1 (TOP1) associate with disease phenotype and severity of organ complications in systemic sclerosis.
- Activated, TOP1-reactive memory B cells and TOP1-secreting plasma cells are found in the circulation of patients with progressive disease and those with pulmonary fibrosis.

WHAT THIS STUDY ADDS

- Novel evidence describing anti-TOP1 monoclonal autoantibodies (ATA) derived from patients with systemic sclerosis, which are heterogeneous and differentially recognise TOP1 and TOP1 in complex with DNA.
- TOP1-DNA complexes enhance the recognition by some but not all anti-TOP1 autoantibodies, a phenomenon observed in most patients.
- The differential recognition of TOP1 and TOP1-DNA complexes affects the immunostimulatory properties of ATA and activation of TOP1-specific B cells.

HOW THIS STUDY MIGHT AFFECT RESEARCH, PRACTICE OR POLICY

- Differential recognition patterns of ATA indicate functional heterogeneity in the B cell response targeting TOP1, which may help to further dissect and understand patient and disease heterogeneity.
- DNA binding by TOP1 could be an important determinant in the activation of the ATA B cell response and thereby offers new insights into potential drivers of disease-relevant immunological processes.

INTRODUCTION

Systemic sclerosis (SSc) is a heterogeneous disease characterised by fibrosis of internal organs and the skin, vasculopathy, and autoimmunity. The disease displays remarkable clinical heterogeneity, ranging from indolent to rapidly progressive disease with irreversible organ damage and subsequent mortality. Clinical management of SSc is complicated by the lack of effective treatments and variation in disease progression, which is difficult to predict [1]. Therefore, identification of pathogenic mechanisms driving disease may improve patient stratification and enable the development of targeted treatment strategies.

Like many other autoimmune diseases, SSc is hallmarked by a break in B cell tolerance towards nuclear proteins [2,3]. Autoantibodies targeting the nuclear enzyme topoisomerase 1 (TOP1) are observed in a subset of patients with SSc and are associated with diffuse cutaneous SSc, a distinct clinical phenotype with the highest mortality among the rheumatic diseases [4,5]. Specifically, anti-TOP1 autoantibodies (ATAs) associate with progressive lung and skin fibrosis and early death, although not all ATA-positive patients show this progressive course of disease [6]. Recently, we could associate measures reflective of an active ATA B cell response to disease progression in patients with ATA$^+$ SSc [7,8]. Specifically, ATA-secreting B cells were found in the circulation of patients with SSc, and their presence was associated with the presence and severity of pulmonary fibrosis [7]. Also, the presence of ATA-immunoglobulin (Ig)M was predictive of disease progression in the early stages of disease [8]. These findings suggest that activated, autoreactive ATA B cells might contribute directly to processes driving fibrosis. This notion is further supported by the beneficial effects of B cell-targeting therapies in SSc [9,10]. Nevertheless, the mechanisms by which ATA B cells could contribute to disease remain unclear [3]. ATA pathogenicity has been debated, with the hypothesis that ATAs directly activate fibroblasts [11–13]. However, whether this affects disease *in vivo* is unclear, primarily because ATA can also be present in indolent disease. ATA B cells, on the other hand, might contribute to disease by the production of cytokines and stimulation of T cells through antigen presentation and co-stimulation [14].

A crucial prerequisite for B cell activation is the recognition of antigen by B cell receptors (BCRs) [15,16]. The same holds for antibody-mediated effector functions, which require antibody-binding to cognate antigens. Epitope structure and conformation can determine and modulate these interactions [17]. TOP1 is a DNA-binding nuclear protein that unwinds negatively supercoiled DNA [18]. During its enzymatic cycle, TOP1 covalently binds DNA to form TOP1-DNA cleavage complexes (TOP1cc), which allows the passing of the other DNA strand through the single-stranded break [18]. TOP1cc is a transient complex under physiological conditions, but stable TOP1cc can be formed if DNA contains lesions, which can occur during cell death induced under inflammatory conditions [19]. The binding of antigen to nucleic acids, a common property among many nuclear antigens targeted in autoimmune diseases, can potentiate antibody effector functions and B cell activation through co-engagement of innate Toll-like receptors (TLRs) with Fc receptors or the BCRs [2,16]. Whether TOP1, as an SSc autoantigen, binds DNA, and how TOP1 and TOP1cc are recognised by human ATAs, warrant detailed analyses to better understand the antigenicity of TOP1 in SSc pathogenesis.

To this end, we set out to determine the molecular and functional characteristics of the interaction between ATAs and TOP1. We generated patient-derived ATA monoclonal antibodies (ATA mAbs), enabling us to study the effect of DNA binding by TOP1 on the interaction with ATAs. We found remarkable heterogeneity in the recognition of TOP1 and TOP1cc among ATA mAbs and ATA in plasma. This heterogeneity affected both antibody functionality and the activation of B cells expressing TOP1-reactive BCRs. Together, these findings show that heterogeneity in the ATA B cell response can impact disease-relevant processes in progressive SSc and contribute to a deeper understanding of disease variability in ATA$^+$ SSc and the processes driving this deleterious disease.

METHODS

The experimental procedures for the recombinant production and purification of human TOP1, the generation of patient-derived ATA mAbs, gel electrophoresis, western blotting, cross-inhibition enzyme-linked immunosorbent assay (ELISA) with ATA mAbs, mass photometry, TOP1-mediated DNA relaxation assay, and the generation of Ramos B cell lines expressing a TOP1-reactive BCR are provided in detail in the Supplementary Methods section.

Patients and healthy individuals

Peripheral blood was obtained from patients with ATA$^+$ and anticentromere protein B autoantibody$^+$ (ACA$^+$) SSc visiting the outpatient clinic of the Department of Rheumatology at Leiden University Medical Center. These patients with SSc were included in the Leiden Combined Care in Systemic Sclerosis cohort [20], fulfilled the American College of Rheumatology/European Alliance of Associations for Rheumatology 2013 classification criteria for SSc, and were either ATA-IgG$^+$ or ACA-IgG$^+$ as measured by routine clinical diagnostic tests. Patients on B cell-depleting therapies or with a history of haematopoietic stem cell transplantation were excluded. Plasma samples of a cross-sectional cohort of patients with ATA-IgG$^+$ SSc (n = 21) collected in a previous study were used (Table 1) [7]. In addition, serum samples of patients with ATA-IgG$^+$ SSc containing high levels of ATA-IgM (n = 9) were selected from another previously reported study (Table 1) [8]. Plasma samples from patients with ACA$^+$ SSc (n = 9) and healthy donors (HDs) (n = 6) were used as controls (Table 1).

Generation of TOP1cc using suicide substrate

To obtain stable TOP1cc, TOP1 was incubated with a suicide substrate (ScS), which is covalently bound by TOP1. ScS was generated as described previously by Kristoffersen et al [21]. Three oligonucleotides (26DL: '5-pAGA AAA ATT TTT CCG AGT GCG AAG-3' [p = phosphorylated 5'], 38SC: 5'-CTA GAG GAT CTA AAA GAC TTA GA-3', 61NCL: 5'-CTT CGC ACT CGG AAA AAT TTT TCT AAG TCT TTT AGA TCC TCT AG-3') were mixed to obtain a 66.67 μM concentration of ScS. The suspension was heated to 80°C for 5 minutes and cooled to room temperature in 3 hours. TOP1cc was formed by incubation of 0.1 mg/mL of TOP1 with 5 μM of ScS for 30 minutes at 37°C.

Anti-TOP1/TOP1cc-antibody ELISAs

To measure the reactivity of ATA mAbs and antibodies in plasma towards TOP1 and TOP1cc, high-binding 384-well microplates (Corning) were coated with 2.5 μg/mL TOP1 or TOP1cc in phosphate buffered saline (PBS) (pH = 8). Plates were blocked using 1% bovine serum albumin (BSA) in PBS (Ig, IgG, IgG subclasses, and IgA) or 1% skim milk in PBS (IgM). Plasma, ATA mAbs, and culture supernatants of single-cell cultured B cells were applied in single or serial dilutions (as indicated in the respective figures) in 1% BSA in PBS with 0.05% Tween (Ig, IgG, IgG subclasses, and IgA) or in 1% skim milk in PBS with 0.05% Tween (IgM). Subsequently, secondary antibodies were added: rabbit anti-human IgG-horseradish peroxidase (HRP) (1:5000, P0214, DAKO), mouse anti-human IgG1 (1:5000, HP6186, Nordic-MUbio), mouse anti-human IgG2 (1:250, HP6014, Nordic-MUbio), mouse anti-human IgG3 (HP6080, 1:2500, Nordic-MUbio), mouse anti-human IgG4 (1:500, MH164-1, Sanquin), goat anti-human IgA-HRP (1:1000, A18781, Novex), goat anti-human-IgM-HRP (1:5000, AP114P, Millipore), and goat anti-human Ig-HRP (1:10000, A80-152P, Bethyl Laboratories). Goat anti-mouse Ig-HRP (1:5000 for IgG1/2, 1:2500 for IgG3/4, P0447, DAKO) was used to detect the IgG subclass-specific secondary antibodies. Pooled plasma samples were used as reference standards. ATA mAbs were used in all plasma ELISAs to control for comparable coating of TOP1 and TOP1cc (ATA mAb 2F8) and as positive controls for the differential recognition of TOP1cc compared with TOP1 (ATA mAbs 7G6 and 9D11). ELISAs were developed using 2,2'-azino-bis(3-ethylbenzothiazoline-6-sulfonic acid) ABTS supplemented with H_2O_2. Optical density was measured at 415 nm with a Spectramax I3 × Multi-Mode Microplate Reader (Molecular Devices) using SoftMax Pro 7 (version 7.0.2, Molecular Devices).

Stimulation of THP-1 cells

To assess the immunostimulatory properties of ATA mAbs, monocytic THP-1 cells (Tohoku Hospital Pediatrics-1 Cells) were stimulated with ATA mAbs in complex with plate-bound TOP1 or TOP1cc. NUNC Maxisorp 96-well plates (ThermoFisher Scientific) were coated with 5 μg/mL TOP1 and TOP1cc. Plates were blocked with PBS containing 1% BSA, and 2.5 μg/mL of lipopolysaccharide (LPS)-depleted (Pierce High-Capacity Endotoxin Removal Spin Columns, ThermoFisher Scientific), sterile-filtered ATA mAbs were subsequently added to the plates. The anti-citrullinated protein mAb 1F2 was used as a negative control [22]. Upon the formation of plate-bound immune complexes, 1 × 10^5 THP-1 cells were added to the plates and stimulated for 24 hours at 37°C in 5% CO_2. Stimulation with 1 μg/mL LPS (Sigma) served as a positive control. Upon stimulation, culture supernatants were collected to determine the secretion of interleukin (IL)-8 by the THP-1 cells.

IL-8 ELISA

Human IL-8 was measured using a commercial ELISA on culture supernatants of THP-1 cells in accordance with the manufacturer's instructions (DY208-05, R&D Systems). Volumes of the ELISA were adapted for the use of high-binding 384-well microplates (Corning): 15 μL for coating, sample, and 3,3', 5,5' tetramethylbenzidine (TMB) substrate solution (555214, BD Biosciences), 75 μL for blocking (1% BSA in PBS), and 7.5 μL for stop solution (1M H_2SO_4). Reactions were developed for

Table 1
Characteristics of patients with ATA$^+$ SSc

	Patients with ATA-IgG$^+$ SSc (n = 21)	Patients with ATA-IgM^{high} SSc (n = 9)	Patients with ACA-IgG$^+$ SSc (n = 9)	Healthy donors (n = 6)
Age (y), median (IQR)	55 (39-65)	53 (36-67)	55 (46-68)	29 (26-36)
Female, n (%)	11 (52)	8 (89)	9 (100)	5 (83)
Duration since first NRP symptom (mo), median (IQR)	56 (31-92.8)	48 (14.5-119)	117 (57-359)	
Diffuse cutaneous SSc, n (%)	7 (33)	3 (33)	0 (0)	
mRSS, median (IQR)	5 (2-7.5)	6 (4-16)	5 (0-9)	
ILD on HRCT, n (%)	14 (66.7)	8 (89)	0 (0)	
Lung fibrosis score, median (IQR)	7 (0-13.5)	[a]	NA	
Current use of immunosuppressive drugs, n (%)	12 (57)	1 (11)	3 (33)	

ACA, anticentromere protein B autoantibody; ATA, antitopoisomerase 1 autoantibody; HRCT, high-resolution computer tomography scan; Ig, immunoglobulin; ILD, interstitial lung disease; mRSS, modified Rodnan skin score; NA, not applicable; NRP, non-Raynaud's phenomenon; SSc, systemic sclerosis.
[a] Lung fibrosis scores were not determined for these patients.

50 minutes, and absorbance was measured with a Spectramax I3 × Multi-Mode Microplate Reader (Molecular Devices) at 450 nm with correction of the absorbance at 570 nm.

Stimulation of primary monocytes

Primary human monocytes were stimulated with ATA mAbs in complex with plate-bound TOP1 or TOP1cc. Monocytes were isolated from peripheral blood mononuclear cells of HDs (n = 4) and patients with ATA^+ SSc (n = 4) by magnetic-activated cell sorting using CD14 MicroBeads (130-097-052, Miltenyi Biotec). Characteristics of these donors/patients are provided in Supplementary Table S1. Plates containing ATA mAbs 2F8 and 9D11 in complex with plate-bound TOP1 or TOP1cc were prepared as described above for THP-1 cell stimulation assays with a coating concentration of 2.5 µg/mL for TOP1 and TOP1cc. Upon the formation of plate-bound immune complexes, 0.5×10^5 primary monocytes were added to the plates and stimulated for 24 hours at 37°C in 5% CO_2. Stimulations were performed in the presence or absence of 100 ng/mL LPS, with 1 µg/mL LPS (Sigma) added as a positive control. Upon stimulation, culture supernatants were collected to determine the secretion of tumour necrosis factor alpha (TNF-α) by the primary monocytes.

TNF-α ELISA

Human TNF-α was measured in culture supernatant of primary monocytes using a commercial ELISA kit (88-7346-88, InVitrogen). Volumes of the ELISA were adapted for the use of high-binding 384-well microplates (Corning): 15 µL for coating, sample, and ABTS, and 75 µL for blocking (1% BSA in PBS). Samples were applied in a dilution of 1:4. Reactions were developed using ABTS, and absorbance was measured with a Spectramax I3 × Multi-Mode Microplate Reader (Molecular Devices) at 415 nm.

Stimulation of Ramos B cell lines expressing a TOP1-reactive BCR

Ramos B cell lines expressing a TOP1-reactive BCR (derived from BCR sequences of 2F8, 7G6, or 9D11 clone) were stimulated with 5 µg/mL TOP1 preincubated (60 minutes, 37°C) with or without 5 µg/mL plasmid DNA (pUC19 DNA, ThermoFisher Scientific) in stimulation medium (Roswell Park Memorial Institute 1640 supplemented with 1% FCS [Bodinco], 10 mM HEPES, 100 units/mL penicillin/streptomycin, and glutamax [all Gibco]) for 5 minutes at 37°C. Stimulation with 5 µg/mL polyclonal AffiniPure F(ab')2 fragment goat anti-human IgG (109-006-097, Jackson ImmunoResearch) was used as a positive control. Stimulated cells were fixed in paraformaldehyde (4%, Biolegend) for 20 minutes at 37°C and subsequently permeabilised (True-Phos Perm Buffer, Biolegend) for 75 minutes at −20°C. Staining was subsequently performed using anti-Syk(pY352)-Alexa Fluor 647 (557817, BD Biosciences) diluted tenfold in PBS, 0.5% BSA, 0.02% NaN_3. Cells were acquired on a BD LSRFortessa 4L flow cytometer (BD Biosciences) and analysed using FlowJo software (version 10.9.0).

Statistical analysis

Data were analysed using Graphpad Prism (version 10.2.3). As indicated in the figure legends, the Mann-Whitney U test, the Wilcoxon matched-pairs signed-rank test, and the Kruskal-Wallis test, combined with Dunn's multiple comparison, were used where appropriate to determine the statistical significance of the data. Correlations were described using Spearman's rank correlation coefficient.

Study approval

This study was approved by the ethical review board of the Leiden University Medical Center (protocol number P17.151) and the Leiden University Biobank Toetsing Commissie (REU/036/SH/sh). Included patients and HDs gave written informed consent to participate in the study.

RESULTS

Generation and characterisation of patient-derived anti-TOP1 monoclonal antibodies

We first generated ATA mAbs based on BCR sequences of TOP1-reactive B cells obtained from 1 patient with ATA^+ SSc. B cells from the peripheral blood of the patient were single-cell sorted based on their reactivity towards full-length human TOP1 conjugated to Alexa Fluor 647 and phycoerythrin (Fig 1A). These sorted cells were subsequently differentiated towards antibody-secreting cells in culture. Secreted antibodies could be detected in a fraction of the culture supernatants (Supplementary Fig S1A-C). By analysing the reactivity of the secreted antibodies towards human TOP1, we identified several TOP1-reactive clones (Fig 1B-D). BCR sequences were determined from 3 of these clones (termed 2F8, 7G6, and 9D11; Table 2) and expressed recombinantly as IgG1 mAbs (Supplementary Fig S1D). Reactivity of the generated ATA mAbs towards TOP1 was verified by ELISA in a concentration-dependent manner (Fig 1E). TOP1 binding by ATA-IgG 2F8 was stronger compared with that of ATA-IgGs 7G6 and 9D11. Specificity of ATA mAbs was further confirmed by western blotting, with all ATA mAbs recognising a single band at the expected height of TOP1 (Fig 1F, Supplementary Fig S1E). No binding was observed to centromeric protein B and double-stranded DNA (Fig 1G,H).

We also performed cross-inhibition assays to determine whether the recombinantly produced ATA mAbs would bind unique or overlapping TOP1 epitopes. The 3 ATA mAbs were generated with murine constant domains to test their capacity to inhibit TOP1 binding by ATA mAbs with a human constant domain. Binding of human ATA mAbs to TOP1 could be blocked by their direct murine counterparts, but not by the respective other mAbs (Fig 1I-K, Supplementary Fig S1F). Together, these data show that we generated 3 ATA mAbs binding unique epitopes of human TOP1.

A subset of ATA mAbs recognise TOP1 better in complex with DNA

TOP1 can form a covalent complex with DNA, termed TOP1cc [18]. To study the effect of DNA binding on the recognition of TOP1 by the ATA mAbs, we next compared mAb reactivity towards TOP1 and TOP1cc. TOP1cc was formed using ScS, a double-stranded DNA ligand that covalently and irreversibly binds to TOP1 [21]. This binding results in a size shift that can be visualised by gel electrophoresis (Fig 2A). By coating of either antigen on an ELISA plate, the recognition of TOP1 and TOP1cc by the ATA mAbs could be compared. ATA mAb 2F8 recognised TOP1 and TOP1cc to a similar extent (Fig 2B,C). In

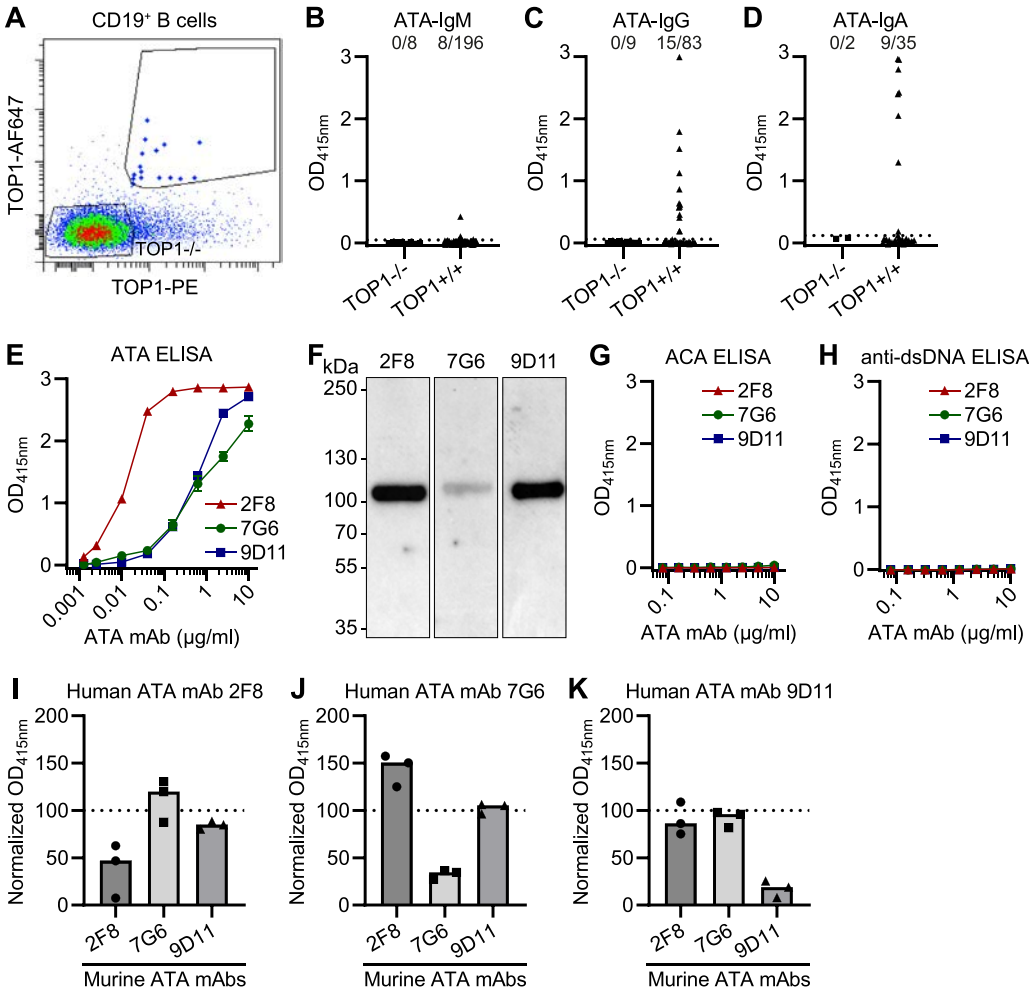

Figure 1. Generation and characterisation of patient-derived ATA mAbs. (A) Gating strategy used to single-cell sort CD19^{+} TOP1$^{+/+}$ B cells binding to TOP1-Alexa Fluor 647 (AF647) and TOP1-PE. (B-D) Reactivity of IgM (B), IgG (C), and IgA (D) secreted by single-cell-sorted TOP1$^{+/+}$ B cells towards TOP1 as assessed by an anti-TOP1-Ig (ATA-IgM), anti-TOP1-IgG and anti-TOP1-IgA ELISA, respectively. Cut-off (mean TOP1$^{-/-}$ B cells + 4 × SD) is represented by a dotted line. Only culture supernatants in which IgM, IgG, or IgA could be detected (Supplementary Fig S1A-C) are depicted. (E) Reactivity of patient-derived ATA mAbs towards TOP1 in an ATA-IgG ELISA. (F) Binding of TOP1 by ATA mAbs on western blot. Molecular weight in kilodaltons (kDa) was estimated using a protein ladder. (G-H) Reactivity of ATA mAbs towards centromere protein B in an anti-centromere protein B antibody-IgG (ACA-IgG) ELISA (G) and towards double-stranded DNA in an anti-double-stranded DNA-IgG (anti-dsDNA-IgG) ELISA (H). (I-K) Binding of ATA mAbs 2F8 (I), 7G6 (J), and 9D11 (K) with a human constant domain (human ATA mAbs) to a TOP1-coated ELISA plate pre-incubated with 5 μg/mL of the indicated ATA mAbs with a murine constant domain (murine ATA mAbs). Binding was normalised to the condition in which no murine mAb was added. Concentrations of human mAbs were in the linear range of the ATA-IgG ELISA; 2F8, 0.04 μg/mL, 7G6 and 9D11, 1 μg/mL. Data are derived from 3 independent experiments. (B-E, G-K) Optical density was measured at 415 nm (OD_{415nm}). (E, G, H) Error bars represent the SD of technical duplicates. (E-H) Data are representative of at least 2 independent experiments. ACA, anti-centromere protein B autoantibody; ATA, anti-TOP1 autoantibody; dsDNA, double-stranded DNA; ELISA, enzyme-linked immunosorbent assay; Ig, immunoglobulin; mAbs, monoclonal antibodies; OD, optical density; PE, phycoerythrin; TOP1, topoisomerase 1.

Table 2
B cell receptor sequence details of patient-derived ATA mAbs

Clone	HC	IGHV	IGHV mutations (#)	IGHV identity (%)	IGHD	IGHJ	IGH-CDR3	LC	IGK/LV	IGK/LV mutations (#)	IGK/LV identity (%)	IGK/LJ	IGK/L-CDR3
2F8	IGHA1	V1-18	14	95.14	D6-6	J4	CARGRDFSSSPYDYW	λ	V3-21	7	97.49	J2/J3	CQVWDRSSDDVIF
7G6	IGHG1	V3-48	26	90.97	D6-6	J5	CATTPRTGRPW	κ	V4-1	12	95.96	J4	CQQYLTPLQIF
9D11	IGHG3	V1-3	28	93.75	D2-15	J4	CARDGGSSVAVISATLDSW	λ	V2-23	8	97.22	J2/J3	CCSYAGSRGVVF

ATA, anti-topoisomerase 1 autoantibody; mAbs, monoclonal antibodies; HC, heavy chain; IGH-CDR3, amino acid sequence of heavy chain complementarity-determining region 3; IGHD, heavy chain D gene; IGHJ, heavy chain J gene; IGHV, heavy chain V gene; IGHV identity (%), similarity of IGHV compared to closest germline IGHV expressed in a percentage; IGHV mutations (#), amount of nucleotide mutations in IGHV compared to closest germline IGHV; IGK/L-CDR3, amino acid sequence of light chain complementarity-determining region 3; IGK/LJ, light chain J gene; IGK/LV, light chain V gene; IGK/LV identity (%), similarity of IGK/LV compared to germline IGK/LV expressed in a percentage; IGK/LV mutations (#), amount of nucleotide mutations in IGK/LV compared to germline IGK/LV; LC, light chain; κ, kappa; λ, lambda.

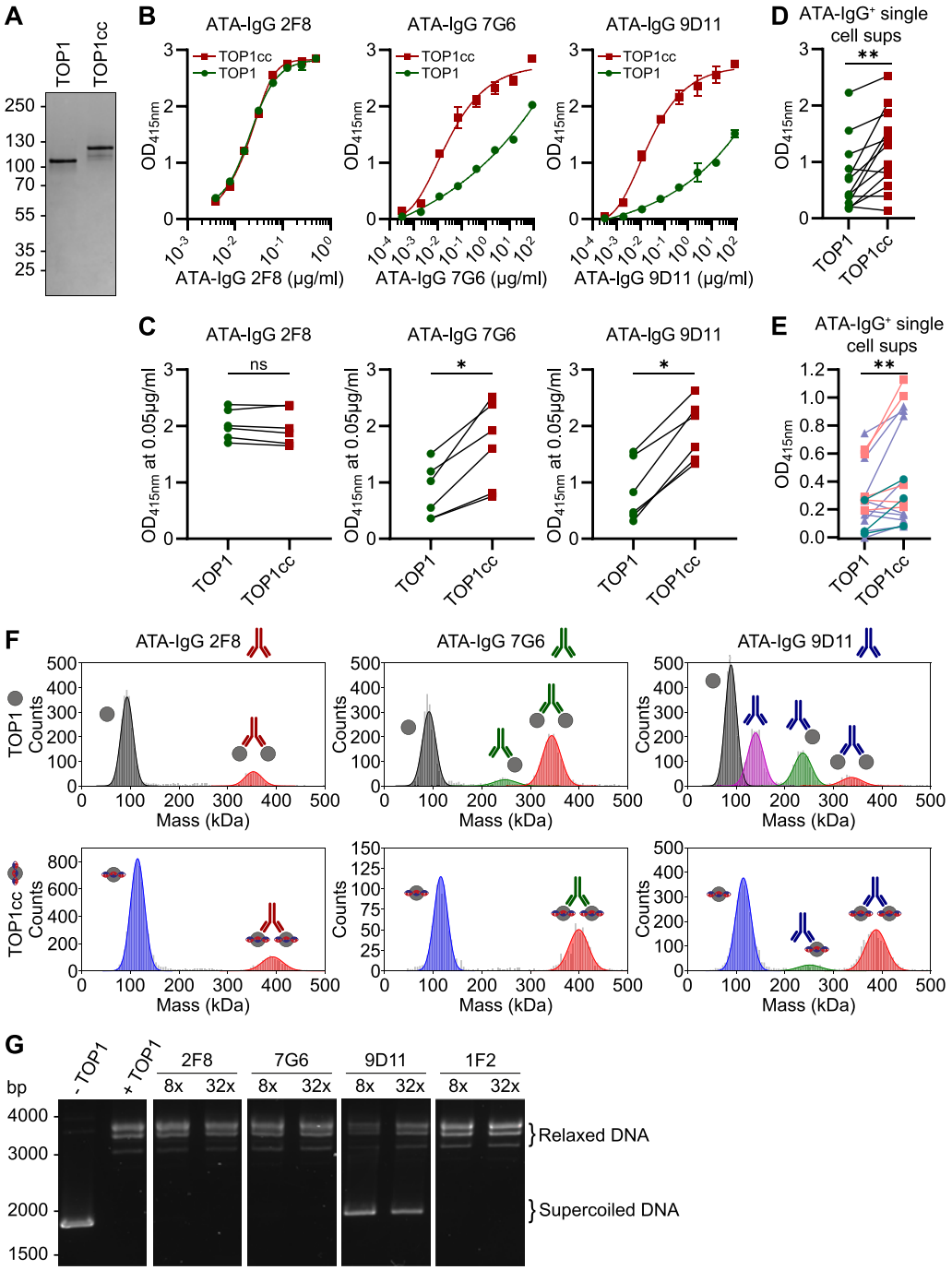

Figure 2. Reactivity of ATA mAbs towards TOP1 and TOP1cc. (A) Gel electrophoresis of TOP1 upon preincubation without or with suicide substrate (TOP1 and TOP1cc, respectively) under non-reducing conditions. Molecular weight in kilodaltons (kDa) was estimated using a protein ladder. (B) Reactivity of ATA mAbs 2F8, 7G6, and 9D11 towards TOP1 and TOP1cc in an anti-TOP1/TOP1cc-IgG ELISA. Data points represent the mean and SD of 2 technical replicates from an individual experiment. (C) Quantification of the binding of 0.05 µg/mL ATA mAbs 2F8, 7G6, and 9D11 to TOP1 and TOP1cc. Data are derived from 6 independent experiments. (D) Reactivity towards TOP1 and TOP1cc of ATA-IgG in culture supernatants (n = 13) of single-cell sorted $CD19^+$ $TOP1^{+/+}$ B cells. Supernatants were derived from $TOP1^{+/+}$ B cells from 1 patient with ATA^+ SSc from whom the recombinantly expressed ATA mAbs were also generated. (E) Reactivity towards TOP1 and TOP1cc of ATA-IgG in culture supernatants (n = 17) of single-cell sorted $CD19^+$ $TOP1^{+/+}$ B cell clones obtained from 3 additional patients with SSc. Data from individual patients are separated by colour and symbol. (F) Representative mass histograms of ATA mAbs incubated with an excess of TOP1 and TOP1cc as obtained by mass photometry. Data are representative of 2 independent experiments. An overview of detected masses can be found in Supplementary Table S2. (G) DNA relaxation assay with TOP1 preincubated with an 8 × and 32 × molar equivalent of the ATA mAbs. A monoclonal antibody reactive towards citrullinated proteins (1F2) was used as negative control. DNA was visualised with a fluorescent DNA stain. Molecular weight of DNA in base pairs (bp) was estimated using a DNA ladder. Data are representative of 2 independent experiments. (B-E) OD was measured at 415 nm (OD_{415nm}). (C-E) Wilcoxon matched-pairs signed-rank test was used to test for significant differences. *$P < .05$, **$P < .005$, ***$P < .001$. ATA, anti-TOP1 autoantibody; ELISA, enzyme-linked immunosorbent assay; Ig, immunoglobulin; mAbs, monoclonal antibodies; ns, not significant; OD, optical density; SSc, systemic sclerosis; TOP1, topoisomerase 1; TOP1cc, TOP1-DNA cleavage complex.

contrast, ATA mAbs 7G6 and 9D11 recognised TOP1cc with higher relative avidity than TOP1 (Fig 2B,C). None of the mAbs reacted to ScS alone (Supplementary Fig S2A). To further substantiate the differential binding of ATA to TOP1 and TOP1cc, we measured the reactivity towards either antigen by IgG in culture supernatants of 13 single-cell sorted TOP1-reactive B cell clones obtained from the same patient (Fig 2D). Only 3 of the 13 clones recognised TOP1 and TOP1cc to a similar extent, whereas the other 10 clones showed enhanced recognition of TOP1cc as compared with TOP1 (Fig 2D). To validate this observation across patients, another 17 ATA-IgG$^+$ culture supernatants of single-cell sorted TOP1$^{+/+}$ B cells were obtained from 3 additional donors. Again, most of these supernatants (12/17) showed enhanced recognition of TOP1cc, while the others recognised TOP1 and TOP1cc to the same extent (5/17) (Fig 2E). Importantly, we noted a strong variation between clones as to the extent to which TOP1cc was differentially recognised.

We next analysed the differential binding under native conditions in solution to exclude that immobilisation of either protein to the ELISA plate would have caused the observed effects. We employed mass photometry to determine the binding stoichiometry of the ATA mAbs to TOP1 and TOP1cc. This single particle interferometric scattering microscopy technique allows to analyse the formation of immune complexes in solution formed upon incubation of ATA mAbs with TOP1 and TOP1cc (Fig 2F, Supplementary Fig S2B,C, Supplementary Table S2). In the presence of antigen excess, ATA-IgG 2F8 bound both TOP1 and TOP1cc and efficiently formed immune complexes containing 2 antigens (Fig 2F). ATA-IgG 7G6 and ATA-IgG 9D11 did not show complete binding to TOP1 (Fig 2F). In these conditions, antibodies binding no or only 1 antigen could be detected, especially for ATA-IgG 9D11. In contrast, nearly complete binding of 7G6 and 9D11 was observed to TOP1cc (Fig 2F). Hence, this independent approach confirmed the finding that certain ATA mAbs differentially recognise TOP1 and TOP1cc.

ATA mAb can inhibit the enzymatic function of TOP1

We further characterised the ATA mAbs by assessing their effect on the enzymatic function of TOP1. Previous work showed that purified immunoglobulins from patients with ATA$^+$ SSc can inhibit the enzymatic function of TOP1 [23,24]. The enzymatic activity of TOP1 can be measured based on the relaxation of supercoiled plasmid DNA, which impairs the mobility of DNA through agarose gels (Fig 2G). Preincubation of TOP1 with ATA-IgG 2F8, ATA-IgG 7G6, and a control mAb did not affect the enzymatic function of TOP1 (Fig 2G). In contrast, supercoiled plasmid DNA was still apparent in the condition in which TOP1 was preincubated with ATA mAb 9D11 (Fig 2G). This indicates that the ATA mAb 9D11 inhibits the enzymatic function of TOP1.

Polyclonal IgG autoantibodies from patients with ATA$^+$ SSc differentially recognise TOP1cc

Differential recognition of TOP1/TOP1cc by ATA-IgG could affect the functionality of ATAs and, hence, influence disease pathogenesis. Therefore, we next assessed differential recognition of TOP1/TOP1cc by polyclonal ATA in the circulation of patients with ATA$^+$ SSc. Half-maximal binding titres of polyclonal IgG to TOP1 and TOP1cc were determined by serial dilutions of patient plasma (Fig 3A). ATA mAbs were taken along in these assays to control for comparable coating concentrations of TOP1 and TOP1cc (ATA mAb 2F8), and as positive controls for the differential recognition of TOP1cc compared with TOP1 (ATA mAbs 7G6 and 9D11). Plasma of all patients with ATA$^+$ SSc (n = 21) showed higher IgG titres to TOP1cc compared with TOP1 (Fig 3B). Patients varied as to the extent of differential TOP1/TOP1cc recognition. The difference between anti-TOP1-IgG and anti-TOP1cc-IgG titres was modest for some patients. For others, much higher dilutions of plasma were needed to reach the same binding signal for TOP1cc in comparison with TOP1 (up to 30,000 difference in dilution factor) (Fig 3C). Again, we excluded ScS recognition as a confounder, as binding to ScS was minimal to undetectable (Supplementary Fig S3A). Also, plasma from patients with ACA$^+$ SSc and HDs generated signals below the limit of detection (Supplementary Fig S3B). Together, these findings indicate that enhanced TOP1cc recognition by a subset of ATAs is a feature commonly present in patients with ATA$^+$ SSc.

To explore the possible clinical relevance of our finding, we assessed the relation between the differential recognition of TOP1cc and clinical disease parameters using the absolute difference between anti-TOP1cc-IgG and anti-TOP1-IgG titres (anti-TOP1cc-IgG titre minus anti-TOP1-IgG titre) as read-out. This difference correlated with anti-TOP1-IgG titres (r_s = 0.91) (Supplementary Fig S3C). In addition, both the anti-TOP1-IgG titre and the difference between anti-TOP1cc-IgG and anti-TOP1-IgG titres were increased in patients with interstitial lung disease and correlated with the lung fibrosis score (r_s = 0.65 and r_s = 0.76, respectively) (Fig 3D,E, Supplementary Fig S3D, E). Similar trends were observed for the modified Rodnan skin score, whereas no differences were observed in patients treated with or without immunosuppressive drugs (Supplementary Fig S3F-I). Together, these data indicate that anti-TOP1-IgG titres and anti-TOP1cc-IgG titres are strongly related and correlate with clinical disease.

Anti-TOP1cc autoantibodies are predominantly present in the IgG1 and IgM compartment

Isotype and subclass usage strongly affects antibody effector functions and provides insights into the underlying B cell response [25,26]. Therefore, we studied the recognition of TOP1 and TOP1cc by antibodies of various subclasses and isotypes in the plasma of patients with ATA$^+$ SSc. The presence of ATA among the IgG subclasses was variable, as IgG1, IgG2, IgG3, and IgG4 anti-TOP1-autoantibodies could be detected in 67%, 81%, 52%, and 95% of the samples (n = 21), respectively (Supplementary Fig S4A-D). Therefore, we limited the analysis to samples in which TOP1 was recognised by multiple IgG subclasses (n = 8 for IgG1/3/4, n = 7 for IgG2) and in which total IgG recognised TOP1cc better than TOP1 (Fig 4A). Enhanced recognition of TOP1cc compared with TOP1 was observed for IgG1 and IgG4, but not for IgG2 and IgG3 (Fig 4A). To compare the relative difference in TOP1cc binding by the IgG subclasses to total IgG, anti-TOP1cc titres were normalised to anti-TOP1 titres by expressing the titres as a ratio (anti-TOP1cc titre divided by anti-TOP1 titre). The relative difference in TOP1cc binding by IgG1 was comparable to total IgG, whereas the ratio between anti-TOP1cc and anti-TOP1 titres for IgG2-4 was lower (Fig 4B). Consequently, the differential recognition of TOP1 upon DNA binding appears most prominent for IgG1.

TOP1-reactive antibodies of the IgA isotype can be detected in almost all patients with ATA-IgG$^+$ SSc [8]. Accordingly, we detected anti-TOP1-IgA in all patients with ATA-IgG$^+$ SSc (n = 21) included in this study (Fig 4C). These IgA antibodies recognised TOP1cc slightly better in comparison with TOP1

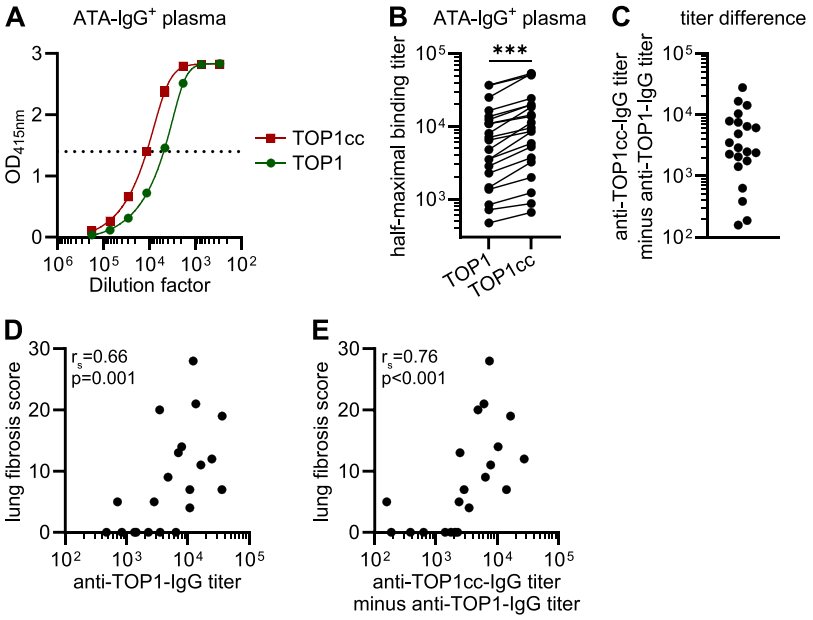

Figure 3. Reactivity of IgG in ATA-IgG$^+$ plasma towards TOP1 and TOP1cc. (A) Binding of IgG in plasma of a patient with ATA$^+$ SSc to TOP1 and TOP1cc in an anti-TOP1/TOP1cc-IgG ELISA. OD was measured at 415 nm (OD_{415nm}). The dotted line represents an OD_{415nm} of 1.4, which was considered the half-maximal signal of the assay. (B) Anti-TOP1/TOP1cc-IgG expressed as half-maximal binding titres (interpolated dilution generating an OD of 1.4 at 415 nm) in plasma of patients with ATA$^+$ SSc (n = 21). Half-maximal binding titres were statistically compared using the Wilcoxon matched-pairs signed-rank test. *P < .05, **P < .005, ***P < .001. (C) Difference between anti-TOP1cc-IgG titre and anti-TOP1-IgG titre in plasma of patients with ATA$^+$ SSc. (D,E) Correlation between the lung fibrosis score and the anti-TOP1-IgG titre (D) and the difference between anti-TOP1cc-IgG and anti-TOP1-IgG titre (E). Correlations are described using Spearman's rank correlation coefficient. ATA, anti-TOP1 autoantibody; ELISA, enzyme-linked immunosorbent assay; Ig, immunoglobulin; OD, optical density; SSc, systemic sclerosis; TOP1, topoisomerase 1; TOP1cc, TOP1-DNA cleavage complex.

(Fig 4C). However, the relative difference in the half-maximal binding titres between TOP1 and TOP1cc was significantly higher in the IgG compartment (Fig 4D).

For IgM, we observed that only 2 of 21 patients with ATA-IgG$^+$ generated higher signals on the anti-TOP1-IgM ELISA compared with controls (Supplementary Fig S4E-G). To prevent interference of non-specific antibodies in the assay, we compared the reactivity of IgM antibodies towards TOP1 and TOP1cc in the 2 patients with SSc who had higher levels of ATA-IgM in comparison with controls, and selected 9 other samples of patients with ATA$^+$ SSc with high levels of ATA-IgM from a previous study (Supplementary Fig S4H, Table 1) [8]. TOP1cc was better recognised than TOP1 by IgM antibodies in these samples (Fig 4E). The relative difference in the half-maximal

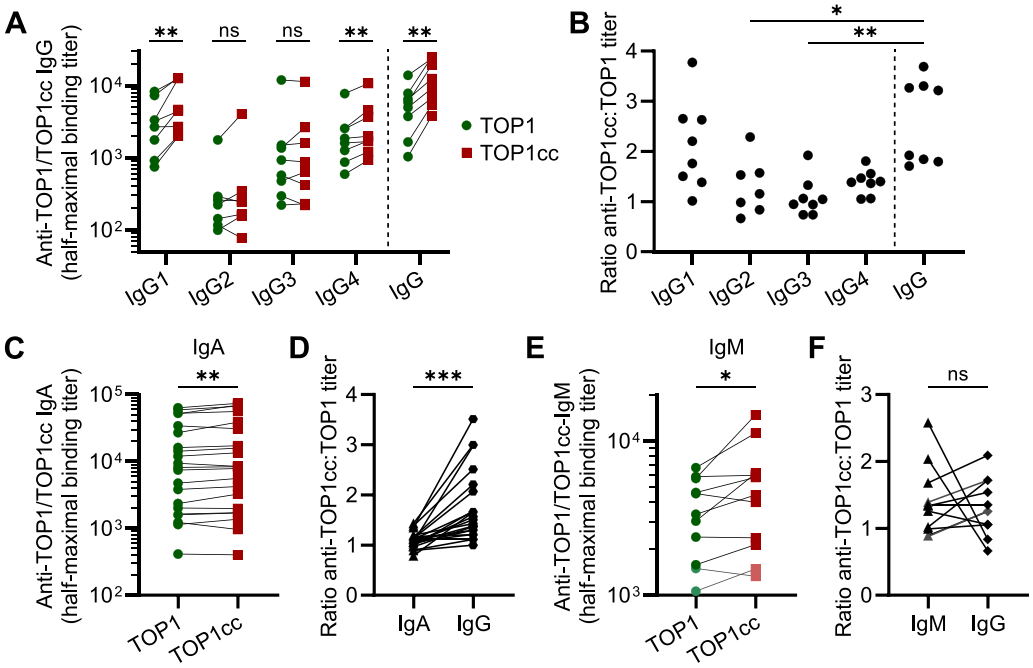

Figure 4. Reactivity towards TOP1 and TOP1cc by IgG subclasses, IgA and IgM in plasma of patients with ATA$^+$ SSc. (A) Half-maximal binding titres of IgG1-4 and total IgG in plasma of patients with ATA-IgG$^+$ SSc (n = 8 for IgG1, 3, 4, n = 7 for IgG2) to TOP1 and TOP1cc. (B) Ratio between anti-TOP1cc and anti-TOP1 titres of IgG1-4 and total IgG in plasma. Ratios of IgG1-4 were compared with total IgG using the Kruskal-Wallis test combined with Dunn's multiple comparison. (C) Reactivity of IgA in plasma of patients with ATA-IgG$^+$ SSc (n = 21) towards TOP1 and TOP1cc. (D) Anti-TOP1cc-IgA/G titres expressed as ratio to anti-TOP1-IgA/G titres. (E) Reactivity of IgM in plasma of patients with ATA-IgM$^+$ SSc (n = 11) towards TOP1 and TOP1cc. These 11 patients had elevated levels of ATA-IgM (see Supplementary Fig S4E-H); 2 were selected from the cohort of 21 patients, and 9 other patients were selected from another study based on high ATA-IgM serum levels. (F) Anti-TOP1cc-IgM/IgG titres expressed as ratio to anti-TOP1-IgA/G titres. (A,C,E) Binding to TOP1 and TOP1cc is expressed as half-maximal binding titre, the interpolated dilution generating an optical density of 1.4 at 415 nm. (C-E) Half-maximal binding titres to TOP1 and TOP1cc were statistically compared using the Wilcoxon matched-pairs signed-rank test. (D,F) Ratio titres were compared using the Mann-Whitney U test. (E,F) The 2 patients with ATA-IgM selected from the cohort of 21 patients are displayed by symbols with dim colours. (A-F) *P < .05, **P < .005, ***P < .001. ATA, anti-TOP1 autoantibody; Ig, immunoglobulin; ns, not significant; SSc, systemic sclerosis; TOP1, topoisomerase 1; TOP1cc, TOP1-DNA cleavage complex.

binding titres to TOP1 and TOP1cc was comparable between IgG and IgM (Fig 4F). Together, these data indicate that the differential recognition of TOP1 and TOP1cc is predominantly found in the IgM compartment and in the IgG1 subclass.

Enhanced induction of cytokine production by anti-TOP1cc mAbs in complex with TOP1cc

The enhanced binding of ATA mAbs to TOP1cc compared with TOP1 may have functional implications on the immunostimulatory capacity of ATAs. To provide supportive evidence for this possibility, we stimulated the monocytic THP-1 cell line with ATA mAbs complexed with plate-bound TOP1 or TOP1cc and subsequently determined the secretion of IL-8, a well-established early activation marker of these cells [27,28]. Minimal secretion of IL-8 by THP-1 cells was detected in conditions with TOP1 and TOP1cc coating to which no antibody or a negative control antibody was added (Fig 5A, Supplementary Fig S5A). The ATA mAb 2F8, which binds to TOP1 and TOP1cc to a similar extent, induced comparable levels of IL-8 if complexed with TOP1cc or TOP1 (Fig 5A, Supplementary Fig S5A). In contrast, ATA mAbs 7G6 and 9D11, which both bind TOP1cc better than TOP1, induced higher production of IL-8 by THP-1 cells when complexed with TOP1cc compared with TOP1 (Fig 5A, Supplementary Fig S5A).

The *in vivo* setting in which ATA-TOP1/TOP1cc immune complexes may form is likely more complex, and human primary cells may be more variable in response to immune complex stimulation. Nonetheless, we opted to validate the differential immunostimulatory potential of ATAs on *ex vivo* isolated cells, choosing monocytes isolated from HDs and patients with ATA$^+$ SSc as a surrogate. Primary monocytes require priming stimuli (eg Toll-like receptor [TLR] ligands) to respond to immune complex stimulation, with TNF-α being a particularly sensitive readout in this setting [29,30]. In line with these considerations, minimal secretion of TNF-α was observed in supernatants of primary monocytes stimulated with ATA mAbs in complex with TOP1, while the cells reacted strongly to LPS stimulation (Supplementary Fig S5B,D). In the presence of LPS, however, ATA mAb immune complexes potently enhanced the LPS-induced TNF-α secretion by monocytes from 2 of 4 HDs and 3 of 4 patients with ATA$^+$ SSc tested (Supplementary Fig S5D,E). As for THP-1 cells, the ability of ATA mAbs to induce activation varied depending on their differential reactivity towards TOP1 and TOP1cc (Fig 5B). ATA mAb 2F8 induced comparable levels of TNF-α in complex with TOP1cc or TOP1, whereas ATA mAb 9D11 induced enhanced secretion of TNF-α when complexed with TOP1cc in both primary monocytes from HDs and patients with ATA$^+$ SSc (Fig 5B). Together, these data provide support for the hypothesis that the differential recognition profile of ATA detected here and, hence, the heterogeneity within the ATA B cell response may have functional consequences for the degree to which inflammatory processes may be affected or modulated by ATA in SSc.

Enhanced activation of B cells expressing TOP1cc-reactive BCR upon stimulation with TOP1-DNA complexes

Previous evidence suggests that the degree of autoreactive B cell activation correlates with SSc disease severity and

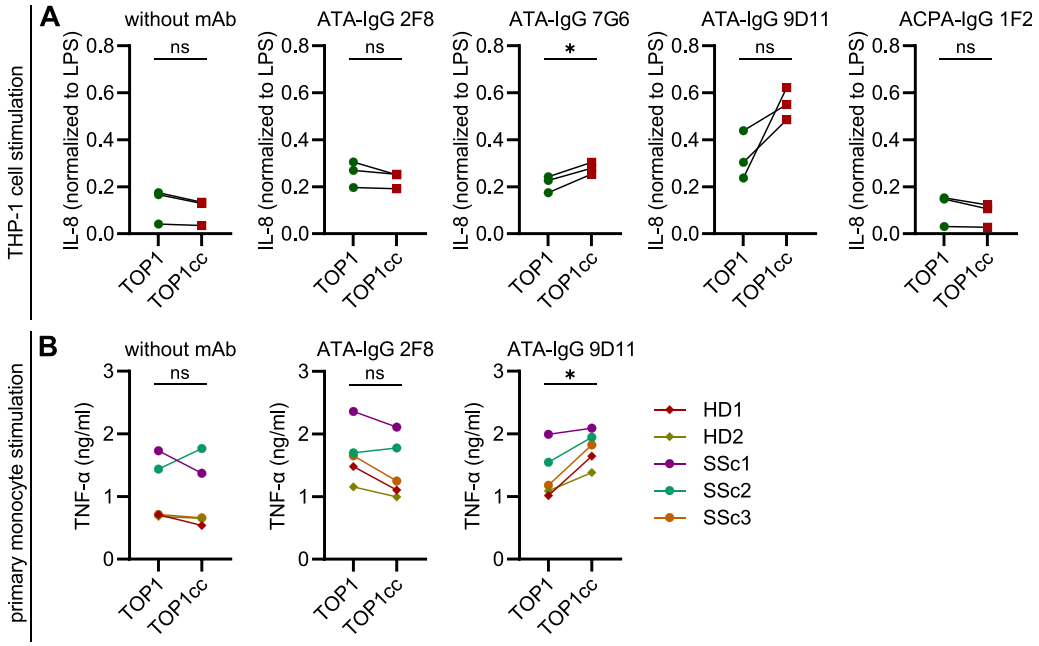

Figure 5. Stimulation of THP-1 cells and primary monocytes with ATA mAbs in complex with TOP1 and TOP1cc. (A) Normalised levels of IL-8 in culture supernatants of THP-1 cells stimulated for 24 hours with ATA mAbs in complex with plate-bound TOP1 and TOP1cc. Conditions to which no mAb or the ACPA-IgG mAb 1F2 was added were used as negative controls. IL-8 levels were normalised to the levels of IL-8 detected in culture supernatant of THP-1 cells stimulated with 1 μg/mL LPS. Data are obtained from 3 independent experiments, which are connected by lines. Two out of 3 experiments were performed in technical duplicate. (B) Levels of TNF-α (ng/mL) in culture supernatants of primed monocytes (100 ng/mL LPS) isolated from HDs and patients with ATA$^+$ SSc upon stimulation with ATA mAbs 2F8 and 9D11 in complex with plate-bound TOP1 and TOP1cc for 24 hours. Conditions to which no mAb was added were used as negative controls. Data from 2 HDs and 3 patients with ATA$^+$ SSc are shown (out of 4 donors tested per group, Supplementary Fig S5B-E) for whom a clear immune complex-mediated signal could be detected in the assay. Experiments were performed in technical duplicate. (A,B) Cytokine levels were compared using a paired t-test. *$P < .05$, **$P < .005$, ***$P < .001$. ACPA, anti-citrullinated protein antibody; ATA, anti-TOP1 autoantibody; mAbs, monoclonal antibodies; HD, healthy donor; Ig, immunoglobulin; IL, interleukin; LPS, lipopolysaccharide; ns, not significant; SSc, systemic sclerosis; TNF-α, tumour necrosis factor alpha; TOP1, topoisomerase 1; TOP1cc, TOP1-DNA cleavage complex; THP-1, Tohoku Hospital Pediatrics-1 cells.

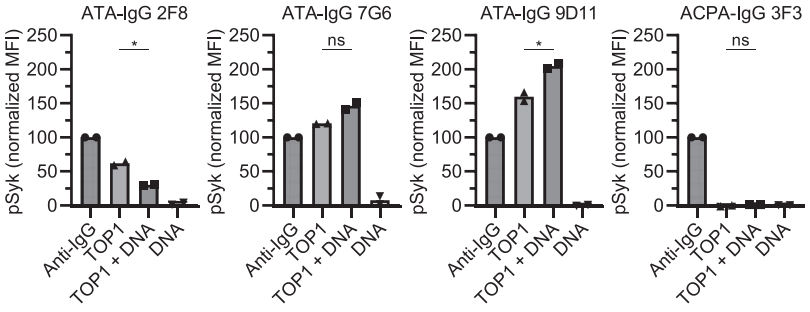

Figure 6. Activation of Ramos B cell lines expressing TOP1-reactive BCRs by TOP1 or TOP1-DNA complexes. Expression of pSyk (pY352) by Ramos B cell lines expressing TOP1-reactive BCRs 2F8, 7G6, or 9D11 upon stimulation with 5 μg/mL anti-IgG, 5 μg/mL TOP1 preincubated with or without 5 μg/mL DNA, or 5 μg/mL DNA only. A Ramos B cell line expressing ACPA-IgG 3F3 was used as a negative control. MFI is shown, normalised to the MFI generated in the corresponding anti-IgG condition upon subtracting the MFI obtained in the unstimulated condition. Data are derived from 2 independent experiments. Differences between TOP1 and TOP1 + DNA were compared using a paired t-test. $^{*}P < .05$, $^{**}P < .005$, $^{***}P < .001$. ACPA, anti-citrullinated protein antibody; ATA, anti-TOP1 autoantibody; BCR, B cell receptor; Ig, immunoglobulin; MFI, median fluorescence intensity; ns, not significant; TOP1, topoisomerase 1; TOP1cc, TOP1-DNA cleavage complex.

progression [7,8]. Therefore, we next investigated the potential functional relevance of the differential recognition of TOP1cc by ATAs on the activation of TOP1-reactive B cells. Three TOP1-reactive B cell lines were generated expressing the BCRs from which 2F8, 7G6, and 9D11 were derived. A fourth B cell line expressing the sequence of an anti-citrullinated protein antibody B cell clone (3F3) served as a control. All B cell lines responded to stimulation with anti-IgG (positive control) as measured by increased expression of pSyk, indicating BCR-mediated activation (Fig. 6, Supplementary Fig S6). Similarly, all TOP1-reactive cell lines, but not the control, responded to stimulation with TOP1 (Fig. 6, Supplementary Fig S6). Notably, B cells expressing BCRs from which the 'TOP1cc-enhanced ATA' clones 7G6 and 9D11 were derived displayed higher expression of pSyk upon stimulation with TOP1 in comparison with anti-IgG (Fig. 6, Supplementary Fig S6). In contrast, a decline of pSyk expression was observed for cells expressing the 2F8 clone. More importantly, however, and in line with observations made using the TOP1-specific mAbs, preincubation of TOP1 with plasmid DNA further enhanced the activation of B cells expressing the 7G6 and 9D11 clones (Fig. 6, Supplementary Fig S6). Importantly, such an effect was not observed for the B cell line expressing the 2F8 BCR. Together, these data show that B cells expressing 'TOP1cc-enhanced ATAs' are particularly sensitive to stimulation by TOP1-DNA complexes, indicating that the differential TOP1/TOP1cc recognition observed might directly impact autoreactive B cell activation.

DISCUSSION

Predictability of disease progression forms a major challenge in the clinical management of SSc due to heterogeneity in clinical presentation and course of disease. To gain insights into the molecular mechanisms driving the disease, we here focused on the ATA B cell response and assessed whether DNA binding by TOP1 would affect its recognition by ATAs. By studying monoclonal and polyclonal ATAs, we observed remarkable heterogeneity among these autoantibodies in the recognition of TOP1 and TOP1cc. In fact, a subset of ATAs recognised TOP1cc better than TOP1, indicating that TOP1cc formation induces conformational changes that enhance the antigenic properties of individual TOP1 epitopes and, consequently, the immunostimulatory properties of ATA immune complexes and the activation of B cells expressing TOP1-reactive BCRs.

Heterogeneity within autoantibody responses has been described for other autoimmune diseases such as rheumatoid arthritis and myasthenia gravis, with evidence in each case for its relevance for disease activity and course [31–35]. Likewise, in SSc, the differential recognition of TOP1 and TOP1cc by ATAs could relate to the disease by various means. We observed that enhanced recognition of TOP1cc can be found in all patients with ATA$^+$ SSc, yet increasingly in patients with interstitial lung disease and in those with higher anti-TOP1-IgG levels in serum. Hence, it is likely that TOP1cc functions as an enhancer of the stimulation of ATA$^+$ B cells. In fact, our data on B cell lines expressing TOP1-reactive BCRs show that TOP1cc preferentially stimulates the subset of B cells expressing ATA with enhanced recognition of TOP1cc epitopes. Interestingly, stimulation of these cells may be further amplified by BCR-mediated internalisation of DNA in complex with TOP1 and subsequent coengagement of TLR9 [36–38]. Consequently, TOP1cc recognition may be relevant for both the initial break of B cell tolerance to TOP1 and, likewise, the continuous activation of ATA B cells in established disease. In this context, it is important that we note the predominant presence of 'TOP1cc-enhanced' ATA within the IgM and the IgG1 subclass compartments. The presence of TOP1cc-enhanced reactivity in the IgM compartment makes the naïve B cell compartment susceptible to strong BCR-mediated stimulation, while TLR stimulation synergises with BCR signalling to induce activation-induced cytidine deaminase, which mediates BCR class-switching [37,39]. Previously, we could show that both the presence of ATA-IgM and ATA-IgG levels in serum associated with progressive disease, supporting this concept [8]. In addition, the presence of ATA-secreting cells in the circulation, a sign of recent B cell activation, is associated with the presence and severity of interstitial lung disease [7]. Together, these results indicate that the formation of TOP1cc could be important for ATA B cell activation and suggest that this process may be relevant to initiate and drive ATA$^+$ disease.

Our findings imply that TOP1 in complex with DNA is the autoantigen primarily targeted by the ATA B cell response. Differential recognition of TOP1 and TOP1cc likely depends on conformational changes that occur when TOP1 binds DNA [40–42]. This conformational change only affects the binding of ATAs that recognise epitopes of TOP1, which are altered and, thus, probably represent a subset of ATA B cells. This is consistent with the finding that ATA mAbs differentially bind to TOP1 and TOP1cc, bind to unique epitopes, and vary in their ability to inhibit the enzymatic function of TOP1. Concerning the latter, it is notable that the activity of the enzyme was affected by those ATA mAbs that preferentially bound to TOP1cc. Our data also indicate that the differential recognition of TOP1cc may enhance ATA functional properties inducing or supporting inflammatory processes. The relevance of these functional

effects, the conformation of the antigen, and the context in which the actual antigen is encountered by ATAs and TOP1-reactive B cells remains to be determined, particularly within affected tissues. It has been described, for example, that TOP1 isolated from nuclei of SSc skin fibroblasts shows reduced enzymatic activity and is more often modified with a small ubiquitin-like modifier (SUMO) [43]. These traits are associated with the presence of TOP1cc, as TOP1cc is SUMOylated in pathways needed to repair DNA lesions trapped in TOP1cc [44]. Another variable could be the source of DNA incorporated in TOP1cc, as human TOP1 can also bind microbial DNA [45]. Microbial DNA is a more potent inducer of TLR9 signalling in comparison with human DNA, which might further enhance the pro-inflammatory potential of TOP1cc [46]. Together, such variables could determine the immunological properties of TOP1, add to the enhanced stimulation of B cells, and indicate the need for molecular analyses of TOP1 in affected tissues.

Our study has limitations. We did not elucidate the exact *in vivo* mechanisms by which ATAs or TOP1-reactive B cells could contribute to disease. Although it is likely that differential recognition of the antigen will modulate downstream effects of ATAs, either as antibody or expressed as BCR by TOP1-reactive B cells, additional studies on antigen conformation, autoantibody reactivity, composition of immune complexes, and ATA B cells *in situ* are warranted. *In vivo* models could also give further insights into such mechanisms. Analysis of IgM reactivity in plasma of patients with ATA^+ SSc towards TOP1 and TOP1cc was biased as we selected patients with high ATA-IgM levels to prevent interference of non-specific antibodies in the assay. In addition, we did not assess the dynamics of ATAs that do or do not differentially recognise TOP1cc. Such analyses will give insights into the relation between the dynamics of this response and disease activity or progression of disease over time.

In conclusion, our data indicate that DNA binding by TOP1, a nuclear autoantigen in SSc, affects the recognition of the antigen by disease-specific autoantibodies. This enhanced antigen binding extends the relevance of the well-appreciated proinflammatory effects of nucleic acid binding by nuclear antigens. Modulation of autoantigen recognition by nucleic acid binding could affect autoreactive B cell responses targeting nuclear proteins in SSc and other autoimmune diseases, thereby modulating their disease processes and course. Finally, autoreactive B cells recognising TOP1cc-enhanced epitopes might be preferential targets for antigen-specific B cell-depleting strategies aimed at further refining recently emerging treatment concepts.

Competing interests

All authors declare they have no competing interests.

Acknowledgements

Flow cytometry was performed at the Flow Cytometry Core Facility (FCF) of the Leiden University Medical Center.

Contributors

SN, DMHvR, ME, BE, AJRH, CMF, JKdVB, REMT, and HUS contributed to conceptualisation. SN, CMW, DMHvR, MJALW, NML, ME, and BE contributed to designing and conducting experiments. SN, CMW, DMHvR, MJALW, RQK, NML, ME, EWNL, CMF, REMT, and HUS contributed to methodology. SN, DMHvR, MJALW, and HUS performed formal analysis. SN, DMHvR, MJALW, ME, BE, AJRH, CMF, JKdVB, REMT, and HUS contributed to data interpretation. REMT and HUS provided supervision. SN and HUS wrote the original draft. All authors contributed to the revision of the manuscript and approved the final version for submission.

Funding

Research presented in this paper was funded by the Dutch Arthritis Foundation (LLP5), the IMI-funded project RTCure (777357), Health~Holland Life Sciences & Health sector programs Target to B! (LSHM18055-5GF) and Immune HealthSeed (LSHM22042-SFG), a European Research Council Advanced grant (AdG2019-884796, to REMT), and a NWO-ZonMW VIDI grant (09150172010067, to HUS).

Patient consent for publication

Not applicable.

Ethics approval

This study was approved by the ethical review board of the Leiden University Medical Center (protocol number P17.151) and the Leiden University Biobank Toetsing Commissie (REU/036/SH/sh).

Provenance and peer review

Not commissioned; externally peer reviewed.

Data availability statement

Data presented in this paper are available upon reasonable request.

Supplementary materials

Supplementary material associated with this article can be found in the online version at doi:10.1016/j.ard.2026.03.016.

Orcid

Sam Neppelenbroek: http://orcid.org/0000-0002-9582-2837
Hans U. Scherer: http://orcid.org/0000-0002-5700-5617

REFERENCES

[1] Pope JE, Denton CP, Johnson SR, Fernandez-Codina A, Hudson M, Nevskaya T. State-of-the-art evidence in the treatment of systemic sclerosis. Nat Rev Rheumatol 2023;19:212–26.
[2] Pisetsky DS. Unique interplay between antinuclear antibodies and nuclear molecules in the pathogenesis of systemic lupus erythematosus. Arthritis Rheumatol 2024;76:1334–43.
[3] Liem SIE, Neppelenbroek S, Fehres CM, Wortel C, Toes REM, Huizinga TWJ, et al. Autoreactive B cell responses targeting nuclear antigens in systemic sclerosis: implications for disease pathogenesis. Semin Arthritis Rheum 2023;58:152136.
[4] Pokeerbux MR, Giovannelli J, Dauchet L, Mouthon L, Agard C, Lega JC, et al. Survival and prognosis factors in systemic sclerosis: data of a French multicenter cohort, systematic review, and meta-analysis of the literature. Arthritis Res Ther 2019;21:86.
[5] Bournia VK, Fragoulis GE, Mitrou P, Mathioudakis K, Tsolakidis A, Konstantonis G, et al. All-cause mortality in systemic rheumatic diseases under treatment compared with the general population, 2015-2019. RMD Open 2021;7:e001694.

[6] Nihtyanova SI, Denton CP. Autoantibodies as predictive tools in systemic sclerosis. Nat Rev Rheumatol 2010;6:112–6.
[7] Wortel CM, Liem SI, van Leeuwen NM, Boonstra M, Fehres CM, Stöger L, et al. Anti-topoisomerase, but not anti-centromere B cell responses in systemic sclerosis display active, Ig-secreting cells associated with lung fibrosis. RMD Open 2023;9:e003148.
[8] Boonstra M, Bakker JA, Grummels A, Ninaber MK, Ajmone Marsan N, Wortel CM, et al. Association of anti-topoisomerase I antibodies of the IgM isotype with disease progression in anti-topoisomerase I-positive systemic sclerosis. Arthritis Rheumatol 2020;72:1897–904.
[9] Bergmann C, Müller F, Distler JHW, Györfi AH, Völkl S, Aigner M, et al. Treatment of a patient with severe systemic sclerosis (SSc) using CD19-targeted CAR T cells. Ann Rheum Dis 2023;82:1117–20.
[10] Goswami RP, Ray A, Chatterjee M, Mukherjee A, Sircar G, Ghosh P. Rituximab in the treatment of systemic sclerosis-related interstitial lung disease: a systematic review and meta-analysis. Rheumatology (Oxford) 2021;60:557–67.
[11] Arcand J, Robitaille G, Koenig M, Senécal JL, Raymond Y. Heparin inhibits the interaction of DNA topoisomerase I/anti-topoisomerase I immune complexes with heparan sulfate on dermal fibroblasts. Arthritis Rheum 2012;64:1632–41.
[12] Hénault J, Robitaille G, Senécal JL, Raymond Y. DNA topoisomerase I binding to fibroblasts induces monocyte adhesion and activation in the presence of anti-topoisomerase I autoantibodies from systemic sclerosis patients. Arthritis Rheum 2006;54:963–73.
[13] Hénault J, Tremblay M, Clément I, Raymond Y, Senécal JL. Direct binding of anti-DNA topoisomerase I autoantibodies to the cell surface of fibroblasts in patients with systemic sclerosis. Arthritis Rheum 2004;50:3265–74.
[14] Rubin SJS, Bloom MS, Robinson WH. B cell checkpoints in autoimmune rheumatic diseases. Nat Rev Rheumatol 2019;15:303–15.
[15] Kwak K, Akkaya M, Pierce SK. B cell signaling in context. Nat Immunol 2019;20:963–9.
[16] Suurmond J, Diamond B. Autoantibodies in systemic autoimmune diseases: specificity and pathogenicity. J Clin Invest 2015;125:2194–202.
[17] Kringelum JV, Nielsen M, Padkjær SB, Lund O. Structural analysis of B-cell epitopes in antibody:protein complexes. Mol Immunol 2013;53:24–34.
[18] Pommier Y, Sun Y, Huang SN, Nitiss JL. Roles of eukaryotic topoisomerases in transcription, replication and genomic stability. Nat Rev Mol Cell Biol 2016;17:703–21.
[19] Sordet O, Goldman A, Redon C, Solier S, Rao VA, Pommier Y. Topoisomerase I requirement for death receptor-induced apoptotic nuclear fission. J Biol Chem 2008;283:23200–8.
[20] Meijs J, Schouffoer AA, Ajmone Marsan N, Kroft LJ, Stijnen T, Ninaber MK, et al. Therapeutic and diagnostic outcomes of a standardised, comprehensive care pathway for patients with systemic sclerosis. RMD Open 2016;2:e000159.
[21] Kristoffersen EL, Jørgensen LA, Franch O, Etzerodt M, Frøhlich R, Bjergbæk L, et al. Real-time investigation of human topoisomerase I reaction kinetics using an optical sensor: a fast method for drug screening and determination of active enzyme concentrations. Nanoscale 2015;7:9825–34.
[22] Kissel T, Reijm S, Slot LM, Cavallari M, Wortel CM, Vergroesen RD, et al. Antibodies and B cells recognising citrullinated proteins display a broad cross-reactivity towards other post-translational modifications. Ann Rheum Dis 2020;79:472–80.
[23] Bankamp L, Preuß B, Pecher AC, Vogel W, Henes J, Klein R. Functional autoantibodies in systemic sclerosis: influence of autologous stem cell transplantation and correlation with clinical outcome. Rheumatology (Oxford) 2023;62:2168–77.
[24] Samuels DS, Tojo T, Homma M, Shimizu N. Inhibition of topoisomerase I by antibodies in sera from scleroderma patients. FEBS Lett 1986;209:231–4.
[25] Lu LL, Suscovich TJ, Fortune SM, Alter G. Beyond binding: antibody effector functions in infectious diseases. Nat Rev Immunol 2017;18:46–61.
[26] Volkov M, Coppola M, Huizinga R, Eftimov F, Huizinga TWJ, van der Kooi AJ, et al. Comprehensive overview of autoantibody isotype and subclass distribution. J Allergy Clin Immunol 2022;150:999–1010.
[27] Fernández N, Renedo M, García-Rodríguez C, Sánchez Crespo M. Activation of monocytic cells through Fc gamma receptors induces the expression of macrophage-inflammatory protein (MIP)-1 alpha, MIP-1 beta, and RANTES. J Immunol 2002;169:3321–8.
[28] Marsh CB, Gadek JE, Kindt GC, Moore SA, Wewers MD. Monocyte Fc gamma receptor cross-linking induces IL-8 production. J Immunol 1995;155:3161–7.
[29] Vogelpoel LT, Hansen IS, Visser MW, Nagelkerke SQ, Kuijpers TW, Kapsenberg ML, et al. FcγRIIa cross-talk with TLRs, IL-1R, and IFNγR selectively modulates cytokine production in human myeloid cells. Immunobiology 2015;220:193–9.
[30] Hoepel W, Chen HJ, Geyer CE, Allahverdiyeva S, Manz XD, de Taeye SW, et al. High titers and low fucosylation of early human anti-SARS-CoV-2 IgG promote inflammation by alveolar macrophages. Sci Transl Med 2021;13:eabf8654.
[31] Niks EH, van Leeuwen Y, Leite MI, Dekker FW, Wintzen AR, Wirtz PW, et al. Clinical fluctuations in MuSK myasthenia gravis are related to antigen-specific IgG4 instead of IgG1. J Neuroimmunol 2008;195:151–6.
[32] Huijbers MG, Vink AF, Niks EH, Westhuis RH, van Zwet EW, de Meel RH, et al. Longitudinal epitope mapping in MuSK myasthenia gravis: implications for disease severity. J Neuroimmunol 2016;291:82–8.
[33] Figueiredo CP, Bang H, Cobra JF, Englbrecht M, Hueber AJ, Haschka J, et al. Antimodified protein antibody response pattern influences the risk for disease relapse in patients with rheumatoid arthritis tapering disease modifying antirheumatic drugs. Ann Rheum Dis 2017;76:399–407.
[34] Nijjar JS, Morton FR, Bang H, Buckley CD, van der Heijde D, Gilmour A, et al. The impact of autoantibodies against citrullinated, carbamylated, and acetylated peptides on radiographic progression in patients with new-onset rheumatoid arthritis: an observational cohort study. Lancet Rheumatol 2021;3:e284–93.
[35] Darrah E, Giles JT, Ols ML, Bull HG, Andrade F, Rosen A. Erosive rheumatoid arthritis is associated with antibodies that activate PAD4 by increasing calcium sensitivity. Sci Transl Med 2013;5:186ra65.
[36] Eckl-Dorna J, Batista FD. BCR-mediated uptake of antigen linked to TLR9 ligand stimulates B-cell proliferation and antigen-specific plasma cell formation. Blood 2009;113:3969–77.
[37] Pone EJ, Zhang J, Mai T, White CA, Li G, Sakakura JK, et al. BCR-signalling synergizes with TLR-signalling for induction of AID and immunoglobulin class-switching through the non-canonical NF-κB pathway. Nat Commun 2012;3:767.
[38] Viglianti GA, Lau CM, Hanley TM, Miko BA, Shlomchik MJ, Marshak-Rothstein A. Activation of autoreactive B cells by CpG dsDNA. Immunity 2003;19:837–47.
[39] Pone EJ, Lou Z, Lam T, Greenberg ML, Wang R, Xu Z, et al. B cell TLR1/2, TLR4, TLR7 and TLR9 interact in induction of class switch DNA recombination: modulation by BCR and CD40, and relevance to T-independent antibody responses. Autoimmunity 2015;48:1–12.
[40] Carey JF, Schultz SJ, Sisson L, Fazzio TG, Champoux JJ. DNA relaxation by human topoisomerase I occurs in the closed clamp conformation of the protein. Proc Natl Acad Sci U S A 2003;100:5640–5.
[41] Takahashi DT, Gadelle D, Agama K, Kiselev E, Zhang H, Yab E, et al. Topoisomerase I (TOP1) dynamics: conformational transition from open to closed states. Nat Commun 2022;13:59.
[42] Woo MH, Losasso C, Guo H, Pattarello L, Benedetti P, Bjornsti MA. Locking the DNA topoisomerase I protein clamp inhibits DNA rotation and induces cell lethality. Proc Natl Acad Sci USA 2003;100:13767–72.
[43] Zhou X, Lin W, Tan FK, Assassi S, Fritzler MJ, Guo X, et al. Decreased catalytic function with altered SUMOylation of DNA topoisomerase I in the nuclei of scleroderma fibroblasts. Arthritis Res Ther 2011;13:R128.
[44] Sun Y, Miller Jenkins LM, Su YP, Nitiss KC, Nitiss JL, Pommier Y. A conserved SUMO pathway repairs topoisomerase DNA-protein cross-links by engaging ubiquitin-mediated proteasomal degradation. Sci Adv 2020;6:eaba6290.
[45] Nitiss JL, Kiianitsa K, Sun Y, Nitiss KC, Maizels N. Topoisomerase assays. Curr Protoc. 2021;1:e250.
[46] Lande R, Gregorio J, Facchinetti V, Chatterjee B, Wang YH, Homey B, et al. Plasmacytoid dendritic cells sense self-DNA coupled with antimicrobial peptide. Nature 2007;449:564–9.

Ann Rheum Dis 85 (2026) 1637–1645

Contents lists available at ScienceDirect

Annals of the Rheumatic Diseases

journal homepage: https://www.sciencedirect.com/journal/annals-of-the-rheumatic-diseases

Osteoarthritis

The epigenomic landscape of primary tissues in osteoarthritis

Peter Kreitmaier[1], Odysseas Sotirios Stergiou[1,2], Georgia Katsoula[1,2,3], Mauro Tutino[1], Norbert Bittner[1], Karan M. Shah[4], Diane Swift[4], Jeremy Mark Wilkinson[4], Eleftheria Zeggini[1,3,*]

[1] *Institute of Translational Genomics, Helmholtz Zentrum München – German Research Center for Environmental Health, Neuherberg, Germany*

[2] *School of Medicine and Health, Graduate School of Experimental Medicine, Technical University of Munich (TUM), Munich, Germany*

[3] *TUM School of Medicine and Health, Technical University of Munich (TUM), TUM University Hospital, Munich, Germany*

[4] *School of Medicine and Population Health, University of Sheffield, Beech Hill Road, Sheffield, UK*

ARTICLE INFO

Article history:
Received 6 October 2025
Received in revised form 27 January 2026
Accepted 28 January 2026

ABSTRACT

Objectives: Osteoarthritis is a complex joint disease, affecting more than 500 million people worldwide. We investigated DNA methylation profiles and integrated these with matching genotype and transcriptomics data in primary tissues of patients with knee osteoarthritis to enhance our understanding of the regulatory framework that modulates gene expression in osteoarthritis.

Methods: We measured matched genotype and methylation from primary chondrocytes of macroscopically intact (low-grade) and degraded (high-grade) disease cartilage as well as synovium, infrapatellar fat pad, and blood samples, for 314 patients who underwent total knee replacement for osteoarthritis. We generated methylation quantitative trait locus (mQTL) maps in cartilage, synovium, fat pad, and blood, as well as expression quantitative trait methylation (eQTM) maps in cartilage and synovium. We integrated these results with genome-wide association studies (GWAS) to identify likely effector genes of osteoarthritis.

Results: We reported widespread associations between genetic variants and methylation as well as between methylation and gene expression. Through colocalisation, we find methylation sites with a potential causal role in osteoarthritis. By tissue-specific integration of colocalisation and eQTM results, we resolved GWAS signals and identified 50 likely effector genes.

Conclusions: We provided the largest genome-wide mQTL maps of low- and high-grade osteoarthritis cartilage and synovium. We further presented the largest cartilage eQTM map for primary cartilage and the first eQTM map in synovium. We found methylation sites with a potential mechanistically causal role in osteoarthritis and associated these with likely effector genes. Together, the presented genome-wide eQTM and mQTL maps constitute relevant resources for osteoarthritis research and beyond.

*Correspondence to Prof Eleftheria Zeggini.

E-mail address: eleftheria.zeggini@helmholtz-munich.de (E. Zeggini).

Handling editor Josef S. Smolen.

J. Mark Wilkinson and Eleftheria Zeggini contributed equally to this work.

https://doi.org/10.1016/j.ard.2026.01.020

WHAT IS ALREADY KNOWN ON THIS TOPIC

- Osteoarthritis is a prevalent joint disease with no curative therapy.
- Genome-wide association studies (GWAS) have identified osteoarthritis risk loci, but enhanced molecular profiles of primary osteoarthritis tissues are required to link these loci to effector genes in a tissue- and disease-specific manner.

WHAT THIS STUDY ADDS

- By combining whole-genome sequencing, DNA methylation, and gene expression data from 314 patients with osteoarthritis with GWAS results, we suggested 50 likely effector genes of genetic risk loci, including 19 novel ones.

HOW THIS STUDY MIGHT AFFECT RESEARCH, PRACTICE OR POLICY

- We prioritised novel targets for further osteoarthritis research.
- We provided publicly available, genome-wide maps of genetic effects on DNA methylation, as well as effects between DNA methylation and gene expression across relevant osteoarthritis tissue types.

INTRODUCTION

Osteoarthritis is a complex joint disease, affecting more than 500 million people worldwide [1], but despite its high prevalence, treatment methods are limited to pain management and total joint replacement. To promote the development of novel, personalised treatment strategies, it is important to better understand the genetic and molecular basis of osteoarthritis. Large genome-wide association studies (GWAS) have generated insights into its complex genetic architecture and found 962 risk loci for osteoarthritis [2]. However, in order to reveal molecular pathways along which genetic variants exert osteoarthritis-relevant effects, it is necessary to link these genetic insights to molecular profiles of primary tissues [3–5].

A relevant regulatory molecular layer is DNA methylation, an epigenetic mark describing the covalent addition of a methyl group to the DNA that has a regulatory role on gene expression. Previous work [6,7] combined DNA methylation of joint primary tissues with genotype data, matched from the same patients with osteoarthritis, to examine genetic effects on methylation, thus providing genome-wide methylation quantitative trait locus (mQTL) maps. These maps have been generated in low-grade (n = 90 patients) [6] and high-grade osteoarthritis cartilage (n = 89 patients) [6], synovium (n = 78 patients) [6], as well as infrapatellar fat pad (n = 68 patients) [7], and constitute a valuable data resource of these tissue types to enable investigation of the causal roles of epigenetic markers in osteoarthritis. Beyond these insights into joint tissues, other osteoarthritis-relevant epigenetic studies have focused on blood methylation profiles of patients with osteoarthritis, in particular on building methylation-based classifiers to predict knee osteoarthritis progression [8].

However, genome-wide mQTL studies in osteoarthritis tissues have been limited in sample size [9] (Supplementary Fig S1). Furthermore, there is a need for genome-wide association maps between molecular layers, particularly between DNA methylation and gene expression in osteoarthritis-relevant tissues.

Here, we investigated primary osteoarthritis tissue samples of 314 patients to (1) map effects of genotype on DNA methylation and identify mQTL, (2) determine associations between gene expression and DNA methylation (expression quantitative trait methylation; eQTM), and (3) apply integrative approaches to find likely effector genes for genetic risk loci.

METHODS

For full details of methods, see Supplementary Methods.

Osteoarthritis-affected individuals and study samples

We studied data from 314 patients who underwent total knee replacement due to osteoarthritis (mean age, 70.57 years; age range, 38-93 years; 181 women and 133 men; mean body mass index [BMI], 32.23 kg/m^2; BMI range, 20-51 kg/m^2; Supplementary Table S1). Inclusion/exclusion criteria were primary osteoarthritis of the affected knee, without use of drugs known to affect bone turnover, such as steroids and bisphosphonates, within 6 months of surgery, and no current cancer diagnosis. Cartilage samples were graded according to the International Cartilage Repair Society (ICRS) macroscopic scoring system (low-grade osteoarthritis cartilage, ICRS score 0 or 1; high-grade cartilage osteoarthritis, ICRS score 3 or 4) [10]. This work was approved by the Oxford National Health Service Research Ethics Committee C (10/H0606/20, 15/SC/0132, and 20/SC/0141), and samples were collected under Human Tissue Authority licence 12182, Sheffield Musculoskeletal Biobank, University of Sheffield, UK. Before participating in the study, all osteoarthritis-affected individuals provided written, informed consent.

Sample extraction

Knee chondrocytes and synoviocytes were isolated by following previously published protocols (Methods, 'Isolation of chondrocytes' and 'Isolation of synoviocytes' sections) [5]. Peripheral blood samples were stored at −80 °C prior to DNA extraction using the QIAamp DNA Blood Maxi Kit [7].

Whole-genome sequencing preprocessing

Whole-genome sequencing (WGS) data preprocessing and variant, as well as sample-level quality control, were described previously [7] (Supplementary Methods).

DNA methylation data

Genome-wide DNA methylation data were obtained from primary chondrocytes of macroscopically intact (low-grade) and degraded (high-grade) cartilage as well as synovium, infrapatellar fat pad, and blood samples. DNA methylation was measured using the Illumina Infinium MethylationEPIC array technology. We preprocessed methylation data from all tissues together using an R package, meffil (https://github.com/perishky/meffil/wiki) [11] (Supplementary Methods). Preprocessing fat pad methylation data and follow-up methylation cis-mQTL analysis have also been described previously [7].

Gene expression data

Gene expression of the same patient cohort was collected and preprocessed as described previously [12]. Of note, tissue-specific RNA sequencing count matrices were normalised using the Trimmed Mean of M-values method. We then retained gene expression data for patients (low-grade cartilage, 227 patients and 16,991 genes; high-grade cartilage, 127 patients and 16,991 genes; synovium, 226 patients and 15,628 genes; fat pad, 45 patients and

15,726 genes) with matching DNA methylation data and performed inverse normal transformation per tissue. We then tissue-specifically estimated PEER factors using the R package peer [13], which we accounted for in the eQTM analysis.

Cis-mQTL analysis

We performed cis-mQTL analysis (cis distance, 1 Mb on either side of the tested methylation site) using FastQTL (https://github.com/francois-a/fastqtl/) [14] in low- (289 patients) and high-grade osteoarthritis cartilage (172 patients), synovium (249 patients), and blood (237 patients) (Supplementary Table S1). We further compared these results with the previously published cis-mQTL map in the infrapatellar fat pad of this patient's cohort (68 patients [7]) to find signals that are tissue-specific and shared between joint tissues (Supplementary Methods).

Trans-mQTL analysis

We performed trans-mQTL analysis using the R package MatrixEQTL [15] in low- and high-grade osteoarthritis cartilage, synovium, and infrapatellar fat pad, as well as blood, using the same methylation and WGS data matrices, as well as including the same covariates in the models as in the cis-mQTL analysis ('Cis-mQTL analysis' section). We considered methylation site-gene pairs of methylation sites and gene transcription starting sites on different chromosomes or with a commonly used [16,17] distance of >5 Mb. To correct for multiple testing, we chose genetic variants with the lowest nominal *P* value per methylation site. Next, we multiplied these nominal *P* values by 10^6 to correct for the number of independent tests when studying common (minor allele frequencies (MAF) >5%) genetic variants on a genome-wide scale. We then performed false discovery rate (FDR) correction on these corrected *P* values to account for tests across methylation sites, regarding methylation sites with q value <5% Storey-Tibshirani FDR as trans-mQTL-targeted [18]. Finally, we considered the largest nominal *P* value of significant mQTL (q value < 0.05) and the lowest nominal *P* value of not significant ones (q value ≥ 0.05) and calculated the average of these 2 nominal *P* values to define a nominal *P* value threshold for trans-mQTLs.

Colocalisation analysis

We performed colocalisation analysis to identify methylation sites that mediate genetic risk for osteoarthritis by integrating mQTL (for low- and high-grade cartilage, synovium, infrapatellar fat pad, and blood) and GWAS summary statistics [2] for knee osteoarthritis (172,256 cases and 1,144,244 controls), total knee replacement (48,161 cases and 958,463 controls), and osteoarthritis at any joint site (489,975 cases and 1,472,094 controls), all aligned to GRCh38. Using the *coloc* R package [19], we ran coloc.abf() to estimate the probability that the same causal variant affects both DNA methylation and osteoarthritis risk. More specifically, we considered a 100 kb (1×10^5 bp) window around the GWAS lead variant. We performed colocalisation for mQTL-targeted methylation sites (q value ≤ 0.05) if the methylation site-specific mQTL index variant was located within this 100 kb window. For the actual analysis, we considered variants within this 100 kb window for which GWAS and cis-mQTL summary statistics were available. A signal was considered significant when the posterior probability that the methylation site and the GWAS signal share the same causal variant exceeded 80% (PP4 >80%).

eQTM analysis

We further integrated methylation and gene expression data matched from the same patients to perform eQTM analysis, thus finding associations between gene expression and methylation levels of close methylation sites (<1 Mb between transcription start site and methylation site). We performed eQTM analysis tissue-specifically in low- (227 patients) and high-grade (127 patients) osteoarthritis cartilage, synovium (226 patients), and infrapatellar fat pad (45 patients) using the R package MatrixEQTL [15] (Supplementary Methods; Supplementary Table S1).

Effector gene analysis

To identify potential effector genes of GWAS risk signals, we overlaid colocalisation results with eQTM maps of the same tissues. More specifically, we tested whether methylation sites with a potential causal role in osteoarthritis (colocalisation posterior probability 'PP4' > .8) are significantly associated with a gene (eQTM q value < 0.05) in the same tissue.

To assess novelty, we tested whether identified likely effector genes have been found in a previous large meta-GWAS for osteoarthritis [2], which integrates 24 orthogonal lines of evidence and reports 700 effector genes (≥3 lines of evidence). If likely effector genes are within these 700, we regard them as confirmed; otherwise, as novel. We further used this effector gene analysis resource [2] to investigate whether mQTL signals have been colocalised with osteoarthritis GWAS risk signals before.

To assess the respective druggability of identified likely effector genes, we overlaid these with the OpenTarget (version 25.09) [20] database using the R package otargen (function: knownDrugsGeneQuery) [21] and filtered for drugs that completed clinical trial phase 2.

Data visualisation

We used the R packages ggplot2 (version 3.4.3) and ggpubr (version 0.4.0) to generate Figures 1, 2, and 3 (Supplementary Methods).

Patient and public involvement statement

There was no involvement of patients and the public in the design, conduct, reporting, or dissemination plans of this research.

RESULTS

Genome-wide mQTL maps in tissues from patients with primary osteoarthritis

We performed mQTL analysis to study the effect of common variants (MAF > 0.05) on methylation in low- (n = 289 patients) and high-grade osteoarthritis cartilage (n = 172), as well as in synovium (n = 249) and blood (n = 237). We found widespread associations (q value < 0.05) between genetic variants and close (<1 Mb; 'cis-mQTL') methylation sites in all tested tissues: low- (207,422 mQTL-targeted methylation sites; Fig 1A; most significant mQTL in Fig 1B) and high-grade cartilage (128,876; Fig 1C; most significant mQTL in Fig 1D), synovium (160,257; Fig 1E; most significant mQTL in Fig 1F) and blood (127,233; Fig 1G; most significant mQTL in Fig 1H).

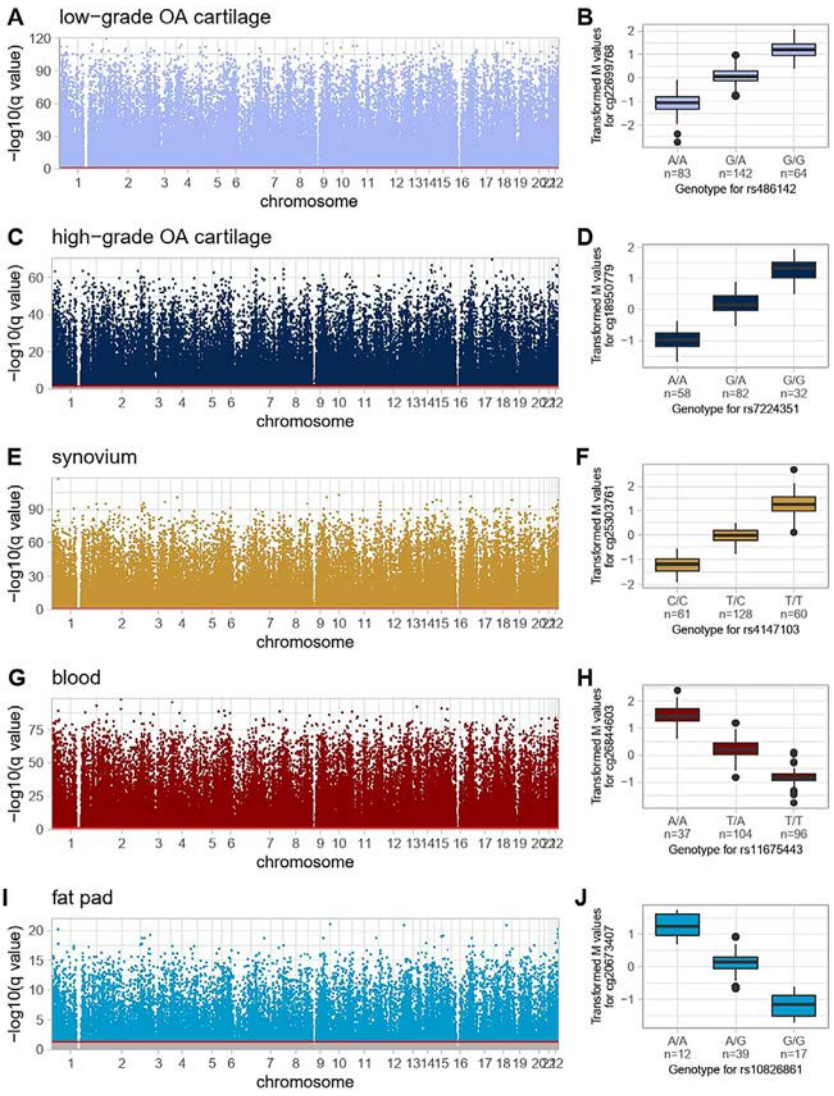

Figure 1. Methylation quantitative trait locus (mQTL) landscapes in cartilage, synovium, blood and fat pad in patients with osteoarthritis. The cis-mQTL maps in (A) low- and (C) high-grade osteoarthritis cartilage, as well as in (E) synovium, (G) blood and (I) fat pad in patients with osteoarthritis. Manhattan plots showing the negative log of the *q* value of the most significant association per methylation site across genetic variants in cis (<1 Mb distance to the tested methylation site). Quantitative trait locus (QTL)-targeted methylation sites (q value < 0.05) are coloured light blue (A), dark blue (C), yellow (E), red (G), and blue (I), otherwise dark grey. Red lines indicate genome-wide significance (q < 0.05). The boxplots exemplify mQTL signals by showing the most significant effects in (B) low-grade osteoarthritis crtilage (rs486142 on cg22699768, with beta = 1.27, SE = 0.02, *P* value = 3.59×10^{-142}), (D) high-grade osteoarthritis cartilage (rs7224351 on cg18950779, with beta = 1.21, SE = 0.03, *P* value = 2.40×10^{-89}), (F) synovium (rs4147103 on cg25303761, with beta = 1.36, SE = 0.02, *P* value = 6.35×10^{-140}), (H) blood (rs11675443 on cg26844603, with beta = −1.22, SE = 0.02, *P* value = 1.75×10^{-118}) and (J) fat pad (rs10826861 on cg20673407, with beta = −1.40, SE = 0.05, *P* value = 4.15×10^{-33}). Of note, the cis-mQTL fat pad map has been published previously [7], and Figures (I) and (J) were included in this earlier work. The boxplots represent the 25th, 50th, and 75th percentiles, and whiskers extend to 1.5 times the IQR. OA, osteoarthritis.

Furthermore, we have generated the first cis-mQTL map in infrapatellar fat pad samples (n = 68 patients; 35,948 cis-mQTL-targeted methylation sites; Fig 1I; most significant mQTL in Fig 1J), which was published previously [7].

In low- and high-grade cartilage as well as synovium, we found cis-mQTL-targeted methylation sites that were not identified in the previous largest mQTL maps [6] in these tissues (low-grade osteoarthritis cartilage, 162,314 of 207,422 quantitative trait locus (QTL)-targeted methylation sites; high-grade osteoarthritis cartilage, 99,818 of 128,876; synovium, 136,315 of 160,257), underlining the novelty of these QTL maps and ultimately the expanded regulatory landscape uncovered by these maps.

We performed follow-up comparative analyses by overlapping cis-mQTL-targeted methylation sites (q < 0.05) in low- and high-grade osteoarthritis cartilage, synovium, and fat pad, identifying signals that are tissue-specific and shared between joint tissues (Supplementary Note S1; Supplementary Fig S2).

We further tested for novel long-range effects of genetic variants on DNA methylation. We found trans-mQTL effects in low- (2836 trans-mQTL-targeted methylation sites; 439 and 2424 DNA methylation sites being targeted by long-range intrachromosomal (>5 Mb) and interchromosomal effects, respectively; $P < 1.82 \times 10^{-10}$; Supplementary Table S2) and high-grade osteoarthritis cartilage (1488 trans-mQTL-targeted methylation sites; 216 and 1279 DNA methylation sites being targeted by long-range intrachromosomal and interchromosomal effects, respectively; $P < 9.55 \times 10^{-11}$; Supplementary Table S3), synovium (1999 trans-mQTL-targeted methylation sites; 307 and 110 DNA methylation sites being targeted by long-range intrachromosomal and interchromosomal effects, respectively; $P < 1.28 \times 10^{-10}$; Supplementary Table S4), blood (1993 trans-mQTL-targeted methylation sites; 260 and 1746 DNA methylation sites being targeted by long-range intrachromosomal and interchromosomal effects, respectively; $P < 1.27 \times 10^{-10}$; Supplementary Table S5) and infrapatellar fat pad (191 trans-mQTL-targeted methylation sites; 25 and 166 DNA methylation sites being targeted by long-range intrachromosomal and interchromosomal effects, respectively; $P < 1.29 \times 10^{-11}$; Supplementary Table S6). Together, these results constitute the largest mQTL data sets for knee osteoarthritis to date and reveal QTL effects in both the short and long-distance ranges.

Genome-wide eQTM maps in tissues from patients with primary osteoarthritis

Next, we integrated DNA methylation with available gene expression data [12] from the same patient cohort and tissue types. We generated eQTM maps to associate methylation sites and expression levels of their proximal genes (<1 Mb) in low- (n = 227 patients) and high-grade osteoarthritis cartilage (n = 127 patients), as well as synovium (n = 226 patients) and infrapatellar fat pad (n = 45). In total, we found 3270 eQTM-targeted genes (q < 0.05) across joint tissues, which showed enrichments (FDR < 0.05) in 100 gene ontology (GO) terms

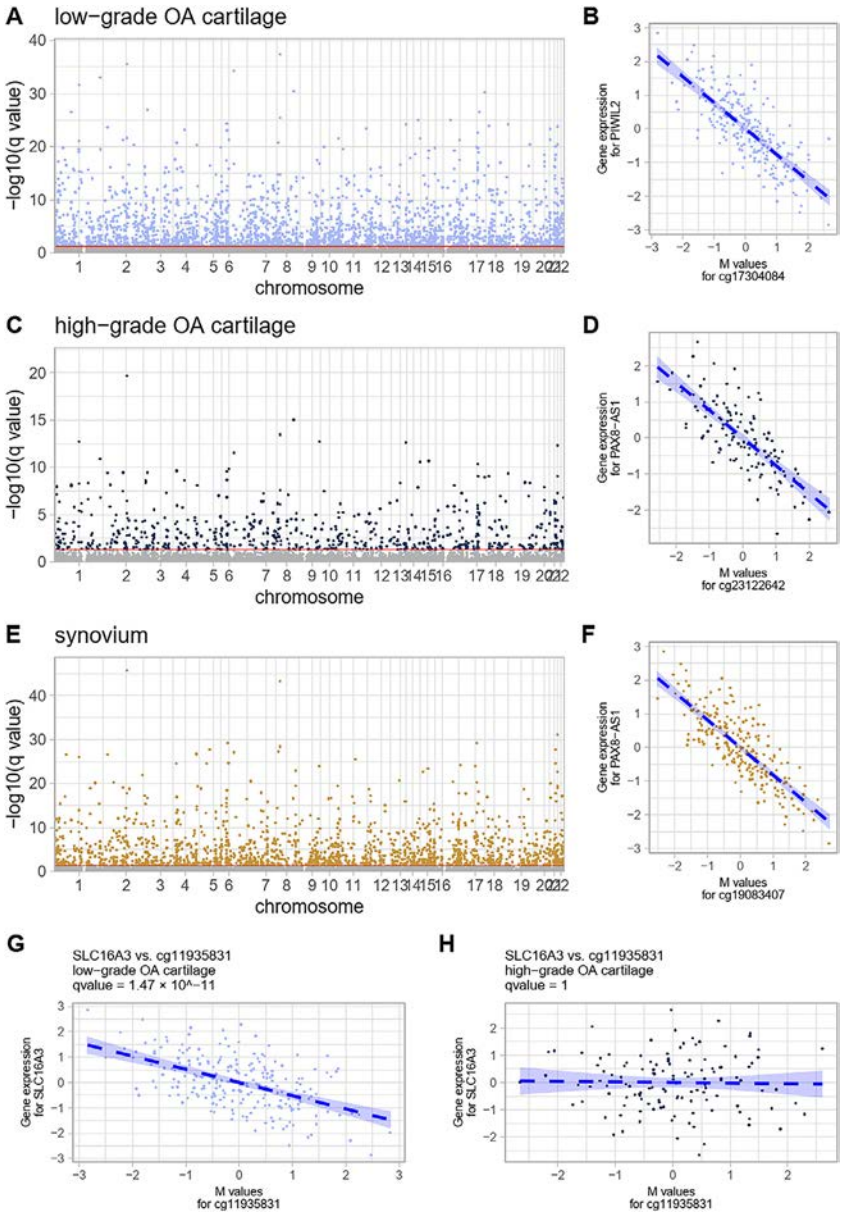

Figure 2. Expression quantitative trait methylation (eQTM) landscapes in cartilage and synovium. The eQTM maps and respective top signals in (A) low- and (C) high-grade osteoarthritis cartilage, as well as in (E) synovium. Manhattan plots showing the negative log of the q value of the most significant association per gene across all tested methylation sites in cis (<1 Mb distance to the tested gene transcription starting site). Methylation-associated genes are shown in light violet (A), dark violet (C), or yellow (E), otherwise dark grey. Red lines indicate genome-wide significance ($q < 0.05$). Scatterplots exemplify eQTM effects by showing the most significant associations between methylation and gene expression levels in (B) low-grade osteoarthritis cartilage (cg17304084 and *PIWIL2* with beta = −0.77, SE = 0.04, *P* value = 2.25×10^{-45}), (D) high-grade osteoarthritis cartilage (cg23122642 and *PAX8-AS1* with beta = −0.77, SE = 0.05, *P* value = 1.90×10^{-27}) and (F) synovium (cg19083407 and *PAX8-AS1* with beta = −0.81, SE = 0.04, *P* value = 1.83×10^{-53}). Furthermore, we show an example for a differential eQTM effect between cg11935831 and *SLC16A3* that is present in (G) low-grade osteoarthritis cartilage (beta = −0.52, SE = 0.06, *P* value = 7.26×10^{-17}, q value = 1.47×10^{-11}), but not (H) high-grade osteoarthritis cartilage (*P* value = .8, q value = 1). In Figures 2B, 2D, 2F, 2G, and 2H, the blue dashed line and shaded region visualise the regression line as well as its 95% CI, respectively. OA, osteoarthritis.

(Supplementary Note S2; Supplementary Table S7). By tissue, we identified genome-wide significant eQTM effects in low- (11,204 methylation sites associated with 2388 genes; Fig 2A; most significant eQTM in Fig 2B; Supplementary Table S8) and high-grade osteoarthritis cartilage (3116 methylation sites associated with 649 genes; Fig 2C; most significant eQTM in Fig 2D; Supplementary Table S9) as well as synovium (7620 methylation sites associated with 1661 genes; Fig 2E; most significant eQTM in Fig 2F; Supplementary Table S10). The fat pad eQTM map revealed effects at nominal significance ($P < .05$) (Supplementary Note S3; Supplementary Fig S3; Supplementary Table S11). To biologically characterise eQTM-targeted genes in a tissue-specific manner, we performed GO enrichment analysis separately in low-grade osteoarthritis cartilage (116 GO terms with FDR < 0.05; Supplementary Table S12) and high-grade osteoarthritis cartilage (5 GO terms with FDR < 0.05; Supplementary Table S13), as well as in synovium (4 GO terms with FDR < 0.05; Supplementary Table S14), and found osteoarthritis-linked terms in cartilage (including terms related to extracellular matrix or innervation) and synovium (including terms related to the cytoskeleton or cell development), suggesting effects between DNA methylation and genes contributing to disease-relevant pathways in primary joint tissues (Supplementary Note S4).

Comparing these eQTM maps between tested osteoarthritis tissues revealed eQTM effects that are present in 1 but not the other tissue type ($q < 0.05$ in 1 tissue and $P > .05$ in the other). For example, we found 4166 eQTM effects (involving 1600 genes) that are present in low-grade osteoarthritis cartilage but not high-grade osteoarthritis cartilage (exemplified using the eQTM effect between *SLC16A3* and cg11935831 being present in low- but not high-grade osteoarthritis cartilage in Fig 2G,H) (Supplementary Table S15). Vice versa, we found 253 eQTM effects (involving 188 genes) in high- but not low-grade osteoarthritis cartilage (Supplementary Table S16). In total, we found 1726 genes that were targeted by a differential eQTM effect between low- and high-grade osteoarthritis cartilage, which were enriched (FDR < 0.05) in 93 GO terms (Supplementary Note S5; Supplementary Table S17). These differences between cartilage sample types suggest eQTM effects are switched on/off during cartilage degeneration. Similarly, we found differences between the synovium and low-grade (3300 eQTM effects involving 1140 genes present in synovium but not low-grade cartilage; 5593 effects for 1626 genes vice versa; 2449 genes involved in total) as well as between the synovium and high-grade osteoarthritis cartilage (4329 eQTM effects involving 1328 genes present in synovium but not high-grade cartilage;

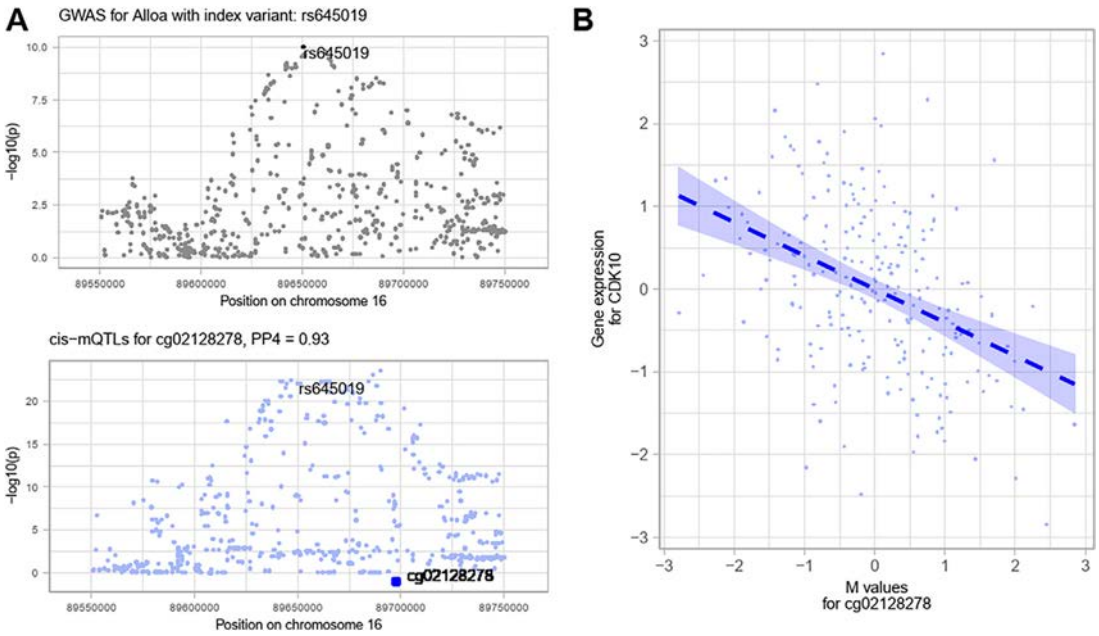

Figure 3. Highlights the likely effector gene *CDK10* in low-grade osteoarthritis cartilage. (A) The methylation quantitative trait locus (mQTL) signal for low-grade osteoarthritis cartilage at cg02128278 colocalises with a GWAS signal (index variant, rs645019) for osteoarthritis at any site (posterior probability, 92.8%). (B) Methylation levels of cg02128278 are negatively associated with *CDK10* expression in low-grade osteoarthritis cartilage (beta, −0.40; SE, 0.06; *P* value, 2.90^{-10}). This exemplifies linking GWAS risk signals to a likely effector gene using methylation. In Figure 3B, the blue dashed line and shaded region visualise the regression line as well as its 95% CI, respectively. GWAS, genome-wide association studies.

964 effects for 335 genes vice versa; 1365 genes involved in total) (Supplementary Tables S18-21). Enrichment analysis found 95 (FDR < 0.05) enriched GO terms in genes targeted by a differential eQTM between cartilage and synovium (Supplementary Note S6; Supplementary Tables S22 and S23). These insights suggest tissue-specific effects between DNA methylation and gene expression in these biological processes.

Furthermore, we found a small number of eQTM effects to be significant in cartilage as well as synovium but show different directions of effect (synovium vs low-grade osteoarthritis cartilage, 50 eQTM effects involving 33 genes; synovium vs high-grade osteoarthritis cartilage, 14 eQTM effects involving 10 genes), suggesting tissue-specific effects between DNA methylation and gene expression.

Together, these results suggest widespread genome-wide effects between DNA methylation and gene expression in knee cartilage and synovium tissue, as well as disease-stage-specific effects.

Linking methylation sites and osteoarthritis GWAS signals

We performed colocalisation analysis by considering GWAS risk signals [2] for osteoarthritis at any site, knee osteoarthritis, and total knee replacement, to identify methylation sites that potentially underlie risk variant effects on osteoarthritis. Applying colocalisation between mQTL and osteoarthritis GWAS risk loci detected 1455 methylation sites with a putative causal role in osteoarthritis. We found osteoarthritis-linked methylation sites in low- (n = 736 methylation sites, colocalising with 166 GWAS signals; Supplementary Table S24) and high-grade osteoarthritis cartilage (n = 473 methylation sites, colocalising with 141 GWAS signals; Supplementary Table S25), synovium (549 methylation sites, colocalising with 144 GWAS signals; Supplementary Table S26), blood (n = 347 methylation sites, colocalising with 123 GWAS signals; Supplementary Table S27) and infrapatellar fat pad (n = 104 methylation sites, colocalising with 64 GWAS signals; Supplementary Table S28). We further found that the majority of these detected methylation sites have not been linked with osteoarthritis GWAS signals in the respective tissue previously [6,7] (low-grade cartilage, mQTL signals from 728 of 736 methylation sites have not been colocalised with osteoarthritis GWAS signals previously; high-grade osteoarthritis cartilage, 469 of 473 methylation sites; synovium, 543 of 549 methylation sites; infrapatellar fat pad, 95 of 104 methylation sites), highlighting the novelty of these colocalisation results. Together, these colocalisation results suggest methylation sites that may mediate genetic osteoarthritis risk in affected tissues.

Resolution of GWAS signals

Next, we tested whether methylation sites with a likely causal role in osteoarthritis (through colocalisation) show genome-wide significant associations with genes (through look-up in the eQTM map of the same tissue). Together, this would suggest molecular mechanisms through which genetic risk signals might exert their osteoarthritis-promoting effects, namely through colocalised methylation sites and methylation-associated effector genes. In total, we identified 50 likely effector genes for GWAS risk signals, of which 31 (62%) were reported in the largest osteoarthritis GWAS [2] to date, and 19 (38%) are novel.

Stratified by tissue, we identified 44 likely effectors in genes of low-grade osteoarthritis cartilage (Supplementary Table S29). Of these 44 genes, 29 were suggested as likely effector genes of genetic variants previously [2], whereas 15 genes are novel. In high-grade osteoarthritis cartilage, we found 8 likely effector genes (Supplementary Table S30). Of these 8 genes, 4 were found as effector genes of genetic variants previously [2], whereas 4 are novel. In the synovium, we detected 13 likely effector genes (Supplementary Table S31). Of these, 3 were identified previously [2], whereas 10 genes are novel. Together, by associating putative osteoarthritis-related methylation sites with genes, we can link GWAS risk signals to likely effector genes. We further compared novel (Supplementary Fig S4) and

confirmed (Supplementary Fig S5) likely effector genes across tissues, thus identifying tissue-specific and shared signals (Supplementary Note S7).

The 31 previously identified effector genes include previously osteoarthritis-associated genes, such as *ALD1A2* [6], *WWP2* [22], or *SMAD3* [23]. For 13 of 31 previously identified effector genes, we, for the first time, suggest mQTL signals that colocalise with osteoarthritis GWAS risk signals, thus providing additional mechanistic insights for these osteoarthritis-relevant genes. These genes include *CYP19A1*, a regulator of the osteoarthritis-linked hormone oestrogen [23]. More specifically, we identified 2 methylation sites in low-grade osteoarthritis cartilage for which mQTL signals colocalise with GWAS risk signals (eg, methylation site cg02325664 with a knee osteoarthritis GWAS risk signal with 95.0% posterior probability and methylation site cg00004322 colocalising with a total knee replacement GWAS risk signal with 97.8% posterior probability, both GWAS signals with lead variant rs146939415 and risk allele C) and that are associated with its *CYP19A1* gene expression levels (cg02325664 with beta, 0.45; *P*, 8.95×10^{-13}; cg00004322 with beta, −0.27; *P*, 4.51×10^{-05}). This proposes a contributing role of these methylation sites in the disease-promoting effect of genetic risk loci through *CYP19A1*.

Similarly, for 17 of 19 novel, likely effector genes (including *GDNF*, which encodes a pain-related neurotrophic factor [24]; *EXOSC6*, component of the RNA exosome complex; *CDK10*, cyclin-dependent kinase), we found for the first time mQTL signals colocalising with osteoarthritis GWAS risk signals. Thus, by linking these GWAS risk signals to DNA methylation sites (through colocalisation analysis) and DNA methylation sites to gene expression (through eQTM association analysis), we suggest, for the first time in these likely effector genes, enhanced molecular insights into how epigenetics and transcriptomics might mediate the osteoarthritis-promoting effect of genetic risk loci in primary tissues.

For 5 (*ZNF641, PDPR, PAM, EXOSC6,* and *CDK10*) of these novel likely effector genes, a previous GWAS study reported 2 lines of evidence supporting their relevance to osteoarthritis, which we now supplement with epigenetic insights.

Together, integrating GWAS, mQTL, and eQTM maps enables additional mechanistic insights into previously identified osteoarthritis effector genes and reveals novel candidates.

To estimate translational potentials, we further performed druggability analysis for the 50 likely effector genes and found links to drugs with at least 1 completed clinical trial phase 2 for 5 genes [20] (Supplementary Table S32). These 5 genes comprise *CDK10*, for which a previous GWAS [2] found a close genetic osteoarthritis risk signal. We identified *CDK10* DNA methylation in low-grade osteoarthritis cartilage for which mQTL signals (for cg02128278, 92.8% posterior probability, Fig 3A; cg08616182, 97.5% posterior probability) colocalise with a GWAS risk signal for osteoarthritis at any site (lead variant, rs645019; risk allele, T). In addition, we associated *CDK10* methylation and gene expression levels (Fig 3B). *CDK10* is involved in the cell cycle, has been associated with cell proliferation [25], and contributes to the regulation of actin cytoskeleton organisation [26]. Of note, *CDK10* is targeted by AT-7519, a drug that has completed clinical trial phase 2. Together, these results suggest translational potential for these likely effector genes.

DISCUSSION

This study provided the largest genome-wide maps of genetic effects on DNA methylation (mQTL maps) in low- and high-grade osteoarthritis cartilage as well as synovium and, for the first time, reports long-range (trans) effects between genetic variants and methylation sites in osteoarthritis tissues. We presented the largest maps of associating DNA methylation sites and genes (eQTM maps) in cartilage and the first in synovium. Integrating osteoarthritis GWAS results, mQTL, and eQTM maps revealed a multitude of methylation sites with a potential causal role in osteoarthritis, as well as 50 likely effector genes in a tissue-specific manner.

We identified novel mQTL, extending our understanding of the genetic effects on the epigenetic profile. Colocalisation of mQTL with GWAS risk signals [2] finds novel methylation sites that putatively mediate the genetic risk of osteoarthritis risk loci, highlighting epigenetic marks that contribute to osteoarthritis risk in primary tissues. We linked these osteoarthritis-related methylation sites to 19 novel likely effector genes, which have not been reported by the largest genetic study for osteoarthritis to date [2]. These novel effector genes include *CDK10*, which encodes a part of the protein kinase CDK10/Cyclin M, which regulates actin cytoskeleton organisation [26]. *EXOSC6* encodes a subunit of the RNA exosome complex, which regulates RNA-processing and RNA-decay functions within the cell [27]. The RNA exosome complex has also been implicated in regulating cytokine production and thereby modulating innate immune signalling and inflammatory responses [28]. Furthermore, depletion of the RNA exosome complex has been linked to disrupted cellular homeostasis and cell senescence [29]. Furthermore, GDNF is a neurotrophic factor that has been linked to skeletal pain in a rat model [24]. More specifically, bone pain involves activation and sensitisation of nonpeptidergic neurones through the GDNF/GFRα1 signalling pathway [24], suggesting a potential osteoarthritis pain-related role.

We suggest that these genes contribute to osteoarthritis pathogenesis through genetically driven changes in DNA methylation and gene expression in disease-relevant tissues.

Our integrative, methylation-focused approach further confirms 31 previously reported effector genes [2], including *ALDH1A2* (linked to the retinoic acid signalling pathway, which regulated genes involved in skeletal [30], organ and limb development [31]), *SMAD3* (mediates the signalling of the osteoarthritis-relevant transforming growth factor β pathway that contributes to skeletal development, cartilage and bone formation, inflammation, remodelling of the extracellular matrix, and changes of the synovial tissue [2]) and *WWP2* (regulator in chondrocytes [22]), highlighting that some findings confirm previous results.

Of note, overlapping the 50 effector genes across tissues revealed tissue-shared as well as tissue-specific signals, suggesting that effector genes mediate genetic risk loci in a tissue-specific manner as well as across joint tissues.

Genome-wide methylation studies in osteoarthritis primary tissues [7,32] often apply rigid, distance-based information, annotating methylation sites to the closest genes for further interpretation, although previous eQTM maps in human tissues found associations between DNA methylation sites and genes to be partly tissue-specific [33] or across moderate distances (per tissue median distance between CpG site and gene transcription start site in Oliva et al [33]: 119-157 kb). Therefore, we generate eQTM maps of tissue (cartilage and synovium) and disease stage (low- and high-grade osteoarthritis cartilage) specifically and annotate methylation sites to genes.

Furthermore, these eQTM maps reveal enrichments of DNA methylation-associated genes in osteoarthritis-relevant GO terms in cartilage as well as in synovium, suggesting that regulatory effects between DNA methylation sites and genes play a role in osteoarthritis-relevant pathways in primary joint tissues.

This study focuses on individuals of European ancestry; it does not reflect global genetic diversity. There is a need to

extend omics studies to diverse populations, particularly including cohorts of non-European ancestry, to enhance maps of genetic and molecular variation and ensure the general applicability of findings [34].

Our study presented the largest genome-wide DNA methylation profiles across tissues and disease stages. We described the effects of genetics on DNA methylation as well as the relationship between DNA methylation and gene expression. We enabled novel insights into the important role of DNA methylation in osteoarthritis and, ultimately, into molecular mechanisms underpinning genetic risk loci. We provided molecular maps of primary tissues in osteoarthritis patients, which represent relevant resources for the musculoskeletal disease research community and beyond.

Acknowledgements

We acknowledge the technical support of the Core Facility Genomics at Helmholtz Munich. We thank Dr Inti Alberto de la Rosa Velasquez, Dr Peter Lichtner, Susanne Wittmann, and Dr Thomas Walzthöni for help with DNA methylation and whole-genome sequencing data generation, as well as whole-genome sequencing data preprocessing.

Contributors

EZ and JMW designed the study. JMW, KMS, and DS collected the clinical data. GK preprocessed the gene expression data. PK, OSS, GK, MT, and NB analysed the data. PK and EZ interpreted the results and drafted the manuscript. All authors reviewed, edited, and approved the final manuscript.

Funding

This work was funded by the Wellcome Trust (206194).

Competing interests

The authors declare no competing interests.

Patient consent for publication

Not applicable.

Ethics approval

This work was approved by Oxford NHS REC C (10/H0606/20, 15/SC/0132 and 20/SC/0141), and samples were collected under Human Tissue Authority license 12182, Sheffield Musculoskeletal Biobank, University of Sheffield, UK. Before participating in the study, all osteoarthritis-affected individuals provided written, informed consent.

Provenance and peer review

Not commissioned; externally peer reviewed.

Data availability statement

Full summary statistics can be obtained online through the MSK portal (http://mskkp.org). All software used in this study is available from free repositories or manufacturers as referenced in the Methods section.

Supplementary materials

Supplementary material associated with this article can be found in the online version at doi:10.1016/j.ard.2026.01.020.

REFERENCES

[1] GBD 2021 Osteoarthritis Collaborators. Global, regional, and national burden of osteoarthritis, 1990-2020 and projections to 2050: a systematic analysis for the Global Burden of Disease Study 2021. Lancet Rheumatol 2023;5:e508–22.
[2] Hatzikotoulas K, Southam L, Stefansdottir L, Boer CG, McDonald ML, Pett JP, et al. Translational genomics of osteoarthritis in 1,962,069 individuals. Nature 2025;641:1217–24.
[3] Katsoula G, Lawrence JEG, Arruda AL, Tutino M, Balogh P, Southam L, et al. Primary cartilage transcriptional signatures reflect cell-type-specific molecular pathways underpinning osteoarthritis. Am J Hum Genet 2024;111:2735–55.
[4] Bittner N, Shi C, Zhao D, Ding J, Southam L, Swift D, et al. Primary osteoarthritis chondrocyte map of chromatin conformation reveals novel candidate effector genes. Ann Rheum Dis 2024;83:1048–59.
[5] Steinberg J, Southam L, Roumeliotis TI, Clark MJ, Jayasuriya RL, Swift D, et al. A molecular quantitative trait locus map for osteoarthritis. Nat Commun 2021;12:1309.
[6] Kreitmaier P, Suderman M, Southam L, Coutinho de Almeida R, Hatzikotoulas K, Meulenbelt I, et al. An epigenome-wide view of osteoarthritis in primary tissues. Am J Hum Genet 2022;109:1255–71.
[7] Kreitmaier P, Park YC, Swift D, Gilly A, Wilkinson JM, Zeggini E. Epigenomic profiling of the infrapatellar fat pad in osteoarthritis. Hum Mol Genet 2024;33:501–9.
[8] Dunn CM, Sturdy C, Velasco C, Schlupp L, Prinz E, Izda V, et al. Peripheral blood DNA methylation-based machine learning models for prediction of knee osteoarthritis progression: biologic specimens and data from the Osteoarthritis Initiative and Johnston County Osteoarthritis Project. Arthritis Rheumatol 2023;75:28–40.
[9] Arruda AL, Katsoula G, Chen S, Reimann E, Kreitmaier P, Zeggini E. The genetics and functional genomics of osteoarthritis. Annu Rev Genomics Hum Genet 2024;25:239–57.
[10] Mainil-Varlet P, Aigner T, Brittberg M, Bullough P, Hollander A, Hunziker E, et al. Histological assessment of cartilage repair: a report by the Histology Endpoint Committee of the International Cartilage Repair Society (ICRS). J Bone Joint Surg Am 2003 85-A Suppl 2:45-57.
[11] Min JL, Hemani G, Davey Smith G, Relton C, Suderman M. Meffil: efficient normalization and analysis of very large DNA methylation datasets. Bioinformatics 2018;34:3983–9.
[12] Katsoula G, Arruda AL, Tutino M, Reimann E, Kreitmaier P, Shah KM, et al. Transcriptome analysis in osteoarthritis primary tissues identifies high-confidence effector genes. medRxiv 2024 12.04.24318411 [Preprint]. 2025 [cited 2025 Oct 4]: [46 p.]. Available from: https://www.medrxiv.org/content/10.1101/2024.12.04.24318411v2.
[13] Stegle O, Parts L, Piipari M, Winn J, Durbin R. Using probabilistic estimation of expression residuals (PEER) to obtain increased power and interpretability of gene expression analyses. Nat Protoc 2012;7:500–7.
[14] Ongen H, Buil A, Brown AA, Dermitzakis ET, Delaneau O. Fast and efficient QTL mapper for thousands of molecular phenotypes. Bioinformatics 2016;32:1479–85.
[15] Shabalin AA. Matrix eQTL: ultra fast eQTL analysis via large matrix operations. Bioinformatics 2012;28:1353–8.
[16] Freimann K, Brümmer A, Warmerdam R, Rupall TS, Hernández-Ledesma AL, Chiou J, et al. Trans-eQTL mapping prioritises USP18 as a negative regulator of interferon response at a lupus risk locus. Nat Commun 2025;16:8795.
[17] Võsa U, Claringbould A, Westra HJ, Bonder MJ, Deelen P, Zeng B, et al. Large-scale cis- and trans-eQTL analyses identify thousands of genetic loci and polygenic scores that regulate blood gene expression. Nat Genet 2021;53:1300–10.
[18] Storey JD, Tibshirani R. Statistical significance for genomewide studies. Proc Natl Acad Sci U S A 2003;100:9440–5.
[19] Giambartolomei C, Vukcevic D, Schadt EE, Franke L, Hingorani AD, Wallace C, Plagnol V. Bayesian test for colocalisation between pairs of genetic association studies using summary statistics. PLoS Genet 2014;10:e1004383.
[20] Ochoa D, Hercules A, Carmona M, Suveges D, Gonzalez-Uriarte A, Malangone C, et al. Open Targets Platform: supporting systematic drug-target identification and prioritisation. Nucleic Acids Res 2021;49:D1302–10.
[21] Feizi A, otargen Ray K. GraphQL-based R package for tidy data accessing and processing from Open Targets Genetics. Bioinformatics 2023;39:btad441.

[22] Mokuda S, Nakamichi R, Matsuzaki T, Ito Y, Sato T, Miyata K, et al. Wwp2 maintains cartilage homeostasis through regulation of Adamts5. Nat Commun 2019;10:2429.
[23] Riancho JA, García-Ibarbia C, Gravani A, Raine EV, Rodríguez-Fontenla C, Soto-Hermida A, et al. Common variations in estrogen-related genes are associated with severe large-joint osteoarthritis: a multicenter genetic and functional study. Osteoarthritis Cartilage 2010;18:927–33.
[24] Nencini S, Ringuet M, Kim DH, Greenhill C, Ivanusic JJ. GDNF, neurturin, and artemin activate and sensitize bone afferent neurons and contribute to inflammatory bone pain. J Neurosci 2018;38:4899–911.
[25] Guen VJ, Gamble C, Lees JA, Colas P. The awakening of the CDK10/cyclin M protein kinase. Oncotarget 2017;8:50174–86.
[26] Guen VJ, Gamble C, Perez DE, Bourassa S, Zappel H, Gärtner J, et al. STAR syndrome-associated CDK10/cyclin M regulates actin network architecture and ciliogenesis. Cell Cycle 2016;15:678–88.
[27] Basu U, Meng FL, Keim C, Grinstein V, Pefanis E, Eccleston J, et al. The RNA exosome targets the AID cytidine deaminase to both strands of transcribed duplex DNA substrates. Cell 2011;144:353–63.
[28] Blin J, Fitzgerald KA. Perspective: the RNA exosome, cytokine gene regulation and links to autoimmunity. Cytokine 2015;74:175–80.
[29] Han X, Xing L, Hong Y, Zhang X, Hao B, Lu JY, et al. Nuclear RNA homeostasis promotes systems-level coordination of cell fate and senescence. Cell Stem Cell 2024;31:694–716 e11.
[30] Underhill TM, Weston AD. Retinoids and their receptors in skeletal development. Microsc Res Tech 1998 Oct 15;43:137–55.
[31] Cunningham TJ, Duester G. Mechanisms of retinoic acid signalling and its roles in organ and limb development. Nat Rev Mol Cell Biol 2015;16:110–23.
[32] Kreitmaier P, Swift D, Wilkinson JM, Zeggini E. Epigenomic differences between osteoarthritis grades in primary cartilage. Osteoarthritis Cartilage 2024;32:1126–33.
[33] Oliva M, Demanelis K, Lu Y, Chernoff M, Jasmine F, Ahsan H, et al. DNA methylation QTL mapping across diverse human tissues provides molecular links between genetic variation and complex traits. Nat Genet 2023;55:112–22.
[34] Arruda AL, Morris AP, Zeggini E. Advancing equity in human genomics through tissue-specific multi-ancestry molecular data. Cell Genom 2024;4:100485.

Ann Rheum Dis 85 (2026) 1646–1655

Contents lists available at ScienceDirect

Annals of the Rheumatic Diseases

journal homepage: https://www.sciencedirect.com/journal/annals-of-the-rheumatic-diseases

Crystal disease

Musculoskeletal ultrasound findings in people with asymptomatic hyperuricemia: baseline analysis from the Transitions in Gout Research (TIGER) study using the OMERACT gout ultrasound semiquantitative scoring system

Sarah Stewart[1], Gregory D. Gamble[1], William J. Taylor[2], Andrew Harrison[2], Tony R. Merriman[3,4], Borislav Mihov[1], Anne Horne[1], Isabel Su[1], Adwoa Dansoa Tabi-Amponsah[1], Lisa K. Stamp[5,6], Janine Haslett[5], Tristan Pascart[7], Mariano Andrés[8], Maria-Luisa Peral-Garrido[9], Tuhina Neogi[10], Eleonora Norkuviene[11], Janitzia Vazquez-Mellado[12], John F. Fitzgerald[13], Lene Terslev[14,15], Hilde Berner Hammer[16,17], Till Uhlig[16,17], Maria-Antonietta D'Agostino[18,19], Julia Martin[20], Mingshu Sun[21], Changgui Li[21], Nicola Dalbeth[1,20,*]

[1] *Department of Medicine, University of Auckland, Auckland, New Zealand*
[2] *Department of Medicine, University of Otago Wellington, Wellington, New Zealand*
[3] *Department of Microbiology and Immunology, University of Otago Dunedin, Dunedin, New Zealand*
[4] *Heersink School of Medicine, University of Alabama at Birmingham, Birmingham, Alabama, United States*
[5] *Department of Medicine, University of Otago Christchurch, Christchurch, New Zealand*
[6] *Health New Zealand-Te Whatu Ora, Wellington, New Zealand*
[7] *Department of Rheumatology, Lille Catholic University, Lille, France*
[8] *Department of Rheumatology, Dr. Balmis General University Hospital, Miguel Hernández University; Alicante Institute for Health and Biomedical Research (ISABIAL), Alicante, Spain*
[9] *Rheumatology Section, Vinalopo University Hospital, Elche, Spain*
[10] *Department of Clinical Epidemiology Research and Training, Boston University School of Medicine, Boston, Massachusetts, United States*
[11] *Rheumatology Department, Lithuanian University of Health Sciences, Kaunas, Lithuania*
[12] *Department of Rheumatology, Hospital General de México, Mexico City, Mexico*
[13] *School of Medicine, UCLA Health, Los Angeles, California, USA*
[14] *Copenhagen Center for Arthritis Research, Rigshospitalet, Glostrup, Denmark*
[15] *Department of Clinical Medicine, University of Copenhagen, Denmark*
[16] *Department of Rheumatology, Center for Treatment for Rheumatic and Musculoskeletal Diseases (REMEDY), Diakonhjemmet Hospital, Oslo, Norway*
[17] *Department of Clinical Medicine, Faculty of Medicine, University of Oslo, Oslo, Norway*
[18] *Division of Rheumatology - Fondazione Policlinico Universitario A. Gemelli IRCCS, Rome, Italy*
[19] *Division of Rheumatology, Università Cattolica del Sacro Cuore, Rome, Italy*
[20] *Te Toka Tumai Auckland, Health New Zealand – Te Whatu Ora, Auckland, New Zealand*
[21] *The Affiliated Hospital of Qingdao University, Qingdao University, Qingdao, China*

*Correspondence to Professor Nicola Dalbeth, Department of Medicine, Faculty of Medical and Health Sciences, University of Auckland, Auckland, New Zealand.
E-mail address: n.dalbeth@auckland.ac.nz (N. Dalbeth).
Handling editor Josef Smolen.

https://doi.org/10.1016/j.ard.2026.03.021

ARTICLE INFO

Article history:
Received 9 November 2025
Received in revised form 2 March 2026
Accepted 20 March 2026

ABSTRACT

Objectives: The objective of this study was to describe the musculoskeletal ultrasound features of asymptomatic hyperuricaemia using the Outcome Measures in Rheumatology (OMERACT) gout semiquantitative scoring system and examine relationships between ultrasound lesions.
Methods: Participants with serum urate ≥0.48 mmol/L, no previous gout flares, and no subcutaneous tophi (n = 269) underwent a standardised ultrasound examination of bilateral patellar tendons, knee, first and second metatarsophalangeal joints (MTPs), and Achilles tendon. Double contour, tophus, and aggregates were scored according to the OMERACT gout ultrasound semiquantitative scoring system (0-3, with score >1 indicating a definite finding), together with erosion, synovial hypertrophy, and power Doppler activity in the scanned joints. In addition to elementary lesion sum scores, the sum of the semiquantitative double contour scores and tophus scores was calculated for each participant (semiquantitative double contour-tophus [SQDT] sum score, maximum 60).
Results: There were 38.7% of participants with at least 1 definite double contour and/or tophus on ultrasound. The median (IQR) SQDT sum score was 2 (0-4). Double contour scores contributed most to the SQDT sum score, followed by first MTP tophus scores. Double contour was associated with synovial hypertrophy at the first and second MTP, and tophus was associated with erosion, synovial hypertrophy, and power Doppler activity at the first MTP.
Conclusions: Definite ultrasound features of gout can be identified in more than one-third of people with asymptomatic hyperuricemia. However, the amount of monosodium urate crystal deposition on ultrasound, assessed using the OMERACT gout ultrasound scoring system, is low. In asymptomatic hyperuricemia without clinical evidence of gout, ultrasound features of gout are associated with subclinical joint damage and inflammation.

WHAT IS ALREADY KNOWN ON THIS TOPIC

- Asymptomatic hyperuricemia is the key precursor to the development of gout.
- Prior studies have reported that ultrasound findings of gout may be present in people with asymptomatic hyperuricemia.

WHAT THIS STUDY ADDS

- We demonstrate that definite musculoskeletal ultrasound features of gout can be identified in more than one-third of people with asymptomatic hyperuricemia.
- However, the amount of monosodium urate (MSU) crystal deposition on ultrasound, assessed using the Outcome Measures in Rheumatology (OMERACT) gout ultrasound scoring system, is low.
- We also demonstrate that in asymptomatic hyperuricemia, ultrasound features of gout are associated with subclinical joint damage and inflammation.

HOW THIS STUDY MIGHT AFFECT RESEARCH, PRACTICE OR POLICY

- This study provides reference data to inform the interpretation of musculoskeletal ultrasound findings in asymptomatic hyperuricemia.
- The study indicates that joint damage and inflammation due to MSU crystal deposition can occur before the development of clinically evident gout in some people with asymptomatic hyperuricemia.
- The low OMERACT ultrasound scores suggest that a threshold of MSU crystal deposition may be required for the development of symptomatic gout, and this will be tested in the long-term follow-up of Transitions in Gout Research study participants.

INTRODUCTION

Gout is caused by monosodium urate (MSU) crystal deposition, which primarily occurs within joints, tendons, and periarticular tissues [1,2]. Asymptomatic hyperuricemia is the key precursor to the development of gout, and there is a concentration-dependent relationship of urate with both MSU crystal formation and incident gout [3–5].

In gout, musculoskeletal ultrasound allows visualisation of the 3 imaging domains of gout: MSU crystal deposition, structural damage, and inflammation [6]. On ultrasound, MSU crystal deposition is visualised most commonly as double contour signs, tophi, and aggregates [7,8]. Prior ultrasound studies have reported that these findings may be present in people with asymptomatic hyperuricemia; 14% to 59% of people with asymptomatic hyperuricemia have ultrasound evidence of MSU crystal deposition [9–20].

The Outcome Measures in Rheumatology (OMERACT) ultrasound working group has developed definitions for ultrasound elementary gout lesions [8,21], together with a semiquantitative ultrasound scoring system for gout [22]. This semiquantitative scoring system was responsive to treatment in people with gout on urate-lowering therapy, with a combined score that summed the semiquantitative double contour scores and tophus scores (SQDT score) found to be the most responsive measure [22].

The aim of this study was to describe the ultrasound features of asymptomatic hyperuricemia using the OMERACT gout semiquantitative scoring system, and to examine relationships between ultrasound lesions using this scoring system.

METHODS

Study design

Baseline visit data from the Transitions in Gout Research (TIGER) study, a multisite prospective cohort study, were analysed. The full protocol of the TIGER study has been published [23], and data describing perceptions of hyperuricemia at the baseline visit have also been reported [24]. In brief, this is a prospective, international, multicentre study of 270 people with

asymptomatic hyperuricemia that aims to understand the risk factors for developing gout in people who already have an increased risk of gout due to elevated serum urate concentrations (serum urate of ≥ 0.48 mmol/L [8 mg/dL]). Baseline visits occurred between June 2019 and August 2024. Participating sites are in Auckland, Wellington and Christchurch (New Zealand), Lille (France), Alicante (Spain), Kaunas (Lithuania), Los Angeles (USA), Qingdao (China), and Mexico City (Mexico). The study was approved by the New Zealand Ministry of Health Southern Health and Disability Ethics Committee (MEC/05/10/130AM16) and by the local ethics committee/institutional review board for each participating centre. All participants provided written informed consent before enrolment in the study. The study was registered with the Australia and New Zealand Clinical Trials Registry (ACTRN12619000915156).

Study participants

Participants were recruited from primary and secondary care, together with public advertising. The inclusion criteria were: serum urate of ≥0.48 mmol/L (8 mg/dL); no current or previous clinical symptoms of gout (including flares or clinically apparent tophi); aged between 18 and 80 years; and able to provide informed consent. The exclusion criteria were: estimated glomerular filtration rate (eGFR) < 30 mL/min/1.73 m² or on renal replacement therapy; serious illness with poor prognosis less than 5 years; other forms of inflammatory arthritis; plans to shift out of area in the next 5 years; previous synovial fluid analysis showing MSU crystals; the presence of subcutaneous tophi; and use of urate-lowering therapy (allopurinol, probenecid, benzbromarone, and febuxostat), canakinumab, or colchicine.

Baseline study visits

The following information was obtained at the baseline visit: demographic and medical history, anthropomorphic measures, swollen (/66) and tender (/68) joint counts, laboratory tests (serum urate and creatinine, with eGFR calculated using the Modification of Diet in Renal Disease formula [25]), questionnaires (including pain score over the last week, using 100 mm visual analogue scale), and bilateral plain weight bearing anterior-posterior radiographs of the feet. The radiographs were scored by a central reader who was blinded to all clinical details, including ultrasound scores for erosion and joint space narrowing according to the Sharp-van der Heijde scoring system modified for gout [26], together with the Kellgren-Lawrence grading scale [27] at each metatarsophalangeal joint (MTP) and the big toe interphalangeal joint. Plain radiographs were available for 240 participants, as 1 site was unable to obtain radiographs due to ethics committee restrictions on medical radiation exposure in asymptomatic individuals.

Ultrasound protocol and scoring

The following sites were scanned by ultrasound: bilateral first and second MTPs (with the feet resting on the examination couch, dorsal longitudinal scanning, from side to side for synovitis, tophi and double contour, and longitudinal scanning of the medial first MTP for tophi and erosions), knee (dorsal scanning of a moderately flexed [suprapatellar recess] or maximally flexed [for double contour, with dorsal longitudinal or transverse scanning of condyles, medial and lateral parapatellar recess]), patellar tendon (entire tendon scanned, recorded as proximal and distal half of tendon from the midpoint of the tendon), and Achilles tendon (entire tendon scanned, recorded as proximal and distal half of tendon from the midpoint of the tendon). Double contour, erosion, synovial hypertrophy and power Doppler activity were assessed at the first and second MTPs and knees. Tophus was assessed at all sites, and aggregates were assessed at the patellar and Achilles tendons. The sites for scanning were selected based on ultrasound expert opinion and prior studies using semiquantitative scoring systems in gout [28,29].

At each centre, ultrasound examinations were performed using a high-end ultrasound machine by an experienced musculoskeletal sonographer unrelated to other study activities. A scanning manual was developed for the study to ensure consistent patient positioning and image acquisition across sites and is shown in Supplementary Material 1. The machine, probe frequency, and sonographer experience/training were recorded on the ultrasound assessment report form and are summarised in Supplementary Material 2.

Ultrasound scans were read locally at the time of scanning on a standardised ultrasound report form, with images at each joint/tendon area recorded for documentation and quality control. The study protocol prespecified analysis of local readers' scores to best reflect 'real world' clinical imaging practice. Before commencing the study, an imaging atlas was developed for each ultrasound gout lesion. This atlas was available to standardise scores of ultrasound lesions across sites. Elementary gout lesions (double contour, tophus, aggregates, and erosion) were assessed according to OMERACT definitions [8,21] and scored according to the OMERACT gout ultrasound scoring system [22]. The definition of aggregates was the following: 'bright hyperechoic, isolated spots too small to fulfil the tophus definition and characterised by maintaining their high degree of reflectivity when the insonation angle is changed' [22]. Although in the OMERACT definitions it is specified to score aggregates only in people with proven gout when other ultrasound gout lesions are also present [22], the TIGER study steering committee decided to include aggregates in the ultrasound protocol, noting that study participants are at increased risk of gout, but limited the sites for scoring aggregates to the patellar and Achilles tendons. Double contour, tophus, and aggregates were graded semiquantitative 0-3 (0 = absent, 1 = possible, 2 = definite but minimal, and 3 = definite and severe). Erosion was graded binary (0 = absent, 1 = present, and defined as present if visible in 2 perpendicular planes, regardless of size). Synovial hypertrophy and power Doppler activity were each scored semiquantitative 0 to 3 using the European Alliance of Associations for Rheumatology (EULAR)-OMERACT rheumatoid arthritis definitions and ultrasound scoring system [30,31]. The scoring sheet is shown in Supplementary Material 3.

Statistical analysis

Data are presented as n (%), mean (SD), or median (IQR) for descriptive purposes. For elementary ultrasound lesions, semiquantitative sum scores for each ultrasound lesion and the proportion of participants with at least 1 definite ultrasound lesion (score > 1) were calculated. The combined SQDT sum score was calculated by summing the double contour scores and tophus scores for all scanned sites, with a maximum score of 60. The relationship between ultrasound lesions was assessed using general linear mixed modelling with a random effect of participant used to provide control for clustering between measurements made on the left and right sides of the same individual and to provide robust confidence intervals. The odds of an ultrasound

score >1 were modelled with a binomial distribution and a logit link function. Bivariate Spearman correlation analysis was also performed. Data were analysed using SAS V.9.4 (SAS Institute). All comparisons were preplanned, so no adjustment for multiple comparisons was made. $P < .05$ was considered statistically significant.

RESULTS

Participant characteristics

Demographic and clinical features of the 269 study participants are shown in Table 1. In this multinational cohort, the mean (SD) age was 48 (18) years, and 81% were men. The mean (SD) serum urate was 0.52 (0.04) mmol/L (8.7 [0.7] mg/dL). There were low levels of pain and radiographic damage, and median (IQR) swollen and tender joint counts were 0 (0,0).

Ultrasound scores

Ultrasound findings are shown in Table 2 and Figures 1 and 2. For the elementary gout lesions, scores >0 were common, particularly for double contour (62.1% participants). There were 77 (28.6%) participants with at least 1 definite (score >1) double contour, 46 (17.1%) with at least 1 definite tophus, and 104 (38.7%) participants with at least 1 definite double contour and/or tophus. The median (IQR) SQDT sum score was 2 (0-4). Definite aggregates were present in 50 (18.6%). There were 83 (30.9%) participants with an SQDT score of 0, including 14 participants (5.2%) with a score of >0 for aggregates, and 8 (3%) participants with at least 1 site with definite aggregates. Ultrasound erosion was present in 32 (11.9%).

Synovial hypertrophy was the most common ultrasound finding; there were 52.8% participants with at least 1 joint with a synovial hypertrophy score >1. However, power Doppler activity was uncommon, with only 5.2% of participants having at least 1 joint with a power Doppler score >1.

Table 1
Participant characteristics

Clinical feature (n = 269)		
Age, y	48 (18)	
Male sex, n (%)	218 (81.0)	
Ethnicity, n (%)	African/Black	5 (1.9)
	East Asian	66 (24.5)
	Hispanic	10 (3.7)
	Māori	11 (4.1)
	Pacific Island	19 (7.1)
	South Asian	36 (13.4)
	White	112 (41.6)
	Other/unknown	10 (3.8)
Country, n (%)	New Zealand	143 (53.2)
	China	65 (24.2)
	France	21 (7.8)
	Spain	21 (7.8)
	Mexico	10 (3.7)
	Lithuania	8 (3.0)
	United States of America	1 (0.4)
Hypertension, n (%)	110 (40.9)	
Cardiovascular disease[a], n (%)	50 (18.6)	
Type 2 diabetes, n (%)	35 (13.0)	
Units of alcohol/day	4.2 (7.6)	
Diuretic use, n (%)	45 (16.7)	
Body mass index, kg/m^2	30.5 (6.5)	
Waist circumference, cm	103 (16)	
Swollen joint count (/66), median (IQR)	0 (0, 0)	
Tender joint count (/68), median (IQR)	0 (0, 0)	
Pain score, mm	12 (21)	
Serum urate, mmol/L	0.52 (0.04)	
eGFR, mL/min/1.73m^2	90 (25)	
SvdH erosion radiographic score (range 0-120)[b]	0.36 (0.97)	
SvdH narrowing radiographic score (range 0-48)[b]	2.52 (2.48)	
Kellgren-Lawrence grade sum scores (range 0-48)[b]	2.92 (2.81)	

eGFR, estimated glomerular filtration rate; SvdH, Sharp-van der Heijde.
Data are mean (SD) unless otherwise specified.
[a] includes chronic heart failure, peripheral vascular disease, myocardial revascularisation, peripheral artery surgery revascularisation (inc. aortic aneurysm), cardiac arrhythmia (atrial fibrillation/flutter), angina, myocardial infarction, or stroke.
[b] n = 240.

Distribution of ultrasound lesions

Figure 1 shows the sites of involvement for the components of the SQDT sum score. Unilateral double contour scores >0 at the first MTP and knee were the most common ultrasound finding. Similarly, double contour scores at the first MTP and knee and 2nd MTP, followed by tophus scores at the 1st MTP and distal patella, were the largest contributors to the SQDT sum score.

Figure 2 shows the sites of involvement for the other ultrasound lesions. Aggregates were most commonly evident in the distal patellar tendon, in a unilateral distribution. The first MTP was most frequently affected by erosion, synovial hypertrophy, and power Doppler activity. Generally, ultrasound lesions were unilateral, except for synovial hypertrophy.

Correlations between ultrasound sum scores

Correlations for the ultrasound sum scores are shown in Supplementary Material 4. There were positive correlations between the sum scores for ultrasound findings of MSU crystal deposition (double contour, tophus, and aggregates), except for double contour and aggregates, with the highest correlations between tophus and aggregates sum scores ($r = 0.34$, $P < .0001$). Erosion sum scores weakly correlated with tophus, synovial hypertrophy, and Doppler activity sum scores. Synovial hypertrophy sum scores weakly correlated with double contour, tophus, and erosion sum scores and power Doppler sum scores with tophus and erosion. There were no significant correlations between screening serum urate results and elementary ultrasound lesions or SQDT scores ($r = -0.12$ to 0.06, $P > .05$ for all comparisons, data not shown).

Association of ultrasound findings of MSU crystal deposition with ultrasound findings of joint damage and inflammation in individual joints

Table 3 shows the analysis of individual joints examining associations between ultrasound findings of MSU crystal deposition and ultrasound findings of joint damage and inflammation. Consistent with the correlation analysis, joint by joint analysis demonstrated an association between double contour sign at the first and second MTPs with synovial hypertrophy; the presence of a definite double contour sign (score > 1) was associated with an odds ratio of 4.00 for the presence of synovial hypertrophy (score > 1) at the first MTP, and 5.11 at the second MTP

Table 2
Ultrasound findings (n = 269)

Number (%) of participants with at least 1 site with an ultrasound lesion		
Ultrasound lesion	N (%) participants with at least 1 site with score >0	N (%) participants with at least 1 site with score >1
Double contour	167 (62.1)	77 (28.6)
Tophus	83 (30.9)	46 (17.1)
Aggregates	80 (29.7)	50 (18.6)
Erosion	32 (11.9)	NA[a]
Synovial hypertrophy	206 (76.6)	142 (52.8)
Power Doppler activity	43 (16.0)	15 (5.6)
Ultrasound sum scores		
Ultrasound lesion (range)	Median (IQR)	Mean (SD)
Double contour (0-18)	1 (0-3)	1.80 (1.89)
Tophus (0-42)	0 (0-1)	0.78 (1.49)
Aggregates (0-24)	0 (0-1)	0.74 (1.43)
Erosion (0-6)	0 (0-0)	0.16 (0.47)
Synovial hypertrophy (0-18)	4 (0-6)	3.84 (3.27)
Power Doppler activity (0-18)	0 (0-0)	0.30 (0.86)
Semiquantitative double contour-tophus (0-60)	2 (0-4)	2.57 (2.47)

[a] erosion scored as binary present/absent.

(Table 3). There was no association observed for the double contour sign with erosion or power Doppler activity.

Similarly, consistent with the correlation analysis, joint by joint analysis demonstrated an association for tophus at the first MTP with erosion, synovial hypertrophy, and power Doppler activity; the presence of a definite tophus (score > 1) was associated with an odds ratio of 3.09 for the presence of erosion, 2.51 for synovial hypertrophy (score > 1), and 19.8 for power Doppler activity (score > 1) at the first MTP (Table 3). Adjustment for synovial hypertrophy in the regression model did not substantially alter the association between tophus and power Doppler activity at the first MTP (adjusted odds ratio [95% CI] 17.06 [4.49-64.75], $P < .0001$). Tophus and erosion were uncommon at the second MTP and knee, so analysis of other associations with tophus at these joints was not possible.

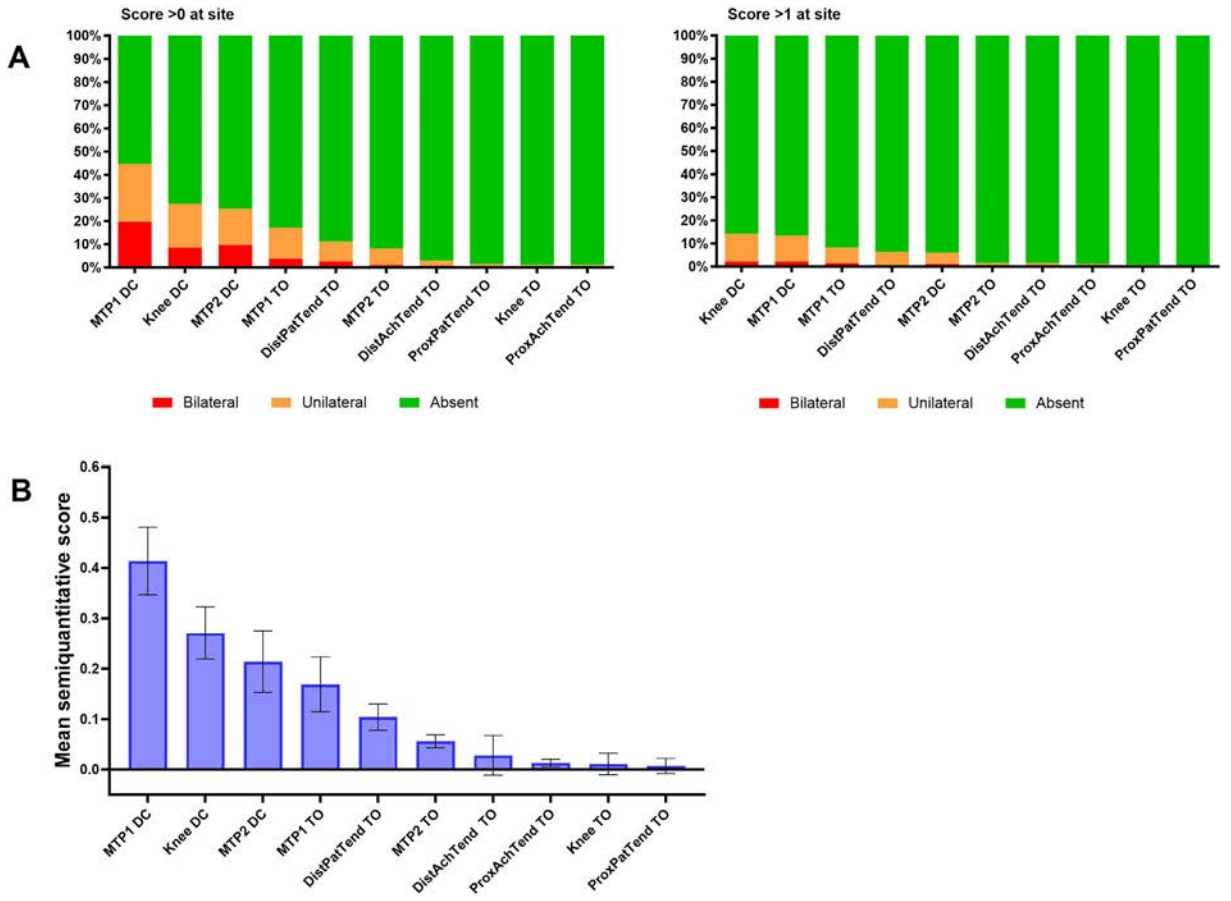

Figure 1. Double contour and tophus scores. (A) Percentage of patients with at least possible (score > 0) or at least definite (score > 1) bilateral or unilateral double contour (DC) and tophus (TO) at joint/tendon sites. (B) Mean (95% CI) score for contributors to semiquantitative DC and TO (SQDT) sum score according to site and gout lesion. MTP, metatarsophalangeal joint.

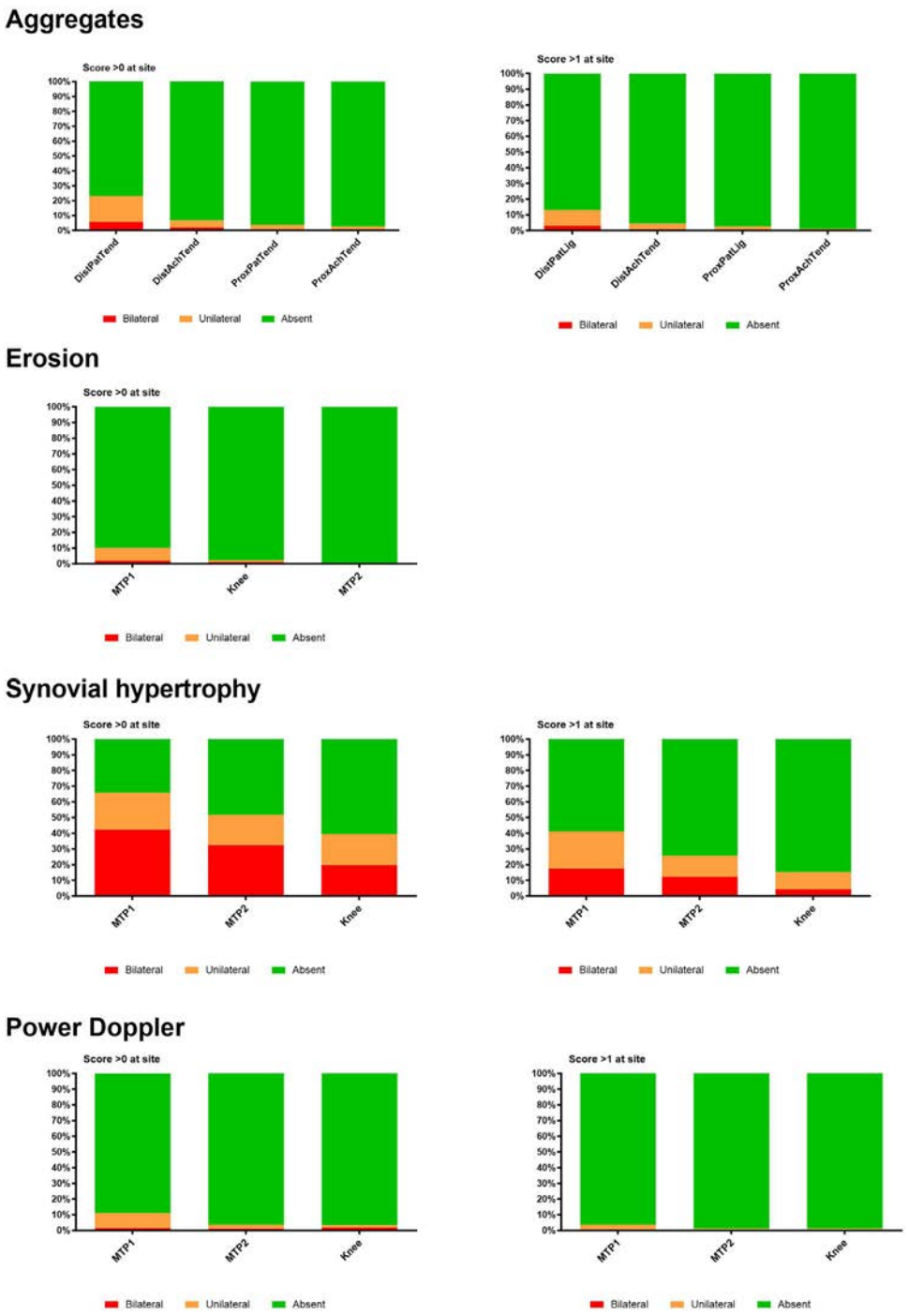

Figure 2. Percentage of patients with other bilateral or unilateral ultrasound lesions. Percentage of patients with at least possible (score > 0) or at least definite (score > 1) bilateral or unilateral ultrasound lesions at joint/tendon sites. MTP, metatarsophalangeal joint.

Association of ultrasound and plain radiographic findings at the first MTP

As the first MTP was most frequently affected on ultrasound and is also a joint that is frequently affected by both gout and osteoarthritis, we undertook additional analysis examining the relationship between ultrasound and plain radiographic findings at this joint, shown in Table 4. On plain radiography, joint space narrowing and features of osteoarthritis were common, but definite erosion was uncommon, affecting only 18 first MTPs (Table 4). There was no association between ultrasound features of MSU crystal deposition (double contour or tophus) or joint inflammation (synovial hypertrophy and Doppler activity) with Sharp-van der Heijde narrowing scores or Kellgren-Lawrence radiographic grade at the first MTP. Consistent with the ultrasound erosion analysis, the presence of a definite ultrasound tophus (score > 1) was associated with an odds ratio of 11.58 for the presence of radiographic erosion at the first MTP. The presence of Doppler activity (score > 1) on ultrasound was also associated with an odds ratio of 11.44 for radiographic erosion at the first MTP. Double contour sign and synovial hypertrophy were not associated with radiographic erosion at this joint.

DISCUSSION

In this multinational study of people with asymptomatic hyperuricemia, ultrasound features of gout were identified, with at least 1 definite double contour or tophus in more than one-

Table 3
Association of ultrasound findings of MSU crystal deposition with ultrasound findings of joint damage and inflammation: joint by joint analysis

Independent variable	Outcome	Joint	Number of events (outcomes)	Odds ratio (95% CI)	*P*
Double contour	Erosion	MTP1	32	0.76 (0.17-3.35)	.72
		MTP2	1	NE	NE
		Knee	9	NE	NE
	Synovial hypertrophy	MTP1	158	4.00 (1.95-8.20)	.0002
		MTP2	102	5.11 (1.94-13.46)	.0010
		Knee	53	1.83 (0.78-4.30)	.17
	Power Doppler activity	MTP1	11	2.66 (0.32-21.85)	.36
		MTP2	3	NE	NE
		Knee	4	NE	NE
Tophus	Erosion	MTP1	32	3.09 (1.06-9.48)	.049
		MTP2	1	NE	NE
		Knee	9	NE	NE
	Synovial hypertrophy	MTP1	158	2.51 (1.15-5.51)	.021
		MTP2	102	1.08 (0.10-11.15)	.95
		Knee	53	NE	NE
	Power Doppler activity	MTP1	11	19.8 (4.87-80.4)	<.0001
		MTP2	3	NE	NE
		Knee	4	NE	NE

MSU, monosodium urate; MTP, metatarsophalangeal joint; NE, not estimable.
Analysis for ultrasound scores >1. Erosion scored as binary present/absent, erosion score of 1 included in this analysis.

third of participants using the OMERACT gout ultrasound scoring system. However, the overall extent of MSU crystal deposition, as assessed using the OMERACT gout scoring system, was low. Despite the low levels of deposition overall, ultrasound tophus scores were associated with other imaging features of MSU crystal deposition, joint damage, and inflammation.

This large multinational study provides precision to prior estimates of MSU crystal deposition on ultrasound in asymptomatic hyperuricemia [9–20]. Variation in the prior estimates may be, in part, due to different methods of scoring or the number of sites scored [32]. The low extent of MSU crystal deposition using the OMERACT gout ultrasound scoring system in this cohort of people with asymptomatic hyperuricaemia is consistent with our previous dual-energy computed tomography (DECT) study, which quantified MSU crystal volume in the feet and ankles [33]. DECT MSU crystal deposition was found in 24% of participants with asymptomatic hyperuricaemia (serum urate > 0.52 mmol/L), and MSU crystal volumes were much lower in people with asymptomatic hyperuricaemia compared with gout-positive control participants, even in those with a gout disease duration <3 years. Patterns of MSU crystal deposition in the TIGER study cohort can be contrasted with those of a study using the OMERACT scoring system in people with gout, which reported that tophus at the first MTP was the most common ultrasound lesion, followed by double contour at the first MTP and knee [28]. In the TIGER study of people with asymptomatic hyperuricaemia, double contour was more common than tophus, potentially reflecting small amounts of MSU crystal deposition on articular cartilage without the larger MSU crystal collections that occur within tophi.

Nevertheless, 17.2% of participants had ultrasound evidence of tophi, despite no history of prior gout flares, no clinically evident subcutaneous tophi, and low levels of pain and plain radiographic erosion scores. In people with gout, clinically evident tophi typically develop more than a decade after the onset of gout in the setting of untreated hyperuricaemia [34], and reflect high volumes of MSU crystal deposition [33]. Prior CT and magnetic resonance imaging research has also demonstrated a close relationship between tophus and bone erosion in people with gout [35–39], and this

Table 4
Association of ultrasound findings with plain radiographic findings: site-by-site analysis at the first metatarsophalangeal joint (n = 240)

Independent variable	Outcome	Number of events (outcomes)	Odds ratio (95% CI)	*P*
Ultrasound double contour	SvdH erosion radiographic score	18	2.44 (0.69-8.61)	.17
	SvdH narrowing radiographic score	109	0.90 (0.37-2.18)	.82
	Kellgren-Lawrence radiographic grade	138	0.88 (0.37-2.08)	.77
Ultrasound tophus	SvdH erosion radiographic score	18	11.58 (4.07-32.96)	<.0001
	SvdH narrowing radiographic score	109	1.93 (0.72-5.17)	.19
	Kellgren-Lawrence radiographic grade	138	1.38 (0.52-3.69)	.52
Ultrasound synovial hypertrophy	SvdH erosion radiographic score	18	1.96 (0.75-5.13)	.17
	SvdH narrowing radiographic score	109	0.69 (0.40-1.19)	.18
	Kellgren-Lawrence radiographic grade	138	0.87 (0.53-1.44)	.60
Ultrasound power Doppler activity	SvdH erosion radiographic score	18	11.44 (3.24-40.45)	.0002
	SvdH narrowing radiographic score	108	2.07 (0.49-8.72)	.32
	Kellgren-Lawrence radiographic grade	137	1.48 (0.35-6.23)	.59

SvdH, Sharp-van der Heijde.
Analysis for ultrasound scores >1 and plain radiography scores/grade >1.

study suggests a similar relationship in asymptomatic hyperuricaemia, both for ultrasound and plain radiographic erosion, particularly at the first MTP. It is noteworthy that erosion was present on ultrasound in 11.9% of participants. Our results indicate that subclinical tophi and joint damage can develop much earlier than previously appreciated in those with elevated serum urate levels without clinical symptoms of gout.

Synovial hypertrophy, particularly at low grade, was the most common ultrasound finding in this study. Of note, neither synovial hypertrophy nor other ultrasound lesions were associated with radiographic features of osteoarthritis. Synovial hypertrophy is very common in the MTPs of healthy individuals [40], and the relevance of these findings in our study population is uncertain, particularly since power Doppler activity scores were very low. On ultrasound, high-grade synovial hypertrophy and Doppler activity in affected joints are characteristic of the acute inflammatory gout flare [41]. Nevertheless, we did observe consistent associations for both double contour and tophus with synovial hypertrophy, and also for tophus and power Doppler activity (independent of synovial hypertrophy), suggesting that MSU crystal deposition contributes to subclinical joint inflammation in people with asymptomatic hyperuricaemia. It will be particularly interesting to determine if the presence of high-grade synovial hypertrophy or Doppler activity at the baseline visit predicts subsequent development of gout in the TIGER study participants during their 5 years of follow-up.

Definitions and scoring of ultrasound aggregates have been controversial, due to low inter-reader agreement, lack of response to change during urate-lowering therapy in some longitudinal studies, and uncertainty about the specificity of aggregates for gout [22,28,42]. In this study, aggregates were scored according to the revised OMERACT gout ultrasound definition [22]. Despite the recent OMERACT gout ultrasound working group recommendation that aggregates should only be scored in patients with other ultrasound lesions indicative of gout (ie, double contour and/or tophus) [22], the protocol prespecified that the presence of aggregates was assessed only at the patellar and Achilles tendons (both proximal and distal) and recorded irrespective of other ultrasound features in this study [23]. There were 14 (5.2%) of participants with a score of >0 for aggregates but no (possible or definite) double contour and tophus. It is noteworthy that aggregate sum scores correlated with tophus sum scores, consistent with the concept that at least some ultrasound aggregates represent small micro-tophi/MSU crystal deposits [28,43].

No significant correlations were observed between screening serum urate results and ultrasound elementary lesion or sum scores. Importantly, all participants had a screening serum urate of at least 0.48 mmol/L, the level at which MSU crystals rapidly form *in vivo* in people with gout [5]. It is possible that once serum urate levels are consistently above the saturation level, MSU crystallisation occurs in a manner that is not concentration dependent with serum urate. However, it should be recognised that the duration of hyperuricemia for each participant could not be accurately recorded before entry into the study, and it is also possible that the duration of serum urate elevation, or some unrelated factor, might contribute to developing ultrasound gout lesions.

Study strengths include the multicentre, multinational cohort study design, large sample size, careful clinical phenotyping including exclusion of people with clinical features of gout using the ACR/EULAR gout classification criteria, standardised ultrasound examination, and scoring using the validated OMERACT definitions and scoring system by experienced sonographers. Despite the attempts to standardise the ultrasound scoring with detailed descriptions and an atlas for the scoring system, there was potential for different scoring between different sonographers across study sites. The decision to use real-time scoring was made to reflect real-life clinical practice, rather than central scoring of ultrasound images which has its own potential biases. Although sonographers were blinded to clinical details, including serum urate levels, they may have been aware that participants were enrolled in a study of people with hyperuricemia, and this knowledge might have influenced the scoring of borderline ultrasound lesions as possible lesions or possible ultrasound lesions as definite. It is also possible that scoring the presence of 1 ultrasound finding may have influenced interpretation and scoring of other possible ultrasound lesions. For this reason, we focused on definite ultrasound lesions (score > 1) in our analysis.

The TIGER study is ongoing, with repeat ultrasound scanning at the time of developing gout or after 5 years of follow-up [23]. The OMERACT scoring systems provide a framework to determine the prognostic relevance of the musculoskeletal ultrasound findings related to the 3 imaging domains of gout: MSU crystal deposition, structural damage, and inflammation, in people with high risk of developing gout due to hyperuricemia.

Competing interests

ND reports financial support was provided by the Health Research Council of New Zealand. ND reports a relationship with Novotech, Medcryst, Arthrosi SK Chemicals, Arthrosi PTC Therapeutics, Protalix, Unlocked Labs, LG Chem, Dexoligo, Therapeutics Shanton Pharma, Avalo, Sobi, Biomarin, and Convergence that includes: consulting or advisory, funding grants, and speaking and lecture fees. All authors declare they have no competing interests.

CRediT authorship contribution statement

Sarah Stewart: Writing – review & editing, Project administration, Methodology, Funding acquisition, Conceptualization. **Gregory D. Gamble:** Writing – review & editing, Methodology, Formal analysis. **William J. Taylor:** Writing – review & editing, Methodology, Conceptualization. **Andrew Harrison:** Writing – review & editing, Investigation. **Tony R. Merriman:** Writing – review & editing, Methodology, Conceptualization. **Borislav Mihov:** Writing – review & editing, Software, Project administration, Investigation. **Anne Horne:** Writing – review & editing, Project administration, Investigation. **Isabel Su:** Writing – review & editing, Project administration, Investigation. **Adwoa Dansoa Tabi-Amponsah:** Writing – review & editing, Project administration. **Lisa K. Stamp:** Writing – review & editing, Project administration, Investigation, Conceptualization. **Janine Haslett:** Writing – review & editing, Project administration, Investigation. **Tristan Pascart:** Writing – review & editing, Investigation, Funding acquisition, Conceptualization. **Mariano Andrés:** Writing – review & editing, Investigation, Funding acquisition, Conceptualization. **Maria-Luisa Peral-Garrido:** Writing – review & editing, Investigation. **Tuhina Neogi:** Writing – review & editing, Methodology, Conceptualization. **Eleonora Norkuviene:** Writing – review & editing, Methodology, Investigation, Funding acquisition. **Janitzia Vazquez-Mellado:** Writing – review & editing, Project administration, Investigation, Funding acquisition. **John F. Fitzgerald:** Writing – review & editing, Methodology, Investigation. **Lene Terslev:** Writing –

review & editing, Resources, Methodology. **Hilde Berner Hammer:** Writing – review & editing, Resources, Methodology. **Till Uhlig:** Writing – review & editing, Resources, Methodology. **Maria-Antonietta D'Agostino:** Writing – review & editing, Resources, Methodology. **Julia Martin:** Writing – review & editing, Resources, Methodology. **Mingshu Sun:** Writing – review & editing, Project administration, Investigation, Funding acquisition, Conceptualization. **Changgui Li:** Writing – review & editing, Project administration, Investigation, Funding acquisition, Conceptualization. **Nicola Dalbeth:** Writing – original draft, Supervision, Project administration, Methodology, Investigation, Funding acquisition, Conceptualization.

Funding

This work is supported by the Health Research Council of New Zealand (grant number 19/232). SS was supported by the Auckland Medical Research Foundation Post-doctoral Fellowship (grant number 1318001). CL is supported by the National Key Research and Development Program of China (2022YFC2503300). MS is supported by an Excellent Physician Scholarship from Simcere Pharma, Nanjing, China. TN is supported by K24 AR070892 and P30 AR072571. TP received funding from Horizon Pharmaceuticals (Amgen) for the French site. The Alicante site's participation in the study was funded by Carlos III Health Institute (Acción Estratégica en Salud 2021, ref. PI21/00544), with co-funding from the European Union.

Patient consent for publication

Not applicable

Ethics approval

The study was approved by the New Zealand Ministry of Health Southern Health and Disability Ethics Committee (MEC/05/10/130AM16) and by the local ethics committee/institutional review board for each participating centre. All participants provided written informed consent prior to enrolment in the study.

Provenance and peer review

Not commissioned; externally peer reviewed.

Supplementary materials

Supplementary material associated with this article can be found in the online version at doi:10.1016/j.ard.2026.03.021.

Orcid

Nicola Dalbeth: http://orcid.org/0000-0003-4632-4476

REFERENCES

[1] Faires JS, McCarty DJ. Acute arthritis in man and dog after intrasynovial injection of sodium urate crystals. Lancet 1962;280(7258):682–5.
[2] Dalbeth N, Kalluru R, Aati O, Horne A, Doyle AJ, McQueen FM. Tendon involvement in the feet of patients with gout: a dual-energy CT study. Ann Rheum Dis 2013;72(9):1545–8.
[3] Campion EW, Glynn RJ, DeLabry LO. Asymptomatic hyperuricemia. Risks and consequences in the Normative Aging Study. Am J Med 1987;82(3):421–6.
[4] Dalbeth N, Phipps-Green A, Frampton C, Neogi T, Taylor WJ, Merriman TR. Relationship between serum urate concentration and clinically evident incident gout: an individual participant data analysis. Ann Rheum Dis 2018;77(7):1048–52.
[5] Kelly B, Gamble GD, Horne A, Doyle AJ, Drake J, Aati O, et al. Relationship between serum urate and changes in dual-energy CT monosodium urate crystal volume over 1 year in people with gout: an individual participant data analysis. Ann Rheum Dis 2025;84(1):136–42.
[6] Grainger R, Dalbeth N, Keen H, Durcan L, Lawrence Edwards N, Perez-Ruiz F, et al. Imaging as an outcome measure in gout studies: report from the OMERACT Gout Working Group. J Rheumatol 2015;42(12):2460–4.
[7] Grassi W, Meenagh G, Pascual E, Filippucci E. "Crystal Clear"—sonographic assessment of gout and calcium pyrophosphate deposition disease. Semin Arthritis Rheum 2006;36(3):197–202.
[8] Gutierrez M, Schmidt WA, Thiele RG, Keen HI, Kaeley GS, Naredo E, et al. International Consensus for ultrasound lesions in gout: results of Delphi process and web-reliability exercise. Rheumatology 2015;54(10):1797–805.
[9] Abhishek A, Courtney P, Jenkins W, Sandoval-Plata G, Jones AC, Zhang W, et al. Brief report: monosodium urate monohydrate crystal deposits are common in asymptomatic sons of patients with gout: the Sons of Gout Study. Arthritis Rheumatol 2018;70(11):1847–52.
[10] De Miguel E, Puig JG, Castillo C, Peiteado D, Torres RJ, Martin-Mola E. Diagnosis of gout in patients with asymptomatic hyperuricaemia: a pilot ultrasound study. Ann Rheum Dis 2012;71(1):157–8.
[11] Estevez-Garcia IO, Gallegos-Nava S, Vera-Pérez E, Silveira LH, Ventura-Ríos L, Vancini G, et al. Levels of cytokines and microRNAs in individuals with asymptomatic hyperuricemia and ultrasonographic findings of gout: a bench-to-bedside approach. Arthritis Care Res (Hoboken) 2018;70(2):1814–21.
[12] Gaber W, Ezzat Y, Abd El Rahman SF. Role of diagnostic ultrasonography in detecting gouty arthritis. The Egyptian Rheumatologist 2013;35(2):71–5.
[13] Reuss-Borst MA, Pape CA, Tausche AK. Hidden gout- ultrasound findings in patients with musculo-skeletal problems and hyperuricemia. Springerplus 2014;3:592.
[14] Pineda C, Amezcua-Guerra LM, Solano C, Rodriguez-Henriquez P, Hernandez-Diaz C, Vargas A, et al. Joint and tendon subclinical involvement suggestive of gouty arthritis in asymptomatic hyperuricemia: an ultrasound controlled study. Arthritis Res Ther 2011;13(1):R4.
[15] Howard RG, Pillinger MH, Gyftopoulos S, Thiele RG, Swearingen CJ, Samuels J. Reproducibility of musculoskeletal ultrasound for determining monosodium urate deposition: concordance between readers. Arthritis Care Res (Hoboken) 2011;63(10):1456–62.
[16] Puig JG, de Miguel E, Castillo MC, Rocha AL, Martinez MA, Torres RJ. Asymptomatic hyperuricemia: impact of ultrasonography. Nucleosides Nucleotides Nucleic Acids 2008;27(6):592–5.
[17] Stewart S, Dalbeth N, Vandal AC, Allen B, Miranda R, Rome K. Ultrasound features of the first metatarsophalangeal joint in gout and asymptomatic hyperuricemia: comparison with normouricemic individuals. Arthritis Care Res 2017;69(6):875–83.
[18] Andrés M, Quintanilla M-A, Sivera F, Sánchez-Payá J, Pascual E, Vela P, et al. Silent monosodium urate crystal deposits are associated with severe coronary calcification in asymptomatic hyperuricemia: an exploratory study. Arthritis Rheumatol 2016;68(6):1531–9.
[19] Keen HI, Davis WA, Latkovic E, Drinkwater JJ, Nossent J, Davis TME. Ultrasonographic assessment of joint pathology in type 2 diabetes and hyperuricemia: the Fremantle Diabetes Study Phase II. J Diabetes Complications 2018;32(4):400–5.
[20] Bhadu D, Das SK, Wakhlu A, Dhakad U. Articular cartilage of knee and first MTP joint are the preferred sites to find double contour sign as an evidence of urate crystal deposition in asymptomatic hyperuricemic individuals. Acta Reumatol Port 2018;43(4):264–8.
[21] Terslev L, Gutierrez M, Christensen R, Balint PV, Bruyn GA, Delle Sedie A, et al. Assessing elementary lesions in gout by ultrasound: results of an OMERACT patient-based agreement and reliability exercise. J Rheumatol 2015;42(11):2149–54.
[22] Christiansen SN, Filippou G, Scire CA, Balint PV, Bruyn GA, Dalbeth N, et al. Consensus-based semi-quantitative ultrasound scoring system for gout lesions: results of an OMERACT Delphi process and web-reliability exercise. Semin Arthritis Rheum 2021;51(3):644–9.
[23] Stewart S, Gamble G, Taylor W, Su I, Merriman T, Mihov B, et al. Development of gout in people with asymptomatic hyperuricemia: study protocol for a 5-year prospective cohort. BMJ Open 2024;14(11):e090415.
[24] Dalbeth N, Stewart S, Gamble GD, Mihov B, Stamp LK, Haslett J, et al. Perceptions about asymptomatic hyperuricemia and views about urate-lowering therapy in people with asymptomatic hyperuricemia. Arthritis Care Res (Hoboken) 2026;78(3):417–23.
[25] Levey AS, Coresh J, Greene T, Marsh J, Stevens LA, Kusek JW, et al. Expressing the Modification of Diet in Renal Disease Study equation for estimating

glomerular filtration rate with standardized serum creatinine values. Clin Chem 2007;53(4):766–72.
[26] Dalbeth N, Clark B, McQueen F, Doyle A, Taylor W. Validation of a radiographic damage index in chronic gout. Arthritis Rheum 2007;57(6):1067–73.
[27] Kellgren JH, Lawrence JS. Radiological assessment of osteo-arthrosis. Ann Rheum Dis 1957;16(4):494–502.
[28] Christiansen SN, Østergaard M, Slot O, Fana V, Terslev L. Retrospective longitudinal assessment of ultrasound gout lesions using the OMERACT semi-quantitative scoring system. Rheumatology (Oxford) 2022;61 (12):4711–21.
[29] Hammer HB, Karoliussen L, Terslev L, Haavardsholm EA, Kvien TK, Uhlig T. Ultrasound shows rapid reduction of crystal depositions during a treat-to-target approach in gout patients: 12-month results from the NOR-Gout study. Ann Rheum Dis 2020;79(11):1500–5.
[30] Wakefield RJ, Balint PV, Szkudlarek M, Filippucci E, Backhaus M, D'Agostino MA, et al. Musculoskeletal ultrasound including definitions for ultrasonographic pathology. J Rheumatol 2005;32(12):2485–7.
[31] D'Agostino MA, Terslev L, Aegerter P, Backhaus M, Balint P, Bruyn GA, et al. Scoring ultrasound synovitis in rheumatoid arthritis: a EULAR-OMERACT ultrasound taskforce-Part 1: definition and development of a standardised, consensus-based scoring system. RMD Open 2017;3(1):e000428.
[32] Peral-Garrido ML, Gómez-Sabater S, Caño R, Bermúdez-García A, Lozano T, Sánchez-Ortiga R, et al. Prevalence of crystal deposits in asymptomatic hyperuricemia according to different scanning definitions: a comparative study. Semin Arthritis Rheum 2024;68:152470.
[33] Dalbeth N, House ME, Aati O, Tan P, Franklin C, Horne A, et al. Urate crystal deposition in asymptomatic hyperuricaemia and symptomatic gout: a dual energy CT study. Ann Rheum Dis 2015;74(5):908–11.
[34] Hench PS. Diagnosis and treatment of gout and gouty arthritis. JAMA 1941;116(6):453–5.
[35] Popovich I, Dalbeth N, Doyle A, Reeves Q, McQueen FM. Exploring cartilage damage in gout using 3-T MRI: distribution and associations with joint inflammation and tophus deposition. Skeletal Radiol 2014;43(7):917–24.
[36] Dalbeth N, Clark B, Gregory K, Gamble G, Sheehan T, Doyle A, McQueen FM. Mechanisms of bone erosion in gout: a quantitative analysis using plain radiography and computed tomography. Ann Rheum Dis 2009;68(8):1290–5.
[37] Dalbeth N, Smith T, Nicolson B, Clark B, Callon K, Naot D, et al. Enhanced osteoclastogenesis in patients with tophaceous gout: urate crystals promote osteoclast development through interactions with stromal cells. Arthritis Rheum 2008;58(6):1854–65.
[38] McQueen FM, Doyle A, Reeves Q, Gao A, Tsai A, Gamble GD, et al. Bone erosions in patients with chronic gouty arthropathy are associated with tophi but not bone oedema or synovitis: new insights from a 3 T MRI study. Rheumatology (Oxford) 2014;53(1):95–103.
[39] Eason A, House ME, Vincent Z, Knight J, Tan P, Horne A, et al. Factors associated with change in radiographic damage scores in gout: a prospective observational study. Ann Rheum Dis 2016;75(1):2075–9.
[40] Padovano I, Costantino F, Breban M, D'Agostino MA. Prevalence of ultrasound synovial inflammatory findings in healthy subjects. Ann Rheum Dis 2016;75(10):1819–23.
[41] Shao Q, Wang J. The Role of ultrasound semi-quantitative scoring in the diagnosis and assessment of gout and hyperuricemia. J Ultrasound Med 2024;43 (2):281–91.
[42] Christiansen SN, Østergaard M, Slot O, Fana V, Terslev L. Ultrasound for the diagnosis of gout-the value of gout lesions as defined by the Outcome Measures in Rheumatology ultrasound group. Rheumatology (Oxford) 2021;60(1):239–49.
[43] Pineda C, Fuentes-Gómez AJ, Hernández-Díaz C, Zamudio-Cuevas Y, Fernández-Torres J, López-Macay A, et al. Animal model of acute gout reproduces the inflammatory and ultrasonographic joint changes of human gout. Arthritis Res Ther 2015;17(1):37.

Ann Rheum Dis 85 (2026) 1656–1665

Contents lists available at ScienceDirect

Annals of the Rheumatic Diseases

journal homepage: https://www.sciencedirect.com/journal/annals-of-the-rheumatic-diseases

Crystal disease

A novel murine model of early calcium pyrophosphate deposition disease based on the *TNFRSF11B* mutation mimics features of the human disease

Chun Wang[1], Claudia M. Gohr[2], Elizabeth Mitton-Fitzgerald[2], Arin K. Oestreich[3,4,5], Yongjia Li[1], Jianqiu Xiao[1], Khushpreet Kaur[1], Farshid Guilak[3,4,5,6], Deborah J. Veis[1,7], Ann K. Rosenthal[2,*], Gabriel Mbalaviele[1]

[1] *Division of Bone and Mineral Diseases, John T Milliken Department of Medicine, Washington University in St. Louis, St. Louis, Missouri, USA*
[2] *Division of Rheumatology, Department of Medicine, Medical College of Wisconsin, and Zablocki VA Medical Center, Milwaukee, Wisconsin, USA*
[3] *Department of Orthopaedic Surgery, Washington University in St. Louis, St. Louis, Missouri, USA*
[4] *Shriners Hospitals for Children, St. Louis, Missouri, USA*
[5] *Center of Regenerative Medicine, Washington University in St. Louis, St. Louis, Missouri, USA*
[6] *Department of Biomedical Engineering, Washington University in St. Louis, Saint Louis, Missouri, USA*
[7] *Department of Pathology and Immunology, Washington University in St. Louis, St. Louis, Missouri, USA*

ARTICLE INFO

Article history:
Received 9 December 2025
Received in revised form 13 February 2026
Accepted 16 February 2026

Handling editor Josef S. Smolen

ABSTRACT

Objectives: Calcium pyrophosphate deposition (CPPD) disease is a common form of arthritis affecting older individuals. This disease is characterised by high levels of pyrophosphate in articular cartilage, resulting in calcium pyrophosphate crystal formation in humans and inflammatory and degenerative arthritis. A loss-of-function mutation in the *TNFRSF11B* locus (also known as *CCAL1*), which encodes osteoprotegerin (OPG) causes familial CPPD. OPG acts as a decoy receptor for RANKL, thereby inhibiting osteoclast differentiation and activity. CPPD currently lacks any animal models. The goal of this study was to develop a murine model of early CPPD by incorporating the *TNFRSF11B* gene mutation in mice and determining its effects on bones, joints and CPPD biomarkers.

Methods: We used CRISPR/Cas9 editing to generate mice carrying the *TNFRSF11B* mutation (Opg^{mt}). Joint and bone phenotypes, bone remodelling biomarkers and key CPPD biomarkers were assessed in wild type (WT; $Opg^{wt/wt}$), $Opg^{wt/mt}$ and $Opg^{mt/mt}$ mice at 6 and 12 months of age.

Results: Male and female mice carrying Opg^{mt} displayed osteopenia and high bone remodelling markers at 6 and 12 months of age. This phenotype was concurrent with increased osteoclast numbers and activity. Female $Opg^{mt/mt}$ mice also displayed significant osteoarthritis features by 12 months of age, including articular cartilage loss in the lateral compartment of the knee based on Mankin structural damage scores. Additionally, biomarkers pathognomonic of CPPD disease, such as pyrophosphate, transforming growth factor (TGF)-β1 levels and ENPP1 activity, were significantly elevated in the joints of both 6- and 12-month-old female mice with OPG^{mt}.

*Correspondence to Dr Ann K Rosenthal, Division of Rheumatology, Department of Medicine, Medical College of Wisconsin, 5000 W National Ave, Milwaukee, WI 53295.

E-mail address: arosenthal@mcw.edu (A.K. Rosenthal).

https://doi.org/10.1016/j.ard.2026.02.014

0003-4967/Published by Elsevier B.V. on behalf of European Alliance of Associations for Rheumatology (EULAR).

Conclusions: Mice carrying Opg^{mt} display bone and joint phenotypes characteristic of early-stage CPPD disease in humans. Opg^{mt} mice represent a novel preclinical model of early CPPD, ideal for exploring potential therapies targeting the disease prior to the development of major joint damage.

WHAT IS ALREADY KNOWN ON THIS TOPIC

- Little is known about the pathogenic mechanisms of calcium pyrophosphate deposition (CPPD) disease. There have been no animal models to date that mimic features of human CPPD.

WHAT THIS STUDY ADDS

- The phenotype of mice carrying mutant osteoprotegerin mimics that of human disease, and to our knowledge, this study presents the first preclinical model of CPPD.
- High levels of osteoclast numbers and activity correlate with increased markers of CPPD in joints of affected mice.

HOW THIS RESEARCH MIGHT AFFECT RESEARCH, PRACTICE OR POLICY

- This work describes a preclinical model of early CPPD that will be useful for identifying drugs that target important pathogenic pathways in this common and disabling arthritis.

INTRODUCTION

Calcium pyrophosphate deposition (CPPD) disease is a common form of arthritis typically affecting older individuals. It is defined by the presence of calcium pyrophosphate (CPP) crystals in articular cartilage and presents clinically as both degenerative and inflammatory arthritis. There are currently no specific treatments targeting CPPD. Work to delineate CPPD aetiology has largely focused on chondrocyte overproduction of pyrophosphate (PPi) [1]. Chondrocytes in affected cartilage produce high levels of extracellular ATP, which is converted by the ectoenzyme ectonucleotide pyrophosphatase phosphodiesterase 1 (ENPP1) into PPi and adenosine monophosphate (AMP) [2,3]. Extracellular PPi accumulates in cartilage matrix where it complexes with calcium to form CPP crystals. CPP crystal formation in human cartilage is likely facilitated by the unique characteristics of ageing chondrocytes in combination with alterations in extracellular matrix due to age or injury [4].

Studies of familial forms of CPPD have contributed to our understanding of CPPD disease pathogenesis. Mutations causing familial CPPD cluster in the 5p and 8q chromosomal regions. The 5p locus (also known as *CCAL2*) encodes ANKH (progressive ankylosis protein homolog) [5], which regulates extracellular PPi levels by modulating extracellular ATP levels in cartilage [3]. Recently, osteoprotegerin (OPG, also known as CCAL1) was identified as the protein encoded by the 8q gene locus. OPG is the protein product of the gene *TNFRSF11B* [6]. OPG is a circulating protein best known for its role in bone metabolism, where it serves as a decoy receptor for receptor activator of NF-κB ligand (RANKL) [7]. Its major function in bone is to negatively modulate osteoclast formation and activity. The CPPD-associated *OPG* mutation occurs at the stop codon, leading to the addition of 19 extra amino acids at the carboxy terminal end of the protein and resulting in its loss of function [8]. Individuals who are heterozygous for the CPPD-associated *OPG* mutation ($OPG^{wt/mt}$) develop severe premature joint degeneration with exuberant CPPD crystal deposition in affected joints [9].

Osteoporosis and increased fracture rates have been recently described in patients with sporadic age-related CPPD disease [10,11]. Interestingly, metabolic conditions such as hemochromatosis, hypomagnesaemia, or hypophosphatasia, which increase risk for CPPD, are also associated with a bone loss phenotype [12–14]. Taken together with the discovery that OPG—a protein critical for normal bone metabolism—causes familial CPPD, we now have ample clinical evidence to propose a role for bone pathology in CPPD. Subchondral bone alterations play key roles in age-related osteoarthritis (OA) [15,16], which shares common features with CPPD. In addition, remodelling processes in subchondral bone can release factors into the adjacent articular cartilage, such as transforming growth factor (TGF)-β1, that contribute to cartilage matrix damage and stimulate PPi formation [17]. Taken together, these observations suggest a possible role for increased osteoclast activity as a critical pathogenic pathway in CPPD.

To our knowledge, there are no animal models of CPPD that focus on pathways leading to CPP crystal formation. We were particularly interested in establishing a model of early CPPD, in which we would not necessarily expect to see crystals but instead could easily measure CPPD biomarkers. This type of model will be useful to study drugs that affect pathways involved in regulation of critical factors contributing to CPPD, and this stage of the disease is logically most amenable to treatment before irrevocable joint damage occurs. We used CRISPR/Cas9 technology to introduce the extra 19 amino acids found in patients with CPPD expressing OPG^{mt} into *Opg* in C57BL/6 mice. Microcomputed tomography (μCT) imaging and histologic scoring was used to measure OA severity and bone phenotypes. We also assessed levels of bone remodelling biomarkers and key CPPD biomarkers in wild type (WT; $Opg^{wt/wt}$), $Opg^{wt/mt}$, and $Opg^{mt/mt}$ mice at 6 and 12 months of age.

METHODS

Mouse model

All animal experiments were performed in accordance with protocols approved by the Institutional Animal Care and Use Committee (IACUC). CRISPR/Cas9 technology was used by the Mouse Genetics Core at Washington University in St. Louis to generate Opg^{mt} mice. The strategy that was used to generate single-stranded oligodeoxynucleotides (ssODN) containing the 19 extra amino acids found at the carboxy terminal end of the human OPG^{mt} is shown in Supplementary Figure S1. Target-specific sgRNA cleavage activity was validated *in vitro* by transfecting N2A cells with ROCHE Xtremegene HP, followed by Sanger sequencing and TIDE analysis (https://tide.nki.nl/) of PCR products. T7 sgRNA and Cas9 templates for *in vitro* transcription were PCR amplified, gel purified and *in vitro* transcribed with the MEGAshortscript T7 kit (sgRNA, Life Technologies) or the T7 mMessage mMachine Ultra kit (Cas9, Life Technologies). After transcription, both RNAs were purified with the Megaclear kit (Life Technologies). A 200 nucleotide ssODN donor DNA was synthesised by IDT. B6/CBA F_1 mice at 3 to 4 weeks of age (JAX Laboratories) were superovulated by intraperitoneal injection of

5 IU pregnant mare serum gonadotropin (Sigma), followed 48 hours later by intraperitoneal injection of 5 IU human chorionic gonadotropin (Millipore). Mouse zygotes were obtained by mating B6/CBA stud males with superovulated B6/CBA females at a 1:1 ratio. One-cell stage fertilised embryos (C57BL/6J) were collected and maintained in M2 medium before microinjections. DNA constructs were microinjected into the pronucleus and/or cytoplasm of each zygote following standard procedures of the Washington University Mouse Genetics Core. Injection concentrations were 50 ng/μL Cas9, 20 ng/μL gRNA and 20 ng/μL ssODN B6/CBA. Injected embryos were transferred into the oviducts of pseudopregnant recipient females. Offspring (F_0 generation) were screened for the presence of the transgene by PCR using genomic DNA extracted from tail biopsies. Positive founders were bred to establish subsequent generations (F_1, F_2) for further studies.

Microcomputed tomography

Before decalcification, the knee joints including femur and tibia were imaged using a μCT 50 scanner (Scanco Medical AG) at a resolution of 10 μm, at 55 kVp, 145 μA, and 300 ms integration time. The distal metaphysis and the middiaphysis of femur were used for μCT analysis of trabecular and cortical bone, respectively.

Histology

The knee joints of 6- and 12-month-old mice were fixed in 10% neutral buffered formalin at room temperature for 24 hours, then decalcified in Immunocal (StatLab) for 3 days; fresh Immunocal was changed every 24 hours. Tissues were processed and paraffin-embedded. Five-μm-thick coronal sections were generated, starting from the anterior side of the knees. These were stained with safranin-O and fast green. Images were taken using a Nanozoomer 2.0 HT whole slide scanner (Hamamatsu Photonics) at 20 × magnification. OA scoring was performed using a modified Mankin scoring system by 2 observers blinded to age, sex and genotype of the mice [18].

Histomorphometry

For static histomorphometry, 5 μm sections were stained with tartrate-resistant acid phosphatase (TRAP) as described previously [19] and imaged as above. Osteoclasts were scored in the distal femur metaphysis using Bioquant Osteo software (v18.2.6; Bioquant Image Analysis Corp) for image analysis.

Osteoclast differentiation and TRAP assay

Bone marrow stromal cells (BMSCs) and bone marrow macrophages (BMMs) were plated in a 96-well plate (2×10^4 total cells/well) at 1:1 ratio in αMEM media containing 10% fetal bovine serum and 20 nM 1,25-dihydroxyvitamin D3 for 7 days. Cytochemical staining for TRAP was used to identify osteoclasts as previously described [20]. Briefly, cells in a 96-well plate were fixed with 3.7% formaldehyde and 0.1% Triton X-100 for 10 minutes at room temperature. Cells were washed with water and incubated with the TRAP staining solution (Leukocyte Acid Phosphatase Kit; Sigma) at 37 °C for 15 minutes followed by washing with water. After drying, pictures were taken using a coupled Olympus microscope and GRYPHAX software. Multinucleated TRAP-positive cells with ≥3 nuclei were scored as osteoclasts using ImageJ.

Biomarker assays

Bone turnover assays

Levels of circulating markers of bone turnover were measured in mouse serum according to manufacturer's directions using Rat-Laps (CTX-1) and Rat/Mouse P1NP enzyme immunoassays (Immunodiagnostic Systems). Twenty microliters of mouse serum were used for the CTX-1 assay and 5 μL of mouse serum was used for the P1NP assay. All serum samples were run in duplicate.

CPPD biomarker assays

PPi, ANK, ENPP1 activity, and TGF-β1 assays were performed on osteochondral units removed from joints from intact unprocessed frozen limbs. These units consisted of a similar size block of articular cartilage and subchondral bone removed from mouse joints cleaned of all visible extra tissues. All assays were run with duplicates of each sample, and results were corrected for wet weight of the sample. Tissue PPi levels were measured in osteochondral units treated with 1.2 M HCl overnight and then dried in an oven until desiccated [21]. Each sample was rehydrated with water and used for the measurement of PPi using a standard radiometric assay [17]. Tissue ENPP1 activity levels were assessed by measuring nucleoside triphosphate pyrophosphohydrolase (NTPPPH) activity. Samples were incubated in 100 μL thymidine 5′-monophosphate p-nitrophenyl ester sodium salt (TMPNP) (Sigma Aldrich) for 2 hours. NTPPPH activity was measured after the addition of 1 N NaOH in a Biotek plate reader at 410 nm. To measure TGF-β1, the osteochondral unit was incubated in TGF-β isolation buffer for 48 hours at 4 °C [22]. After incubation, the supernatant was dialysed against 4 mM HCl for 3 hours and then neutralised with 0.5 N NaOH. The neutralised samples were assayed with the Mouse Transforming Growth (TGF-β1) ELISA kit (Abbexa). ANK levels were measured using Mouse Progressive Ankylosis Protein (ANK) ELISA kit (Abexxa). The samples were snap-frozen and pulverised, then resuspended in phosphate-buffered saline and assayed for levels of ANK protein.

Statistical analysis

Statistical analysis was performed using GraphPad Prism 9.0 software either using Student's *t* test or one-way analysis of variance with Tukey's multiple comparisons test based on the data type. Parameters that were deemed nonparametric, including serum and osteochondral unit biomarkers, were analysed using Kruskal-Wallis with Dunn's multiple comparison post-hoc test. Values are expressed as mean ± SEM. $P < .05$ was considered statistically significant.

RESULTS

Mice expressing OPG^{mt} are osteopenic

WT (*Opg*$^{wt/wt}$) mice and mice carrying 1 or 2 mutant *Opg* alleles (hereafter referred to as *Opg*$^{wt/mt}$ and *Opg*$^{mt/mt}$, respectively) were born at the expected Mendelian ratios, developed normally and were all fertile. At both 6 and 12 months of age, *Opg*$^{wt/wt}$, *Opg*$^{wt/mt}$ and *Opg*$^{mt/mt}$ mice of the same sex displayed comparable body weights (Supplementary Fig S2). We assessed the bone phenotypes of *Opg*$^{wt/wt}$, *Opg*$^{wt/mt}$ and *Opg*$^{mt/mt}$ mice. Male *Opg*$^{wt/mt}$ mice exhibited no reduction in trabecular bone at 6 months of age compared to *Opg*$^{wt/wt}$ controls (Fig 1A-C). By contrast, male *Opg*$^{mt/mt}$ mice and female *Opg*$^{wt/mt}$ and *Opg*$^{mt/mt}$

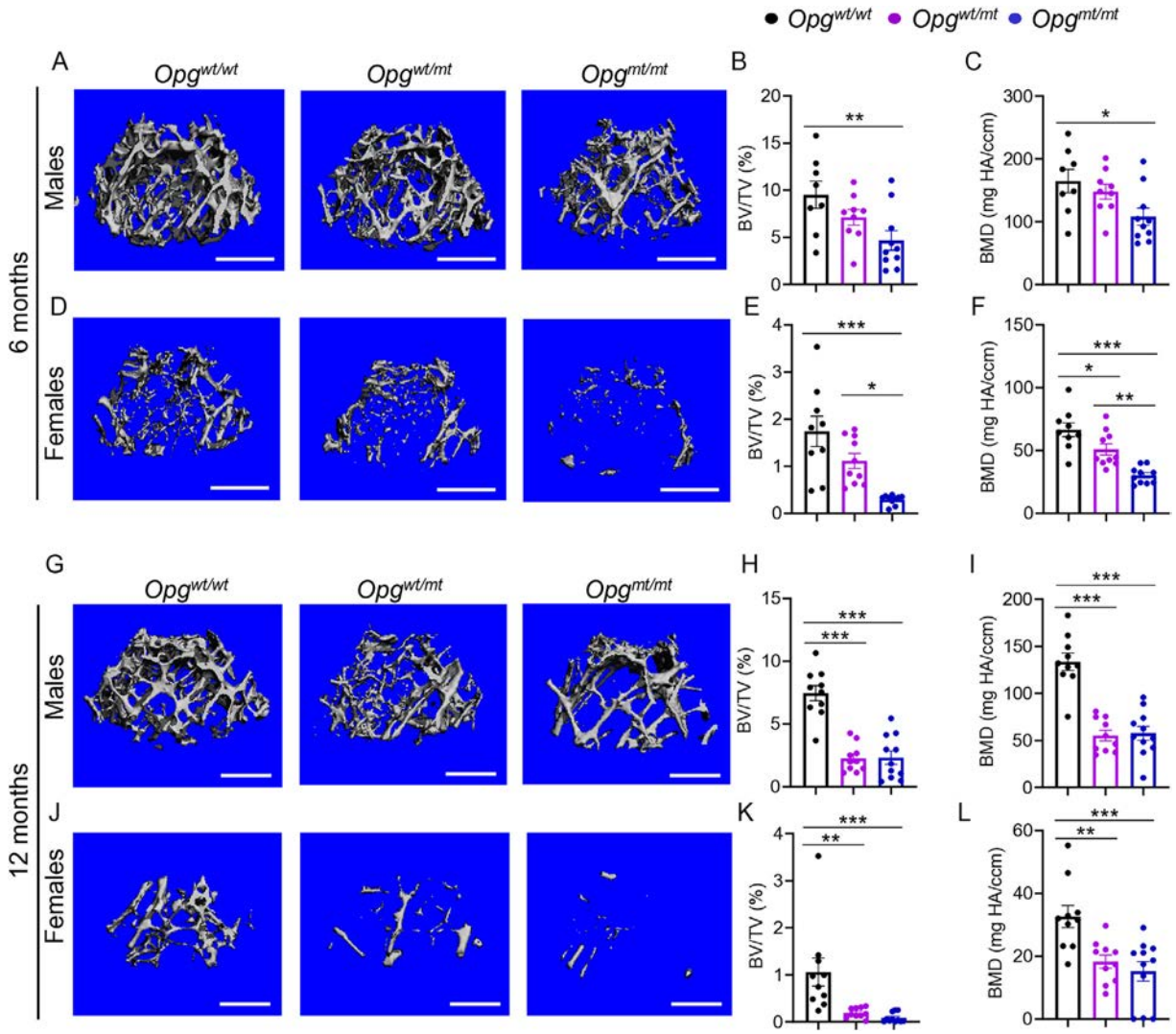

Figure 1. Expression of OPG^{mt} causes trabecular bone loss in 6- and 12-month-old mice. Analysis of trabecular bone was performed using μCT scanning in 6- and 12-month-old mice (n = 9-11). Representative images of bone from all 3 genotypes and both sexes of mice are shown in panels A, D, G, and J. Bone volume/total volume (BV/TV) measurements are displayed in panels B, E, H, and K. At 6 months, male mice with *Opg*$^{mt/mt}$ had significantly reduced bone mineral density (BMD) and lower BV/TV. Both female *Opg*$^{wt/mt}$ and *Opg*$^{mt/mt}$ mice (E, F) showed significantly lower values of both BV/TV and BMD. At 12 months, both male and female *Opg*$^{wt/mt}$ and *Opg*$^{mt/mt}$ mice had significantly reduced BV/TV and BMD compared with their *Opg*$^{wt/wt}$ counterparts (H, I, K, L). Scale bar: 500 μm. $^{*}P < .05$, $^{**}P < .01$, $^{***}P < .001$. mt, mutant; OPG, osteoprotegerin; wt, wild type.

mice at the age of 6 months and 12 months showed significantly reduced trabecular bone volume/total volume and bone mineral density compared to *Opg*$^{wt/wt}$ controls as assessed by μCT scanning (Fig 1A-L). Similar trends were observed for other bone parameters, including trabecular number and trabecular spacing (Supplementary Fig S3). Significant changes in cortical bone parameters occurred at 6 months of age in male and female *Opg*$^{mt/mt}$ mice. Both *Opg*$^{wt/mt}$ and *Opg*$^{mt/mt}$ mice exhibited these changes at 12 months (Supplementary Fig S4). To rule out potential off-target effects from CRISPR/Cas9-based editing, we assessed bone parameters in an independent line of *Opg*$^{mt/mt}$ mice. In this second line, trabecular and cortical bone parameters were similarly reduced in 6-month-old *Opg*$^{mt/mt}$ mice compared to *Opg*$^{wt/wt}$ counterparts (Supplementary Fig S5). These findings demonstrate significant reduction of bone density in all mice carrying OPG^{mt} compared to *Opg*$^{wt/wt}$ controls.

OPG^{mt} promotes osteoclast differentiation and activity in vivo and in vitro

We previously demonstrated that recombinant OPG^{mt} ineffectively blocks osteoclastogenesis in *in vitro* models [8]. Here, we found that male and female *Opg*$^{wt/mt}$ and *Opg*$^{mt/mt}$ mice carrying *Opg*^{mt} had significantly higher osteoclast number and bone surface area compared to *Opg*$^{wt/wt}$ mice at 6 months of age (Fig 2A-D). Evidence of increased bone remodelling was assessed using plasma levels of CTX-1 (biomarker of bone resorption) and P1NP (biomarker of bone formation) in 12-month-old mice. Although serum CTX-1 levels were similar across male genotypes at 12 months of age, P1NP levels showed a small but significant increase in *Opg*$^{mt/mt}$ males compared to *Opg*$^{wt/wt}$ controls (Fig 3E). In contrast, the levels of both CTX-1 and P1NP were significantly higher in female 12-month-old *Opg*$^{mt/mt}$ mice relative to their *Opg*$^{wt/wt}$ counterparts (Fig 3F). Similar patterns of CTX-1 and P1NP levels across genotypes and sexes were seen at 6 months of age (Supplementary Fig S6). To further determine the impact of OPG^{mt} on osteoclastogenesis, we cocultured *Opg*$^{wt/wt}$ BMMs, serving as osteoclast precursors, with either *Opg*$^{wt/wt}$ BMSCs or *Opg*$^{mt/mt}$ BMSCs in the presence of 1,25-dihydroxyvitamin D3, a well-known inducer of RANKL expression by mesenchymal cells [23]. Osteoclast differentiation was significantly increased in *Opg*$^{wt/wt}$ BMM−*Opg*$^{mt/mt}$ BMSC cocultures compared to *Opg*$^{wt/wt}$ BMM−*Opg*$^{wt/wt}$ BMSC cocultures (Fig 2G, H). Collectively, these results demonstrate that

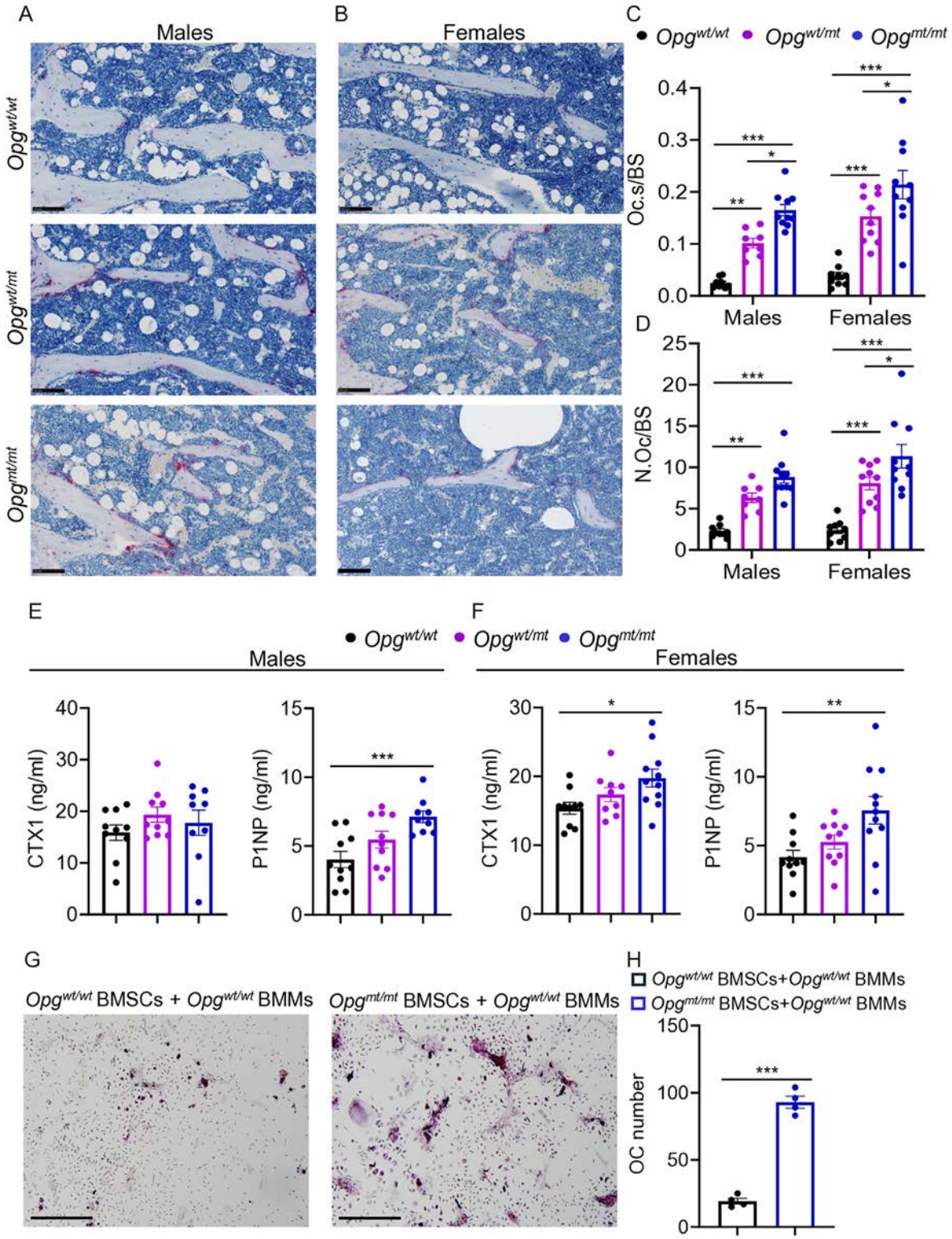

Figure 2. OPG^{mt} promotes osteoclast differentiation and activity *in vivo* and *in vitro*. Osteoclast numbers in bones of 6-month-old mice were scored from femoral specimens stained for tartrate-resistant acid phosphatase (TRAP) activity (n = 8-11). Images are representative TRAP-stained samples from males (A) and females (B). Panels C and D show osteoclast surface area (Oc.S/BS) and osteoclast number (N.Oc/BS) per bone surface area. Serum levels of bone remodelling markers including CTX-1 and P1NP are shown in E, F. P1NP but not CTX-1 levels were elevated in male *Opg*$^{mt/mt}$ mice, whereas female *Opg*$^{mt/mt}$ mice had higher levels of both biomarkers. Panel G shows representative images of cocultures stained for TRAP activity from *Opg*$^{wt/wt}$ bone marrow stromal cells (BMSCs) cocultured with either *Opg*$^{wt/wt}$ or *Opg*$^{mt/mt}$ bone marrow macrophages (BMMs). The number of TRAP-positive multinucleated cells with at least 3 nuclei (osteoclasts)/well was significantly increased in cocultures with *Opg*$^{mt/mt}$ (H; n = 4). Scale bar: 100 μm (A, B), 200 μm (G). *P < .05, **P < .01, ***P < .001. mt, mutant; OPG, osteoprotegerin; wt, wild type.

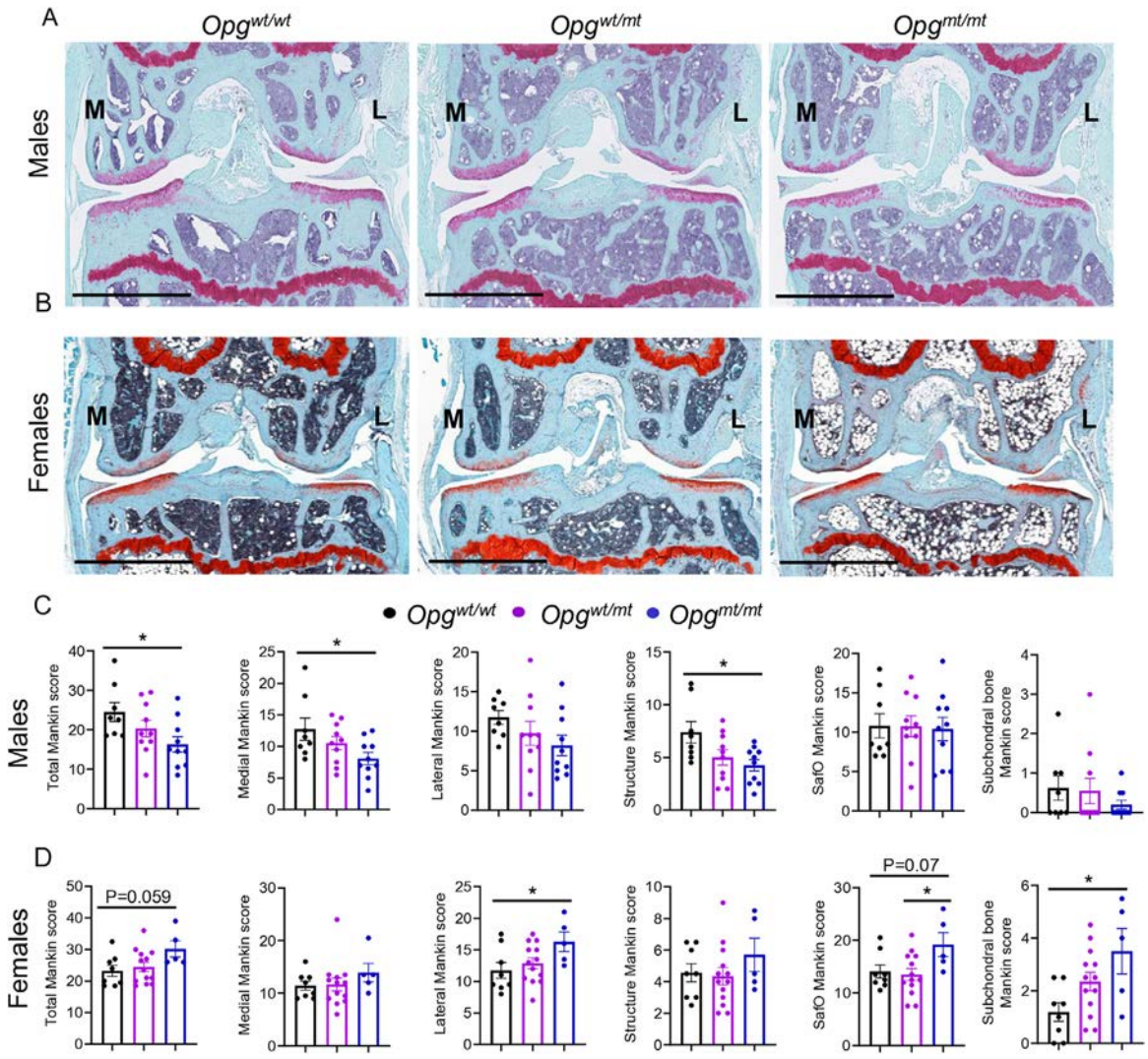

Figure 3. Expression of OPG^{mt} causes arthritis in 12-month-old female mice. Knee joints from 12-month-old male and female mice (n = 5-13) were sectioned and stained as described in Methods. Modified Mankin scores were assessed with reviewers blinded to the genotype and sex. Representative images of the knees are shown in panels A and B. Arthritis scores are shown in males (C) and females (D). Female *Opg*$^{mt/mt}$ mice had significantly higher scores than *Opg*$^{wt/wt}$ mice at 12 months of age. Scale bar: 1 mm. M = medial compartment; L = lateral compartment. *$P < .05$. mt, mutant; OPG, osteoprotegerin; wt, wild type.

OPG^{mt} is ineffective at inhibiting osteoclast formation both *in vitro* and *in vivo*.

Female Opg$^{mt/mt}$ mice exhibit cartilage damage by 12 months of age

Knee joints from *Opg*$^{wt/wt}$, *Opg*$^{wt/mt}$ and *Opg*$^{mt/mt}$ mice were analysed for the development of OA using the modified Mankin scoring system [18]. At 6 months of age, OA was not detected in either males or females across all genotypes (Supplementary Fig S7A-D). Twelve-month-old male *Opg*$^{wt/wt}$ and *Opg*$^{wt/mt}$ mice had similar arthritis scores, and *Opg*$^{mt/mt}$ mice did not exhibit signs of OA (Fig 3A, C). Unlike 12-month-old *Opg*$^{wt/mt}$ and *Opg*$^{wt/wt}$ female littermates, *Opg*$^{mt/mt}$ females exhibited significant OA pathology characterised by loss of safranin-O staining in the cartilage and subchondral bone changes in the lateral knee compartment (Fig 3B, D). Total Mankin scores approached but did not achieve statistical significance, in part due to interanimal variability. Taken together, these data show that *Opg*$^{mt/mt}$ female mice had significant evidence of knee OA, which was not observed in similarly aged *Opg*$^{wt/wt}$ female mice or *Opg*$^{mt/mt}$ male mice.

CPPD biomarkers are elevated in female mice with Opg^{mt}

Although human CPPD is characterised by the presence of CPP crystals in cartilage matrix, murine articular cartilage has considerably less extracellular matrix than large animal cartilage and is therefore unlikely to allow formation of CPP crystals. There are, however, multiple biomarkers of CPP crystal formation that are critical in the development of CPPD arthritis, are quantifiable in tissue and are extremely valuable for preclinical studies of early CPPD. The biomarker most strongly associated with CPPD is PPi, which is essential for crystal formation. Alongside PPi, we also measured other factors with major roles in CPPD, including NTPPH activity, which reflects activity levels of ENPP1, the ecto-enzyme that produces PPi from ATP [24]; ANK protein, which regulates levels of extracellular ATP and PPi in cartilage; and TGF-β1, which is the strongest known stimulant of PPi production by chondrocytes. At 12 months of age, only NTPPPH activity was increased in male *Opg*$^{mt/mt}$ mice (Fig 4A). ANK levels were comparable across all genotypes in 12-month-old female mice (Fig 4B). In contrast, all other biomarkers were elevated in females expressing OPG^{mt}, except for PPi, which showed higher levels in heterozygote females and smaller

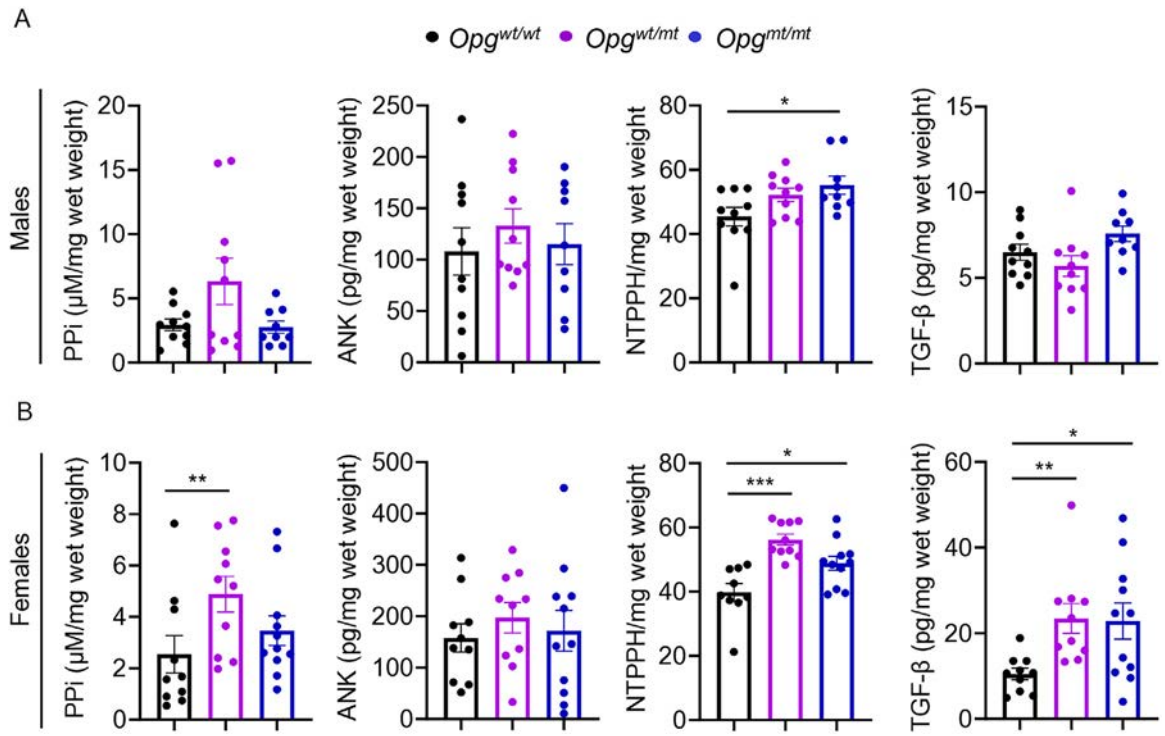

Figure 4. CPPD biomarkers are elevated in 12-month-old mice with OPG^{mt}. Levels of calcium pyrophosphate deposition disease biomarkers were measured in osteochondral units corrected for wet weight from 12-month-old male (A) and female (B) mice (n = 9-11). PPi levels were significantly increased in female *Opg*$^{wt/mt}$ mice, and there was a similar trend in male *Opg*$^{wt/mt}$ mice. Ectonucleotide pyrophosphatase phosphodiesterase 1 activity was measured as NTPPPH activity, which was increased in *Opg*$^{mt/mt}$ male and both *Opg*$^{wt/mt}$ and *Opg*$^{mt/mt}$ female mice. TGF-β1 levels were increased in female *Opg*$^{wt/mt}$ and *Opg*$^{mt/mt}$ mice. *P <.05, ***P <.001. ANK, progressive ankylosis protein; mt, mutant; NTPPPH, nucleoside triphosphate pyrophosphohydrolase; OPG, osteoprotegerin; Ppi, pyrophosphate; TGF, transforming growth factor; wt, wild type.

increases in *Opg*$^{mt/mt}$ mice. The phenotype observed in 6-month-old mice expressing OPG^{mt} was unexpected, as significant differences in CPPD markers were primarily seen in *Opg*$^{wt/mt}$ mice, but not in *Opg*$^{mt/mt}$ mice, when compared to *Opg*$^{wt/wt}$ controls (Supplementary Fig S8A, B). Despite this variability, the findings align with the presence of overt OA in female *Opg*$^{mt/mt}$ mice at 12 months of age.

DISCUSSION

We show here that mice that are heterozygous or homozygous carrying OPG^{mt} have both bone and joint phenotypes consistent with human CPPD. The bone phenotype is characterised by reduced trabecular and cortical bone and associated with increased numbers of osteoclasts. These data are consistent with our *in vitro* studies showing that this mutation impairs OPG function, thus facilitating excess osteoclastogenesis and bone loss. We also see strong evidence for OA in the 12-month-old *Opg*$^{mt/mt}$ female mice. This pattern of OA with lateral compartment dominance is often seen in age-related murine OA models [25]. The joint damage correlates with high levels of CPPD biomarkers, including PPi, ENPP1 activity and TGF-β1.

This model clearly mimics early human CPPD disease and has characteristics that are particularly useful as a preclinical model. Humans and mice carrying this *OPG* mutation develop both arthritis and osteoporosis and demonstrate high levels of articular PPi. We approached this project knowing that rodent cartilage, which has little extracellular matrix, is highly unlikely to produce CPP crystals, in contrast to human cartilage, which has ample extracellular matrix in which crystals can form. We chose not to define CPPD by the presence of crystals in this model for several additional reasons. Most importantly, elevated PPi levels are critical for CPP crystal formation and pathognomonic for this disease. In contrast to crystals themselves, PPi levels are easily measurable and represent a key pharmacologic target for new therapies. For example, agents that block enzymes that stimulate PPi production, such as ENPP1, are already in clinical trials for cancer [26], and drugs that focus on osteoclast activity, such as denosumab, are currently available. In addition, we feel strongly that early disease represents the disease phase most likely to be amenable to therapy. In humans, CPP crystals damage cartilage by replacing the extracellular matrix-rich midzone of articular cartilage. Agents that dissolve existing crystals, for example, may actually leave empty spaces in cartilage that would result in further biomechanical damage, as human cartilage is not capable of repair. There is also evidence that breaking up existing CPP crystal deposits may induce a vigorous inflammatory response [27]. Taken together, these findings suggest that once significant crystal formation occurs, treatments focused on removing crystals are unlikely to reverse and may actually exacerbate joint damage.

The mechanism through which this loss-of-function mutation in OPG contributes to CPPD remains to be fully elucidated. Osteoclast activity is clearly increased throughout the bone in mice with this mutation as well as humans with age-related osteoporosis [28]. One potential mechanism that may lead to subsequent joint degeneration is through excess osteoclast activity at the osteochondral junction. Channels at the cartilage-bone interface increase with age and OA [29] and facilitate the transfer of substances from one tissue to another. Osteoclasts in subchondral bone can promote joint damage by releasing factors from bone matrix that stimulate PPi production by chondrocytes. TGF-β1 is an excellent candidate for such a factor [30]. In addition, PPi itself is a bioactive molecule. PPi suppresses

hydroxyapatite crystal formation and affects osteoblasts and bone remodelling [31]. PPi from cartilage may filter to subchondral bone and affect osteoblast behaviour, including increasing levels of RANKL, which cannot be effectively blocked due to defective OPG [31]. This type of positive feedback loop may promote joint damage even in the absence of crystal formation [32] (Fig 5). Alternatively, or in addition, osteoclast activity near the joint may result in increased levels of proteases and cytokines that cause cartilage matrix damage and further facilitate arthritis. However, the high PPi levels in mice carrying the *OPG* mutation suggest that this model has features unique to early CPPD disease that are not seen in typical OA.

The bone phenotype in this model is similar in males and females carrying OPG^{mt}, but the OA pattern shows sexual dimorphism. Age-related and familial CPPD occurs equally in men and women [1]. However, dramatic differences in males and females are seen in a variety of murine models of degenerative and inflammatory arthritis. Many models of posttraumatic OA show more consistent and severe OA in males than in females, which remains largely unexplained [33]. Age-associated murine OA models are less commonly used but also show some sexual dimorphism [34]. In our model, we saw more OA in female mice expressing OPG^{mt} than in their male counterparts. One potential explanation for this is the decline in oestrogen levels at 6 months of age in female mice [35]. This results in reduced bone formation and increased bone destruction, similar to what occurs in postmenopausal women. Although males expressing OPG^{mt} have no evidence of an OA phenotype at 12 months, we will need to study older mice to determine if these mice eventually develop more OA than their WT counterparts but do it more slowly.

Although the bone phenotype was clearly more dramatic in the homozygotes than the heterozygote mutant mice, some biomarkers of CPPD did not appear to show a gene-based dose-response. For example, PPi levels were higher in the osteochondral units of heterozygotes than homozygotes in both sexes and at both 6 months and 12 months of age. This pattern was also seen with ENPP1 activity at some time points in the female mice. Although this observation will require further study to assess its mechanism, it may ultimately provide some additional information about interactions between the OPG^{wt} and OPG^{mt} proteins that apply to arthritis in human CPPD disease, which has a dramatic joint phenotype in heterozygous individuals. This may also reflect a timing issue, such that PPi levels rise before significant arthritis occurs. Examining arthritis in all 3 genotypes at an older age may show a longitudinal relationship between arthritis and PPi levels that may contribute to our understanding of this phenomenon. Furthermore, the dramatic bone loss seen in female homozygous mice may be an additional cause of worsened joint damage.

Several factors should be considered in the interpretation of these findings. There are clearly differences between human and murine joints that limit the translation of mouse models to human arthritis. However, our model shares many similarities with early human CPPD. As murine cartilage is very difficult to remove from underlying subchondral bone in mature mice, we used the osteochondral unit to measure tissue levels of the key biomarkers of CPPD. Although not ideal, it was important to measure levels in this unit, as levels of the CPP biomarkers likely reside in both cartilage and subchondral bone as joint disease develops. We also only aged mice to 12 months. Although the 12-month-old mice mimic the early onset joint degeneration that occurs in humans expressing OPG^{mt}, many murine studies of age-related OA use 18- to 24-month-old mice [34]. Finally, as described above, we did not examine the murine joints for CPP crystals, as previous studies have shown that mice may not form CPP crystals [36]. Although the mechanisms involved are not clear, important differences that may explain this phenomenon include factors such as the minimal cartilage thickness in mice, differences in local temperature or pH, or the relatively short lifespan of mice. However, further work should be done in this area.

This preclinical model of early CPPD presents exciting opportunities for translation. In our opinion, targeting pathways of excess PPi production in the early phases of CPPD may be highly effective in preventing the irreversible damage seen in human CPPD. Both pharmacologic and genetic strategies can also be used to further confirm and explore the pathways delineated in Figure 5. Using OA and the CPPD biomarkers as endpoints, we hope to rapidly identify potential drugs that may be safe and useful in the treatment of this common and debilitating disease.

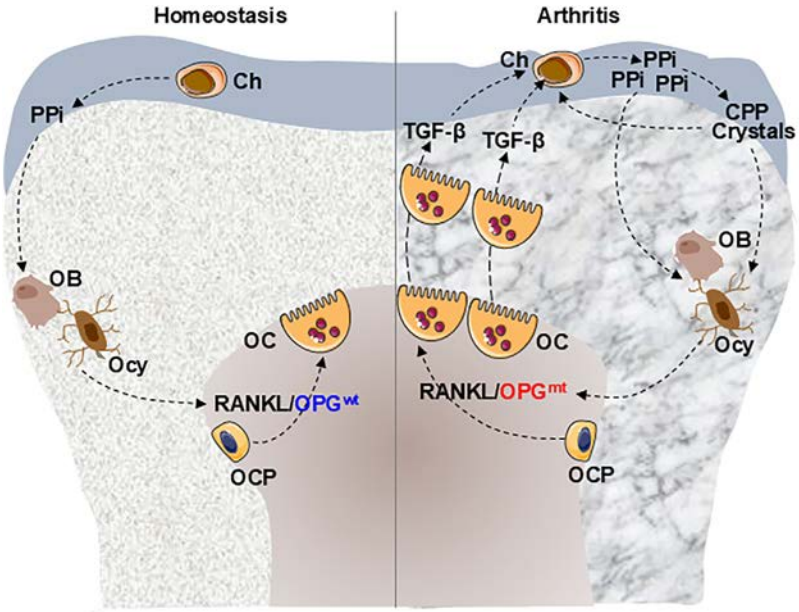

Figure 5. Proposed pathogenic mechanisms through which OPG^{mt} causes human calcium pyrophosphate deposition disease. In healthy joints, OPG^{wt} regulates RANKL activity to control osteoclast (OC) formation from osteoclast precursors (OCP). This is illustrated on the left side of the figure (Homeostasis). In contrast, OPG^{mt} is a weak RANKL inhibitor, leading to excessive OC formation, as shown on the right side of the figure (Arthritis). This effect causes release of TGF-β from bone matrix into the adjacent cartilage, which stimulates PPi production by chondrocytes (Ch). The excess PPi diffuses back into the subchondral bone triggering osteoblasts (OB) and osteocytes (Ocy) to produce more RANKL, thereby creating a positive feedback loop that accelerates both cartilage and bone destruction. CPP, calcium pyrophosphate; OPG, osteoprotegerin; PPi, pyrophosphate; RANKL, receptor activator of NF-κB ligand; TGF, transforming growth factor.

Competing interests

AKR reports financial support from National Institute on Aging. GM reports financial support from National Institute of Aging and a relationship with Aclaris Therapeutics, Inc that includes: equity or stocks. DJV reports financial support from National Institute of Aging. AKO reports financial support from National Institute of Arthritis and Musculoskeletal and Skin Diseases. All other authors declare that they have no known competing financial interests or personal relationships that could have appeared to influence the work reported in this paper.

CRediT authorship contribution statement

Chun Wang: Writing – review & editing, Methodology, Formal analysis, Data curation. **Claudia M. Gohr:** Writing – review & editing, Writing – original draft, Methodology, Formal analysis, Data curation. **Elizabeth Mitton-Fitzgerald:** Writing – review & editing, Writing – original draft, Formal analysis, Data curation, Conceptualization. **Arin K. Oestreich:** Writing – review & editing, Validation, Methodology, Formal analysis, Data curation. **Yongjia Li:** Writing – review & editing, Formal analysis. **Jianqiu Xiao:** Writing – review & editing, Formal analysis, Data curation. **Khushpreet Kaur:** Writing – review & editing, Formal analysis. **Farshid Guilak:** Writing – review & editing, Supervision, Methodology, Investigation, Formal analysis, Data curation. **Deborah J. Veis:** Writing – review & editing, Writing – original draft, Supervision, Methodology, Investigation, Data curation, Conceptualization. **Ann K. Rosenthal:** Writing – review & editing, Writing – original draft, Validation, Supervision, Project administration, Methodology, Investigation, Funding acquisition, Formal analysis, Data curation, Conceptualization. **Gabriel Mbalaviele:** Writing – review & editing, Writing – original draft, Supervision, Methodology, Investigation, Funding acquisition, Formal analysis, Data curation, Conceptualization.

Funding

This work was funded by the National Institutes of Health grants R01 AG077732 (Rosenthal, Mbalaviele, Veis), R01 AI161022 (Mbalaviele, Veis), K01 AR079045 (Oestreich), P30 AR073752, and Shriners Hospitals for Children. MicroCT and histology/histomorphometry services were provided by the Washington University Musculoskeletal Research Center cores, supported by NIH grants P30 AR074992 (Guilak) and S10 OD028573 (Guilak). Some of this work was supported by resources and facilities at the Clement J Zablocki VA Medical Center in Milwaukee, WI.

Patient consent for publication

No applicable.

Ethics approval

All animal experiments were performed in concordance with protocol number 25-0227 approved by the Washington University School of Medicine IACUC on September 22, 2025.

Provenance and peer review

Not commissioned; externally peer reviewed.

Supplementary materials

Supplementary material associated with this article can be found in the online version at doi:10.1016/j.ard.2026.02.014.

Orcid

Ann K. Rosenthal: http://orcid.org/0000-0003-3911-2846

REFERENCES

[1] Rosenthal AK, Ryan LM. Calcium pyrophosphate deposition disease. N Engl J Med 2016;374(26):2575–84.
[2] Costello JC, Rosenthal AK, Kurup IV, Masuda I, Medhora M, Ryan LM. Parallel regulation of extracellular ATP and inorganic pyrophosphate: roles of growth factors, transduction modulators, and ANK. Connect Tissue Res 2011;52(2):139–46.
[3] Rosenthal AK, Gohr CM, Mitton-Fitzgerald E, Lutz MK, Dubyak GR, Ryan LM. The progressive ankylosis gene product ANK regulates extracellular ATP levels in primary articular chondrocytes. Arthritis Res Ther 2013;15(5):R154.
[4] Jubeck B, Muth E, Gohr CM, Rosenthal AK. Type II collagen levels correlate with mineralization by articular cartilage vesicles. Arthritis Rheum 2009;60(9):2741–6.
[5] Ho AM, Johnson MD, Kingsley DM. Role of the mouse *ank* gene in control of tissue calcification and arthritis. Science 2000;289(5477):265–70.
[6] Williams CJ, Qazi U, Bernstein M, et al. Mutations in osteoprotegerin account for the CCAL1 locus in calcium pyrophosphate deposition disease. Osteoarthritis Cartilage 2018;26(6):797–806.
[7] Simonet WS, Lacey DL, Dunstan CR, et al. Osteoprotegerin: a novel secreted protein involved in the regulation of bone density. Cell 1997;89(2):309–19.
[8] Mitton-Fitzgerald E, Gohr CM, Williams CJ, Ortiz A, Mbalaviele G, Rosenthal AK. Effects of the TNFRSF11B mutation associated with calcium pyrophosphate deposition disease in osteoclastogenesis in a murine model. Arthritis Rheumatol 2021;73(8):1543–9.
[9] Ramos YFM, Bos SD, van der Breggen R, et al. A gain of function mutation in *TNFRSF11B* encoding osteoprotegerin causes osteoarthritis with chondrocalcinosis. Ann Rheum Dis 2015;74(9):1756–62.
[10] Abhishek A, Doherty S, Maciewicz R, Muir K, Zhang W, Doherty M. Association between low cortical bone mineral density, soft-tissue calcification, vascular calcification and chondrocalcinosis: a case-control study. Ann Rheum Dis 2014;73(11):1997–2002.
[11] Tedeschi SK, Hayashi K, Rosenthal A, et al. Fractures in patients with acute calcium pyrophosphate crystal arthritis versus matched comparators in a large cohort study. Arthritis Rheumatol 2024;76(6):936–41.
[12] Valenti L, Varenna M, Fracanzani AL, Rossi V, Fargion S, Sinigaglia L. Association between iron overload and osteoporosis in patients with hereditary hemochromatosis. Osteoporos Int 2009;20(4):549–55.
[13] Rondanelli M, Faliva MA, Tartara A, et al. An update on magnesium and bone health. Biometals 2021;34(4):715–36.
[14] Shapiro JR, Lewiecki EM. Hypophosphatasia in adults: clinical assessment and treatment considerations. J Bone Miner Res 2017;32(10):1977–80.
[15] Henrotin Y, Pesesse L, Sanchez C. Subchondral bone and osteoarthritis: biological and cellular aspects. Osteoporos Int 2012;23(Suppl 8) S847-51.
[16] Liu Y, Xie HQ, Shen B. Type H vessels - a bridge connecting subchondral bone remodelling and articular cartilage degeneration in osteoarthritis development. Rheumatology (Oxford) 2023;62(4):1436–44.
[17] Rosenthal AK, Cheung HS, Ryan LM. Transforming growth factor β1 stimulates inorganic pyrophosphate elaboration by porcine cartilage. Arthritis Rheum 1991;34(7):904–11.
[18] Furman BD, Strand J, Hembree WC, Ward BD, Guilak F, Olson SA. Joint degeneration following closed intraarticular fracture in the mouse knee: a model of posttraumatic arthritis. J Orthop Res 2007;25(5):578–92.
[19] Wang C, Qu C, Alippe Y, et al. Poly-ADP-ribosylation-mediated degradation of ARTD1 by the NLRP3 inflammasome is a prerequisite for osteoclast maturation. Cell Death Dis 2016;7(3):e2153.
[20] Bonar SL, Brydges SD, Mueller JL, et al. Constitutively activated NLRP3 inflammasome causes inflammation and abnormal skeletal development in mice. PLoS One 2012;7(4):e35979.
[21] Murali SK, Andrukhova O, Clinkenbeard EL, White KE, Erben RG. Excessive osteocytic FGF23 secretion contributes to pyrophosphate accumulation and mineralization defect in *Hyp* mice. PLoS Biol 2016;14(4):e1002427.
[22] Albro MB, Nims RJ, Cigan AD, et al. Accumulation of exogenous activated TGF-β in the superficial zone of articular cartilage. Biophys J 2013;104(8):1794–804.

[23] Takahashi N, Udagawa N, Kobayashi Y, Suda T. Generation of osteoclasts in vitro, and assay of osteoclast activity. Methods Mol Med 2007;135:285–301.
[24] Terkeltaub R, Rosenbach M, Fong F, Goding J. Causal link between nucleotide pyrophosphohydrolase overactivity and increased intracellular inorganic pyrophosphate generation demonstrated by transfection of cultured fibroblasts and osteoblasts with plasma cell membrane glycoprotein-1. Relevance to calcium pyrophosphate dihydrate deposition disease. Arthritis Rheum 1994;37(6):934–41.
[25] Armstrong AR, Carlson CS, Rendahl AK, Loeser RF. Optimization of histologic grading schemes in spontaneous and surgically-induced murine models of osteoarthritis. Osteoarthritis Cartilage 2021;29(4):536–46.
[26] Ruiz-Fernández de Córdoba B, Martínez-Monge R, Lecanda F. ENPP1 immunobiology as a therapeutic target. Clin Cancer Res 2023;29(12):2184–93.
[27] Bennett RM, Lehr JR, McCarty DJ. Crystal shedding and acute pseudogout. An hypothesis based on a therapeutic failure. Arthritis Rheum 1976;19(1):93–7.
[28] Wang R, Yang Y, Zhang Z, et al. Major vault protein (MVP) suppresses aging- and estrogen deficiency-related bone loss through Fas-mediated apoptosis in osteoclasts. Cell Death Dis 2023;14(9):604.
[29] Boyde A. The bone cartilage interface and osteoarthritis. Calcif Tissue Int 2021;109(3):303–28.
[30] Crane JL, Cao X. Bone marrow mesenchymal stem cells and TGF-β signaling in bone remodeling. J Clin Invest 2014;124(2):466–72.
[31] Bourne LE, Davies BK, Millan JL, et al. Evidence that pyrophosphate acts as an extracellular signalling molecule to exert direct functional effects in primary cultures of osteoblasts and osteoclasts. Bone 2023;176:116868.
[32] van der Kraan PM. Differential role of transforming growth factor-beta in an osteoarthritic or a healthy joint. J Bone Metab 2018;25(2):65–72.
[33] Dvir-Ginzberg M, Maatuf YH, Mobasheri A. Do we understand sex-related differences governing dimorphic disease mechanisms in preclinical animal models of osteoarthritis? Osteoarthritis Cartilage 2024;32(9):1054–7.
[34] Obeidat AM, Ishihara S, Li J, et al. Intra-articular sprouting of nociceptors accompanies progressive osteoarthritis: comparative evidence in four murine models. Front Neuroanat 2024;18:1429124.
[35] Blenck CL, Harvey PA, Reckelhoff JF, Leinwand LA. The importance of biological sex and estrogen in rodent models of cardiovascular health and disease. Circ Res 2016;118(8):1294–312.
[36] Luisetto R, Scanu A. The translational value of calcium pyrophosphate deposition disease experimental mouse models. Front Med (Lausanne) 2024;11:1417318.

Ann Rheum Dis 85 (2026) 1666–1677

Contents lists available at ScienceDirect

Annals of the Rheumatic Diseases

journal homepage: https://www.sciencedirect.com/journal/annals-of-the-rheumatic-diseases

Epidemiology

How long do people with rheumatic and musculoskeletal diseases stay healthy and in work across Europe? Analysis of data from SHARE and ELSA

Ross Wilkie *, Oluwasikemi Onamusi, Jessica Potts, Marty Lynch

School of Medicine, Keele University, Staffordshire, UK

ARTICLE INFO

Article history:
Received 5 November 2025
Received in revised form 9 February 2026
Accepted 10 February 2026

ABSTRACT

Objectives: This study aims to estimate the extent of the reduction in healthy working life expectancy (HWLE), from age 50, for people with rheumatic and musculoskeletal diseases (RMDs) in 19 countries across Europe and highlight the need to target extending working lives through interventions and policy.

Methods: Data were from 2 longitudinal studies (Survey of Health, Ageing and Retirement in Europe [2004-2022], English Longitudinal Study of Ageing [2002-2023]) that collect information in people aged 50 years and over. 'Healthy' and 'working' were defined as no limiting long-standing illness and employment/self-employment, respectively. RMDs were identified from self-report of ever having received a doctor diagnosis of arthritis or rheumatism. Age-adjusted discrete time 3-state models were fitted using IMaCh software, a maximum likelihood modelling programme using interpolation of Markov Chains, to estimate HWLE from transition probabilities between each healthy and working state based on RMD status (overall, by sex, education, and physical activity), stratified by 19 countries.

Results: In 6 countries, HWLE in the population with RMDs was around 50% or less than for the population without RMDs. The lowest HWLE for populations with RMDs was in Austria 2.60 (1.49, 3.71) years which was 42.9% of HWLE for the population without RMDs. HWLE was lower in populations with RMDs with lower than upper secondary education in all countries and in populations with RMDs categorised as physically inactive in 16 countries.

Conclusions: The differences observed in HWLE demonstrate the substantial societal burden associated with RMDs. However, differences by country, sex, education and physical activity indicate that there are opportunities for interventions and policies to increase HWLE.

INTRODUCTION

Across Europe, the relationship between rheumatic and musculoskeletal diseases (RMDs) and work is demanding more attention from policymakers, employers, health professionals, and people with these conditions [1–6]. Health professionals are urged to increasingly consider work in their assessment and management because, in addition to benefits to employers and society, good quality work is beneficial for individual's physical health, mental health and well-being, is an indicator of healthy ageing and often a requirement for continuing independence [1,7]. In addition to this invigorated approach to work, there is an even greater need to focus on workers aged 50 and over [8]; across Europe there are targets to encourage people to work until they are older with state retirement age in some countries (eg, Denmark) increasing [8]. The high and increasing prevalence of RMDs in adults aged 50 years onwards indicates that they will have an increasing impact on work [9]. Plans to extend

*Correspondence to Prof Ross Wilkie, School of Medicine, Keele University, Staffordshire, UK.
E-mail address: r.wilkie@keele.ac.uk (R. Wilkie).
Handling editor Josef S. Smolen.

https://doi.org/10.1016/j.ard.2026.02.010

WHAT IS ALREADY KNOWN ON THIS TOPIC

- With the prevalence of rheumatic and musculoskeletal diseases (RMDs) increasing with age, the impact of RMDs on being healthy and in work is greater in older workers. Now with policies encouraging people to work until they are older, there will be a greater number of adults with RMDs who are expected to remain in work.
- Healthy Working Life Expectancy (HWLE) is a population health indicator that estimates the average number of years from age 50 that people in a population are healthy and in work. This captures whether populations and those with RMDs are in a position to extend working lives and is important for identifying potential demand on healthcare and employers to manage health-related work issues and the development of employment opportunities. Identifying associations with different levels of HWLE can contribute to the development of policies and interventions to improve health and work for people with RMDs.

WHAT THIS STUDY ADDS

- This study has identified that the amount of time that the population of people with RMDs are healthy and in work is lower than that of the population without RMDs in 18 of 19 European countries. In 6 countries, HWLE for populations with RMDs was around 50% or less than for the population without RMDs.
- For people with RMDs, HWLE was lower in all countries in the populations with educational attainment lower than upper secondary education and in 16 countries in populations categorised as physically inactive.

HOW THIS STUDY MIGHT AFFECT RESEARCH, PRACTICE OR POLICY

- The extent that HWLE is lower in populations with RMDs in almost all countries indicates the need for policies (local, national, international), interventions and clinical approaches focusing on improving health and work for people with RMDs.
- Differences by sex, education, and physical inactivity, as well as country, highlight the role of enhancing job opportunities and support to keep people healthy and in work, including occupational health and retraining. The study indicates the need for larger datasets to further identify how HWLE can increase for populations with RMDs.

working life mean that there will be a greater number of adults with RMDs who are expected to remain in work. This will lead to an additional demand on healthcare and healthcare professionals to improve individuals' capacity to stay in work. Capturing whether populations and those with RMDs are in a position to extend working lives is important for identifying potential demand on healthcare (eg, greater need for nonpharmacological approaches to reduce the impact of pain linked to working practice) and employers (eg, through offering vocational rehabilitation and workplace accommodations) to manage health-related work issues and the development of employment opportunities (eg, increased access to jobs with less physical demands and include potential for flexibility [10].

Healthy working life expectancy (HWLE) is a measure of the average number of years that people in populations are healthy and in work from age 50 [11,12]; higher HWLE corresponds to longer working lives in good health, a key component of populations being able to extend working lives. Measurement of HWLE is encouraged by the European Commission and allows identification of factors that lead to lower and higher amounts of health and work in populations; variation is linked to health conditions, as well as demographic, lifestyle, and workplace factors [13,14]. There has been one previous study, which focused on the most common RMD in adults aged 50 and over, and estimated that adults aged 50 with osteoarthritis worked on average for 4.32 years less than those who did not have osteoarthritis in England [15]. However, there are no estimates of HWLE for people with RMDs in other countries in Europe and comparing estimates by country can contribute to the identification of targets and development of policies to extend working lives for people with RMDs.

In this study, we focused on HWLE from age 50 in adults with RMDs. Nationally representative data from 19 countries was used to estimate (i) HWLE in adults with and without RMDs and (ii) the association of one modifiable factor with HWLE, in this instance the role of physical (in)activity, and socioeconomic status (educational attainment) and sex, and (iii) identify how estimates differ between European countries. The overall aim is to inform health professionals in rheumatology of the extent of the reduction in healthy working life for people with RMDs and the potential need to target extending working lives through interventions and policy.

METHODS

Patient and public involvement

Methods were coproduced with people with RMDs through:

(1) actively listening to people's experiences of RMDs through qualitative interviews in previous studies. The need (i) to reduce work loss and improve work capacity is a concern for people with RMDs, (ii) for dynamic approaches and treatments to improve work capacity, either through public health, primary or secondary care was identified, and (iii) to provide data that would highlight the amount of time and work that is lost to encourage policymakers to develop policies and clinicians to focus on work.

(2) responding to the documented information needs of user-led and user-centred organisations (eg, people with arthritis/rheumatism in Europe) wishing to promote musculoskeletal health, influence policy, and advocate service improvements; these documents advocated measurement of health and work in populations to encourage change at policy level and by clinicians.

(3) convening dedicated workshops with people with RMDs to select factors that explain differences in health and work; education and physical activity were highlighted. For example, people with higher qualifications were observed as being able to retrain or modify their work roles more than people with less qualifications who were in roles that did not enable modifications. Those who were physically active were seen to be more able to better cope with the physical demands of work.

Study design and participants

Data used were from 2 longitudinal studies that collect information in people aged 50 years and over: the Survey of Health, Ageing and Retirement in Europe (SHARE) research infrastructure programme [16,17] provided data from surveys conducted in 18 countries and the English Longitudinal Study of Ageing (ELSA) [17] provided data for England. Full details of the study design, including ethical approval, and methods of data collected have been published [16–21]. SHARE and ELSA are

harmonised datasets where data collection was similar, and the same constructs were measured using the same items (albeit translated into relevant languages) to produce data for comparisons. Briefly, self-reported SHARE data were collected via interview questionnaires in a representative sample of community-dwelling adults aged 50 years and older in each participating country every 2 years. Mortality-linked data were obtained from the SHARE programme wave 1–9 (2004/2005–2021/2022), except for wave 3 (SHARELIFE), which did not follow the longitudinal SHARE questionnaire. SHARE wave 1 (or other first survey timepoint; countries did not all participate in every wave) was used as the baseline wave for identification of self-reported fixed (time-invariant) covariates sex, education, and date of birth. Similarly, ELSA data were obtained from the UK Data Service (England) waves 1–10 (2002-2021/2023). We analysed data by country. SHARE and ELSA participants may have joined the study at baseline or through sample refreshment to account for national cohort ageing or study attrition. Participants in each national sample who responded to at least one survey wave (while aged 50 years or over) were included in this study and their first non-zero cross-sectional survey weight was used as their survey weight for this study.

Assessment of health and work states

Health and work states were self-reported in each survey wave. Health was defined by the presence or absence of limiting long-standing illness, obtained from a combination of 2 survey items: "Some people suffer from chronic or long-term health problems. By long-term we mean it has troubled you over a period of time or is likely to affect you over a period of time. Do you have any long-term health problems, illness, disability or infirmity?" If so, "For the past six months at least, to what extent have you been limited because of a health problem in activities people usually do?" (In England, these items were: "Do you have any long-standing illness, disability or infirmity?" and, if so, "(Does this/Do these) illness(es) or disability(ies) limit your activities in any way?").

Work was defined, in SHARE data, as self-report of current employment situation as being employed or self-employment. In England, work was defined as participating in paid work or self-employment within the month preceding the survey.

At each survey wave, respondents were classified according to whether they were healthy or not healthy, and whether they were working or not working, or whether they had died.

RMDs were identified from self-report of ever having received a doctor diagnosis of arthritis or rheumatism. We assumed that the development of arthritis was irreversible; that is, once reported, arthritis would continue to be present, and that arthritis would not have been present before a negative survey response [22,23].

Covariates

Age was included in transition probability models and was calculated as the number of years from date of birth to date of observation (either survey date or death date). Sex (male/female) was identified by self-report. Educational attainment was categorised using 1997 International Standard Classification of Education (ISCED-97) codes: upper secondary education or higher was defined as high level of educational attainment; no, or less than upper secondary, educational attainment was defined as low educational attainment. Physical inactivity was defined as participating in less than 2 vigorous or moderate physical activities per week; physically active was defined as 2 or more. This was measured using 2 items; vigorous activity was measured using the item "How often do you engage in vigorous physical activity (such as sports, heavy housework, or a job) that involves physical labour?" Moderate activity was measured using "How often do you engage in activities that require a low or moderate level of energy such as gardening, cleaning the car, or doing a walk? Validity of the measurement of physical activity similarly across countries was addressed during survey development [16–19].

Handling of missing data is outlined in Supplementary Material File.

Statistical analysis

A multistate model was defined comprising 2 living states (healthy and working, and otherwise) and an absorbing mortality state; that is a 3-state model where healthy and not in work, not healthy and in work, and not healthy and not in work are combined into a not 'healthy and in work' state (Supplementary Fig). Interpolated Markov Chain multistate modelling was performed to estimate HWLE with 95% confidence intervals, using IMaCh software version 0.99r19. Guidance on the use of IMaCh software and code is available at https://euroreves.ined.fr/imach/wiki/index.php/Documentation. This approach uses multinomial logistic regression to model the probabilities of transition from and to each HWLE state (or transition to the dead vital state) over discrete time intervals (interpolation steps) based on the transitions observed in the data. Maximum likelihood estimates of transition probability model parameters were found by evaluating the product of the transition probabilities for each step contained within each observed transition (health and work states at consecutive observed time points) or sequence of transitions (where more than one transition was observed for an individual). HWLE was estimated according to the health and work state occupied at age 50 years and averaged (weighted by the prevalence of occupying each health and work state at age 50 years) to estimate HWLE for the population. Further details are provided elsewhere [11,12]. The prevalence of state occupation at age 50 was taken as the mean of the forward and backward stable prevalences from the IMaCh transition model, weighted by the years to convergence.

First of all, HWLE was estimated overall for all the countries, and then by sex and education. HWLE was then estimated for those with and without arthritis for each country and then by sex, education and physical inactivity. Estimates are presented for 19 countries.

RESULTS

Sample characteristics

Table 1 describes the sample sizes for each of the 19 countries; Supplementary Table S1a and S1b provides further detail.

HWLE varied across the 19 countries (Table 2). HWLE was highest in Switzerland (10.98; 95% CI: 10.64-11.32) years from age 50) and lowest in Romania (5.28 years; 4.08, 6.48); that is, if everyone were to live their healthy working years consecutively, in Switzerland, on average people from age 50 were healthy and in work until they were 60.98 years old, while in Romania it was 55.28 years. Supplementary Table S2a and S2b shows estimates of HWLE for each country overall and stratified by sex, educational attainment, and physical inactivity.

Table 1

Observed and weighted numbers and percentages of variables at baseline wave.

(A)				Austria	Belgium	Czech_Republic	Denmark	England	Estonia	France	Germany	Greece
Baseline wave				1	1	2	1	1	4	1	1	1
No. of survey wave timepoints analysed				8	8	7	8	10	6	8	8	6
Calendar year period of survey time points				2004-2022	2004-2022	2006-2022	2004-2022	2002-2023	2010-2022	2004-2022	2004-2022	2004-2022
Total participants			Observed sample size	1534	3694	2618	1660	10,488	6791	2988	2924	2836
			Weighted sample size	2,763,714	3,668,946	3,581,609	1,867,472	10,679	499,727	20,785,265	30,505,708	3,926,132
Age	Median		Observed	64 (57-72)	63 (55-72)	62 (56 -70)	61 (55-72)	64 (56-73)	65 (58-74)	62 (55-73)	63 (56-70)	61 (54-71)
	(IQR)		Weighted	63 (56-73)	64 (56-74)	62 (55-71)	61 (55-72)	64 (56-73)	63 (56-73)	64 (56-74)	64 (56-72)	64 (55-72)
Sex	Female		Observed sample size	896 (58.4%)	1991 (53.9%)	1495 (57.1%)	906 (54.6%)	5579 (53.2%)	4047 (59.6%)	1677 (56.1%)	1569 (53.7%)	1599 (56.4%)
			Weighted sample size	1,551,545 (56.1%)	2,027,194 (55.3%)	1,978,938 (55.3%)	1,006,739 (53.9%)	5702 (53.4%)	305,857 (61.2%)	11,604,436 (55.8%)	16,879,063 (55.3%)	2,156,633 (54.9%)
	Male		Observed sample size	638 (41.6%)	1703 (46.1%)	1123 (42.9%)	754 (45.4%)	4909 (46.8%)	2744 (40.4%)	1311 (43.9%)	1355 (46.3%)	1237 (43.6%)
			Weighted sample size	1,212,169 (43.9%)	1,641,752 (44.7%)	1,602,671 (44.7%)	860,733 (46.1%)	4977 (46.6%)	193,870 (38.8%)	9,180,829 (44.2%)	13,626,645 (44.7%)	1,769,499 (45.1%)
RMDs			Observed sample size	164 (10.7%)	827 (22.4%)	417 (15.9%)	432 (26.0%)	3215 (30.7%)	1915 (28.2%)	912 (30.5%)	341 (11.7%)	467 (16.5%)
			Weighted sample size	295,173 (10.7%)	882,692 (24.1%)	563,351 (15.7%)	489,398 (26.2%)	3263 (30.6%)	138,966 (27.8%)	6,433,085 (31.0%)	3,696,600 (12.1%)	700,659 (17.8%)
Sex + RMDs	Male + RMDs		Observed sample size	43 (26.2%)	281 (34.0%)	148 (35.5%)	147 (34.0%)	1192 (37.1%)	584 (30.5%)	309 (33.9%)	125 (36.7%)	118 (25.3%)
			Weighted sample size	83,999 (28.5%)	287,476 (32.6%)	194,595 (34.5%)	167,280 (34.2%)	1199 (36.7%)	39,492 (28.4%)	2,180,084 (33.9%)	1,252,960 (33.9%)	186,967 (26.7%)
	Female + RMDs		Observed sample size	121 (73.8%)	546 (66.0%)	269 (64.5%)	285 (66.0%)	2023 (62.9%)	1331 (69.5%)	603 (66.1%)	216 (63.3%)	349 (74.7%)
			Weighted sample size	211,174 (71.5%)	595,216 (67.4%)	368,756 (65.5%)	322,118 (65.8%)	2064 (63.3%)	99,474 (71.6%)	4,253,001 (66.1%)	2,443,640 (66.1%)	513,692 (73.3%)
Education	Less than high school + RMDs		Observed sample size	67 (40.9%)	499 (60.3%)	278 (66.7%)	131 (30.3%)	1822 (56.7%)	661 (34.5%)	579 (63.5%)	81 (23.8%)	368 (78.8%)
			Weighted sample size	119,763 (40.6%)	515,952 (58.5%)	314,850 (55.9%)	150,528 (30.8%)	1859 (57.0%)	48,320 (34.8%)	4,150,987 (64.5%)	1,009,305 (27.3%)	563,374 (80.4%)
	Less than high school + no RMDs		Observed sample size	428 (31.2%)	1396 (48.7%)	1205 (54.7%)	287 (23.4%)	3159 (43.4%)	1408 (28.9%)	1011 (48.7%)	426 (16.5%)	1347 (56.9%)
			Weighted sample size	769,791 (31.2%)	1,345,843 (48.3%)	1,348,031 (44.7%)	323,984 (23.5%)	3244 (43.7%)	100,354 (27.8%)	7,145,276 (49.8%)	4,776,742 (17.8%)	1,935,146 (60.0%)
Physical inactivity	Inactive + RMDs		Observed sample size	66 (40.2%)	345 (41.7%)	180 (43.2%)	101 (23.4%)	1602 (49.8%)	703 (36.7%)	323 (35.4%)	95 (27.9%)	200 (42.8%)
			Weighted sample size	120,978 (41.0%)	381,210 (43.2%)	208,701 (37.0%)	116,468 (23.8%)	1633 (50.0%)	50,422 (36.3%)	2,370,318 (36.8%)	1,174,606 (31.8%)	300,728 (42.9%)
	Inactive + no RMDs		Observed sample size	439 (32.0%)	721 (25.1%)	864 (39.3%)	198 (16.1%)	2467 (33.9%)	1311 (26.9%)	663 (31.9%)	538 (20.8%)	621 (26.2%)
			Weighted sample size	815,525 (33.0%)	719,978 (25.8%)	1,054,829 (34.9%)	223,281 (16.2%)	2535 (34.2%)	94,448 (26.2%)	4,620,090 (32.2%)	6,179,886 (23.1%)	879,151 (27.3%)

(B)			Hungary	Italy	Netherlands	Poland	Portugal	Romania	Slovenia	Spain	Sweden	Switzerland
Baseline wave			4	1	1	2	4	7	4	1	1	1
No. of survey wave timepoints analysed			4	8	6	6	5	3	6	8	8	8
Calendar year period of survey time points			2011-2022	2004-2022	2004-2022	2006-2022	2011-2022	2017-2022	2011-2022	2004-2022	2004-2022	2004-2022
Total participants		Observed sample size	2997	2527	2854	2412	1915	1592	2719	2281	2973	941
		Weighted sample size	3,860,758	21,724,321	5,202,962	12,252,857	3,831,766	5,835,238	765,280	765,280	3,293,191	2,442,040
Age	Median (IQR)	Observed	63 (57-71)	63 (57-70)	61 (55-70)	61 (55-71)	64 (56-71)	63 (58 -70)	64 (57-73)	66 (57-74)	63 (57-72)	63 (56-72)
		Weighted	62 (56-72)	64 (57-73)	61 (55-71)	60 (54-71)	64 (56-73)	63 (57-71)	63 (56-73)	65 (56-74)	63 (56-73)	62 (55-73)
Sex	Female	Observed sample size	1694 (56.5%)	1409 (55.8%)	1524 (53.4%)	1351 (56.0%)	1073 (56.0%)	930 (58.4%)	1539 (56.6%)	1326 (58.1%)	1592 (53.5%)	507 (53.9%)
		Weighted sample size	2,290,998 (59.3%)	12,010,584 (55.3%)	2,784,930 (53.5%)	7,059,560 (57.6%)	2,124,906 (55.5%)	3,444,778 (59.0%)	422,588 (55.2%)	7,688,530 (54.8%)	1,781,202 (54.1%)	1,330,592 (54.5%)
	Male	Observed sample size	1303 (43.5%)	1118 (44.2%)	1330 (46.6%)	1061 (44.0%)	842 (44.0%)	662 (41.6%)	1180 (43.4%)	955 (41.9%)	1381 (46.5%)	434 (46.1%)
		Weighted sample size	1,569,760 (40.7%)	9,713,737 (44.7%)	2,418,032 (46.5%)	5,193,297 (42.4%)	1,706,860 (44.5%)	2,390,460 (41.0%)	342,692 (44.8%)	6,330,161 (45.2%)	1,511,989 (45.9%)	1,111,448 (45.5%)
RMDs		Observed sample size	1194 (39.8%)	801 (31.7%)	265 (9.3%)	829 (34.4%)	553 (28.9%)	255 (16.0%)	272 (10.0%)	692 (30.3%)	287 (9.7%)	101 (10.7%)
		Weighted sample size	1,515,734 (39.3%)	6,867,196 (31.6%)	497,739 (9.6%)	4,084,331 (33.3%)	978,821 (25.5%)	889,607 (15.2%)	71,491 (9.3%)	3,918,119 (27.9%)	328,430 (10.0%)	267,232 (10.9%)
Sex + RMDs	Male + RMDs	Observed sample size	425 (35.6%)	254 (31.7%)	74 (27.9%)	299 (36.1%)	175 (31.6%)	70 (27.5%)	79 (29.0%)	197 (28.5%)	79 (27.5%)	29 (28.7%)
		Weighted sample size	485,364 (32.0%)	2,064,609 (30.1%)	128,260 (25.8%)	1,371,005 (33.6%)	234,942 (24.0%)	224,676 (25.3%)	19,007 (26.6%)	1,168,859 (29.8%)	85,936 (26.2%)	70,767 (26.5%)
	Female + RMDs	Observed sample size	769 (64.4%)	547 (68.3%)	191 (72.1%)	530 (63.9%)	378 (68.4%)	185 (72.5%)	193 (71.0%)	495 (71.5%)	208 (72.5%)	72 (71.3%)
		Weighted sample size	1,030,370 (68.0%)	4,802,587 (69.9%)	369,479 (74.2%)	2,713,326 (66.4%)	743,879 (76.0%)	664,931 (74.7%)	52,484 (73.4%)	2,749,260 (70.2%)	242,494 (73.8%)	196,465 (73.5%)
Education	Less than high school + RMDs	Observed sample size	487 (40.8%)	680 (84.9%)	152 (57.4%)	474 (57.2%)	494 (89.3%)	157 (61.6%)	125 (46.0%)	639 (92.3%)	162 (56.4%)	68 (67.3%)
		Weighted sample size	598,091 (39.5%)	5,788,307 (84.3%)	289,627 (58.2%)	2,318,224 (56.8%)	876,549 (89.6%)	565,981 (63.6%)	30,579 (42.8%)	3,540,239 (90.4%)	193,362 (58.9%)	178,483 (66.8%)
	Less than high school + no RMDs	Observed sample size	456 (25.3%)	1282 (74.3%)	1471 (56.8%)	669 (42.3%)	1026 (75.3%)	630 (47.1%)	820 (33.5%)	1313 (82.6%)	1404 (52.3%)	423 (50.4%)
		Weighted sample size	645,602 (27.5%)	10,889,740 (73.3%)	2,690,030 (57.2%)	3,418,101 (41.8%)	2,168,600 (76.0%)	2,473,425 (50.0%)	229,194 (33.0%)	8,043,656 (79.6%)	1,554,809 (52.4%)	1,112,942 (51.2%)
Physical inactivity	Inactive + RMDs	Observed sample size	543 (45.5%)	344 (42.9%)	76 (28.7%)	432 (52.1%)	286 (51.7%)	119 (46.7%)	105 (38.6%)	227 (32.8%)	66 (23.0%)	26 (25.7%)
		Weighted sample size	757,234 (50.0%)	3,145,155 (45.8%)	144,123 (29.0%)	2,185,056 (53.5%)	496,525 (50.7%)	398,353 (44.8%)	30,368 (42.5%)	1,251,498 (31.9%)	87,341 (26.6%)	65,979 (24.7%)
	Inactive + no RMDs	Observed sample size	564 (31.3%)	600 (34.8%)	457 (17.7%)	612 (38.7%)	686 (50.4%)	467 (34.9%)	649 (26.5%)	379 (23.9%)	406 (15.1%)	139 (16.5%)
		Weighted sample size	738,390 (31.5%)	5,584,635 (37.6%)	896,866 (19.1%)	3,106,093 (38.0%)	1,613,039 (56.5%)	1,587,977 (32.1%)	172,108 (24.8%)	2,326,352 (23.0%)	468,721 (15.8%)	379,893 (17.5%)

RMDs, rheumatic and musculoskeletal diseases.

Table 2

Estimates (and 95% CI) of healthy working life expectancy for adults aged 50 years and over (including adults with and without arthritis, stratified by sex, education, and physical inactivity)

		Austria	Belgium	Czech Republic	Denmark	England	Estonia	France	Germany	Greece
Overall		5.82 (5.43, 6.21)	7.08 (6.79, 7.37)	7.13 (6.87, 7.39)	9.57 (9.23, 9.91)	10.56 (10.35, 10.77)	8.33 (8.01, 8.65)	7.28 (7.02, 7.54)	6.90 (6.54, 7.26)	9.67 (9.22, 10.12)
RMDs	No RMDs	6.05 (5.65, 6.45)	7.68 (7.37, 7.99)	7.55 (7.28, 7.82)	10.47 (10.10, 10.84)	11.55 (11.31, 11.79)	9.21 (8.87, 9.55)	7.70 (7.40, 8.00)	7.43 (7.06, 7.80)	9.94 (9.48, 10.40)
	RMDs	2.60 (1.49, 3.71)	4.95 (4.39, 5.51)	5.25 (4.64, 5.86)	6.53 (5.88, 7.18)	6.92 (6.50, 7.34)	4.54 (3.96, 5.12)	5.86 (5.38, 6.34)	3.96 3.25, 4.67)	6.14 (4.57, 7.71)
	Difference (%) in HWLE between no RMD and RMD	3.45 (43.0%)	2.73 (64.5%)	2.3 (69.5%)	3.94 (62.4%)	4.63 (59.9%)	4.67 (49.3%)	1.84 (76.1%)	3.47 (53.3%)	3.8 (61.8%)
Sex + RMDs	Male + RMDs	3.55 (2.27, 4.83)	5.29 (4.66, 5.92)	6.28 (5.62, 6.94)	7.67 (6.95, 8.39)	8.18 (7.71, 8.65)	4.16 (3.58, 4.74)	5.88 (5.35, 6.41)	3.96 (3.17, 4.75)	10.13 (8.56, 11.70)
	Female + RMDs	2.43 (1.38, 3.48)	4.75 (4.18, 5.32)	4.85 (4.22, 5.48)	5.88 (5.19, 6.57)	5.89 (5.46, 6.32)	4.78 (4.15, 5.41)	5.76 (5.24, 6.28)	3.93 (3.21, 4.65)	5.67 (4.17, 7.17)
	Male + no RMDs	7.09 (6.58, 7.60)	8.07 (7.69, 8.45)	7.94 (7.60, 8.28)	11.46 (11.00, 11.92)	12.69 (12.39, 12.99)	8.76 8.31, 9.21)	7.83 (7.47, 8.19)	7.67 (7.18, 8.16)	12.70 (12.23, 13.17)
	Female + no RMDs	5.36 (4.89, 5.83)	7.23 (6.82, 7.64)	7.11 (6.73, 7.49)	9.38 (8.88, 9.88)	10.32 (10.01, 10.63)	9.66 (9.19, 10.13)	7.66 (7.26, 8.06)	7.22 (6.75, 7.69)	7.52 (6.91, 8.13)
Education + RMDs	High school + RMDs	2.97 (1.81, 4.13)	5.57 (4.99, 6.15)	6.11 (5.46, 6.76)	7.06 (6.41, 7.71)	7.51 (7.09, 7.93)	4.85 (4.25, 5.45)	6.13 (5.64, 6.62)	4.15 (3.43, 4.87)	6.90 (5.26, 8.54)
	Less than high school + RMDs	1.38 (0.56, 2.20)	3.41 (2.75, 4.07)	3.53 (2.90, 4.16)	4.70 (3.61, 5.79)	5.65 (5.11, 6.19)	2.49 (1.89, 3.09)	5.10 (4.47, 5.73)	2.29 (1.44, 3.14)	5.82 (4.20, 7.44)
	High school + no RMDs	6.59 (6.19, 6.99)	8.21 (7.88, 8.54)	8.18 (7.87, 8.49)	10.80 (10.42, 11.18)	11.97 (11.72, 12.22)	9.73 (9.37, 10.09)	8.05 (7.74, 8.36)	7.63 (7.25, 8.01)	10.59 (10.08, 11.10)
	Less than high school + no RMDs	3.71 (2.94, 4.48)	6.23 (5.67, 6.79)	5.79 (5.32, 6.26)	7.96 (6.90, 9.02)	10.18 (9.72, 10.64)	5.89 (5.00, 6.78)	6.46 (5.89, 7.03)	4.79 (3.68, 5.90)	8.82 (8.11, 9.53)
Physical inactivity + RMDs	Active + RMDs	2.79 (1.67, 3.91)	5.24 (4.67, 5.81)	5.41 (4.82, 6.00)	6.97 (6.32, 7.62)	8.40 (7.97, 8.83)	5.00 (4.40, 5.60)	6.23 (5.75, 6.71)	3.96 (3.25, 4.67)	6.59 (4.98, 8.20)
	Inactive + RMDs	2.18 (1.01, 3.35)	4.04 (3.32, 4.76)	4.49 (3.55, 5.43)	4.69 (3.56, 5.82)	5.16 (4.66, 5.66)	2.96 (2.31, 3.61)	4.92 (4.28, 5.56)	3.27 (2.39, 4.15)	6.83 (5.21, 8.45)
	Active + no RMDs	6.35 (5.94, 6.76)	7.82 (7.49, 8.15)	7.69 (7.41, 7.97)	10.73 (10.35, 11.11)	12.25 (12.00, 12.50)	9.67 (9.30, 10.04)	7.99 (7.67, 8.31)	7.57 (7.18, 7.96)	9.91 (9.40, 10.42)
	Inactive + no RMDs	5.22 (4.41, 6.03)	6.93 (6.32, 7.54)	7.10 (6.44, 7.76)	8.58 (7.49, 9.67)	9.08 (8.64, 9.52)	7.13 (6.36, 7.90)	7.01 (6.48, 7.54)	6.76 (5.94, 7.58)	9.97 (9.24, 10.70)

		Hungary	Italy	Netherlands	Poland	Portugal	Romania	Slovenia	Spain	Sweden	Switzerland
Overall		8.26 (7.66, 8.86)	7.22 (6.84, 7.60)	8.15 (7.71, 8.59)	6.13 (5.69, 6.57)	7.90 (7.06, 8.74)	5.28 (4.08, 6.48)	6.42 (6.02, 6.82)	5.98 (5.62, 6.34)	10.70 (10.41, 10.99)	10.98 (10.64, 11.32)
RMDS	No RMDs	9.37 (8.86, 9.88)	7.64 (7.24, 8.04)	8.32 (7.89, 8.75)	6.54 (6.09, 6.99)	8.05 (7.22, 8.88)	5.35 (4.14, 6.56)	6.57 (6.17, 6.97)	6.38 (5.99, 6.77)	11.11 (10.81, 11.41)	11.47 (11.10, 11.84)
	RMDs	4.70 (2.73, 6.67)	5.36 (4.57, 6.15)	3.82 (3.25, 4.39)	4.60 (3.72, 5.48)	8.05 (6.17, 9.93)	4.96 (1.31, 8.61)	3.17 (1.44, 4.90)	3.62 (2.93, 4.31)	7.37 (6.56, 8.18)	8.13 (7.34, 8.92)
	Difference (%) in HWLE between no RMD and RMD	4.67 (50.2%)	2.28 (70.2%)	4.50 (45.9%)	1.94 (70.3%)	0.00 (100.0%)	0.39 (92.7%)	3.40 (48.3%)	2.76 (56.7%)	3.74 (66.3%)	3.34 (70.9%)
Sex +RMDs	Male +RMDs	7.04 (5.73, 8.35)	7.74 (6.92, 8.56)	4.65 (3.83, 5.47)	5.91 (4.93, 6.89)	9.29 (6.95, 11.63)	5.03 (1.30, 8.76)	3.16 (1.42, 4.90)	5.09 (4.27, 5.91)	8.21 (7.38, 9.04)	8.59 (7.70, 9.48)
	Female + RMDs	4.19 (2.86, 5.52)	4.58 (3.78, 5.38)	3.67 (3.11, 4.23)	3.78 (2.94, 4.62)	7.76 (5.86, 9.66)	5.17 (1.51, 8.83)	3.07 (1.34, 4.80)	3.30 (2.62, 3.98)	6.90 (6.07, 7.73)	7.75 (6.96, 8.54)
	Male + no RMDs	10.73 (10.15, 11.31)	9.23 (8.79, 9.67)	9.58 (9.07, 10.09)	7.81 (7.23, 8.39)	9.29 (8.30, 10.28)	6.54 (5.13, 7.95)	7.08 (6.60, 7.56)	7.29 (6.79, 7.79)	11.97 (11.60, 12.34)	12.49 (12.02, 12.96)
	Female + no RMDs	7.84 (7.17, 8.51)	6.21 (5.67, 6.75)	7.01 (6.44, 7.58)	5.50 (4.97, 6.03)	6.96 (5.96, 7.96)	5.00 (3.61, 6.39)	6.06 (5.50, 6.62)	5.70 (5.21, 6.19)	10.26 (9.84, 10.68)	10.48 (10.01, 10.95)
Education +RMDs	High school + RMDs	5.15 (3.97, 6.33)	8.03 (7.13, 8.93)	4.20 (3.41, 4.99)	4.80 (3.93, 5.67)	10.26 (7.66, 12.86)	5.96 (1.95, 9.97)	3.63 (1.82, 5.44)	4.88 (4.04, 5.72)	7.62 (6.81, 8.43)	8.56 (7.75, 9.37)
	Less than high school + RMDs	3.44 (2.56, 4.32)	3.94 (3.18, 4.70)	3.64 (3.05, 4.23)	4.19 (2.95, 5.43)	8.13 (6.29, 9.97)	4.38 (0.91, 7.85)	1.77 (0.49, 3.05)	3.15 (2.50, 3.80)	5.87 (4.86, 6.88)	6.36 (5.37, 7.35)
	High school + no RMDs	10.05 (9.54, 10.56)	9.85 (9.34, 10.36)	9.32 (8.83, 9.81)	6.90 (6.45, 7.35)	8.94 (7.54, 10.34)	6.21 (4.89, 7.53)	7.30 (6.91, 7.69)	8.55 (7.97, 9.13)	11.48 (11.16, 11.80)	11.79 (11.40, 12.18)
	Less than high school + no RMDs	5.98 (4.86, 7.10)	5.87 (5.39, 6.35)	6.40 (5.76, 7.04)	5.13 (4.03, 6.23)	7.62 (6.74, 8.50)	4.03 (2.48, 5.58)	3.67 (2.80, 4.54)	5.37 (4.93, 5.81)	9.86 (9.24, 10.48)	10.38 (9.64, 11.12)
Physical inactivity +RMDs	Active + RMDs	5.17 (3.88, 6.46)	6.01 (5.20, 6.82)	3.49 (2.87, 4.11)	4.73 (3.84, 5.62)	8.77 (6.92, 10.62)	5.26 (1.64, 8.88)	3.29 (1.57, 5.01)	4.13 (3.41, 4.85)	7.41 (6.60, 8.22)	7.67 (6.86, 8.48)
	Inactive + RMDs	4.66 (3.57, 5.75)	4.10 (3.20, 5.00)	4.08 (3.44, 4.72)	4.40 (3.35, 5.45)	6.73 (4.40, 9.06)	4.54 (0.15, 8.93)	3.37 (1.25, 5.49)	2.75 (1.98, 3.52)	6.02 (4.92, 7.12)	7.13 (6.12, 8.14)
	Active +no RMDs	9.86 (9.24, 10.48)	7.78 (7.32, 8.24)	8.48 (8.03, 8.93)	6.87 (6.38, 7.36)	8.27 (7.36, 9.18)	5.57 (4.36, 6.78)	6.52 (6.11, 6.93)	6.75 (6.34, 7.16)	11.27 (10.96, 11.58)	11.61 (11.22, 12.00)
	Inactive + no RMDs	8.62 (7.94, 9.30)	7.36 (6.77, 7.95)	6.98 (5.81, 8.15)	5.89 (5.09, 6.69)	7.22 (5.98, 8.46)	4.37 (2.01, 6.73)	7.18 (6.15, 8.21)	5.06 (4.33, 5.79)	10.11 (9.24, 10.98)	10.75 (9.97, 11.53)

HWLE, Healthy working life expectancy; RMDs, rheumatic and musculoskeletal diseases.

Comparing HWLE between populations with and without RMDs in 19 countries across Europe

In 18 of the 19 countries, HWLE was lower for the populations with RMDs than in the populations without RMDs (Fig 1). In Portugal, HWLE was similar in both populations with and without RMDs. In 6 of the 19 countries, HWLE in the populations with RMDs was around 50% or less, from age 50 years, of the populations without RMDs. The lowest HWLE for populations with RMDs was for Austria: 2.60 (1.49, 3.71) years, which was 43.0% of HWLE for the population without RMD. The other countries were Netherlands (45.9%), Slovenia (48.3%), Estonia (49.3%), Hungary (50.2%), and Germany (53.3%). In a further 6 countries, HWLE for the population with RMDs was greater than a third less than for the population without RMD: Spain (56.7%), England (59.9%), Greece (61.8%), Denmark (62.4%), Belgium (64.5%), and Sweden (66.3%). The greatest difference in HWLE between populations with and without RMDs was in Estonia and Hungary (both 4.67 years).

Of the countries showing a difference, the country with the smallest difference in HWLE between populations with and without RMDs was France; HWLE for the population with RMDs was 76.1% of the population without RMDs. The country with the highest HWLE for the population with RMDs was Switzerland (8.13 [7.34, 8.92] years).

Comparing HWLE by sex for the population within countries with RMDs

In populations with RMDs, HWLE was higher in men than in women in 17 countries (Fig. 2); the greatest difference (56%) was in Greece where men with RMDs on average were healthy and in work for 10.13 (8.56, 11.70) years and women for 5.67 (4.17, 7.17) years. HWLE was higher for women than for men in Estonia and Romania. The lowest HWLE for women with RMDs was in Austria (2.43 [1.38, 3.48] years) and for men with RMDs was in Slovenia (3.16 [1.42, 4.90] years).

Comparing HWLE by education for the population within countries with RMDs

In populations with RMDs, HWLE was lower in all countries for populations with lower education. Austria had the lowest HWLE for populations with RMDs with high education (2.97 [1.81, 4.13] years) as well as for the population with RMDs with low education (1.38 [0.56, 2.20] years). Portugal had the highest HWLE for populations with RMDs and high education (10.26 [7.66, 12.86] years) and for RMDs and low education (8.13 [6.29, 9.97]years). The greatest difference, within a country, in HWLE between populations with high and low education for

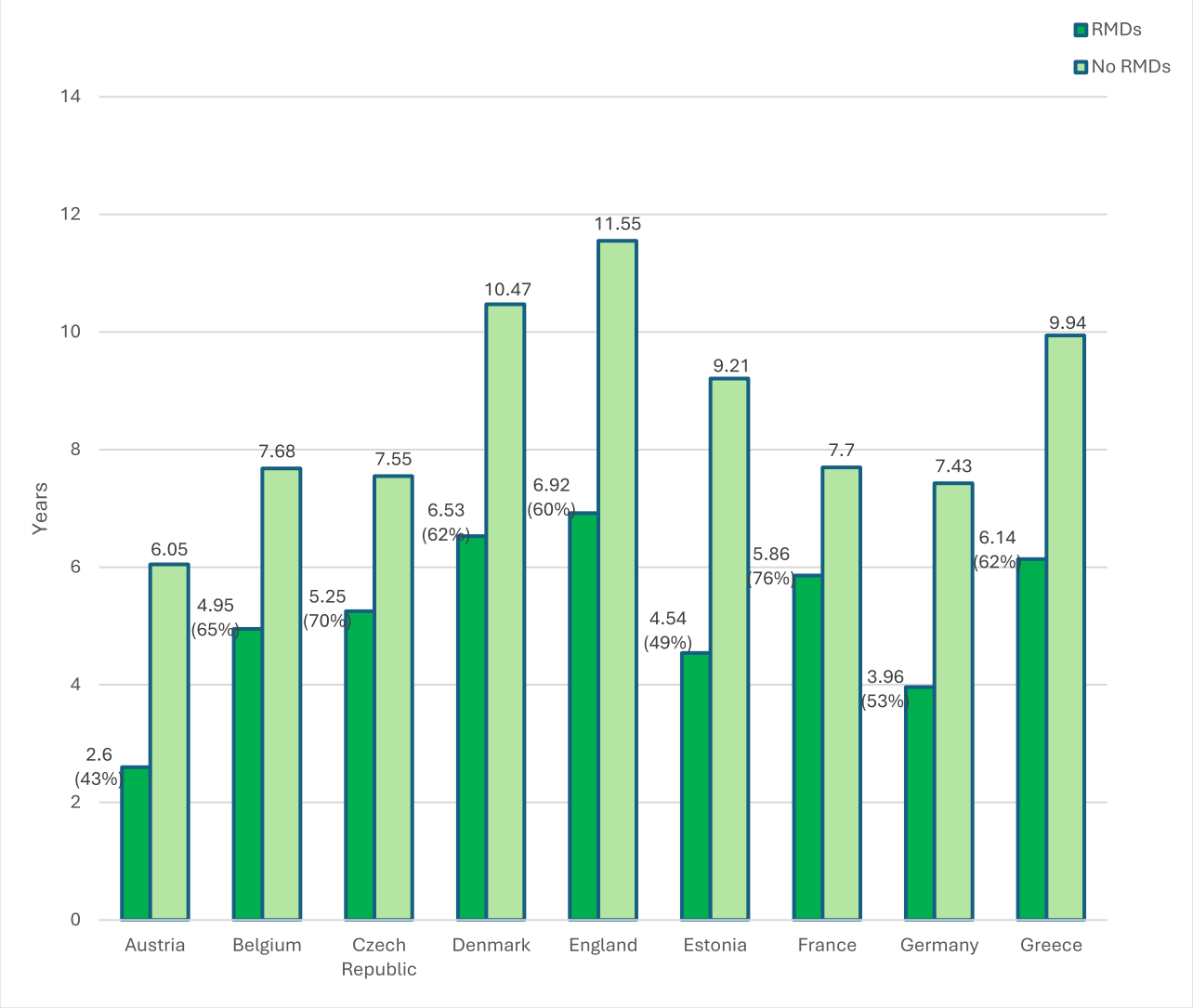

Figure 1. (A) Healthy working life expectancy for adults over 50 with or without RMDs stratified by country. (B) Healthy working life expectancy for adults over 50 with or without RMDs stratified by country. RMDs, rheumatic and musculoskeletal diseases.

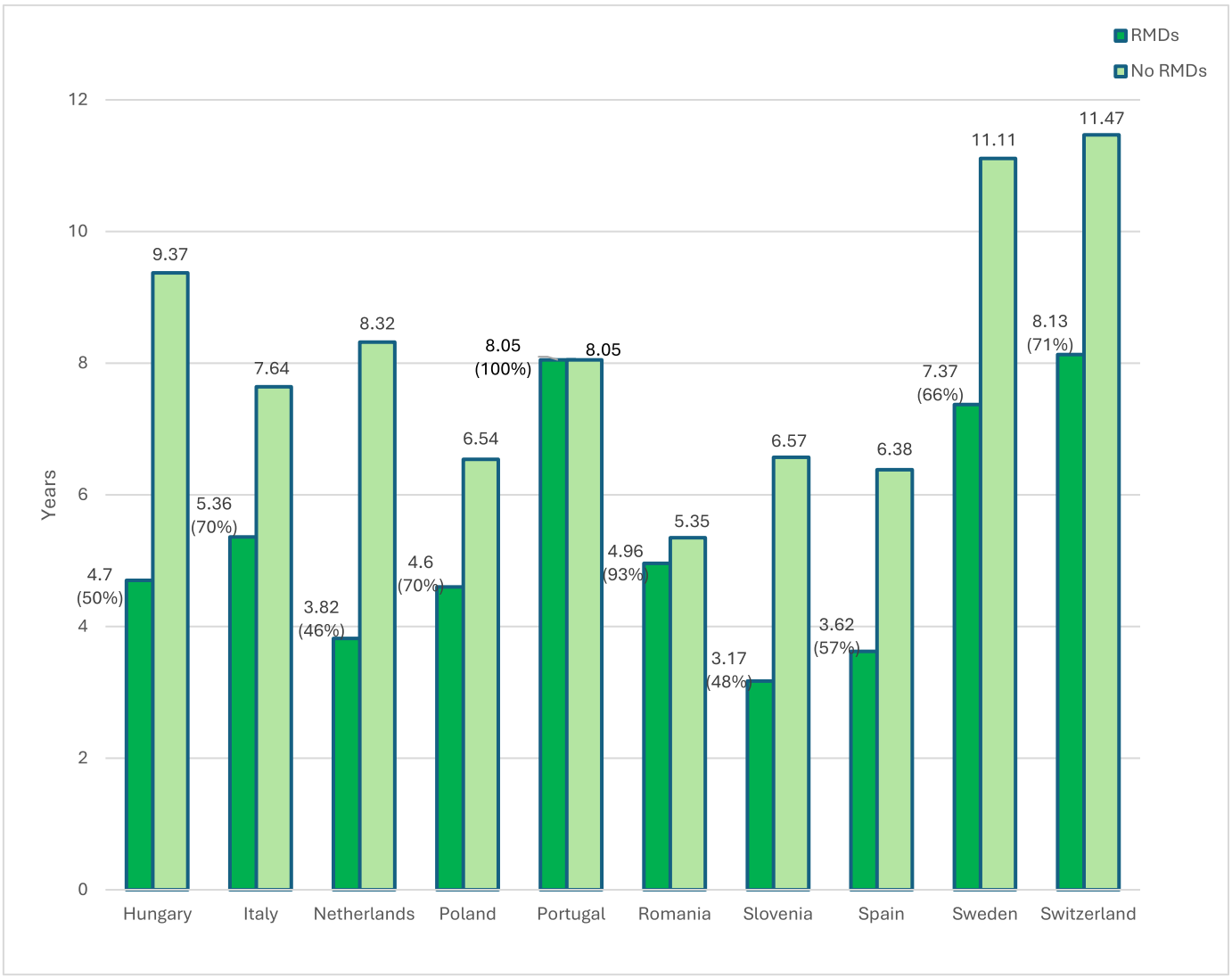

Figure 1. Continued.

those with RMDs, was for Italy (4.09 years; 8.03 [7.13, 8.93] years compared to 3.94 [3.18, 4.70] years).

Comparing HWLE by physical activity for the population within countries with RMDs

For those with RMDs, HWLE was higher in the populations who were categorised as being physically active in 16 countries. In Slovenia, Netherlands, and Greece, in the population with RMDs, HWLE was similar in the populations who were categorised as physically active and physically inactive. In 4 countries (Denmark, England, Estonia, and Spain), in the populations with RMDs who were physically inactive, HWLE was approximately one-third or less than that of the population of those who had RMDs and were physically active.

DISCUSSION

Key findings

This study has used nationally representative longitudinal data from 19 countries across Europe to estimate the average amount of time that adults who have RMDs are healthy and in work from age 50. These results indicate that RMDs are associated with a significant reduction in length of healthy working life; in 6 countries, the number of years that the population with RMDs were healthy and in work was around a half, or less, than that of the population without RMDs. This could indicate the extent of the role that joint pain, fatigue, and related disability, as well as other symptoms and morbidities that people with RMDs experience, have on being healthy and in work. HWLE will differ due to a range of factors and the differences in the amount of HWLE in populations with RMDs by country indicate differences in disability pension schemes and support for people with RMDs in the workplace to compensate for the mismatch in work capacity.

Differences by sex, education, and physical (in)activity, as well as country, highlight the role of broader factors (including retraining and workplace support) and indicate there are opportunities to improve the number of years that people can be healthy and in work. Levels of job access, differences in available occupations in each country, caring responsibilities, menopause and differences in state pension age will contribute to variation by sex [24]. For example, in 2023, state retirement age was 5 years higher for men than for women in Austria and Poland (65 years compared to 60 years). As well as indicating the relationship HWLE has with educational level, education acts as a proxy for socioeconomic status [25]. Lower education

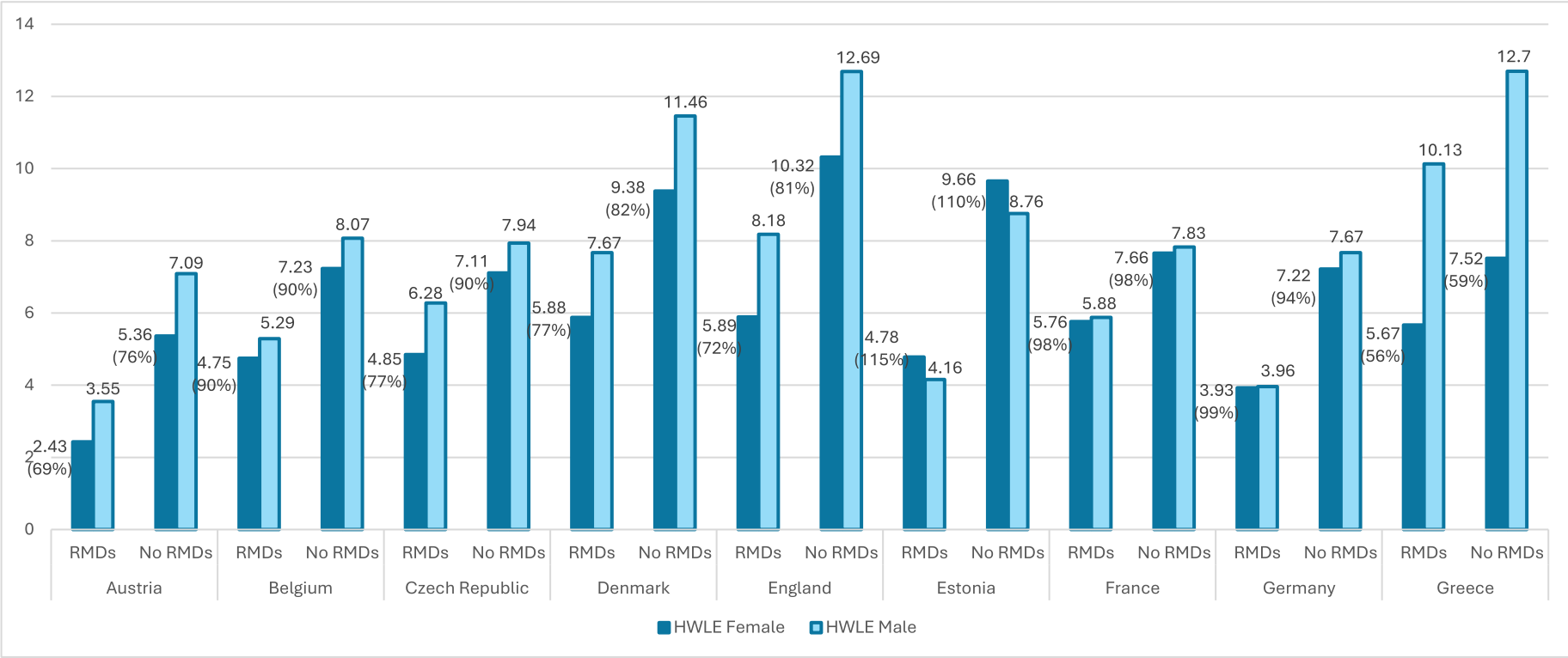

Figure 2. (A) Healthy working life expectancy (HWLE) for females and males with or without RMDs stratified by country. (B) HWLE for females and males with or without RMDs stratified by country. RMDs, rheumatic and musculoskeletal diseases.

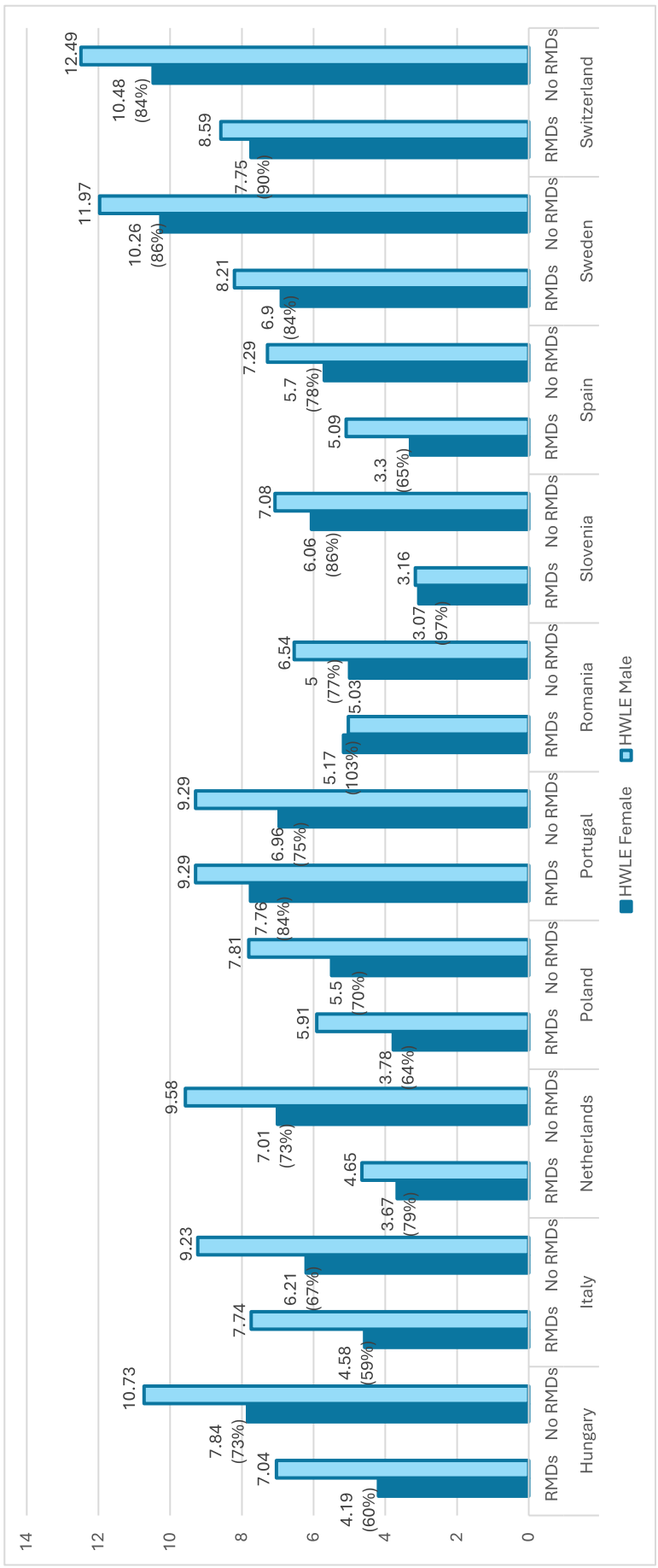

Figure 2. Continued.

is associated with occupations with less skill, latitude, and decision authority and a higher likelihood of environmental exposures to harmful conditions including adverse ergonomic and physical demands [26]. People with lower education are more likely to be in jobs where there is a mismatch between their capacity to meet job demands [26]. Lower educational attainment reduces the ability to adapt or change roles, and there is less opportunity to manage the impacts of joint pain and disability on employment [24,26].

Physical activity is associated with longer healthy working lives in people with and without RMDs; in 16 countries, HWLE was less for the physically inactive RMD population compared to the active. While this is an association, it suggests that this may be one opportunity to increase healthy working life through interventions. Physical activity has long been acknowledged as being beneficial for physical and mental health and also for maintaining work participation for people with RMDs [27]. Through its wider effect on health, increasing physical activity would be expected to achieve an increase in health subsequently increasing HWLE. Notably, HWLE was higher for people with RMDs who were inactive compared to active in Greece, the Netherlands, and Slovenia. In these countries, the prevalence of RMDs was much lower than in the countries where HWLE is lower with inactivity; this could suggest that doctor-diagnosed arthritis differs by country and that diagnosis is given when arthritis is more severe in Greece, the Netherlands, and Slovenia. This may also indicate that activity levels act to some extent as a proxy for the severity of arthritis (more severe pain and disability will lead to less activity).

Comparison with other studies

The results are comparable to others focusing on HWLE. Cross-country variation in HWLE reported using the Sullivan method (which tends to underestimate estimates compared to IMaCh) are lower than in this study (eg, HWLE for men in England in this study is 8.24 [7.85, 8.64] and was 5.07 [4.84, 5.29] when using the Sullivan method) [28]. Previously published estimates of HWLE in England who reported having a doctor diagnosis of osteoarthritis (6.56 [5.99, 7.12] years) were lower than those in this study [15]; this is explained by more recent waves of data used in this study, in which state pension age has increased, as well as no observed deaths in more recent ELSA waves; this systematically underrepresents mortality transitions relative to alive-to-alive transitions. However, because HWLE is primarily experienced at younger ages from age 50, when mortality rates are relatively low compared to later ages, this potential upwards bias in HWLE is likely to be small. The differences within country between men and women with RMDs might be explained by the availability of jobs that allow people with RMDs to work through the prevention of pain and disability to remain healthy and in work. Lower HWLE for women may also reflect cultural expectation that women will stop working earlier or focus on unpaid work such as caring responsibilities [29].

Strengths and limitations

The strengths of this study include the use of nationally representative longitudinal datasets with sufficient sample sizes for comparison of HWLE by country. HWLE was estimated using multistate models which consider the transition between states between time points and is considered the best approach for generating health expectancy estimates [30]. However, these methods demand large sample sizes across multiple dimensions: sufficient participants and waves to generate adequate total transitions, sufficient observations within each subgroup of interest (eg, participants with or without particular characteristics), and sufficient observations of specific transition types within each subgroup (eg, participants with particular combinations of characteristics making particular transitions). Given these demands, examination of dataset characteristics and model outputs suggested that representativeness may be more limited in Greece, Portugal, and Romanian SHARE survey datasets, and that cautious interpretation is warranted of arthritis-stratified results for Portugal, and arthritis by activity status in Slovenia. Representativeness appeared most robust for Belgium, Czech Republic, England (ELSA), Estonia, and France. We have not reported the estimates for 10 other countries (Croatia, Finland, Israel, Latvia, Lithuania, Luxemburg, Bulgaria, Malta, Cyprus, Slovakia) because of limited sample sizes and transitions to provide detailed estimates. We have also not presented estimates of years spent in other health and work states because of sample constraints; we have provided estimates of the proportion of those with RMDs who are not healthy or not in work in Supplementary Table S1a and S1b. Previous analysis of ELSA data indicated that, in the population with RMDs, with the lower HWLE, there was 1 year longer in the not healthy and working state, and substantially higher number of years spent in the not healthy and not working state compared to those without RMDs [15]. The definition of health focuses on capacity to work and alignment with the recommended Global Activity Limitation Indicator (GALI) [31]. One limitation is that the definition of work is broad and does not differentiate between amounts of work (eg, full-time vs part-time). For the health definition, it was not possible to incorporate the temporality aspect of the recommended GALI [31].

Self-report of doctor-diagnosed arthritis excludes those who have joint pain but do not seek healthcare for it; this may misclassify those with osteoarthritis who are less likely to seek healthcare, instead viewing their symptoms as an inevitable part of ageing that healthcare cannot improve. The binary variable masks the heterogeneity, in terms of type, severity and time since diagnosis of RMDs. There is an assumption that self-reported ‘doctor-diagnosed arthritis’ indicates a similar severity, type, and distribution of arthritis in each country; differences in diagnosis may explain some of the differences by country. However, this operationalisation is likely to capture RMDs that lead to significant functional limitation, as evidence suggests most persons with limiting symptoms do seek healthcare advice for it [32]. Exclusion of those with missing data may have impacted the representativeness of HWLE estimates. Not having an ‘other’ option for sex may have contributed to a small amount of missing data.

Implications

Knowledge about the differences in HWLE reported in this manuscript will be crucial for the design of policies aimed at increasing the length of working life for people with RMDs, particularly when people will be expected to work until they are older because of population ageing and pension policies encouraging extension to working life. The lower HWLE in adults with RMDs suggests that extending the length of work participation will be difficult for many people who experience pain, and functional limitation, from RMDs. The much lower level of HWLE in most countries across Europe among populations with RMDs indicates the need for policies to focus on supporting people with RMDs to remain in/return to work to reduce the inequality.

This would be encouraged by having work participation as a treatment goal to encourage a focus on work for working-age adults and to utilise opportunities (treatment of RMDs or how to improve work) for people with RMDs [1]. The higher levels for some countries and strata indicate there is potential for HWLE to increase. Policy issues that impact at macrolevel and on economic conditions may be beyond the scope of the RMD community but targeting the need to support health and work must continue to be a priority. Policy focusing on individual factors that target work expectations and culture and lifestyle factors, such as known detriments to health (eg, obesity), would reduce the impact on people with RMDs. The further reduction in HWLE linked to sex and education indicates a focus on supporting women and those who are in occupations linked to lower socioeconomic status and where workers have less latitude to manage pain and disability. This can include initiatives to promote job availability and fair hiring practices, facilitate training and retraining opportunities for workers with RMDs, and encourage employer flexibility to adapt jobs and workplaces. A focus on maintaining health in the worker, which would include maintenance of physical activity, would contribute to increases in the ability of people with RMDs to work for longer. This should include adults aged less than 50 when RMDs begin to influence work participation.

A key implication for research is that there is a need for larger sample sizes to model the transitions that occur and datasets that provide information across health, work, and lifestyle factors. This will provide a greater understanding of how health, sociodemographic, workplace, and environmental factors combine to drive being healthy and in work; this includes understanding why absenteeism (work absence) and presenteeism (reduced productivity while at work due to illness or for other reasons) occur.

In conclusion, the findings indicate that people with RMDs have substantially reduced ability to work until they are older. The magnitude of these differences suggests the need for policy approaches across Europe and within countries to support longer healthy working lives. Variations by country, sex, education, and physical activity levels suggest that HWLE could be improved through targeted interventions addressing modifiable factors.

FUNDING

This work was supported by European Alliance of Associations for Rheumatology Health Professionals grants (HPR 044 & HPR 047) and through a NIHR Policy Research Programme grant (NIHR204670). The views expressed are those of the author(s) and not necessarily those of the NIHR or the Department of Health and Social Care.

Competing interests

All authors declare they have no competing interests.

CRediT authorship contribution statement

Ross Wilkie: Writing – review & editing, Writing – original draft, Investigation, Funding acquisition, Conceptualization. **Oluwasikemi Onamusi:** Writing – review & editing, Writing – original draft, Formal analysis, Data curation. **Jessica Potts:** Writing – review & editing, Writing – original draft, Formal analysis, Data curation. **Marty Lynch:** Writing – review & editing, Writing – original draft, Methodology, Funding acquisition, Formal analysis, Data curation.

Patient consent for publication

Not applicable.

Ethical approval

This study involved secondary analysis of data from the English Longitudinal Study of Ageing (ELSA) and the Survey of Health, Ageing and Retirement in Europe (SHARE). Ethical approval for each wave of both studies was obtained from the relevant national and institutional research ethics committees, and all participants provided informed consent. No additional ethical approval was required for the present analysis.

Provenance and peer review

Not commissioned; externally peer reviewed.

Supplementary materials

Supplementary material associated with this article can be found in the online version at doi:10.1016/j.ard.2026.02.010.

Orcid

Ross Wilkie: http://orcid.org/0000-0003-4825-714X
Oluwasikemi Onamusi: http://orcid.org/0009-0006-9018-1248
Jessica Potts: http://orcid.org/0000-0002-9333-5787
Marty Lynch: http://orcid.org/0000-0003-4882-6875

REFERENCES

[1] Boonen A, Webers C, Butink M, Barten B, Betteridge N, Black DC, et al. 2021 EULAR points to consider to support people with rheumatic and musculoskeletal diseases to participate in healthy and sustainable paid work. Ann Rheum Dis 2023;82:57–64.
[2] van der Zwan R, de Beer P. The disability employment gap in European countries: what is the role of labour market policy? J Eur Soc Policy 2021;31:473–86.
[3] Bevan S, Quadrello T, McGee R. Reducing temporary work absence through early intervention: the case of MSDs in the EU. Lancaster: The Work Foundation 2013.
[4] EULAR. EULAR strategy, 2023. [cited 2026 March 2]. Available from: https://www.eular.org/eular-strategy
[5] European Agency for Safety and Health at Work-EU-OSHA. Work-related musculoskeletal disorders: prevalence, costs and demographics in the EU. 2019. [cited 2026 March 2]. Available from: https://osha.europa.eu/sites/default/files/Work-related_MSDs_prevalence_costs_and_demographics_in_the_EU_report.pdf
[6] European Agency for Safety and Health at Work, IKEI, Panteia, Kok JD, Vroonhof P, et al. Work-related musculoskeletal disorders - prevalence, costs and demographics in the EU, Publications Office; 2019. [cited 2026 March 2]. Available from: https://data.europa.eu/doi/10.2802/66947
[7] Waddell G, Kim Burton A. Is work good for your health and well-being?. The Stationary Office; 2006. [cited 2026 March 2]. Available from: https://huddersfield.box.com/s/kmyygl6clmsap4m3femp6wb7joaxd87d.
[8] OECD. Pensions at a Glance 2023: OECD and G20 Indicators. Paris: OECD Publishing; 2023 https://doi.org/10.1787/678055dd-en.
[9] GBD 2021 Other Musculoskeletal Disorders Collaborators. Global, regional, and national burden of other musculoskeletal disorders, 1990-2020, and projections to 2050: a systematic analysis of the Global Burden of Disease Study 2021. Lancet Rheumatol. 2023;5(11):e670–82. doi: 10.1016/S2665-9913(23)00232-1.

[10] Murphy LB, Cisternas MG, Pasta DJ, Helmick CG, Yelin EH. Medical expenditures and earnings losses among US adults with arthritis in 2013. Arthritis Care Res (Hoboken) 2018;70:869–76. doi: 10.1002/acr.23425.
[11] Lievre A, Jusot F, Barnay T, Sermet C, Brouard N, Robine JM, et al. Healthy working life expectancies at age 50 in Europe: a new indicator. J Nutr Health Aging 2007;11:508–14.
[12] Parker M, Bucknall M, Jagger C, Wilkie R. Population-based estimates of healthy working life expectancy in England at age 50 years: analysis of data from the English Longitudinal Study of Ageing. Lancet Public Health 2020;5: e395–403. doi: 10.1016/S2468-2667(20)30114-6.
[13] Futures of big tech in Europe. Publications Office of the European Union; 2024. [cited 2026 March 2] https://op.europa.eu/en/publication-detail/-/publication/db955dcf-af69-11ee-b164-01aa75ed71a1/language-en.
[14] Lynch M, Bucknall M, Jagger C, Kingston A, Wilkie R. Demographic, health, physical activity, and workplace factors are associated with lower healthy working life expectancy and life expectancy at age 50. Sci Rep. 2024 Mar 11;14(1):5936. doi: 10.1038/s41598-024-53095-z.
[15] Lynch M, Bucknall M, Jagger C, Wilkie R. Healthy working life expectancy at age 50 for people with and without osteoarthritis in local and national English populations. Sci Rep. 2022 Feb 14;12(1):2408. doi: 10.1038/s41598-022-06490-3.
[16] Börsch-Supan A, Brandt M, Hunkler C, Kneip T, Korbmacher J, Malter F, et al. Data resource profile: the survey of health, ageing and retirement in Europe (SHARE). Int J Epidemiol 2013;42:992–1001. doi: 10.1093/ije/dyt088.
[17] Bergmann M, Kneip T, De Luca G, Scherpenzeel A. Survey participation in the Survey of Health, Ageing and Retirement in Europe (SHARE), Wave 1-7. 2019. Based on Release 7.0.0. SHARE Work. Pap. Ser., 41-2019. Munich: MEA, Max Planck Institute for Social Law and Social Policy; 2019. [cited 2026 March 2]. Available from: https://share-eric.eu/fileadmin/user_upload/SHARE_Working_Paper/WP_Series_41_2019_Bergmann_et_al.pdf
[18] Bergmann M, Wagner M, Börsch-Supan A. Share wave 9 methodology: from the share corona survey 2 to the share main wave 9 interview. In: Bergmann M, Wagner M, Börsch-Supan A, editors. Munich: SHARE-ERIC; 2024.
[19] Banks J, Batty G, David, Breedvelt J, Coughlin K, Crawford R, et al. (2026). English Longitudinal Study of Ageing: Waves 0-11, 1998-2024. [data collection]. 49th Edition. UK Data Service. SN: 5050, http://doi.org/10.5255/UKDA-SN-5050-36
[20] Scholes S, Taylor R, Cheshire H, Cox K, Lessof C. Technical report (ELSA wave 2): retirement, health and relationships of the older population in England. ELSA. 2008. [cited 2026 March 2]. Available from: https://ifs.org.uk/publications/technical-report-elsa-wave-2-retirement-health-and-relationships-older-population.
[21] Bridges S, Hussey D, Blake M. The Dynamics of Ageing: The 2012 English Longitudinal Study of Ageing (Wave 6) Technical Report. 2015. [cited 2026 March 2]. Available from: https://www.ucl.ac.uk/population-health-sciences/sites/population_health_sciences/files/5050_elsa_w6_technical_report_v1.pdf.
[22] Wilkie R, Phillipson C, Hay EM, Pransky G. Anticipated significant work limitation in primary care consulters with osteoarthritis: a prospective cohort study. BMJ Open 2014;4:e005221.
[23] Loeser RF, Goldring SR, Scanzello CR, Goldring MB. Osteoarthritis: a disease of the joint as an organ. Arthritis Rheum 2012;64:1697–707.
[24] Eurostat. Pensions and labour market participation-main characteristics. 2024. [cited 2026 March 2]. Available from: https://ec.europa.eu/eurostat/statistics-explained/index.php?title=Pensions_and_labour_market_participation_-_main_characteristics#Recent_trends_in_statutory_pension_ages_in_the_EU
[25] Khalatbari-Soltani S, Maccora J, Blyth FM, Joannès C, Kelly-Irving M. Measuring education in the context of health inequalities. Int J Epidemiol 2022;51(3):701–8.
[26] Lynch M, Wilkie R. Increasing inequalities in healthy working lives. Lancet Public Health 2023;8(8):e578–9. doi: 10.1016/S2468-2667(23)00155-X.
[27] Gwinnutt JM, Wieczorek M, Balanescu A, Bischoff-Ferrari HA, Boonen A, Cavalli G, et al. 2021 EULAR recommendations regarding lifestyle behaviours and work participation to prevent progression of rheumatic and musculoskeletal diseases. Ann Rheum Dis 2023;82:48–56.
[28] Boissonneault M, Rios P. Changes in healthy and unhealthy working-life expectancy over the period 2002-17: a population-based study in people aged 51-65 years in 14 OECD countries. Lancet Healthy Longev 2021;2:e629–38.
[29] Cislaghi B, Bhatia A, Hallgren EST, Horanieh N, Weber AM, Darmstadt GL. Gender norms and gender equality in full-time employment and health: a 97-country analysis of the World values survey. Front Psychol 2022 May 31;13:689815.
[30] Dudel C. Healthy and unhealthy working-life expectancy: opportunities and challenges. Lancet Healthy Longev 2021;2(10):e604–5.
[31] Robine JM, Jagger C, Euro-REVES Group. Creating a coherent set of indicators to monitor health across Europe: the Euro-REVES 2 project. Eur J Public Health 2003;13(3 Suppl):6–14.
[32] Paskins Z, Sanders T, Hassell AB. What influences patients with osteoarthritis to consult their GP about their symptoms? A narrative review. BMC Fam Pract 2013;14:195.

Ann Rheum Dis 85 (2026) 1678–1679

Contents lists available at ScienceDirect

Annals of the Rheumatic Diseases

journal homepage: https://www.sciencedirect.com/journal/annals-of-the-rheumatic-diseases

Letter

Criterion validity of the EULAR Antiphospholipid Syndrome Disease Activity Score (EAPSDAS)

The EULAR Antiphospholipid Syndrome Disease Activity Score (EAPSDAS) is a newly developed clinical measure [1,2] that measures antiphospholipid syndrome (APS) disease activity based on new or worsening thrombotic/microvascular/nonthrombotic (TMN) manifestations and separately scores obstetric manifestations. Either the maximum TMN score or the average TMN score during an observation period can be calculated. In initial tests of construct validity, TMN scores were highly correlated with physician ratings of APS activity in patient vignettes [1]. Here, we examined the criterion validity of the TMN maximum score, using mortality as the criterion. We tested the hypothesis that TMN maximum scores over the study period would be higher in patients who died from APS than in patients who died from other causes and those who survived during observation.

We performed a nested case-control study within the Euro-Phospholipid cohort, which was a prospective 10-year observational study of clinical manifestations and outcomes in 1000 patients with primary or secondary APS [3]. We limited our study to patients with primary APS, because the development of the EAPSDAS was focused on this group, and to patients observed during the last 5 years of the study (2004-2009). New/worsening TMN manifestations during this period were scored independently by 3 study investigators (MGT, GJP-E, SS), and the maximum TMN score was determined. Discrepancies were resolved by consensus. Mortality and causes of death had previously been recorded [3] and were used to classify cases (death due to APS) and 2 groups of controls (death from other causes; alive). We used Wilcoxon rank-sum tests to compare maximum TMN scores between groups.

The 459 patients had a median (25th, 75th percentile) age of 49 (42, 60) years, and 78% were women. The median TMN maximum score was 0 (0, 39). During the observation period, 12 patients died from manifestations of APS, including stroke (n = 4), myocardial infarction (n = 3), pulmonary embolism (n = 3), haemorrhage (n = 1), and catastrophic APS (n = 1). Fifteen patients died from other causes (infections in 8), and 432 patients survived; 10 patients were lost to follow-up during observation.

TMN maximum scores were significantly higher among patients who died from APS (median 87 [25th, 75th percentile 86, 87]) than among those who survived (median 0 [25th, 75th percentile 0, 0]) and those who died from other causes (median 0 [25th, 75th percentile 0, 65]) (Table). Although age and sex distributions were similar between cases and controls, we also compared TMN maximum scores within sex/age subgroups to control for potential confounding. Results were similar in these subgroups (Table).

Strengths of the study include the use of data from the largest cohort to date of patients with primary APS with information on all new thrombotic, microvascular, and nonthrombotic manifestations scored using the EAPSDAS, and the inclusion of multiple European centres, supporting the generalizability of our findings. A limitation is the lack of information on the exact time new manifestations occurred, which precludes calculation of the average TMN score. We controlled for age and sex but not for comorbidities such as cardiovascular risk factors [4] and APS-related treatments (eg, anticoagulants and/or antiplatelets), because the associations of cardiovascular risk factors and treatments with death is largely through, and not independent of, APS events.

In showing a strong association with disease-specific mortality, these results support the criterion validity of the TMN scale of the EAPSDAS. As with other time-adjusted disease activity scores (eg, Systemic Lupus Erythematosus Disease Activity Index) [5], validating the TMN maximum score against mortality suggests an association between disease activity and long-

Table
Comparison of maximum TMN scores during observation in patients based on cause of death

	Number	Maximum TMN score, median (25^{th}, 75^{th})			*P*	*P*
		Alive	Death from other causes	Death due to APS	Death due to APS vs alive	Death due to APS vs death from other causes
All	453	0 (0, 0)	0 (0, 65)	87 (86, 87)	<.0001	<.0001
Men	68	0 (0, 61)	0 (0, 0)	86 (85, 87)	<.0001	<.0001
Women aged 18-44 y	128	0 (0, 39)	0 (0, 0)	87 (85, 95)	<.0001	<.0001
Women aged 45-64 y	167	0 (0, 0)	39 (0, 82)	87 (87, 87)	<.0001	<.0001
Women aged 65 y or older	44	0 (0, 47)	0 (0, 32.5)	87 (85, 87)	<.0001	<.0001

APS, antiphospholipid syndrome; TMN, thrombotic/microvascular/nonthrombotic.
Data on age or sex were missing for 46 patients.

https://doi.org/10.1016/j.ard.2026.02.001
Received 9 January 2026; Revised 2 February 2026; Accepted 2 February 2026

term survival. This may help identify groups at high risk requiring aggressive, targeted therapies [6]. Additional studies are needed to examine the validity of average TMN scores over time and of the obstetric scale.

Competing interests

MGT: grants to the institution from AbbVie, Boehringer Ingelheim, DEMO, Faran, GSK, and UCB; participation in advisory boards for GSK, Lilly, and UCB; honoraria for presentations by GSK and Otsuka Pharmaceutical. AT: participation in advisory boards from UCB and Galapagos. MMW: consultant to Advanced Clinical LLC. RC, GJP-E, SS: none declared.

Contributors

MGT: study conception and design, supervision, data analysis, interpretation of data, manuscript writing, guarantor. RC: data curation, data acquisition. GJP-E and SS: data acquisition, data analysis. AT: data acquisition. MMW: study conception and design, methodology, data analysis, interpretation of data, manuscript writing. All authors critically revised the manuscript and approved its final version.

Funding

None.

Patient consent for publication

Not applicable.

Ethics approval

This EAPSDAS validation study was approved by the Institutional Review Board of Laiko Hospital, Athens, Greece (protocol number 148, 14-03-22). The Euro-Phospholipid study (1999-2009) was approved by the Data Ethics Committee of the Hospital Clínic of Barcelona, Spain.

Provenance and peer review

Not commissioned; externally peer-reviewed.

Data availability statement

All data relevant to the study are included in this article, and the accompanying methodology article is published simultaneously.

Orcid

Maria G. Tektonidou: http://orcid.org/0000-0003-2238-0975
Ricard Cervera: http://orcid.org/0000-0001-6085-492X
Guillermo J. Pons-Estel: http://orcid.org/0000-0002-0647-929X
Savino Sciascia: http://orcid.org/0000-0003-1266-9441
Angela Tincani: http://orcid.org/0000-0003-4355-9333
Michael M. Ward: http://orcid.org/0000-0003-1857-9367

REFERENCES

[1] Tektonidou MG, Cervera R, Tincani A, Pons-Estel GJ, Sciascia S, Alijotas-Reig J, et al. Development and validation of a EULAR disease activity score in antiphospholipid syndrome. Ann Rheum Dis 2025. doi: 10.1016/j.ard.2025.10.006.
[2] Tektonidou MG, Cervera R, Tincani A, Pons-Estel GJ, Sciascia S, Stamm T, et al. Methodology of the development of the EULAR Antiphospholipid Syndrome Disease Activity Score (EAPSDAS). EULAR Rheumatol Open 2025. doi: 10.1016/j.ero.2025.07.009.
[3] Ahmadzadeh Y, Magder LS, de Andrade DCO, Paredes-Ruiz D, Tektonidou MG, Pengo V, et al. Predictors of mortality in antiphospholipid antibody-positive patients: prospective results from Antiphospholipid Syndrome Alliance for Clinical Trials and International Networking clinical database and repository. Arthritis Care Res (Hoboken) 2025;77:760–6. doi: 10.1002/acr.25503.
[4] Bolla E, Semb AG, Petri M, Sfikakis PP, Artim-Esen B, Hernandez-Molina G, et al. Cardiovascular risk factor control in antiphospholipid syndrome, and differences between primary and systemic lupus erythematosus-related antiphospholipid syndrome (SURF-SLE and APS project): a cross-sectional study of 1003 individuals from 11 countries. Lancet Rheumatol 2025. doi: 10.1016/S2665-9913(25)00257-7.
[5] Ibañez D, Urowitz MB, Gladman DD. Summarizing disease features over time: I. Adjusted mean SLEDAI derivation and application to an index of disease activity in lupus. J Rheumatol 2003;30(9):1977–82.
[6] Lopez-Pedrera C, Pérez-Sánchez C, Tektonidou MG. Towards precision medicine in antiphospholipid syndrome. Lancet Rheumatol 2025;7 e5(8)76-89. doi: 10.1016/S2665-9913(25)00094-3.

Maria G. Tektonidou *
Rheumatology Unit, First Department of Propaedeutic Internal Medicine, Joint Academic Rheumatology Program, Medical School, National and Kapodistrian University of Athens, Athens, Greece

Ricard Cervera
Department of Autoimmune Diseases, Hospital Clínic, IDIBAPS, University of Barcelona, Barcelona, Catalonia, Spain

Guillermo J. Pons-Estel
Department of Rheumatology, Grupo Oroño-Centro Regional de Enfermedades Autoinmunes y Reumáticas (GO-CREAR), Rosario, Argentina

Savino Sciascia
University Center of Excellence on Nephrologic, Rheumatologic and Rare Diseases (ERK-Net, ERN Reconnet and RITA-ERN Member), University of Turin, Turin, Italy

Angela Tincani
Rheumatology and Clinical Immunology Unit-ERN ReCONNET, ASST-Spedali Civili and University of Brescia, Brescia, Italy

Michael M. Ward
Verier Outcomes Research, Rockville, MD, USA

*__Correspondence to__ Prof Maria G. Tektonidou, Rheumatology Unit, First Department of Propaedeutic Internal Medicine, Joint Academic Rheumatology Program, Medical School, National and Kapodistrian University of Athens, Laiko Hospital, 17 Agiou Thoma Street, Goudi, 115 27 Athens, Greece.
E-mail addresses: mtektonidou@gmail.com, mtektonidou@med.uoa.gr (M.G. Tektonidou).

Ann Rheum Dis 85 (2026) 1680–1682

Contents lists available at ScienceDirect

Annals of the Rheumatic Diseases

journal homepage: https://www.sciencedirect.com/journal/annals-of-the-rheumatic-diseases

Letter

MRI structural lesions in axSpA: distinguishing outcome measures from diagnostic thresholds

Inhibiting development and progression of structural damage is a priority for patients with axial spondyloarthritis (axSpA) [1]. To address this concern, the measurement of structural damage is important. Radiographs have traditionally been used to measure structural damage, but their sensitivity is low. Magnetic resonance imaging (MRI) has emerged as an alternative to allow earlier and more sensitive detection of structural lesions, such as erosions, fat lesions, or ankylosis, in axSpA. Consequently, MRI has been increasingly used in research studies, including clinical trials, to assess structural damage over time.

Currently, no outcome measurement instruments have been formally validated for quantifying MRI structural lesions in axSpA. Individual groups have proposed and started to use different methods for measuring MRI structural damage. Some approaches focus on counting individual lesions, such as the Spondyloarthritis Research Consortium of Canada (SPARCC) MRI sacroiliac joint (SIJ) structural score (SPARCC-SSS), which uses a count for each lesion type, but without an overall or aggregated score [2]. Building on this, the total number of structural lesions has been reported as an outcome [3]. In parallel, dichotomous lesion thresholds, such as '≥5 fat lesions or erosions,' '≥3 SIJ quadrants with erosions,' or '≥5 fat lesions' on MRI of the SIJ or spine have been proposed to maximise discrimination between axSpA and non-axSpA chronic back pain and can therefore be useful for diagnostic or classification purposes in studies [4,5].

The lack of consensual and validated instruments has caused substantial heterogeneity in how MRI structural lesions are assessed across studies. Moreover, the proposed measures are often applied irrespective of the study type or objective. This may also happen due to a lack of agreement in the field on the specific measurement instruments to use [3,6]. It is essential to point out that the abovementioned approaches serve different purposes. Structural lesion counts quantify the structural burden or progression in patients with axSpA and are therefore best regarded as outcome measures. The specific count variable may differ—for example, the measures listed in the Table and scoring systems such as the SPARCC-SSS and Canada-Denmark MRI scoring system of the spine (CANDEN), which apply

Table
MRI structural lesions in axSpA and examples of their use as outcome measure or as a diagnostic threshold

Structural lesions	Use as an outcome measure	Use as diagnostic threshold (dichotomous threshold with high specificity for axSpA and good discriminatory capacity)
MRI-SIJ		
Erosions	0-40	≥3 erosions ≥3 SIJ quadrants with erosions ≥1 erosion present in ≥2 consecutive slices
Fat lesions	0-40	≥3 fat lesions ≥5 erosions or fat lesions ≥5 SIJ quadrants with fat lesions ≥1 fat lesion present in ≥3 consecutive slices ≥1 deep fat lesion (>1 cm depth)
(partial) Ankylosis	0-24[a]	
Total structural lesions[b]	0-104	
MRI spine		
Erosions	0-92	
Fat lesions	0-92	≥5 fat lesions
Bone spurs	0-92	
Ankylosis	0-46	
Total structural lesions[c]	0-322	

axSpA; axial spondyloarthritis; MRI; magnetic resonance imaging; SIJ, sacroiliac joint.
[a] Difference in scoring from the original Spondyloarthritis Research Consortium of Canada (SPARCC) sacroiliac joint structural score because of scoring 6 slices, in alignment with the assessment of bone marrow oedema following the SPARCC scoring system.
[b] Total structural lesions considering erosions, fat lesions, and (partial) ankylosis.
[c] Total structural lesions considering erosions, fat lesions, bone spurs and ankylosis.

https://doi.org/10.1016/j.ard.2026.03.008
Received 13 November 2025; Revised 6 January 2026; Accepted 10 March 2026

different ranges—but the underlying principle remains the same [2,3,6–8]. In contrast, dichotomous thresholds such as '≥5 fat lesions or erosions' are markers of disease presence. These binomial thresholds were 'tailor-made,' namely for optimally distinguishing patients with chronic back pain due to axSpA from those with pain due to other causes. This means that binomial thresholds cannot be used to monitor the severity or degree of abnormalities in patients with axSpA over time, as their binary nature obscures true quantitative change.

To promote methodological consistency, we emphasise the importance of distinguishing existing measures of MRI structural lesions by their intended use. When using imaging outcomes in longitudinal studies of structural progression, researchers should select lesion-count scores designed for outcome assessment (Table, left column). For diagnostic or classification studies, especially those differentiating axSpA from non-axSpA chronic back pain, dichotomous thresholds that are discriminatory between groups should be used (Table, right column).

Contributors

SR wrote the first version of the paper. All authors discussed the content and reviewed it until its final version, which was approved by all. SR is guarantor.

Funding

The authors have not declared a specific grant for this research from any funding agency in the public, commercial or not-for-profit sectors.

Competing interests

SR has received consultancy fees from AbbVie, Alfasigma, Eli Lilly, Johnson & Johnson, MSD, Novartis, Pfizer, and UCB; speaker fees from Eli Lilly, Novartis, and UCB; and research grants from AbbVie, Alfasigma, Eli Lilly, MSD, Novartis, Pfizer, and UCB. FAvG has received consultancy fees from Novartis, MSD, AbbVie, Bristol Myers Squibb, and Eli Lilly; research grants from Stichting vrienden van Sole Mio, Stichting ASAS, Novartis, and UCB; and is a member of the Assessment of SpondyloArthritis international Society (ASAS) and ASAS treasurer. MdH has received consultancy fees from UCB Pharma. MvL has no competing interests to declare. DvdH has received consulting fees from AbbVie, Alfasigma, ArgenX, BMS, Eli-Lilly, Grey-Wolf Therapeutics, Janssen, Novartis, Pfizer, Takeda, and UCB Pharma and is director of Imaging Rheumatology bv, an Associate editor of *Annals of the Rheumatic Diseases*, and an editorial board member of *Journal of Rheumatology*. RL has received speaker/consultancy fees from AbbVie, UCB, Novartis, Galapagos, and Janssen.

Patient consent for publication

Not applicable.

Ethics approval

Not applicable.

Provenance and peer review

Not commissioned; externally peer reviewed.

Data availability statement

Not applicable.

Orcid

Sofia Ramiro: http://orcid.org/0000-0002-8899-9087
Floris A. van Gaalen: http://orcid.org/0000-0001-8448-7407
Manouk de Hooge: http://orcid.org/0000-0002-0652-9808
Miranda van Lunteren: http://orcid.org/0000-0002-0601-4863
Désirée van der Heijde: http://orcid.org/0000-0002-5781-158X
Robert Landewé: http://orcid.org/0000-0002-0577-6620

REFERENCES

[1] Garrido-Cumbrera M, Poddubnyy D, Gossec L, Gálvez-Ruiz D, Bundy C, Mahapatra R, et al. The European map of axial spondyloarthritis: capturing the patient perspective-an analysis of 2846 patients across 13 countries. Curr Rheumatol Rep 2019;21(5):19.
[2] Maksymowych WP, Wichuk S, Chiowchanwisawakit P, Lambert RG, Pedersen SJ. Development and preliminary validation of the spondyloarthritis research consortium of Canada magnetic resonance imaging sacroiliac joint structural score. J Rheumatol 2015;42(1):79–86.
[3] Sepriano A, Ramiro S, van der Heijde D, Dougados M, Claudepierre P, Feydy A, et al. Imaging outcomes for axial spondyloarthritis and sensitivity to change: a five-year analysis of the DESIR cohort. Arthritis Care Res (Hoboken) 2022;74(2):251–8.
[4] de Hooge M, van den Berg R, Navarro-Compán V, Reijnierse M, van Gaalen F, Fagerli K, et al. Patients with chronic back pain of short duration from the SPACE cohort: which MRI structural lesions in the sacroiliac joints and inflammatory and structural lesions in the spine are most specific for axial spondyloarthritis? Ann Rheum Dis 2016;75(7):1308–14.
[5] Maksymowych WP, Lambert RG, Baraliakos X, Weber U, Machado PM, Pedersen SJ, et al. Data-driven definitions for active and structural MRI lesions in the sacroiliac joint in spondyloarthritis and their predictive utility. Rheumatology (Oxford) 2021;60(10):4778–89.
[6] López-Medina C, Molto A, Sepriano A, Ramiro S, Tournadre A, Dougados M. Sensitivity to change of structural outcomes in axial spondyloarthritis after 10 years of follow up. Data from the DESIR cohort. RMD Open 2024;10(3):e004400.
[7] Krabbe S, Østergaard M, Pedersen SJ, Weber U, Kröber G, Makysmowych W, et al. Canada-Denmark MRI scoring system of the spine in patients with axial spondyloarthritis: updated definitions, scoring rules and inter-reader reliability in a multiple reader setting. RMD Open 2019;5(2):e001057.
[8] Madari Q, Sepriano A, Ramiro S, Molto A, Claudepierre P, Wendling D, et al. 5-year follow-up of spinal and sacroiliac MRI abnormalities in early axial spondyloarthritis: data from the DESIR cohort. RMD Open 2020;6(1):e001093.

Sofia Ramiro *
Department of Rheumatology, Leiden University Medical Center, Leiden, the Netherlands
Department of Rheumatology, Zuyderland Medical Center, Heerlen, the Netherlands

Floris A. van Gaalen
Department of Rheumatology, Leiden University Medical Center, Leiden, the Netherlands

Manouk de Hooge
Department of Rheumatology, Leiden University Medical Center, Leiden, the Netherlands
Department of Rheumatology, Ghent University Hospital, Gent, Belgium

Miranda van Lunteren
Department of Rheumatology, Leiden University Medical Center, Leiden, the Netherlands

Désirée van der Heijde
Department of Rheumatology, Leiden University Medical Center, Leiden, the Netherlands

Robert Landewé
Department of Rheumatology, Amsterdam University Medical Center, Amsterdam, the Netherlands
Department of Rheumatology, Zuyderland Medical Center, Heerlen, the Netherlands

*__Correspondence to__ Dr Sofia Ramiro
E-mail address: sofiaramiro@gmail.com (S. Ramiro).

Ann Rheum Dis 85 (2026) e75–e76

Contents lists available at ScienceDirect

Annals of the Rheumatic Diseases

journal homepage: https://www.sciencedirect.com/journal/annals-of-the-rheumatic-diseases

Correspondence

Correspondence on 'How long do people with rheumatic and musculoskeletal diseases stay healthy and in work across Europe? Analysis of data from SHARE and ELSA' by Wilkie et al

To the Editor,

We read with interest the paper by Wilkie et al [1], which estimates healthy working-life expectancy (HWLE) for people with rheumatic and musculoskeletal diseases (RMDs) across 19 European countries [1]. It is an important study and a timely reminder of the scale of the work-related disadvantage associated with RMDs. However, it identifies the burden more clearly than the remedy. That distinction matters if cross-country differences are to inform policy.

Caution begins with the exposure definition. RMD status was based on self-report of ever having received a doctor's diagnosis of 'arthritis or rheumatism', and once recorded, was treated as irreversible [1]. As the authors acknowledge, this binary variable obscures heterogeneity in diagnosis, severity, and duration, and may also reflect differences in diagnostic practice across countries [1]. Clinically, this is not a minor caveat. 'Arthritis or rheumatism' is not a single entity, and a broad administrative category is a poor substitute for disease phenotype when the question is why one country appears to sustain work better than another. Some of the observed variation in work sustainability may therefore reflect differences in who is classified as having RMD in the first place.

Interpretation is further complicated by the outcome structure. The model combines 3 distinct states: healthy and not at work, not healthy and at work, and not healthy and not at work, into a single residual category [1]. The authors are clear that this simplification reflects sample constraints [1]. Even so, the price is interpretive ambiguity, a problem well recognised in studies using work participation as an outcome domain [2,3]. A reduction in HWLE driven mainly by labour-market exit is not the same problem as one driven mainly by deterioration in health status, even if both reduce the same summary measure. The policy implications are plainly different: one points towards pension rules, job design, and workplace accommodation; the other towards disease control, rehabilitation, and clinical support [2,3]. When these pathways are not separated, the policy signal is inevitably blurred.

This becomes more important when sample limitations are considered. The authors note that representativeness may be more limited in Greece, Portugal, and Romania; that some stratified estimates require particular caution; and that results for 10 additional countries could not be presented because sample sizes and transitions were insufficient [1]. These acknowledgements strengthen confidence in the authors' judgement, but should also temper confidence in the precision of cross-national ranking. When both the case definition and transition modelling are partly constrained by the data, international contrasts should be interpreted with caution.

Similar care is needed when interpreting physical inactivity. The association with lower HWLE is clinically plausible and important. However, the paper notes that inactivity may partly serve as a proxy for pain, disability, or disease severity and highlights countries where the expected pattern is not observed [1]. In this setting, inactivity cannot yet be assumed to be a straightforward intervention target [4,5]. What is robustly shown is association; what remains uncertain is how much of that association is independently modifiable.

None of this diminishes the value of the study. On the contrary, it makes an important contribution by quantifying the loss of healthy working years associated with RMDs across Europe [1]. But its principal strength is descriptive. The paper convincingly shows that the burden is large. It is less able, at least in its present form, to show which levers should be pulled, in which countries, and for what precise reason. That distinction matters to clinicians, employers, and policymakers alike.

CRediT authorship contribution statement

Robert Weglowski: Conceptualization, Investigation, Writing – original draft, Writing – review & editing. **Lukasz Szarpak:** Conceptualization, Resources, Supervision, Writing – original draft, Writing – review & editing. **Mahdi Al-Jeabory:** Conceptualization, Data curation, Writing – original draft, Writing – review & editing.

Funding

No specific funding was received for this work.

Competing interests

All authors declare they have no competing interests.

https://doi.org/10.1016/j.ard.2026.03.009
Received 9 March 2026; Accepted 10 March 2026

Patient consent for publication

Not applicable.

Ethics approval

Not applicable. This correspondence is based on the interpretation of previously published data and did not involve original human participant research or new data collection.

Provenance and peer review

Not commissioned; not peer reviewed.

Orcid

Lukasz Szarpak: http://orcid.org/0000-0002-0973-5455

REFERENCES

[1] Wilkie R, Onamusi O, Potts J, Lynch M. How long do people with rheumatic and musculoskeletal diseases stay healthy and in work across Europe? Analysis of data from SHARE and ELSA. Ann Rheum Dis 2026 Mar 5;S0003-4967(26)00085-3. doi: 10.1016/j.ard.2026.02.010.

[2] Boonen A, Webers C, Butink M, Barten B, Betteridge N, Black DC, et al. 2021 EULAR points to consider to support people with rheumatic and musculoskeletal diseases to participate in healthy and sustainable paid work. Ann Rheum Dis 2023;82(1):57–64. doi: 10.1136/ard-2022-222678.

[3] Boonen A, Putrik P, Marques ML, Alunno A, Abasolo L, Beaton D, et al. EULAR points to consider (PtC) for designing, analysing and reporting of studies with work participation as an outcome domain in patients with inflammatory arthritis. Ann Rheum Dis 2021;80(9):1116–23. doi: 10.1136/annrheumdis-2020-219523.

[4] Gwinnutt JM, Wieczorek M, Balanescu A, Bischoff-Ferrari HA, Boonen A, Cavalli G, et al. 2021 EULAR recommendations regarding lifestyle behaviours and work participation to prevent progression of rheumatic and musculoskeletal diseases. Ann Rheum Dis 2023;82(1):48–56. doi: 10.1136/annrheumdis-2021-222020.

[5] Butink MHP, Webers C, Verstappen SMM, Falzon L, Betteridge N, Wiek D, et al. Non-pharmacological interventions to promote work participation in people with rheumatic and musculoskeletal diseases: a systematic review and meta-analysis from the EULAR taskforce on healthy and sustainable work participation. RMD Open 2023;9(1):e002903. doi: 10.1136/rmdopen-2022-002903.

Robert Weglowski[1], Lukasz Szarpak[2,3,*], Mahdi Al-Jeabory[4,5]

[1] *Clinical Department of Trauma and Orthopedic Surgery, The John Paul II Catholic University of Lublin, Radzyn Podlaski, Poland*

[2] *Institute of Medical Sciences, The John Paul II Catholic University of Lublin, Lublin, Poland*

[3] *Henry JN Taub Department of Emergency Medicine, Baylor College of Medicine, Houston, TX, USA*

[4] *Department of Trauma and Orthopedic Surgery, Silesian Center for Rheumatology, Ustron, Poland*

[5] *Clinical Department of Orthopedics, Faculty of Medical Sciences in Zabrze, Medical University of Silesia, Katowice, Silesia, Poland*

*__Correspondence to__ Prof Lukasz Szarpak, Henry JN Taub Department of Emergency Medicine, Baylor College of Medicine, Houston, TX, USA.
E-mail address: lukasz.szarpak@gmail.com (L. Szarpak).

Ann Rheum Dis 85 (2026) e77–e78

Contents lists available at ScienceDirect

Annals of the Rheumatic Diseases

journal homepage: https://www.sciencedirect.com/journal/annals-of-the-rheumatic-diseases

Correspondence

Response to correspondence on "How long do people with rheumatic and musculoskeletal diseases stay healthy and in work across Europe?"

We thank Weglowski and colleagues [1] for their thoughtful engagement with our study [2].

We agree that the analysis is principally descriptive. Healthy working life expectancy (HWLE) is a population indicator that quantifies the average number of years that a population spends in both healthy and in work from age 50 years, and estimates are descriptive rather than causal. The substantial variation we observed, with HWLE for populations with rheumatic and musculoskeletal diseases (RMDs) falling to around half that of populations without RMDs in several countries, demonstrates the scale of disadvantage associated with these conditions across Europe. This variation, even allowing for differences in measurement and case ascertainment, signals that policy-relevant differences exist and merit further attention.

Our study reported HWLE; however, it was not feasible to report time spent in the other health and work states: healthy and not working, not healthy and working, and not healthy and not working. In other studies where such reporting was possible, time spent in the unhealthy but still working state was generally limited, suggesting that health status is an important aspect of maintaining work participation [3–5].

HWLE does not clearly distinguish whether reductions primarily arise from health deterioration or labour market exit. Weglowski et al [1] are clear that both health and work are important to the conversation of extending working lives [1]. We agree that understanding pathways out of healthy work requires recognising that both health and work play a role and furthermore that these roles interact. Whether a given job remains sustainable depends on functional capacity and broader psychosocial factors, including those in the workplace. The availability of suitable job roles also varies by context. This is why we examined HWLE rather than healthy life expectancy or working life expectancy alone. Neither measure alone provides a clear policy signal about the population's readiness to extend working lives, making HWLE better suited for this purpose. Understanding why populations differ in HWLE, and what can be done to improve it, requires studies that examine transitions between health and work states, informed by descriptive findings such as these.

The broad self-reported category of 'arthritis or rheumatism' used in this study grouped together a wide range of musculoskeletal conditions, varying in terms of duration, severity, and impact on work and health, and we treated onset as irreversible once reported [6]. This operationalisation reflects what the survey data provide and aligns with how musculoskeletal conditions are often recorded in population work-related statistics, but it is indeed a limitation, particularly for condition-specific interpretation. Further work is needed to understand how different factors influence staying in or exiting from healthy work and how these pathways differ across condition types and between populations with and without RMDs. This includes understanding the role of factors such as physical inactivity, which may act as intervention targets, markers of severity, or both.

The findings provide a foundation, as Weglowski et al [1] also suggested; they quantify the burden, identify variation associated with RMDs by country and sociodemographic factors, and suggest that opportunities for improvement exist. Realising those opportunities will require larger data sets amenable to modelling transitions in greater detail and studies designed to identify which specific factors function as modifiable policy levers in different contexts.

Competing interests

All authors declare they have no competing interests.

CRediT authorship contribution statement

Ross Wilkie: Conceptualization, Writing – review & editing. **Oluwasikemi Onamusi:** Writing – review & editing. **Jessica Potts:** Writing – review & editing. **Marty Lynch:** Conceptualization, Writing – review & editing.

Funding

This research did not receive any specific grant from funding agencies in the public, commercial, or not-for-profit sectors.

Patient consent for publication

Not applicable.

Ethics approval

Not applicable.

DOI of original article: http://dx.doi.org/10.1016/j.ard.2026.03.009.

https://doi.org/10.1016/j.ard.2026.03.028
Received 23 March 2026; Accepted 24 March 2026

Orcid

Marty Lynch: http://orcid.org/0000-0003-4882-6875

REFERENCES

[1] Weglowski R, Szarpak L, Al-Jeabory M. Correspondence on "How long do people with rheumatic and musculoskeletal diseases stay healthy and in work across Europe? Analysis of data from SHARE and ELSA" by Wilkie et al. Ann Rheum Dis; 2026. doi: 10.1016/j.ard.2026.03.009.

[2] Wilkie R, Onamusi O, Potts J, Lynch M. How long do people with rheumatic and musculoskeletal diseases stay healthy and in work across Europe? Analysis of data from SHARE and ELSA. Ann Rheum Dis. https://doi.org/10.1016/j.ard.2026.02.010.

[3] Parker M, Bucknall M, Jagger C, Wilkie R. Population-based estimates of healthy working life expectancy in England at age 50 years: analysis of data from the English Longitudinal Study of Ageing. Lancet Public Health 2020;5(7):e395–403. doi: 10.1016/S2468-2667(20)30114-6.

[4] Hambisa MT, Tawiah R, Jagger C, Kiely KM. Gender, education, and cohort differences in healthy working life expectancy at age 50 years in Australia: a longitudinal analysis. Lancet Public Health 2023;8(8):e610–7. doi: 10.1016/S2468-2667(23)00129-9.

[5] Yang M, Lee J, Lynch M, Wilkie R, van Tongeren M, Kang MY. Educational and gender disparities in healthy working life expectancy among middle-aged and older adults in South Korea. Occup Environ Med 2025;82(6):293–9. doi: 10.1136/oemed-2025-110239.

[6] Wilkie R, Phillipson C, Hay EM, Pransky G. Anticipated significant work limitation in primary care consulters with osteoarthritis: a prospective cohort study. BMJ Open 2014;4(9):e005221. doi: 10.1136/bmjopen-2014-005221.

Ross Wilkie, Oluwasikemi Onamusi, Jessica Potts, Marty Lynch*
School of Medicine, Keele University, Staffordshire, UK

*Correspondence to Dr Marty Lynch, School of Medicine, Keele University, Staffordshire, UK.
E-mail address: m.e.lynch@keele.ac.uk (M. Lynch).

Ann Rheum Dis 85 (2026) e79–e80

Contents lists available at ScienceDirect

Annals of the Rheumatic Diseases

journal homepage: https://www.sciencedirect.com/journal/annals-of-the-rheumatic-diseases

Correspondence

Correspondence on 'Psoriatic dactylitis: the association with HLA genetic susceptibility markers' by 'Kharouf et al.'

Dear Editor,

I read with great interest the fascinating recent report by Kharouf et al, 'Psoriatic dactylitis: the association with HLA genetic susceptibility markers' [1]. Human leukocyte antigen (HLA) class I, including specific HLA-B alleles—particularly HLA-B27—is a known susceptibility marker for psoriatic arthritis (PsA) occurrence [2]. In their large cohort (n = 1216), in addition to HLA-B27, HLA-C alleles—especially HLA-C2—are suggested to be associated with the dactylitis domain of PsA [1]. Such a novel association with HLA-C is intriguing; further validation is essential [3]. HLA-C locus alleles likely influence the clinical features of PsA, but additional subanalyses may be needed to explore this interesting finding, as detailed below.

In regression models, the risk is approximately 2 for HLA-B*27 (odds ratio [OR] 1.94, 95% CI 1.49-2.53), HLA-C*02 (OR 1.63, 95% CI 1.17-2.25), and the haplotype HLA-B*27/C*02 (OR 1.88, 95% CI 1.32-2.67). The study showed a positive association between PsA dactylitis (both tender and nontender) and the presence of HLA-B*27, HLA-C*02, and HLA-B*27/C*02 genetic markers. Most (93.4%) of their cohort experienced dactylitis resolution during follow-up. Interestingly, analyses of both univariable and multivariable models, except for HLA-B27, found no allele or haplotype that was significantly associated [1]. Adjusting for potential confounders, such as age, sex, calendar decade, PsA duration, and use of antirheumatic drugs, is important, but I believe the most relevant factor to adjust for is ethnicity.

In the study cohort, most (85%) participants were of White ancestry (n = 1033). Among them, the frequency of HLA-B*27 was about 1 in 5 patients (n = 191) across various European ancestry subgroups (18.5%; range = 5.1%-25%), and approximately 1 in 2 White patients had dactylitis (49.7%; range = 45.9%-58.3%) [S3, ref 1]. However, in the non-White ethnic group (n = 183), the HLA-B*27 frequency was low, roughly 1 in 15 patients (n = 10), while about 1 in 3 had dactylitis (range = 32.3%-42.0%) [S2, ref 1]. Notably, within the study cohort, White ancestry, which was enriched for HLA-B*27, showed only a modest increase in PsA dactylitis compared to non-White groups. This may suggest a role for non-HLA-B*27 factors, such as other HLA genetic susceptibility markers (eg, HLA-C), especially in non-White populations. Therefore, a supplementary note should be added to detail the frequency of other non-HLA-B27 types, including the HLA-C alleles linked with increased risk (OR) of dactylitis, specifically HLA-C*02 and HLA-B*27/C*02. Before evaluating the risk of these HLA-C-specific alleles and haplotypes alongside HLA-B27 for PsA, clinical phenotypes and specific features like psoriatic dactylitis, data on missing class I HLA typing across different ethnic groups need to be completed.

In summary, the connection between HLA genetic susceptibility markers, especially HLA-C, and its influence on the phenotype of PsA remains unclear and requires further research.

Competing interests

The author declares no competing interests.

CRediT authorship contribution statement

Suhail Aamar: Conceptualization, Data curation, Resources, Writing – original draft, Writing – review & editing.

Funding

None.

Patient consent for publication

Not applicable.

Ethics approval

Not applicable.

Provenance and peer review

Not commissioned; externally peer reviewed.

Orcid

Suhail Aamar: http://orcid.org/0000-0003-1671-8220.

REFERENCES

[1] Kharouf F, Abarza VC, Mehta P, Gao S, Ganatra D, Pereira D, et al. Psoriatic dactylitis: the association with HLA genetic susceptibility markers. Ann Rheum Dis 2026;S0003-4967(26):00086-5. Epub ahead of print. doi: 10.1016/j.ard.2026.02.011.

[2] Queiro R, Morante I, Cabezas I, Acasuso B. HLA-B27 and psoriatic disease: a modern view of an old relationship. Rheumatology (Oxford) 2016 Feb 1;55(2):221–9.

https://doi.org/10.1016/j.ard.2026.03.012
Received 10 March 2026; Accepted 12 March 2026

[3] Queiro R, Gonzalez S, López-Larrea C, Alperi M, Sarasqueta C, Riestra JL, et al. HLA-C locus alleles may modulate the clinical expression of psoriatic arthritis. Arthritis Res Ther 2006 Dec 13;8(6):R185.

Suhail Aamar [1,2,*]

[1] *Rheumatology Clinic, Hadassah-Hebrew University Medical Center, Mount Scopus Hospital, Jerusalem, Israel*

[2] *Rheumatology Unit, Assuta Ashdod University Hospital; Faculty of Health Sciences, Ben-Gurion University of the Negev, Beer-Sheva, Israel*

*__Correspondence to__ Dr Suhail Aamar, Rheumatology Clinic, Hadassah Mount Scopus, Jerusalem, Israel.
E-mail address: suhail_aamar@hotmail.com

Ann Rheum Dis 85 (2026) e81–e83

Contents lists available at ScienceDirect

Annals of the Rheumatic Diseases

journal homepage: https://www.sciencedirect.com/journal/annals-of-the-rheumatic-diseases

Correspondence

Response to correspondence on "Psoriatic dactylitis: the association with HLA genetic susceptibility markers" by Kharouf et al

We thank Dr Aamar for the careful reading of our work [1] and for raising important considerations regarding the role of ethnicity in the interpretation of human leukocyte antigen (HLA) associations in psoriatic arthritis (PsA).

We agree that population structure is relevant in genetic association studies, particularly given known variability in HLA allele frequencies across ancestral groups [2]. This was acknowledged in our manuscript as a limitation, as the cohort is predominantly of White ancestry, which may limit generalizability and preclude robust ancestry-stratified analyses.

However, we would qualify the assertion that ethnicity represents the most relevant confounder in our time-to-resolution models. For ethnicity to act as a confounder, it would need to be associated not only with HLA allele distribution but also independently with the rate of resolution of tender dactylitis. Although the former is well established [2,3], the latter remains uncertain. We therefore consider this an important hypothesis rather than an established source of confounding.

To address this point directly, however, we performed a sensitivity analysis further adjusting the multivariable Cox models for ethnicity (White vs other). The results were materially unchanged (Table 1), including the association between *HLA-B*27* and slower resolution of tender dactylitis, which remained statistically significant. Estimates for the remaining alleles and haplotypes were also not meaningfully altered. These findings are consistent with the primary analysis.

We also agree that additional descriptive data on the distribution of relevant alleles across ethnic groups may be informative. The frequencies of *HLA-C*02* and the *HLA-B*27/C*02* haplotype across ethnic strata, alongside *HLA-B*27* and dactylitis history, are provided in Table 2. These alleles were more frequent in White participants than in other groups. However, given the limited sample size in non-White strata, particularly within certain subgroups, these findings should be interpreted with caution.

Finally, we agree that the relationship between HLA class I alleles—particularly HLA-C—and specific PsA phenotypes such as dactylitis remains incompletely defined. Our findings are consistent with prior studies [3–6] but require replication, particularly in larger and more diverse cohorts with detailed ancestry characterization.

In summary, although ethnicity is an important consideration in genetic studies of PsA, our sensitivity analysis does not support a material confounding effect on the association between *HLA-B*27* and the resolution of tender dactylitis. We provide additional data on the distribution of *HLA-C**02 and *HLA-B*27/C*02*, which were more frequent in White participants; however, the limited representation of non-White strata precludes robust inference regarding ancestry-specific effects. As we noted in the original manuscript, this represents an important limitation of our study; larger, population-based studies are required to address this.

We thank the author for the thoughtful and constructive remarks and believe that such scientific dialogue contributes meaningfully to the advancement of the field.

DOI of original article: http://dx.doi.org/10.1016/j.ard.2026.03.012.

https://doi.org/10.1016/j.ard.2026.03.031
Received 25 March 2026; Accepted 27 March 2026

Table 1
Results of the univariable and separate multivariable Cox regression analyses for each allele or haplotype for the time to resolution of tender dactylitis

Variable	Univariable model			Multivariable model*		
	HR	95% CI	*P* value	HR	95% CI	*P* value
Alleles						
*HLA-B*08*	0.98	0.76-1.26	0.87	0.99	0.69-1.40	.94
*HLA-B*15*	1.16	0.86-1.55	0.33	1.10	0.76-1.59	.60
*HLA-B*27*	**0.72**	**0.56-0.94**	**0.02**	**0.75**	**0.57-0.98**	**.04**
*HLA-B*40*	1.32	0.80-2.18	0.27	1.50	0.89-2.51	.13
*HLA-B*51*	0.81	0.54-1.22	0.32	0.86	0.54-1.37	.64
*HLA-C*02*	0.78	0.59-1.05	0.10	0.84	0.58-1.21	.34
*HLA-C*03*	1.19	0.89-1.60	0.24	1.41	0.97-2.03	.07
*HLA-C*12*	1.04	0.83-1.31	0.71	0.97	0.78-1.21	.80
Haplotypes						
*HLA-B*08/C*07*	0.99	0.76-1.28	0.92	1.00	0.73-1.36	.98
*HLA-B*27/C*01*	0.98	0.67-1.42	0.91	0.98	0.67-1.43	.91
*HLA-B*27/C*02*	0.76	0.53-1.09	0.13	0.80	0.55-1.17	.25
*HLA-B*38/C*12*	1.03	0.76-1.38	0.85	0.96	0.72-1.30	.80
*HLA-B*44/C*05*	1.06	0.80-1.40	0.71	1.05	0.75-1.46	.77
*HLA-B*44/C*16*	0.90	0.63-1.29	0.58	0.97	0.59-1.62	.92
*HLA-B*57/C*06*	0.97	0.71-1.33	0.84	0.99	0.72-1.36	.95

CI, confidence interval; DMARD, disease-modifying antirheumatic drug; HLA, human leukocyte antigen; HR, hazard ratio; PsA, psoriatic arthritis

* Adjusted for age, sex, ethnicity (White versus non-White), calendar decade (with 1978-1988 as the reference; other categories: 1989-1999, 2000-2010, and 2011-2024), PsA duration, and background use of conventional synthetic DMARDs as well as biologic or targeted synthetic DMARDs, all measured at the time when dactylitis was recorded.
Bold values indicate statistical significance ($p < 0.05$).

Table 2
Frequency of *HLA-B*27*, *HLA-C*02*, and *HLA-B*27/C*02* and history of dactylitis across ethnic groups

Variable	White (n = 1033)	South Asian (n = 69)	Chinese (n = 31)	Other (n = 83)
*HLA-B*27*, *n* (%)	191 (18.5%)	5 (7.2%)	0 (0.0%)	5 (6.0%)
*HLA-C*02*, *n* (%)	128 (12.4%)	3 (4.3%)	0 (0.0%)	2 (2.4%)
*HLA-B*27/C*02*, *n* (%)	101 (9.8%)	3 (4.3%)	0 (0.0%)	1 (1.2%)
Dactylitis ever, *n* (%)	513 (49.7%)	29 (42.0%)	10 (32.3%)	32 (38.6%)

HLA, human leukocyte antigen.

CONTRIBUTORS

All authors made significant contributions to the conception, design, and execution of this study. All authors reviewed and approved the final manuscript.

FUNDING

The Gladman Krembil Psoriatic Arthritis Program is funded by a grant from the Krembil Foundation and the Schroeder Arthritis Institute. DP is supported by a grant from the Krembil Foundation. VC is supported by Dr Dafna D. Gladman, Chair in Psoriatic Arthritis Research, a joint Hospital-University Named Chair between the University of Toronto, the University Health Network, and the UHN Foundation.

Competing interests

DP has received research grants for AbbVie, Eli Lilly, Johnson and Johnson, Novartis, Pfizer, UCB, and has received honoraria for advisory board member roles from AbbVie, Biocad, Bristol-Myers Squibb, Eli Lilly, Janssen, Moonlake, Novartis, Pfizer, and UCB. DG has received grants and/or consulting fees from AbbVie, Amgen, AstraZeneca, Bristol-Myers Squibb, Eli Lilly, Fresenius Kabi, Johnson and Johnson, Novartis, Pfizer, and UCB. VC has received research grants from AbbVie, Eli Lilly, and Johnson and Johnson, and has received honoraria for advisory board member roles from AbbVie, Bristol-Myers Squibb, Eli Lilly, Fresenius Kabi, Johnson and Johnson, Novartis, Takeda, and UCB. His spouse is an employee of AstraZeneca. All other authors declare they have no competing interests.

Patient consent for publication

Not applicable.

Ethics approval

This research study was approved by the University Health Network Research Ethics Board (REB Study#: 08-0630). All individuals have provided written informed consent for this research study and its publication.

Provenance and peer review

Not commissioned; externally peer reviewed.

Data availability statement

The data underlying this article will be shared on reasonable request to the corresponding author.

Orcid

Fadi Kharouf: http://orcid.org/0000-0002-3540-0341

REFERENCES

[1] Kharouf F, Abarza VC, Mehta P, Gao S, Ganatra D, Pereira D, et al. Psoriatic dactylitis: the association with HLA genetic susceptibility markers. Ann Rheum Dis 2026 S0003-4967(26)00086-5. doi: 10.1016/j.ard.2026.02.011.
[2] Arrieta-Bolaños E, Hernández-Zaragoza DI, Barquera R. An HLA map of the world: a comparison of HLA frequencies in 200 worldwide populations reveals diverse patterns for class I and class II. Front Genet 2023;14:866407. doi: 10.3389/fgene.2023.866407.
[3] Chandran V. Genetic determinants of psoriatic arthritis. University of Toronto; 2014.
[4] Queiro R, Gonzalez S, López-Larrea C, Alperi M, Sarasqueta C, Riestra JL, et al. HLA-C locus alleles may modulate the clinical expression of psoriatic arthritis. Arthritis Res Ther 2006;8(6):R185. doi: 10.1186/ar2097.
[5] FitzGerald O, Haroon M, Giles JT, Winchester R. Concepts of pathogenesis in psoriatic arthritis: genotype determines clinical phenotype. Arthritis Res Ther 2015;17(1):115. doi: 10.1186/s13075-015-0640-3.
[6] Haroon M, Winchester R, Giles JT, Heffernan E, FitzGerald O. Certain class I HLA alleles and haplotypes implicated in susceptibility play a role in determining specific features of the psoriatic arthritis phenotype. Ann Rheum Dis 2016;75(1):155–62. doi: 10.1136/annrheumdis-2014-205461.

Fadi Kharouf
Gladman Krembil Psoriatic Arthritis Program, Centre for Prognosis Studies in the Rheumatic Diseases, Schroeder Arthritis Institute, Krembil Research Institute, University Health Network, Toronto, Ontario, Canada
Division of Rheumatology, Department of Medicine, University of Toronto, Toronto, Ontario, Canada
Rheumatology Unit, Department of Medicine, Hadassah Medical Center and Faculty of Medicine, Hebrew University of Jerusalem, Israel

Virginia Carrizo Abarza
Gladman Krembil Psoriatic Arthritis Program, Centre for Prognosis Studies in the Rheumatic Diseases, Schroeder Arthritis Institute, Krembil Research Institute, University Health Network, Toronto, Ontario, Canada
Division of Rheumatology, Department of Medicine, University of Toronto, Toronto, Ontario, Canada

Pankti Mehta
Gladman Krembil Psoriatic Arthritis Program, Centre for Prognosis Studies in the Rheumatic Diseases, Schroeder Arthritis Institute, Krembil Research Institute, University Health Network, Toronto, Ontario, Canada
Division of Rheumatology, Department of Medicine, University of Toronto, Toronto, Ontario, Canada
Institute of Medical Science, University of Toronto, Toronto, Ontario, Canada

Shangyi Gao
Gladman Krembil Psoriatic Arthritis Program, Centre for Prognosis Studies in the Rheumatic Diseases, Schroeder Arthritis Institute, Krembil Research Institute, University Health Network, Toronto, Ontario, Canada

Darshini Ganatra
Gladman Krembil Psoriatic Arthritis Program, Centre for Prognosis Studies in the Rheumatic Diseases, Schroeder Arthritis Institute, Krembil Research Institute, University Health Network, Toronto, Ontario, Canada

Daniel Pereira
Gladman Krembil Psoriatic Arthritis Program, Centre for Prognosis Studies in the Rheumatic Diseases, Schroeder Arthritis Institute, Krembil Research Institute, University Health Network, Toronto, Ontario, Canada

Richard J. Cook
Department of Statistics and Actuarial Science, University of Waterloo, Waterloo, Ontario

Denis Poddubnyy
Gladman Krembil Psoriatic Arthritis Program, Centre for Prognosis Studies in the Rheumatic Diseases, Schroeder Arthritis Institute, Krembil Research Institute, University Health Network, Toronto, Ontario, Canada
Division of Rheumatology, Department of Medicine, University of Toronto, Toronto, Ontario, Canada
Institute of Medical Science, University of Toronto, Toronto, Ontario, Canada

Dafna D. Gladman
Gladman Krembil Psoriatic Arthritis Program, Centre for Prognosis Studies in the Rheumatic Diseases, Schroeder Arthritis Institute, Krembil Research Institute, University Health Network, Toronto, Ontario, Canada
Division of Rheumatology, Department of Medicine, University of Toronto, Toronto, Ontario, Canada
Institute of Medical Science, University of Toronto, Toronto, Ontario, Canada

Vinod Chandran*
Gladman Krembil Psoriatic Arthritis Program, Centre for Prognosis Studies in the Rheumatic Diseases, Schroeder Arthritis Institute, Krembil Research Institute, University Health Network, Toronto, Ontario, Canada
Division of Rheumatology, Department of Medicine, University of Toronto, Toronto, Ontario, Canada
Institute of Medical Science, University of Toronto, Toronto, Ontario, Canada
Department of Laboratory Medicine and Pathobiology, University of Toronto, Toronto, Ontario, Canada

*Correspondence to: Dr Vinod Chandran, University of Toronto, Department of Medicine, Division of Rheumatology, Toronto, Ontario, Canada.
E-mail address: vinod.chandran@uhn.ca (V. Chandran).

Ann Rheum Dis 85 (2026) e84–e85

Contents lists available at ScienceDirect

Annals of the Rheumatic Diseases

journal homepage: https://www.sciencedirect.com/journal/annals-of-the-rheumatic-diseases

Correspondence

Correspondence on 'Final validation of the hierarchical framework for outcomes in axial spondyloarthritis: longitudinal determinants of health-related quality of life'

Dear Editor,

We read with interest the 10-year longitudinal analysis by Ortolan et al. [1] in the Devenir des Spondylarthropathies Indifférenciées Récentes (DESIR) cohort. Their effort to move beyond cross-sectional associations and to examine how disease activity, physical function and health-related quality of life (HRQoL) relate over time is important. We are less convinced, however, the study justifies the claim of 'final validation'. What the analysis shows is that, within one early axial spondyloarthritis (axSpA) cohort and with a selected set of patient-reported instruments, the Axial Spondyloarthritis Disease Activity Score (ASDAS) and Bath Ankylosing Spondylitis Functional Index (BASFI), remain closely linked to later HRQoL. That is not the same as establishing a definitive hierarchy of outcome generation in axSpA.

The main difficulty lies in the status assigned to ASDAS. The model still assumes that ASDAS can be read largely as an upstream inflammatory construct and BASFI as its downstream functional consequence. That assumption has become harder to defend. Recent work suggests that ASDAS in treated axSpA is shaped not only by inflammation, but also by illness perception and central sensitisation [2]. The recent Assessment of SpondyloArthritis International Society (ASAS) consensus definition of difficult-to-manage and treatment-refractory axSpA makes the same point in more practical terms: treatment-refractory disease requires objective evidence of inflammatory activity and exclusion of noninflammatory explanations for persistent symptoms [3]. Against that background, the proposed sequence from ASDAS to BASFI and then to HRQoL looks less like a settled biological pathway than a model built around a mixed construct.

There is also a more basic issue of measurement proximity. ASDAS, BASFI, SF-36 and ankylosing spondylitis quality of life (ASQoL) are all heavily patient-derived and conceptually adjacent. Pain, fatigue, limitation, and perceived health run through all of them. Under those conditions, it is not surprising that BASFI appears to account for much of the association between ASDAS and later HRQoL. The question is whether this reflects mechanism or simply overlap between instruments that interrogate neighbouring domains in different language. This matter because current ASAS-Outcomes Measures in Rheumatology (OMERACT) work no longer treats axSpA outcomes as reducible to disease activity and physical function alone. The updated core set includes fatigue and overall functioning and health among the mandatory domains, with the ASAS Health Index selected to capture the latter [4]. A framework confined largely to ASDAS and BASFI therefore seems narrower than the field's current outcome architecture.

The omission of structural damage further limits the model. Recent data confirm that spinal damage remains independently associated with physical function, even if its contribution is smaller than that of disease activity or mobility [5]. Once imaging-defined inflammation, radiographic progression, spinal mobility, and the broader disease spectrum are left outside the model, the residual direct effect attributed to ASDAS becomes difficult to interpret. It is unlikely to represent one coherent pathway. More probably, it absorbs what the framework does not measure.

For the same reason, the clinical inference should be stated more cautiously. Recent guidance places the primary goal of management on optimising HRQoL through comprehensive management of all disease manifestations, prevention of structural damage, and preservation of physical function, work productivity and social participation and explicitly recommends that follow-up should be holistic and supported by, rather than solely reliant on, disease indices [6]. Seen in that light, the study by Ortolan et al. [1] offers a useful longitudinal description of how selected patient-reported domains move together over time, but it does not provide a final account of outcome generation in axSpA. The proposed hierarchy is informative, but incomplete.

Contributors

XQ wrote the original draft of the manuscript and contributed to investigation, formal analysis, and conceptualisation. C Li and C Luo contributed to investigation and conceptualisation and assisted with writing through review and editing. BC contributed to methodology, investigation, and conceptualisation and assisted with writing through review and editing.

Funding

This research did not receive any specific grant from funding agencies in the public, commercial, or not-for-profit sectors.

Handling editor Josef Smolen.

https://doi.org/10.1016/j.ard.2026.04.003
Received 6 April 2026; Accepted 7 April 2026

Competing interests

All authors declare they have no competing interests.

Patient consent for publication

Not applicable.

Ethics approval

Not applicable.

Provenance and peer review

Not commissioned; externally peer reviewed.

Orcid

Bo Chen: http://orcid.org/0009-0000-5599-4813

REFERENCES

[1] Ortolan A, van der Heijde D, Gossec L, Ramiro S. Final validation of the hierarchical framework for outcomes in axial spondyloarthritis: longitudinal determinants of health-related quality of life. Ann Rheum Dis 2026;85(2):308–18. doi: 10.1016/j.ard.2025.10.016.

[2] Kieskamp SC, van der Kraan Y, Arends S, Wink F, Bos R, Stewart R, et al. Interrelationships of disease activity, central sensitization, psychosocial and lifestyle factors in axial spondyloarthritis. Rheumatology (Oxford) 2025;64(6):3547–55. doi: 10.1093/rheumatology/keaf102.

[3] Poddubnyy D, Navarro-Compán V, Torgutalp M, Arends S, Aydin SZ, Battista S, et al. The assessment of spondyloarthritis international society (ASAS) consensus-based expert definition of difficult-to-manage, including treatment-refractory, axial spondyloarthritis. Ann Rheum Dis 2025;84(4):538–46. doi: 10.1016/j.ard.2025.01.035.

[4] Navarro-Compán V, Boel A, Boonen A, Mease PJ, Dougados M, Kiltz U, et al. Instrument selection for the ASAS core outcome set for axial spondyloarthritis. Ann Rheum Dis 2023;82(6):763–72. doi: 10.1136/annrheumdis-2022-222747.

[5] Penteado MPS, Resende GG, R da Cruz Lage, Jr Tavares WC, de Souza Bueno Filho JS, Ferreira GA. The burden of spine structural damage on function in patients with axial spondyloarthritis: adaptation-mediated uncoupling? J Rheumatol 2024;51(8):765–71. doi: 10.3899/jrheum.2024-0022.

[6] Zhao SS, Harrison SR, Thompson B, Yates M, Eddison J, Chan A, et al. The 2025 British Society for Rheumatology guideline for the treatment of axial spondyloarthritis with biologic and targeted synthetic DMARDs. Rheumatology (Oxford) 2025;64(6):3242–54. doi: 10.1093/rheumatology/keaf089.

Xia Qu, Chunlian Li, Cheng Luo, Bo Chen*

***Correspondence to** Dr Bo Chen, Department of Orthopedics, The Affiliated Traditional Chinese Medicine Hospital, Southwest Medical University, NO.182, Chunhui Road, Longmatan District, Luzhou, Sichuan, People's Republic of China
E-mail address: spinecb@163.com (B. Chen).

Ann Rheum Dis 85 (2026) e86–e87

Contents lists available at ScienceDirect

Annals of the Rheumatic Diseases

journal homepage: https://www.sciencedirect.com/journal/annals-of-the-rheumatic-diseases

Correspondence

Response to correspondence on 'Final validation of the hierarchical framework for outcomes in axial spondyloarthritis: longitudinal determinants of health-related quality of life'

We appreciate the interest shown by Qu et al. [1] in our work, 'Final validation of the hierarchical framework for outcomes in axial spondyloarthritis: longitudinal determinants of health-related quality of life' [2], and welcome the opportunity to respond.

Our conclusion of 'final validation' builds on a series of previous longitudinal studies that have validated the individual components of the hierarchical framework of outcomes in axial spondyloarthritis (axSpA) proposed by Machado et al. [3]. Specifically, 2 longitudinal studies [4,5] of the same Devenir des Spondylarthropathies Indifférénciées Récentes (DESIR) cohort, in which we conducted our analysis, demonstrated that (1) disease activity, structural damage, and spinal inflammation contribute to spinal mobility [4]; and (2) disease activity is the main contributor to disability (ie, loss of function), together with spinal mobility [5]. In both studies, contextual factors were considered in the associations, and their importance was confirmed in subsequent studies [4–6]. Starting from this, we continued and completed the validation of the hierarchical model. The choice of the DESIR cohort has been particularly relevant, as it includes the whole spectrum of axSpA (both radiographic and nonradiographic) and has followed patients for 10 years, providing robustness to our results. Furthermore, the relationships across the outcomes described above have been consistently reported in other cohorts, supporting the generalisability of our findings [7,8].

Illness perception and central sensitisation related to neuropathic and nociplastic pain can contribute to higher Axial Spondyloarthritis Disease Activity Score (ASDAS) scores. However, this can likely influence the magnitude, but not the presence of the association noted consistently throughout literature between disease activity and health-related quality of life (HRQoL) [9]. Of note, the DESIR cohort does not represent a trial population but rather reflects usual clinical care, and approximately 25% of its patients present with nociplastic pain; our results, therefore, indirectly incorporate the influence of this pain mechanism.

Usual instruments to assess HRQoL include Short Form (SF)-36 and Ankylosing Spondylitis Quality of Life. According to the Assessment of SpondyloArthritis international Society (ASAS)-Outcome Measures in Rheumatology core domain set [10], HRQoL is a proxy for overall functioning and health. According to the ASAS core outcome set, such a domain is assessed with the ASAS-HI, but the SF-36 is also endorsed [11]. The SF-36 has been widely used throughout medicine and allows comparisons across conditions; we chose this score to obtain an overview in the current analysis. Furthermore, we appreciate the remark about a possible redundancy in the instruments for disease activity, function, and HRQoL. Although some degree of conceptual proximity between patient-reported outcomes is unavoidable, consistent longitudinal associations across studies suggest that these relationships are not merely driven by measurement overlap. Moreover, it is well known that HRQoL is heavily influenced by both disease- and non–disease-related factors [8,9]. Accordingly, our analysis was adjusted for all contextual factors that, to the best of our knowledge, could influence these measures, thereby isolating the relationship between axSpA outcomes as much as possible.

Structural damage was not included in the model because, in this inception cohort of patients with axSpA, it has been demonstrated that structural damage was very low and progressed very slowly, probably due to a timely diagnosis and a prompt treatment [12,13]. For similar reasons, and given that the relationship between structural damage and spinal mobility has already been demonstrated [3,4], we considered that adding spinal mobility would contribute little to the model.

Taken together, these findings support the validity of the proposed framework while acknowledging that it represents a simplified -yet clinically meaningful- model of complex outcome interactions in axSpA. We demonstrated a direct relationship between disease activity and HRQoL, which makes the ASDAS a good target for treatment. We recognise nevertheless, the importance of non-pharmacological interventions for the preservation of physical function, work productivity and social participation, aimed at attaining a higher HRQoL. Our results underline how a prolonged control of disease activity over time might influence HRQoL, while accounting for the full range of contextual factors.

Competing interest

The authors declare the following financial interests/personal relationships, which may be considered as potential

DOI of original article: http://dx.doi.org/10.1016/j.ard.2026.04.003.

https://doi.org/10.1016/j.ard.2026.04.009
Received 21 April 2026; Accepted 22 April 2026

competing interests: AO reports relationships with AbbVie, Johnson & Johnson MedTech, Eli Lilly and Company, Novartis, and UCB Pharma SA that include consulting or advisory services. DvdH reports relationships with AbbVie, Alfasigma SpA, Argenx BV, Bristol Myers Squibb, Eli Lilly and Company, Grey Wolf Therapeutics Limited, Janssen Pharmaceuticals Inc, Novartis, Pfizer, Takeda Pharmaceuticals International AG, and UCB Pharma SA that include consulting or advisory services. LG reports relationships with AbbVie, Eli Lilly and Company, and Novartis that include consulting or advisory services and grant funding; a relationship with Biogen Inc that includes grant funding; and relationships with Amgen Inc, Bristol Myers Squibb, Celltrion Pharm Inc, Janssen Pharmaceuticals Inc, Merck Sharp & Dohme, Pfizer, Sandoz Inc, and UCB Pharma SA that include consulting or advisory services. SR reports relationships with AbbVie, Alfasigma SpA, Merck Sharp & Dohme, and Pfizer that include consulting or advisory services and grant funding; relationships with Novartis and UCB Pharma SA that include grant funding and speaking and lecture fees; a relationship with Eli Lilly and Company that includes consulting or advisory services and speaking and lecture fees; and a relationship with Janssen Pharmaceuticals Inc that includes consulting or advisory services.

Contributors

AO wrote the original draft, curated the data, and contributed to conceptualisation. DvdH and LG reviewed and edited the manuscript, contributed to visualisation and validation, supervised the work, and were involved in conceptualisation and data curation. SR reviewed and edited the manuscript, contributed to visualisation and validation, supervised the work, was involved in conceptualisation, and contributed to project administration. All authors participated in the development of the study and read and approved the final manuscript.

Funding

The Devenir des Spondylarthropathies Indifférenciées Récentes cohort was funded by unrestricted grants from (in order of decreasing support) Pfizer France, AbbVie, Biogen, UCB, Novartis, Lilly, Galapagos, MSD, Celltrion HealthCare, and Fresenius.

Patient consent for publication

Not applicable.

Ethics approval

Not applicable.

Provenance and peer review

Not applicable.

Orcid

Augusta Ortolan: http://orcid.org/0000-0002-3131-0939
Désirée van der Heijde: http://orcid.org/0000-0002-5781-158X
Laure Gossec: http://orcid.org/0000-0002-4528-310X
Sofia Ramiro: http://orcid.org/0000-0002-8899-9087

REFERENCES

[1] Qu X, Li C, Luo C, Chena B. Correspondence on 'Final validation of the hierarchical framework for outcomes in axial spondyloarthritis: longitudinal determinants of health-related quality of life'. Ann Rheum Dis. 2026;in press.
[2] Ortolan A, van der Heijde D, Gossec L, Ramiro S. Final validation of the hierarchical framework for outcomes in axial spondyloarthritis: longitudinal determinants of health-related quality of life. Ann Rheum Dis. 2026;85 (2):308–18.
[3] Machado P, Landewé R, Braun J, Hermann KG, Baraliakos X, Baker D, et al. A stratified model for health outcomes in ankylosing spondylitis. Ann Rheum Dis. 2011;70(10):1758–64.
[4] Carvalho PD, Ruyssen-Witrand A, Fonseca J, Marreiros A, Machado PM. Determining factors related to impaired spinal and hip mobility in patients with axial spondyloarthritis: longitudinal results from the DESIR cohort. RMD Open 2020;6(3):e001356.
[5] Carvalho PD, Ruyssen-Witrand A, Marreiros A, Machado PM. Long-term association between disease activity and disability in early axial spondyloarthritis: results from a prospective observational study of inflammatory back pain. Arthritis Care Res (Hoboken) 2022;74(5):768–75.
[6] Portier E, Benattar L, Resche-Rigon M, Dougados M, Gossec L, Molto A. Different disease activity trajectories in early axial spondyloarthritis lead to significantly different long-term outcomes: a trajectory-based analysis of the DESIR cohort over 10 years. RMD Open 2024;10(4):e004910.
[7] Machado P, Landewé R, Braun J, Hermann KG, Baker D, van der Heijde D. Both structural damage and inflammation of the spine contribute to impairment of spinal mobility in patients with ankylosing spondylitis. Ann Rheum Dis. 2010;69(8):1465–70.
[8] Poddubnyy D, Fedorova A, Listing J, Haibel H, Baraliakos X, Braun J, et al. Physical function and spinal mobility remain stable despite radiographic spinal progression in patients with ankylosing spondylitis treated with TNF-α inhibitors for up to 10 years. J Rheumatol. 2016;43(12):2142–8.
[9] Drouet J, López-Medina C, Granger B, Fautrel B, Landewe RBM, Molto A, et al. Disease activity and widespread pain are main contributors to patient-reported global health in axial spondyloarthritis: an analysis of 6064 patients. Rheumatol Int. 2024;44(8):1455–68.
[10] Navarro-Compán V, Boel A, Boonen A, Mease P, Landewé R, Kiltz U, et al. The ASAS-OMERACT core domain set for axial spondyloarthritis. Semin Arthritis Rheum 2021;51(6) 1342-9.
[11] Navarro-Compán V, Boel A, Boonen A, Mease PJ, Dougados M, Kiltz U, et al. Instrument selection for the ASAS core outcome set for axial spondyloarthritis. Ann Rheum Dis. 2023;82(6):763–72.
[12] Dougados M, Serrand C, Alonso S, Berenbaum F, Claudepierre P, Combe B, al et. Ten-year clinical outcome of recent-onset axial spondyloarthritis: results from the DESIR inception cohort. Joint Bone Spine 2024;91(3):105678.
[13] Ramiro S, van der Heijde D, Sepriano A, van Lunteren M, Moltó A, Feydy A, et al. Spinal radiographic progression in early axial spondyloarthritis: five-year results from the DESIR cohort. Arthritis Care Res (Hoboken) 2019;71 (12):1678–84.

Augusta Ortolan [1,2], Désirée van der Heijde [2], Laure Gossec [3,4], Sofia Ramiro [2,5,*]
[1] *Rheumatology and Clinical Immunology Unit, Fondazione Policlinico Universitario Agostino Gemelli IRCCS (Istituto di Ricovero e Cura a Carattere Scientifico), Rome, Italy*
[2] *Department of Rheumatology, Leiden University Medical Centre, Leiden, The Netherlands*
[3] *Institut National de la Santé Et de la Recherche Médicale, Institut Pierre Louis d'Epidé miologie et de Santé Publique, Sorbonne Université, Paris, France*
[4] *Rheumatology Department, Hopital Universitaire Pitie Salpetriere, Assistance Publique - Hopitaux de Paris, Paris, France*
[5] *Department of Rheumatology, Zuyderland Medical Centre, Heerlen, The Netherlands*

*Correspondence to Dr Sofia Ramiro
E-mail address: sofiaramiro@gmail.com (S. Ramiro).